# Multicarrier DS-CDMA Communication Systems Using Smart Antennas[1]

by

**Bin Hu**
School of Electronics and Computer Sciences
University of Southampton, SO17 1BJ, UK
Email: bh202r@ecs.soton.ac.uk

**Supervisors: Dr. Lie Liang Yang and Prof. Lajos Hanzo**

School of Electronics and Computer Sciences
University of Southampton, SO17 1BJ, UK
Email: lly@ecs.soton.ac.uk and lh@ecs.soton.ac.uk

[1]Last changed: Date: April 2006

UNIVERSITY OF SOUTHAMPTON

ABSTRACT

Faculty of Engineering and Applied Science
School of Electronics and Computer Science

Mini-Thesis submitted in candidature for upgrading from the degree of Master of Philosophy to the degree of Doctor of Philosophy

**Multicarrier DS-CDMA Communication Systems Using Smart Antennas**

by Bin Hu

Multi-Carrier Direct Sequence Code Division Multiple Access (MC DS-CDMA) constitutes an attractive scheme based on a combination of Direct Sequence Code Division Multiple Access (DS-CDMA) and Orthogonal Frequency Division Multiplexing (OFDM). Hence, MC DS-CDMA benefits from the advantages of both DS-CDMA and OFDM, resulting in a high spectral efficiency and substantial frequency diversity gain provided by the frequency selective fading channels. On the other hand, smart antennas are capable of increasing both the performance and the user-load of wireless systems, because they radiate and receive energy in the intended directions, hence reducing the interference between wireless users and improving the system's user-load. In this thesis the benefits of smart antennas are investigated in the context of a generalized MC DS-CDMA system, which includes the subclasses of both multitone DS-CDMA and orthogonal MC DS-CDMA as special cases.

Firstly, in Chapter 2 the philosophy of the generalized multicarrier DS-CDMA system invoking smart antennas was described and characterized, where a $(M \times L)$-dimensional antenna array was employed by the generalized MC DS-CDMA system considered for the sake of achieving both SNR gain and spatial diversity. Four optimum combining schemes, which are based on the Minimum Variance Distortionless Response (MVDR), the Maximum Signal-to-Interference-plus-Noise Ratio (MSINR), the Minimum Mean-Square Error (MMSE) and the Minimum Power Distortionless Response (MPDR) principles, were introduced. In the context of optimum combining, the signals received by the antennas are appropriately weighted and combined in order to combat the effect of the multipath fading on the desired signal and for the sake of mitigating the effects of the interfering signals. The family of optimum combiners designed for DS-CDMA and MC-CDMA systems was reviewed first. Then the derivation of the optimum array weight vector employed by the proposed MC DS-CDMA system was provided. The novelty of this part is that we exploit optimum combining techniques in the context of generalized MC DS-CDMA systems employing smart antennas for the sake of achieving frequency, time and spatial diversity. From the simulation results and the accompanying analysis we found that in the proposed MC DS-CDMA system supporting four users 4 dB SNR gain was achieved at a BER of $10^{-4}$ by joint subcarrier processing based optimum combiners.

Secondly, four downlink space-time transmitter processing schemes based on the principles of beamforming, Beam Selection Transmit Diversity (BSTD), Space-Time Transmit Diversity (STTD) and Steered Space-Time Spreading (SSTS) were invoked for the downlink of generalized MC DS-CDMA systems in Chapter 3, in order to enhance the achievable performance. Specific discussions concerning the downlink beamforming-aided generalized Multicarrier DS-CDMA system were first

provided. Then a BSTD scheme constituted by an amalgam of beamforming and Selection Transmit Diversity (STD) was discussed and analyzed, followed by the characterization of the STTD scheme. Finally, SSTS, based on both STTD and beamforming, was adopted for employment in the generalized MC DS-CDMA system. The novel contribution of the second part of this thesis is that the four downlink space-time transmitter processing schemes are investigated comparatively in the context of the smart antennas aided MC DS-CDMA system. Furthermore, an interference coefficient based user-grouping technique is proposed for reducing the effects of multiuser interference caused by the employment of both Time and Frequency (TF)-domain spreading. The system employing the interference coefficient based user grouping technique is shown to substantially outperform the system refraining from user grouping. Our simulation results also show that in the proposed MC DS-CDMA system supporting a single user and employing an antenna array having four antenna elements, the STTD scheme achieves the poorest performance, followed by the beamforming shceme, which achieves a 1.7 dB SNR gain compared to the STTD scheme at a BER of $10^{-5}$. The SSTS scheme outperforms both the STTD and beamforming schemes and achieves a 1.9 dB SNR gain compared to the STTD scheme. The BSTD scheme achieves the best BER performance and attains a 3.4 dB SNR gain compared to the STTD scheme.

Thirdly, a range of adaptive space-time processing schemes are investigated in the context of a generalized MC DS-CDMA system supported by a $(M \times L)$-dimensional antenna array in Chapter 4, where knowledge of the Direction of Arrival (DOA), of the channel amplitudes or of the channel-induced phase-rotations is required. A brief introduction to the literature of adaptive space-time processing is provided first, followed by portraying the philosophy of the Least-Mean-Square (LMS) and Recursive-Least-Square (RLS) algorithms. Then the LMS-based Adaptive Space-Time Detector (ASTD) and the RLS-based ASTD are developed for the adaptive uplink of the generalized MC DS-CDMA system. Furthermore, the Parallel Interference Canceller (PIC) technique is employed for improving the convergence rate of the ASTDs. The simulation results demonstrate that the RLS-based ASTD has a higher convergence rate than that of the LMS-based ASTD, which is achieved at the expense of a higher computational complexity. With the advent of the proposed PIC technique we are able to increase the achievable convergence rate of the ASTD, while maintaining the required BER performance. We may also conclude that when the spatial signals arriving at the different elements of the antenna array become less correlated, the spatial diversity gain becomes higher, hence the achievable BER performance improves. At a BER of $10^{-5}$, the ASTDs employing a $(4 \times 1)$-dimensional antenna array $(M = 4, L = 1)$ achieve a 5.0 dB SNR gain compared to that using a $(2 \times 2)$-dimensional antenna array $(M = 2, L = 2)$ and a 6.7 dB SNR gain against that of a $(1 \times 4)$-dimensional antenna array $(M = 1, L = 4)$.

Finally, in Chapter 5 the performance of subspace-based blind and group-blind space-time Multi-User Detection (MUD) invoked for a generalized MC DS-CDMA system is studied, which does not require any training sequence and hence achieves an increased spectrum efficiency. After a detailed discourse on subspace-based both totally blind and group-blind MUDs, we concentrated our investigations on blind and group-blind space-time MUD invoked for a smart antenna aided generalized MC

DS-CDMA system. Two adaptive subspace tracking algorithms, namely the Projection Approximation Subspace Tracking deflation (PASTd) algorithm and the Noise-Averaged Hermitian-Jacobi Fast Subspace Tracking (NAHJ-FST) algorithm, are employed for the sake of reducing the computational complexity imposed. As expected, the group-blind MUD benefitting from the knowledge of more intracell users' signature waveforms attained a better BER performance. The NAHJ-FST tracking algorithm exhibits a faster convergence and a better steady-state performance than that of the PASTd tracking algorithm. The blind and group-blind space-time MUDs equipped with the subspace based CIR estimator perform only slightly worse than the scheme exploiting the perfect knowledge of the CIRs, which implied that the associated performance degradation imposed by the channel estimator error is negligible. Furthermore, our simulation results suggested that increasing the number of AEs is capable of providing an increased degree of freedom and hence of substantially improving the attainable performance at the expense of a higher system complexity. It was shown that when employing an antenna array having $M = 2$ correlated AEs, the group-blind space-time MUD benefitting from the knowledge of $\tilde{K} = 8$ intracell users' spreading codes attained a 5.0 dB SNR gain at a BER of $2 \times 10^{-3}$, compared to the blind space-time MUD.

Acknowledgements

First of all I would like to express my heartfelt gratitude to Professor Lajos Hanzo for his outstanding supervision and support throughout my research. His guidance, inspiration and encouragement have greatly benefited me not only in work but also in life. Most importantly, I would like to thank him for his invaluable friendship.

I would also like to offer my heartfelt thanks to Dr. Lie-Liang Yang. His outstanding supervision, his encouragement and enthusiasm deserve my uttermost acknowledge and gratitude.

Many thanks also to my colleagues and the staff of the Communications Group, both past and present, for their support, help and discussions throughout my research. I would like to thank Hua Wei, Song Ni, Feng Guo, Soon X Ng, Wei Liu and all other colleagues and staff, too numerous to mention here explicitly. Special thanks are also due to Denise Harvey for her help in the administrative matters.

I would like to thank my parents in China for their love and support. Finally, to my beloved wife, Jinxia Li, for her love, support and care for me.

## LIST OF PUBLICATIONS

1) B. Hu, L. L. Yang and L. Hanzo, "Performance of the Smart Antenna Aided Multicarrier DS-CDMA Uplink", *IEEE Vehicular Technology Conference, Fall 2004*, Vol. 1, 26-29 Sept. 2004, pp. 191 - 195, Los Angeles, USA.

2) B. Hu, L. L. Yang and L. Hanzo, "Performance of the Smart Antenna Aided Generalized Multicarrier DS-CDMA Downlink Using Both Time-Domain Spreading and Steered Space-Time Spreading", *IEEE Vehicular Technology Conference, Fall 2005*, Vol. 1, 28-25 Sept. 2005, pp. 458 - 462, Dallas, USA.

3) B. Hu, L. L. Yang and L. Hanzo, "Adaptive Detection of Generalized Multicarrier DS-CDMA Employing Smart Antennas", In Proceedings of the IEE International Conference on 3G Mobile Communication Technologies 2005, London, UK, 7-9 November 2005.

4) B. Hu, L. L. Yang and L. Hanzo, "Differential Space-Time Modulation Schemes for Smart Antenna Aided Generalized Multicarrier DS-CDMA Systems", *to appear in Proceedings of IEEE Wireless Communications and Networking Conference 2006*, Las Vegas, USA, 3-6 April 2006.

5) B. Hu, W. Liu, L. L. Yang and L. Hanzo, "Multiuser Decorrelating Based Long-Range Frequency-Domain Channel Transfer Function Prediction in Multicarrier DS-CDMA Systems", *Accepted by IEEE International Symposium on Spread Spectrum Techniques (ISSSTA) 2006*, Manaus-Amazonia, Brazil, 28-31 August 2006.

6) B. Hu, L. L. Yang and L. Hanzo, "Subspace-Based Blind and Group-Blind Space-Time Multiuser Detection for the Generalized Multicarrier DS-CDMA Uplink", *submitted to IEEE Vehicular Technology Conference, Fall 2006*, Montreal, Canada, 25-28 September 2006.

7) B. Hu, L. L. Yang and L. Hanzo, "Downlink Differential Space-Time Spreading and Space-Time Steering Aided Generalized Multicarrier DS-CDMA", *submitted to IEEE Transactions on Wireless Communications*, October 2005.

8) B. Hu, L. L. Yang and L. Hanzo,"Adaptive Detection in the Generalized Multicarrier DS-CDMA Uplink Using Both Receiver Diversity and Receiver Beamforming", *submitted to IEEE*

*Transactions on Vehicular Technology*, January 2006.

9) B. Hu, L. L. Yang and L. Hanzo,"Time- and Frequency-Domain Spread Generalized Multicarrier DS-CDMA Using Subspace-Based Blind and Group-Blind Space-Time Multiuser Detection", *submitted to IEEE Transactions on Vehicular Technology*, February 2006.

10) B. Hu, L. L. Yang and L. Hanzo,"Time-Frequency-Space Diversity Aided Generalized Multicarrier DS-CDMA", *submitted to IEE Proc. Communications*, March 2006.

11) B. Hu, L. L. Yang and L. Hanzo, "Downlink Beamforming, Beam-Selection Transmit Diversity and Steered Space-Time Spreading Aided MC DS-CDMA", *submitted to IEEE Transactions on Vehicular Technology*, March 2006.

# List of Symbols

## General notation

- The superscript * is used to indicate complex conjugation. Therefore, $a^*$ represents the complex conjugate of the variable $a$.
- The superscript $^T$ is used to indicate matrix transpose operation. Therefore, $\mathbf{a}^T$ represents the transpose of the matrix $\mathbf{a}$.
- The superscript $^H$ is used to indicate complex conjugate transpose operation. Therefore, $\mathbf{a}^H$ represents the complex conjugate transpose of the matrix $\mathbf{a}$.
- The notation $\otimes$ denotes the convolutional process. Therefore, $a \otimes b$ represents the convolution between variables $a$ and $b$.
- The notation $\hat{x}$ represents the estimate of $x$.

## Special symbols

$U$: number of bits involved in the serial-to-parallel (S/P) converter;

$V$: number of subcarriers, used for the transmission of a bit. Hence, the total number of subcarriers is $UV$;

$T_b$: the bit duration;

$T_s$: the symbol duration;

$T_c$: the chip duration;

$\Delta = 1/T_s$: the spacing between two adjacent subcarrier frequencies;

$f_{uv}$: subcarrier frequency corresponding to the $v$th subcarrier of the set conveying the $u$th bit;

$\phi_{k,uv}$: phase angles corresponding to the $K$th user's subcarrier determined by $u$ and $v$;

$K$: total number of users supported by the MC DS-CDMA system;

$c_k(t)$: DS spreading waveform of the $k$th user, $1 \leq\leq K$;

$N_e$: T-domain spreading factor (gain) of the signals;

$P/V$: the transmitted power of each subcarrier;

$b_{ku}(t)$: the $u$th bit of the $k$th user;

$P_{T_c}(t)$: the rectangular chip waveform;

$\nabla = \Delta U$: the maximum possible frequency spacing for the $V$ number of subcarriers, which convey the same data bit;

$W_s$: the total bandwidth available;

$T_{c1}$: the chip-duration of a corresponding single-carrier DS-CDMA signal occupying the bandwidth of $W_s$;

$W_{ds} = 2/T_c$: the 'null-to-null' bandwidth of the subcarrier signals;

$T_m$: maximum delay spread of a wireless communication channel;

$L_p$: number of resolvable of paths associated with each subcarrier signal;

$M$: number of $\frac{\lambda}{2}$-spaced antenna arrays;

$L$: number of antenna elements in a $\frac{\lambda}{2}$-spaced antenna array;

$h_{uv,ml}^{(k)}$: the Spatio-Temporal Channel Impulse Response (ST-CIR) between the $uv$th subcarrier of the $k$th user and the $l$th $\frac{\lambda}{2}$-spaced array of the $m$th antenna;

$\tau_k$: signal delay of $k$th user;

$\varphi_{uv,ml}^{(k)}$: phase angle, which is the result of the channel-induced phase rotation, modelled by a random variable uniformly distributed in $[0, 2\pi]$;

$\alpha_{uv,ml}^{(k)}(t)$: Rayleigh faded envelope's amplitude corresponding to the $uv$th subcarrier signal and to the $l$th array of the $m$th antenna;

$d$: inter-element spacing of the $\frac{\lambda}{2}$-spaced antenna array;

$\lambda$: wavelength of the transmitted signal at the radio frequency;

$\psi_m^{(k)}$: average Direction-Of-Arrival (DOA) from the $k$th transmitter to the $m$th $\frac{\lambda}{2}$-spaced antenna array;

$\kappa_m^{(k)} B$: angular spread, where $B$ represents the maximum angular spread, while $-\frac{1}{2} \leqslant \kappa_m^{(k)} \leqslant \frac{1}{2}$ is a uniformly distributed random variable;

$\mathbf{a}_{uv,m}^{(k)}(t)$: complex array vector in the $uv$th subcarrier of the $k$th user and the $m$th $\frac{\lambda}{2}$-spaced antenna array;

$\mathbf{h}_{uv,m}^{(k)}(t)$: ST-CIR vector in the $uv$th subcarrier of the $k$th user and the $m$th $\frac{\lambda}{2}$-spaced antenna array;

$s_k(t)$: the transmitted signal of user $k$;

$\mathbf{r}(t)$: the received baseband equivalent signal vector at the $\frac{\lambda}{2}$-spaced antenna array's output;

$\mathbf{n}(t)$: the Additive White Gaussian Noise (AWGN) vector;

$N_0$: the double-sided power spectral density of a complex valued low-pass-equivalent AWGN signal;

$\mathbf{r}_k(t)$: the response of the $k$th user's transmitted signal to the spatial-temporal channels;

$\theta_{uv}^{(k)}$: a random variable uniformly distributed in $[0, 2\pi]$;

$\mathbf{z}_u$: a $VML$-length vector containing the entire set of $VML$ number of decision variables in the context of the $u$th data bit after multicarrier demodulation and DS despreading;

$\mathbf{z}_{uv}$: an $ML$-length vector containing the $ML$ number of variables in the context of the $v$th subcarrier;

$\mathbf{z}_{uv,m}$: an $L$-length vector including the $m$th $\frac{\lambda}{2}$-spaced array's response to the $v$th subcarrier signal;

$\mathbf{I}$: a unity matrix;

$E_b = PT_s$: the energy per bit;

$\mathbf{n}_{uv}$: an AWGN vector having zero mean and a variance of $\frac{VN_0}{E_b}\mathbf{I}$;

$\mathbf{i}_{u'v'}^{(s)}$: the self-interference contributed by the subcarrier indexed by $u'$, $v'$ of the reference signal;

$\mathbf{i}_{uv}^{(k)}$: the multiuser interference engendered by the subcarrier signal determined by $u$ and $v$ of the $k$th interfering user;

$\mathbf{i}_{u'v'}^{(k)}$: the MUI term imposed by the subcarrier determined by $u'$ and $v'$ associated with the $k$th interfering user;

$\mathbf{R}_d$: the autocorrelations of the desired signals;

$\mathbf{d}_m$: a vector related to the DOA of the desired user's signal and to the received signal's angular spread;

$\mathbf{R}_j$: the covariance matrix of the composite interference given by the sum of the self-interference and multiuser interference;

$\mathbf{R}_n$: the covariance matrix of the AWGN noise;

$\sigma_i^2$: the variance of the interference in the context of a single element;

$\mathrm{Re}\{x\}$: the real part of $x$;

$\mathrm{sgn}(x)$: a sign function;

$\mathbf{w}$: the array weight vector;

$\alpha$: a constant;

$\mathbf{w}_{MSINR}$: the array weight vector that maximizes the output SINR;

$\mathbf{R}_{uu}$: the correlation matrix of the interference-plus-noise;

$\mathbf{w}_{MVDR}$: the array weight vector derived based on the MVDR criterion;

$\mathbf{w}_{ML}$: the array weight vector derived based on the Maximum Likelihood (ML) criterion;

$\mathbf{r}_{zs_1}$: the cross-correlation between the received signal $\mathbf{z}$ and the desired signal $s_1(t)$;

$\mathbf{R}_{zz}$: the auto-correlation of the received signal;

$\mathbf{w}_{MMSE}$: the array weight vector derived based on the MMSE criterion;

$\sigma_1^2$: the power of the desired user;

$\mathbf{w}_{MPDR}$: the array weight vector derived based on the MPDR criterion;

$\mathbf{a}_m$: the steering vector of the desired user;

$\mathbf{w}_v^{(k)}$: a BS transmit weight vector applied to the signal associated with the $v$th subcarrier of the $k$th user;

$\mathbf{c}_k'$: the $k$th user's orthogonal code in discrete form, which will be used for F-domain spreading;

$\rho_{1k}$: the interference coefficient between the $k$th user and the first user;

$\mathbf{w}_{v,m^{(k)}}^{(k)}$: the transmit weight vector generated by the beamformer according to the channel quality information between the $k$th mobile user and $m^{(k)}$th $\frac{\lambda}{2}$-spaced array;

$\mathbf{h}_{uv,m^{(k)}}^{(1)}(t)$: the ST-CIRs between the first user and the $m^{(k)}$th antenna array which is selected to transmit the $k$th user's signal;

$a_{uv,m^{(k)}l}^{(1)}(t)$: the CIR with respect to the $uv$th subcarrier of the reference user and the $l$th element of the $m^{(k)}$th array;

$c_{k,m}(t)$: the $k$th user's orthogonal STS codes corresponding to the $m$th $\frac{\lambda}{2}$-spaced transmitter antenna array;

$\mathbf{s}_k(t)$: the transmitted signal vector;

$\mathbf{B}_{ku}$: matrix mapped from the $u$th sub-block data bits, according to the requirements of STS;

$\mathbf{u}(n)$: the input vector or the received signal vector;

$\mathbf{w}(n)$: the weight vector;

$d(n)$: the desired signal $d(n)$;

$\hat{d}(n)$: the estimate of the desired response $d(n)$;

$e(n)$: the estimation error;

$J(\mathbf{w}_n)$: the mean-square error based on the weight vector $\mathbf{w}(n)$;

$\delta_d^2$: the variance of the desired signal $d(n)$;

$\mathbf{p}$: the cross-correlation vector between the input vector $\mathbf{u}(n)$ and the desired signal $d(n)$;

$\mathbf{R}$: the autocorrelation matrix;

$\mathbf{w}_o$: the optimum weight vector;

$J_{\min}$: the minimum mean-square error

$\nabla J(\mathbf{w}_n)$: the gradient vector of the mean-square error $J(\mathbf{w}_n)$;

$\mu$: the step-size parameter chosen to optimize both the convergence rate and the mean-squared error;

$\Delta\mathbf{w}(n)$: the correction term;

$\lambda_{\max}$: the largest eigenvalue of the autocorrelation matrix $\mathbf{R}$;

tr[$\mathbf{R}$]: the trace of the matrix $\mathbf{R}$;

$\beta(n,i)$: the forgetting factor satisfying $0 < \beta(n,i) \leq 1$;

$\nabla_k J$: the $k$th component of the gradient vector $\nabla J$;

$e_{\min}(i)$: the estimation error when $J(\mathbf{w})$ achieves its minimum value;

$\mathbf{\Phi}(n)$: the autocorrelation matrix of the received signal in the form of $\sum_{i=1}^{n} \lambda^{n-i}\mathbf{u}(i)\mathbf{u}^H(i)$;

$\mathbf{P}(n)$: the inverse of the autocorrelation matrix $\mathbf{\Phi}(n)$;

$\mathbf{k}(n)$: the RLS gain vector, which is the result of the received signal vector $\mathbf{u}(n)$ transformed by the inverse of the received signal's correlation matrix $\mathbf{\Phi}(n)$;

$\xi(n)$: the *a priori* estimation error;

$\sigma_u^2$; the variance of a data sample $u(n)$;

$\delta$: a small value compared to $0.01\sigma_u^2$;

$N_a$: the total number of antenna elements in the $M$ antenna arrays;

$\tilde{d}(n)$: the decided data fed back from the data decision unit of the receiver;

$\mathbf{x}_{uv,l}$: the output signal vector arriving from the chip matched filter;

$\hat{\mathbf{w}}_{kj}(n)$: the MMSE/PIC ASTD's weight vector indexed by the $j$th PIC iteration during the $n$th bit interval of the $k$th user;

$y_j(n)$: the output signal of the LMS-based MMSE/PIC ASTD;

$\hat{i}_{j-1}(n)$: the estimate of the MAI during the $(j-1)$th iteration of the $n$th received bit;

$\beta_k$: the interference coefficient quantifying the interference imposed by the $k$th user;

$\kappa$: the number of strong interfering users;

$\hat{\mathbf{w}}_F(n)$: the final weight vector during the $n$th bit interval;

$\xi_j(n)$: the *a priori* estimation error computed in the $j$th PIC iteration;

$A_k$: the received signal's amplitude;

$\mathbf{I}_N$: the $N \times N$-dimensional identity matrix;

$\mathbf{c}_k$: the normalized signature waveform of the $k$th user;

$\mathbf{U}_s$: the *signal space*;

$\mathbf{\Lambda}_s$: a diagonal matrix containing the largest $K$ eigenvalues of the autocorrelation matrix $\mathbf{R}$;

$\mathbf{U}_n$: the *noise space*;

$\mathbf{\Lambda}$: a diagonal matrix constituted by the eigenvalues of the autocorrelation matrix $\mathbf{R}$;

$\mathbf{U}$: the unitary matrix that is used to diagonalize the autocorrelation matrix $\mathbf{R}$;

$\mathbf{X}$: the received signal matrix;

$\mathbf{w}_k$: the MUD's weight vector optimized for detecting user $k$;

$\mathcal{R}$: the correlation matrix of the signature waveforms;

$[\mathcal{R}^{-1}]_{ij}$: the $(i,j)$th element of the matrix $\mathcal{R}^{-1}$;

$\mathbf{d}_1$: the decorrelating detector's weight vector;

$\mathbf{m}_1$: the linear MMSE detector's weight vector;

$h_k(t)$: The CIR corresponding to the $k$th user;

$M_F$: the number of data bits in the transmitted data frame;

$L_k$: the total number of paths in the channel experienced by the $k$th user;

$\tau_{kl}$: the delay of the $l$th path of the $k$th user;

$m$: the smoothing factor employed in subspace-based blind MUDs;

$\mathbf{1}_l$: a vector having all-zero elements, except for the $l$th element, which is one;

$\tilde{K}$: the number of intracell users communicating within the cell of the reference user;

$\mathbf{H}_k$: the FDCTF corresponding to the $k$th user;

$\mathbf{F}$: the DFT matrix;

$\mathbf{F}_L$: an $(V \times L)$-dimensional matrix, which is given by the first $L$ columns of the DFT matrix $\mathbf{F}$;

$\gamma$: the forgetting factor used in NAHJ-FST algorithm;

$\Theta$: a Givens rotation;

$T_{c'}$: the OFDM-chip-duration;

$\mathbf{C'}_k = diag\{\mathbf{c'}_k\}$: the F-domain spreading code matrix;

$\mathbf{T}_L$: the acyclic left shift operator processing vectors of length $2N$;

$\mathbf{T}_R$: the acyclic right shift operator processing vectors of length $2N$;

$\mathbf{P}$: the composite signature waveform matrix;

$h_{km}(t)$: the Spatio-Temporal CIR between the $k$th user and the $m$th antenna element.

# Contents

# Chapter 1

# Introduction

During the last two decades, numerous wireless communication systems have been proposed [5–11] and analyzed in order to efficiently utilize the available spectrum, since the radio spectrum is a scarce resource. On the other hand, the growth in subscriber numbers as well as the demand for high-rate multimedia services constitute other important factors to be taken into account in the design of wireless communication systems. Predominantly using Time-Division Multiple-Access (TDMA), the Second Generation (2G) mobile telephone systems employ a fixed number of time slots, one per active user, which imposes a hard upper limit on the total number of users supported. As a successful example of TDMA systems, the Global System for Mobile Communication (GSM) supports eight Time Slots (TS) within each 200 kHz channel. However, even if all the eight TSs could be allocated to a single user, as in the Generic Packet Radio System known as GPRS, the system is not particularly suitable for high data rate multimedia applications. In order to support a variety of multimedia applications, both variable bit rate and packet transmission capabilities are essential. There is also a need for sufficient flexibility to ensure that different services may be jointly supported within the same propagation environment. The main design aim of the third generation (3G) systems was to provide global support for a variety of multimedia services at a quality similar to that experienced over fixed networks, while ensuring a high spectral efficiency. Code-Division Multiple-Access (CDMA) [6–9] constitutes an attractive solution for the construction of mobile communication systems exhibiting a high capacity, while supporting a variety of multimedia applications. MultiCarrier (MC) CDMA [7–9, 12–36] combines the benefits of both Direct-Sequence (DS) CDMA techniques as well as Orthogonal Frequency Division Multiplex (OFDM) [9, 18, 37, 38] techniques and it may be expected to outperform both the original CDMA and OFDM techniques. There are three main categories of multicarrier CDMA, such as MultiCarrier Code Division Multiple Access (MC CDMA), MC DS-CDMA, and MultiTone CDMA (MT CDMA) [39]. In this thesis, a generalized MC DS-CDMA system [40–42] is studied, which includes the subclasses of multitone DS-CDMA [43] and orthogonal MC DS-CDMA [12] as special cases. Apart from novel multi-access methods, smart antenna techniques, including beamforming [6,44–46], Beam Selection Transmit Diversity (BSTD) [47], Space-Time Transmit Diversity (STTD) [48] and Steered Space-Time Spreading (SSTS) [49] are employed for improving both the

achievable system coverage and user-load in Chapter 3, respectively. In Chapter 4, training sequence based adaptive space-time detection schemes are proposed for employment in the uplink of a generalized MC DS-CDMA system invoking both receiver diversity and receiver beamforming for improving the achievable performance of the system, where no knowledge of the Direction of Arrival (DOA), of the channel amplitudes or of the channel-induced phase-rotations is available. In contrast to the training sequence based adaptive space-time detection schemes of Chapter 4, the subspace-based blind and group-blind space-time multiuser detectors invoked for a smart antenna aided generalized MC DS-CDMA system in Chapter 5 does not require any training sequence and hence achieves an increased spectrum efficiency. The benefits of employing a generalized MC DS-CDMA system invoking smart antennas are explored in a multiuser mobile communications context. The emphasis is on the signal processing algorithms that are implemented at the base station.

## 1.1 Mobile Radio Propagation

Before commencing our study of a generalized MC DS-CDMA system supported by smart antennas, we provide a brief introduction to mobile radio channels. Unlike the wired channels that are stationary and predictable, mobile radio channels [10, 50–59] are described by random processes. The radio channel between the mobile subscriber (MS) and the base station (BS) is affected by various propagation phenomena. The first is the gradual reduction of the average received signal power as a function of the distance from the BS, which is attributable to path loss. Generally, the longer the distance between the MS and BS, the lower the mean signal strength at the receiver. The second phenomenon is fast fading, which occurs due to the sometimes constructive, sometimes destructive interference between two or more echoes of the transmitted signal, which arrive at the receiver at slightly different times. Since the phases of these multipath components are random, the sum of their contributions varies widely. The transmitted signal is diffracted and reflected by the surrounding buildings and other objects between the MS and BS, which results in multiple versions of the transmitted signal arriving at the receiver with different shifts in arrival time, amplitudes and phases. Fast-fading may be further classified into several different categories. While the phenomenon of multipath delay spread leads to time dispersion and frequency selective fading, the Doppler spread leads to frequency dispersion and time selective fading. The multipath delay spread and Doppler spread are independent of one another. The coherence bandwidth, which is related to the reciprocal of the multipath delay spread, is defined as the bandwidth over which the channel can be considered to have a constant gain and linear phase response. If the channel's coherence bandwidth is higher than the bandwidth of the transmitted signal, a flat fading channel is encountered. Conversely, frequency-selective fading occurs, if the signal's bandwidth is higher than the channel's coherence bandwidth. Depending on how rapidly the transmitted baseband signal fluctuates according to the symbol-duration, a channel may be categorized either as a fast-fading or slow-fading channel. For a fast fading channel, the coherence time, which is related to the reciprocal of the channel's frequency-domain Doppler spread and during which the channel's response does not appreciably change, is less than a symbol period. By contrast,

| Year | Author | Contribution |
|---|---|---|
| '82 | Lee [60] | In this model the effective scatterers are evenly spaced on a circular ring surrounding the mobile. The correlation coefficient of the signals between any two elements of the array is predicted using a discrete AOA model. |
| '94 | Norklit and Anderson [61] | The Uniform Sectored Distribution (USD) model presented assumes that scatters are uniformly distributed within a maximum angular distribution of $\Theta_{BW}$ and a radial range of $\Delta R$ centered about the mobile. |
| '95 | Zetterberg and Ottersten [62] | A statistical channel model provides a general formula for the received signal's correlation matrix, grouping scatters into different clusters, within which the delay differences are not resolvable. |
| '95 | Raleigh and Paulraj [63] | Raleigh's time-varying vector channel model is presented to provide both small-scale Rayleigh fading and theoretical spatial correlation properties. |
| '96 | Aszetly [64] | A Discrete Uniform Distribution model is proposed for evenly spaced scatterers within a narrow beamwidth centered about the line of sight path of the mobile. |
| '96 | Petrus, Reed and Rappaport [65] | The Geometrically Based Single Bounce Microcell (GBSBM) Model provided is used in a macrocellular environment, assuming that the scatterers lie within a ring surrounding the mobile. |
| '96 | Liberti and Rappaport [66] | A Geometrically Based Single Bounce Elliptical Model (GBSBEM) is proposed for macrocellular environments, where the scatterers are assumed to be uniformly distributed within an ellipse. |
| '96 | Mogensen [67] | Two spatial channel models are introduced, namely The typical urban (TU) model and the bad urban (BU) model. |
| '96 | Klein and Mohr [68] | The extended tap-delay-line model considered is an extension of the traditional statistical tap-delay-line model and includes AOA information. |
| '96 | Litva and Lo [69] | A comprehensive discussion on spatial and temporal channel models is provided. |
| '97 | Lu, Lo and Litva [70] | A spatio-temporal model is presented, which is based on the distribution of the scatters in elliptical subregions, corresponding to a range of excess delays. |

**Table 1.1:** Contributions on spatial channel models.

slow fading implies that the coherence time is significantly higher than a symbol period. In this thesis, we assume that the signalling rate is significantly higher than the maximum Doppler frequency, implying that typically slow fading radio channels are considered here.

A comprehensive overview of contributions on spatial channel models is provided in Tables 1.1 and 1.2.

| Year | Author | Contribution |
|---|---|---|
| '98 | Ertel, Rappaport, Sowerby, Cardieri and Reed [71] | A review of a number of spatial propagation models is provided. |
| '00 | Zwick, Fischer, Didascalou and Wiesbeck [72] | A stochastic model derived for the spatial indoor mobile propagation channel is developed. |
| '02 | Zwick, Fischer and Wiesbeck [73] | A physical wave propagation based stochastic model is designed for indoor scenarios, which is extendable to urban environments. In this model, a large number of parameters is required for characterizing the large number of effects considered. |
| '03 | Reed, Smith, Rodriguez and Calcev [74] | The spatial channel model described characterizes the associated delay spread, angular spread and log-normal shadow fading, which is used for multiple antenna aided systems. |

**Table 1.2:** Contributions on spatial channel models.

## 1.2 Generalized Multicarrier DS-CDMA

In this section, we will provide a brief introduction to the philosophy of generalized MC DS-CDMA systems [40–42], which include the subclasses of multitone DS-CDMA [43] and orthogonal MC DS-CDMA [12] as special cases. Since the study of generalized MC DS-CDMA techniques requires the understanding of DS-CDMA, MC CDMA, MT-CDMA, and orthogonal MC DS-CDMA, these four techniques will be reviewed first.

### 1.2.1 Overview of DS-CDMA

In single-carrier DS-CDMA systems multiple users simultaneously share the same bandwidth, while employing unique, user-specific spreading codes [6, 7]. The length of the spreading code is termed as the spreading factor, which is closely related to the achievable spreading gain. The performance of DS-CDMA systems is limited by the multiple-access interference (MAI) imposed by the overlapping spectra of the signals transmitted by the different users. By correlating the received signal with an appropriately delayed version of the spreading code assigned to the desired user, we can suppress the MAI by a factor proportional to the processing gain, resulting in a noise-like signal at the correlator's output. However, the performance of DS-CDMA systems typically degrades as the number of active users increases. This soft capacity limit is unique to CDMA systems due to the dynamic sharing of the available bandwidth.

If multipath propagation occurs and the received signal experiences small-scale fading, then the performance reduction imposed by MAI may be severe. The near-far phenomenon occurs when the total interference power received by the BS overwhelms the desired signal. The classical way of coping with this problem is to employ prompt and accurate power control so that all users' signals are received with approximately equal power. In open-loop power control schemes [75] a MS decides its

transmit power according to the received signal power arriving from the BS, based on the assumption that the transmitter path and the receiver path have similar attenuations. This conveniently simple principle has however a limited validity in frequency division duplex (FDD) CDMA systems, where the uplink and downlink signals are transmitted at different frequencies. In closed-loop power control schemes [76, 77], the BS invokes several metrics based on the received signal power, the ratio of the signal energy per bit to noise density ($E_b/N_o$), and the bit error ratio (BER), and based on these metrics it transmits appropriate power adjustment commands to each MS. Naturally, a certain fraction of the downlink capacity has to be dedicated to these commands in closed-loop power control schemes. Having an increased processing delay is another drawback of closed-loop power control schemes, which is undesirable in low-delay interactive voice communications.

Again, in multipath propagation environments different versions of the transmitted signal arrive at the receiver at different times. This implies that the Channel Impulse Response (CIR) exhibits scattered multipath components in the time-domain (T-domain) and this phenomenon results in inter-symbol interference (ISI). In DS-CDMA systems typically RAKE receivers are used to resolve the multiple paths that arrive with delay differences greater than one chip interval. Then, the despread components corresponding to the individual resolvable paths that are fading independently can be combined for the sake of exploiting the associated multipath diversity. A system having shorter chip duration or wider bandwidth is capable of resolving smaller delay differences and hence gathers more of the transmitted energy scattered in the T-domain.

Compared to TDMA and FDMA systems, DS-CDMA systems have an important benefit, since they are capable of achieving a near-unity frequency reuse factor [78]. An obvious advantage of the universal frequency reuse is the associated increase in the system's capacity per unit bandwidth and geographic area, which is seven times higher in comparison to 7-cell clusters. Another important advantage of DS-CDMA systems is the ability to use soft handovers, which implies that the MS simultaneously communicates with both the old and the new target BS in the interest of rendering the handover as seamless as possible. This is in contrast to conventional multiple access systems using hard handovers. This soft handover makes seamless communications possible and also mitigates the effect of multipath fading during the hand over period using cell site diversity [79], which allows both the old and the new target BS to combine their signals in the interest of improving the attainable received signal integrity.

### 1.2.2 Overview of MC CDMA

Unlike in DS-CDMA, where the spreading sequences are applied in the T-domain, in the context of MC CDMA we apply them in the F-domain, mapping a different chip of a spreading sequence onto each individual subcarrier. The transmitter schematic of the $k$th user is shown in Figure 1.1 for the MC CDMA system considered, which corresponds to Figure 19.1 of [8]. This scheme was referred to in Section 19.2.1 of [8] as the F-domain spreading assisted multicarrier CDMA (MC CDMA) scheme. At the transmitter side, the binary data stream having a bit duration of $T_b$ is Serial-to-Parallel (S/P) converted to $U$ parallel sub-streams. The bit duration of each sub-stream, which we refer to as

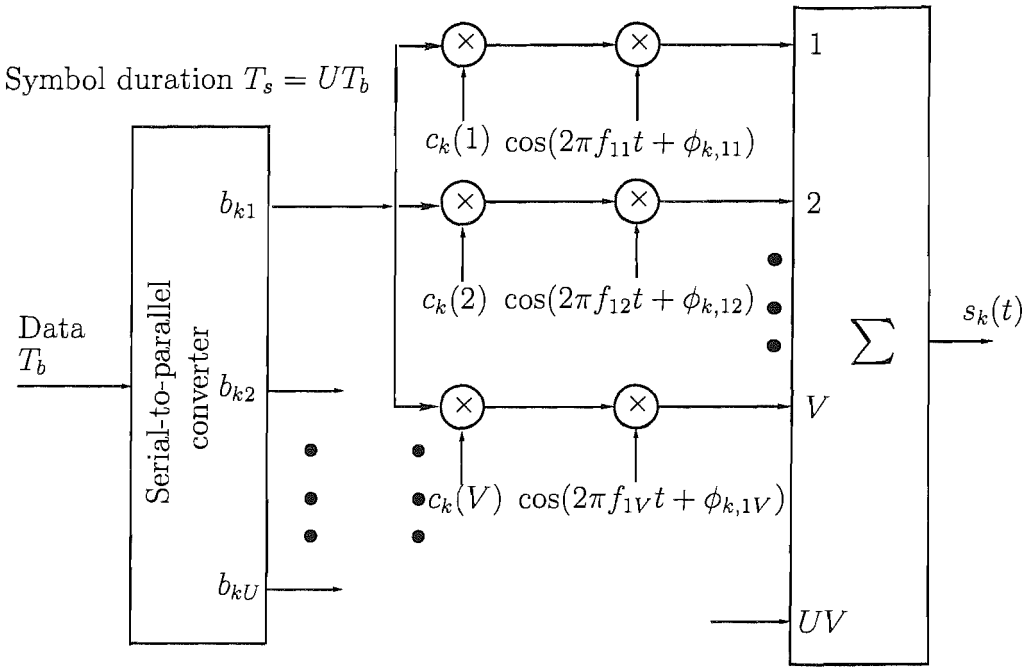


**Figure 1.1:** The $k$th user's transmitter schematic for the multicarrier CDMA system using F-domain spreading.

the symbol duration, becomes $T_s = UT_b$, as seen in Figure 1.2 associated with $U = 2$. After S/P conversion, the data of the $u$th sub-stream, where we have $u = 1, 2, \ldots, U$, simultaneously modulates a group of $V$ subcarrier frequencies $\{f_{u1}, f_{u2}, \ldots, f_{uV}\}$ using Binary Phase Shift Keying (BPSK). Since each of the $U$ data bits is spread to $V$ subcarriers, a total of $UV$ subcarriers are required in the MC CDMA system considered. It is worth mentioning that if the $V$ subcarriers conveying replicas of the same bit are faded independently, $V$th-order diversity is achieved at the cost of a $V$-fold effective throughput reduction. However, this $V$-fold throughput reduction may be eliminated by spreading bits to the $V$ subcarriers using orthogonal spreading codes, rather than simply copying them. This spreading process is demonstrated in Figure 1.2 in conjunction with the F-domain spreading code $[+1 - 1]$. All the subcarriers are rendered orthogonal for the duration of the symbol period by setting the frequency separation of the nearest-neighbour subcarriers equal to a multiple of the symbol rate. Finally, the $UV$ number of subcarrier signals are superimposed on each other, in order to form the complex modulated signal, as seen in Figure 1.1.

The MC CDMA detector consists of two main parts. The first part carries out multicarrier demodulation, while in the second part the demodulated components spread over the F-domain are combined for the sake of achieving diversity. It is essential that each subcarrier experiences flat fading, so that the orthogonality of the subcarriers is retained. In the downlink, where synchronous transmissions are automatically maintained, MC CDMA is capable of achieving a better performance than DS-CDMA, since depending on the propagation environment, the DS-CDMA receiver may not be as effective at combining the received signal energy scattered in the T-domain, as the MC CDMA receiver, which

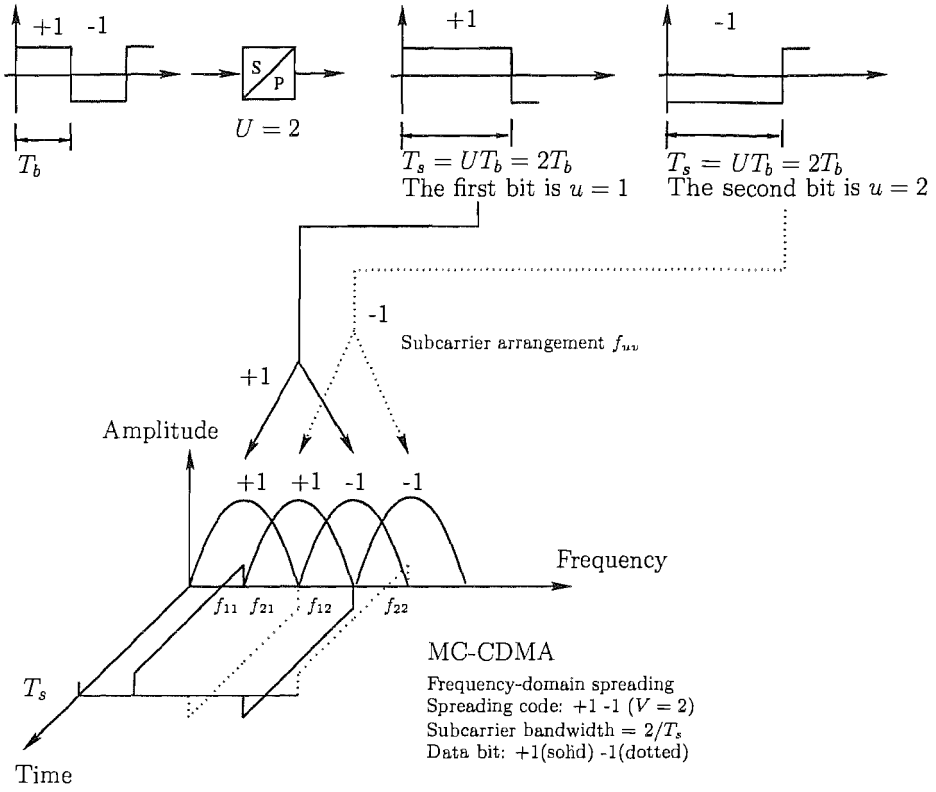


**Figure 1.2:** T-domain signal waveforms and the corresponding power spectra associated with MC CDMA using the F-domain spreading code $[+1 - 1]$, $(V = 2)$ and S/P conversion in conjunction with $U = 2$ bits.

combines the energy scattered in the F-domain. By contrast, in the uplink, where asynchronous transmissions are assumed, the performance of MC CDMA systems will be severely degraded, as the number of active users increases. However, Multi-User Detection (MUD) may be used in the uplink for the sake of improving the achievable performance of MC CDMA systems.

### 1.2.3 Multitone CDMA

In [43], a novel multiple access communications system referred to as multitone DS-CDMA was proposed for the sake of combating the effects of both multipath and multiple access interference, while exhibiting a multiple access capability. The block diagram of a multitone DS-CDMA communications system is portrayed in Figure 1.3 [43], which shows that the input symbol stream having a rate of $1/T_b$ is first split into $V$ parallel streams, each having a symbol duration of $T_s = VT_b$, as shown in Figure 1.4 associated with $V = 2$. This scheme was also discussed in Figure 19.10 of Section 19.2.4 in [8]. The $v$th symbol stream modulates a tone having a frequency of $f_v$, and the carriers $f_v$, $v = 1, 2, \ldots, V$ are orthogonal to each other over the symbol duration, which are given by $f_v = f_0 + v/T_s$, $v = 1, 2, \ldots, V$. The corresponding power spectra is shown in Figure 1.4. The spectra associated with the different tones overlap with each other, but nonetheless the modulating

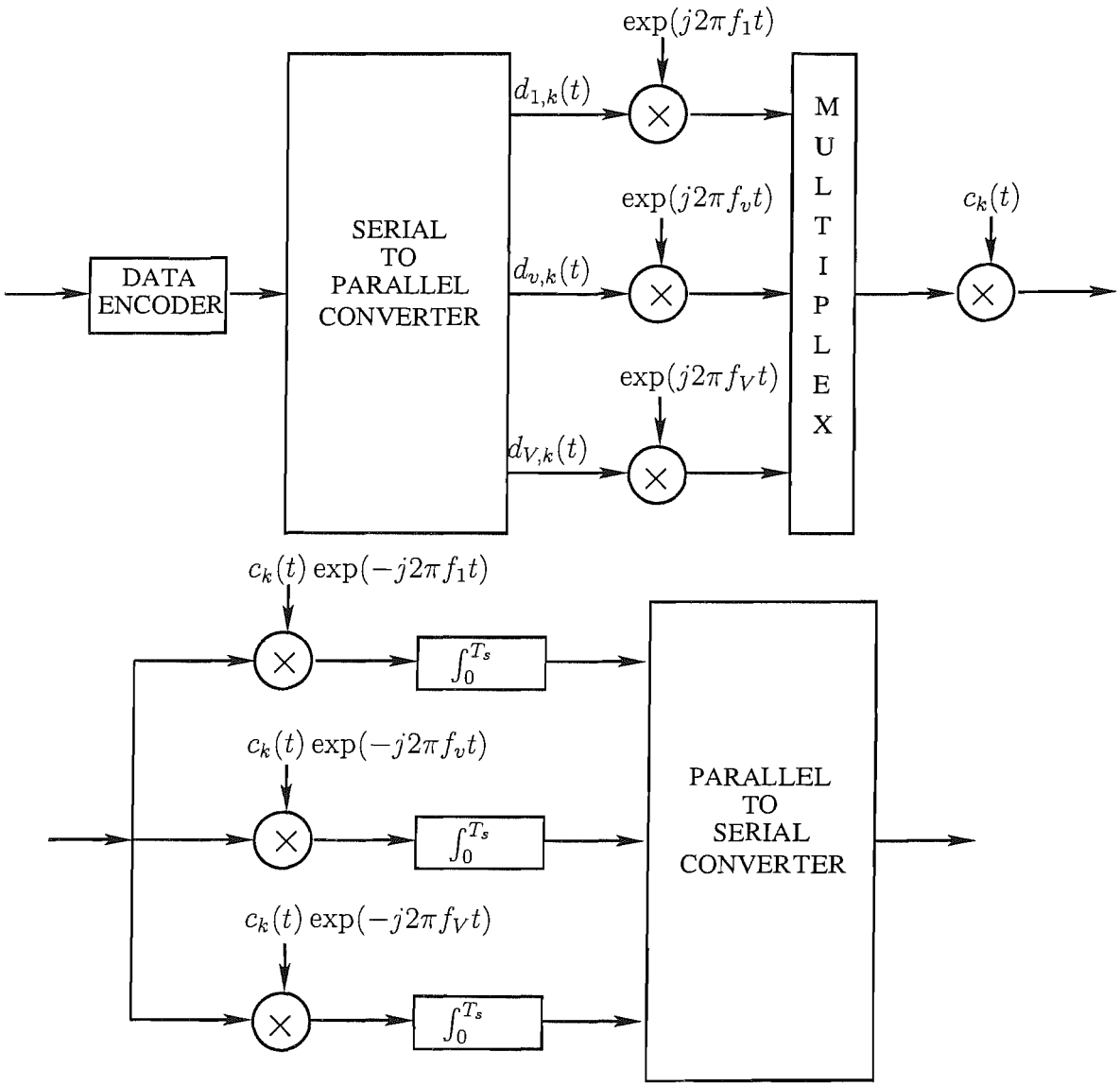


**Figure 1.3:** Block diagram of a multitone DS-CDMA communications system.

symbol associated with each tone can be recovered, as long as the frequency-selective fading channel does not destroy the F-domain orthogonality of the parallel streams portrayed in Figure 1.3. As seen in Figure 1.3, after mapping the extended-duration parallel symbols to the $V$ number of subcarriers, DS T-domain spreading is imposed on the multitone signal, where each symbol is T-domain spread by multiplying it with the spreading sequence $c_k(t)$ associated with the $k$th user. The T-domain spreading sequence $c_k(t)$ has a chip duration of $T_c = T_s/N_e$, where $N_e$ is the number of chips. As seen in Figure 1.4 associated with the spreading gain $N_e = 4$, the resulting spectrum of each subcarrier no longer satisfies the orthogonality condition.

The conventional MT-CDMA receiver of Figure 1.3 demodulates the different subcarriers and

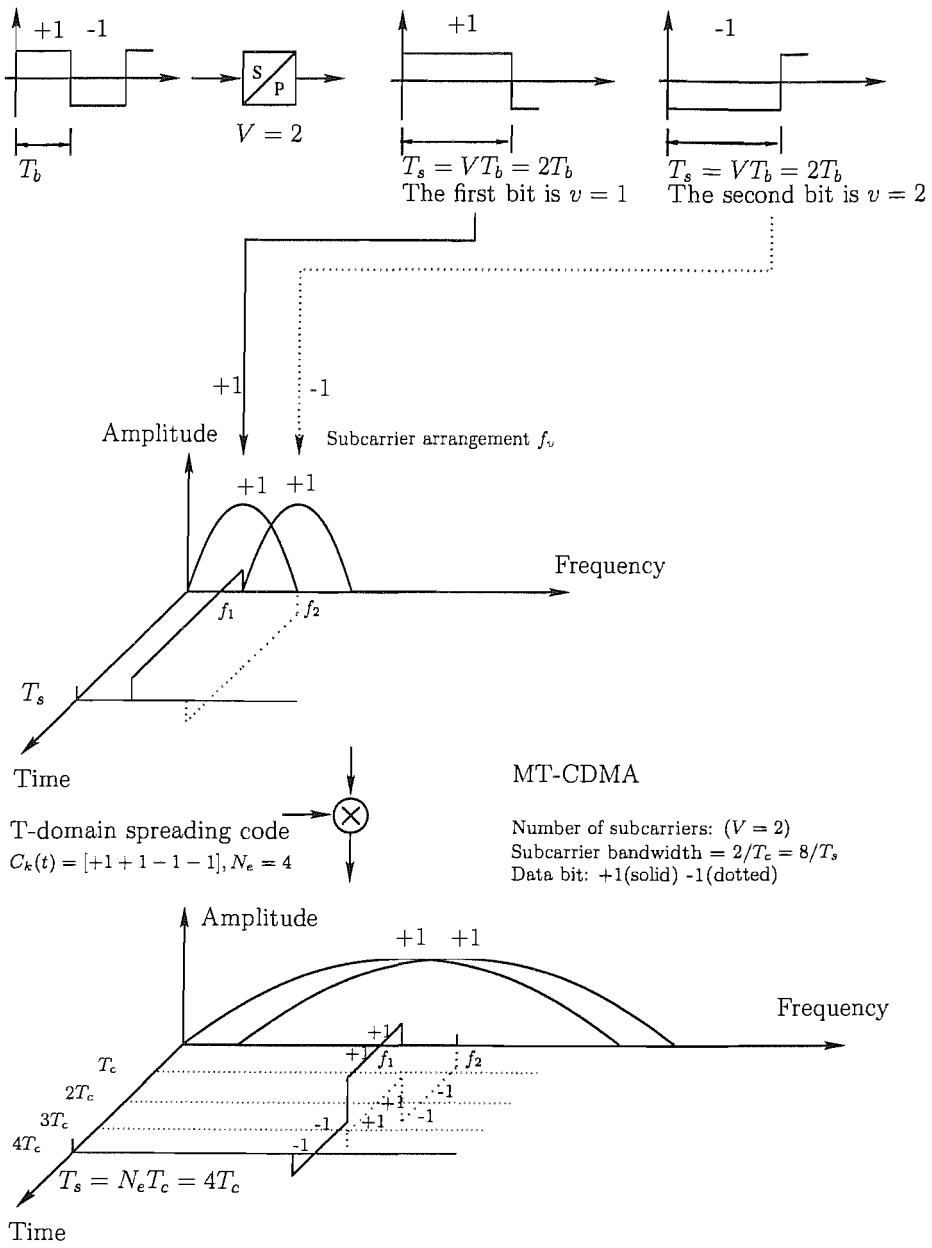


**Figure 1.4:** T-domain signal waveforms and the corresponding power spectra associated with MT-CDMA having $V = 2$ subcarriers, using the T-domain spreading code $[+1 + 1 - 1 - 1]$, $(N_e = 4)$, and S/P conversion in conjunction with $U = 2$ bits.

then uses a bank of RAKE receivers, one per subcarrier, to produce the decision variables. The longer symbol period which was extended by a factor corresponding to the number of subcarriers implies that the spreading codes are proportionally longer than in DS-CDMA. However, in MT-CDMA, due to the wideband nature of the channel, the subchannels tend to be exposed to frequency-selective fading, which results in the loss of subcarrier orthogonality and hence increases the inter-subcarrier interference.

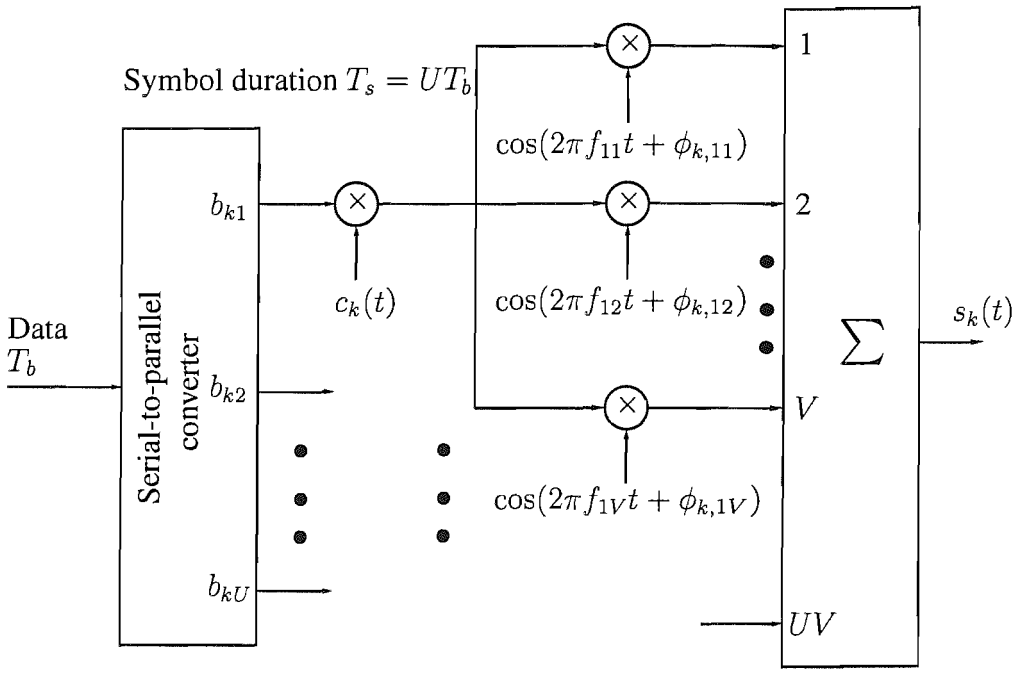


**Figure 1.5:** The $k$th user's transmitter schematic for the generalized multicarrier DS-CDMA system.

### 1.2.4 Multicarrier DS-CDMA

In [12], an orthogonal MC DS-CDMA system was proposed for efficiently exploiting the transmission bandwidth and for mitigating the effects of frequency selective multipath interference, while achieving both frequency and time diversity. In this system, the modulating symbol stream generated at the rate of $1/T_b$ was serial to parallel converted to $U$ parallel streams having a symbol duration of $T_s = UT_b$, as seen in Figure 1.6 associated with $U = 2$, and then the symbols conveyed by each parallel stream were DS spread by the spreading sequence $c_k(t)$ associated with the $k$th user, as seen in Figure 1.5. The T-domain signal waveform is shown in Figure 1.6 in conjunction with the T-domain spreading code $[+1 + 1 - 1 - 1]$. This scheme was also characterized in Figure 19.7 of Section 19.2.3 in [8]. After DS spreading the chip duration of each branch became $T_c = T_s/N_e$, where $N_e$ is the number of chips. Then, these DS-spread streams modulate $V$ number of orthogonal subcarriers, generating overlapping subbands. Here, the spacing between two adjacent subcarrier frequencies is $1/T_c = N_e/T_s$. The corresponding power spectra is shown in in Figure 1.6 associated with $N_e = 4$. Finally, the signal branches are superimposed for the sake of producing the baseband MC DS-CDMA signal.

In the receiver, the received signal is first multicarrier demodulated and then despread by using the spreading code assigned to the desired user. Finally, the decision variables are obtained by diversity combining. The achievable performance difference of SC DS-CDMA and MC DS-CDMA depends on both the propagation environment and on the number of subcarriers. Explicitly, in a flat-fading environment both systems would perform similarly. However, as the number of resolvable multipath

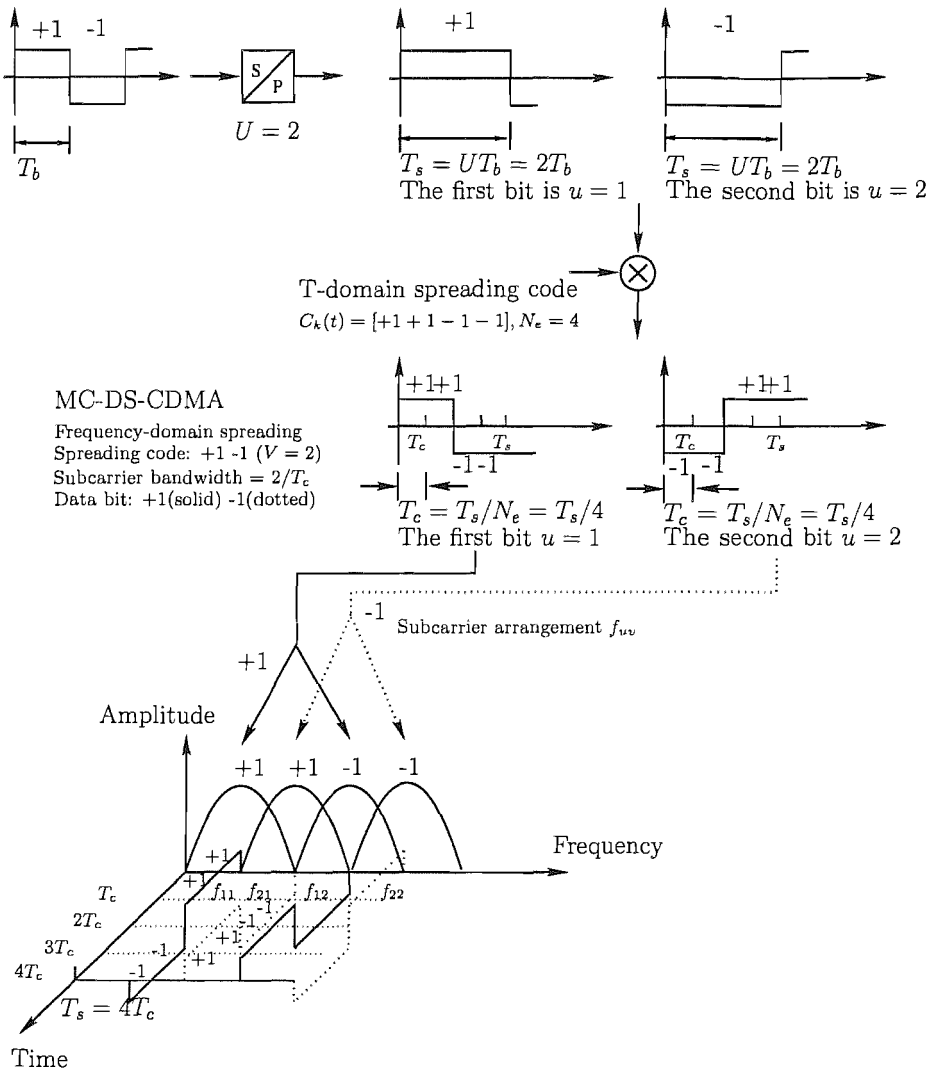


**Figure 1.6:** T-domain signal waveforms and the corresponding power spectra associated with MC-DS-CDMA having $V = 2$ subcarriers, employing the F-domain spreading code of $[+1 - 1]$ as well as the T-domain spreading code of $[+1 + 1 - 1 - 1]$, $(N_e = 4)$, and S/P conversion in conjunction with $U = 2$ bits.

components increases, SC DS-CDMA benefits more substantially from the associated higher-order diversity gain [12], because the number of resolvable paths experienced by each subcarrier of MC DS-CDMA is reduced by a factor corresponding to the number of subcarriers.

In [40–42], a generalized MC DS-CDMA system was presented, in which the spacing between adjacent subcarriers was programmable. The transmitter schematic of the $k$th user is shown in Figure 1.5 for the generalized MC DS-CDMA system considered. At the transmitter side, the binary data stream having a bit duration of $T_b$ is serial-to-parallel (S/P) converted to $U$ parallel sub-streams. The new bit duration of each sub-stream, which we refer to as the symbol duration becomes $T_s = UT_b$. After S/P conversion, each substream is spread using a DS spreading sequence waveform $c_k(t)$. Then,

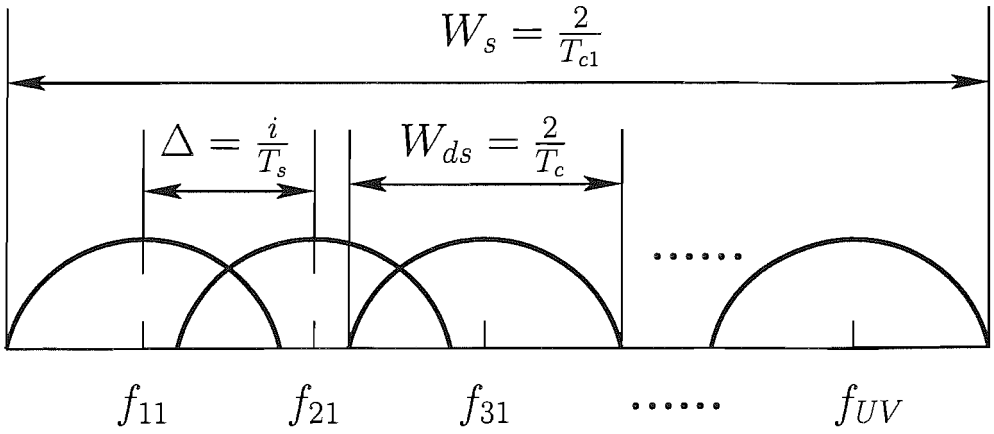


**Figure 1.7:** Stylized spectrum of the generalized multicarrier DS-CDMA signal.

the DS spread-spectrum signal of the $u$th sub-stream, where we have $u = 1, 2, \ldots, U$, modulates a group of subcarrier frequencies $\{f_{u1}, f_{u2}, \ldots, f_{uV}\}$ using Binary Phase Shift Keying (BPSK). Since each of the $U$ data bits is copied to $V$ subcarriers, a total of $UV$ number of subcarriers are required in the MC DS-CDMA system considered. Finally, the $UV$ number of subcarrier signals are superimposed, in order to form the complex modulated signal. The stylised spectrum arrangement of the generalized MC DS-CDMA system considered here is shown in Figure 1.7, where we assume that $W_s = 2/T_{c1}$ is the total bandwidth available, $T_{c1}$ represents the chip-duration of the corresponding single-carrier DS-CDMA signal occupying the bandwidth of $W_s$, while $W_{ds} = 2/T_c$ represents the 'null-to-null' bandwidth of the subcarrier signals. The spacing between two adjacent subcarrier frequencies is assumed to be $\Delta$, which is assumed to be a variable assuming values in the form of $\Delta = i/T_s$, with $i = 0, 1, 2, \ldots$ being an integer. Let $N_e = T_s/T_c$ be the spreading gain of the DS-spread subcarrier signals. It was shown in [41, 42] that the generalized MC DS-CDMA scheme incorporates the family of multitone DS-CDMA arrangements [43], if we assume $\Delta = 1/T_s$. Similarly, if it is configured to satisfy $\Delta = N_e/T_s$, the generalized MC DS-CDMA scheme considered incorporates also the class of orthogonal MC DS-CDMA [12] systems. Furthermore, there is no overlap between the main-lobes of the modulated subcarrier signals after DS spreading, provided that the criterion of $\Delta = 2N_e/T_s$ is obeyed.

### 1.2.5 System Features Comparison

Table 1.3 summarizes the features of various CDMA systems in the spirit of Table 1 in [80]. Observing Figures 1.1, 1.3 and 1.5 shows that MC CDMA employs spreading in the F-domain, while the MT-CDMA and MC DS-CDMA schemes carry out DS spreading in the T-domain. In contrast to the MT-CDMA scheme of Figure 1.3, where DS T-domain spreading is carried out after the multicarrier modulation generating the multitone signal, the MC DS-CDMA scheme of Figure 1.5 performs DS T-domain spreading before the multicarrier modulation stage. Hence, in the family of MT-CDMA

| Multiple-access scheme | SC DS-CDMA | MC CDMA | MC DS-CDMA | MT-CDMA |
|---|---|---|---|---|
| Symbol duration at subcarrier | $T_b$ | $UT_b$ | $UT_b$ | $VT_b$ |
| Number of subcarriers | 1 | $V$ | $V$ | $V$ |
| Processing gain | $N_e$ | $V$ | $N_e$ | $N_e$ |
| Chip duration | $T_b/N_e$ | | $UT_b/N_e$ | $VT_b/N_e$ |
| Subcarrier separation | | $1/(UT_b)$ | $N_e/UT_b$ | $1/(VT_b)$ |
| Required band-width (main-lobe) | $2N_e/T_b$ | $(UV+1)$ $/(UT_b)$ | $(UV+1)N_e$ $/(UT_b)$ | $(V-1+2N_e)$ $/(VT_b)$ |

**Table 1.3:** Comparison of various CDMA systems.

arrangements we have a subcarrier separation of $\Delta = 1/T_s$, while in the class of orthogonal MC DS-CDMA systems we have $\Delta = N_e/T_s$. A comprehensive overview of contributions on Multicarrier CDMA techniques is provided in Tables 1.4 and 1.5.

## 1.3 Smart Antennas

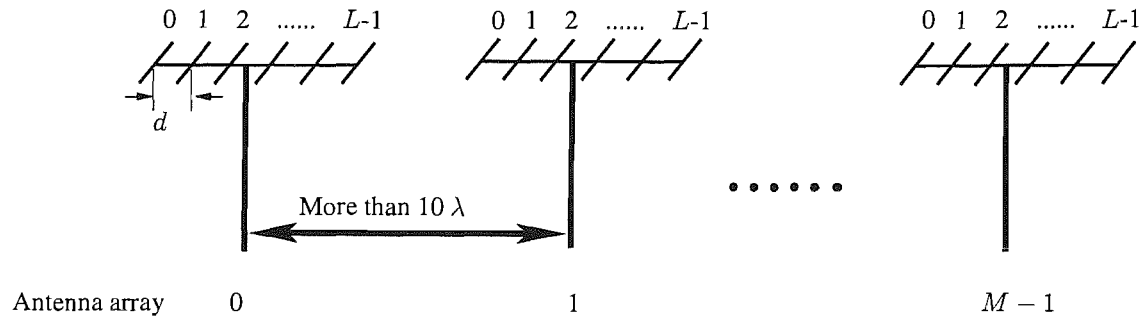


**Figure 1.8:** Multiple antenna configuation to be used in the generalized MC DS-CDMA system considered.

In wireless communications smart antennas have been used for improving the achievable performance of wireless systems, since they are capable of radiating and receiving energy in and from the intended directions, respectively, which potentially reduces the interference amongst wireless users [6, 45, 46, 87–112]. However, the various types of spatial processing techniques have different advantages and disadvantages in different systems [6, 113, 114]. Spatial transmit diversity [7], beamforming [6, 8, 115], Space Division Multiple Access (SDMA) [9], Bell Laboratory's Layered

| Year | Author | Contribution |
|---|---|---|
| '93 | Yee, Linnartz and Fettweis [81] | A novel digital modulation/multiple access technique referred to as MC CDMA is presented, where each data symbol is spread to multiple narrowband subcarriers by using F-domain spreading codes. This scheme is evaluated in an indoor wireless multipath radio channel. |
| '93 | Fazel and Papke [82] | The concept of combining OFDM with the classic multiple access technique of CDMA is proposed, where the performance of convolutionally-coded CDMA/OFDM is investigated. |
| '93 | Chouly, Brajal and Jourdan [83] | A novel design technique is introduced that applies the orthogonal multicarrier transmission scheme to DS-CDMA systems. More explicitly, in synchronous mode, each data symbol is spread to multiple subcarriers by using F-domain spreading code. |
| '93 | Vandendorpe [84] | The multitone CDMA scheme proposed spreads the S/P-converted data streams using spreading codes, which results in the loss of subcarriers' orthogonality, while more users may be accommodated. |
| '94 | Dasilva and Sousa [20] | Multicarrier DS-CDMA is proposed in conjunction with specific spreading codes and chip pulse shapes, which minimize the effects of multiple-access interference in the case of quasi-synchronous operation. |
| '95 | Vandendorpe [43] | The performance of multitone CDMA systems is analyzed in an indoor wireless channel, demonstrating that the larger symbol duration associated with multitone transmission is favorable in terms of multipath interference reduction. |
| '96 | Sourour and Nakagawa [12] | The proposed multicarrier DS-CDMA system spreads the S/P-converted data in T-domain and transmits them using orthogonal subcarriers, efficiently utilizing the available transmission bandwidth, while reducing the multipath interference as well as achieving both frequency and time diversity. |
| '97 | Prasad and Hara [80] | An overview of multiple access schemes based on a combination of CDMA and multicarrier techniques, such as MC CDMA, MC DS-CDMA and MT-CDMA, is presented. |

**Table 1.4:** Contributions on multicarrier CDMA techniques.

| Year | Author | Contribution |
|---|---|---|
| '02 | Yang and Hanzo [41] | A class of generalized MC DS-CDMA schemes is defined and its performance is considered when communicating over multipath Nakagami-$m$ fading channels. This scheme includes the subclasses of multitone DS-CDMA and orthogonal MC DS-CDMA as special cases. |
| '03 | Yang and Hanzo [42] | The investigation of generalized MC DS-CDMA is extended by considering two additional types of chip waveforms, namely, the time-domain half-sine and raised-cosine chip waveforms, in addition to the rectangular chip waveform. |
| '03 | Hanzo, Yang, Kuan and Yen [8] | A detailed discussion of multicarrier CDMA schemes is provided, including the family of MC CDMA and the class of frequency-hopping assisted MC CDMA schemes. The performance of different MC CDMA systems is investigated, when communicating over frequency-selective Rayleigh fading channels. |
| '05 | Nguyen [85] | This paper studies the effect of chip waveform shaping on the performance of band-limited MC DS-CDMA systems. The performance criterion is the average multiple access interference at the output of a correlation receiver. |
| '05 | Sadler and Manikas [86] | Reception of asynchronous MC DS-CDMA in time-varying, multipath radio channels with use of a receiving antenna array is investigated in this paper. A blind implementation of the modified MMSE receiver is proposed which applies subspace methods to estimate the composite channel vectors for each user. |

**Table 1.5:** Contributions on multicarrier CDMA techniques.

Space-Time (BLAST) system [116–118] and their hybrids can be used to improve the system's coverage, capacity and link quality. In beamforming schemes, $\lambda/2$-spaced antenna elements are employed to form a spatially selective transmitter/receiver beam, resulting in the mitigation of cochannel interference and hence providing SNR gain. In contrast with beamforming schemes, spatial diversity schemes position the multiple antennas far apart, so that the transmitted signals of the different antennas experience independent fading, hence attaining the maximum achievable diversity gain. In SDMA schemes, the unique, user-specific "spatial signature" of the individual users is exploited for the sake of differentiating amongst them, resulting in the improvement of the user-load. Different from SDMA schemes, BLAST schemes employ multiple antennas for the sake of increasing the throughput of a wireless system in terms of the number of bits per symbol, instead of supporting more users. A comprehensive overview of contributions on smart antenna techniques is provided in Tables 1.6 and 1.7. With the advent of using smart antennas, the BS becomes capable of reducing or suppressing the interference imposed by co-channel users. Hence achieving both spatial diversity and beamforming gain provides an improved desired signal level. An array having $M$ antenna elements generally provides an increased directional antenna gain plus additional diversity gain for the sake of

| Year | Author | Contribution |
|---|---|---|
| '90 | Swales, Beach, Edwards and McGeehan [100] | A multiple-beam adaptive base-station antenna is proposed, which is capable of resolving the angular distribution of the mobile users, and then using this information to direct beams toward the desired mobile users. |
| '91 | Anderson, Millnert, Viberg and Wahlberg [101] | An application of adaptive antenna techniques is presented for the sake of additionally increasing the channel capacity. An antenna array is employed at the base station to obtain directional sensitivity. |
| '96 | Foschini [116] | The concept of the BLAST architecture is introduced. |
| '97 | Paulraj and Papadias [95] | An overview of space-time signal processing techniques is provided. The space-time signal processing techniques introduced aim for enhancing the capacity and quality of wireless communication systems by using antenna arrays. |
| '97 | Godara [94, 115] | A comprehensive treatment of the use of an antenna arrays to enhance the efficiency of mobile communications systems is provided in Part I. Furthermore, a comprehensive treatment of different beam-forming schemes, adaptive algorithms and direction-of-arrival estimation methods is detailed in Part II. |
| '98 | Affes and Mermelstein [45] | A Spatio-Temporal Array-Receiver (STAR) using a new space/time structural approach is proposed for asynchronous CDMA, offering a high potential for increasing the achievable capacity at a relatively low computational complexity. |
| '98 | Wong, Lok, Lehnert and Zoltowski [119] | A linear receiver is designed for direct-sequence spread spectrum multiple-access communication systems. The receiver consists of the conventional matched filter followed by a tapped delay line combined with antenna arrays. |
| '98 | Wolniansky, Foschini, Golden and Valenzuela [117] | A wireless communication architecture known as the vertical BLAST scheme is introduced, which shows that the rich-scattering wireless channel is capable of supporting high capacities if the multipath channel is exploited to its full potential. |
| '99 | Li and Sollenberger [92] | Adaptive antenna arrays are investigated in the context of OFDM systems subjected to cochannel interference. |
| '99 | Dell'Anna and Aghvami [46] | The performance of an array of antennas combined with a Rake receiver at the base station of a wideband CDMA system is investigated in the context of single-user reception. |

**Table 1.6:** Contributions on Smart Antenna techniques.

mitigating the effects of multipath fading. The attainable diversity gain depends on the correlation of the fading encountered by the different antennas [113]. In this thesis, it is assumed that the BS is equipped with the hybrid antenna array portrayed in Figure 1.8, while the mobile terminals only have a single antenna.

| Year | Author | Contribution |
|---|---|---|
| '00 | Onggosanusi, Sayeed and Veen [120] | A canonical space-time characterization of mobile wireless channels is introduced in terms of a fixed basis that is independent of the true channel parameters. |
| '01 | Herscovici and Christodoulou [96] | An overview of the application of smart antennas designed for DS-CDMA systems is presented. |
| '02 | Zekavat, Nassar and Shattil [97] | A novel combination of smart antenna arrays and MC CDMA systems is introduced. |
| '02 | Trees [44] | An overview of various optimum beamforming schemes is provided. |
| '02 | Blogh and Hanzo [6] | Intelligent antenna arrays and beamforming are introduced and a range of adaptive beamforming algorithms is detailed. |
| '02 | Hanzo, Wong and Yee [7] | An overview of Space-Time Coded TDMA, CDMA, MC-CDMA and OFDM Systems is provided. |
| '03 | Hanzo, Munster, Choi and Keller [9] | SDMA schemes designed for OFDM and MC CDMA systems are proposed and investigated. |
| '04 | Fredrick, Wang and Itoh [121] | A new method for reducing mutual coupling in a smart antenna array using patch antenna elements is proposed. |
| '05 | Ioannides and Balanis [122] | In this paper, the performance of smart antennas with Uniform Circular Arrays (UCAs) is examined. A profound justification for this selection is the symmetry possessed by uniform circular arrays. |
| '06 | Uthansakul and Bialkowski [123] | A spatial beamformer is proposed in this paper, which steers a beam in azimuth over a wide frequency band without frequency filters or tap-delay networks, by using a rectangular array antenna. |

**Table 1.7:** Contributions on Smart Antenna techniques.

### 1.3.1 Optimum Beamforming

Optimum beamforming is a spatial filtering technique [6, 44], where the spatially selective array patterns are generated as a function of the channel or its parameters. In the uplink of wireless systems using smart antennas the signals received by the multiple antenna elements at the BS are appropriately weighted and linearly combined by the optimum beamformer in order to generate the decontaminated desired signal. The optimum linear combining schemes considered in this thesis are based on the following designs: Minimum Variance Distortionless Response (MVDR) [44, 96, 119], the Maximum Signal-to-Interference-plus-Noise Ratio (MSINR) [44, 119, 124, 125], the Minimum Mean-Square Error (MMSE) [44, 96, 119, 125] and the Minimum Power Distortionless Response (MPDR) [44] optimization criteria, respectively. The MVDR [44, 119] approach constitutes a well-known beamforming optimization criterion, which is capable of providing the minimum-variance unbiased estimate of the transmitted signal. In other words, with the aid of the MVDR based scheme, the desired signal arriving from a specific direction will pass through the optimum combiner without distortion, while the variance of the interference-plus-noise is minimized. When using optimum combining schemes

based on the Maximum Signal-to-Interference-plus-Noise Ratio (MSINR) [44, 119, 124, 125] criterion, the array's weight vector is optimized by maximizing the SINR at the output of the beamformer. In the MMSE beamformer [44, 119, 125], the mean-square error between the beamformer output and the desired signal generated either from the training signal, form the decision-directed receiver output or from a combination of both is minimized. Finally, let us consider the beamformer based on the MPDR criterion [44], which is closely related to the MVDR beamformer. However, in the context of the MVDR design, the assumed steering direction is different from the actual direction. Additionally, we assume that we know the statistics of the total received signal, but do not know the statistics of the users' signal and noise components. The performance of the generalized MC DS-CDMA systems using the above-mentioned optimum linear combining schemes will be investigated and compared, when operating in various propagation environments.

### 1.3.2 Transmit Processing

The antenna arrays installed at the base-station may be used both in the DownLink (DL) as well as in the UpLink (UL) for enhancing the system's attainable performance. There are two fundamental approaches to preprocess each user's signal at the base station's transmitter [126]. The so-called open loop methods [48,127,128] do not require any knowledge of the radio channel at the transmitter, while the family of closed loop methods exploit the characteristics of the channel [47, 129, 130]. The open loop techniques that rely on no channel information are desirable for the sake of implementational simplicity, but they are outperformed by the more sophisticated closed loop techniques, as long as the channel information is correct and up-to-date, rather than outdated. Various Transmit Diversity (TD) schemes have been proposed in the literature [48,126–132] for the sake of mitigating the performance degradation inflicted by multipath fading. Space-Time Transmit Diversity (STTD) schemes [48] belong to the open-loop family and they are capable of exploiting the extra space diversity provided by employing additional diversity antennas. Selection Transmit Diversity (STD) [129, 130] is a representative of the family of closed loop proposals, since it operates by selecting the specific antenna for transmission, which has the best instantaneous channel quality and hence this technique is expected to be superior to STTD in most cases, as long as the transmit-antenna-specific channel quality information can be correctly fed back to the transmitter without excessive latency [129], [130]. On the other hand, beamforming, or spatial filtering [6, 133], constitutes an effective solution to the suppression of MAI, where the antenna gain is increased in the direction of the desired user, whilst reducing the gain towards the interfering users. Let us now briefly consider downlink beamforming. There are techniques, which simply direct the main lobe to the desired user without considering the interference imposed upon other users [134, 135]. Other techniques form the beam with a high gain towards the desired user, while creating transmission nulls in the directions of the undesired users [132,136]. Both techniques are capable of achieving user-load improvements in the downlink by reducing the effects of MAI. Using the antenna arrays shown in Figure 1.8, both TD and beamforming can be implemented at the Base Station (BS). The Beam Selection Transmit Diversity (BSTD) scheme of [47] constitutes a combination of STD and beamforming. In [49], a novel technique based on a combination of diver-

sity and beamforming was presented, which was referred to as steered space-time spreading (SSTS). The achievable performance improvements are a function of both the antenna spacing and the specific techniques used for attaining TD and beamforming. In order to maintain a reliable performance in fast-fading channels, where attaining accurate channel estimation is challenging, Differential Space-Time Modulation (DSTM) schemes were proposed in [137–139], as extensions of the traditional Differential Phase Shift Keying (DPSK) scheme. In contrast to the above-mentioned STTD scheme of [48], the BSTD scheme of [47], the SSTS scheme of [49] and many other arrangements proposed in [126, 136, 140], DSTM schemes of [137–139] were capable of reliable data detection without any CSI, which is an attractive feature in fast-fading channels. Furthermore, a Differential Space-Code Modulation (DSCM) scheme was proposed in [141], which combined the merits of the DSTM arrangement of [137–139] and spread spectrum techniques, for the sake of suppressing the effects of co-channel interference encountered in DS-CDMA systems. A summary of the acontributions on transmit processing techniques is provided in Tables 1.8 and 1.9.

### 1.3.3 Adaptive Detection

Recently, numerous research contributions on space-time signal processing using an adaptive array have been pursued in the literatures [126, 132, 134, 136, 150–152]. The philosophy of adaptive beamforming is different from that of optimum beamformers, since optimum beamforming requires channel information, such as the DOA, and other interference-related parameters to produce their tap weights. By contrast, adaptive beamformers recursively update their tap weights according to the received data. Hence adaptive beamformers are capable of providing an attractive tradeoff between the achievable performance, the complexity imposed and the need for side information. The adaptive beamformer typically operates in two successive modes, the first being the training mode, during which a training sequence is used, while the second is the decision directed mode, where the adaptive receiver is updated using the data decisions. Provided that these decisions are error-free, the beamformer substantially benefits from the availability of 100 % training information. In [153], an adaptive Minimum Mean-Square Error (MMSE) beamformer based on the Least-Mean-Square (LMS) algorithm was employed in a smart antenna aided system. Choi presented an alternative adaptive beamforming algorithm having a lower complexity [154]. In [155], Sigdel modified the adaptive beamforming algorithm proposed by Choi in [154] and used it in a MC CDMA system aided by antenna arrays. In this thesis, we developed an adaptive beamformer based on the LMS and Recursive-Least-Square (RLS) algorithm. The LMS algorithm is a widely used technique, which was proposed by Widrow and Hoff in [156]. In [157], Haykin extended the employment of the method of steepest decent to derive the LMS algorithm and studied its characteristics. An attractive feature of the LMS algorithm is its simplicity, although it has a low convergence speed. The RLS algorithm [157], developed from the method of least squares, is another important tool often used in adaptive filtering. Given the least-square estimate of the tap-weight vector of the adaptive filtering at iteration $n-1$, the updated estimate of this vector at iteration $n$ may be computed upon the arrival of new received data. An important feature of the RLS algorithm is that it utilizes not only the information provided

| Year | Author | Contribution |
|---|---|---|
| '96 | Naguib and Paulraj [135] | An antenna array aided BS receiver structure designed for DS-CDMA is proposed, which simply direct the main lobe to the desired user without considering the interference imposed upon other users. |
| '98 | Proposed TDOC: 662/98 to ETSI SMG2 UMTS Standards [48] | STTD schemes belonging to the open-loop family are presented and they are capable of exploiting the extra space diversity provided by employing additional diversity antennas. |
| '98 | Ho, Stüber and Austin [133] | The performance and feasibility of switched-beam smart antennas is investigated. Switched-beam smart antenna aided systems are shown to either increase the capacity or extend the radio coverage by increasing the carrier-to-interference ratio. |
| '98 | Liang and Chin [136] | A new downlink beamforming technique is proposed that converts the downlink beamforming problem into a virtual uplink one and takes into account the data rate information of all users, thus forming a beam with a high gain towards the desired user, while creating transmission nulls in the directions of the undesired users. |
| '99 | Rajan and Gray [128] | Three open loop schemes contrived for performing transmit diversity are examined, including OTD, TSTD and STD. These schemes do not require any knowledge of the radio channel at the transmitter. |
| '99 | Thompson, Grant and Mulgrew [130] | A number of transmit diversity schemes proposed for the downlink in CDMA networks are discussed, including STTD, OTD, TSTD, STD, Delay Diversity (DD), Phase Sweeping Transmit Diversity (PSTD) and Pre-RAKE techniques. |
| '00 | Correia, Hottinen and Wichman [129] | The detrimental effects of channel estimation errors on the performance of STTD combined with WCDMA is evaluated. Comparison is made with the STD scheme in the context of different fading channel models. |
| '01 | Zhou, Chin, Liang and Ko [47] | The BSTD scheme, which constitutes a combination of STD and beamforming, is proposed. |
| '02 | Choi [134] | A semiblind downlink beamforming technique based on the reciprocity of wireless channels and designed for CDMA systems equipped with a transmit antenna array is introduced. |
| '02 | Soni, Buehrer and Benning [49] | A novel technique based on a combination of diversity and beamforming is presented, which is referred to as SSTS. |
| '04 | Soni and Buehrer [142] | A comprehensive investigation of the performance and practical implementation issues of open-loop transmit diversity schemes for the IS-2000 third-generation cellular CDMA standard is provided. |
| '05 | Cai, Giannakis and Zoltowski [143] | In this paper, channels spatial correlation and the temporal covariance of the interference are exploited to design multiantenna transmitters. |
| '06 | Wang and Wang [144] | Linear Dispersion (LD) codes are designed for uplink multiuser channels with multiple antennas at the base station and each mobile unit. |

**Table 1.8:** Contributions on transmit processing techniques.

| Year | Author | Contribution |
|---|---|---|
| '00 | Tarokh and Jafarkhani [137] | A differential detection aided transmit diversity method is presented, where neither the receiver nor the transmitter has access to any channel state information. |
| '00 | Hughes [138] | Unitary group code based Differential Space-Time Modulation (DSTM) techniques that do not require channel estimates at the transmitter or receiver are proposed to exploit the presence of multiple transmit antennas, for the sake of improving the performance attained for transmissions over multipath radio channels. |
| '00 | Hochwald and Sweldens [139] | A framework devised for differential modulation combined with multiple antennas communicating over fading channels is presented as a natural extension of standard Differential Phase-Shift Keying (DPSK), where neither the transmitter nor the receiver has access to any channel information. |
| '01 | Liu, J. Li, H. B. Li and Larsson [141] | A novel coding and modulation scheme, referred to as Differential Space-Code Modulation (DSCM), is designed for interference suppression. It is shown that DSCM significantly outperforms DSTM [137–139] in the typical scenario, where interference is present. |
| '01 | Liu, Giannakis and Hughes [145] | A novel diagonal unitary matrix group based double differential space-time block coding approach is derived for time-selective fading channels. The proposed transceiver has a low complexity and is applicable to an arbitrary number of transmit and receive antennas. |
| '02 | Lampe and Schober [146] | Bit-interleaved coded Differential Space-Time Modulation (DSTM) designed for transmission over spatially correlated Ricean flat fading channels is discussed. |
| '02 | H. B. Li and J. Li [147] | Two differential receivers and a coherent receiver specifically devised for space-time-coded CDMA systems that utilize DSCM transmission are considered. The proposed differential/coherent receivers are fading resistant to MUI. |
| '02 | Schober and Lampe [148] | Differential Modulation Diversity (DMD) based on diagonal signals is introduced. DMD is capable of exploiting both space- and time-diversity and hence DSTM combined with diagonal signaling, which is limited to exploiting space-diversity only can be considered as a special case. |
| '03 | Lampe, Schober and Fischer [149] | Powerful coding techniques specially designed for Differential Space-Time Modulation (DSTM) communicating over Rayleigh flat fading channels and combined with noncoherent detection operating without channel state information at the receiver are investigated. |

**Table 1.9:** Contributions on Differential Space-Time Modulation (DSTM).

by the current received data, but also that of all past data. The resultant convergence rate of the RLS algorithm is therefore higher than that of the LMS algorithm. However, this convergence rate improvement is achieved at the expense of a higher computational complexity than that of the LMS algorithm. In order to reduce the overhead introduced by the training sequence, iterative Interference Cancellation (IC) schemes may be employed for improving the attainable convergence rate of the LMS/RLS adaptive receiver. In [158], Hamouda presented a combined adaptive MMSE/PIC receiver. The proposed system made use of the available knowledge of the training sequence for all the users to jointly cancel the Multiple Access Interference (MAI) and increased the attainable convergence speed at the expense of a higher complexity. An outline of publications on adaptive detection techniques is given in Table 1.10.

### 1.3.4 Blind Detection

In contrast to the training sequence based adaptive MUDs discussed in Section 1.3.3, the Minimum-Output-Energy (MOE) based blind adaptive MUD [168] does not require any training sequence and hence achieves an increased spectral efficiency. However, its performance is suboptimum in the high-SNR region. In [1, 2], Wang and Poor proposed a novel blind MUD for single-carrier DS-CDMA systems based on the philosophy of signal subspace estimation, which benefits from a lower computational complexity and a better performance compared to the MOE based blind MUD. Group-blind MUDs having the prior knowledge of all signature waveforms of the intracell users were then proposed in [169] for the uplink of a single-carrier DS-CDMA system, which exhibited a significant performance improvement over that of the blind MUDs advocated in [1, 2]. Furthermore, Spasojevic *et al.* [170] proposed a nonlinear group-blind multiuser detector for DS-CDMA systems. A Genetic Algorithm (GA) based blind multiuser detector was proposed and investigated by Yen and Hanzo [171]. Recently, a novel Expectation-Maximization (EM) algorithm based blind multiuser detector was proposed by Li, Georghiades and Wang [172], which exhibited a low computational complexity, that was on the order of $O(K^2)$ per bit, where $K$ is the number of users. In [26], an adaptive algorithm was proposed in the context of MC CDMA for exploiting the correlation between the noise and the interference for the sake of rejecting the MAI. However, this frequency-domain MMSE multiuser detector performs well only in specific situations, where the number of subcarriers is low and only a few dominant interferers exist [173]. A subspace-based MMSE receiver was proposed in [173] for a MC DS-CDMA system, which is similar to that advocated in [1, 174], where the orthogonality between the noise subspace and the desired signal vector was exploited for blindly extracting both the timing and channel information.

The history of blind multiuser detectors designed for CDMA systems is summarized in Table 1.11.

## 1.4 Outline of the Report

In this thesis, a generalized MC DS-CDMA system supported by smart antennas is investigated in the context of both the uplink and downlink. The outline of this thesis is as follows:

| Year | Author | Contribution |
|---|---|---|
| '90 | Godara [153] | An adaptive MMSE based receiver is investigated in the context of smart antenna aided systems, where an improved LMS algorithm is proposed for adaptive beamforming. |
| '93 | Pateros and Saulnier [159] | An adaptive MMSE receiver has been investigated when considering frequency-selective fading channels. |
| '95 | Miller [160] | An adaptive MMSE receiver is considered for detecting DS-CDMA signals. The focus of the paper is on the multiuser interference rejection capability of the receiver. |
| '96 | Haykin [157] | A detailed treatment of linear Finite Impulse Response (FIR) adaptive filters is provided, including the method of steepest descent, the LMS algorithm, frequency-domain adaptive filters, the singular value-decomposition (SVD) and the RLS algorithm. |
| '97 | Honig, Shensa, Miller and Milstein [161] | Adaptive MMSE receivers are investigated, when communicating over flat fading channels. |
| '98 | Barbosa and Miller [162] | The performance of adaptive MMSE receivers has been investigated, when considering both flat and frequency-selective fading channels, where adaptive MMSE receivers were implemented based either on the principles of the LMS or the RLS algorithm. |
| '00 | Miller, Honig and Milstein [163] | The performance of the MMSE receiver invoked for detection of DS-CDMA is considered in various fading channel models. Several modifications to the basic MMSE receiver structure are reviewed and shown to represent different approximations of a single common form. |
| '00 | Choi [154] | A novel adaptive beamforming algorithm imposing a low detection complexity is proposed. |
| '01 | Hamouda and Mclane [158] | A combined adaptive MMSE/PIC receiver designed for DS-CDMA systems is presented. The proposed system suppresses the MAI and increases the attainable convergence speed at the expense of a higher complexity by employing the classic PIC operation. |
| '02 | Sigdel, Ahmed and Fernando [155] | The adaptive beamforming algorithm proposed in [154] is modified for employment in MC CDMA systems. |
| '05 | Joshi, Dietrich and Stutzman [164] | In this paper, results of an experimental investigation of adaptive beamforming in the presence of interferers are presented. |
| '05 | Chen and Chi [165] | In this paper, a RAKE receiver design with adaptive antenna arrays is proposed for the WCDMA Frequency-Division Duplexing (FDD) uplink. The RLS-based adaptive beamforming scheme is proposed and can be built with the existing one-dimensional RAKE receiver. |
| '05 | El-Keyi, Kirubarajan and Gershman [166] | A novel approach to implement the robust MVDR beamformer is proposed. |
| '05 | Chen, Ahmad and Hanzo [167] | An adaptive beamforming technique is proposed based on directly minimizing the BER. It is demonstrated that this minimum BER (MBER) approach utilizes the antenna array elements more intelligently than the standard MMSE approach. |

**Table 1.10:** Contributions on adaptive detection techniques.

| Year | Author | Contribution |
|---|---|---|
| '95 | Honig, Madhow and Poor [168] | The so-called Minimum-Output-Energy (MOE) based blind adaptive MUD is proposed, which does not require any training sequence and hence achieves an increased spectral efficiency. |
| '98 | Wang and Poor [1] | A subspace-based linear blind MUD is proposed for single-carrier DS-CDMA systems, which benefits from a lower computational complexity and a better performance compared to the MOE based blind MUD. |
| '98 | Wang and Poor [2] | Subspace-based blind MUDs are developed for the joint suppression of MAI and ISI in dispersive CDMA channels. |
| '99 | Wang and Host-Madsen [169] | Group-blind MUDs benefitting from the prior knowledge of all known signature waveforms are proposed for the uplink of a single-carrier DS-CDMA system, which exhibit a significant performance improvement over that of the blind MUDs advocated in [1, 2]. |
| '99 | Lok, Wong and Lehnert [26] | Blind adaptive signal reception is proposed for MC CDMA systems communicating in Rayleigh fading channels. |
| '00 | Namgoong, Wong and Lehnert [173] | A subspace-based MMSE receiver is proposed for a MC DS-CDMA system, where the orthogonality between the noise subspace and the desired signal vector was exploited for blindly extracting both the timing and channel information. |
| '01 | Spasojevic, Wang and Host-Madsen [170] | A nonlinear group-blind multiuser detector is presented for DS-CDMA systems. |
| '01 | Yen and Hanzo [171] | Genetic algorithm assisted blind MUDs are invoked for synchronous CDMA. |
| '03 | Reynolds and Wang [175] | Transmitter optimization for blind and group-blind multiuser detectors is investigated. |
| '04 | Li, Georghiades and Wang [172] | Sequential Expectation-Maximization (EM) algorithm based blind MUDs are proposed, which exhibit a low computational complexity. |
| '05 | Ding and Ward [176] | A new approach to blind and semi-blind channel estimation is presented for Space-Time Block Codes (STBCs). |
| '05 | Kang and Champagne [177] | This paper provides a systematic study of the subspace-based blind channel estimation method. A generalized subspace-based channel estimator is proposed by minimizing a novel cost function, which incorporates the set of kernel matrices of the signals sharing the target channel via a weighted sum of projection errors. |
| '06 | Kotoulas, Koukoulas and Kalouptsidis [178] | In this paper, a novel algorithm based on subspace projections is developed for blindly estimating the discrete orders of a linear Finite-Impulse-Response (FIR) MIMO system, the number of subsystems that attain each order as well as the total number of inputs. |
| '06 | Tugnait and Luo [179] | In this paper, a MultiStep Linear Prediction (MSLP) approach is presented for blind channel estimation for short-code DS-CDMA signals in time-varying multipath channels using a receiver antenna array. |

**Table 1.11:** Contributions on blind multiuser detection

- Chapter 2: In this chapter, antenna arrays are studied in the context of the uplink at the base station receiver. We present a generalized MC DS-CDMA system supported by smart antennas for the sake of improving the attainable performance of the uplink of the system. Four different beamformers based on the MVDR, MSINR, MMSE and MPDR array element optimization criteria are studied with the aid of different antenna array models. Furthermore, various antenna array models are investigated in the proposed generalized MC DS-CDMA system.

- Chapter 3: Both transmit diversity and transmit beamforming are invoked in the downlink transmissions of the base station for the sake of improving the attainable system user-load and link quality. Four different space-time transmitter processing schemes based on the principles of transmit beamforming, Beam Selection Transmit Diversity (BSTD), Space-Time Transmit Diversity (STTD) and Steered Space-Time Spreading (SSTS) are studied in order to enhance the achievable downlink performance of generalized MC DS-CDMA systems. Furthermore, the generalized MC DS-CDMA system employs both Time and Frequency (TF)-domain spreading, where a novel user-grouping technique is employed for reducing the effects of multiuser interference.

- Chapter 4: Adaptive space-time detection schemes are proposed for employment in the uplink of a generalized MC DS-CDMA system invoking both receiver diversity and receiver beamforming for improving the achievable performance of the system. No knowledge of the Direction of Arrival (DOA), of the channel amplitudes or of the channel-induced phase-rotations is available. Two adaptive detection schemes, namely the LMS and the RLS algorithms are invoked. The convergence rate of the LMS/RLS-detection aided adaptive receiver is improved using the proposed adaptive Minimum Mean Square Error/Parallel Interference Canceller (MMSE/PIC) space-time processing schemes having a low complexity.

- Chapter 5: Subspace-based blind and group-blind space-time multiuser detection is investigated in the context of a smart antenna aided generalized MC DS-CDMA system communicating over a dispersive Space-Time (ST) Rayleigh fading channel, where the channel estimates are attained by using subspace-based blind techniques. Two low-complexity subspace tracking algorithms, namely the Projection Approximation Subspace Tracking deflation (PASTd) algorithm and the Noise-Averaged Hermitian-Jacobi Fast Subspace Tracking (NAHJ-FST) algorithm are investigated for the sake of reducing the computational complexity. Furthermore, in the generalized MC DS-CDMA system considered, smart antennas are employed, in order to provide increased degrees of freedom and hence to improve the attainable performance and user-load.

- Chapter 6: Chapter 6 concludes this thesis and presents future research directions.

## 1.5 The Novel Contributions

**The novel contributions of this thesis are listed below:**

- Optimum combining techniques are exploited in the context of the uplink of generalized MC DS-CDMA systems employing novel, generic smart antennas capable of achieving both beamforming and diversity gains [180, 181].
- Four downlink space-time transmitter processing schemes are investigated in the context of the novel generic smart antenna aided MC DS-CDMA system. Furthermore, an interference coefficient based user-grouping technique is proposed for reducing the effects of multiuser interference caused by the employment of TF-domain spreading [182–185].
- Adaptive space-time detection schemes amalgamating uplink receiver diversity and receiver beamforming are designed for improving the achievable performance of the family of generalized MC DS-CDMA systems. These novel adaptive space-time detectors require appropriate receiver algorithms and are capable of receiving energy from the intended directions of the desired users, which potentially reduces the interference amongst wireless users, as well as additionally mitigating the effects of fading [186, 187].
- The benefits of subspace-based blind and group-Blind space-time MUDs are combined with those of the smart antenna aided generalized MC DS-CDMA system for the sake of improving the achievable performance of the system by jointly performing multiuser detection in the space-time-frequency domain, while achieving both frequency and spatial diversity [188, 189].

# Chapter 2

# Multicarrier DS-CDMA Systems Using Smart Antennas - Uplink

## 2.1 Introduction

In recent years numerous research contributions have appeared on the topic of MC DS-CDMA scheme, based on a combination of DS-CDMA and OFDM. In [43], a novel multiple access communications system referred to as multitone DS-CDMA was proposed for the sake of combating the effects of both multipath and multiple access interference, while exhibiting a multiple access capability. The block diagram of a multitone DS-CDMA communications system portrayed in Figure 2.1 of [43] shows that the input symbol stream having a rate of $1/T_b$ is first split into $V$ parallel streams, each having a symbol duration of $T_s = T_b \cdot V$. The $v$th symbol stream modulates a tone having a frequency of $f_v$, and the carriers $f_v$, $v = 1, 2, \ldots, V$ are orthogonal to each other over the symbol duration, which are given by $f_v = f_0 + v/T_s$, $v = 1, 2, \ldots, V$. The spectra associated with the different tones overlap with each other, but the modulating symbol associated with each tone can be recovered as long as the channel does not destroy the orthogonality of the parallel streams. As seen in Figure 2.1, after multiplexing the $V$ number of subcarriers, DS spreading is imposed on the multitone signal, where each symbol is spread by multiplying it with the spreading sequence $c_k(t)$ associated with the $k$th user. The spreading sequence $c_k(t)$ has a chip duration of $T_c = T_s/N_e$, where $N_e$ is the number of chips. In [12], an orthogonal MC DS-CDMA system was proposed for efficiently exploiting the transmission bandwidth and for mitigating the effects of frequency selective multipath interference, while achieving both frequency and time diversity. In this system, the modulating symbol stream generated at the rate of $1/T_b$ was serial to parallel converted to $U$ parallel streams having a symbol duration of $T_s = T_b \cdot U$, and then the symbol conveyed by each parallel stream was DS spread by the spreading sequence $c_k(t)$ associated with the $k$th user. After DS spreading the chip duration of each branch became $T_c = T_s/N_e$, where $N_e$ is the number of chips. Then, these DS-spread streams modulate $V$ number of orthogonal subcarriers, generating overlapping subbands. Here, the spacing between two adjacent subcarrier frequencies is $1/T_c = N_e/T_s$. In this chapter, we will discuss a gen-

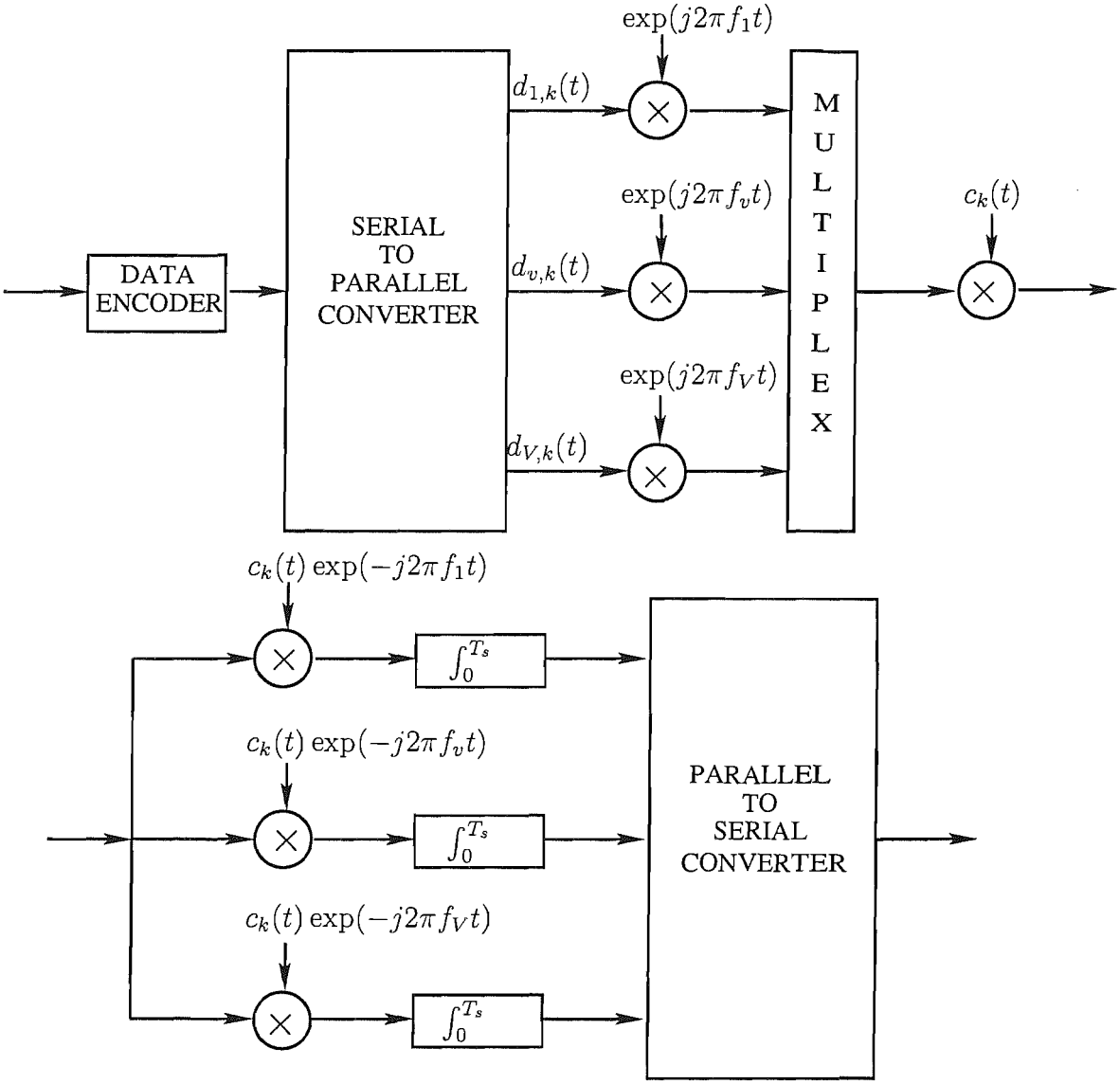


**Figure 2.1:** Block diagram of a multitone DS-CDMA communications system.

eralized MC DS-CDMA system [40–42], which includes the subclasses of multitone DS-CDMA [43] and orthogonal MC DS-CDMA [12] as special cases.

Chapter 2 has following structure. In Section 2.2 the philosophy of the Generalized Multicarrier DS-CDMA System will be described and characterized. In Section 2.3 a range of linear combining based antenna array weight optimization schemes are invoked for deriving the decision variables, while their performance will be studied in Section 2.3.6, in the context of a DS-CDMA system, a MC-CDMA system and a generalized MC DS-CDMA system.

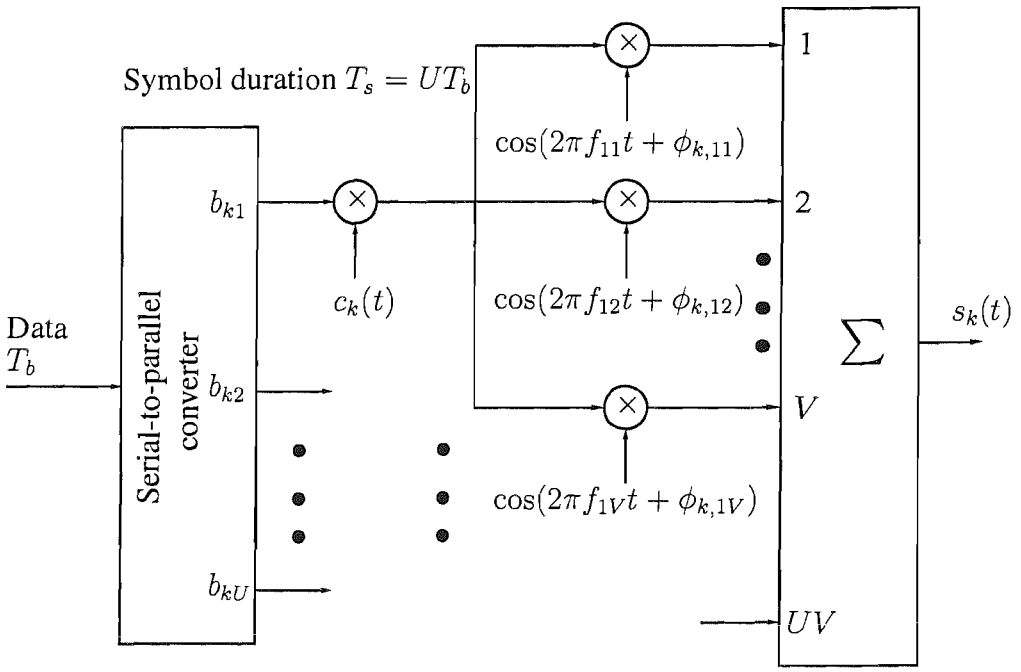


**Figure 2.2:** The $k$th user's transmitter schematic for the generalized multicarrier DS-CDMA system.

## 2.2 Generalized Multicarrier DS-CDMA Systems

### 2.2.1 Transmitted Signal

In this chapter, a generalized MC DS-CDMA system [40–42] is considered, which includes the subclasses of multitone DS-CDMA [43] and orthogonal MC DS-CDMA [12] as special cases. The transmitter schematic of the $k$th user is shown in Figure 2.2 for the generalized MC DS-CDMA system considered. At the transmitter side, the binary data stream having a bit duration of $T_b$ is Serial-to-Parallel (S/P) converted to $U$ parallel sub-streams. The new bit duration of each sub-stream, which we refer to as the symbol duration becomes $T_s = UT_b$. After S/P conversion, each substream is spread using a DS spreading sequence waveform $c_k(t)$. Then, the DS spread-spectrum signal of the $u$th sub-stream, where we have $u = 1, 2, \ldots, U$, modulates a group of subcarrier frequencies $\{f_{u1}, f_{u2}, \ldots, f_{uV}\}$ using Binary Phase Shift Keying (BPSK). Since each of the $U$ data bits is conveyed with the aid of $V$ subcarriers, a total of $UV$ number of subcarriers are required in the MC DS-CDMA system considered. Finally, the $UV$ number of subcarrier signals are added in order to form the complex modulated signal. Therefore, the transmitted signal of user $k$ can be expressed as

$$s_k(t) = \sum_{u=1}^{U}\sum_{v=1}^{V}\sqrt{\frac{2P}{V}}b_{ku}(t)c_k(t)\cos(2\pi f_{uv}t + \phi_{k,uv}), \tag{2.1}$$

where $P/V$ represents the transmitted power of each subcarrier, while $\{b_{ku}(t)\}$, $c_k(t)$, $\{f_{uv}\}$ and $\{\phi_{k,uv}\}$ represent the data stream, the DS spreading waveform, the subcarrier frequency set and the

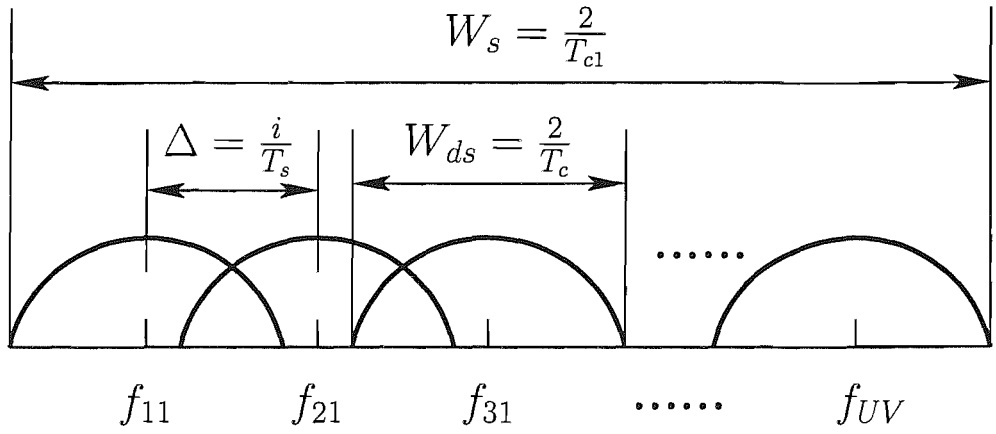


**Figure 2.3:** Stylized spectrum of the generalized multicarrier DS-CDMA signal.

phase angles introduced in the carrier modulation process. The data stream's waveform $b_{ku}(t) = \sum_{i=-\infty}^{\infty} b_{ku}[i]P_{T_s}(t - iT_s)$ consists of a sequence of mutually independent rectangular pulses of duration $T_s$ and of amplitude +1 or -1 with equal probability. The spreading sequence $c_k(t) = \sum_{j=-\infty}^{\infty} c_{kj}P_{T_c}(t-jT_c)$ denotes the signature sequence waveform of the $k$th user, where $c_{kj}$ assumes values of +1 or -1 with equal probability, while $P_{T_c}(t)$ is the rectangular chip waveform, which is defined over the interval $[0, T_c)$.

### 2.2.2 Modulation Parameters

The stylized spectrum arrangement of the generalized MC DS-CDMA systems considered here is shown in Figure 2.3, where we assume that $W_s = 2/T_{c1}$ is the total bandwidth available, $T_{c1}$ represents the chip-duration of a corresponding single-carrier DS-CDMA signal occupying the bandwidth of $W_s$, while $W_{ds} = 2/T_c$ represents the 'null-to-null' bandwidth of the subcarrier signals. The spacing between two adjacent subcarrier frequencies is assumed to be $\Delta$, which is assumed to be a variable assuming values in the form of $\Delta = i/T_s$, with $i = 0, 1, 2, \ldots$ being an integer.

Let $N_e = T_s/T_c$ be the spreading gain of the DS-spread subcarrier signals. It can be shown that the generalized MC DS-CDMA scheme of Figure 2.2 incorporates the family of multitone DS-CDMA arrangements [43], if we assume $\Delta = 1/T_s$. Similarly, if it is configured to satisfy $\Delta = N_e/T_s$, the generalized MC DS-CDMA scheme considered incorporates also the class of orthogonal MC DS-CDMA [12] systems. Furthermore, there is no overlap between the main-lobes of the modulated subcarrier signals after DS spreading, provided that the criterion of $\Delta = 2N_e/T_s$ is obeyed. Explicitly, the difference between the systems proposed in [43] and [12] is that the spacing between two adjacent subcarrier frequencies $\Delta$ of multitone DS-CDMA scheme [43] is $1/T_s$, while that of the orthogonal MC DS-CDMA scheme [12] is $N_e/T_s$.

The subcarrier frequencies of Figure 2.3 are arranged according to

$$f_{uv} = \frac{1}{T_c} + \Delta\left[(v-1)U + u - 1\right],\ u = 1, 2, \ldots, U;\ v = 1, 2, \ldots, V. \tag{2.2}$$

When using the above-mentioned subcarrier frequency arrangement, the frequency spacing between the $uv$-th subcarrier and the $u(v+1)$-st subcarrier, which convey the same data bit as it can be inferred from Figure 2.2, is $\nabla = \Delta U$. This implies that under the constraint of having a total bandwidth of $W_s = 2/T_{c1}$, $\nabla = \Delta U$ is the maximum possible frequency spacing for the $V$ number of subcarriers used in (2.1), which convey the same data bit. Therefore, with the advent of spacing the replicas of the same bit far apart in the frequency-domain, the receiver is capable of achieving the maximum frequency-domain diversity gain as a benefit of the independent frequency-selective fading of the subcarriers, when combining the corresponding subcarrier signals. Let $N_1 = T_b/T_{c1}$ be the spreading gain of a corresponding single-carrier DS-CDMA system having a bandwidth of $W_s = 2/T_{c1}$. Then, according to Figure 2.3, the system's total transmission bandwidth, the subcarrier spacing $\Delta$ and the DS spreading bandwidth of the subcarrier signal obey the relationship of $W_s = (UV-1)\Delta + W_{ds}$, or

$$\frac{2}{T_{c1}} = (UV-1)\Delta + \frac{2}{T_c}. \tag{2.3}$$

Multiplying both sides of the above equation by the symbol duration of $T_s = UT_b$, and taking into account that we have $T_s = N_e T_c$ as well as that $T_s = UT_b = UN_1 T_{c1}$, the processing gain, $N_e = T_s/T_c$ associated with the subcarrier signal can be expressed as

$$N_e = UN_1 - \frac{(UV-1)\Delta T_s}{2}, \tag{2.4}$$

which implies that for a given total system bandwidth of $W_s = 2/T_{c1}$ and for a given number of subcarriers, $UV$, $N_e$ decreases, as $\Delta$ increases.

Let the maximum delay spread of a wireless communication channel be $T_m$, which implies that the coherence bandwidth of the wireless channel is assumed to be $(\Delta f) \approx 1/T_m$ [190]. Under the above-mentioned fading channel assumptions, the number of resolvable of paths associated with each subcarrier signal can be expressed as

$$L_p = \lfloor \frac{T_m}{T_c} \rfloor + 1, \tag{2.5}$$

where $\lfloor x \rfloor$ denotes the largest integer less than $x$. Upon expressing $T_c$ from (2.3) as

$$T_c = \frac{2T_{c1}}{2 - (UV-1)\Delta T_{c1}}, \tag{2.6}$$

and substituting it into (2.5), we obtain

$$\begin{aligned} L_p &= \left\lfloor \frac{T_m}{2T_{c1}} [2 - (UV-1)\Delta T_{c1}] \right\rfloor + 1 \\ &\approx \lfloor (L_1 - 1)\,[1 - 0.5(UV-1)\Delta T_{c1}] \rfloor + 1, \end{aligned} \tag{2.7}$$

where $L_1 = \lfloor T_m/T_{c1} \rfloor + 1$ represents the number of resolvable paths of a corresponding single-carrier DS-CDMA signal namely one, which uses a null-to-null bandwidth of $W_s = 2/T_{c1}$. Again, the frequency spacing of the generalized MC DS-CDMA system between two adjacent subcarriers was denoted by $\Delta = i/T_s$, where $i$ is an integer. Equation (2.7) can be expressed as

$$\begin{aligned} L_p &= \left\lfloor \frac{T_m}{2T_{c1}} [2 - (UV-1)\Delta T_{c1}] \right\rfloor + 1 \\ &\approx \left\lfloor (L_1 - 1)\left(1 - \frac{(UV-1)i}{2UN_1}\right) \right\rfloor + 1. \end{aligned} \tag{2.8}$$

Equations (2.7) and (2.8) show that the number of resolvable paths of the subcarrier signals is a function of the total number of subcarriers $UV$, that of the number of bits $U$ invoked in the S/P conversion stage of Figure 2.2 as well as that of the frequency spacing between two adjacent subcarriers. These parameters can be optimized during the system design stage or may be reconfigured on-line, in order to satisfy specific system requirements. The generalized MC DS-CDMA systems considered here are configured such that each subcarrier signal is guaranteed to experience flat-fading. Then, the frequency-selective diversity gain is attained by combining the $V$ number of independently faded subcarrier signals, jointly conveying a given bit. Specifically, according to (2.5), the flat-fading condition of each subcarrier signal is satisfied, if the chip-duration, $T_c$, is higher than the delay-spread, i.e. when $T_c > T_m$. Since any two of the subcarriers conveying the same data bit is spaced at least by $U\Delta$ Hz, the condition of independently faded subcarrier signals can be achieved, provided that we have this frequency spacing higher than the coherence bandwidth of $(\Delta f)_m \approx 1/T_m$, i.e., when

$$U\Delta > \frac{1}{T_m}. \tag{2.9}$$

Having outline the transmitter's schematic, let us now consider the receiver model.

### 2.2.3 Receiver Model

We assume that at a base-station (BS) there are $M$ number of receiver antennas, as shown in Figure 2.4, which are located sufficiently far apart so that a MC DS-CDMA signal experiences independent fading, when it reaches the different antennas. Each of the $M$ antennas consists of an antenna array having $L$ number of linearly elements separated by a distance of $d$, which is usually half a wavelength. Hence, the total number of antenna elements of the $M$ antennas is $ML$. Based on the these assumptions, the Spatio-Temporal (ST) Channel Impulse Response (CIR) $h^{(k)}_{uv,ml}$ between the $uv$th

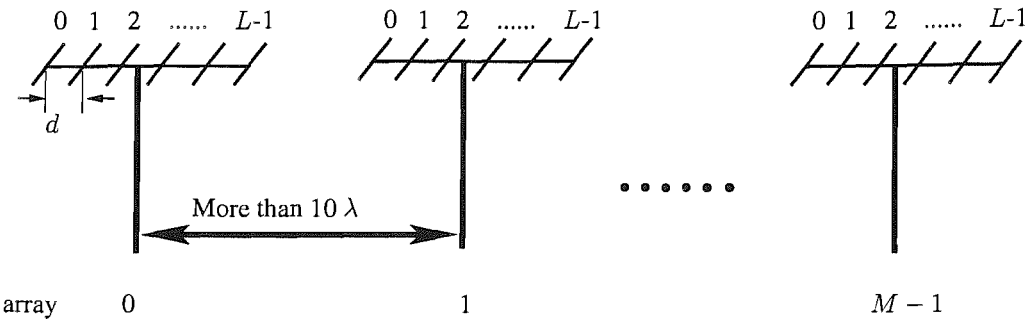


**Figure 2.4:** Multiple antenna configuation to be used in the generalized MC DS-CDMA system considered.

subcarrier of the $k$th user and the $l$th array of the $m$th antenna can be expressed as

$$h_{uv,ml}^{(k)} = \alpha_{uv,ml}^{(k)}(t) \exp\left(j\left[\varphi_{uv,ml}^{(k)} + 2\pi\frac{d}{\lambda} l \sin(\psi_m^{(k)} + \kappa_m^{(k)} B)\right]\right) \delta(t - \tau_k), \quad (2.10)$$
$$m = 0, 1, \ldots, M-1;\ l = 0, 1, \ldots, L-1;$$
$$u = 1, 2, \ldots, U;\ v = 1, 2, \ldots, V;$$
$$k = 1, 2, \ldots, K.$$

The variables used in (2.10) are described as follows:

- $\tau_k$: signal delay, which takes account of the users' different distance-related channel delay and of their asynchronous transmissions.
- $\varphi_{uv,ml}^{(k)}$: phase angle, which is the result of the channel-induced phase rotation, modelled by a random variable uniformly distributed in $[0, 2\pi]$. When the spatial signals arriving at the elements of an antenna array are perfectly correlated, the channel-induced phase angle $\varphi_{uv,ml}^{(k)}$ is independent of the array's element index of $l$, i.e. we have $\varphi_{uv,ml}^{(k)} = \varphi_{uv,m}^{(k)}$;
- $\alpha_{uv,ml}^{(k)}(t)$: Rayleigh faded envelope's amplitude corresponding to the $uv$th subcarrier signal and to the $l$th array of the $m$th antenna. When the spatial signals arriving at the elements of an antenna array are perfectly correlated, the fading envelope's amplitude $\alpha_{uv,ml}^{(k)}(t)$ becomes independent of the array's element index of $l$, i.e. we have $\alpha_{uv,ml}^{(k)}(t) = \alpha_{uv,m}^{(k)}(t)$;
- $d$: inter-element spacing of the antenna array;
- $\lambda$: wavelength of the transmitted signal at the radio frequency;
- $\psi_m^{(k)}$: average Direction-Of-Arrival (DOA) from the $k$th transmitter to the $m$th antenna;
- $\kappa_m^{(k)} B$: spatial angle spread, where $B$ represents the maximum angular spread, while $-\frac{1}{2} \leqslant \kappa_m^{(k)} \leqslant \frac{1}{2}$ is a uniformly distributed random variable.

Let the ST-CIR vector of the $L$ array elements be formulated as:

$$\begin{aligned}\mathbf{h}_{uv,m}^{(k)}(t) &= \left[h_{uv,m0}^{(k)}(t), h_{uv,m1}^{(k)}(t), \ldots, h_{uv,m(L-1)}^{(k)}(t)\right]^T \\ &= \mathbf{a}_{uv,m}^{(k)}(t)\delta(t-\tau_k),\end{aligned} \tag{2.11}$$

where

$$\begin{aligned}\mathbf{a}_{uv,m}^{(k)}(t) = &\left[\alpha_{uv,m0}^{(k)}(t)\exp\left(j\varphi_{uv,m0}^{(k)}\right),\right. \\ &\alpha_{uv,m1}^{(k)}(t)\exp\left(j\left[\varphi_{uv,m1}^{(k)} + 2\pi\frac{d}{\lambda}\sin(\psi_m^{(k)} + \kappa_m^{(k)}B)\right]\right), \ldots, \\ &\left.\alpha_{uv,m(L-1)}^{(k)}(t)\exp\left(j\left[\varphi_{uv,m(L-1)}^{(k)} + 2\pi\frac{d}{\lambda}(L-1)\sin(\psi_m^{(k)} + \kappa_m^{(k)}B)\right]\right)\right]^T.\end{aligned} \tag{2.12}$$

is the $L$-dimensional complex array vector in the $uv$th subcarrier of the $k$th user and the $m$th antenna. Where, $2\pi\frac{dl}{\lambda}\sin(\psi_m^{(k)})$ is the phase delays of a plane wave with wavelength $\lambda$ and angle of incidence, namely, DOA from the $k$th transmitter to the $l$th array element of the $m$th antenna array with respect to the first element, and $\kappa_m^{(k)}B$ is the effect of the angular spread. When we assume that the array elements are separated by half a wavelength, i.e. that we have $d = \lambda/2$, then, (2.12) may be simplified to

$$\begin{aligned}\mathbf{a}_{uv,m}^{(k)}(t) = &\left[\alpha_{uv,m0}^{(k)}(t)\exp\left(j\varphi_{uv,m0}^{(k)}\right),\right. \\ &\alpha_{uv,m1}^{(k)}(t)\exp\left(j\left[\varphi_{uv,m1}^{(k)} + \pi\sin(\psi_m^{(k)} + \kappa_m^{(k)}B)\right]\right), \ldots, \\ &\left.\alpha_{uv,m(L-1)}^{(k)}(t)\exp\left(j\left[\varphi_{uv,m(L-1)}^{(k)} + (L-1)\pi\sin(\psi_m^{(k)} + \kappa_m^{(k)}B)\right]\right)\right]^T.\end{aligned} \tag{2.13}$$

Based on (2.11), the ST-CIRs corresponding to the entire set of $ML$ elements of the $M$ antennas can be written as

$$\begin{aligned}\tilde{\mathbf{h}}_{uv}^{(k)}(t) &= \left[\left(\mathbf{h}_{uv,0}^{(k)}(t)\right)^T, \left(\mathbf{h}_{uv,1}^{(k)}(t)\right)^T, \ldots, \left(\mathbf{h}_{uv,(M-1)}^{(k)}(t)\right)^T\right]^T \\ &= \tilde{\mathbf{a}}_{uv}^{(k)}(t)\delta(t-\tau_k) \\ &= \left[\left(\mathbf{a}_{uv,0}^{(k)}(t)\right)^T, \left(\mathbf{a}_{uv,1}^{(k)}(t)\right)^T, \ldots, \left(\mathbf{a}_{uv,(M-1)}^{(k)}(t)\right)^T\right]^T \delta(t-\tau_k),\end{aligned} \tag{2.14}$$

which is a $ML \times 1$-dimensional vector.

We assume that $K$ asynchronous MC DS-CDMA users are supported by the system, where all of them use the same $U$, $V$, $\Delta$ and $N_e$ values, and that the average power received from each user at the base station is also the same, implying perfect power control. Consequently, when $K$ number of single-user signals obeying the form of (2.1) are transmitted over the spatio-temporal channels characterized by (2.14), the received baseband equivalent signal vector at the antenna arrays output

can be expressed as

$$\mathbf{r}(t) = \sum_{k=1}^{K} \mathbf{r}_k(t) + \mathbf{n}(t), \tag{2.15}$$

where $\mathbf{r}(t)$ is a $ML \times 1$-dimensional vector, and $\mathbf{n}(t) = \mathbf{n}_c(t) + j\mathbf{n}_s(t)$ is the $ML \times 1$-dimensional additive white Gaussian noise (AWGN) vector having a zero mean and covariance of

$$\mathrm{E}\left\{\mathbf{n}(t_1)\mathbf{n}^H(t_2)\right\} = 2N_0\mathbf{I} \cdot \delta(t_1 - t_2), \tag{2.16}$$

with the superscript $H$ denoting the conjugate transpose operation, while $N_0$ represents the double-sided power spectral density of a complex valued low-pass-equivalent AWGN signal. In (2.15) $\mathbf{r}_k(t)$ represents the response of the $k$th user's transmitted signal to the spatial-temporal channels, which is a $ML \times 1$-dimensional vector that can be expressed as

$$\begin{aligned} \mathbf{r}_k(t) &= s_k(t) \otimes \tilde{\mathbf{h}}_{uv}^{(k)}(t) \\ &= \sum_{u=1}^{U}\sum_{v=1}^{V} \sqrt{\frac{2P}{V}}\, b_{ku}(t - \tau_k)c_k(t - \tau_k)\tilde{\mathbf{a}}_{uv}^{(k)}(t) \exp\left(j\left[2\pi f_{uv}t + \theta_{uv}^{(k)}\right]\right), \end{aligned} \tag{2.17}$$

where we have $\theta_{uv}^{(k)} = \phi_{k,uv} - 2\pi f_{uv}\tau_k$, which is a random variable uniformly distributed in $[0, 2\pi]$. In the above equation, we assumed that for a given antenna index $m$, all the subcarrier signals arrive from the same direction. i.e. the DOA is only dependent on the user's location, but it is independent of the subcarrier frequencies. We note that this assumption is valid only, if the bandwidth of the MC DS-CDMA system considered is significantly lower than the carrier frequency $f_c$.

Let us assume that the first user corresponding to $k = 1$ is the user-of-interest, which is referred to as the reference user. The receiver block diagram designed for detecting the information arriving from the reference user is shown in Figure 2.5, where the superscript and subscript denoting the reference user of $k = 1$ has been omitted for notational convenience. As shown in Figure 2.5, the MC DS-CDMA detector consists of two main parts, the first part carries out multicarrier demodulation and DS despreading in the context of each array element and each of the $M$ antennas. Each antenna array element provides $V$ number of outputs, which correspond to the $V$ number of subcarriers conveying the signals representing the same data bit. Therefore, associated with each transmitted data bit, such as bit $u$, we have a total of $VML$ output variables, as shown in Figure 2.5, which carry the information of the same transmitted data bit. Hence, the second task, namely, the task of the second section of the receiver seen in Figure 2.5 is to combine these $VML$ number of variables according to an efficient combining algorithm, and this process will be discussed in detail during our forthcoming discourse in Section 2.3.

Let

$$\mathbf{z}_u = \left[\mathbf{z}_{u1}^T, \mathbf{z}_{u2}^T, \ldots, \mathbf{z}_{uV}^T\right]^T, \tag{2.18}$$

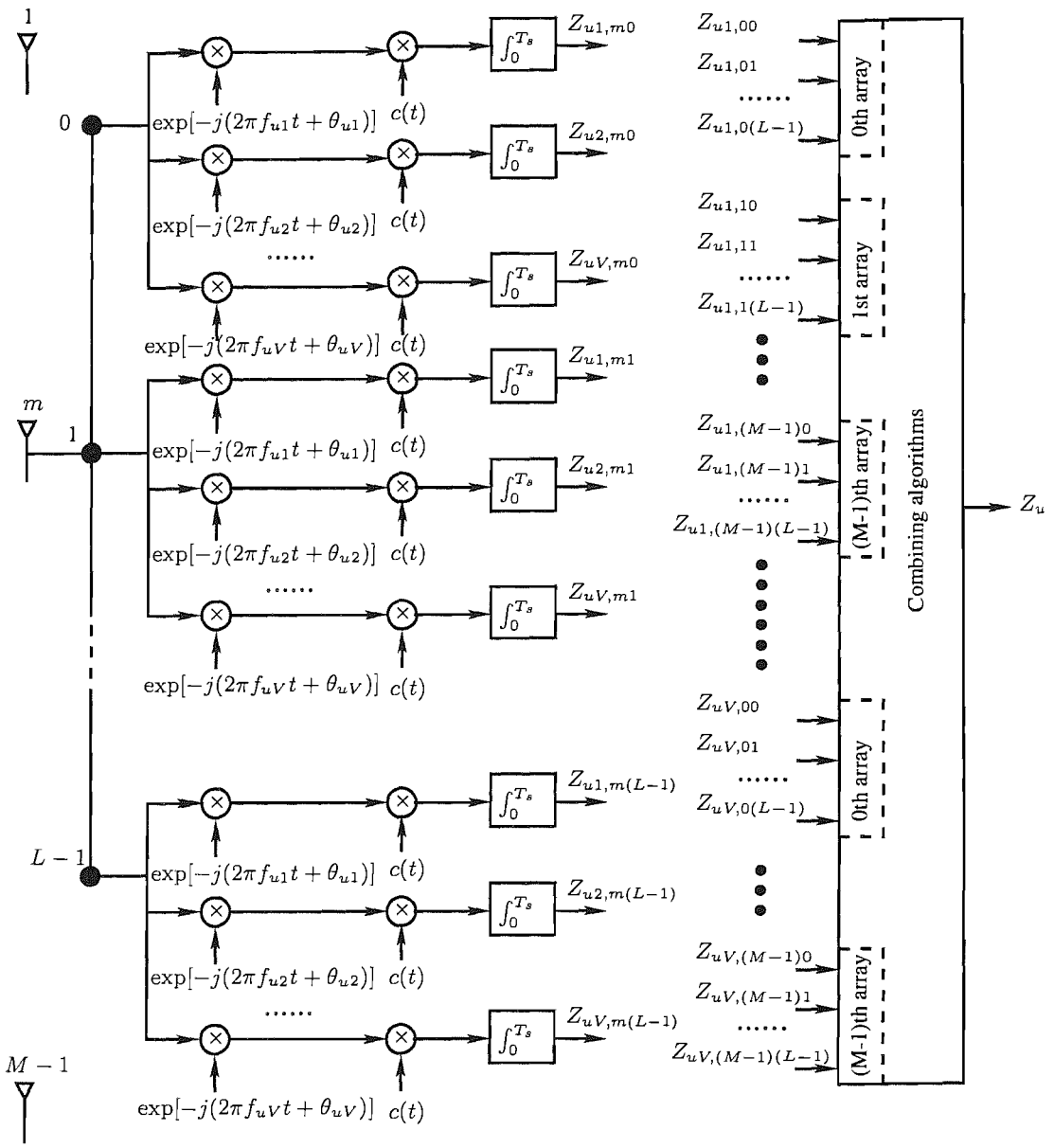


**Figure 2.5:** Receiver block diagram of the generalized MC DS-CDMA system considered. The receiver employs beamforming, receiver diversity combining and multicarrier-spreading-assisted frequency-selective diversity combining.

be a $VML$-length vector containing the entire set of $VML$ number of decision variables in the context of the $u$th data bit after multicarrier demodulation and DS despreading. These $VML$ number of variables are denoted in Figure 2.5 as $\{z_{uv,ml}\}$ for $v = 1, 2, \ldots, V$; $m = 0, 1, \ldots, (M-1)$; $l = 0, 1, \ldots, (L-1)$, where

$$\mathbf{z}_{uv} = \left[\mathbf{z}_{uv,0}^T, \mathbf{z}_{uv,1}^T, \ldots, \mathbf{z}_{uv,(M-1)}^T\right]^T, \; v = 1, 2, \ldots, V \tag{2.19}$$

is an $ML$-length vector containing the $ML$ number of variables in the context of the $v$th subcarrier, where $v = 1, 2, \ldots, V$. In other words, the vector $\mathbf{z}_{uv}$ contains the $ML$ number of antenna arrays' outputs in response to the $v$th subcarrier signal. Finally, in (2.19)

$$\mathbf{z}_{uv,m} = \left[z_{uv,m0}, z_{uv,m1}, \ldots, z_{uv,m(L-1)}\right]^T, \quad v = 1, 2, \ldots, V;\ m = 0, 1, \ldots, M-1 \tag{2.20}$$

represents an $L$-length vector, which includes the $m$th antenna's response to the $v$th subcarrier signal after multicarrier demodulation and DS despreading.

We assume that the receiver is capable of acquiring perfect time-domain synchronization. The attenuations and phases of the ST CIR taps are assumed to be perfectly estimated. Furthermore, in this chapter we assume that the DOA of the reference user's signal is also known at the base-station. In order to render our investigations as realistic as possible, in our forthcoming discourse the antenna array assisted MC DS-CDMA systems will be investigated without the knowledge of the spatio-temporal channel. Returning to Figure 2.5, after multicarrier demodulation and DS despreading, the antenna array outputs corresponding to the 0th bit $b_u[0]$ and the $v$th subcarrier can be expressed as

$$\mathbf{z}_{uv} = \int_0^{T_s} \mathbf{r}(t)c(t)\exp\left(-j[2\pi f_{uv}t + \theta_{uv}]\right)dt,\ v = 1, 2, \ldots, V, \tag{2.21}$$

where we assumed that the reference signal's transmission delay was $\tau_1 = 0$ for simplicity.

### 2.2.4 Statistical Properties of $\mathbf{z}_u$

In this section we characterize the properties of the decision variable $\mathbf{z}_u$ expressed in (2.18). Let us first derive the components of $\mathbf{z}_u$. We assume that the ST CIR taps given by $\tilde{\mathbf{a}}_{uv}^{(k)}$ of Equation (2.14) remain constant for a symbol duration of $T_s$. Upon substituting the received signal vector $\mathbf{r}(t)$ of (2.15) into (2.21), it can be shown that $\mathbf{z}_{uv}$ expressed in terms of the $v$th subcarrier of $b_u$ can be written as

$$\mathbf{z}_{uv} = \sqrt{\frac{2P}{V}}T_s \left[ b_u[0]\tilde{\mathbf{a}}_{uv} + \mathbf{n}_{uv} + \underbrace{\sum_{u'=1}^{U}\sum_{v'=1}^{V}}_{v'\neq v,\ \text{if } u'=u} \mathbf{i}_{u'v'}^{(s)} + \sum_{k=2}^{K}\mathbf{i}_{uv}^{(k)} + \sum_{k=2}^{K}\underbrace{\sum_{u'=1}^{U}\sum_{v'=1}^{V}}_{v'\neq v,\ \text{if } u'=u} \mathbf{i}_{u'v'}^{(k)} \right], \tag{2.22}$$

where $b_u[0]\tilde{\mathbf{a}}_{uv}$ represents the desired array outputs obtained by substituting (2.15) into (2.21) and setting $k = 1$, $u' = u$, $v' = v$, while $\tilde{\mathbf{a}}_{uv}$ is given by (2.14) associated with the reference user corresponding to $k = 1$. In (2.22) $\mathbf{n}_{uv}$ is contributed by $\mathbf{n}(t)$ of (2.15), that can be expressed as

$$\mathbf{n}_{uv} = \frac{1}{\sqrt{\frac{2P}{V}}T_s}\int_0^{T_s} \mathbf{n}(t)c(t)\exp\left(-j[2\pi f_{uv}t + \theta_{uv}]\right)dt, \tag{2.23}$$

which is an $ML \times 1$-dimensional AWGN vector having zero mean and a covariance of

$$\mathrm{E}\left\{\mathbf{n}_{uv}\mathbf{n}_{uv}^{H}\right\} = \frac{VN_0}{E_b}\mathbf{I}, \tag{2.24}$$

where $E_b = PT_s$ represents the energy per bit, while $\mathbf{I}$ is an $ML \times ML$-dimensional unity matrix. The term $\mathbf{i}_{u'v'}^{(s)}$ in (2.22) represents the self-interference contributed by the subcarrier indexed by $u'$, $v'$ of the reference signal. To expound further, $\mathbf{i}_{u'v'}^{(s)}$ can be expressed as

$$\begin{aligned}\mathbf{i}_{u'v'}^{(s)} &= \frac{1}{T_s}\int_0^{T_s} b_{u'}(t)c(t)\tilde{\mathbf{a}}_{u'v'}\exp\left(j\left[2\pi f_{u'v'}t + \theta_{u'v'}\right]\right) \\ &\quad \times c(t)\exp\left(-j\left[2\pi f_{uv}t + \theta_{uv}\right]\right)dt \\ &= \frac{b_{u'}[0]\tilde{\mathbf{a}}_{u'v'}}{T_s}\int_0^{T_s}\exp\left(j\left[2\pi(f_{u'v'} - f_{uv})t + \vartheta_{u'v'}\right]\right)dt,\end{aligned} \tag{2.25}$$

where $\vartheta_{u'v'} = \theta_{u'v'} - \theta_{uv}$. It can be shown that (2.25) can be simplified as

$$\mathbf{i}_{u'v'}^{(s)} = b_{u'}[0]\tilde{\mathbf{a}}_{u'v'}\mathrm{sinc}\left[\pi\left(f_{u'v'} - f_{uv}\right)T_s\right]\exp\left(j\left[\pi(f_{u'v'} - f_{uv})T_s + \vartheta_{u'v'}\right]\right), \tag{2.26}$$

where $\mathrm{sinc}(x) = \sin(x)/x$. Furthermore, it can be shown that

$$\mathbf{i}_{u'v'}^{(s)} = \mathbf{0}, \tag{2.27}$$

provided that we have $(f_{u'v'} - f_{uv}) = \frac{n}{T_s}$, implying that the subcarrier signals are orthogonal before the DS spreading, where $n \geq 1$ represents an integer.

The multiuser interference (MUI) term $\mathbf{i}_{uv}^{(k)}$ in (2.22) is engendered by the subcarrier signal determined by $u$ and $v$ of the $k$th interfering user, which can be expressed as

$$\begin{aligned}\mathbf{i}_{uv}^{(k)} = \frac{1}{T_s}\int_0^{T_s} b_{ku}(t-\tau_k)c_k(t-\tau_k)\tilde{\mathbf{a}}_{uv}^{(k)}\exp\left(j\left[2\pi f_{uv}t + \theta_{uv}^{(k)}\right]\right) \\ \times c(t)\exp\left(-j\left[2\pi f_{uv}t + \theta_{uv}\right]\right)dt,\end{aligned} \tag{2.28}$$

that can be further simplified to

$$\mathbf{i}_{uv}^{(k)} = \frac{\tilde{\mathbf{a}}_{uv}^{(k)}\exp\left(j\vartheta_{uv}^{(k)}\right)}{T_s}\int_0^{T_s} b_{ku}(t-\tau_k)c_k(t-\tau_k)c(t)dt, \tag{2.29}$$

where we have $\vartheta_{uv}^{(k)} = \theta_{uv}^{(k)} - \theta_{uv}$.

Finally, the MUI term $\mathbf{i}_{u'v'}^{(k)}$ in (2.22) is imposed by the subcarrier determined by $u'$ and $v'$ associated with the $k$th interfering user, where $\mathbf{i}_{u'v'}^{(k)}$ can be expressed as

$$\begin{aligned}\mathbf{i}_{u'v'}^{(k)} = \frac{1}{T_s}\int_0^{T_s} b_{ku'}(t-\tau_k)c_k(t-\tau_k)\tilde{\mathbf{a}}_{u'v'}^{(k)}\exp\left(j\left[2\pi f_{u'v'}t + \theta_{u'v'}^{(k)}\right]\right) \\ \times c(t)\exp\left(-j\left[2\pi f_{uv}t + \theta_{uv}\right]\right)dt,\end{aligned} \tag{2.30}$$

which can be written as

$$\mathbf{i}_{u'v'}^{(k)} = \frac{\tilde{\mathbf{a}}_{u'v'}^{(k)} \exp(\vartheta_{u'v'}^{(k)})}{T_s} \int_0^{T_s} b_{ku'}(t-\tau_k) c_k(t-\tau_k) c(t) \exp\left(j2\pi[f_{u'v'} - f_{uv}]t\right) dt, \tag{2.31}$$

where, again, we have $\vartheta_{u'v'}^{(k)} = \theta_{u'v'}^{(k)} - \theta_{uv}$.

We have assumed that the MC DS-CDMA signal experiences independent fading, when it reaches each element of the different antennas. Hence, after ignoring the common factor of $\sqrt{2P/V}T_s$ in (2.23), the array outputs expressed in the context of bit $b_u[0]$ can be written as

$$\mathbf{z}_u = \begin{bmatrix} \mathbf{z}_{u1} \\ \mathbf{z}_{u2} \\ \vdots \\ \mathbf{z}_{uV} \end{bmatrix}, \tag{2.32}$$

$$= \tilde{\mathbf{a}}_u b_u[0] + \mathbf{n}_u + \mathbf{j}_u, \tag{2.33}$$

$$= \begin{bmatrix} \tilde{\mathbf{a}}_{u1} \\ \tilde{\mathbf{a}}_{u2} \\ \vdots \\ \tilde{\mathbf{a}}_{uV} \end{bmatrix} b_u[0] + \begin{bmatrix} \mathbf{n}_{u1} \\ \mathbf{n}_{u2} \\ \vdots \\ \mathbf{n}_{uV} \end{bmatrix} + \begin{bmatrix} \mathbf{j}_{u1} \\ \mathbf{j}_{u2} \\ \vdots \\ \mathbf{j}_{uV} \end{bmatrix}, \tag{2.34}$$

$$\mathbf{z}_u = \begin{bmatrix} \mathbf{z}_{u1,0} \\ \mathbf{z}_{u1,1} \\ \vdots \\ \mathbf{z}_{u1,M-1} \\ \mathbf{z}_{u2,0} \\ \mathbf{z}_{u2,1} \\ \vdots \\ \mathbf{z}_{u2,M-1} \\ \vdots \\ \mathbf{z}_{uV,0} \\ \mathbf{z}_{uV,1} \\ \vdots \\ \mathbf{z}_{uV,M-1} \end{bmatrix} = \begin{bmatrix} \mathbf{a}_{u1,0} \\ \mathbf{a}_{u1,1} \\ \vdots \\ \mathbf{a}_{u1,M-1} \\ \mathbf{a}_{u2,0} \\ \mathbf{a}_{u2,1} \\ \vdots \\ \mathbf{a}_{u2,M-1} \\ \vdots \\ \mathbf{a}_{uV,0} \\ \mathbf{a}_{uV,1} \\ \vdots \\ \mathbf{a}_{uV,M-1} \end{bmatrix} b_u[0] + \begin{bmatrix} \mathbf{n}_{u1,0} \\ \mathbf{n}_{u1,1} \\ \vdots \\ \mathbf{n}_{u1,M-1} \\ \mathbf{n}_{u2,0} \\ \mathbf{n}_{u2,1} \\ \vdots \\ \mathbf{n}_{u2,M-1} \\ \vdots \\ \mathbf{n}_{uV,0} \\ \mathbf{n}_{uV,1} \\ \vdots \\ \mathbf{n}_{uV,M-1} \end{bmatrix} + \begin{bmatrix} \mathbf{j}_{u1,0} \\ \mathbf{j}_{u1,1} \\ \vdots \\ \mathbf{j}_{u1,M-1} \\ \mathbf{j}_{u2,0} \\ \mathbf{j}_{u2,1} \\ \vdots \\ \mathbf{j}_{u2,M-1} \\ \vdots \\ \mathbf{j}_{uV,0} \\ \mathbf{j}_{uV,1} \\ \vdots \\ \mathbf{j}_{uV,M-1} \end{bmatrix}, \tag{2.35}$$

where $\mathbf{a}_{uv,m}$ is in the form of (2.12). When assuming a time-invariant channel during the detection

of bit $b_u[0]$, $\mathbf{a}_{uv,m}$ can be expressed as

$$\begin{aligned}\mathbf{a}_{uv,m} = & \left[\alpha_{uv,m0}\exp\left(j\varphi_{uv,m0}\right),\right. \\ & \alpha_{uv,m1}\exp\left(j\left[\varphi_{uv,m1}+2\pi\frac{d}{\lambda}\sin(\psi_m+\kappa_m B)\right]\right),\ldots, \\ & \left.\alpha_{uv,m(L-1)}\exp\left(j\left[\varphi_{uv,m(L-1)}+2\pi\frac{d}{\lambda}(L-1)\sin(\psi_m+\kappa_m B)\right]\right)\right]^T.\end{aligned} \tag{2.36}$$

In (2.35) $\mathbf{a}_{uv,m}$ is independent of $\tilde{\mathbf{a}}_{u'v',m'}$ for $u \neq u'$, $v \neq v'$ or $m \neq m'$. Each row of (2.35), i.e., $\mathbf{z}_{uv,m}$ can be modelled as an independently distributed random vector having a common covariance matrix. Furthermore, $\tilde{\mathbf{a}}_u$, $\mathbf{n}_u$ and $\mathbf{j}_u$ in (2.33) are assumed to be the mutually independent random vectors.

The correlation matrix $\mathbf{R}_{zz}$ of $\mathbf{z}_u$ can be expressed as

$$\mathbf{R}_{zz} = E\left[\mathbf{z}_u\mathbf{z}_u^H\right], \tag{2.37}$$

where the superscript $H$ represents the conjugate transpose operation. Upon substituting the decision variable $\mathbf{z}_u$ of (2.35) into (2.37) and exploiting the statistical independence of the derived signal and the noise, $\mathbf{R}_{zz}$ can be expressed as

$$\mathbf{R}_{zz} = \mathbf{R}_d + \mathbf{R}_{uu}, \tag{2.38}$$

where $\mathbf{R}_d$ contains the autocorrelations of the desired signals hosted by the matrix $\tilde{\mathbf{a}}_u$ in (2.33), which can be expressed as

$$\mathbf{R}_d = E\left[\tilde{\mathbf{a}}_u\tilde{\mathbf{a}}_u^H\right]. \tag{2.39}$$

Upon substituting $\tilde{\mathbf{a}}_u$ given by the first term of (2.35) into (2.39) and exploiting the property the property that $\tilde{\mathbf{a}}_{uv,m}$ is independent of $\tilde{\mathbf{a}}_{u'v',m'}$ for $u \neq u'$, $v \neq v'$ or $m \neq m'$, $\mathbf{R}_d$ can be expressed as

$$\begin{aligned}\mathbf{R}_d = \mathrm{diag}\Big\{ & E\left[\mathbf{a}_{u1,0}\mathbf{a}_{u1,0}^H\right], E\left[\mathbf{a}_{u1,1}\mathbf{a}_{u1,1}^H\right],\ldots,E\left[\mathbf{a}_{u1,M-1}\mathbf{a}_{u1,M-1}^H\right], \\ & E\left[\mathbf{a}_{u2,0}\mathbf{a}_{u2,0}^H\right], E\left[\mathbf{a}_{u2,1}\mathbf{a}_{u2,1}^H\right],\ldots,E\left[\mathbf{a}_{u2,M-1}\mathbf{a}_{u2,M-1}^H\right], \\ & \cdots\cdots\cdots\cdots \\ & E\left[\mathbf{a}_{uV,0}\mathbf{a}_{uV,0}^H\right], E\left[\mathbf{a}_{uV,1}\mathbf{a}_{uV,1}^H\right],\ldots,E\left[\mathbf{a}_{uV,M-1}\mathbf{a}_{uV,M-1}^H\right]\Big\},\end{aligned} \tag{2.40}$$

where diag $\{\ldots\}$ represents a diagonal matrix. When the ST-CIR is independent of the index of $l$, we have

$$E\left[\mathbf{a}_{uv,m}\mathbf{a}_{uv,m}^H\right] = (\alpha_{uv,m})^2 E\left[\mathbf{d}_m\mathbf{d}_m^H\right], \tag{2.41}$$

where $\mathbf{d}_m$ is an $L$-length vector related the DOA of the desired user's signal and to the received

signal's angular spread. Hence $\mathbf{d}_m$ can be expressed as

$$\mathbf{d}_m = \left[1, \exp\left(j2\pi\frac{d}{\lambda}\sin(\psi_m + \kappa_m B)\right), \ldots, \exp\left(j2\pi\frac{d}{\lambda}(L-1)\sin(\psi_m + \kappa_m B)\right)\right]^T. \tag{2.42}$$

In (2.38) $\mathbf{R}_{uu}$ represents the covariance matrix of the interference-plus-noise, which is given by

$$\begin{aligned}\mathbf{R}_{uu} &= E\left[(\mathbf{n}_u + \mathbf{j}_u)(\mathbf{n}_u + \mathbf{j}_u)^H\right] \\ &= \mathbf{R}_n + \mathbf{R}_j,\end{aligned} \tag{2.43}$$

where we have

$$\begin{aligned}\mathbf{R}_n &= E\left[\mathbf{n}_u \mathbf{n}_u^H\right] \\ &= \frac{VN_0}{E_b}\mathbf{I},\end{aligned} \tag{2.44}$$

while $\mathbf{R}_j$ represents the covariance matrix of the composite interference given by the sum of the self-interference and multiuser interference. Let us now derive this matrix.

### 2.2.5 Properties of $\mathbf{R}_j$

In order to derive $\mathbf{R}_j$, the following assumptions are stipulated for convenience. Firstly, as we have shown in the context of Equations (2.25) to (2.27), the self-interference is zero corresponding to $\mathbf{i}_{u'v'}^{(s)} = \mathbf{0}$, when the difference between the frequency, $f_{u'v'}$, of the interfering subcarrier signal and the frequency, $f_{uv}$, of the desired subcarrier obeys $f_{u'v'} - f_{uv} = n/T_s$, where $n$ is an integer. This condition can be readily satisfied during the system design stage. Therefore, our first assumption is that there is no self-interference, i.e. we have $\mathbf{i}_{u'v'}^{(s)} = \mathbf{0}$. Secondly, we assume that random DS spreading sequences are employed by each of the $K$ users. Under this assumption, it has been shown in [135] that the covariance matrix of the composite interference given by the sum of the self-interference and multiuser interference is proportional to an identity matrix, provided that the spreading factor and the number of users supported are sufficiently high. This assumption implies that the interference is 'angularly' white. Based on the above assumptions, it can be shown, by referring to (2.22) as well as (2.32) - (2.35) that we have

$$\mathbf{R}_j = E[\mathbf{j}_u \mathbf{j}_u^H] = \sigma_i^2 \mathbf{I}, \tag{2.45}$$

where $\sigma_i^2$ represents the variance of the interference in the context of a single element of the antenna array of Figure 2.5. Based on (2.22) as well as Equations (2.27), (2.29) and (2.31), for given values

$u$, $v$ and for the $l$th element of the $m$th array, the corresponding interference can be expressed as

$$i_{uv,ml} = \sum_{k=2}^{K} {i_{uv,ml}}^{(k)} + \sum_{k=2}^{K} \underbrace{\sum_{u'=1}^{U} \sum_{v'=1}^{V}}_{v' \neq v, \text{ if } u'=u} {i_{u'v',ml}}^{(k)}, \tag{2.46}$$

where ${i_{uv,ml}}^{(k)}$ can be derived from (2.29) in the following form

$$i_{uv,ml}^{(k)} = \frac{\alpha_{uv,ml}^{(k)} \exp\left(j\vartheta_{uv}^{(k)}\right)}{T_s} \int_0^{T_s} b_{ku}(t-\tau_k) c_k(t-\tau_k) c(t) dt, \tag{2.47}$$

where, for convenience, $\vartheta_{uv}^{(k)}$ has absorbed all the different types of phases. Upon using the Gaussian approximation [41], $i_{uv,ml}^{(k)}$ can be modelled by a Gaussian random variable having zero mean and a variance given by

$$\text{Var}\left[i_{uv,ml}^{(k)}\right] = \frac{2\Omega}{3N_e}, \tag{2.48}$$

where we have $\Omega = E\left[\left(\alpha_{uv,ml}^{(k)}\right)^2\right]$.

Similarly, ${i_{u'v',ml}}^{(k)}$ in (2.46) can be derived from (2.31), which can be expressed as

$$\begin{aligned} i_{u'v'}^{(k)} = \frac{\alpha_{u'v',ml}^{(k)} \exp(\vartheta_{u'v'}^{(k)})}{T_s} \int_0^{T_s} & b_{ku'}(t-\tau_k) c_k(t-\tau_k) c(t) \\ & \times \exp\left(j2\pi[f_{u'v'} - f_{uv}]t\right) dt. \end{aligned} \tag{2.49}$$

The variance of $i_{u'v'}^{(k)}$ can be obtained by following the approach in [41]. It can be shown that, when the frequency spacing between two adjacent subcarriers is $\lambda/T_s$, the averaged variance of $i_{u'v'}^{(k)}$ can be expressed as

$$\begin{aligned} \bar{i}_{u'v'}^{(k)} &= 2\Omega \times \bar{i}_M \\ &= 2\Omega \times \frac{1}{UV(UV-1)} \sum_{v=1}^{UV} \sum_{\substack{u=1 \\ u \neq v}}^{UV} \frac{N_e}{2\pi^2(u-v)^2\lambda^2} \left[1 - \text{sinc}\left(\frac{2\pi(u-v)\lambda}{N_e}\right)\right]. \end{aligned} \tag{2.50}$$

Finally, the variance of $\sigma_i^2$ can be derived based on (2.46), (2.48) and (2.50), which can be expressed as

$$\sigma_i^2 = 2\Omega \times \left[\frac{(K-1)}{3N_e} + K(UV-1)\bar{i}_M\right]. \tag{2.51}$$

Upon substituting (2.44) and (2.45) into (2.43), it can be shown that the interference-plus-noise

covariance matrix $\mathbf{R}_{uu}$ can be written as

$$\begin{aligned}\mathbf{R}_{uu} &= \frac{VN_0}{E_b}\mathbf{I} + \sigma_i^2\mathbf{I}, \qquad (2.52)\\ &= \frac{VN_0}{E_b}\mathbf{I} + 2\Omega \times \left[\frac{(K-1)}{3N_e} + K(UV-1)\bar{i}_M\right]\mathbf{I}\\ &= 2\Omega \times \left[\left(\frac{2\Omega E_b}{VN_0}\right)^{-1} + \frac{(K-1)}{3N_e} + K(UV-1)\bar{i}_M\right] \times \mathbf{I}\\ &= 2\Omega \times \frac{1}{\gamma_c} \times \mathbf{I}. \qquad (2.53)\end{aligned}$$

Note that in (2.53) the term

$$\gamma_c = \left[\left(\frac{2\Omega E_b}{VN_0}\right)^{-1} + \frac{(K-1)}{3N_e} + K(UV-1)\bar{i}_M\right]^{-1} \qquad (2.54)$$

represents the average output Signal-to-Interference-plus-Noise Ratio ratio (SINR) in the context of a single element of the antenna array of Figure 2.5.

Having characterized the statistical properties of the antenna array's outputs $\mathbf{z}_u$, in the following section we derive the optimum antenna array weight vector, in order to generate the decision variable for the information bit $b_u[0]$.

## 2.3 Optimum Combining Schemes

For the sake of maintaining a low detection complexity, in this section a range of linear combining based antenna array weight optimization schemes are invoked for deriving the decision variables. In the context of linear combining schemes, the decision variable related to the information bit $b_u[0]$ can be expressed as [44]

$$z_u = \mathrm{Re}\left\{\mathbf{w}^H\mathbf{z}_u\right\}, \qquad (2.55)$$

where $\mathrm{Re}\{x\}$ represents the real part of $x$, while $\mathbf{w}$ is the array weight vector to be determined below. Specifically, four types of optimum combining schemes are considered for deriving the array weight vector $\mathbf{w}$. More explicitly, these optimum combining schemes are based on the Minimum Variance Distortionless Response (MVDR) [44], the Maximum Signal-to-Interference-plus-Noise Ratio (SINR) [44], the Minimum Mean-Square Error (MMSE) [44] and the Minimum Power Distortionless Response (MPDR) principles [44].

Having obtained the decision variable $z_u$, $u = 1, 2, \ldots, U$ in (2.55), the corresponding information bit $b_u[0]$ is classified according to

$$b_u[0] = \mathrm{sgn}(z_u),\ u = 1, 2, \ldots, U, \qquad (2.56)$$

where $\mathrm{sgn}(x)$ is a sign function, which is defined as

$$\mathrm{sgn}(x) = \begin{cases} +1 & \text{if } x > 0, \\ -1 & \text{if } x \leq 0. \end{cases} \tag{2.57}$$

### 2.3.1 Weight Vector Optimization

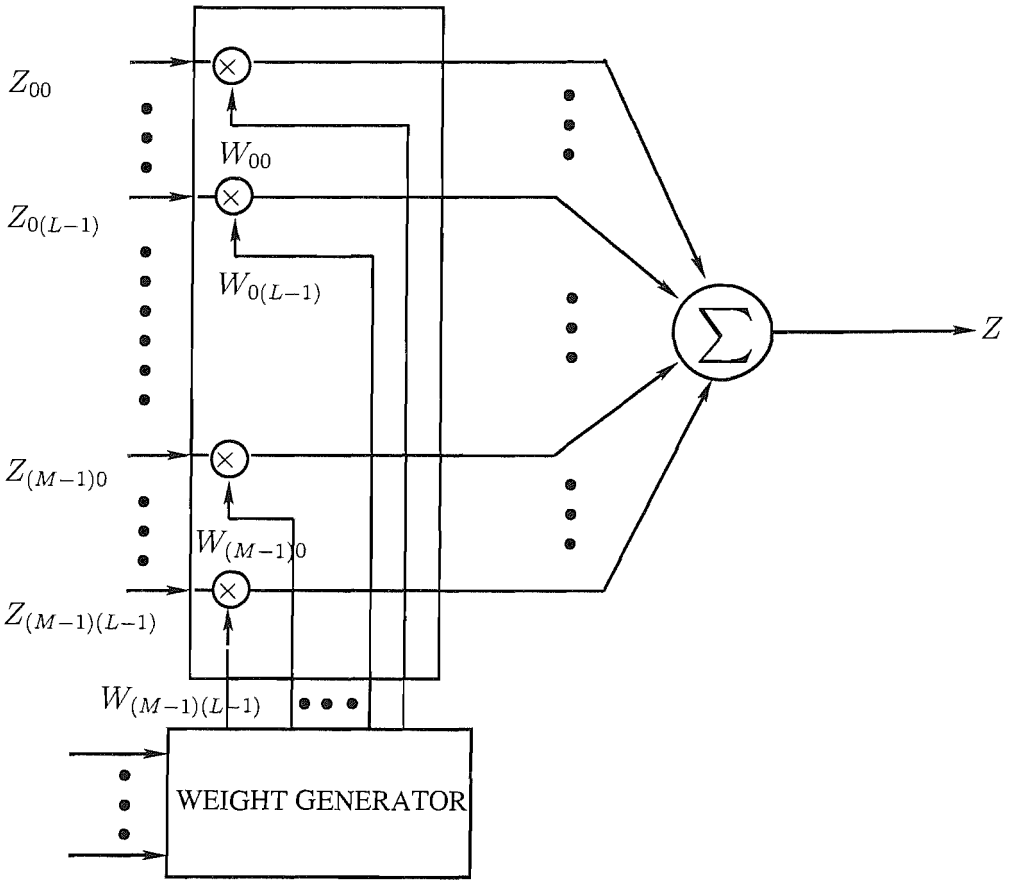


**Figure 2.6:** In the context of the optimum combining, the signals received by the antennas are appropriately weighted and combined in order to combat the effect of the multipath fading on the desired signal and for the sake of mitigating the effects of the interfering signals, where the optimum weight vector is derived from the channel information perfectly estimated.

In this section we first outline the basic philosophy of optimum combiners classically used in digital mobile radio systems dispensing with DS-spreading and study the achievable BER performance of these optimum combiners, when both the desired and interfering signals are subject to non-dispersive Rayleigh fading. Then, the family of optimum combiners designed for DS-CDMA systems are reviewed and their BER performance is characterized, when communicating over non-dispersive Rayleigh fading environments. Finally, we focus our attention on the derivation of the

optimum array weight vector employed by the proposed MC DS-CDMA system using the multiple antenna arrays shown in Figure 2.4.

In the context of the optimum combining [44], the signals received by the antennas are appropriately weighted and combined in order to combat the effect of the multipath fading on the desired signal and for the sake of mitigating the effects of the interfering signals as seen in the Figure 2.6, where the optimum weight vector is derived from the channel information which is assumed to be perfectly estimated in this chapter. In most systems the same interfering signals may contaminate each of the receiving antennas. However, Maximal Ratio Combining (MRC) [44] of the spatial-domain signals is only effective in terms of combating the multipath fading of the desired signal. Hence, it is expected that the family of optimum combining schemes is capable of achieving a better BER performance, than the MRC scheme, when the interfering signals imposed on the individual receive antenna elements are not independent.

#### 2.3.1.1 Optimum Combining Schemes for Digital Mobile Radio Systems using no DS-spreading

In [191], an optimum combining scheme based on the Maximum Signal to Interference-plus-Noise Ratio (MSINR) criterion has been proposed for employment in digital mobile radio systems using no DS-spreading, where the terminology MSINR explicitly indicates that the combiner maximized the SINR. The corresponding received signal vector $\mathbf{r}$ can be expressed as [191]

$$\begin{aligned}\mathbf{r}(t) &= \mathbf{r}_1(t) + \mathbf{n}(t) + \sum_{k=2}^{K} \mathbf{r}_k(t) \\ &= \sqrt{P_1}\mathbf{a}_1 s_1 + \mathbf{n}(t) + \sum_{k=2}^{K} \sqrt{P_k}\mathbf{a}_k s_k(t), \end{aligned} \tag{2.58}$$

and the variables $\mathbf{r}_1$, $\mathbf{n}(t)$, $\mathbf{r}_k$ denote the received desired signal, noise, and $k$th interfering signal vectors, respectively, where $(K-1)$ is the number of interferers. Correspondingly, the signals $s_1$ and $s_k(t)$ denote the desired and $k$th interfering signals having an equal transmitted power of $E[s_1^2(t)] = 1$ and $E[s_k^2(t)] = 1$ for $2 \leq k \leq K$. The variables $P_1$ and $P_k$ denote the the desired and $k$th interfering signals' transmitted power, while $\tilde{\mathbf{a}}_1$ and $\tilde{\mathbf{a}}_k$ are the desired and $k$th interfering signal complex-valued non-dispersive CIR respectively. The correlation matrix of the received composite signal constituted

by the interference-plus-noise is given by [191]

$$\begin{aligned}\mathbf{R}_{uu} &= E\left[\left(\mathbf{n}(t)+\sum_{k=2}^{K}\mathbf{r}_k(t)\right)^*\left(\mathbf{n}(t)+\sum_{k=2}^{K}\mathbf{r}_k(t)\right)^T\right] \\ &= E\left[\mathbf{n}^*(t)\mathbf{n}^T(t)\right]+E\left[\left(\sum_{k=2}^{K}\mathbf{r}_k(t)\right)^*\left(\sum_{k=2}^{K}\mathbf{r}_k(t)\right)^T\right]+2E\left[\mathbf{n}^*(t)\left(\sum_{k=2}^{K}\mathbf{r}_k(t)\right)^T\right] \\ &= \sigma^2\mathbf{I}+\sum_{k=2}^{K}P_kE\left[\mathbf{a}_k^*\mathbf{a}_k^T\right]+2E\left[\mathbf{n}^*(t)\left(\sum_{k=2}^{K}\mathbf{r}_k(t)\right)^T\right], \qquad (2.59)\end{aligned}$$

where $E\left[\left(\sum_{k=2}^{K}\mathbf{r}_k(t)\right)^*\left(\sum_{k=2}^{K}\mathbf{r}_k(t)\right)^T\right]=\sum_{k=2}^{K}P_kE\left[\mathbf{a}_k^*\mathbf{a}_k^T\right]$, and $E\left[\mathbf{n}^*(t)\mathbf{n}^T(t)\right]=\sigma^2\mathbf{I}$, $\sigma^2$ is the noise power and $\mathbf{I}$ is the identity matrix of rank $ML$, with $ML$ being the total number of the antenna elements, as seen in Figure 2.5. The superscripts * and $T$ denote conjugate and transpose, respectively. Assuming that the noise and the interfering signals are uncorrelated, this means $E\left[\mathbf{n}^*(t)\left(\sum_{k=2}^{K}\mathbf{r}_k(t)\right)^T\right]=\mathbf{0}$. Then, it can be shown that we have [191]

$$\mathbf{R}_{uu}=\sigma^2\mathbf{I}+\sum_{k=2}^{K}P_kE\left[\mathbf{a}_k^*\mathbf{a}_k^T\right], \qquad (2.60)$$

Finally, the array weights that maximize the output SINR have been derived in [191], which can be expressed as

$$\mathbf{w}_{MSINR}=\alpha\mathbf{R}_{uu}^{-1}\mathbf{a}_1, \qquad (2.61)$$

where $\alpha$ is a constant, and the superscript -1 denotes the inverse of the matrix. In practice the correlation matrix $\mathbf{R}_{uu}$ of the interference-plus-noise has to be determined for a limited-duration signal segment, for example during instances, where no desired signal is received, i.e. during unallocated time slots. The dimension of $\mathbf{R}_{uu}$ is determined by the number of array weights required and in general the complexity of the associated matrix inversion is cubically proportional to the size of $\mathbf{R}_{uu}$. However, it is possible to invoke the computationally efficient Recursive Least Squares (RLS) algorithm for updating $\mathbf{R}_{uu}$, when new received samples become available [7]. It was shown in [191] that since the optimum combining scheme is capable of efficiently suppressing the interfering signals, the optimum combiner is expected to obtain a better performance, than the MRC scheme. It was also shown in [191] that for a fixed average received SINR the achievable BER performance improves, as the interference power becomes a larger proportion of the total noise-plus-interference power, and this enhanced performance may be further improved as the number of the antennas is increased.

### 2.3.1.2 Optimum Combining Schemes for DS-CDMA Systems

In DS-CDMA wireless systems, each user supported within a cell spreads the information signal using a DS spreading sequence. Hence, the users supported within a cell interfere with each other, unless perfect channel conditions prevail, potentially resulting in intracell interference. Furthermore, multiuser interference is also imposed by the users roaming in the adjacent cells, resulting in inter-cell interference. The optimum combiner described by Equations (2.58)-(2.61) for multiple antenna aided systems using no DS-spreading was found unsuitable for DS-CDMA systems for the following reasons [125]. First, after despreading, the correlation matrix of the interference-plus-noise becomes different from the correlation matrix given in (2.60). In [125], a new approach referred to as code-filtering has been proposed, which may be interpreted as a beamforming technique, where the base station's adaptive processor exploits the temporal/spatial structure and properties of the received signal for determining the weights of the beamformer. The signal is contaminated by both interference and noise. Then the beamformer attempts to restore the signal's original properties at its output and thus reduces the effects of interference, by exploiting both the temporal and spatial structure of the received signal. Since in the code-filtering approach the input signals will be despread by their spreading sequences, the received signals are convolved with the corresponding spreading sequences, which maybe interpreted as filtering by a circuit having an identical impulse response, hence it is referred to as the code-filtering approach. This approach has been used in adaptive beamforming, which can be modified in order to derive the optimum combiner. Since each of the subcarrier signals in the generalized MC DS-CDMA system considered experiences flat fading, for the sake of simplicity we assume that the DS-CDMA signals considered here also experience flat fading. Consequently, we can formulate the complex baseband received signal vector at an $ML$-element antenna array for the $k$th user as [125]

$$\mathbf{r}_k(t) = \sqrt{P_k} b_k(t - \tau_k) c_k(t - \tau_k) e^{j\phi_k} \mathbf{a}_k \tag{2.62}$$

where $\mathbf{a}_k$ represents the $k$th user's complex-valued non-dispersive CIR vector having a length of $ML$, where $ML$ is the number of the antenna elements, while $P_k$ represents the $k$th user's transmitted power, $c_k(t)$ represents the spreading code employed by the $k$th user, $\phi_k = \omega_c \tau_k$, and $\omega_c$ is the carrier frequency. The composite received signal of the $K$ number of users can be expressed as

$$\mathbf{r}(t) = \sum_{k=1}^{K} \mathbf{r}_k(t) + \mathbf{n}(t), \tag{2.63}$$

where the vector $\mathbf{n}(t)$ is the $ML \times 1$-dimensional AWGN vector having zero mean and a covariance of $\sigma_n^2$, and again, $ML$ is the total number of antenna elements of the array seen in Figure 2.5. Without loss of generality, let us assume that the first user is the desired user to be detected and the first user's time delay $\tau_1$ is perfectly estimated. Then the total received signal can be written as

$$\mathbf{r}(t) = \sqrt{P_1} b_1(t - \tau_1) c_1(t - \tau_1) e^{j\phi_1} \mathbf{a}_1 + \mathbf{i} + \mathbf{n}(t), \tag{2.64}$$

where $\mathbf{i}$ represents the multiple-access interference (MAI) imposed by the undesired users, which can be expressed as

$$\mathbf{i} = \sum_{k=2}^{K} \sqrt{P_k} b_k(t-\tau_k) c_k(t-\tau_k) e^{j\phi_k} \mathbf{a}_k. \tag{2.65}$$

Upon correlating $\mathbf{r}(t)$ of (2.64) with $c_1(t-\tau_1)$, the post-correlation signal vector associated with the $n$th bit can be expressed as

$$\mathbf{z}(n) = \frac{1}{\sqrt{T_b}} \int_{(n-1)T+\tau_1}^{nT+\tau_1} \mathbf{r}(t) c_1^*(t-\tau_1) dt \tag{2.66}$$

$$= \sqrt{T_b P_1} b_1(n) e^{j\phi_1} \mathbf{a}_1 + \mathbf{i}_1 + \mathbf{n}_1, \tag{2.67}$$

where we have

$$\mathbf{n}_1 = \frac{1}{\sqrt{T_b}} \int_{(n-1)T+\tau_1}^{nT+\tau_1} \mathbf{n}(t) c_1^*(t-\tau_1) dt, \tag{2.68}$$

which is due to the Gaussian noise $\mathbf{n}(t)$, hence $\mathbf{n}_1$ can be modelled as a complex Gaussian random variable vector having a zero mean and a covariance matrix $\sigma_n^2 T_c \mathbf{I}$, where $\mathbf{I}$ is an identity matrix of rank $ML$. Furthermore, in (2.67)

$$\mathbf{i}_1 = \sum_{k=2}^{K} \sqrt{P_k} i_{1,k} e^{j\phi_k} \mathbf{a}_k \tag{2.69}$$

is contributed by the MAI of (2.65), where we have

$$i_{1,k} = \frac{1}{\sqrt{T_b}} \int_{(n-1)T+\tau_1}^{nT+\tau_1} b_k(t-\tau_k) c_k(t-\tau_k) c_1^*(t-\tau_1) dt, \tag{2.70}$$

which is an i.i.d random variable having zero mean and a covariance of $\frac{\rho_{1,k}^2}{G} T_c$, where $\rho_{1,k}$ is the cross-correlation factor between the 1st user's and the $i$th interfering user's spreading code. Furthermore, $T_b$ is the bit duration, $T_c$ is the chip duration, and $G = T_b/T_c$ represents the spreading gain. We assume that the chip waveform is rectangular. However, our results can be readily extended to the cases using various types of chip waveforms, such as time-domain raised-cosine waveform signals. Assuming that the noise and the interfering signals are uncorrelated, with the aid of (2.67), (2.68) and (2.69), the correlation matrix of the post-correlation interference-plus-noise can be readily derived [125],

$$\mathbf{R}_{uu} = \frac{1}{T_c} E\left[ (\mathbf{n}_1 + \mathbf{i}_1)^* (\mathbf{n}_1 + \mathbf{i}_1)^T \right] = \sigma_n^2 \mathbf{I} + \sum_{k=2}^{K} \frac{\rho_{1,k}^2}{G} P_k \mathbf{a}_k^* \mathbf{a}_k^T. \tag{2.71}$$

Finally, similar to the optimum combiner based on the MSINR criterion invoked in the context of wireless systems using no DS-spreading, the weights that maximize the output SINR in DS-CDMA

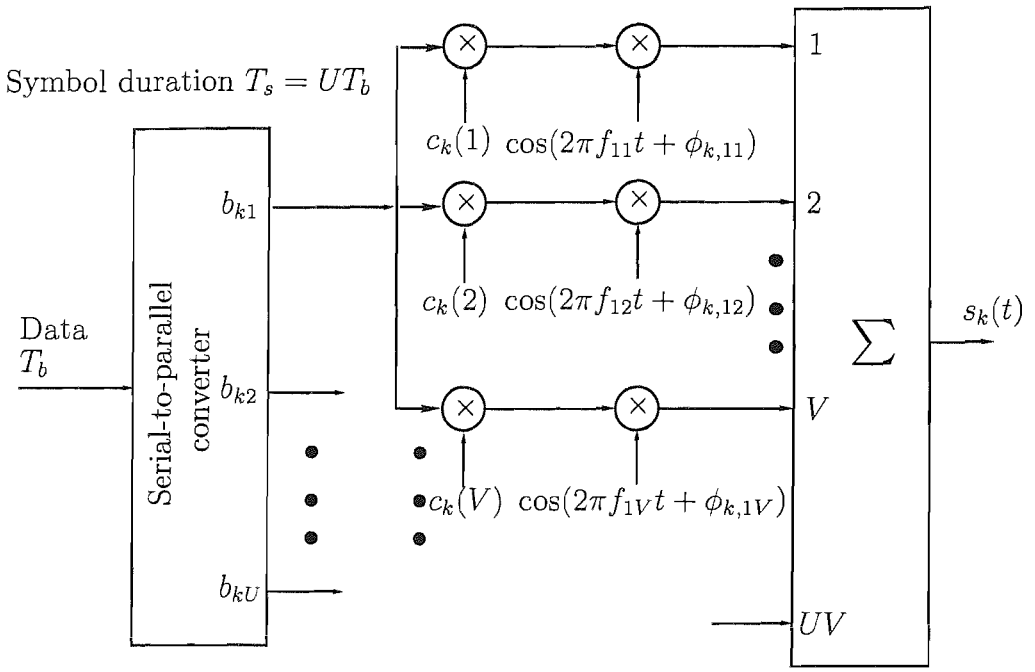


**Figure 2.7:** The $k$th user's transmitter schematic for the multicarrier CDMA system.

systems can be expressed as [125],

$$\mathbf{w}_{MSINR} = \alpha \mathbf{R}_{uu}^{-1} \mathbf{a}_1. \tag{2.72}$$

Similarly to the optimum weight vector $\mathbf{w}_{MSINR}$ of (2.61) devised for digital mobile radio systems using no DS-spreading, the optimum weight vector $\mathbf{w}_{MSINR}$ of (2.72) devised for DS-CDMA systems is determined by the inversion of the correlation matrix $\mathbf{R}_{uu}^{-1}$ of the interference-plus-noise signal and by the desired user's complex-valued non-dispersive CIR vector $\mathbf{a}_1$. However, the correlation matrix $\mathbf{R}_{uu}$ in (2.72) is derived from the post-correlation interference-plus-noise signal, while the correlation matrix $\mathbf{R}_{uu}$ in (2.61) is directly obtained from the interference-plus-noise signal.

### 2.3.1.3 Optimum Combining Schemes for MC-CDMA Systems

In this section, first the MC-CDMA system of [39] is discussed briefly. The transmitter schematic of the $k$th user is shown in Figure 2.7 for the MC-CDMA system considered. At the transmitter side, the binary data stream having a bit duration of $T_b$ is serial-to-parallel (S/P) converted to $U$ parallel sub-streams. The bit duration of each sub-stream, which we refer to as the symbol duration, remains $T_s = UT_b$. After S/P conversion, the data of the $u$th sub-stream, where we have $u = 1, 2, \ldots, U$, modulates a group of subcarrier frequencies $\{f_{u1}, f_{u2}, \ldots, f_{uV}\}$ using Binary Phase Shift Keying (BPSK). Since each of the $U$ data bits is conveyed with the aid of $V$ subcarriers, a total of $UV$ number of subcarriers are required in the MC-CDMA system considered. Finally, the $UV$ number of subcarrier signals are added, in order to form the complex modulated signal as seen in Figure 2.7.

Therefore, the transmitted signal of user $k$ can be expressed as

$$s_k(t) = \sum_{u=1}^{U}\sum_{v=1}^{V}\sqrt{\frac{P_k}{V}}b_{ku}(t)c_k(v)\cos(2\pi f_{uv}t + \phi_{k,uv}), \tag{2.73}$$

where $P$ represents the transmitted power per bit, while $\{b_{ku}(t)\}$, $c_k(v)$, $\{f_{uv}\}$ and $\{\phi_{k,uv}\}$ represent the data stream, the frequency-domain spreading code of the $k$th user, the subcarrier frequency set and the phase angles introduced in the carrier modulation process. The data stream's waveform $b_{ku}(t) = \sum_{i=-\infty}^{\infty} b_{ku}[i]P_{T_s}(t - iT_s)$ consists of a sequence of mutually independent rectangular pulses of duration $T_s$ and of amplitude +1 or -1 with equal probability, while $P_{T_s}(t)$ is the rectangular chip waveform, which is defined over the interval $[0, T_s)$.

Let us assume that the first user corresponding to $k = 1$ is the user-of-interest, which is referred to as the reference user. The receiver block diagram designed for detecting the information arriving from the reference user is shown in Figure 2.8, where the superscripts and subscripts denoting the reference user associated with $k = 1$ has been omitted for notational convenience. As shown in Figure 2.8, the MC-CDMA detector also consists of two main parts, the first part carries out multicarrier demodulation in the context of each array element and each of the $M$ antennas. Each antenna array element provides $V$ number of outputs, which correspond to the $V$ number of subcarriers conveying the signals representing the same data bit. Therefore, associated with each transmitted data bit, such as bit $u$, we have a total of $VML$ output variables, as shown in Figure 2.8, which carry the information of the same transmitted data bit. Hence, the second task, namely, the task of the second section of the receiver of Figure 2.8 is to combine these $VML$ number of variables according to an efficient combining algorithm, which will be discussed in detail during our forthcoming discourse in this section.

In Section 2.3.1.2 the optimum MSINR linear combiner designed for DS-CDMA systems was described. In the context of MC-CDMA systems, we can use a similar approach to that employed in systems dispensing with DS-spreading for deriving the post-demodulation interference-plus-noise correlation matrix, in order to determine the array weight vector $\mathbf{w}_{MSINR}$. For simplicity, let us assume $U = 1$, then, in MC-CDMA systems using antenna arrays which we depicted in Figure 2.8, the received signals at the output of the antenna array can be expressed as

$$\begin{aligned}\mathbf{r}(t) &= \sum_{k=1}^{K}\mathbf{r}_k(t) + \mathbf{n}(t) \\ &= \sum_{k=1}^{K}\sum_{v=1}^{V}\sqrt{\frac{P_k}{V}}b_k(t-\tau_k)c_k(v)\mathbf{a}_v^{(k)}\exp\left(j\left[2\pi f_v t + \theta_v^{(k)}\right]\right) + \mathbf{n}(t)\end{aligned} \tag{2.74}$$

where, for simplicity, we assumed encountering flat fading by each subcarrier signal. Here, the channel model $\mathbf{h}_{v,m}^{(k)}(t)$ employed is described by (2.14) in Section 2.2.3, correspondingly, the response of the $k$th user's transmitted signal to the spatial-temporal channels $\mathbf{r}_k(t) = s_k(t) \otimes \tilde{\mathbf{h}}_v^{(k)}(t) = \sum_{v=1}^{V}\sqrt{\frac{P_k}{V}}\, b_k(t-\tau_k)c_k(v)\tilde{\mathbf{a}}_v^{(k)}(t)\exp\left(j\left[2\pi f_v t + \theta_v^{(k)}\right]\right)$. In (2.74), $\mathbf{r}(t)$ is the composite mul-

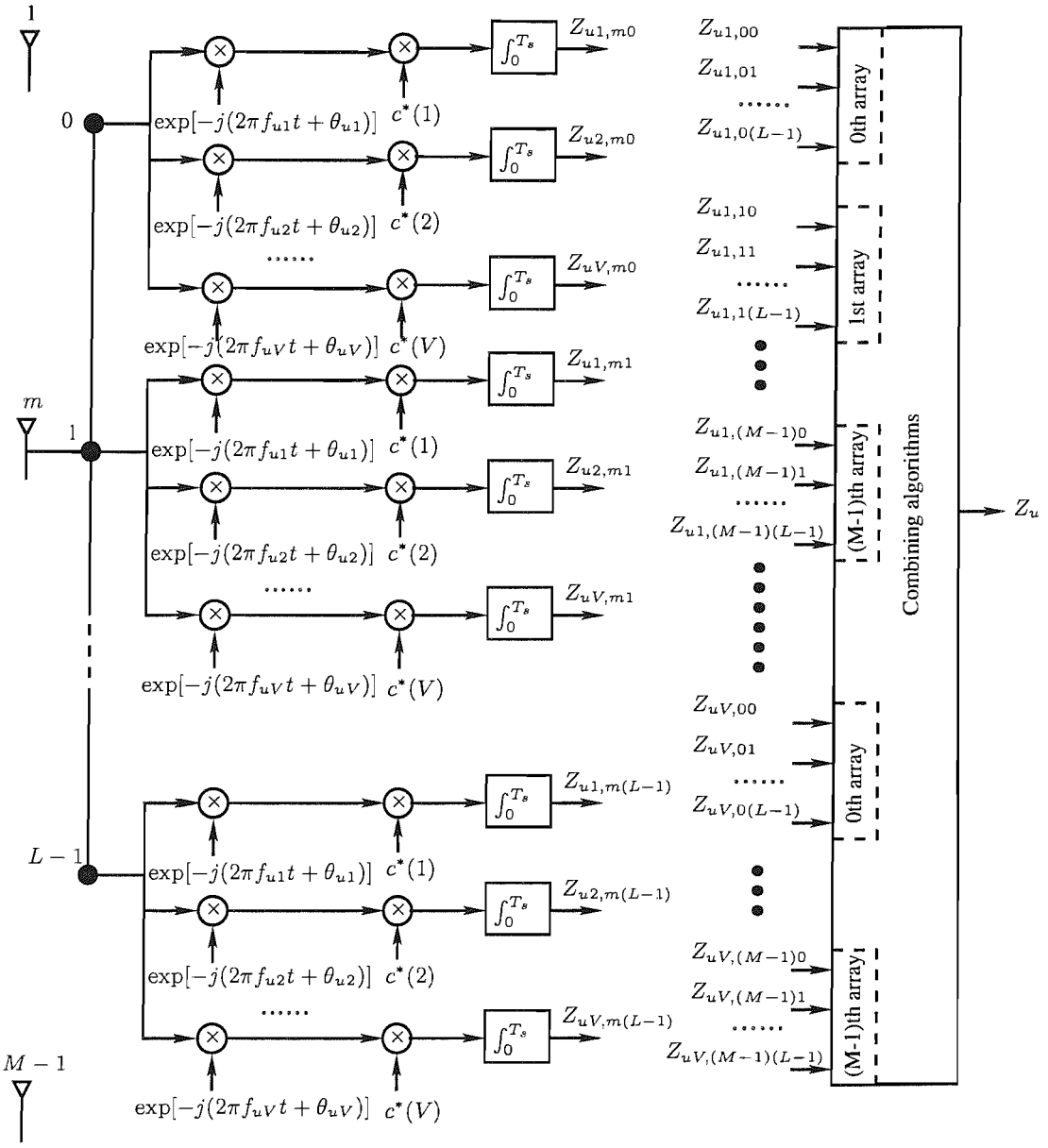


**Figure 2.8:** Receiver block diagram of the MC-CDMA system considered. The receiver employs beamforming, receiver diversity combining and multicarrier-spreading-assisted frequency-selective diversity combining.

tiuser signal at the output of array described by a $ML \times 1$-dimensional vector, $K$ is the number of users, $c_k$ is the frequency-domain spreading code of the $k$th user, $b_k(t - \tau_k)$ is the data bit of the $k$th user, while $P_k$ is the $k$th user's transmitted power, $f_v$ is the frequency of the $v$th subcarrier, and finally, $\tau_k$ is the $k$th user's transmission delay. Furthermore, in (2.74), $\mathbf{a}_v^{(k)}$ is the $ML \times 1$-dimensional channel impulse response vector corresponding to the $v$th subcarrier of the $k$th user, where the CIR taps are typically modelled by an i.i.d Rayleigh distributed random variable, while the phase by an

i.i.d uniform random variable spread across the interval of $[0, 2\pi]$. Recall from Figure 2.8 that $ML$ is the total number of antenna elements, without loss of generality, we assume that the receiver is synchronized with the desired user 1.

Similarly to (2.18) in the generalized MC DS-CDMA system, let

$$\mathbf{z}_u = \left[\mathbf{z}_{u1}^T, \mathbf{z}_{u2}^T, \ldots, \mathbf{z}_{uV}^T\right]^T, \tag{2.75}$$

be a $VML$-length vector containing the entire set of $VML$ number of decision variables in the context of the $u$th data bit after multicarrier demodulation. These $VML$ number of variables are denoted in Figure 2.8 as $\{z_{uv,ml}\}$ for $v = 1, 2, \ldots, V$; $m = 0, 1, \ldots, (M-1)$; $l = 0, 1, \ldots, (L-1)$, where

$$\mathbf{z}_{uv} = \left[\mathbf{z}_{uv,0}^T, \mathbf{z}_{uv,1}^T, \ldots, \mathbf{z}_{uv,(M-1)}^T\right]^T, \; v = 1, 2, \ldots, V \tag{2.76}$$

is an $ML$-length vector containing the $ML$ number of variables in the context of the $v$th subcarrier, where $v = 1, 2, \ldots, V$. In other words, the vector $\mathbf{z}_{uv}$ contains the $ML$ number of antenna arrays' outputs in response to the $v$th subcarrier signal. Finally, in (2.76)

$$\begin{aligned} \mathbf{z}_{uv,m} &= \left[z_{uv,m0}, z_{uv,m1}, \ldots, z_{uv,m(L-1)}\right]^T, \\ & v = 1, 2, \ldots, V; \; m = 0, 1, \ldots, M-1 \end{aligned} \tag{2.77}$$

represents an $L$-length vector, which includes the $m$th antenna's response to the $v$th subcarrier signal after multicarrier demodulation. Again, for simplicity, let us assume $U = 1$, then, after the multicarrier demodulation in the context of each array element and each of the $M$ antennas as shown in Figure 2.8, the $ML \times 1$-dimensional post-demodulation vector of decision variables corresponding to the $v$th subcarrier can be expressed as

$$\begin{aligned} \mathbf{z}_v(n) &= \frac{1}{T_s}\int_{lT_s}^{(l+1)T_s} \mathbf{r}(t)c_1^*(v)\exp\left(-j\left[2\pi f_v t + \theta_v^{(1)}\right]\right)dt \\ &= \sqrt{\frac{P_1}{V}}b_1(n)\mathbf{a}_v^{(1)} + \mathbf{i}_v + \mathbf{n}_v \\ &= \sqrt{\frac{P_1}{V}}b_1(n)\mathbf{a}_v^{(1)} + \sum_{k=2}^{K}\sqrt{\frac{P_k}{V}}b_k(n)\mathbf{a}_v^{(k)}c_k(v)c_1^*(v)\exp\left(j\left[\theta_v^{(k)} - \theta_v^{(1)}\right]\right) + \mathbf{n}_v \end{aligned} \tag{2.78}$$

where, we have $\mathbf{i}_v = \sum_{k=2}^{K}\sqrt{\frac{P_k}{V}}b_k(n)\mathbf{a}_v^{(k)}c_k(v)c_1^*(v)\exp\left(j\left[\theta_v^{(k)} - \theta_v^{(1)}\right]\right)$ and $1/T_s$ is used to normalize the signals. Furthermore, $\mathbf{n}_v$ is contributed by the AWGN noise, which can be expressed as

$$\mathbf{n}_v = \frac{1}{T_s}\int_{lT_s}^{(l+1)T_s} \mathbf{n}(t)c_1^*(v)\exp\left(-j\left[2\pi f_v t + \theta_v^{(1)}\right]\right)dt \tag{2.79}$$

Here, $E\left[\mathbf{n}_v^*\mathbf{n}_v^T\right] = E\left[\mathbf{n}^*(t)\mathbf{n}^T(t)\right] = \sigma_n^2\mathbf{I}$, $\sigma_n^2$ is the noise power and $\mathbf{I}$ is the identity matrix of rank $ML$. We assume that the received signals are uncorrelated and wide-sense stationary. First,

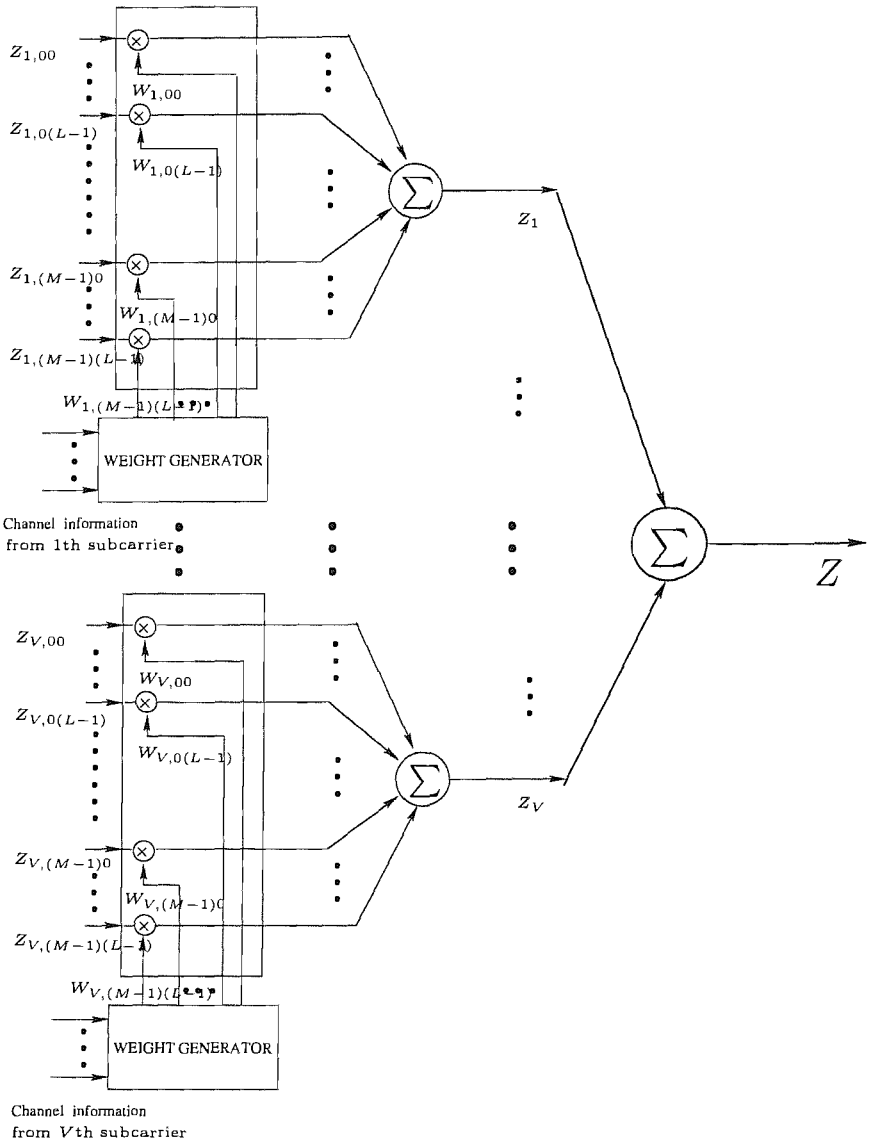


**Figure 2.9:** In the context of the individual subcarrier-based optimum combining scheme, the signals received by the antennas are separately weighted and combined, where the optimum weight vector for the $v$th subcarrier is correspondingly derived from the channel information of the $v$ subcarrier.

the received signals associated with the $V$ number of subcarriers on the schematic of Figure 2.8 can be processed separately as in Figure 2.9, since they are uncorrelated with each other. Following the subcarrier-based processing, the $V$ number of subcarrier signals representing bit $n$ are then combined based on the MRC principle. To elaborate a little further, in the context of the separate subcarrier-based processing scheme of Figure 2.9, the interference-plus-noise correlation matrix corresponding to the $v$th subcarrier is similar to that of the scheme using no DS-spreading, exactly because each

subcarrier is treated separately, which can be expressed as

$$\begin{aligned}\mathbf{R}_{uu,v} &= E\left[(\mathbf{n}_v+\mathbf{i}_v)^*(\mathbf{n}_v+\mathbf{i}_v)^T\right] \\ &= E\left[\mathbf{n}_v^*\mathbf{n}_v^T\right]+E\left[\mathbf{i}_v^*\mathbf{i}_v^T\right]+2E\left[\mathbf{n}^*\mathbf{i}_v^T\right] \\ &= \sigma_n^2\mathbf{I}+\sum_{k=2}^{K}\frac{P_k}{V}(\mathbf{a}_v^{(k)})^*(\mathbf{a}_v^{(k)})^T \end{aligned} \tag{2.80}$$

Where we have $E\left[\mathbf{i}_v^*\mathbf{i}_v^T\right]=\sum_{k=2}^{K}\frac{P_k}{V}(\mathbf{a}_v^{(k)})^*(\mathbf{a}_v^{(k)})^T$ and $E\left[\mathbf{n}^*(t)\mathbf{i}_v^T\right]=\mathbf{0}$ because of the uncorrelation between the interfering signals and noise. Based on (2.80), the optimum weight vector derived according to the MSINR criterion of Equation (2.119) for the $v$th subcarrier can be expressed as

$$\mathbf{w}_{v,MSINR}=\alpha\mathbf{R}_{uu,v}^{-1}\mathbf{a}_v^{(1)}. \tag{2.81}$$

Hence, the optimum combiners' output corresponding to the $v$th subcarrier is given by

$$z_v=\mathbf{w}_{v,MSINR}^*\mathbf{z}_v \tag{2.82}$$

The operations carried out by the combiner can also be seen in Figure 2.9. Finally, the decision variable $z$ can be obtained by combining all the subcarrier signal $z_v$, $v=1,2,\ldots,V$, according to the MRC principle, which can be expressed as

$$z=\sum_{v=1}^{V}z_v \tag{2.83}$$

Above, the optimum combiner designed for the MC-CDMA system of Figure 2.8 was derived by processing the received signal of the $ML\times 1$-dimensional vector if each subcarrier is treated separately. However, the optimum combiner can be derived by jointly processing the $VML$-dimensional received signal vector as seen in Figure 2.10. Then the post-demodulation signals of the $VML$-dimensional vector can be derived from (2.78) in the following form

$$\begin{aligned}\mathbf{z} &= \left[\mathbf{z}_1^T,\mathbf{z}_2^T,\ldots,\mathbf{z}_V^T\right]^T \\ &= \sqrt{\frac{P_1}{V}}b_1\mathbf{a}^{(1)}+\mathbf{i}+\mathbf{n}, \end{aligned} \tag{2.84}$$

where $\mathbf{z}_v$ is an $ML\times 1$-dimensional vector in (2.78), $\mathbf{a}^{(1)}$ is the 1st user's channel impulse response $VML$-dimensional spatio-temporal vector, $\mathbf{i}$ is the $VML$-dimensional interference vector and $\mathbf{n}$ is the $VML$-dimensional noise vector. If we assume that the received signals of the $V$ subcarriers and $ML$ array elements are uncorrelated, similar to the derivation of the individual subcarrier-based optimized post-demodulation interference-plus-noise correlation matrix $\mathbf{R}_{uu,v}$ of rank $ML$, the jointly optimized post-demodulation interference-plus-noise correlation matrix $\mathbf{R}_{uu}$ of rank $VML$ can be

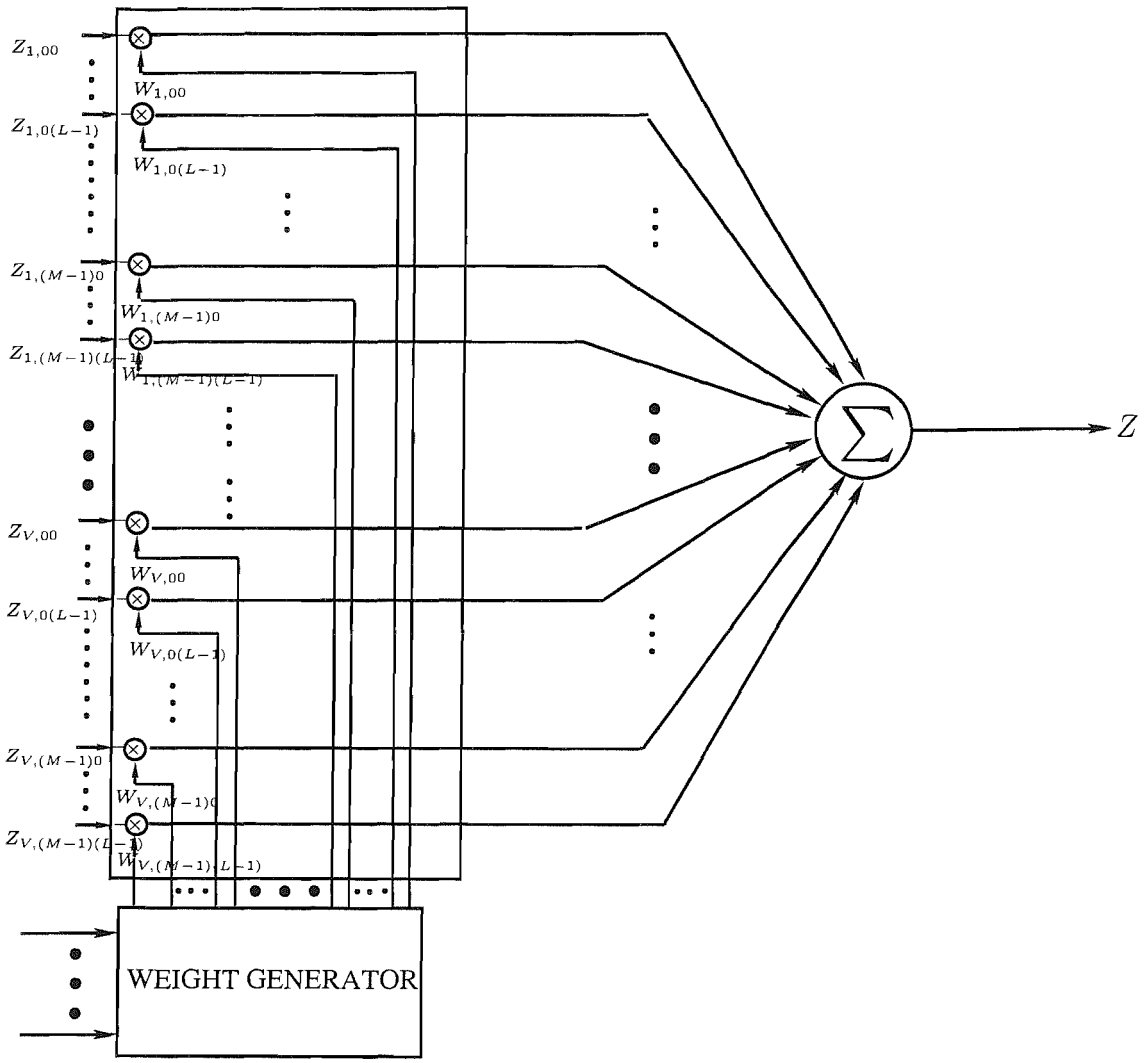


**Figure 2.10:** In the context of the joint processing aided optimum combining scheme, the signals received by the antennas are jointly weighted and combined, where the optimum weight vector is derived from the channel information of all the $V$ number of subcarriers.

derived as

$$\begin{aligned}\mathbf{R}_{uu} &= E\left[(\mathbf{n}+\mathbf{i})^*(\mathbf{n}+\mathbf{i})^T\right] \\ &= E\left[\mathbf{n}^*\mathbf{n}^T\right] + E\left[\mathbf{i}^*\mathbf{i}^T\right] + 2E\left[\mathbf{n}^*\mathbf{i}^T\right] \\ &= \sigma_n^2\mathbf{I} + \sum_{k=2}^{K}\frac{P_k}{V}(\mathbf{a}^{(k)})^*(\mathbf{a}^{(k)})^T \end{aligned} \tag{2.85}$$

where $\sigma_n^2$ is the noise power and $\mathbf{I}$ is the identity matrix of rank $VML$, $P_k$ is the the $k$th user's transmitted power, and $\mathbf{a}^{(k)}$ is the $VML$-dimensional channel impulse response vector corresponding

to the $k$th user, where the CIR taps are typically modelled by an i.i.d Rayleigh distributed random variable, while the phase by an i.i.d uniform random variable spread across the interval of $[0, 2\pi]$. The composite and properties of the matrix $\mathbf{R}_{uu}$ in (2.85) is almost the same as that of the matrix $\mathbf{R}_{uu,v}$ in (2.80) except that the rank of the matrix $\mathbf{R}_{uu,v}$ in (2.80) is $VML$ while the rank of the matrix $\mathbf{R}_{uu}$ in (2.85) is $ML$. Consequently, the $VML$-dimensional jointly optimized weight vector based on the MSINR criterion invoked for the MC-CDMA scheme of Figure 2.8 can be expressed as

$$\mathbf{w}_{MSINR} = \alpha \mathbf{R}_{uu}^{-1} \mathbf{a}^{(1)}. \tag{2.86}$$

It is worth noting that the optimum weight vector of this jointly optimized scenario is similar to the subcarrier-based approach of Equation (2.81), only the interference-plus-noise correlation matrix $\mathbf{R}_{uu}$ is different, obeying Equation (2.85), instead of Equation (2.80).

#### 2.3.1.4 Optimum Combining Schemes for MC DS-CDMA Systems

In the context of the generalized MC DS-CDMA scheme of Figure 2.5, the approach of determining the optimum weight vector similar to those used in DS-CDMA systems and in MC-CDMA systems. In the generalized MC DS-CDMA scheme, the transmitted data stream can be spread in both time-domain and the frequency-domain in order to increase the user-load of the generalized MC DS-CDMA system and achieve a higher frequency diversity [192]. In order to elaborate further on frequency-domain spreading, let us assume that after the time-domain DS-spreading in Figure 2.2, the parallel data bits of the $V$ subcarriers are replaced by the $V$ chip values of $\{+1, -1, \ldots, +1\}$ of a spreading code invoking for spreading the data in the frequency-domain across $V$ number of different subcarriers. The resultant bandwidth is again the same as that of the MC DS-CDMA scheme only employing the time-domain spreading. Then, the transmitted MC DS-CDMA signal benefits from both time-domain spreading and frequency-domain spreading. At the receiver, the MC DS-CDMA is despread using both time-domain spreading code-having a length of $N_e = T_s/T_c$-and the frequency-domain spreading code-associated with a length of $V$ in Figure 2.2. The total processing gain will be the product of the time-domain spreading code's processing gain and the frequency-domain spreading code's processing gain, namely $N_e \cdot V$. Furthermore, the maximum number of users supported by the MC DS-CDMA system is also determined by the above product of $N_e \cdot V$, which is determined by the system bandwidth.

As shown in Figure 2.5, after multicarrier demodulation and DS despreading, the antenna array outputs $\mathbf{z}_{uv}$ corresponding to the $n$th bit $b_u[n]$ and the $v$th subcarrier can be expressed as in (2.21). For simplicity, we assume that the number of bits involved in the S/P converter is $U = 1$. Then, after multicarrier demodulation and time-domain despreading, the resultant signal vector corresponding to

$v$th subcarrier can be expressed as

$$\begin{aligned}
\mathbf{z}_v[n] &= \frac{1}{T_s}\int_{lT_s}^{(l+1)T_s} \mathbf{r}(t)c_1^*(t-\tau_1)s_1^*(v)\exp\left(-j\left[2\pi f_v t+\theta_v^{(1)}\right]\right)dt \\
&= \sqrt{\frac{P_1}{V}}\sqrt{G}b_1[n]\mathbf{a}_v^{(1)}+\mathbf{i}_v+\mathbf{n}_v \\
&= \sqrt{\frac{P_1}{V}}\sqrt{G}b_1[n]\mathbf{a}_v^{(1)} \\
&\quad +\sum_{k=2}^{K}\sqrt{\frac{P_k}{V}}\frac{\rho_{1,k}}{\sqrt{G}}b_k[n]\mathbf{a}_v^{(k)}s_k(v)s_1^*(v)\exp\left(j\left[\theta_v^{(k)}-\theta_v^{(1)}\right]\right)+\mathbf{n}_v \qquad (2.87)
\end{aligned}$$

where $\mathbf{r}(t)$ is described in (2.15), and $\mathbf{i}_v = \sum_{k=2}^{K}\sqrt{\frac{P_k}{V}}\frac{\rho_{1,k}}{\sqrt{G}}b_k[n]\mathbf{a}_v^{(k)}s_k(v)s_1^*(v)\exp\left(j\left[\theta_v^{(k)}-\theta_v^{(1)}\right]\right)$, in which $\frac{\rho_{1,k}}{\sqrt{G}}$ comes from the time-domain despreading. $\mathbf{z}_v$ is a $ML\times 1$-dimensional vector of $v$th subcarrier signal used for detecting the $n$th bit of the user-of interest, $K$ is the number of users, $s_k(v)$ is the frequency-domain spreading code assigned to $v$th subcarrier of the $k$th user, $b_k[n]$ is the $n$th data bit of the $k$th user, and $\rho_{1,k}$ is the cross-correlation factor between the time-domain spreading codes of the 1st user and the $k$th interfering user. Again, $T_b$ is the bit duration, $T_c$ is the chip duration, and $G = T_b/T_c$ is time spread gain. Furthermore, in (2.87), $\mathbf{a}_v^{(k)}$ is the $ML\times 1$-dimensional complex-valued non-dispersive CIR vector corresponding to the $v$th subcarrier of the $k$th user, the fading amplitude is usually modelled by an i.i.d Rayleigh distributed random variable, while the fading-induced phase can be modelled as a random variable uniformly distributed in the interval of $[0, 2\pi]$. Similar to the separate subcarrier-based processing employed in the MC-CDMA systems of Figure 2.8, the received signal associated with the $V$ number of subcarriers of the generalized MC DS-CDMA systems of Figure 2.5 can be processed separately. Then, the $V$ number of subcarrier signals are combined based on the MRC principles. In the context of the separate subcarrier-based processing MC DS-CDMA scheme of Figure 2.5, since in this scheme each subcarrier is first treated separately, hence the interference-plus-noise correlation matrix is similar to that of the DS-CDMA scheme given in Equation (2.71), which can be expressed as

$$\begin{aligned}
\mathbf{R}_{uu,v} &= E\left[(\mathbf{n}_v+\mathbf{i}_v)^*(\mathbf{n}_v+\mathbf{i}_v)^T\right] \\
&= E\left[\mathbf{n}_v^*\mathbf{n}_v^T\right]+E\left[\mathbf{i}_v^*\mathbf{i}_v^T\right]+2E\left[\mathbf{n}^*\mathbf{i}_v^T\right] \\
&= \sigma_n^2\mathbf{I}+\sum_{k=2}^{K}\frac{\rho_{1,k}^2}{G}\frac{P_k}{V}(\mathbf{a}_v^{(k)})^*(\mathbf{a}_v^{(k)})^T. \qquad (2.88)
\end{aligned}$$

where $\sigma_n^2$ is the noise power and $\mathbf{I}$ is the identity matrix of rank $ML$, $P_k$ is the the $k$th user's transmitted power, and $\rho_{1,k}^2/G$ comes from the time-domain despreading, in which $G = T_b/T_c$ is time spread gain while $\rho_{1,k}$ is the cross-correlation factor between the time-domain spreading codes of the 1st user and the $k$th interfering user. $\mathbf{a}_v^{(k)}$ is the $ML$-dimensional channel impulse response vector corresponding to the $v$th subcarrier of the $k$th user, where the CIR taps are typically modelled by an i.i.d Rayleigh distributed random variable, while the phase by an i.i.d uniform random variable

spread across the interval of $[0, 2\pi]$. The composite and properties of the matrix $\mathbf{R}_{uu}$ in (2.88) is similar to that of the matrix $\mathbf{R}_{uu,v}$ in (2.80) except that the effect of the time-domain despreading $\rho_{1,k}^2/G$ is presented in (2.85). Based on (2.88), the optimum weight vector derived according to the MSINR criterion for the $v$th subcarrier of the generalized MC DS-CDMA scheme of Figure 2.5 can be expressed as

$$\mathbf{w}_{v,MSINR} = \alpha \mathbf{R}_{uu,v}^{-1} \mathbf{a}_v^{(1)}. \tag{2.89}$$

Hence, the optimum combiners' output corresponding to the $v$th subcarrier of the generalized MC DS-CDMA scheme of Figure 2.5 is given by

$$z_v = \mathbf{w}_{v,MSINR}^H \mathbf{z}_v. \tag{2.90}$$

Finally, the decision variable $z$ can be obtained by combining the $v$th subcarrier signal $z_v$ of the generalized MC DS-CDMA scheme of Figure 2.5 according to the MRC principle, which can be expressed as

$$z = \sum_{v=1}^{V} z_v, \tag{2.91}$$

Above, the optimum combiner adopted for the generalized MC DS-CDMA system of Figure 2.5 was derived by processing the $V$ number of received subcarrier signals hosted by the $ML \times 1$-dimensional vector separately. However, the optimum combiner can also be derived by jointly processing the received signal of the $VML$-dimensional received signal vectors of the $V$ subcarriers and $ML$ array elements. Then the post-despreading signals of the $VML$-dimensional vector can be derived from (2.87) as follows:

$$\begin{aligned} \mathbf{z} &= \left[\mathbf{z}_1^T, \mathbf{z}_2^T, \ldots, \mathbf{z}_V^T\right]^T \\ &= \sqrt{\frac{P_1}{V}} \sqrt{G} b_1 \mathbf{a}^{(1)} + \mathbf{i} + \mathbf{n} \end{aligned} \tag{2.92}$$

where $\mathbf{z}_v$ is an $ML$-dimensional vector in (2.87), $\mathbf{a}^{(1)}$ is the 1st user's $VML$-dimensional spatio-temporal channel impulse response vector, $\mathbf{i}$ is the $VML$-dimensional interference vector, and $\mathbf{n}$ is the $VML$-dimensional noise vector. If we assume that the received signals of the $V$ subcarriers and $ML$ array elements are uncorrelated, the joint optimum post-despreading interference-plus-noise correlation matrix $\mathbf{R}_{uu}$ of rank $VML$ can be derived as

$$\begin{aligned} \mathbf{R}_{uu} &= E\left[(\mathbf{n}+\mathbf{i})^* (\mathbf{n}+\mathbf{i})^T\right] \\ &= \sigma_n^2 \mathbf{I} + \sum_{k=2}^{K} \frac{\rho_{1,k}^2}{G} \frac{P_i}{V} (\mathbf{a}_v^{(k)})^* (\mathbf{a}_v^{(k)})^T. \end{aligned} \tag{2.93}$$

Consequently, the $VML$-dimensional jointly optimized weight vector based on the MSINR criterion

used for optimizing the MC DS-CDMA system of Figure 2.5 can be expressed as

$$\mathbf{w}_{MSINR} = \alpha \mathbf{R}_{uu}^{-1} \mathbf{a}^{(1)} \tag{2.94}$$

Having discussed the MSINR array weight optimization criterion, in the next section we consider the minimum variance distortionless Response approach.

### 2.3.2 Minimum Variance Distortionless Response Criterion

In this section, the optimum combiner is derived based on Minimum Variance Distortionless Response (MVDR) criterion. The MVDR approach constitutes a well known beamforming optimization criterion [44], which is capable of providing the minimum variance unbiased estimate of the transmitted signal. In other words, with the aid of the MVDR based scheme, the desired signal arriving from a specific direction will pass through the optimum combiner without distortion, while the variance of the interference-plus-noise is minimized. More explicity, this corresponds to minimizing the power of the interference-plus-noise at the array's output, provided that the desired signal is distortionless. In the optimum beamformer using the MVDR criterion, the array output signal $\mathbf{z} = s_1\mathbf{a}_1 + \mathbf{i} + \mathbf{n}$ arriving at the input of the receiver is processed by the beamformer having a weight vector $\mathbf{w}^H$, producing the signal $z = \mathbf{w}^H\mathbf{z}$, which was decontaminated by the beamformer, where the dimensions of both $\mathbf{z}$ and $\mathbf{w}$ are $ML \times 1$, where again, $ML$ is the number of the antenna array elements. The MVDR criterion leads to the following optimization problem [44]:

$$\min\left(E\left[|z_n|^2\right]\right) = \min_{\mathbf{w}}\left(\mathbf{w}^H\mathbf{R}_{uu}\mathbf{w}\right) \tag{2.95}$$

where we have $z_n = \mathbf{w}^H\mathbf{z}(n)$, $E\left[|z_n|^2\right]$ is the mean square value of the interference-plus-noise at the output of the ML-element array and $\mathbf{R}_{uu}$ is the correlation matrix of the interference-plus-noise expressed in the form of $\mathbf{u} = \mathbf{i} + \mathbf{n}$. The condition of no distortion at the output of the MVDR beamformer is given by

$$\mathbf{w}^H\mathbf{a}_1 = 1, \tag{2.96}$$

which physically indicates that the desired signal is detected with a unity gain. With the aid of the Lagrange multiplier $\lambda$ [44], the minimization problem of Equation (2.95) can be solved by imposing the constraint of Equation (2.96). The target function that we minimize is then formulated as [44]

$$j = \mathbf{w}^H\mathbf{R}_{uu}\mathbf{w} + \lambda(\mathbf{w}^H\mathbf{a}_1 - 1) + \lambda^*(\mathbf{a}_1^H\mathbf{w} - 1) \tag{2.97}$$

Following the basic approach of Lagrangian optimization [44] and taking the partial derivative of $\mathbf{j}$ with respect to $\mathbf{w}^H$ we set the derivative to zero, yielding

$$0 = \frac{\partial j}{\partial \mathbf{w}^H} = \mathbf{R}_{uu}\mathbf{w} + \lambda\mathbf{a}_1. \tag{2.98}$$

Hence, we have

$$\mathbf{w} = -\lambda \mathbf{R}_{uu}^{-1} \mathbf{a}_1. \tag{2.99}$$

The constraint in (2.96) can be used for deriving $\lambda$, giving

$$\mathbf{w}^H \mathbf{a}_1 = -\lambda \mathbf{a}_1^H \mathbf{R}_{uu}^{-1} \mathbf{a}_1 = 1. \tag{2.100}$$

Therefore, we arrive at

$$\lambda = -\frac{1}{\mathbf{a}_1^H \mathbf{R}_{uu}^{-1} \mathbf{a}_1}. \tag{2.101}$$

Substituting $\lambda$ in (2.96) into (2.99), it can be shown that the solution to the MVDR optimization problem can be expressed as [44]

$$\mathbf{w}_{MVDR} = \frac{\mathbf{R}_{uu}^{-1} \mathbf{a}_1}{\mathbf{a}_1^H \mathbf{R}_{uu}^{-1} \mathbf{a}_1} \tag{2.102}$$

### 2.3.2.1 Maximum Likelihood Combining Criterion

In the context of the Maximum Likelihood (ML) beamformer, we consider the same model as in the previous section, except that we now assume that the composite interference $\mathbf{i}$ is a complex Gaussian random vector, hence the total undesired signal vector $\mathbf{u} = \mathbf{i} + \mathbf{n}$ has a multivariate complex Gaussian distribution. Thus, the distribution function of the signal vector input to the beamformer can be expressed as [125]

$$f(\mathbf{z}) = \rho\ (\mathbf{z}|s_1) = \frac{1}{(2\pi)|\mathbf{R}_{uu}|} \exp\left(-[\mathbf{z} - s_1\mathbf{a}_1]^H \mathbf{R}_{uu}^{-1} [\mathbf{z} - s_1\mathbf{a}_1]\right), \tag{2.103}$$

Where $s_1$ is the estimate of the desired signal $s_1$, and the $s_1$ which maximizes the distribution function $f(\mathbf{z})$ is the maximum likelihood to the desired signal $s_1$. Here, maximizing $f(\mathbf{z})$ means minimizing $[\mathbf{z} - s_1\mathbf{a}_1]^H \mathbf{R}_{uu}^{-1} [\mathbf{z} - s_1\mathbf{a}_1]$. Hence, in order to maximize (2.103), we take the partial derivative of $[\mathbf{z} - s_1\mathbf{a}_1]^H \mathbf{R}_{uu}^{-1} [\mathbf{z} - s_1\mathbf{a}_1]$ with respect to $s_1$ and set the result to zero, yielding

$$0 = \frac{\partial\left([\mathbf{z} - s_1\mathbf{a}_1]^H \mathbf{R}_{uu}^{-1} [\mathbf{z} - s_1\mathbf{a}_1]\right)}{\partial s_1} = -2\mathbf{a}_1^H \mathbf{R}_{uu}^{-1} \mathbf{z} + 2s_1 \mathbf{a}_1^H \mathbf{R}_{uu}^{-1} \mathbf{a}_1. \tag{2.104}$$

Consequently, the estimate $s_1$ that maximizes $f(\mathbf{z})$ is given by

$$s_1 = \frac{(\mathbf{R}_{uu}^{-1} \mathbf{a}_1)^H \mathbf{z}}{\mathbf{a}_1^H \mathbf{R}_{uu}^{-1} \mathbf{a}_1} = \mathbf{w}_{ML}^H \mathbf{z}. \tag{2.105}$$

Since $\tilde{\mathbf{a}}_1^H \mathbf{R}_{uu}^{-1} \tilde{\mathbf{a}}_1$ is constant scalar, the optimum weight vector which results in the most likely estimate of $s_1$ - hence the terminology $ML$ - has the form of

$$\mathbf{w}_{ML} = \frac{\mathbf{R}_{uu}^{-1} \mathbf{a}_1}{\mathbf{a}_1^H \mathbf{R}_{uu}^{-1} \mathbf{a}_1}, \tag{2.106}$$

which is identical to the weight vector of (2.102) derived for the MVDR-based beamformer. In other words, the MVDR beamformer provides the ML estimate of the desired signal $s_1$, provided that the direction of arrival (DOA) of the desired signal $s_1$ is known and that the total undesired signal vector of $\mathbf{u} = \mathbf{i} + \mathbf{n}$ including the interference and the noise obeys a multivariate complex Gaussian distribution. However, in most cases, the MVDR beamformer does not provide the ML estimate of the signal's DOA. Below we compare the achievable beamformer gains of the MVDR and MRC solution. For the MVDR scheme, the output SINR is given by [44]

$$(SINR)_{MVDR} = \frac{E\{|\mathbf{w}_{MVDR}^H s_1 \mathbf{a}_1|^2\}}{E\{|\mathbf{w}_{MVDR}^H \mathbf{u}|^2\}} = \frac{\sigma_1^2 |\mathbf{w}_{MVDR}^H \mathbf{a}_1|^2}{\mathbf{w}_{MVDR}^H \mathbf{R}_{uu} \mathbf{w}_{MVDR}}, \tag{2.107}$$

where $\sigma_1^2$ is the power of the desired user. The weight vector of $\mathbf{w}_{MVDR}$ is distortionless, this means that the desired user's power will not be distorted after weighting and combining. Hence, after substituting (2.96) and (2.102) into (2.107), it can be shown that (2.107) can be simplified to

$$(SINR)_{MVDR} = \sigma_1^2 \mathbf{a}_1^H \mathbf{R}_{uu}^{-1} \mathbf{a}_1. \tag{2.108}$$

The SINR of the beamformer's input signal is $SINR = \sigma_1^2/\sigma_u^2$, where we assume that we have $\mathbf{R}_{uu} = \sigma_u^2 \rho_{uu}$, with $\rho_{uu}$ being the normalized version of the matrix $\mathbf{R}_{uu}$ upon division by $\sigma_u^2$. Therefore, the beamformer's gain can be expressed as

$$A_{MVDR} = \frac{(SINR)_{MVDR}}{SINR} = \sigma_u^2 \mathbf{a}_1^H \mathbf{R}_{uu}^{-1} \mathbf{a}_1 = \mathbf{a}_1^H \rho_{uu}^{-1} \mathbf{a}_1. \tag{2.109}$$

In physical terms Equation (2.109) indicates that the lower the correlation coefficients of the interference-plus-noise, the higher the spatial diversity, then the higher the beamformer gain. In the context of the MRC, the weight vector is given by $\mathbf{w}_c = \alpha \mathbf{a}_1$, where $\alpha$ is a constant constant and we set $\alpha = 1/\tilde{\mathbf{a}}_1^H \mathbf{a}_1$ . The variance of the beamformer's output noise is $\alpha^2 \mathbf{a}_1^H \mathbf{R}_{uu} \mathbf{a}_1$. For the MRC $\alpha^2 \tilde{\mathbf{a}}_1^H \mathbf{R}_{uu} \mathbf{a}_1$. For

$$(SINR)_{MRC} = \frac{E\{|\mathbf{w}_{MRC}^H s_1 \mathbf{a}_1|^2\}}{E\{|\mathbf{w}_{MRC}^H \mathbf{u}|^2\}} = \frac{\sigma_1^2 |\mathbf{a}_1^H \mathbf{a}_1|^2}{\mathbf{a}_1^H \mathbf{R}_{uu} \mathbf{a}_1}. \tag{2.110}$$

Then, the corresponding array gain is given by

$$A_{MRC} = \frac{(SINR)_{MRC}}{SINR} = \frac{1}{\alpha^2 \mathbf{a}_1^H \rho_{uu} \mathbf{a}_1}. \tag{2.111}$$

It can be shown that when the interference-plus-noise contributions impinging at the different array elements are uncorrelated, the correlation matrix $\mathbf{R}_{uu}$ will be a diagonal matrix. In this scenario it can be seen from Equation (2.108) and Equation (2.110) that the MVDR and MRC combiners are equivalent and their corresponding array gains in Equation (2.109) and Equation (2.111) are also identical, i.e. we have $A_{MVDR} = A_{MRC}$. Otherwise, by comparing Equation (2.109) and Equation (2.111) we can see that when the interference and/or the noise arriving at the different array elements are correlated, we have $A_{MVDR} \geq A_{MRC}$.

### 2.3.3 Maximum Signal-to-Interference-plus-Noise Ratio Criterion

In this section we discuss the optimum combiner based on the Maximum Signal-to-Interference-plus-Noise Ratio (MSINR) criterion. According to this criterion, the weight vector is optimized by maximizing the SINR at the output of the beamformer. For simplicity, we assume that the signal input into the combiner is identical to that used in the previous sections, namely, $\mathbf{z} = s_1\mathbf{a}_1 + \mathbf{u}$. Let us assume that the optimum weight vector is expressed as $\mathbf{w}_o$. Then, the output SINR is given by [44]

$$\begin{aligned}(SINR)_o &= \frac{E\{|\mathbf{w}_o^H s_1\mathbf{a}_1|^2\}}{E\{|\mathbf{w}_o^H\mathbf{u}|^2\}} = \frac{\sigma_1^2|\mathbf{w}_o^H\mathbf{a}_1|^2}{\mathbf{w}_o^H\mathbf{R}_{uu}\mathbf{w}_o} \\ &= \frac{\sigma_1^2|(\mathbf{R}_{uu}^{1/2}\mathbf{w}_o)^H(\mathbf{R}_{uu}^{-1/2}\mathbf{a}_1)|^2}{\mathbf{w}_o^H\mathbf{R}_{uu}\mathbf{w}_o}. \end{aligned} \tag{2.112}$$

where $\sigma_1^2 = E\{|s_1|^2\}$ is the power of the desired user, $E\{|\mathbf{w}_o^H\mathbf{u}|^2\} = E\{\mathbf{w}_o^H\mathbf{u}\mathbf{u}^H(t)\mathbf{w}_o\} = \mathbf{w}_o^H\mathbf{R}_{uu}\mathbf{w}_o$, and $\mathbf{w}_o^H\mathbf{a}_1 = \mathbf{w}_o^H(\mathbf{R}_{uu}^{1/2})^H\mathbf{R}_{uu}^{-1/2}\mathbf{a}_1 = (\mathbf{R}_{uu}^{1/2}\mathbf{w}_o)^H(\mathbf{R}_{uu}^{-1/2}\mathbf{a}_1)$, in which $(\mathbf{R}_{uu}^{1/2})^H\mathbf{R}_{uu}^{-1/2} = \mathbf{I}$. According to the Schwarz' inequality [44], when the condition of

$$\mathbf{R}_{uu}^{1/2}\mathbf{w}_o = \mathbf{R}_{uu}^{-1/2}\mathbf{a}_1, \tag{2.113}$$

is satisfied, we have

$$\begin{aligned}(SINR)_o &= \frac{\sigma_1^2|(\mathbf{R}_{uu}^{1/2}\mathbf{w}_o)^H(\mathbf{R}_{uu}^{-1/2}\mathbf{a}_1)|^2}{\mathbf{w}_o^H\mathbf{R}_{uu}\mathbf{w}_o} \\ &= \frac{\sigma_1^2|\mathbf{a}_1^H(\mathbf{R}_{uu}^{-1/2})^H\mathbf{R}_{uu}^{-1/2}\mathbf{a}_1|^2}{\mathbf{w}_o^H(\mathbf{R}_{uu}^{1/2})^H\mathbf{R}_{uu}^{1/2}\mathbf{w}_o} \\ &= \frac{\sigma_1^2|\mathbf{a}_1^H\mathbf{R}_{uu}^{-1}\mathbf{a}_1|^2}{(\mathbf{R}_{uu}^{-1/2}\mathbf{a}_1)^H\mathbf{R}_{uu}^{-1/2}\mathbf{a}_1} \\ &= \sigma_1^2\mathbf{a}_1^H\mathbf{R}_{uu}^{-1}\mathbf{a}_1 \\ &\triangleq (SINR)_{max} \end{aligned} \tag{2.114}$$

Multiple $\mathbf{R}_{uu}^{-1/2}$ on both sides of (2.113), we have $\mathbf{R}_{uu}^{-1/2}\mathbf{R}_{uu}^{1/2}\mathbf{w}_o = \mathbf{R}_{uu}^{-1/2}\mathbf{R}_{uu}^{-1/2}\mathbf{a}_1$, then, we can derive the weight vector that maximizes the SINR at the output of the combiner, which is given by:

$$\mathbf{w}_{MSINR} = \alpha\mathbf{R}_{uu}^{-1}\mathbf{a}_1, \tag{2.115}$$

where $\alpha$ represents a nonzero constant.

### 2.3.4 Minimum Mean-Square Error Criterion

In the previous section we have discussed the MSINR beamformer. Let us now turn our attention to the Minimum Mean-Square Error (MMSE) beamformer. The MMSE beamformer minimizes the mean-square error of $E[|e(t)|^2]$ between the beamformer output $\mathbf{w}^H\mathbf{z}$ and the desired signal $s_1$. Let

the error signal be expressed as

$$e(t) = s_1 - \mathbf{w}^H \mathbf{z}. \tag{2.116}$$

Then the mean square error $\epsilon(\mathbf{w})$ is given by

$$\begin{aligned} \epsilon(\mathbf{w}) &= E[|e(t)|^2] \\ &= E[(s_1 - \mathbf{w}^H\mathbf{z})(s_1 - \mathbf{w}^H\mathbf{z})^*] \\ &= E[s_1^* s_1 - 2\mathbf{w}^H s_1^* \mathbf{z} - \mathbf{w}^H \mathbf{z}\mathbf{z}^H \mathbf{w}] \\ &= \sigma_1^2 - \mathrm{R_e}\{2\mathbf{w}^H \mathbf{r}_{zs_1} - \mathbf{w}^H \mathbf{R}_{zz}\mathbf{w}\}, \end{aligned} \tag{2.117}$$

where $\mathbf{r}_{zs_1} = E[\mathbf{z}s_1]$, represents the cross-correlation between the received signal $\mathbf{z}$ and the desired signal $s_1$. Furthermore, $\mathbf{R}_{zz} = E[\mathbf{z}\mathbf{z}]$ represents the auto-correlation of the received signal, or the signal vector input into the beamformer. After taking the partial derivative of $\epsilon(\mathbf{w})$ with respect to $\mathbf{w}^H$ and setting it to zero we have

$$0 = \frac{\partial \epsilon(\mathbf{w})}{\partial \mathbf{w}^H} = -2(\mathbf{R}_{zz}\mathbf{w} - \mathbf{r}_{zs_1}), \tag{2.118}$$

and hence, the optimum weight vector based on the MMSE criterion can be expressed as

$$\mathbf{w}_{MMSE} = \mathbf{R}_{zz}^{-1}\mathbf{r}_{zs_1}. \tag{2.119}$$

As before, the complexity of the matrix inversion depends cubically on the dimensionality of $\mathbf{R}_{zz}$, which in turn depends on the number of array weights to be determined. The RLS algorithm [44] may be invoked for updating $\mathbf{R}_{zz}^{-1}$ directly, as decision variable samples become available. Below several specific cases are considered in the context of the MMSE beamformer. First, for the wireless system dispensing with DS-spreading, the received signal vector $\mathbf{r}$ is given in (2.58). Hence, the auto-correlation matrix $\mathbf{R}_{rr}$ of the received signal vector can be expressed as

$$\mathbf{R}_{rr} = P_1 E\left[\mathbf{a}_1^* \mathbf{a}_1^T\right] + \sigma^2 \mathbf{I} + \sum_{k=2}^{K} P_k E\left[\mathbf{a}_k^* \mathbf{a}_k^T\right], \tag{2.120}$$

where $P_1 E\left[\mathbf{a}_1^* \mathbf{a}_1^T\right]$ is proportional to the power $P_1$ of the desired signal and to the variance $E\left[\mathbf{a}_1^* \mathbf{a}_1^T\right]$ of the variance $E\left[\tilde{\mathbf{a}}_1^* \mathbf{a}_1^T\right]$ of the $\sum_{k=2}^{K} P_k E\left[\mathbf{a}_k^* \mathbf{a}_k^T\right]$ is due to the interfering signals. Consequently, the optimum weight vector based on the MMSE criterion adopted for wireless system using no DS-spreading can be expressed as

$$\mathbf{w}_{MMSE} = \mathbf{R}_{rr}^{-1}\mathbf{r}_{rs_1} = \alpha \mathbf{R}_{rr}^{-1}\mathbf{a}_1, \tag{2.121}$$

where, again, $\alpha$ is a nonzero constant. Different from the optimum weight vector $\mathbf{w}_{MSINR}$ in (2.61) based on the MSINR criterion, the optimum weight vector $\mathbf{w}_{MMSE}$ based on the MMSE criterion is determined by the auto-correlation matrix $\mathbf{R}_{rr}$ of the received signal, instead of the correlation matrix

$\mathbf{R}_{uu}$ of interference-plus-noise.

In the context of single-carrier DS-CDMA systems, after the correlation or matched filtering operation, the output signal $\mathbf{z}(n)$ was given in (2.67). Here, the auto-correlation matrix $\mathbf{R}_{zz}$ of $\mathbf{z}(n)$ can be expressed as

$$\mathbf{R}_{zz} = E\left[\mathbf{z}^*\mathbf{z}^T\right] = GP_1\mathbf{a}_1^*\mathbf{a}_1^T + \sigma_n^2\mathbf{I} + \sum_{k=2}^{K}\frac{\rho_{1,k}^2}{G}P_k\mathbf{a}_k^*\mathbf{a}_k^T. \tag{2.122}$$

Here, $\mathbf{R}_{zz} = GP_1\mathbf{a}_1^*\mathbf{a}_1^T + \mathbf{R}_{uu}$, in which $\mathbf{R}_{uu}$ is the correlation matrix of the post-correlation interference-plus-noise signal of (2.71). Thus, according to (2.119), the optimum weight vector based on the MMSE criterion adopted for a DS-CDMA system can be expressed as

$$\mathbf{w}_{MMSE} = \alpha\mathbf{R}_{zz}^{-1}\mathbf{a}_1, \tag{2.123}$$

where $\alpha$ is a nonzero constant. Different from the optimum weight vector $\mathbf{w}_{MSINR}$ in (2.72) based on the MSINR criterion, the optimum weight vector $\mathbf{w}_{MMSE}$ based on the MMSE criterion for DS-CDMA system is determined by the auto-correlation matrix $\mathbf{R}_{zz}$ of the post-correlation signal, instead of the correlation matrix $\mathbf{R}_{uu}$ of post-correlation interference-plus-noise.

For a MC-CDMA system employing frequency-domain spreading but no DS-spreading, and using separate subcarrier-based processing of the $ML$ array elements, the post-demodulation signal $\mathbf{z}_v(n)$ was expressed in (2.78). Hence, the auto-correlation matrix $\mathbf{R}_{zz,v}$ of the post-demodulation signal $\mathbf{z}_v(n)$ can be expressed as

$$\mathbf{R}_{zz,v} = E\left[\mathbf{z}_v^*\mathbf{z}_v^T\right] = \frac{P_1}{V}(\mathbf{a}_v^{(1)})^*(\mathbf{a}_v^{(1)})^T + \sigma_n^2\mathbf{I} + \sum_{k=2}^{K}\frac{P_k}{V}(\mathbf{a}_v^{(k)})^*(\mathbf{a}_v^{(k)})^T. \tag{2.124}$$

Here, $\mathbf{R}_{zz,v} = \frac{P_1}{V}(\mathbf{a}_v^{(1)})^*(\mathbf{a}_v^{(1)})^T + \mathbf{R}_{uu,v}$, in which $\mathbf{R}_{uu,v}$ is the correlation matrix of the post-correlation interference-plus-noise signal corresponding to the $v$th subcarrier of (2.80). Therefore, according to (2.119) the separate subcarrier-based optimum weight vector invoking the MMSE criterion for the frequency-domain spreading aided MC-CDMA system of Figure 2.7 is given by

$$\mathbf{w}_{MMSE} = \alpha\mathbf{R}_{zz,v}^{-1}\mathbf{a}_v^{(1)}. \tag{2.125}$$

Different from the individual subcarrier-based optimum weight vector $\mathbf{w}_{MSINR}$ in (2.81) based on the MSINR criterion for the MC-CDMA system, the individual subcarrier-based optimum weight vector $\mathbf{w}_{MMSE}$ based on the MMSE criterion for MC-CDMA system is determined by the auto-correlation matrix $\mathbf{R}_{zz,v}$ of the post-demodulation signal corresponding to the $v$th subcarrier, instead of the correlation matrix $\mathbf{R}_{uu,v}$ of post-demodulation interference-plus-noise signal corresponding to the $v$th subcarrier.

When using the jointly optimized approach, the $VML$-dimensional signal vector $\mathbf{z}$ was formulated in (2.84). Hence, the auto-correlation matrix $\mathbf{R}_{zz}$ of the post-demodulation signal $\mathbf{z}$ can be

expressed as

$$\mathbf{R}_{zz} = E\left[\mathbf{z}^*\mathbf{z}^T\right] = \frac{P_1\pi}{2}(\mathbf{a}^{(1)})^*(\mathbf{a}^{(1)})^T + V\sigma_n^2\mathbf{I} + \sum_{k=2}^{K}\frac{P_k}{V}(\mathbf{a}^{(k)})^*(\mathbf{a}^{(k)})^T. \tag{2.126}$$

Here, $\mathbf{R}_{zz} = \frac{P_1\pi}{2}(\mathbf{a}^{(1)})^*(\mathbf{a}^{(1)})^T + \mathbf{R}_{uu}$, in which $\mathbf{R}_{uu}$ is the correlation matrix of the post-demodulation interference-plus-noise signal of (2.85). Therefore, according to (2.119) the jointly optimized weight vector based on the MMSE criterion invoked for the frequency-domain spreading aided MC-CDMA system of Figure 2.7 is given by

$$\mathbf{w}_{MMSE} = \alpha\mathbf{R}_{zz}^{-1}\mathbf{a}^{(1)}. \tag{2.127}$$

Different from the joint processing aided optimum weight vector $\mathbf{w}_{MSINR}$ in (2.86) based on the MSINR criterion for the MC-CDMA system, the joint processing aided optimum weight vector $\mathbf{w}_{MMSE}$ based on the MMSE criterion for MC-CDMA system is determined by the auto-correlation matrix $\mathbf{R}_{zz}$ of the post-demodulation signal, instead of the correlation matrix $\mathbf{R}_{uu}$ of post-demodulation interference-plus-noise signal.

Finally, for the generalized MC DS-CDMA system of Figure 2.5, the received signal vector $\mathbf{z}$ associated with the $V$ subcarriers, $M$ receiver antenna arrays and the L elements of each antenna array, was given in (2.92). With the aid of $\mathbf{z}$ in (2.92), the auto-correlation matrix $\mathbf{R}_{zz}$ of $\mathbf{z}$ can be expressed as

$$\begin{aligned}\mathbf{R}_{zz} &= E\left[\mathbf{z}^*\mathbf{z}^T\right] \\ &= \frac{P_1\pi}{2V}G(\mathbf{a}^{(1)})^*(\mathbf{a}^{(1)})^T \\ &\quad +\sigma_n^2\mathbf{I} + \sum_{k=2}^{K'}\frac{\rho_{1,k}^2}{G}\frac{P_i}{V}(\mathbf{a}_v^{(k)})^*(\mathbf{a}_v^{(k)})^T + \frac{1}{V}\sum_{k=K'+1}^{K}\frac{\rho_{1,k}^2}{G}\frac{P_i}{V}(\mathbf{a}_v^{(k)})^*(\mathbf{a}_v^{(k)})^T,\end{aligned} \tag{2.128}$$

where we have $1 \leq K' \leq K$. In this system, the interfering users can be classified to two group according to their time-domain and frequency-domain spreading sequences. In the first group, the interfering users employ the same frequency-domain spreading code as the 1st user, while employing a different time-domain spreading code. Here, the number of the interfering users in this group is assumed to be $K' - 1$. While the interfering users belong to the second group invoke the different frequency-domain spreading code. Because the interfering users belonging to the first group employ the same frequency-domain spreading code as the 1st user, the effect of the multicarrier demodulation to their signal will be same to that of the desired user's signal but different from that of the interfering users' signal belonging to the second group. the parameter $\frac{1}{V}$ in $\frac{1}{V}\sum_{k=K'+1}^{K}\frac{\rho_{1,k}^2}{G}\frac{P_i}{V}(\mathbf{a}_v^{(k)})^*(\mathbf{a}_v^{(k)})^T$ is just the result of the multicarrier demodulation to the different frequency-domain spreading code. Again, $\mathbf{R}_{zz} = \frac{P_1\pi}{2V}G(\mathbf{a}^{(1)})^*(\mathbf{a}^{(1)})^T + \mathbf{R}_{uu}$, in which $\mathbf{R}_{uu}$ is the correlation matrix of the post-demodulation interference-plus-noise signal of (2.93). Consequently, based on (2.119), the jointly optimized weight vector based on the MMSE criterion and invoked for the generalized MC DS-

CDMA system of Figure 2.5 can be expressed as

$$\mathbf{w}_{MMSE} = \alpha \mathbf{R}_{zz}^{-1} \mathbf{a}^{(1)}, \tag{2.129}$$

where $\mathbf{R}_{zz}$ is given in (2.128). Different from the joint processing aided optimum weight vector $\mathbf{w}_{MSINR}$ in (2.94) based on the MSINR criterion for the generalized MC DS-CDMA system, the joint processing aided optimum weight vector $\mathbf{w}_{MMSE}$ based on the MMSE criterion for the generalized MC DS-CDMA system is determined by the auto-correlation matrix $\mathbf{R}_{zz}$ of the post-demodulation signal, instead of the correlation matrix $\mathbf{R}_{uu}$ of post-demodulation interference-plus-noise signal. In (2.128), the auto-correlation matrix was derived by simultaneously considering all the $VML$ signals of the $V$ subcarriers and $ML$ antenna elements related to a transmitted information bit. When we consider beamforming on a separate subcarrier-by-subcarrier basis the received signal vector corresponding to the $v$th subcarrier is given in (2.87). Hence, for the $v$th subcarrier, the auto-correlation matrix can be expressed as

$$\mathbf{R}_{zz,v} = G\frac{P_1}{V}(\mathbf{a}_v^{(1)})^*(\mathbf{a}_v^{(1)})^T + \sigma_n^2\mathbf{I} + \sum_{k=2}^{K} \frac{\rho_{1,k}^2}{G}\frac{P_k}{V}(\mathbf{a}_v^{(k)})^*(\mathbf{a}_v^{(k)})^T. \tag{2.130}$$

Here, $\mathbf{R}_{zz,v} = G\frac{P_1}{V}(\mathbf{a}_v^{(1)})^*(\mathbf{a}_v^{(1)})^T + \mathbf{R}_{uu,v}$, in which $\mathbf{R}_{uu,v}$ is the correlation matrix of the post-demodulation interference-plus-noise signal corresponding to the $v$th subcarrier of (2.88). Then, the separate subcarrier-by-subcarrier optimum weight vector derived on the basis of the MMSE criterion for the $v$th subcarrier of the generalized MC DS-CDMA system of Figure 2.5 is given by

$$\mathbf{w}_{MMSE} = \alpha \mathbf{R}_{zz,v}^{-1} \mathbf{a}_v^{(1)}, \tag{2.131}$$

where $\mathbf{R}_{zz,v}$ is given by (2.130). Different from the individual subcarrier-based optimum weight vector $\mathbf{w}_{MSINR}$ in (2.89) based on the MSINR criterion for the generalized MC DS-CDMA system, the individual subcarrier-based optimum weight vector $\mathbf{w}_{MMSE}$ based on the MMSE criterion for the generalized MC DS-CDMA system is determined by the auto-correlation matrix $\mathbf{R}_{zz}$ of the post-demodulation signal corresponding to the $v$th subcarrier, instead of the correlation matrix $\mathbf{R}_{uu}$ of post-demodulation interference-plus-noise signal corresponding to the $v$th subcarrier.

Note that, from the assumption of encountering uncorrelated signal and noise, the cross-correlation of the received signal $\mathbf{z}$ and the desired signal $\mathbf{r}_{zs_1} = E[\mathbf{z}s_1]$ in (2.119) can be simplified to

$$\mathbf{r}_{zs_1} = \sigma_1^2 \mathbf{a}_1 \tag{2.132}$$

where $\sigma_1^2$ is the power of the desired user, $\mathbf{a}_1$ is the complex-valued non-dispersive CIR vector of the desired user. Hence, From Euqation (2.120), (2.122), (2.124), (2.126), (2.128) and (2.130), the relationship between the auto-correlation matrix of the received signal and that of the interference-

plus-noise can be expressed as

$$\mathbf{R}_{zz} = \sigma_1^2 \mathbf{a}_1 \mathbf{a}_1^H + \mathbf{R}_{uu}. \tag{2.133}$$

where $\sigma_1^2$ is the power of the desired user and $\mathbf{a}_1$ is the complex-valued non-dispersive CIR vector of the desired user. According to the matrix inversion lemma [193], when the positive-definite $M$-by-$M$ matrix $\mathbf{A}$ have the form $\mathbf{A} = \mathbf{B}^{-1} + \mathbf{C}\mathbf{D}^{-1}\mathbf{C}^H$, where $\mathbf{B}$ is positive-definite $M$-by-$M$, $\mathbf{C}$ is $M$-by-$N$ and $\mathbf{D}$ is positive-definite $M$-by-$M$, then inverse is $\mathbf{A}^{-1} = \mathbf{B} - \mathbf{B}\mathbf{C}(\mathbf{D} + \mathbf{C}^H\mathbf{B}\mathbf{C})^{-1}\mathbf{C}^H\mathbf{B}$. Hence, from (2.133) we obtain

$$\begin{aligned}
\mathbf{R}_{zz}^{-1} &= \mathbf{R}_{uu}^{-1} - \mathbf{R}_{uu}^{-1}\mathbf{a}_1(\sigma_1^{-2} + \mathbf{a}_1^H\mathbf{R}_{uu}^{-1}\mathbf{a}_1)^{-1}\mathbf{a}_1^H\mathbf{R}_{uu}^{-1} \\
&= \mathbf{R}_{uu}^{-1} - \sigma_1^2\mathbf{R}_{uu}^{-1}\mathbf{a}_1(1 + \sigma_1^2\mathbf{a}_1^H\mathbf{R}_{uu}^{-1}\mathbf{a}_1)^{-1}\mathbf{a}_1^H\mathbf{R}_{uu}^{-1} \\
&= \mathbf{R}_{uu}^{-1} - \frac{\sigma_1^2\mathbf{R}_{uu}^{-1}\mathbf{a}_1\mathbf{a}_1^H\mathbf{R}_{uu}^{-1}}{1 + \sigma_1^2\mathbf{a}_1^H\mathbf{R}_{uu}^{-1}\mathbf{a}_1},
\end{aligned} \tag{2.134}$$

Upon substituting (2.132) and (2.134) into (2.119), the optimum weight vector of all systems based on the MMSE criterion can be expressed as

$$\begin{aligned}
\mathbf{w}_{MMSE} &= \mathbf{R}_{zz}^{-1}\mathbf{r}_{zs_1} \\
&= \sigma_1^2\left(\mathbf{R}_{uu}^{-1}\mathbf{a}_1 - \frac{\sigma_1^2\mathbf{R}_{uu}^{-1}\mathbf{a}_1\mathbf{a}_1^H\mathbf{R}_{uu}^{-1}\mathbf{a}_1}{1 + \sigma_1^2\mathbf{a}_1^H\mathbf{R}_{uu}^{-1}\mathbf{a}_1}\right) \\
&= \frac{\sigma_1^2}{1 + \sigma_1^2\mathbf{a}_1^H\mathbf{R}_{uu}^{-1}\mathbf{a}_1}\mathbf{R}_{uu}^{-1}\mathbf{a}_1.
\end{aligned} \tag{2.135}$$

Noting that the matrix $\mathbf{R}_{zz}$ of all systems can be expressed as (2.133), the optimum weight vector $\mathbf{w}_{MMSE}$ in (2.133) is available for all systems.

### 2.3.5 Minimum Power Distortionless Response Criterion

Finally, let us consider the beamformer based on the Minimum Power Distortionless Response (MPDR) criterion [44], which is closely related to the MVDR beamformer. However, in contrast to the MVDR scheme, the MPDR arrangement has two characteristics, which are different from that of the MVDR scheme. First, the spatial beamformer filter is a distortionless filter, i.e. we have

$$\mathbf{w}^H\mathbf{a}_m = 1, \tag{2.136}$$

where $\mathbf{a}_m$ represents the steering vector [44]. Ideally, we would like the steering vector to exactly match to the signal vector, i.e. we would like the condition $\mathbf{a}_m = \mathbf{a}_1$ to be satisfied. However, in many cases this may not be true. Secondly, in the context of the MPDR scheme, the auto-correlation matrix of the received signal vector, $\mathbf{R}_{zz}$, is required for deriving the optimum weight vector. By contrast, in case of the MVDR beamformer, $\mathbf{R}_{uu}$ and $\mathbf{a}_1$ are required for deriving the optimum weight vector, as we have seen in Equation (2.102). According to the MPDR criterion, the total received power is minimized subject to the constraint of (2.136). Following a derivation similar to that in the context of

the MVDR model, we obtain the optimum array weight vector in the form of [44]:

$$\mathbf{w}_{MPDR} = \frac{\mathbf{R}_{zz}^{-1}\mathbf{a}_m}{\mathbf{a}_m^H \mathbf{R}_{zz}^{-1}\mathbf{a}_m}. \tag{2.137}$$

In (2.137), if we have $\mathbf{a}_m = \mathbf{a}_1$, then $\tilde{\mathbf{a}}_m = \tilde{\mathbf{a}}_1$, then $\mathbf{R}_{zz}^{-1}$ can be derived from $\mathbf{R}_{uu}^{-1}$ as in (2.134). Substituting (2.134) into (2.137), we can see that the MPDR beamformer is equivalent

$$\mathbf{w}_{MPDR} = \frac{\mathbf{R}_{uu}^{-1}\mathbf{a}_1}{\mathbf{a}_1^H \mathbf{R}_{uu}^{-1}\mathbf{a}_1} = \mathbf{w}_{MVDR}. \tag{2.138}$$

However, when we have $\tilde{\mathbf{a}}_m \neq \tilde{\mathbf{a}}_1$, beamformer solutions result in different. In practical applications, $\mathbf{R}_{zz}$ is usually estimated from $\mathbf{R}_{zz}$ is usually estimated from $\tilde{\mathbf{a}}_1$, instead of $\mathbf{a}_m$, although the results of [44] suggest that deriving the optimum weight vector from $\mathbf{R}_{zz}$ may result in a significant receiver performance degradation, when we have $\mathbf{a}_m \neq \tilde{\mathbf{a}}_1$.

### 2.3.6 Comparison of Various Optimum Combining Schemes

In our simulations, we will focus on the generalized MC DS-CDMA scheme of Section 2.3.1.4. The parameters used in our analysis are defined as follows:

$$\Gamma = \frac{\text{mean received desired signal power per antenna}}{\text{mean received interference plus noise power per antenna}} \tag{2.139}$$

$$\Gamma_1 = \frac{\text{mean received desired signal power per antenna}}{\text{mean received noise power per antenna}} \tag{2.140}$$

$$\Gamma_k = \frac{\text{mean received } k\text{th interferer signal power per antenna}}{\text{mean received noise power per antenna}}, k = 2, 3, \ldots, K. \tag{2.141}$$

The relationship among these parameters is

$$\Gamma = \frac{\Gamma_1}{1 + \sum_{k=2}^{K} \Gamma_k} \tag{2.142}$$

First we consider a single-carrier DS-CDMA system communicating over a single-path non-dispersive Rayleigh fading channel using 31-chip Gold codes as their spreading sequences, as seen in Figure 2.11. There are 16 users in this system, namely, the desired user and 15 interfering users. Here we assume that $\Gamma_k = 0, k = 2, 3, \ldots, K$. Furthermore we use a $3 \times 1$-dimensional linear antenna array ($M = 1, L = 3$), having an element-spacing of $\lambda/2$. We observe from Figure 2.11 that the performance of each beamformer is better than that of the MRC, since the MRC can not suppress the interference. It can also be seen that the performance of the MSINR beamformer is similar to that of the MVDR beamformer, while the performance of MMSE beamformer is almost the same as that of the MPDR beamformer. Finally, the performance of the MVDR or MSINR beamformer is better than that of the MPDR or MMSE beamformer. Note in (2.102) and (2.115), that the optimum weight vector of the MSINR or MVDR beamformer is determinated by the interference-plus-noise correla-

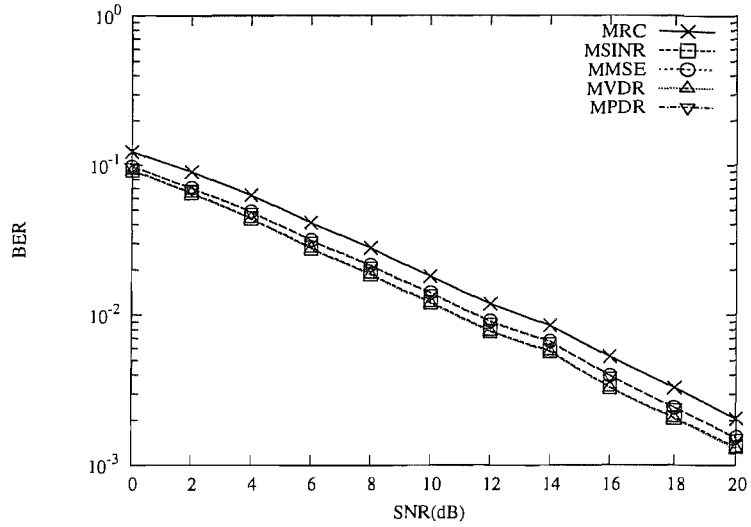


**Figure 2.11:** BER versus SNR performance of the uplink of a DS-CDMA wireless system supporting 16 users using 31-chip Gold codes as spreading sequences, using a $1 \times 3$-dimensional antenna array ($M = 1, L = 3$), different optimum combiners based on beamforming schemes of Section 2.3.1.

tion matrix $\mathbf{R}_{uu}$, while the optimum weight vector of the MMSE or MPDR scheme is based on the entire post-decorrelation signal's correlation matrix $\mathbf{R}_{zz}$, as seen in (2.123) and (2.137) respectively. Hence the presence of the entire post-decorrelation signal's correlation matrix $\mathbf{R}_{zz}$ may result in a more dramatic effect on the array weight vector than that of the interference-plus-noise correlation matrix $\mathbf{R}_{uu}$, as observed in Equation (2.71).

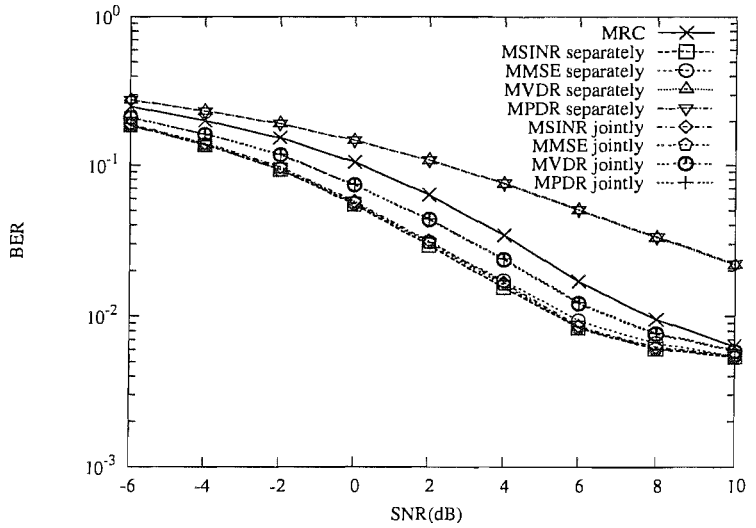


**Figure 2.12:** BER versus SNR performance of the uplink of a MC-CDMA wireless system supporting 4 users using 4-chip Walsh codes as frequency spreading sequences, employing a $1 \times 3$-dimensional antenna array ($M = 1, L = 3$), different optimum combiners based on beamforming schemes of Section 2.3.1.

Let us now discuss the achievable performance of a non-dispersive MC-CDMA system in a Rayleigh fading channel contaminated by AWGN, as seen in the Figure 2.12. In these simulations we adopted 4-chip Walsh codes as frequency-domain spreading sequences, we have four subcarriers, and correspondingly four users. We assume that $\Gamma_k = 0, i = 2, 3, \ldots, K$ and we use a $3 \times 1$-dimensional linear antenna array ($M = 1, L = 3$), having an element-spacing of $\lambda/2$. Figure 2.12 shows that when using the MSINR combiner of Section 2.3.3, the joint subcarrier processing based optimum MSINR combiner is capable of achieving a slightly better performance than the individual subcarrier-based optimum MSINR combiner. When using the MMSE combiner of Section 2.3.4, the joint subcarrier processing aided optimum MMSE combiner is also capable of achieving a better performance than its subcarrier-based optimum MMSE combiner counterpart. The performance of the optimum MVDR and MPDR combiner separately processing the subcarrier signals is the worst. From (2.102) and (2.137) we infer that when separately processing the subcarrier signals in MC-CDMA, the optimum weight vector of the MVDR or MPDR is not entirely determined by the $ML \times 1$-dimensional vector $\mathbf{R}_{uu}^{-1}\mathbf{a}_1$ or $\mathbf{R}_{zz}^{-1}\mathbf{a}_m$, but also by the scalar factors $\tilde{\mathbf{a}}_1^H\mathbf{R}_{uu}^{-1}\tilde{\mathbf{a}}_1$ $\mathbf{a}_m^H\mathbf{R}_{zz}^{-1}\mathbf{a}_m$. By contrast, the optimum weight vector of the MSINR or MMSE beamformer is entirely determined by the $ML \times 1$-dimensional vector $\mathbf{R}_{uu}^{-1}\mathbf{a}_1$ or $\mathbf{R}_{zz}^{-1}\mathbf{a}_m$. Hence, after combining the signals $z_v$ in (2.82), the presence of the scalars $\mathbf{a}_1^H\mathbf{R}_{uu}^{-1}\mathbf{a}_1$ or $\mathbf{a}_m^H\mathbf{R}_{zz}^{-1}\mathbf{a}_m$ may result in dramatically scaling the decision variable $z$ in (2.83). Furthermore, the performance of the optimum MVDR and MPDR combiner separately processing the subcarrier signals is even worse than that of the MRC scheme. When employing the joint subcarrier processing based optimum MVDR or MPDR combiner, we arrive at the decision variable $z = \mathbf{w}_{MVDR}^H\mathbf{z}$ directly, without invoking the combining procedure described in (2.83). Hence, the joint subcarrier processing based optimum MVDR or MPDR combiner is capable of achieving a significantly better performance, than the individual subcarrier-based optimum MVDR or MPDR combiner. However, scaling by the scalar factors of $\mathbf{a}_1^H\mathbf{R}_{uu}^{-1}\mathbf{a}_1$ or $\mathbf{a}_m^H\mathbf{R}_{zz}^{-1}\mathbf{a}_m$ is still present, although its effect is less dominant in the joint subcarrier processing based optimum MVDR or MPDR combiner, because after the summation operation in (2.83) the scaling by the scalars $\mathbf{a}_1^H\mathbf{R}_{uu}^{-1}\mathbf{a}_1$ or $\mathbf{a}_m^H\mathbf{R}_{zz}^{-1}\mathbf{a}_m$ is enhanced. The performance of the joint subcarrier processing based optimum MVDR or MPDR combiner is worse than that of the joint subcarrier based processing aided optimum MSINR and MMSE combiners. Finally, in this simulation, we have $\mathbf{a}_m = \mathbf{a}_1$. Hence the performance of the MVDR optimum combiner is similar to that of the MPDR optimum combiner.

Below we will discuss the performance of the generalized MC DS-CDMA system communicating over a single-path non-dispersive Rayleigh fading channel contaminated by AWGN employing 31-chip Gold codes as time-domain spreading sequences and 4-chip Walsh codes as frequency-domain spreading codes. We have four subcarriers, as seen in Figures 2.13, 2.14, 2.15 and 2.16. Specifically, in Figures 2.13 and 2.14, we assume that we have $\Gamma_k = 0, i = 2, 3, \ldots, K$, and we use a $3 \times 1$-dimensional linear antenna array ($M = 1, L = 3$), having an element-spacing of $\lambda/2$. Four users are supported in this scenario, namely, the desired user and three interfering users, all adopting the same Gold code as their time-domain spreading sequence, but using different Walsh codes as their frequency-domain spreading codes. It transpires from Figures 2.13 and 2.14, that the

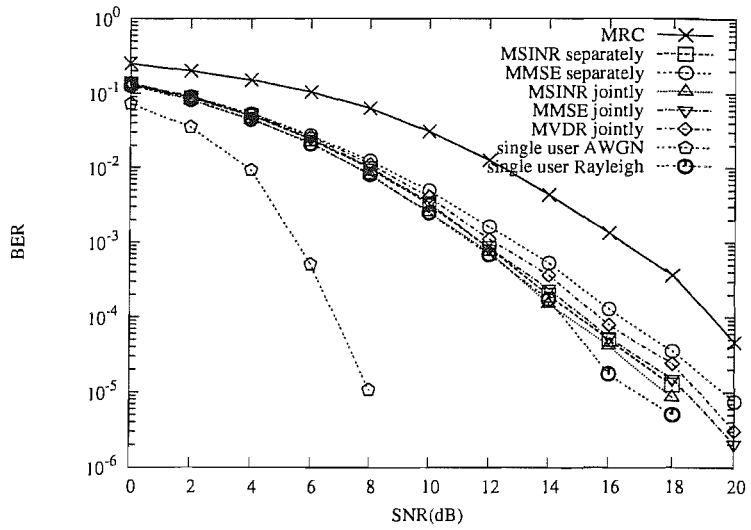


**Figure 2.13:** BER versus SNR performance of the uplink of a generalized MC DS-CDMA wireless system supporting 4 users using 31-chip Gold codes as time spreading sequences and 4-chip Walsh codes as frequency spreading sequences, using a $1 \times 3$-dimensional antenna array ($M = 1, L = 3$), different optimum combiners based on beamforming schemes of Section 2.3.1. The four users use the same Gold code as time spreading sequence while using different Walsh codes as frequency spreading sequences.

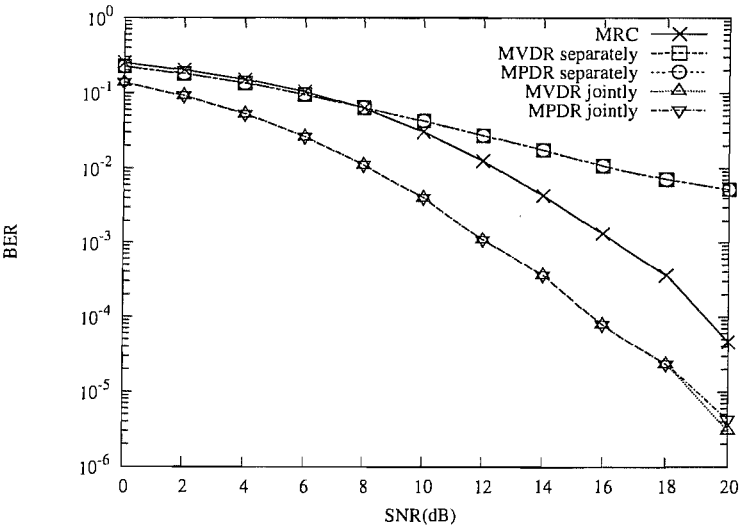


**Figure 2.14:** BER versus SNR performance of the uplink of a generalized MC DS-CDMA wireless system supporting 4 users using 31-chip Gold codes as time spreading sequences and 4-chip Walsh codes as frequency spreading sequences, employing a $1 \times 3$-dimensional antenna array ($M = 1, L = 3$), different optimum combiners based on beamforming schemes of Section 2.3.1. The four users use the same Gold code as time spreading sequence while using different Walsh codes as frequency spreading sequences.

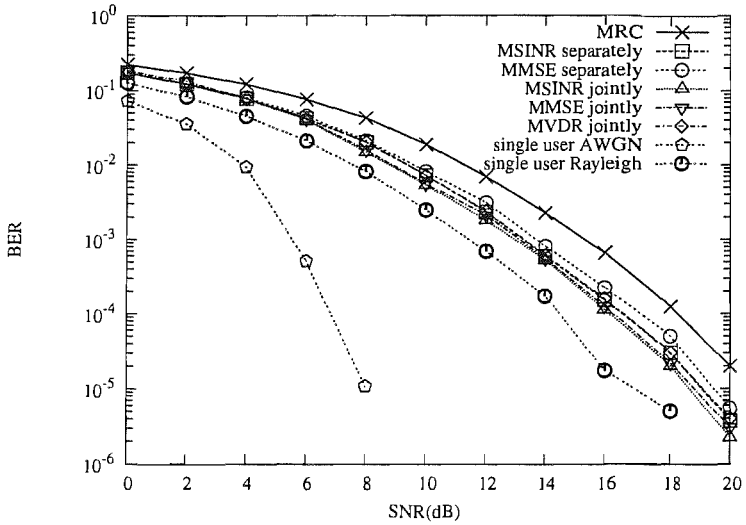


**Figure 2.15:** BER versus SNR performance of the uplink of a generalized MC DS-CDMA wireless system supporting 62 users using 31-chip Gold codes as time spreading sequences and 4-chip Walsh codes as frequency spreading sequences, using a $1 \times 3$-dimensional antenna array ($M = 1, L = 3$), different optimum combiners based on beamforming schemes of Section 2.3.1.

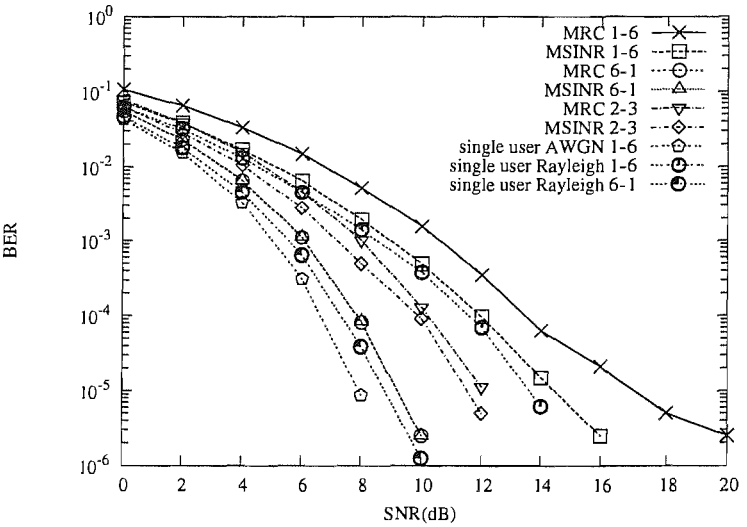


**Figure 2.16:** BER versus SNR performance of the uplink of a generalized MC DS-CDMA wireless system supporting 16 users using 31-chip Gold codes as time spreading sequences and 4-chip Walsh codes as frequency spreading sequences, using different antenna arrays, different optimum combiners based on beamforming schemes of Section 2.3.1.

performance of the joint subcarrier processing based optimum MSINR combiner is better than that of the joint subcarrier processing based optimum MMSE combiner. Furthermore, the performance of the individual subcarrier-based optimum MSINR combiner is better than that of the individual subcarrier-based optimum MMSE combiner. Again, note in (2.115), that the optimum weight vector of the MSINR beamformer is determinated by the interference-plus-noise correlation matrix $\mathbf{R}_{uu}$, while the optimum weight vector of the MMSE scheme is based on the entire post-decorrelation signal's correlation matrix $\mathbf{R}_{zz}$, as seen in (2.129) and (2.131), respectively. Hence the presence of the entire post-decorrelation signal's correlation matrix $\mathbf{R}_{zz}$ may result in a more substantial effect on the array weight vector than that of the interference-plus-noise correlation matrix $\mathbf{R}_{uu}$, as observed in Equations (2.93) and (2.88). Figures 2.13 and 2.14 also demonstrate that the performance of the joint subcarrier processing based optimum combiner is better than that of the individual subcarrier-based optimum combiner. However, the matrix $\mathbf{R}_{uu}$ processed by the joint subcarrier processing based optimum combiner is $VML \times VML$-dimensional, while the $V$ matrices $\mathbf{R}_{uu,v}$ processed by the individual subcarrier-based optimum combiner are $ML \times ML$-dimensional. Hence, the computational complexity imposed by the inversion of the matrix $\mathbf{R}_{uu}$ on the joint subcarrier processing based optimum combiner is significantly higher than that of the inversion of the matrix $\mathbf{R}_{uu,v}$ carried out $V$ times by the individual subcarrier-based optimum combiner. In Figure 2.15 we support 62 users, namely, the desired user and 61 interfering users. We can classify the 61 interfering users into two groups by assigning them different spreading sequences. In the first group, the interfering users employ the same 4-chip Walsh code as that adopted by the desired user as their frequency-domain spreading sequence, but they employ different 31-chip Gold codes as their time-domain spreading codes. By contrast, all the interfering users belonging to the other user group employ a different, but to this group common, 4-chip Walsh code as their frequency-domain spreading sequence, in spite of the Gold codes employed by them as their time-domain spreading sequences. Again, we assume having $\Gamma_k = 0, i = 2, 3, \ldots, K$ and we use a $3 \times 1$-dimensional linear antenna array ($M = 1, L = 3$), having an element-spacing of $\lambda/2$. The performance of this scenario is similar to that of the former generalized MC DS-CDMA system supporting four users characterized in Figure 2.13, except that the performance difference among the various optimum combiners decreases. The reason for this performance trend is that upon increasing the number of users, the correlation matrix of the interference-plus-noise becomes similar to an identity matrix, and accordingly, the weighting process imitates MRC. Therefore the associated performance difference decreases. In Figure 2.16 we support 16 users, namely, the desired user and 15 interfering users. The interfering users employ the same 4-chip Walsh code as that adopted by the desired user as their frequency-domain spreading sequence, but invoke different 31-chip Gold codes as their time-domain spreading codes. Again, we assume that we have $\Gamma_k = 0, i = 2, 3, \ldots, K$. In this scenario, we consider three different antenna arrays. The first antenna array is a $6 \times 1$-dimensional linear antenna array associated with ($M = 1, L = 6$), having an element-spacing of $\lambda/2$. The second is a $6 \times 1$-dimensional linear antenna array ($M = 6, L = 1$), having an array-spacing of $10\lambda$. The third is a $6 \times 1$-dimensional array ($M = 2, L = 3$), having an element-spacing of $\lambda/2$ and an array-spacing of $10\lambda$. The number of the arrays is denoted by $M$

and $L$ is the number of elements in the array, as seen in Figure 2.4. Figure 2.16 shows that when the spatial signals arriving at the elements of an antenna array are less correlated, the attainable spatial diversity becomes higher, hence, the performance is better. Figure 2.16 also demonstrates that when the correlation between the signals arriving at the different elements of an antenna array decreases, the performance difference between the MRC scheme and the optimum combiner also reduces. Therefore, the system employing a 6 $\times$ 1-dimensional linear antenna array ($M = 6, L = 1$) having an array-spacing of $10\lambda$ achieves the best result. By contrast, there is no appreciable difference between the performance of the MRC scheme and the MSINR beamformer. Furthermore, the system adopting a 6 $\times$ 1-dimensional antenna array ($M = 2, L = 3$), having an element-spacing of $\lambda/2$ and an array-spacing of $10\lambda$ achieves a mediocre performance. On the same note, the difference between the performance of the MRC scheme and the MSINR beamformer is also mediocre. Finally, the performance of the system using a 6 $\times$ 1-dimensional linear antenna array ($M = 1, L = 6$), having an element-spacing of $\lambda/2$ is the worst and the associated performance difference between the MRC scheme and the MSINR beamformer is the highest. In Figures 2.17, 2.18 and 2.19, we consider a generalized MC DS-CDMA system serving 4 users, where the joint subcarrier processing based optimum MSINR combining scheme of Section 2.3.3 was employed. Different antenna arrays were employed in these simulations, namely a single antenna ($M = 1, L = 1$), a 1 $\times$ 2-dimensional antenna array ($M = 1, L = 2$), a 1 $\times$ 3-dimensional antenna array ($M = 1, L = 3$), a 1 $\times$ 4-dimensional antenna array ($M = 1, L = 4$), a 1 $\times$ 6-dimensional antenna array ($M = 1, L = 6$), a 1 $\times$ 8-dimensional antenna array ($M = 1, L = 8$), a 2 $\times$ 1-dimensional antenna array ($M = 2, L = 1$), a 3 $\times$ 1-dimensional antenna array ($M = 3, L = 1$), a 4 $\times$ 1-dimensional antenna array ($M = 4, L = 1$), a 6 $\times$ 1-dimensional antenna array ($M = 6, L = 1$), a 8 $\times$ 1-dimensional antenna array ($M = 8, L = 1$), a 2 $\times$ 2-dimensional antenna array ($M = 2, L = 2$), a 2 $\times$ 3-dimensional antenna array ($M = 2, L = 3$), a 2 $\times$ 4-dimensional antenna array ($M = 2, L = 4$), a 3 $\times$ 2-dimensional antenna array ($M = 3, L = 2$) and a 4 $\times$ 2-dimensional antenna array ($M = 4, L = 2$). Figures 2.17, 2.18 and 2.19 confirms that when the spatial signals arriving at the different elements of the antenna array become less correlated, the achievable spatial diversity gain becomes higher, hence, the achievable performance improves.

## 2.4 Conclusions

In this chapter we have proposed four different beamformers based on the MVDR, MSINR, MMSE and MPDR array element optimization criteria, which were invoked for a DS-CDMA system, MC-CDMA system, and a generalized MC DS-CDMA system. In Section 2.1, we provided a brief introduction to various research contributions on MC DS-CDMA schemes. Following a rudimentary overview of Multitone DS-CDMA [43] and orthogonal MC DS-CDMA [12], we outlined the basic philosophy of generalized MC DS-CDMA [40–42].

In Section 2.2 the philosophy of the Generalized Multicarrier DS-CDMA system was detailed and characterized. The transmitter schematic was portrayed in Figure 2.2 for the generalized MC DS-CDMA system considered, while the corresponding stylized spectrum arrangement was shown

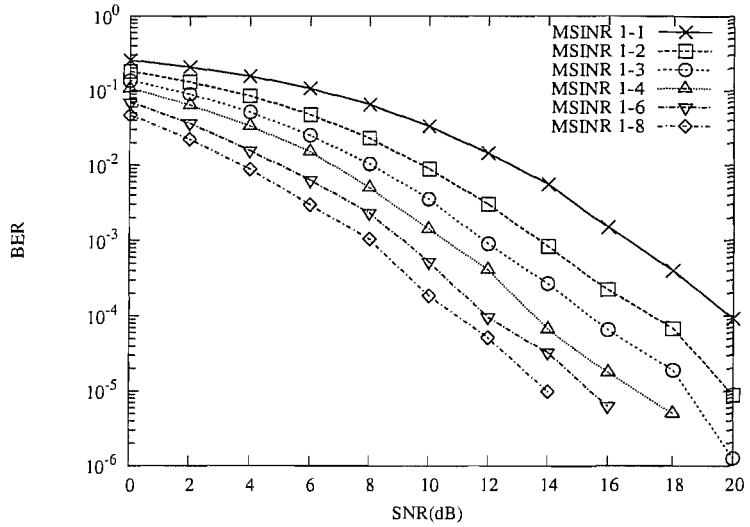


**Figure 2.17:** BER versus SNR performance of the uplink of a generalized MC DS-CDMA wireless system supporting 4 users using 31-chip Gold codes as time spreading sequences and 4-chip Walsh codes as frequency spreading sequences, using different antenna arrays, where the joint subcarrier processing based optimum MSINR combining scheme of Section 2.3.3 was employed.

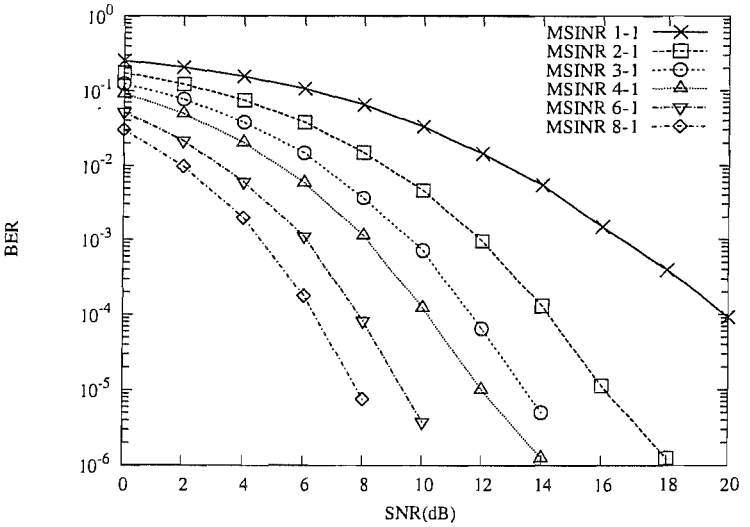


**Figure 2.18:** BER versus SNR performance of the uplink of a generalized MC DS-CDMA wireless system supporting 4 users using 31-chip Gold codes as time spreading sequences and 4-chip Walsh codes as frequency spreading sequences, using different antenna arrays, where the joint subcarrier processing based optimum MSINR combining scheme of Section 2.3.3 was employed.

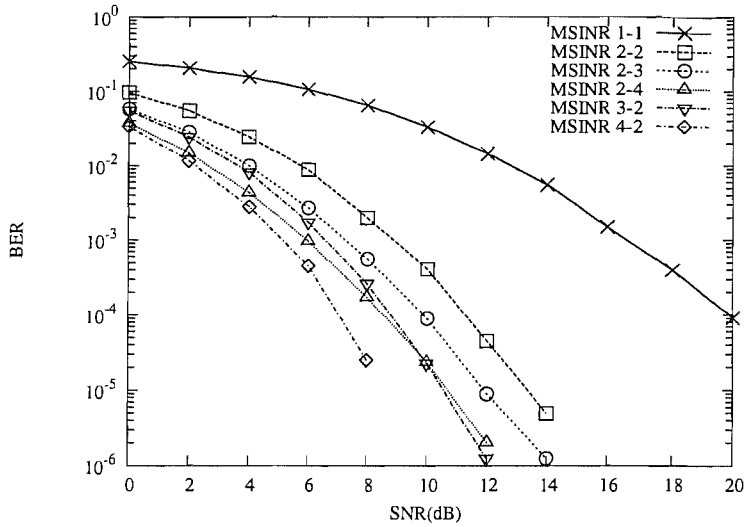


**Figure 2.19:** BER versus SNR performance of the uplink of a generalized MC DS-CDMA wireless system supporting 4 users using 31-chip Gold codes as time spreading sequences and 4-chip Walsh codes as frequency spreading sequences, using different antenna arrays, where the joint subcarrier processing based optimum MSINR combining scheme of Section 2.3.3 was employed.

in Figure 2.3. The $(M \times L)$-dimensional antenna array seen in Figure 2.4 was employed by the generalized MC DS-CDMA system considered for the sake of achieving both an SNR gain and spatial diversity gain. Finally, Figure 2.5 portrayed the receiver block diagram designed for detecting the information arriving from the reference user. In Section 2.2.4 we characterized the properties of the decision variable $\mathbf{z}_u$ expressed in Equation (2.18), while in Section 2.2.5 we derived the covariance matrix $\mathbf{R}_j$ of the composite interference given by the sum of the self-interference and multiuser interference.

Having provided the detailed system model of the generalized MC DS-CDMA system, we invoked a range of linear combining based antenna array weight optimization schemes in order to derive the decision variables in Section 2.3. In the context of optimum combining [44] the signals received by the antennas are appropriately weighted and combined in order to combat the effect of multipath fading on the desired signal and for the sake of mitigating the effects of interfering signals, as seen in the Figure 2.6. In Section 2.3.1, we first outlined the basic philosophy of optimum combiners classically used in digital mobile radio systems dispensing with DS-spreading, where the array weights that maximized the output SINR were expressed in Equation (2.61) [191]. Then, the family of optimum combiners designed for DS-CDMA systems was reviewed. We provided the expression of the weights that maximized the output SINR, as seen in Equation (2.72) [125]. Finally, we focused our attention on the derivation of the optimum array weight vector employed by the proposed MC DS-CDMA system. The individual subcarrier-based optimum combiner adopted for the generalized MC DS-CDMA system of Figure 2.5 was first derived by separately processing the $V$ number of received subcarrier signals hosted by the $(ML \times 1)$-dimensional vector. The operations

carried out by this individual subcarrier-based optimum combiner was portrayed in Figure 2.9. On the other hand, the optimum combiner can also be derived by jointly processing the received signal of the $VML$-dimensional received signal vectors of the $V$ subcarriers and $ML$ array elements, as seen in Figure 2.10. In Section 2.3.2 the optimum combiner based on the MVDR criterion was derived, which constitutes a well-known beamforming optimization criterion [44] and is capable of providing the minimum variance unbiased estimate of the transmitted signal. In Section 2.3.3 we discussed the optimum combiner based on the MSINR criterion, where the weight vector is optimized by maximizing the SINR at the output of the beamformer [44]. In Section 2.3.4 we focused our attention on the MMSE beamformer, which is capable of minimizing the mean-square error between the beamformer output and the desired signal. The beamformer based on the MPDR criterion [44] was considered in Section 2.3.5, which is closely related to the MVDR beamformer.

In Section 2.3.6, the BER performance of these four optimum combining schemes was studied and compared in the context of a DS-CDMA system, a MC-CDMA system and a generalized MC DS-CDMA system. We employed several different antenna array models in our simulations. From the simulation results and the accompanying analysis we concluded that as expected, the performance of the different beamformers is different. For example, the MVDR optimum combiner is the best one in the context of a DS-CDMA system, while the individual subcarrier-based optimum MVDR combiner exhibits the poorest performance in the context of the MC-CDMA system of Figure 2.7 or in the generalized MC DS-CDMA system of Figure 2.2. When the number of the users increases, the correlation matrix $\mathbf{R}_{uu}$ or $\mathbf{R}_{zz}$ becomes reminiscent of an identity matrix. Accordingly, the weighting process becomes reminiscent of the MRC scheme. Having investigated a range of different antenna array models in Figure 2.20(a), we found that when the spatial signals arriving at the different elements of the antenna array become less correlated, the achievable spatial diversity gain becomes higher, hence the achievable performance improves. Furthermore, when the correlation of the signals arriving at the different elements of the antenna array decreases, the performance difference between the MRC scheme and the optimum combiners will reduce. A summary of the associated results is provided in Table. 2.1 for the sake of characterizing and comparing the attainable BER performance of all optimum combining schemes invoked for the uplink of the generalized MC DS-CDMA system supporting four users. The four users employ the same Gold code as their time-domain spreading sequence, while using different Walsh codes as frequency-domain spreading sequences. Finally, the computational complexity of the corresponding optimum beamforming aided generalized MC DS-CDMA systems is provided in Figure 2.20(b).

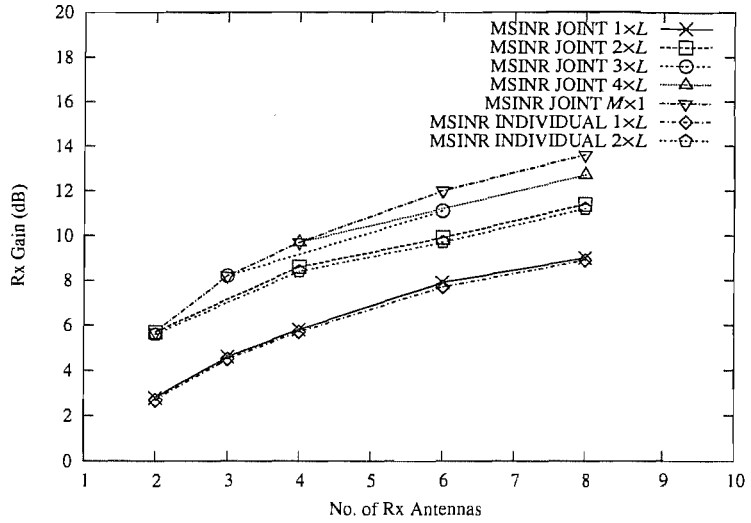


(a)

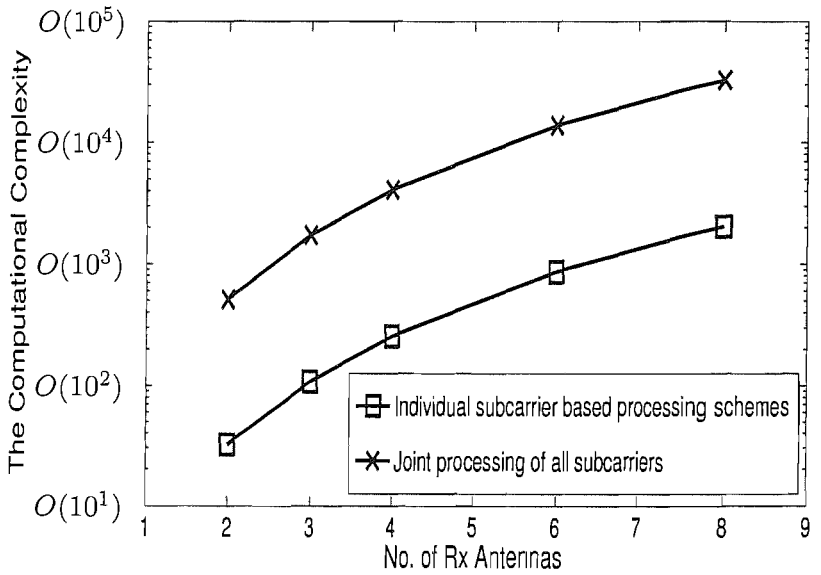


(b)

**Figure 2.20:** (a) Receive (Rx) gain versus the number of receive antennas for the various antenna array types employed for the uplink of the MSINR-aided generalized MC DS-CDMA system supporting four users at a BER of $10^{-4}$. These results were extracted from Figures 2.17, 2.18 and 2.19. (b) The computational complexity versus the number of receive antennas for the various antenna array types employed for the uplink of the optimum beamforming-aided generalized MC DS-CDMA system employing $V = 4$ subcarriers based on both individual subcarrier based processing and on using joint processing of all subcarriers, as outlined in Section 2.3.1.4. Since the corresponding Rx gain recorded in Figure 2.20(a) for the joint processing of all subcarriers is only marginally better than that of the substantially less complex individual subcarrier processing, the latter is recommended for practical implementations.

| Scheme | | $E_b/N_0$(dB) required at BER=$10^{-2}$ | $E_b/N_0$(dB) required at BER=$10^{-4}$ | Figure No. |
|---|---|---|---|---|
| MRC | | 12.5 | 19.2 | Figure 2.13 |
| MSINR | Jointly | 8.1 | 14.6 | Figure 2.13 |
| | Separately | 8.2 | 15.0 | Figure 2.13 |
| MVDR | Joint | 8.3 | 15.8 | Figure 2.14 |
| | Separately | 16.0 | N/A | Figure 2.14 |
| MMSE | Joint | 8.2 | 15.2 | Figure 2.13 |
| | Separately | 8.5 | 16.4 | Figure 2.13 |
| MPDR | Joint | 8.4 | 15.8 | Figure 2.14 |
| | Separately | 16.1 | N/A | Figure 2.14 |

**Table 2.1:** Summary of the required $E_b/N_0$ values for the various optimum combining schemes characterized in Figures 2.13 and 2.14 invoked for the uplink of the generalized MC DS-CDMA system supporting four users, employing a $(1 \times 3)$-dimensional antenna array ($M = 1, L = 3$). The four users employ the same Gold code as their time-domain spreading sequence, while using different Walsh codes as frequency-domain spreading sequences.

# Chapter 3

# Multicarrier DS-CDMA Systems Using Smart Antennas - Downlink

## 3.1 Introduction

In chapter 2 we presented a generalized MC DS-CDMA system [41,42] supported by smart antennas for the sake of improving the attainable uplink performance of the system at the base station. However, the antenna arrays installed at the base-station may also be used both in the downlink as well as in the uplink for enhancing the system's performance. More explicitly, it is possible to steer a transmitting array in the same way as the one used for reception, so as to minimize the downlink interference inflicted upon co-channel mobiles. There are two fundamental approaches to preprocess each user's signal at the base station's downlink transmitter. The so-called open loop methods do not require any knowledge of the radio channel at the transmitter, while the family of closed loop methods exploit the characteristics of the channel. The open loop techniques that rely on no channel information are desirable for the sake of simplicity, but they are outperformed by the more sophisticated closed loop techniques, as long as the channel information is correct and up-to-date, rather than outdated. Various transmit diversity (TD) schemes have been proposed in the literature [48, 126–134, 136] for the sake of mitigating the performance degradation inflicted by multipath fading. Again, the family of TD schemes may be divided into the classes of open loop TD and the closed loop TD, and the open-loop family may be further classified as Orthogonal Transmit Diversity (OTD) [128], Time Switched Transmit Diversity (TSTD) [128], and Space-Time Transmit Diversity (STTD) [48]. Both the OTD and TSTD schemes use multiple transmit antennas for providing spatial interleaving against fading, hence they have a similar performance [127], provided that the different antennas experience independent fading. Upon exploiting the extra space diversity provided by employing additional diversity antennas, STTD schemes [48] are capable of outperforming both OTD and TSTD [131]. Selection Transmit Diversity (STD), a representative of closed loop proposals, selects the specific antenna for transmission, which has the best instantaneous channel quality and hence this technique is expected to be superior to STTD in most cases, as long as the transmit antenna specific channel quality infor-

mation can be correctly fed back to the transmitter without excessive latency [129, 130]. On the other hand, in addition to channel-induced fading, the received signal at the MS is also corrupted by MAI. Beamforming, or spatial filtering [6] constitutes an effective solution to this problem, where the antenna gain is increased in the direction of the desired user, whilst reducing the gain towards interfering users. The simplest approach to beamforming is represented by the switched-beam technique, which measures a particular user's uplink power received, for example, by a bank of narrow beams, and then uses the highest-power beam for downlink transmission to that particular user [133]. In [126], Zhou provided a comparison between switched-beam transmission and STD, where the results indicated that conventional beamforming is capable of outperforming STD in interference-limited scenarios, but only if some grade of temporal diversity is also available. Let us now briefly consider downlink beamforming. There are techniques, which simply direct the main lobe to the desired user without considering the interference imposed upon other users [134, 135], and methods which form the beam with a high gain towards the desired user, while creating nulls in the directions of the undesired users [132, 136]. They are both capable of achieving user-load improvements in the downlink by reducing the effects of MAI.

Using the antenna arrays shown in Figure 2.4, both TD and beamforming can be implemented at the Base Station (BS). The $M$ antenna arrays having an array-spacing of $10\lambda$ are widely separated from each other for the sake of forming a transmit diversity scheme, since the system experiences low correlation among these arrays, while the $L$ elements having an element-spacing of $\lambda/2$ create a beamforming antenna array. The beam selection transmit diversity (BSTD) scheme of [47] constitutes a combination of STD and beamforming, while the downlink eigenbeamformer [194] represents an alternative approach, which combines the gain of spatial filtering with beam selection diversity. In [49], three techniques have been described, based on diversity, spatial beamforming, and a combination of diversity as well as beamforming, which was referred to as Steered Space-Time Spreading (SSTS).

However, the SSTS scheme of [49] and many other transmit diversity schemes, such as those proposed in [48, 126, 136, 140], are based on the assumption that perfect Channel State Information (CSI) is available at the receiver. The estimation accuracy of the CSI has a grave impact on the attainable detection performance. Naturally, the estimation of these parameters increases the complexity imposed and typically requires a substantial channel sounding overhead, which wastes valuable bandwidth. Furthermore, when the Channel Impulse Response (CIR) fades rapidly, its estimation based on the previous symbols might be insufficiently accurate for the reliable detection of the forthcoming symbols. By contrast, Differential Space-Time Modulation (DSTM) schemes [137–139], introduced as extensions of the traditional Differential Phase Shift Keying (DPSK) scheme, were capable of reliable data detection without any CSI, which is an attractive feature in fast fading channels. Hence, DSTM schemes obviate the need for channel estimation at the receiver, while retaining the desirable benefits of space-time coding techniques. However, the performance of DSTM systems degrades significantly in the presence of even relatively mild interference and breaks down completely, when strong interference is inflicted [141]. To suppress the effects of co-channel interference when communicating

over flat fading channels, a Differential Space-Code Modulation (DSCM) scheme was proposed by combining the merits of the DSTM and spread spectrum techniques in [141].

In this chapter, we will continue our discourse by considering the generalized MC DS-CDMA system of Chapter 2. Four different downlink space-time transmitter processing schemes based on the principles of beamforming, BSTD, STTD and SSTS are proposed, in order to enhance the achievable performance of generalized MC DS-CDMA systems. Furthermore, we combine the merits of DSTM and the generalized MC DS-CDMA system of [41] to propose a novel Differential Space-Time Spreading (DSTS) scheme as well as a Differential Steered Space-Time Spreading (DSSTS) scheme for the sake of improving the downlink performance of generalized MC DS-CDMA systems communicating in rapidly fading channels. The proposed DSSTS scheme amalgamates the benefits of DSTS and beamforming. Our focus is on the performance enhancements that can be obtained on the downlink of a generalized MC DS-CDMA system with the aid of an antenna array architecture that supports a combination of beamforming and transmit diversity. The achievable performance improvements are a function of both the antenna spacing and the specific techniques used for attaining TD and beamforming. In our system, we employ 32-chip Walsh-Hadamard (WH) codes as Time-Domain (T-domain) spreading codes and 4-chip WH codes as Frequency-Domain (F-domain) spreading sequences. Since all users are synchronous in the downlink, the interference amongst users invoking different 32-chip WH codes as their user-specific time-domain spreading codes becomes zero after despreading in time-domain. However, the transmitted data stream can be spread both in the time-domain and in the frequency-domain in order to increase the user-load of the generalized MC DS-CDMA system and for the sake of achieving a higher frequency diversity [192]. Therefore, after despreading, the interference amongst the users employing the same 32-chip WH code as their time-domain spreading sequence, but invoking different 4-chip WH codes as frequency-domain spreading codes may become high. For the sake of mitigating this phenomenon, we can combine beamforming techniques with the careful assignment of the T-domain WH spreading codes.

The rest of this chapter has the following structure. In Section 3.2 the philosophy of the downlink beamforming-aided generalized Multicarrier DS-CDMA system is described and characterized. A BSTD scheme constituted by an amalgam of beamforming and STD is discussed and analyzed in the context of the generalized MC DS-CDMA system in Section 3.3. Then STTD is analyzed and its concept is extended for employment in the generalized MC DS-CDMA system considered. Based on STTD and beamforming, SSTS is adopted for employment in the generalized MC DS-CDMA system in Section 3.5. In Section 3.6 the downlink DSTS and DSSTS schemes are invoked for generalized Multicarrier DS-CDMA systems communicating over rapidly fading channels, both of which obviate the need for channel estimation at the receiver, while retaining the desirable benefits of space-time coding techniques. Finally, the performance of these schemes will be studied and compared in Section 3.7, again, in the context of the generalized MC DS-CDMA system concept advocated.

## 3.2 System Model for Downlink Communication - Beamforming

In the context of coherent beamforming, the signals that will be transmitted by several BS transmit antennas are appropriately weighted before transmission based on the channel information fed back from the MS with the aid of the uplink in order to steer the transmitted energy in the direction of the desired user. The beamforming schemes steering energy in the direction of the desired user are referred to as the user-specific beamforming. By contrast, the beamforming schemes, where a set of predefined beams shared by a number of roughly co-located users is termed as the fixed beamforming. In the context of downlink beamforming, if the downlink channel is in the same frequency band as the uplink, we can estimate the direction of a specific user and then calculate the required transmit beamformer weights from the received uplink signals. In this section, we assume that the direction of the desired user can be perfectly estimated. It can be shown that in the absence of scattering the beamforming gain of the coherent beamformer is linearly proportional to the number of array elements of $L$. When scattering is present, the attainable beamforming gain depends on the phase-coherence accuracy of the closely spaced transmit antennas. It can be shown that the attainable beamforming gain in environments having a small angular spread is higher than that in the context of larger angular spreads, since the grade of phase coherence between the array elements decreases.

The downlink transmission model of the space-time MC DS-CDMA system considered is similar to the uplink model described in Section 2.2. However, maintaining a sufficiently high spatial separation of users in the downlink is more difficult than that on the uplink. This is because in the context of downlink transmissions the mobiles cannot necessarily be expected to cooperate for the sake of carrying out joint detection or joint adaptive interference cancellation. Therefore, an attractive technique of achieving spatial separation in the downlink is to reduce the interference imposed on the $K$ users by performing spatial processing prior to transmission in the base-station transmitter equipped with antenna arrays. At the mobile receiver the processing is simply restricted to the temporal and frequency domains. Furthermore, in contrast to the uplink, each mobile user receives all the signals intended for the other users but distorted by its own radio channel. As in Chapter 2, let us assume that the first user is the desired user to be detected and the first user's time delay $\tau_1$ is perfectly estimated.

### 3.2.1 Transmitted Signal - Downlink

The block diagram of the downlink BS transmitter schematic configured for transmitting to the $k$th user is shown in Figure 3.1 for the generalized MC DS-CDMA system employing a transmit antenna array, which has $L$ number of linearly spaced elements separated by a distance of half a wavelength. At the transmitter side, the binary data stream having a bit duration of $T_b$ is Serial-to-Parallel (S/P) converted to $U$ parallel sub-streams. The new bit duration of each sub-stream, which we refer to as the symbol duration, becomes $T_s = UT_b$. After S/P conversion, each substream is spread using an $N$-chip DS spreading sequence waveform $c_k(t)$. Then, the DS spread signal of the $u$th sub-stream, where we have $u = 1, 2, \ldots, U$, simultaneously modulates a group of parallel subcarrier frequencies $\{f_{u1}, f_{u2}, \ldots, f_{uV}\}$ using Binary Phase Shift Keying (BPSK). A total of $UV$ number of

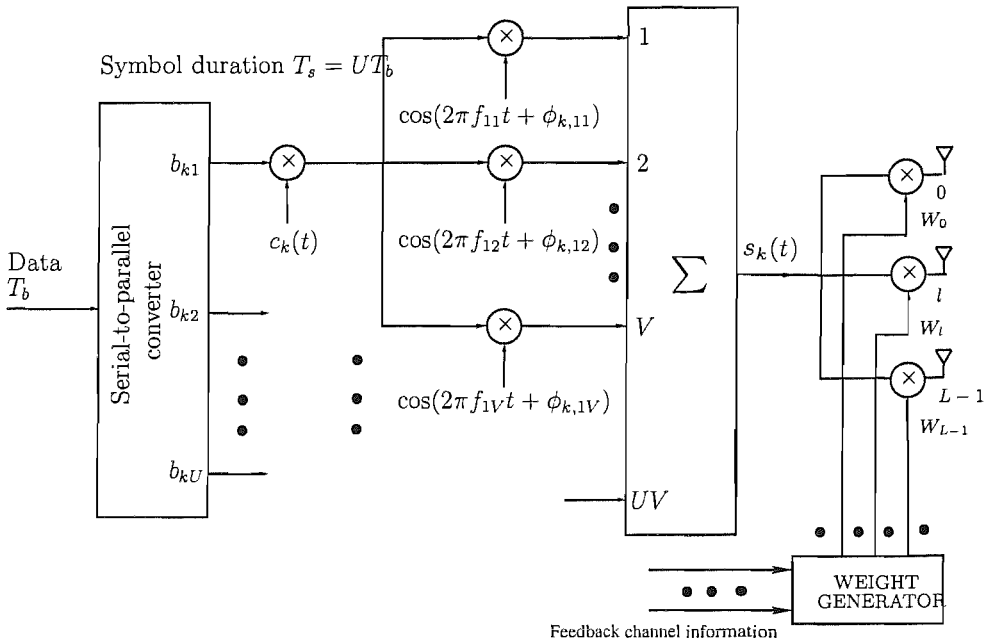


**Figure 3.1:** The $k$th user's transmitter schematic for the downlink of the generalized multicarrier DS-CDMA system. In contrast to Figure 2.2, where the transmitted signal $s_k(t)$ of user $k$ is transmitted from a single antenna, in This figure, a BS transmit weight vector $\mathbf{w}_v^{(k)}$ is applied to the signal associated with the $v$th subcarrier of the $k$th user at the BS's downlink transmit beamformer.

subcarriers are required by the MC DS-CDMA system considered and the $UV$ subcarrier signals are superimposed on each other in order to form the complex modulated signal. The baseband downlink MC DS-CDMA signal prior to transmit beamforming is identical to the uplink transmit signal, as described in Equation (2.1). In contrast to Figure 2.2, where the transmitted signal $s_k(t)$ of user $k$ is transmitted from a single antenna, in Figure 3.1 a BS transmit weight vector $\mathbf{w}_v^{(k)}$ is applied to the signal associated with the $v$th subcarrier of the $k$th user at the BS's downlink transmit beamformer, so that the $(L \times 1)$-dimensional MC DS-CDMA signal vector of the $k$th user at the beamformer's output becomes

$$\begin{aligned} \mathbf{s}_k(t) &= (\mathbf{w}_v^{(k)})^H \bullet s_k(t) \\ &= \sum_{u=1}^{U}\sum_{v=1}^{V} \sqrt{\frac{2P_k}{VL}} (\mathbf{w}_v^{(k)})^H b_{ku}(t) c_k(t) \cos(2\pi f_{uv} t + \phi_{k,uv}), \end{aligned} \tag{3.1}$$

where $\mathbf{w}_v^{(k)}$ is a $(L \times 1)$-dimensional BS downlink transmit weight vector generated by the beamformer according to the perfect known channel information corresponding to the $v$th subcarrier of the $k$th user, while $P_k/V$ represents the transmitted power of each subcarrier, and the factor of $L$ in the denominator of (3.1) is due to the beamforming using an antenna array having $L$ elements. Furthermore, in (3.1) $\{b_{ku}(t)\}$, $c_k(t)$, $\{f_{uv}\}$ and $\{\phi_{k,uv}\}$ represent the data stream, the DS spreading waveform, the subcarrier frequency set and the phase angles introduced in the carrier modulation

process. The data stream's waveform $b_{ku}(t) = \sum_{i=-\infty}^{\infty} b_{ku}[i]P_{T_s}(t - iT_s)$ consists of a sequence of mutually independent rectangular signalling pulses of duration $T_s$ and of amplitude +1 or -1 with equal probability. The spreading sequence $c_k(t) = \sum_{j=-\infty}^{\infty} c_{kj}P_{T_c}(t - jT_c)$ denotes the signature sequence waveform of the $k$th user, where $c_{kj}$ assumes values of +1 or -1 with equal probability, while $P_{T_c}(t)$ is the rectangular chip waveform, which is defined over the interval $[0, T_c)$. We assume that $N_e = T_s/T_c = UT_b/T_c$, which represents the spreading gain of the DS-spread subcarrier signals.

The stylised spectral arrangement on the downlink is also identical to that on the uplink, which was shown in Figure 2.3. The subcarrier frequencies of the downlink are also arranged according to $f_{uv} = \frac{1}{T_c} + \Delta\left[(v-1)U + u - 1\right]$, $u = 1, 2, \ldots, U$; $v = 1, 2, \ldots, V$, so that the specific subcarrier frequencies conveying the $V$ number of repeated replicas of the same data bit are separated by the maximum possible frequency spacing for the sake of experiencing independent fading. More explicitly, with the advent of maximum spacing the $V$ replicas of the same bit are far apart in the frequency-domain, hence the receiver becomes capable of achieving the maximum frequency-domain diversity gain as a benefit of the independent frequency-selective fading of the subcarriers, when combining the corresponding subcarrier signals.

### 3.2.2 Receiver Model - Downlink

For each mobile user, the multiplexed transmitted signal intended for all of the $K$ active users is received, and it is subjected to distortion by the wireless channel associated with the particular user. Assuming that the transmitter antenna array shown in Figure 2.4 is configured by the base-station for downlink transmission, the Spatio-Temporal (ST) Channel Impulse Response (CIR) $h_{uv,l}^{(k)}$ between the $uv$th subcarrier of the $k$th user and the $l$th BS downlink transmit antenna can be expressed in the same form as Equation (2.10)in conjunction with $M = 1$. Consequently, the signal received by the first user, who is the desired user, due to the BS's transmission intended for the $k$th user is given by

$$\begin{aligned} r_k(t) &= \mathbf{s}_k(t) \otimes \mathbf{h}_{uv}^{(1)}(t) \qquad (3.2) \\ &= \sum_{u=1}^{U}\sum_{v=1}^{V} \sqrt{\frac{2P_k}{VL}}\, b_{ku}(t-\tau_1)c_k(t-\tau_1)(\mathbf{w}_v^{(k)})^H \mathbf{a}_{uv}^{(1)}(t) \exp\left(j\left[2\pi f_{uv}t + \theta_{uv}^{(k)}\right]\right), \end{aligned}$$

where we have $\theta_{uv}^{(k)} = \phi_{k,uv} - 2\pi f_{uv}\tau_1$, which is a random variable uniformly distributed in $[0, 2\pi]$. In the above equation, we assumed that all the subcarrier signals arrive from the same direction. i.e. the DOA is only dependent on the user's location, but it is independent of the subcarrier frequencies. We note that this assumption is valid only, if the bandwidth of the MC DS-CDMA system considered is significantly lower than the carrier frequency $f_c$. In (3.2) the ST-CIRs corresponding to the entire set of $L$ elements of the BS's downlink transmit antenna array $\mathbf{h}_{uv}^{(1)}(t)$ is the same as in Equation (2.14) associated with $M = 1$, except that only the first user is considered. Hence $\mathbf{h}_{uv}^{(1)}(t)$ can now be

expressed as

$$\begin{aligned}\mathbf{h}_{uv}^{(1)}(t) &= \left[h_{uv,0}^{(1)}(t), h_{uv,1}^{(1)}(t), \ldots, h_{uv,(L-1)}^{(1)}(t)\right]^T \\ &= \mathbf{a}_{uv}^{(1)}(t)\delta(t-\tau_1) \\ &= \left[a_{uv,0}^{(1)}(t), a_{uv,1}^{(1)}(t), \ldots, a_{uv,(L-1)}^{(1)}(t)\right]^T \delta(t-\tau_1), \end{aligned} \tag{3.3}$$

which is an $(L \times 1)$-dimensional vector, where $a_{uv,l}^{(1)}(t)$ is the CIR with respect to the $uv$th subcarrier of the first user and the $l$th BS downlink array element. Based on the assumption that the array elements are separated by half a wavelength, i.e. that we have $d = \lambda/2$, we can simplify $\mathbf{a}_{uv}^{(1)}(t)$ to

$$\begin{aligned}\mathbf{a}_{uv}^{(1)}(t) &= \alpha_{uv}^{(1)}(t)\mathbf{d}^{(1)} \\ &= \alpha_{uv}^{(1)}(t)\,[1, \\ &\qquad \exp\left(j\left[\pi \sin(\psi^{(1)} + \kappa^{(1)}B)\right]\right), \ldots, \\ &\qquad \exp\left(j\left[(L-1)\pi \sin(\psi^{(1)} + \kappa^{(1)}B)\right]\right)\Big]^T. \end{aligned} \tag{3.4}$$

The total received signal of the first user is the superposition of all the $K$ users' transmissions plus the AWGN, hence we have

$$r(t) = \sum_{k=1}^{K} r_k(t) + n(t), \tag{3.5}$$

where $n(t)$ is an AWGN process having a zero mean and a covariance of

$$\mathrm{E}\left[n(t_1)n^*(t_2)\right] = 2N_0\delta(t_1 - t_2), \tag{3.6}$$

with $N_0$ representing the double-sided power spectral density of a complex valued low-pass-equivalent AWGN signal.

The receiver front-end of the downlink is shown in Figure 3.2, where the superscript and subscript denoting the reference user of $k = 1$ have been omitted for notational convenience. Observing both Figure 2.5 and Figure 3.2 suggests that the receiver of the downlink is similar to that of the uplink, except that each mobile receiver has only a single antenna. As shown in Figure 3.2, the receiver essentially consists of two main parts. The first part carries out multicarrier demodulation and DS despreading, providing $V$ number of outputs, which correspond to the $V$ number of subcarriers conveying the repeated replicas representing the same data bit. Therefore, associated with each transmitted data bit, such as bit $u$, we have a total of $V$ output variables, as shown in Figure 3.2, which carry the information of the same transmitted data bit. In the second part, after combining these $V$ number of variables with the aid of a MRC scheme, the decision variable related to the information bit $b_u[0]$ can be derived. This process will be discussed in detail during our forthcoming discourse in Section 3.2.3.

In our forthcoming discourse we assume that the receiver is capable of acquiring perfect time-

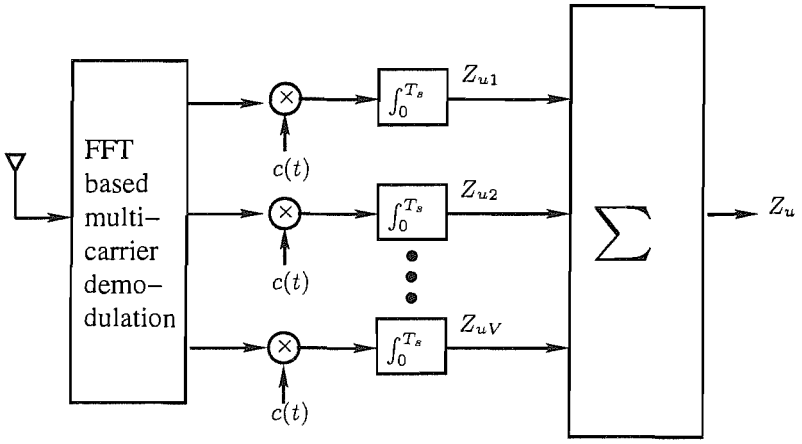


**Figure 3.2:** Receiver block diagram of mobile users in the generalized MC DS-CDMA system considered. The receiver employs multicarrier-spreading-assisted frequency-selective diversity combining. Observing both Figure 2.5 and this figure suggests that the receiver of the downlink is similar to that of the uplink, except that each mobile receiver has only a single antenna.

domain synchronization. The attenuations and phases of the ST CIR taps are assumed to be perfectly estimated. Furthermore, in this chapter we assume that the DOA of the reference user's signal is also known at the base-station. Returning to Figure 3.2, after multicarrier demodulation and DS despreading, the outputs corresponding to the 0th bit $b_u[0]$ and the $v$th subcarrier can be expressed as

$$z_{uv} = \int_0^{T_s} r(t)c(t)\exp\left(-j[2\pi f_{uv}t + \theta_{uv}]\right)dt,\ v = 1, 2, \ldots, V, \tag{3.7}$$

where for the sake of simplicity we assumed that the reference signal's transmission delay was $\tau_1 = 0$.

### 3.2.3 Statistical Analysis

In this section we first characterize the properties of the decision variable $z_{uv}$ expressed in (3.7). Let us first derive the components of $z_{uv}$. We assume that the ST CIR taps given by $\mathbf{a}_{uv}^{(1)}$ of Equation (3.3) remain constant over a symbol duration of $T_s$. Upon substituting the received signal vector $r(t)$ of (3.5) into (3.7), it can be shown that $z_{uv}$ expressed in terms of the $v$th subcarrier of $b_u$ can be written

as

$$z_{uv} = \sqrt{\frac{2P}{VL}}T_s \Bigg[ b_u[0](\mathbf{w}_v^{(1)})^H \mathbf{a}_{uv} + \underbrace{\sum_{u'=1}^{U}\sum_{v'=1}^{V}}_{v'\neq v,\ \text{if } u'=u} (\mathbf{w}_v^{(1)})^H \mathbf{i}_{u'v'}^{(s)} + n_{uv} + \sum_{k=2}^{K}\sqrt{\frac{P_k}{P}}(\mathbf{w}_v^{(k)})^H \mathbf{i}_{uv}^{(k)} + \sum_{k=2}^{K}\underbrace{\sum_{u'=1}^{U}\sum_{v'=1}^{V}}_{v'\neq v,\ \text{if } u'=u} \sqrt{\frac{P_k}{P}}(\mathbf{w}_v^{(k)})^H \mathbf{i}_{u'v'}^{(k)} \Bigg], \tag{3.8}$$

where $b_u[0](\mathbf{w}_v^{(1)})^H \mathbf{a}_{uv}$ represents the desired output obtained by substituting (3.5) into (3.7) and setting $k = 1$, $u' = u$, $v' = v$, while $\mathbf{a}_{uv}$ is given by (3.3) associated with the reference user corresponding to $k = 1$. In (3.8) $n_{uv}$ is contributed by $n(t)$ of (3.5), which can be expressed as

$$n_{uv} = \frac{1}{\sqrt{\frac{2P}{VL}}T_s}\int_0^{T_s} n(t)c(t)\exp\left(-j[2\pi f_{uv}t + \theta_{uv}]\right)dt, \tag{3.9}$$

which is an AWGN process having zero mean and a covariance of

$$\mathrm{E}\left[n_{uv}n_{uv}^*\right] = \frac{VLN_0}{E_b}, \tag{3.10}$$

where $E_b = PT_s$ represents the energy per bit. The term $(\mathbf{w}_v^{(1)})^H \mathbf{i}_{u'v'}^{(s)}$ in (3.8) represents the self-interference contributed by the subcarrier indexed by $u'$, $v'$ of the reference signal. As shown in Equation (2.27), $\mathbf{i}_{u'v'}^{(s)} = \mathbf{0}$, provided that we have $(f_{u'v'} - f_{uv}) = \frac{n}{T_s}$, implying that the subcarrier signals are orthogonal before the DS spreading, where $n \geq 1$ represents an integer. Therefore, we can conclude that

$$(\mathbf{w}_v^{(1)})^H \mathbf{i}_{u'v'}^{(s)} = 0. \tag{3.11}$$

The Multi-User Interference (MUI) term $(\mathbf{w}_v^{(k)})^H \mathbf{i}_{uv}^{(k)}$ in (2.22) is engendered by the subcarrier signal determined by $u$ and $v$ of the $k$th interfering user, where $\mathbf{i}_{uv}^{(k)}$ is similar to Equation (2.29), except that all users are synchronous and all $K$ transmitted signals are impaired by the radio channel $\mathbf{a}_{uv}$ associated with the desired user $k = 1$. Thus, the term $\mathbf{i}_{uv}^{(k)}$ can be expressed as

$$\mathbf{i}_{uv}^{(k)} = \frac{\mathbf{a}_{uv}\exp\left(j\vartheta_{uv}^{(k)}\right)}{T_s}\int_0^{T_s} b_{ku}(t)c_k(t)c(t)dt, \tag{3.12}$$

where we have $\vartheta_{uv}^{(k)} = \theta_{uv}^{(k)} - \theta_{uv}$.

Finally, the MUI term $(\mathbf{w}_v^{(k)})^H \mathbf{i}_{u'v'}^{(k)}$ in (3.8) is imposed by the subcarrier determined by $u'$ and $v'$

associated with the $k$th interfering user. In the downlink situation, $\mathbf{i}_{u'v'}^{(k)}$ can be expressed as

$$\mathbf{i}_{u'v'}^{(k)} = \frac{\tilde{\mathbf{a}}_{u'v'} \exp(\vartheta_{u'v'}^{(k)})}{T_s} \int_0^{T_s} b_{ku'}(t) c_k(t) c(t) \exp\left(j2\pi[f_{u'v'} - f_{uv}]t\right) dt, \tag{3.13}$$

where, again, we have $\vartheta_{u'v'}^{(k)} = \theta_{u'v'}^{(k)} - \theta_{uv}$. Similar to the self-interference term $\mathbf{i}_{u'v'}^{(s)}$ formulated in Equation (2.27), $\mathbf{i}_{u'v'}^{(k)} = \mathbf{0}$ can be derived, which results in

$$(\mathbf{w}_v^{(k)})^H \mathbf{i}_{u'v'}^{(k)} = 0. \tag{3.14}$$

Let

$$\mathbf{z}_u = [z_{u1}, z_{u2}, \ldots, z_{uV}]^T \tag{3.15}$$

be a $V$-length vector containing the entire set of $V$ number of decision variables in the context of the $u$th data bit after multicarrier demodulation and DS despreading. These $V$ number of variables are denoted in Figure 3.2 as $z_{uv}$ for $v = 1, 2, \ldots, V$, which is expressed in Equation (3.8). Therefore, after ignoring the common factor of $\sqrt{2P/VLT_s}$ in (3.8), we have

$$\mathbf{z}_u = (\mathbf{W}^{(1)})^H \mathbf{a}_u b_u[0] + \mathbf{n}_u + \mathbf{j}_u, \tag{3.16}$$

where $\mathbf{a}_u = [\mathbf{a}_{u1}^T, \mathbf{a}_{u2}^T, \cdot, \mathbf{a}_{uV}^T]^T = [a_{u1,0}, \cdot, a_{u1,L-1}, \cdots, a_{uV,0}, \cdot, a_{uV,L-1}]^T$, and $\mathbf{a}_{uv}$ was expressed in Equation (3.4). In (3.16), the matrix $\mathbf{W}^{(k)}$ can be expressed as

$$\mathbf{W}^{(k)} = \begin{bmatrix} \mathbf{w}_1^{(k)} & \mathbf{0} & \ldots & \mathbf{0} \\ \mathbf{0} & \mathbf{w}_2^{(k)} & \ldots & \mathbf{0} \\ \vdots & \vdots & \ddots & \vdots \\ \mathbf{0} & \mathbf{0} & \ldots & \mathbf{w}_V^{(k)} \end{bmatrix}, \quad k = 1, 2, \ldots, K \tag{3.17}$$

where, $\mathbf{0} = [0, 0, \ldots, 0]^T$ is an $L$-dimensional vector. In (3.16), $\mathbf{n}_u = [n_{u1}, n_{u2}, \ldots, n_{uV}]^T$ is an $L$-dimensional vector, where $n_{uv}$ was expressed in (3.9), while $\mathbf{j}_u = \left[\sum_{k=2}^K \sqrt{\frac{P_k}{P}} (\mathbf{w}_1^{(k)})^H \mathbf{i}_{u1}^{(k)}, \sum_{k=2}^K \sqrt{\frac{P_k}{P}} (\mathbf{w}_2^{(k)})^H \mathbf{i}_{u2}^{(k)}, \ldots, \sum_{k=2}^K \sqrt{\frac{P_k}{P}} (\mathbf{w}_V^{(k)})^H \mathbf{i}_{uV}^{(k)}\right]$ is a $L$-dimensional vector corresponding to the interfering signals.

The $(V \times V)$-dimensional autocorrelation matrix $\mathbf{R}_u$ of the $V$-length decision variable set $\mathbf{z}_u$ of the $u$th data bit after multicarrier demodulation and DS despreading seen in Equation (3.16) can be expressed as

$$\mathbf{R}_u = E\left[\mathbf{z}_u \mathbf{z}_u^H\right]. \tag{3.18}$$

Upon substituting the decision variable $\mathbf{z}_u$ of (3.16) into (3.18) and exploiting the statistical independence of the devised signal and the noise, $\mathbf{R}_u$ can be expressed as

$$\mathbf{R}_u = \mathbf{R}_d + \mathbf{R}_n, \tag{3.19}$$

where $\mathbf{R}_d$ contains the autocorrelations of the desired signals hosted by the matrix $(\mathbf{W}^{(1)})^H\mathbf{a}_u$ of (3.16), which can be expressed as

$$\mathbf{R}_d = E\left[((\mathbf{W}^{(1)})^H\mathbf{a}_u)((\mathbf{W}^{(1)})^H\mathbf{a}_u)^H\right]. \tag{3.20}$$

Upon substituting $(\mathbf{W}^{(1)})^H\mathbf{a}_u$ given by the first term of (3.16) into (3.20) and exploiting the property that $\mathbf{a}_{uv}$ is independent of $\mathbf{a}_{u'v'}$ for $u \neq u'$ or $v \neq v'$, we have $E\left[\mathbf{a}(1)_{uv}(t) \cdot \mathbf{a}(1)_{u'v'}(t)\right] = 0$ for $u \neq u'$ or $v \neq v'$. Hence $\mathbf{R}_d$ can be expressed as

$$\begin{aligned}\mathbf{R}_d = \text{diag}\Big\{&E\left[(\mathbf{w}_1^{(1)})^H\mathbf{a}_{u1}\mathbf{a}_{u1}^H\mathbf{w}_1^{(1)}\right],\\ &E\left[(\mathbf{w}_2^{(1)})^H\mathbf{a}_{u2}\mathbf{a}_{u2}^H\mathbf{w}_2^{(1)}\right],\\ &\cdots,\\ &E\left[(\mathbf{w}_1^{(1)})^H\mathbf{a}_{u1}\mathbf{a}_{u1}^H\mathbf{w}_1^{(1)}\right]\Big\},\end{aligned} \tag{3.21}$$

where $\mathbf{w}_v^{(1)} = [w_{v,0}^{(1)}, w_{v,1}^{(1)}, \ldots, w_{v,L-1}^{(1)}]^T$. Consequently, we have

$$\begin{aligned}E\left[(\mathbf{w}_v^{(1)})^H\mathbf{a}_{uv}\mathbf{a}_{uv}^H\mathbf{w}_v^{(1)}\right] &= E\left[(\mathbf{w}_v^{(1)})^H\mathbf{a}_{uv}\mathbf{a}_{uv}^H\mathbf{w}_v^{(1)}\right]\\ &= (\mathbf{w}_v^{(1)})^H E\left[\mathbf{a}_{uv}\mathbf{a}_{uv}^H\right]\mathbf{w}_v^{(1)}\\ &= (\alpha_{uv})^2(\mathbf{w}_v^{(1)})^H E\left[\mathbf{d}\mathbf{d}^H\right]\mathbf{w}_v^{(1)},\end{aligned} \tag{3.22}$$

where $\mathbf{d}$ was formulated in (2.42) in conjunction with $M = 1$.

In (3.19) $\mathbf{R}_n$ represents the covariance matrix of the interference-plus-noise, which is given by

$$\begin{aligned}\mathbf{R}_n &= E\left[(\mathbf{n}_u + \mathbf{j}_u)(\mathbf{n}_u + \mathbf{j}_u)^H\right]\\ &= \mathbf{R}_N + \mathbf{R}_J,\end{aligned} \tag{3.23}$$

where we have

$$\begin{aligned}\mathbf{R}_N &= E\left[\mathbf{n}_u\mathbf{n}_u^H\right]\\ &= \frac{VLN_0}{E_b}\mathbf{I},\end{aligned} \tag{3.24}$$

while $\mathbf{R}_J$ represents the covariance matrix of the composite interference given by the sum of the self-interference and multiuser interference.

In order to derive $\mathbf{R}_J$, the following assumptions are stipulated for convenience. As we have shown in the context of Equation (3.11), the self-interference is zero corresponding to $(\mathbf{w}_v^{(1)})^H\mathbf{i}_{u'v'}^{(s)} = 0$, when the difference between the frequency $f_{u'v'}$ of the interfering subcarrier signal and the frequency $f_{uv}$ of the desired subcarrier obeys $f_{u'v'} - f_{uv} = n/T_s$, where $n$ is an integer. This condition can be readily satisfied during the system design stage. Similarly, the MUI term $(\mathbf{w}_v^{(k)})^H\mathbf{i}_{u'v'}^{(k)}$ is zero according to Equation (3.14).

Based on this assumption, it can be shown by referring to (3.8) as well as to (3.16) that we have

$$\mathbf{R}_J = E[\mathbf{j}_u \mathbf{j}_u^H], \tag{3.25}$$

where $\mathbf{j}_u$ is a $V \times 1$-dimensional vector. Substituting (3.11) and (3.14) into (3.8), we have $\mathbf{j}_u = \sum_{k=2}^{K} \sqrt{\frac{P_k}{P}} (\mathbf{W}^{(k)})^H \mathbf{i}_u^{(k)}$, where $\mathbf{i}_u^{(k)} = [(\mathbf{i}_{u1}^{(k)})^T, (\mathbf{i}_{u2}^{(k)})^T, \ldots, (\mathbf{i}_{uV}^{(k)})^T]^T$ is a $(VL \times 1)$-dimensional vector. Following the approach of [41], $\mathbf{R}_J$ can be expressed as

$$\begin{aligned} \mathbf{R}_J = \sum_{k=2}^{K} \frac{P_k}{P} \bullet \mathrm{diag}\Big\{ & E\left[(\mathbf{w}_1^{(k)})^H \mathbf{i}_{u1}^{(k)} (\mathbf{i}_{u1}^{(k)})^H \mathbf{w}_1^{(k)}\right], \\ & E\left[(\mathbf{w}_2^{(k)})^H \mathbf{i}_{u2}^{(k)} (\mathbf{i}_{u2}^{(k)})^H \mathbf{w}_2^{(k)}\right], \\ & \ldots, \\ & E\left[(\mathbf{w}_v^{(k)})^H \mathbf{i}_{uv}^{(k)} (\mathbf{i}_{uv}^{(k)})^H \mathbf{w}_V^{(k)}\right] \Big\}, \end{aligned} \tag{3.26}$$

where we have

$$\begin{aligned} E\left[(\mathbf{w}_v^{(k)})^H \mathbf{i}_{uv}^{(k)} (\mathbf{i}_{uv}^{(k)})^H \mathbf{w}_v^{(k)}\right] &= E\left[(\mathbf{w}_v^{(k)})^H \mathbf{i}_{uv}^{(k)} (\mathbf{i}_{uv}^{(k)})^H \mathbf{w}_v^{(k)}\right] \\ &= (\mathbf{w}_v^{(k)})^H E\left[\mathbf{i}_{uv}^{(k)} (\mathbf{i}_{uv}^{(k)})^H\right] \mathbf{w}_v^{(k)}. \end{aligned} \tag{3.27}$$

In this chapter we assume that orthogonal WH codes are used as DS spreading codes. Therefore, based on the assumption of orthogonal multicarrier signals, of synchronous transmissions of the $K$ simultaneous user signals as well as slow flat-fading of each subcarrier, there is no interference between the different users and the different subcarrier signals. Then, (3.12) can be simplified to

$$\mathbf{i}_{uv}^{(k)} = \mathbf{0}. \tag{3.28}$$

Substituting (3.28) into (3.8), we have

$$z_{uv} = \sqrt{\frac{2P}{VL}} T_s \left[ b_u[0] (\mathbf{w}_v^{(1)})^H \mathbf{a}_{uv} + n_{uv} \right]. \tag{3.29}$$

Consequently, the Equation (3.26) can be simplified to

$$\mathbf{R}_J = \mathrm{diag}\{0, 0, \ldots, 0\}. \tag{3.30}$$

In this situation, the MRC criterion based beamformer, which constitutes an effective solution to maximizing the antenna gain in the direction of the desired user, is the optimum beamformer. Let $\mathbf{w}_v^{(1)} = \mathbf{a}_{uv}$ in (3.29), then the term $z_{uv}$ can be expressed as

$$z_{uv} = \sqrt{\frac{2P}{VL}} T_s \left[ L b_u[0] \|a_{uv}\|^2 + n_{uv} \right]. \tag{3.31}$$

After MRC combining, the decision variable $z_u$ may be expressed as

$$\begin{aligned} z_u &= \sum_{v=1}^{V} z_{uv} \\ &= \sum_{v=1}^{V} \sqrt{\frac{2P}{VL}} T_s \left[ L b_u[0] \|a_{uv}\|^2 + n_{uv} \right], \end{aligned} \tag{3.32}$$

which suggests that the receiver is capable of achieving the maximum possible beamforming gain indicated by the multiplicative factor $L$ in the square bracket.

### 3.2.4 User-load Improvement Using TF-Domain Spreading - Beamforming

In Sections 3.2.1, 3.2.2 and 3.2.3 the DS spreading used by the MC DS-CDMA system was carried out in the TD based on orthogonal WH DS-spreading codes. However, as proposed for MC-CDMA schemes in [25, 80], spreading in the F-domain can also be employed for exploiting the attainable diversity gain in the F-domain. In the generalized MC DS-CDMA scheme considered, the transmitted data stream can be spread in both the T-domain and the F-domain in order to support more users or to achieve the maximum attainable frequency diversity gain [192]. In order to elaborate further on F-domain spreading, let us assume that after the T-domain DS-spreading seen in Figure 3.3, the identical data bits of the $V$ subcarriers are multiplied by the $V$ chip values of $\{+1, -1, \ldots, +1\}$ of a spreading code invoked for spreading the data in the F-domain across the $V$ number of subcarriers. The resultant bandwidth is again the same as that of the MC DS-CDMA scheme employing the T-domain only spreading. In this case, the transmitted MC DS-CDMA signal benefits from both time-domain spreading and frequency-domain spreading. At the receiver, the MC DS-CDMA signal is first despread using the T-domain orthogonal WH DS-spreading code, then despread by the F-domain spreading code of length-$V$, as shown in Figure 3.4. When using both T-domain and F-domain spreading, the total processing gain becomes the product of the T-domain spreading code's processing gain and the F-domain spreading code's processing gain, namely $N_e \cdot V$. Furthermore, the maximum number of users supported by the MC DS-CDMA system is also determined by the above product of $N_e \cdot V$, which is determined by the total system bandwidth.

#### 3.2.4.1 System Model - Beamforming

The transmitter schematic of the broadband MC DS-CDMA system using TF-domain spreading is shown in Figure 3.3, which is similar to that seen in Figure 3.1, except that the $V$-depth F-domain repetition scheme of Figure 3.1 is now replaced by the F-domain spreading arrangement associated with an orthogonal spreading code of length $V$. Specifically, let $\{c'_k[0], c'_k[1], \ldots, c'_k[V-1]\}$ be the $k$th user's orthogonal code in discrete form, which will be used for F-domain spreading. By contrast, the $k$th user's T-domain orthogonal codes have been expressed in Section 3.2.1 as $c_k(t)$ in continuous form. As shown in Figure 3.3, the binary data stream having a bit duration of $T_b$ is Serial-to-Parallel (S/P) converted to $U$ parallel sub-streams. After S/P conversion, each substream is spread

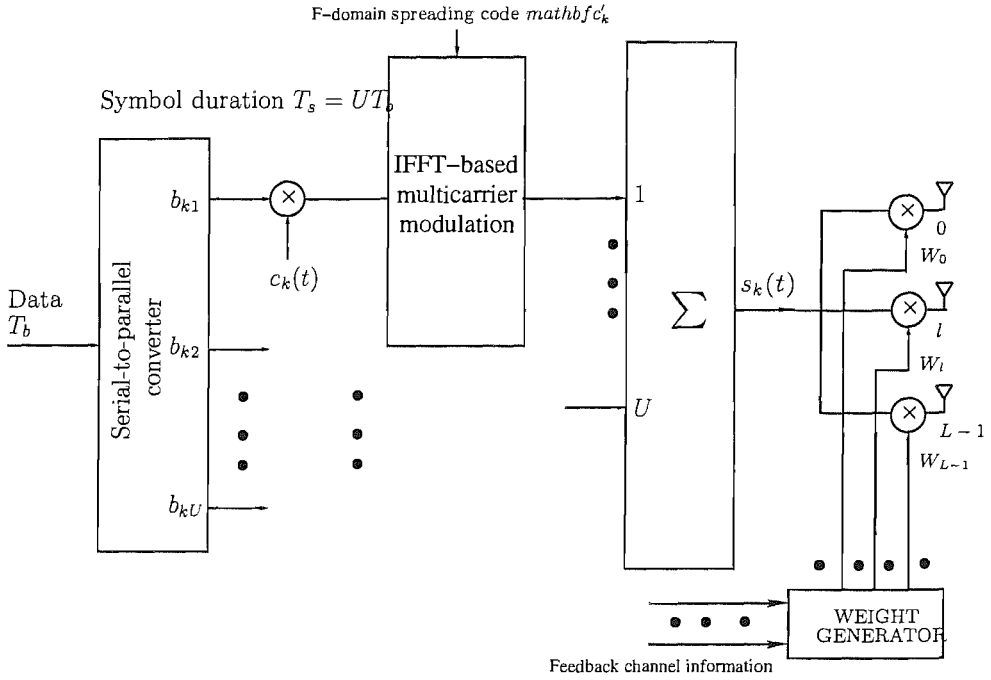


**Figure 3.3:** The $k$th user's BS transmitter schematic for the downlink of the generalized multicarrier DS-CDMA system using TF-domain spreading. This schematic is similar to that seen in Figure 3.1, except that the $V$-depth F-domain repetition scheme of Figure 3.1 is now replaced by the F-domain spreading arrangement associated with an orthogonal spreading code of length $V$.

using an $N_e$-chip DS spreading sequence waveform $c_k(t)$. Then, in the broadband MC DS-CDMA system using TF-domain spreading, instead of employing data repetition over $V$ subcarriers, the $U$ sub-block signals of user $k$ generated after T-domain spreading are now further spread across the F-domain using the above F-domain spreading codes. According to our analysis provided in Sections 3.2.1 and 3.2.2, the total number of orthogonal codes that can be used for T-domain spreading is $N_e$ and the maximum number of users supported by these orthogonal codes is $\mathcal{K}_{max} = N_e$. By contrast, the total number of orthogonal codes that can be used for F-domain spreading is $V$. This implies that even if $V$ number of users share the same set of T-domain spreading codes, these $V$ user signals might be distinguishable with the aid of the associated $V$ number of F-domain spreading codes. Explicitly, the total number of users that may be supported is $V\mathcal{K}_{max} = VN_e$. Therefore, the orthogonal spreading codes can be assigned as follows. If the number of users is in the range of $0 \leq K \leq \mathcal{K}_{max}$, these users will be assigned the required orthogonal T-domain spreading codes and the same F-domain orthogonal spreading code. The resultant scheme is the same as the one we studied in Sections 3.2.1 as well as 3.2.2. However, when the number of users is in the range of $v\mathcal{K}_{max} \leq K \leq (v+1)\mathcal{K}_{max}$, $v = 1, 2 \ldots, V-1$, then the same orthogonal T-domain code has to be assigned to $v$ or $(v+1)$ users, but these $v$ or $(v+1)$ users are assigned different F-domain spreading codes. These $v$ or $(v+1)$ users employing the same orthogonal T-domain code are identified by their corresponding F-domain spreading codes. Since the subcarrier signals across which F-domain

spreading takes place encounter independent fading, the orthogonality of the F-domain spreading codes cannot be retained in frequency-selective fading channels. Hence, multiuser interference is inevitably introduced, which degrades the attainable BER performance, when increasing the number of users sharing the same T-domain spreading code.

In the generalized MC DS-CDMA system using both T-domain spreading and F-domain spreading, the signals transmitted from the downlink antenna array at the BS associated with using transmitter beamforming can be expressed as

$$\begin{aligned} \mathbf{s}_k(t) &= (\mathbf{w}_v^{(k)})^H \bullet s_k(t) \\ &= \sum_{u=1}^{U}\sum_{v=1}^{V}\sqrt{\frac{2P_k}{VL}}(\mathbf{w}_v^{(k)})^H b_{ku}(t)c_k(t)c'_k[v-1]\cos(2\pi f_{uv}t+\phi_{k,uv}), \end{aligned} \tag{3.33}$$

where $P_k/V$ represents the transmitted power of each subcarrier, while $\mathbf{w}_v^{(k)}$ is the $(L \times 1)$-dimensional BS downlink transmitter beamforming weight vector generated for the $v$th subcarrier of the $k$th user by the beamformer according to the perfectly estimated channel information. In (3.33), the T-domain spreading sequence $c_k(t) = \sum_{j=-\infty}^{\infty} c_{kj} P_{T_c}(t - jT_c)$ denotes the signature sequence waveform of the $k$th user, where $c_{kj}$ assumes values of +1 or -1 with equal probability, while $P_{T_c}(t)$ is the rectangular chip waveform, which is defined over the interval $[0, T_c)$.

Let $1 \leq K' \leq V$ be the number of users sharing the same T-domain spreading code. We also assume that any T-domain spreading code is shared by the same $K'$ number of users. Then, when the $K'\mathcal{K}_{max}$ signals expressed in the form of (3.33) are transmitted over frequency-selective fading channels, the complex-valued low-pass equivalent received signal can be expressed as

$$\begin{aligned} r(t) &= \sum_{k=1}^{K'\mathcal{K}_{max}} \mathbf{s}_k(t) \otimes \mathbf{h}_{uv}^{(1)}(t) + n(t) \\ &= \sum_{k=1}^{K'\mathcal{K}_{max}}\sum_{u=1}^{U}\sum_{v=1}^{V}\sqrt{\frac{2P_k}{VL}}\, b_{ku}(t-\tau_1)c_k(t-\tau_1)(\mathbf{w}_v^{(k)})^H \mathbf{a}_{uv}^{(1)}(t) \\ &\quad \times c'_k[v-1]\exp\left(j\left[2\pi f_{uv}t + \theta_{uv}^{(k)}\right]\right) + n(t). \end{aligned} \tag{3.34}$$

The receiver of the generalized MC DS-CDMA system using TF-domain spreading is shown in Figure 3.4, which is similar to that seen in Figure 3.2. The receiver portrayed in Figure 3.4 consists of two main parts. The first part carries out multicarrier demodulation and DS despreading, then provides $V$ number of outputs, which correspond to the $V$ number of subcarriers conveying the repeated replicas representing the same data bit. This part is the same as the first part seen in Figure 3.2. However, in the second part, instead of being combined with the aid of an MRC scheme, the $V$ number of variables are despread by the desired user's F-domain WH spreading codes. Following the derivations provided in Section 3.2.2, the decision variable $z_{uv}$ corresponding to the subcarrier $uv$

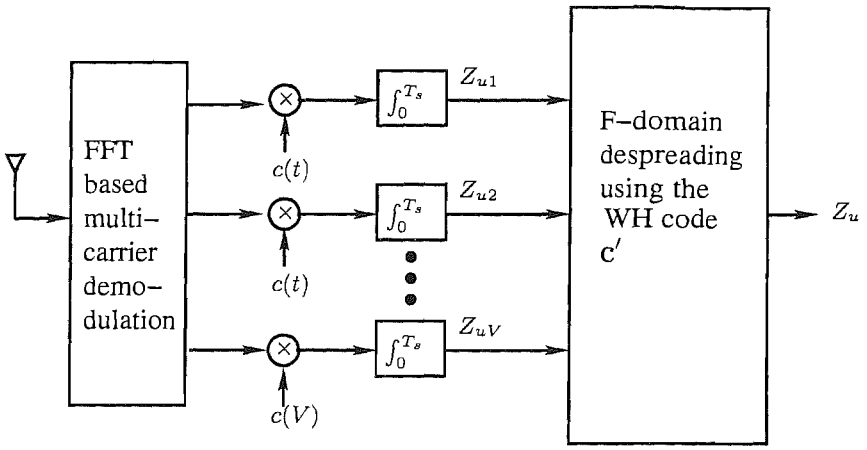


**Figure 3.4:** Receiver block diagram of mobile users in the generalized MC DS-CDMA system employing TF-domain spreading.

can now be expressed as

$$z_{uv} = \sqrt{\frac{2P}{VL}} T_s \left[ \sum_{k=1}^{K'} \left( \sqrt{\frac{P_k}{P}} (\mathbf{w}_v^{(k)})^H \mathbf{a}_{uv}^{(1)}(t) \times c'_k[v-1] b_{ku}[0] \right) + n_{uv} \right], \tag{3.35}$$

where $n_{uv}$ is an AWGN process having zero mean and a variance of $\frac{VLN_0}{E_b}$.

Let $\beta_{kv} = (\mathbf{w}_v^{(k)})^H \mathbf{a}_{uv}^{(1)}(t)$, and

$$\mathbf{z}_u = [z_{u1}\ z_{u2}\ \ldots\ z_{uV}]^T, \tag{3.36}$$

$$\mathbf{C} = \begin{pmatrix} \beta_{11}c'_1[0] & \beta_{21}c'_2[0] & \ldots & \beta_{K'1}c'_{K'}[0] \\ \beta_{12}c'_1[1] & \beta_{22}c'_2[1] & \ldots & \beta_{K'2}c'_{K'}[1] \\ \vdots & \vdots & \ddots & \vdots \\ \beta_{1V}c'_1[V-1] & \beta_{2V}c'_2[V-1] & \ldots & \beta_{K'V}c'_{K'}[V-1] \end{pmatrix}, \tag{3.37}$$

$$\mathbf{P} = \text{diag}\left\{ 1, \sqrt{\frac{P_2}{P}}, \ldots, \sqrt{\frac{P_{K'}}{P}} \right\}, \tag{3.38}$$

$$\mathbf{b} = [b_{1u}\ b_{2u}\ \ldots\ b_{K'u}]^T, \tag{3.39}$$

$$\mathbf{n} = [n_{u1}\ n_{u2}\ \ldots\ n_{uV}]^T. \tag{3.40}$$

Then (3.35) can be written in a matrix form as

$$\mathbf{z}_u = \sqrt{\frac{2P}{VL}} T_s \left[ \mathbf{CPb} + \mathbf{n} \right]. \tag{3.41}$$

Based on (3.41) the multiuser MC DS-CDMA signals can be detected by invoking a range of different detection algorithms [195]. In this section, we investigate two detection algorithms, namely the single-user correlation based detector, and the multiuser decorrelating detector [195]. In the context

of the single-user correlation based detector, the decision variable $z_u$ of the desired user is obtained by multiplying both sides of (3.41) with $\mathbf{c}'_1 = [c'_1[0], c'_1[1], \ldots, c'_1[V-1]]$, which can be expressed as

$$z_u = \sqrt{\frac{2P}{VL}} T_s \left[ \sum_{v=1}^{V} \beta_{1v} b_{1u} + \sum_{k=2}^{K'} \sum_{v=1}^{V} \sqrt{\frac{P_k}{P}} c'_1[v-1] c'_k[v-1] \beta_{kv} b_{ku} + \mathbf{c}'_1 \mathbf{n} \right], \tag{3.42}$$

where we have

$$\beta_{1v} = (\mathbf{w}_v^{(1)})^H \mathbf{a}_{uv}^{(1)}(t) = L \|\alpha_{uv}\|^2, \tag{3.43}$$

and $\mathbf{w}_v^{(1)} = \mathbf{a}_{uv}^{(1)}$ is generated by the MRC beamformer [7] .

From (3.42) we infer that multiuser interference is inevitably introduced, since the orthogonality of the F-domain spreading codes cannot be retained in frequency-selective fading channels. However, the desired signal is not contaminated by the signal of the users employing different orthogonal T-domain spreading codes, provided that synchronous transmission of all the $K'\mathcal{K}_{max}$ user signals is maintained as well as slow flat-fading of each subcarrier is encountered. Only the users sharing the same T-domain spreading code as the desired user will interfere with the desired user. Therefore, the interference $\sum_{k=2}^{K'} \sum_{v=1}^{V} \sqrt{\frac{P_k}{P}} c'_1[v-1] c'_k[v-1] \beta_{kv} b_{ku}$ can be reduced, if we carefully select the $K'-1$ users, which have the lowest interference coefficient with respect to the desired user, from the total number of $K'\mathcal{K}_{max}$ users to share the same T-domain spreading code with the desired user, where the interference coefficient is defined as $\rho_{1k} = \sqrt{\frac{P_k}{P}} \beta_{kv} = \sqrt{\frac{P_k}{P}} (\mathbf{w}_v^{(k)})^H \mathbf{a}_{uv}^{(1)}(t)$, $k = 1, 2, \ldots, K'\mathcal{K}_{max}$. The interference coefficient can be derived off-line based on the assumption that $\mathbf{a}_{uv}^{(1)}(t)$ defined in (3.4) is perfectly estimated and that $\mathbf{w}_v^{(k)} = \mathbf{a}_{uv}^{(k)}(t)$, which is also perfectly estimated. Then we have

$$\begin{aligned} \rho_{1k} &= \sqrt{\frac{P_k}{P}} (\mathbf{a}_{uv}^{(k)}(t))^H \mathbf{a}_{uv}^{(1)}(t) \\ &= \sqrt{\frac{P_k}{P}} (\alpha_{uv}^{(k)}(t))^* \alpha_{uv}^{(1)}(t) (\mathbf{d}^{(k)})^H \mathbf{d}^{(1)}, \end{aligned} \tag{3.44}$$

where $\alpha_{uv}^{(k)}(t)$ is the Rayleigh faded envelope's amplitude corresponding to the $k$th user's $uv$th subcarrier signal and to the $m$th antenna array. Since the $UV$ subcarriers of the $k$th user are expected to encounter independent fading, it is reasonable to remove the term $(\alpha_{uv}^{(k)}(t))^* \alpha_{uv}^{(1)}(t)$ from the interference coefficient $\rho_{1k}$. Hence we arrive at

$$\rho_{1k} = \sqrt{\frac{P_k}{P}} (\mathbf{d}^{(k)})^H \mathbf{d}^{(1)}, \tag{3.45}$$

where $\mathbf{d}^{(K)}$ was expressed in (3.4). It will be shown based on our simulation results that after the corresponding interference coefficient based user grouping operation, which is referred to as regrouping for brevity, the BER performance of the system may be significantly improved.

Below we will demonstrate the benefits of user regrouping with the aid of an example, noting that the grouping has to be updated every time, when a new user joins or disjoin the system. In these

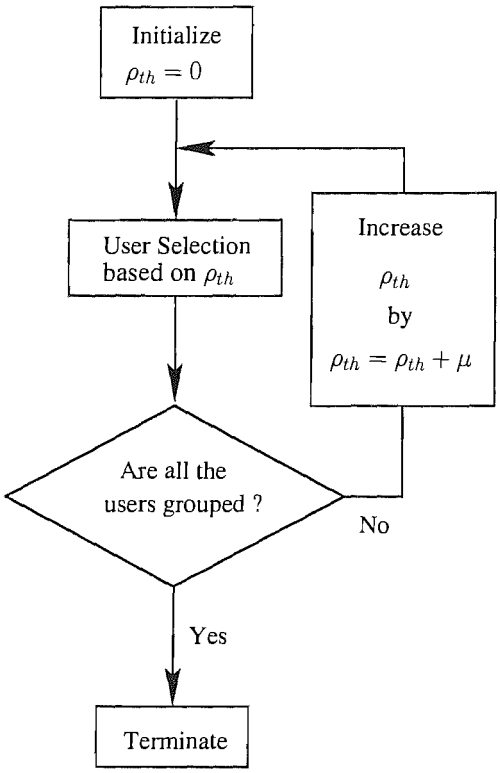


**Figure 3.5:** The schematic of the user grouping technique.

simulations, we employed 4-chip WH codes as the T-domain spreading code, while using 2-chip WH code as the F-domain spreading sequences. A $(1 \times 2)$-dimensional antenna array $(M = 1, L = 2)$ was employed in the BS's transmitter. The total number of users was $K = 8$, i.e. the system operated at its full user load. Furthermore, perfect power control was assumed, which implies that we have $P_0 = P_1 = \ldots = P_K$. The $K = 8$ users' DOAs are $\psi^{(1)} = 2.61$, $\psi^{(2)} = 0.58$, $\psi^{(3)} = 4.75$, $\psi^{(4)} = 3.33$, $\psi^{(5)} = 5.85$, $\psi^{(6)} = 2.41$, $\psi^{(7)} = 4.11$, $\psi^{(8)} = 0.42$. Based on the assumption that no angular spread is encountered, we have, for example,

$$\rho_{12} = (\mathbf{d}^{(2)})^H \mathbf{d}^{(1)} = [1, \exp(-j\pi \sin(\psi^{(2)}))] \times \begin{bmatrix} 1 \\ \exp(j\pi \sin(\psi^{(1)})) \end{bmatrix} = 1.99. \quad (3.46)$$

The matrix of interference coefficients is given by

$$\rho = \begin{pmatrix} \rho_{11} & \rho_{12} & \cdots & \rho_{18} \\ \rho_{21} & \rho_{22} & \cdots & \rho_{28} \\ \vdots & \vdots & \ddots & \vdots \\ \rho_{81} & \rho_{82} & \cdots & \rho_{88} \end{pmatrix} = \begin{pmatrix} 2.00 & 1.99 & 1.42 & 0.93 & 0.22 & 1.93 & 0.98 & 1.97 \\ 1.99 & 2.00 & 1.51 & 0.81 & 0.09 & 1.96 & 1.09 & 1.95 \\ 1.42 & 1.51 & 2.00 & 0.57 & 1.23 & 1.73 & 1.92 & 1.19 \\ 0.93 & 0.81 & 0.57 & 2.00 & 1.86 & 0.45 & 1.07 & 1.19 \\ 0.22 & 0.09 & 1.23 & 1.86 & 2.00 & 0.28 & 1.61 & 0.52 \\ 1.93 & 1.96 & 1.73 & 0.45 & 0.28 & 2.00 & 1.39 & 1.83 \\ 0.98 & 1.09 & 1.92 & 1.07 & 1.61 & 1.39 & 2.00 & 0.70 \\ 1.97 & 1.95 & 1.19 & 1.19 & 0.52 & 1.83 & 0.70 & 2.00 \end{pmatrix} \quad (3.47)$$

Observe from Equation (3.47) that the user grouping operation should be jointly optimized for all users, since the interference is mutual. In our user grouping scheme, we first set a threshold value $\rho_{th}$, for example $\rho_{th} = 1.20$ in this case. In the absence of any prior knowledge, the initial value of $\rho_{th}$ was set to 0. When the $k_1$th user has an interference coefficient of $\rho_{k_1 k_2} \leq \rho_{th}$ with respect to the $k_2$th user, they are termed here as the users interfering with each other. Furthermore, when the $k_1$th user shares the same T-domain spreading code with the $k_2$th user, they are deemed to be in the same T-domain user group and they are differentiated by their F-domain sequences. Table 3.1 indicates the number of users interfering with each user, as well as their F-domain interference coefficients. Based on Table 3.1, we found that it is more difficult for the users subjected to a lower number of interferers to find a beneficial T-domain user group imposing a low interference, than for the users having a high number of interferers. Therefore, the users having fewer interferers are assigned a higher priority in selecting the specific interferers belonging to the same T-domain user group and vice versa. In this case, we observe in Equation (3.47) that the 3rd user and the 6th user have the highest priorities, since both of them has a low number of interferers. By observing column 3 and row 8 of Equation (3.47), we infer that for the 3rd user, the 8th user was selected to be in the same T-domain group owing to their low F-domain interference coefficient of 1.19, since the 8th user has four interfering users in Table 3.1, while the 4th user has six interfering users. This selection procedure will continue, until all users have been grouped. However, when the threshold value $\rho_{th}$ was set too low, some users cannot be allocated to a T-domain user group imposing an interference coefficient lower than $\rho_{th}$. In this scenario, the threshold value $\rho_{th}$ was increased by a step size of $0 < \mu < L$. Based on the new threshold value, another T-domain user group allocation attempt was initiated. The flow chart of the user grouping operation is portrayed in Figure 3.5. The computational complexity of the user grouping operation is heavily dependent on the step-size parameter $\mu$. The larger the step size $\mu$, the sooner the user grouping is completed and hence the lower the computational complexity. However, the average interference between users of the same group increased upon increasing $\mu$.

By employing the user grouping technique associated with $\rho_{th} = 1.20$, we assign the 1st user and the 7th user to the same T-domain spreading code, where the corresponding interference coefficient seen at position (1,7) of (3.47) is 0.98. Similarly, the 2nd user and the 4th user are seen in (3.47) to have an interference coefficient of 0.81, the 3rd user and the 8th user exhibit an interference coefficient

of 1.19, and finally, the 5th user and the 6th user have an interference coefficient of 0.28. The average interference coefficient is 0.81. By contrast, without user regrouping, the first user and the 5th user would share the same T-domain spreading code and the corresponding interference coefficient is 0.22. The second user would share the same T-domain spreading code with the 6th user in conjunction with an interference coefficient of 1.96, the third user would share the same T-domain spreading code with the 7th user along with an interference coefficient of 1.92, while the 4th user would share the same T-domain spreading code with the 8th user, which exhibit an interference coefficient of 1.19. Accordingly, the average interference coefficient is 1.33. As expected, the proposed user regrouping technique decreased the average interference between the users sharing the same T-domain spreading codes and hence improved the achievable system performance.

| User No. | Number of Interfering users | Interfering users (Interference coefficient) |
|---|---|---|
| User 1 | 3 | 4(0.93), 5(0.22) and 7(0.98) |
| User 2 | 3 | 4(0.81), 5(0.09) and 7(1.09) |
| User 3 | 2 | 4(0.93) and 8(1.19) |
| User 4 | 6 | 1(0.93), 2(0.81), 3(0.57), 6(0.45), 7(1.07) and 8(1.19) |
| User 5 | 4 | 1(0.22), 2(0.09), 6(0.28) and 8(0.52) |
| User 6 | 2 | 4(0.45) and 5(0.28) |
| User 7 | 4 | 1(0.98), 2(1.90), 4(1.07) and 8(0.70) |
| User 8 | 4 | 3(1.19), 4(1.19), 5(0.52) and 7(0.70) |

**Table 3.1:** The table of interfering users and their interference coefficients generated based on the threshold value $\rho_{th} = 1.20$.

In the context of the multiuser decorrelating detector [195], the vector of decision variables $\mathbf{z'}_u = \left[z'_{1u}\ z'_{2u}\ \cdots\ z'_{K'u}\right]^T$ of the $K'$ users is obtained by multiplying both sides of (3.41) with the matrix $(\mathbf{C}^H\mathbf{C})^{-1}\mathbf{C}^H$, which can be expressed as

$$\begin{aligned}\mathbf{z'}_u &= \sqrt{\frac{2P}{VL}}T_s\left[(\mathbf{C}^H\mathbf{C})^{-1}\mathbf{C}^H\mathbf{C}\mathbf{P}\mathbf{b} + (\mathbf{C}^H\mathbf{C})^{-1}\mathbf{C}^H\mathbf{n}\right] \\ &= \sqrt{\frac{2P}{VL}}T_s\left[\mathbf{P}\mathbf{b} + \mathbf{n'}\right], \end{aligned} \tag{3.48}$$

where

$$\mathbf{n'} = (\mathbf{C}^H\mathbf{C})^{-1}\mathbf{C}^H\mathbf{n}. \tag{3.49}$$

Hence, according to Equation (3.48), the decision variable $z'_{1u}$ for the first user is given by

$$z'_{1u} = \sqrt{\frac{2P}{VL}}T_s(b_{1u} + n'_1), \tag{3.50}$$

where $n'_1$ is the first element of the noise vector $\mathbf{n'}$ of (3.49). It can be shown from Equation (3.50) that the multiuser interference is fully eliminated.

## 3.3 Beam Selection Transmit Diversity - Downlink

In [47] Zhou has presented a novel beam selection transmit diversity (BSTD) scheme designed for the downlink. This BSTD arrangement is a hybrid space-time processing scheme, which uses both beamforming and selection transmit diversity (STD). The antenna arrays used for BSTD are identical to those shown in Figure 2.4. The $M$ antenna arrays having an array-spacing of more than $10\lambda$ are sufficiently widely separated in order to achieve transmit diversity, since the arrays may be expected to encounter independent fading, while the $L$ elements have an element-spacing of $\lambda/2$ within the antenna arrays. In the context of the BSTD space-time processing scheme, one of the antenna arrays benefitting from the best channel state is selected in order to form a beam toward the desired mobile user for signal transmission.

### 3.3.1 Transmitter Model - Beam Selection Transmit Diversity

In this section, a baseband system model using the BSTD scheme invoked for improving the attainable performance of the generalized MC DS-CDMA system is described. Again, the BSTD scheme may be viewed as a hybrid of a beamforming scheme and a STD scheme. Moreover, it can be shown that the BSTD is equivalent to the conventional beamforming arrangement, if we assume that the number of antenna arrays is $M = 1$. Furthermore, when the number of the array elements per antenna array is $L = 1$, the BSTD scheme is degenerated to the STD arrangement.

The BS downlink transmitter schematic of the $k$th user is shown in Figure 3.6 for the generalized MC DS-CDMA system employing $M$ antenna arrays and using the BSTD arrangement of [47]. Similar to the BS transmitter schematic of the beamforming scheme seen in Figure 3.1, the binary data stream having a bit duration of $T_b$ is Serial-to-Parallel (S/P) converted to $U$ parallel sub-streams. After S/P conversion, each substream is spread using an $N$-chip DS spreading sequence waveform $c_k(t)$. Then, the DS spread signal of the $u$th sub-stream, where we have $u = 1, 2, \ldots, U$, simultaneously modulates a group of parallel subcarrier frequencies $\{f_{u1}, f_{u2}, \ldots, f_{uV}\}$ using Binary Phase Shift Keying (BPSK). In contrast to the beamforming scheme seen in Figure 3.1, where only a single antenna array having $L$ array elements is used, the BSTD scheme of Figure 3.6 employs $M$ antenna arrays and one of the antenna arrays benefitting from the best channel quality is selected to form a beam towards the desired mobile user for signal transmission. Without loss of generality, we assume that the first user corresponding to $k = 1$ is the desired user, who is referred to as the reference user. As shown in Figure 3.7, the $m^{(1)}$th array, which is assumed to have the best channel quality for the desired user, is selected to form a beam toward the desired user. Let the transmit weight vector for the $v$th subcarrier of the $k$th user be expressed as $\mathbf{w}_{v,m^{(k)}}^{(k)}$, which is generated for the $m^{(k)}$th array based on the related channel information. Then, the $k$th user's transmitted signal can be expressed as

$$\begin{aligned} \mathbf{s}_k(t) &= (\mathbf{w}_{v,m^{(k)}}^{(k)})^H \bullet s_k(t) \\ &= \sum_{u=1}^{U}\sum_{v=1}^{V} \sqrt{\frac{2P_k}{VL}} (\mathbf{w}_{v,m^{(k)}}^{(k)})^H b_{ku}(t) c_k(t) \cos(2\pi f_{uv} t + \phi_{k,uv}), \end{aligned} \tag{3.51}$$

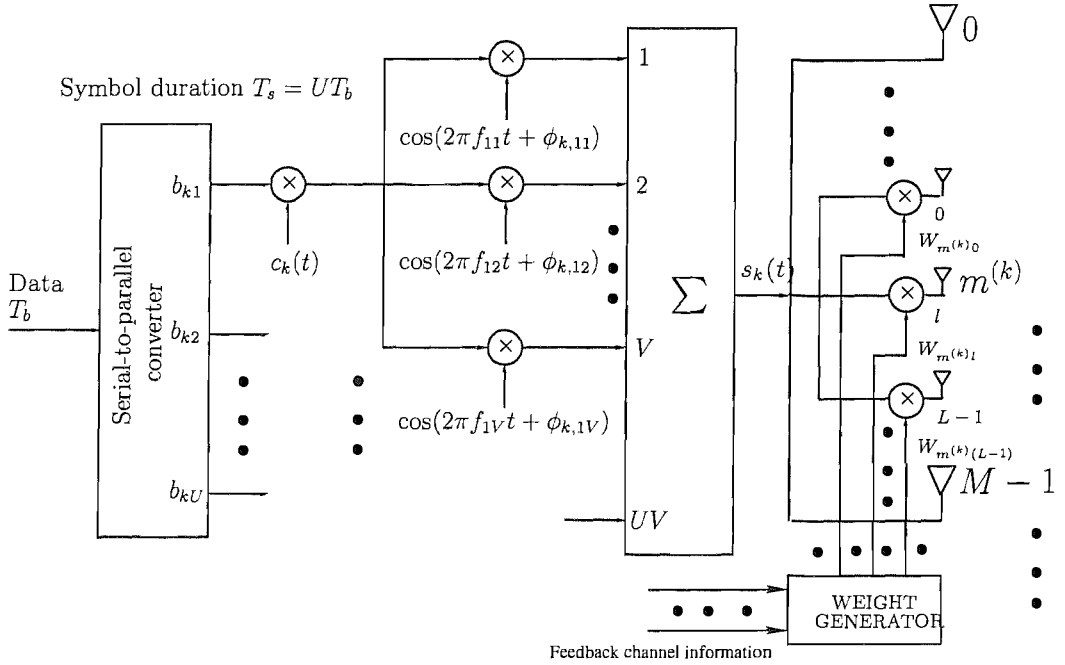


**Figure 3.6:** The downlink transmitter schematic of the generalized multicarrier DS-CDMA system, where the transmitter space-time processing scheme using the BSTD is employed. In contrast to the beamforming scheme seen in Figure 3.1, where only a single antenna array having $L$ array elements is used, the BSTD scheme employs $M$ antenna arrays and one of the antenna arrays benefitting from the best channel quality is selected to form a beam towards the desired mobile user for signal transmission.

where $s_k(t)$ is identical to (2.1), $\mathbf{w}^{(k)}_{v,m^{(k)}}$ is the $(L \times 1)$-dimensional transmit weight vector generated by the beamformer according to the channel quality information between the $k$th mobile user and $m^{(k)}$th array, $P_k/V$ represents the transmitted power of each subcarrier, while the factor of $L$ in the denominator of (3.51) indicates that the total transmit power is shared by $L$ array elements, as indicated by the power divider block of Figure 3.7. Furthermore, in (3.51) $\{b_{ku}(t)\}$, $c_k(t)$, $\{f_{uv}\}$ and $\{\phi_{k,uv}\}$ represent the data stream, the DS spreading waveform, the subcarrier frequency set and the phase angles introduced in the carrier modulation process, respectively. The data stream's waveform $b_{ku}(t) = \sum_{i=-\infty}^{\infty} b_{ku}[i]P_{T_s}(t - iT_s)$ consists of a sequence of mutually independent rectangular pulses of duration $T_s$ and of amplitude +1 or -1 with equal probability. The spreading sequence $c_k(t) = \sum_{j=-\infty}^{\infty} c_{kj}P_{T_c}(t - jT_c)$ denotes the signature sequence waveform of the $k$th user, where $c_{kj}$ assumes values of +1 or -1 with equal probability, while $P_{T_c}(t)$ is the rectangular chip waveform, which is defined over the interval $[0, T_c)$. The stylised spectral arrangement on the downlink is also identical to that shown in Figure 2.3. Hence the receiver is capable of achieving the maximum frequency-domain diversity gain as a benefit of the independent frequency-selective fading of the subcarriers, when combining the corresponding subcarrier signals.

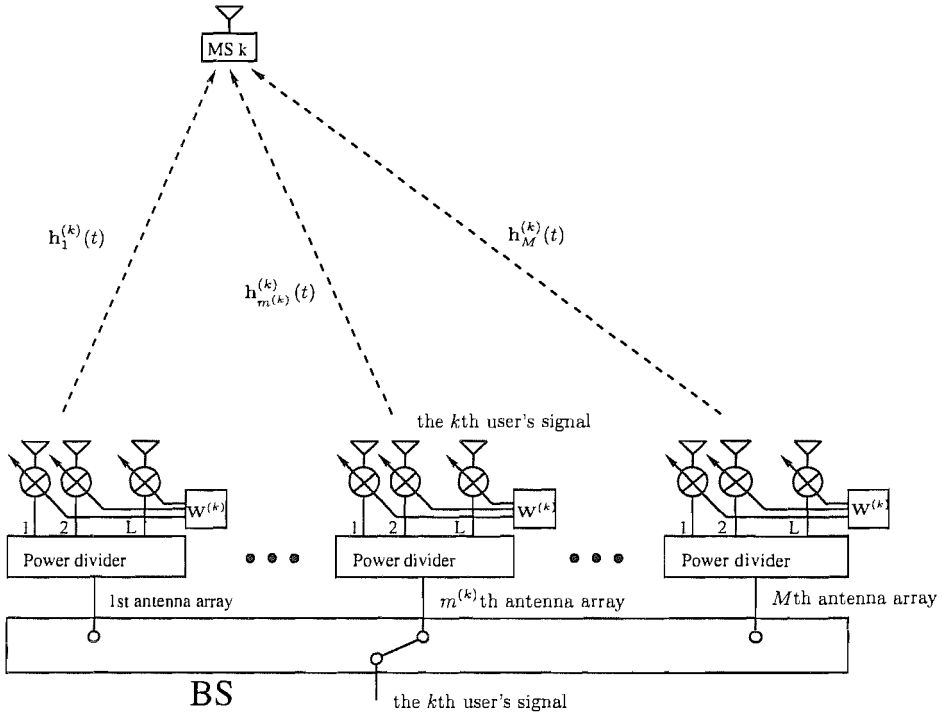


**Figure 3.7:** BS downlink transmitter array configuration for the BSTD scheme.

### 3.3.2 Receiver Model - Beam Selection Transmit Diversity

Based on the assumption that the $m^{(k)}$th array is selected to transmit the $k$th user's signal, the ST-CIRs corresponding to the $m^{(k)}$th antenna array $\mathbf{h}^{(1)}_{uv,m^{(k)}}(t)$ for the reference user can be formulated by modifying (3.3), leading to

$$\begin{aligned}\mathbf{h}^{(1)}_{uv,m^{(k)}}(t) &= \left[h^{(1)}_{uv,m^{(k)}0}(t), h^{(1)}_{uv,m^{(k)}1}(t), \ldots, h^{(1)}_{uv,m^{(k)}(L-1)}(t)\right]^T \\ &= \mathbf{a}^{(1)}_{uv,m^{(k)}}(t)\delta(t-\tau_1) \\ &= \left[a^{(1)}_{uv,m^{(k)}0}(t), a^{(1)}_{uv,m^{(k)}1}(t), \ldots, a^{(1)}_{uv,m^{(k)}(L-1)}(t)\right]^T \delta(t-\tau_1), \end{aligned} \quad (3.52)$$

which is an $(L \times 1)$-dimensional vector, where $a^{(1)}_{uv,m^{(k)}l}(t)$ is the CIR with respect to the $uv$th sub-carrier of the reference user and the $l$th element of the $m^{(k)}$th array. Based on the assumption that the array elements are separated by half a wavelength, i.e. that we have $d = \lambda/2$, we can simplify $\mathbf{a}^{(1)}_{uv,m^{(k)}}(t)$ of (3.52) to

$$\begin{aligned}\mathbf{a}^{(1)}_{uv,m^{(k)}}(t) &= \Big[\alpha^{(1)}_{uv,m^{(k)}}(t), \\ &\quad \alpha^{(1)}_{uv,m^{(k)}}(t)\exp\left(j\left[\pi\sin(\psi^{(1)}_{m^{(k)}} + \kappa^{(1)}_{m^{(k)}}B)\right]\right), \ldots, \\ &\quad \alpha^{(1)}_{uv,m^{(k)}}(t)\exp\left(j\left[(L-1)\pi\sin(\psi^{(1)}_{m^{(k)}} + \kappa^{(1)}_{m^{(k)}}B)\right]\right)\Big]^T, \end{aligned} \quad (3.53)$$

which is similar to (3.4) except that it corresponds to the $m^{(k)}$th antenna array.

The total received signal for the reference user is constitutedly the superposition of all the $K$ users' transmissions plus the AWGN, hence the received signal can be expressed as

$$\begin{aligned} r(t) &= \sum_{k=1}^{K} r_k(t) + n(t) \\ &= \sum_{k=1}^{K}\sum_{u=1}^{U}\sum_{v=1}^{V} \sqrt{\frac{2P_k}{VL}}\, b_{ku}(t-\tau_1)c_k(t-\tau_1)(\mathbf{w}_{v,m^{(k)}}^{(k)})^H \mathbf{a}_{uv,m^{(k)}}^{(1)}(t) \\ &\quad \times \exp\left(j\left[2\pi f_{uv}t + \theta_{uv}^{(k)}\right]\right) + n(t), \end{aligned} \tag{3.54}$$

where $r_k(t)$ is similar to (3.2), and we have $\theta_{uv}^{(k)} = \phi_{k,uv} - 2\pi f_{uv}\tau_1$, which is a random variable uniformly distributed in $[0, 2\pi]$. In the above equation, we assumed that all the subcarrier signals arrive from the same direction. In (3.54), $n(t)$ is an AWGN process having a zero mean and a variance of $2N_0\delta(t_1 - t_2)$, where $N_0$ represents the double-sided power spectral density of a complex valued low-pass-equivalent AWGN process.

The receiver is the same as that seen in Figure 3.2, where the superscript and subscript denoting the reference user of $k = 1$ has been omitted for notational convenience. Based on the assumption of orthogonal multicarrier signals, orthogonal WH DS spreading codes, synchronous transmission of the $K$ user signals as well as slow flat-fading of each subcarrier, there is no interference between the different users and the different subcarrier signals. The decision variable related to the information bit $b_u[0]$ can be derived following the same approach presented in Section 3.2.2. Therefore, according to the derivation of (3.8), the decision variable corresponding to the 0th bit $b_u[0]$ and the $v$th subcarrier can be expressed as

$$\begin{aligned} z_{uv} &= \int_0^{T_s} r(t)c(t)\exp\left(-j[2\pi f_{uv}t + \theta_{uv}]\right) dt \\ &= \sqrt{\frac{2P}{VL}}T_s\left[b_u[0](\mathbf{w}_{v,m^{(1)}}^{(1)})^H \mathbf{a}_{uv,m^{(1)}} + n_{uv}\right], \end{aligned} \tag{3.55}$$

where $b_u[0](\mathbf{w}_{v,m^{(1)}}^{(1)})^H \mathbf{a}_{uv,m^{(1)}}$ represents the desired output, while $\mathbf{a}_{uv,m^{(1)}}$ is given by (3.53) for the reference user corresponding to $k = 1$. In (3.55) $n_{uv}$ is contributed by $n(t)$ of (3.54), which is an AWGN process having zero mean and a variance of $\frac{VLN_0}{E_b}$. After the MRC combining stage of Figure 3.2, we arrive at the decision variable $z_u$ expressed as

$$z_u = \sum_{v=1}^{V} \sqrt{\frac{2P}{VL}}T_s\left[Lb_u[0]\|a_{uv,m^{(1)}}\|^2 + n_{uv}\right], \tag{3.56}$$

which is similar to (3.32) corresponding to the $m^{(1)}$th antenna array.

### 3.3.3 User-load Extension Using TF-Domain Spreading - Beam Selection Transmit Diversity

As in Section 3.2.4, spreading in the F-domain across the $V$ subcarriers, which conveyed identical replicas of the same bit in Figure 2.3, can also be employed in order to support more users in the generalized MC DS-CDMA system using BSTD. The resultant bandwidth is again the same as that of the MC DS-CDMA scheme employing the time-domain-only spreading, while the total number of users supported becomes $VK_{max} = VN_e$, which is $V$ times higher than the number of the users supported by the MC DS-CDMA scheme employing the time-domain-only spreading.

Explicitly, the transmitter schematic of the broadband MC DS-CDMA scheme using TF-domain spreading is similar to that seen in Figure 3.6, except that the $V$-depth FD repetition scheme of Figure 3.6 is now replaced by the F-domain spreading associated with an orthogonal spreading code of length $V$. Similarly, let $\{c'_k[0], c'_k[1], \ldots, c'_k[V-1]\}$ be the $k$th user's orthogonal code in discrete form, while the $k$th user's T-domain orthogonal code has been expressed in Section 3.2.1 as $c_k(t)$ in continuous form. The assignment of the orthogonal spreading codes is identical to that described in Section 3.2.4, hence, the transmitted signals of the $k$th user can be expressed as

$$\begin{aligned} \mathbf{s}_k(t) &= (\mathbf{w}^{(k)}_{v,m^{(k)}})^H \bullet s_k(t) \qquad (3.57) \\ &= \sum_{u=1}^{U}\sum_{v=1}^{V} \sqrt{\frac{2P_k}{VL}} (\mathbf{w}^{(k)}_{v,m^{(k)}})^H b_{ku}(t) c_k(t) c'_k[v-1] \cos(2\pi f_{uv} t + \phi_{k,uv}), \end{aligned}$$

which is the same as (3.33). In (3.57) $P_k/V$ represents the transmitted power of each subcarrier, while $\mathbf{w}^{(k)}_{v,m^{(k)}}$ is the $(L \times 1)$-dimensional BS downlink transmit weight vector generated by the beamformer with the aid of the channel quality information corresponding to the $v$th subcarrier of the $k$th user on the $m^{(k)}$th antenna array.

Let $1 \leq K' \leq V$ be the number of users sharing the same T-domain spreading code. We also assume that any T-domain spreading code is shared by the same $K'$ number of users. Then, when the $K'K_{max}$ signals expressed in the form of (3.57) are transmitted over frequency-selective fading channels, the complex-valued low-pass equivalent received signal can be expressed as

$$\begin{aligned} r(t) &= \sum_{k=1}^{K'K_{max}} \mathbf{s}_k(t) \otimes \mathbf{h}^{(1)}_{uv,m^{(k)}}(t) + n(t) \\ &= \sum_{k=1}^{K'K_{max}} \sum_{u=1}^{U}\sum_{v=1}^{V} \sqrt{\frac{2P_k}{VL}}\, b_{ku}(t-\tau_1) c_k(t-\tau_1) (\mathbf{w}^{(k)}_{v,m^{(k)}})^H \mathbf{a}^{(1)}_{uv,m^{(k)}}(t) \\ &\quad \times c'_k[v-1] \exp\left(j\left[2\pi f_{uv} t + \theta^{(k)}_{uv}\right]\right) + n(t), \qquad (3.58) \end{aligned}$$

which is identical to (3.58) corresponding to the $m^{(k)}$th antenna array. Following the derivations provided in Section 3.2.4, the decision variable $z_{uv}$ corresponding to the subcarrier $uv$ can now be

expressed as

$$z_{uv} = \sqrt{\frac{2P}{VL}} T_s \left[ \sum_{k=1}^{K'} \left( \sqrt{\frac{P_k}{P}} (\mathbf{w}_{v,m^{(k)}}^{(k)})^H \mathbf{a}_{uv,m^{(k)}}^{(1)}(t) \times c'_k[v-1] b_{ku}[0] \right) + n_{uv} \right], \tag{3.59}$$

where $n_{uv}$ is an AWGN process having zero mean and a variance of $\frac{VLN_0}{E_b}$.

Let $\beta_{kv} = (\mathbf{w}_{v,m^{(k)}}^{(k)})^H \mathbf{a}_{uv,m^{(k)}}^{(1)}(t)$, then (3.59) can be written in a matrix form as

$$\mathbf{z}_u = \sqrt{\frac{2P}{VL}} T_s \left[ \mathbf{C}\mathbf{P}\mathbf{b} + \mathbf{n} \right], \tag{3.60}$$

which is the same as (3.41). In the context of the single-user correlation based detector, the decision variable $z_u$ of the desired user is obtained by combining $\mathbf{z}_u = [z_{u1}, z_{u2}, \ldots, z_{uV}]$ with $\mathbf{c}'_1 = [c'_1[0], c'_1[1], \ldots, c'_1[V-1]]$, which can be expressed as

$$z_u = \sqrt{\frac{2P}{VL}} T_s \left[ \sum_{v=1}^{V} \beta_{1v} b_{1u} + \sum_{k=2}^{K'} \sum_{v=1}^{V} \sqrt{\frac{P_k}{P}} c'_1[v-1] c'_k[v-1] \beta_{kv} b_{ku} + \mathbf{c}'_1 \mathbf{n} \right], \tag{3.61}$$

where we have $\mathbf{n} = [n_{u1}, n_{u2}, \ldots, n_{uV}]^T$ and

$$\beta_{1v} = (\mathbf{w}_{v,m^{(1)}}^{(1)})^H \mathbf{a}_{uv,m^{(1)}}^{(1)}(t) = L \| \alpha_{uv,m^{(1)}} \|^2, \tag{3.62}$$

while $\mathbf{w}_{v,m^{(1)}}^{(1)} = \mathbf{a}_{uv,m^{(1)}}^{(1)}$ in (3.62) is generated by the MRC beamformer [7] of Figure 3.6.

As we have discussed previously in Section 3.2.4, the interference $\sum_{k=2}^{K'} \sum_{v=1}^{V} \sqrt{\frac{P_k}{P}} c'_1[v-1] c'_k[v-1] \beta_{kv} b_{ku}$ can be reduced, if we carefully select the $K'$ users, which have the lowest interference coefficient with respect to the desired user, from all the $K'\mathcal{K}_{max}$ users in order to share the same T-domain spreading code with the desired user. The interference coefficient of $\rho_{1k} = \sqrt{\frac{P_k}{P}} \beta_{kv} = \sqrt{\frac{P_k}{P}} (\mathbf{w}_{v,m^{(k)}}^{(k)})^H \mathbf{a}_{uv,m^{(1)}}^{(1)}(t)$, $k = 1, 2, \ldots, K'\mathcal{K}_{max}$, can be derived before transmissions based on the assumption that $\mathbf{a}_{uv,m^{(1)}}^{(1)}(t)$ is perfectly estimated and provided that $\mathbf{w}_{v,m^{(k)}}^{(k)} = \mathbf{a}_{uv,m^{(k)}}^{(k)}(t)$ is also perfectly estimated, which is generated by the MRC beamformer [7] of Figure 3.6. With the advent of this user regrouping operation, the achievable BER performance may be substantially improved. Note that when a new user joins or disjoins the system, the grouping has to be updated.

Naturally, the achievable detection performance can also be improved, if the single-user detector is replaced by a more sophisticated multiuser detector, such as the decorrelating MUD [195] or an MMSE based MUD [195]. Specifically, when the multiuser decorrelating detector is employed, the vector of decision variables $\mathbf{z}'_u = \left[ z'_{1u}\ z'_{2u}\ \ldots\ z'_{K'u} \right]^T$ derived for the $K'$ users is obtained by

multiplying both sides of (3.60) with the matrix $(\mathbf{C}^H\mathbf{C})^{-1}\mathbf{C}^H$, which can be expressed as

$$\begin{aligned}\mathbf{z'}_u &= \sqrt{\frac{2P}{VL}}T_s\left[(\mathbf{C}^H\mathbf{C})^{-1}\mathbf{C}^H\mathbf{C}\mathbf{P}\mathbf{b} + (\mathbf{C}^H\mathbf{C})^{-1}\mathbf{C}^H\mathbf{n}\right] \\ &= \sqrt{\frac{2P}{VL}}T_s\left[\mathbf{P}\mathbf{b} + \mathbf{n'}\right], \end{aligned} \tag{3.63}$$

which is identical to (3.48) and again, we have

$$\mathbf{n'} = (\mathbf{C}^H\mathbf{C})^{-1}\mathbf{C}^H\mathbf{n}. \tag{3.64}$$

Obviously, according to Equation (3.63), the decision variable $z'_{1u}$ for the first user is given by

$$z'_{1u} = \sqrt{\frac{2P}{VL}}T_s(b_{1u} + n'_1), \tag{3.65}$$

where $n'_1$ is the first element of the noise vector $\mathbf{n'}$ of (3.64). It can be shown from Equation (3.65) that the multiuser interference is fully eliminated.

## 3.4 Space Time Transmit Diversity - Downlink

The well-known family of orthogonal transmit diversity (OTD) schemes [128] achieves diversity gain by recovering the received signal energy from two independently fading paths arriving from two transmit antennas to the receiver. The OTD scheme relies on the assistance of both an interleaver and a channel decoder. In the context of the OTD, the channel coded symbols are demultiplexed into two different streams, which are then transmitted using two WH codes, mapping the resultant signals to two transmit antennas. The total achievable diversity gain of this scheme depends on the power of the convolutional or turbo code that is employed. In addition to the conventionally transmitted pilot signal of single-antenna systems, an auxiliary pilot is transmitted on the second antenna in order to aid coherent detection at the receiver. The so-called Time Switched Transmit Diversity (TSTD) scheme [128] has a similar performance to that of the OTD arrangement [128]. In the STTD scheme of [48], the symbols to be transmitted are first space-time coded and then transmitted via two widely separated antennas [48], hence the system is capable of achieving second order diversity without requiring channel coding and interleaving, which are inevitably required in the OTD scheme of [128]. Upon exploiting the extra space diversity provided by the additional diversity antennas, STTD is capable of outperforming both OTD and TSTD [131]. Moveover, in the OTD and TSTD based schemes, the benefits of path diversity become less significant, since the interleaver associated with the error correction coding scheme provides sufficient temporal diversity, leading to potentially reduced performance gains at high vehicular speeds [128]. By contrast, the STTD scheme is capable of achieving significant gains in single-path Rayleigh fading channels. Therefore, below we will only focus our attention on the employment of the STTD scheme. We will demonstrate that additional antennas may be added to this diversity configuration in order to achieve additional diversity gains on the downlink. However, the largest incremental diversity gains are obtained, when increasing the

number of antennas from one to two. Furthermore, the STD scheme, which constitutes a representative of the closed-loop transmit diversity schemes and selects the specific antenna having the best instantaneous channel state for signal transmission may be expected to have a superior performance in comparison to that of the open-loop STTD scheme, as long as the antenna selection decision can be correctly and sufficiently promptly fed back to the transmitter [129,130].

### 3.4.1 Transmitter Model of Space Time Transmit Diversity

Alamouti proposed a simple transmit diversity scheme employing a space-time block code [140], which was capable of achieving a substantial diversity gain by simultaneously transmitting two symbols with the aid of two antennas. The system considered in this section is a generalized MC DS-CDMA scheme [40–42] using $U \cdot V$ number of subcarriers, $M$ number of transmitter antennas having an antenna-spacing of $10\lambda$ and a single receiver antenna. The transmitter schematic of the $k$th user employing $M$ transmit antennas is shown in Figure 3.8, where real-valued data symbols using real-valued spreading [196,197] were considered. However, the analysis provided here may be extended to MC DS-CDMA systems using both complex-valued data symbols as well as complex-valued spreading. The frequency arrangement of the $U \cdot V$ subcarriers in this system is the same as that seen in Figure 2.3. As shown in Figure 3.8, at the transmitter side a block of $U \cdot M$ data bits each having a bit duration of $T_b$ is S-P converted to $U$ parallel sub-blocks. The new bit duration of each sub-stream, which we refer to as the symbol duration, becomes $T_s = UT_b$ as seen in Figure 3.8. In contrast with Figure 2.2, Figure 3.8 suggests that the STTD scheme employs orthogonal STS codes for spreading the signal in the T-domain, instead of the WH codes used by the beamforming scheme in Figure 2.2. Each parallel sub-block has $M$ data bits, which are space-time spread using the schemes of [196–198] - with the aid of $M$ orthogonal spreading codes - for example $M$ modified WH codes - $\{c_{k,1}(t), c_{k,2}(t), \ldots, c_{k,M}(t)\}$, $k = 1, 2, \ldots, K$ and mapped to $M$ transmitter antennas. More specifically, these $M$ modified WH codes having length of $MN_e$ were derived from the assigned WH code having a length of $N_e$ for the $k$th user by concatenating $M$ identical replicas of the original code. For $M = 2$ and 4, we have

$$\begin{aligned} c_{k,1}(t) &= [1,1]c_k(t) = [c_k(t), c_k(t)], \\ c_{k,2}(t) &= [1,-1]c_k(t) = [c_k(t), -c_k(t)], \end{aligned} \tag{3.66}$$

and

$$\begin{aligned} c_{k,1}(t) &= [1,1,1,1]c_k(t) = [c_k(t), c_k(t), c_k(t), c_k(t)], \\ c_{k,2}(t) &= [1,-1,1,-1]c_k(t) = [c_k(t), -c_k(t), c_k(t), -c_k(t)], \\ c_{k,3}(t) &= [1,1,-1,-1]c_k(t) = [c_k(t), c_k(t), -c_k(t), -c_k(t)], \\ c_{k,4}(t) &= [1,-1,-1,1]c_k(t) = [c_k(t), -c_k(t), -c_k(t), c_k(t)]. \end{aligned} \tag{3.67}$$

The symbol duration of the Space-Time Spreading (STS) [196–198] signals is $MT_s$, and the discrete period of the orthogonal codes is $MT_s/T_c = MN_e$, where $N_e = T_s/T_c$ and $T_c$ represents

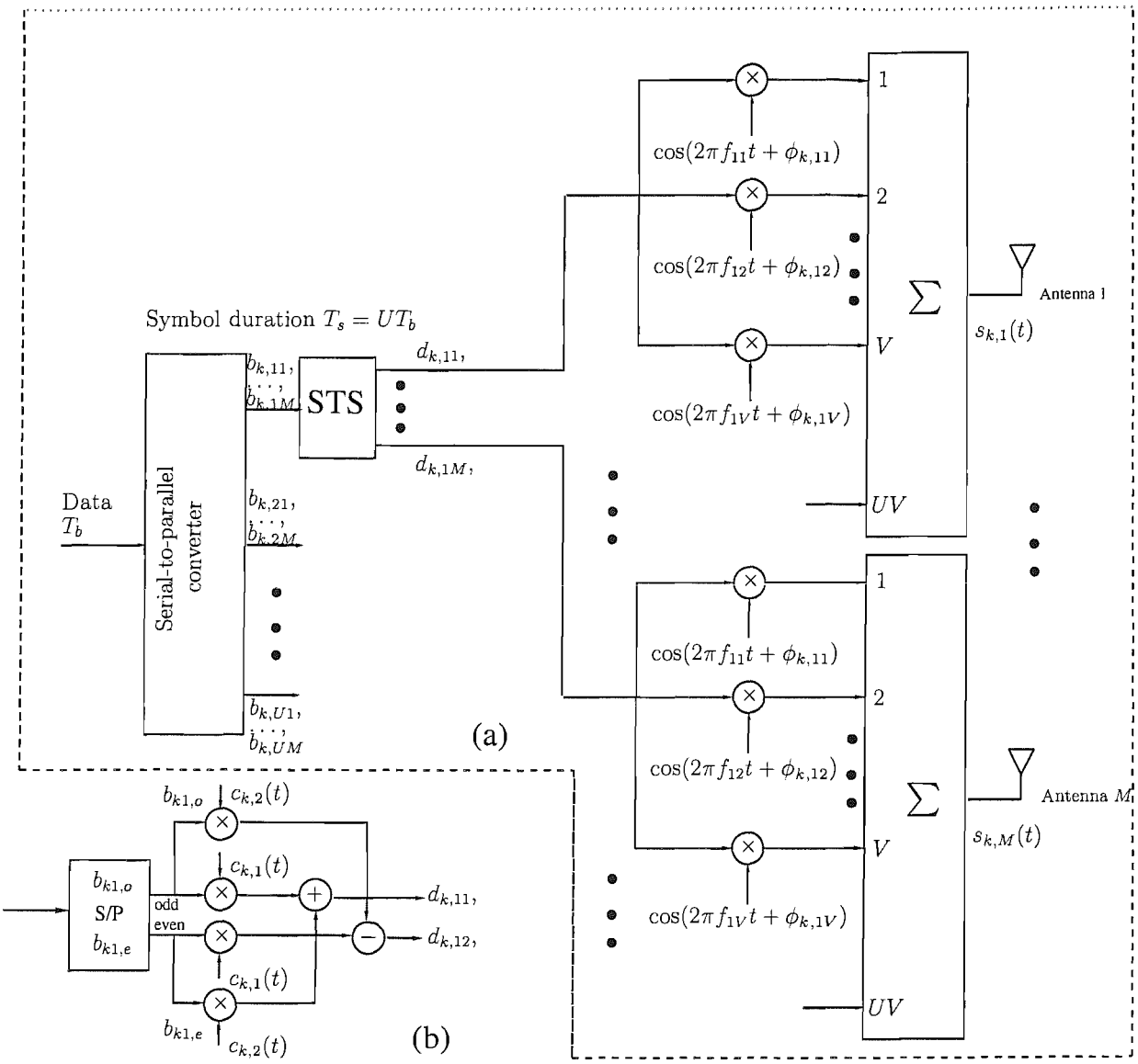


**Figure 3.8:** (a) The $k$th user's transmitter schematic for the downlink of the generalized multicarrier DS-CDMA system associated with STTD; (b) The block diagram of STS using $M = 2$. Observing Figure 2.2 and this figure suggests that the STTD scheme employs orthogonal STS codes for spreading the signal in the T-domain, instead of the WH codes used in Figure 2.2. Another difference between these two figures is that the STTD scheme uses $M$ antennas to attain transmit diversity gain, while the transmit schematic seen in Figure 2.2 only employs a single transmit antenna.

the chip-duration of the orthogonal STS codes. The orthogonal STS codes obey the relationship of $\sum_{l=0}^{MN_e} c_{i,m}[l]c_{j,n}[l] = 0$, when $i \neq j$ or $m \neq n$. As seen in Figure 3.8(a), following STS, each STS block generates $M$ parallel signals to be mapped to the $M$ downlink BS transmitter antennas. A detailed STS processing for the case of $M = 2$ is provided in Figure 3.8(b), where the odd bit $b_{k1,o}$ and the even bit $b_{k1,e}$ are space-time (ST) spread using the schemes of [196–198] with the aid of

two orthogonal spreading codes $\{c_{k,1}(t), c_{k,2}(t)\}$, $k = 1, 2, \ldots, K$. As shown in Figure 3.8(b), the resultant STS signals are $d_{k,11} = b_{k1,o}c_{k,1}(t) + b_{k1,e}c_{k,2}(t)$ and $d_{k,12} = b_{k1,e}c_{k,1}(t) - b_{k1,o}c_{k,2}(t)$. The specific $U$ STS signals of Figure 3.8, which are output by the $U$ STS blocks and which will be transmitted using the same antenna from the set $1, 2, \ldots, M$ then modulate a group of subcarrier frequencies $\{f_{u1}, f_{u2}, \ldots, f_{uV}\}$ using Binary Phase Shift Keying (BPSK). Since each of the $U$ data bits is spread to and hence conveyed with the aid of $V$ subcarriers, a total of $UV$ number of subcarriers are required in the MC DS-CDMA system considered. Finally, the $UV$ number of subcarrier signals are superimposed on each other in order to form the complex modulated signal. As shown in Figure 2.3, the subcarrier frequency arrangement according to Equation (2.2) guarantees that the same STS signal is spread to and hence transmitted by the specific $V$ subcarriers having the maximum possible frequency spacing, so that they experience independent fading and hence achieve the maximum attainable frequency diversity. Observing Figure 2.2 and Figure 3.8 suggests that the STTD scheme of Figure 3.8 employs orthogonal STS codes for spreading the signal in the T-domain, instead of the WH codes used in Figure 2.2. Another difference between these two figures is that the STTD scheme uses $M$ antennas to attain transmit diversity gain, while the transmit schematic seen in Figure 2.2 only employs a single transmit antenna.

The general form of the $k$th user's transmitted signal corresponding to the $M$ transmitter antennas can be expressed as

$$\mathbf{s}_k(t) = \sum_{u=1}^{U}\sum_{v=1}^{V}\sqrt{\frac{2P_k}{V}\frac{1}{MM}}\mathbf{B}_{ku}\mathbf{c}_k\cos(2\pi f_{uv}t + \phi_{k,uv}), \tag{3.68}$$

where $P_k/V$ represents the transmitted power of each subcarrier, while the factor of $MM$ in the denominator suggests that the STS scheme using $M$ orthogonal codes and $M$ transmitter antennas distributes its total transmit power proportionally. In (3.68) $\mathbf{s}_k(t) = [s_{k1}(t)\ s_{k2}(t)\ \ldots\ s_{kM}(t)]^T$ represents the transmitted signal vector of the $M$ transmitter antennas, while $\mathbf{c}_k$ is an $(M \times 1)$-dimensional vector constituted by the orthogonal STS codes, which can be expressed as

$$\mathbf{c}_k = [c_{k,1}(t), c_{k,2}(t), \ldots, c_{k,M}(t)]^T. \tag{3.69}$$

In (3.68) $\mathbf{B}_{ku}$ is an $(M \times M)$-dimensional matrix mapped from the $u$th sub-block data bits, according to the requirements of STS [196, 197]. Specifically, the matrix $\mathbf{B}_{ku}$ can be expressed as

$$\mathbf{B}_{ku} = \begin{pmatrix} a_{11}b'_{k,11} & a_{12}b'_{k,12} & \cdots & a_{1M}b'_{k,1M} \\ a_{21}b'_{k,21} & a_{22}b'_{k,22} & \cdots & a_{2M}b'_{k,2M} \\ \vdots & \vdots & \ddots & \vdots \\ a_{M1}b'_{k,M1} & a_{M2}b'_{k,M2} & \cdots & a_{MM}b'_{k,MM} \end{pmatrix}, \ u = 1, 2, \ldots, U, \tag{3.70}$$

where $a_{ij}$ represents the sign of the element at the $i$th row and the $j$th column, which is determined by the STS design rule [196, 197], while $b'_{k,ij}$ in $\mathbf{B}_{ku}$ is the data bit assigned to the $(i, j)$th element, which is one of the $M$ input data bits $\{b_{k,u1}, b_{k,u2}, \ldots, b_{k,uM}\}$ of user $k$. For $M = 2$ and 4, the

corresponding $\mathbf{B}_{ku}$ matrices are given by [196]

$$\begin{pmatrix} b_{k,u1} & b_{k,u2} \\ b_{k,u2} & -b_{k,u1} \end{pmatrix}, \text{ and } \begin{pmatrix} b_{k,u1} & b_{k,u2} & b_{k,u3} & b_{k,u4} \\ b_{k,u2} & -b_{k,u1} & -b_{k,u4} & b_{k,u3} \\ b_{k,u3} & b_{k,u4} & -b_{k,u1} & -b_{k,u2} \\ b_{k,u4} & -b_{k,u3} & b_{k,u2} & -b_{k,u1} \end{pmatrix}, \; u = 1, 2, \ldots, U. \tag{3.71}$$

Equation (3.68) represents the general form of the transmitted signals using STS, regardless of the value of $M$. However, the study conducted in [196] has shown that STS schemes using $M = 2, 4, 8$ constitute attractive schemes, since they are capable of providing maximal transmit diversity without requiring extra STS codes. Note that for the specific values of $M = 2, 4$ the above mentioned attractive STS schemes have been unambiguously specified with the aid of (3.71). In this treatise, we only investigate these attractive STS schemes and our results are mainly based on MC DS-CDMA systems using two or four transmitter antennas.

For the case of $M = 2$, the MC DS-CDMA signals transmitted by antenna 1 and 2 can be simply expressed as

$$\begin{aligned} \mathbf{s}_k(t) &= \begin{pmatrix} s_{k1}(t) \\ s_{k2}(t) \end{pmatrix} \\ &= \sqrt{\frac{2P_k}{4V}} \begin{pmatrix} \sum_{u=1}^{U}\sum_{v=1}^{V}[c_{k,1}b_{k,u1} + c_{k,2}b_{k,u2}]\cos(2\pi f_{uv}t + \phi_{k,uv}) \\ \sum_{u=1}^{U}\sum_{v=1}^{V}[c_{k,1}b_{k,u2} - c_{k,2}b_{k,u1}]\cos(2\pi f_{uv}t + \phi_{k,uv}) \end{pmatrix}. \end{aligned} \tag{3.72}$$

By contrast, for the case of $M = 4$, the MC DS-CDMA signals transmitted by antenna 1, 2, 3 and 4 can be expressed as

$$\begin{aligned} \mathbf{s}_k(t) = \begin{pmatrix} s_{k1}(t) \\ s_{k2}(t) \\ s_{k3}(t) \\ s_{k4}(t) \end{pmatrix} &= \sqrt{\frac{2P_k}{16V}} \\ \times \begin{pmatrix} \sum_{u=1}^{U}\sum_{v=1}^{V}[c_{k,1}b_{k,u1} + c_{k,2}b_{k,u2} + c_{k,3}b_{k,u3} + c_{k,4}b_{k,u4}]\cos(2\pi f_{uv}t + \phi_{k,uv}) \\ \sum_{u=1}^{U}\sum_{v=1}^{V}[c_{k,1}b_{k,u2} - c_{k,2}b_{k,u1} - c_{k,3}b_{k,u4} + c_{k,4}b_{k,u3}]\cos(2\pi f_{uv}t + \phi_{k,uv}) \\ \sum_{u=1}^{U}\sum_{v=1}^{V}[c_{k,1}b_{k,u3} + c_{k,2}b_{k,u4} - c_{k,3}b_{k,u1} - c_{k,4}b_{k,u2}]\cos(2\pi f_{uv}t + \phi_{k,uv}) \\ \sum_{u=1}^{U}\sum_{v=1}^{V}[c_{k,1}b_{k,u4} - c_{k,2}b_{k,u3} + c_{k,3}b_{k,u2} - c_{k,4}b_{k,u1}]\cos(2\pi f_{uv}t + \phi_{k,uv}) \end{pmatrix}. \end{aligned} \tag{3.73}$$

Observing Equations (3.72) and (3.73) suggests that upon using the STS technique, the STTD scheme

transmits the same bit, i.e. $b_{k,u1}$, through the $M$ number of transmit antennas, which are located sufficiently far apart so that the three replicas of bit $b_{k,u1}$ experience independent fading and hence attain a transmit diversity gain. By contrast, in Equation (3.1) the beamforming scheme employs an antenna array having $L$ antenna elements, which are separated by a distance of half a wavelength for the sake of achieving angular selectivity and hence attain an increased SNR gain.

### 3.4.2 Receiver Model of Space Time Transmit Diversity

Based on the assumptions that $M$ transmitter antennas, which are located sufficiently apart since then have an antenna-spacing of more than $10\lambda$, are activated at the BS, the ST-CIR $h_{uv,m}^{(k)}$ between the $uv$th subcarrier of the $k$th user and the $m$th antenna can be expressed as

$$\begin{aligned} h_{uv,m}^{(k)} &= \alpha_{uv,m}^{(k)}(t)\exp(j\varphi_{uv,m}^{(k)})\delta(t-\tau_k), \\ & \quad m = 0,1,\ldots,M-1; \\ & \quad u = 1,2,\ldots,U;\ v = 1,2,\ldots,V; \\ & \quad k = 1,2,\ldots,K, \end{aligned} \tag{3.74}$$

which is identical to (2.10) in conjunction with $L = 1$. In (3.74) $\alpha_{uv,m}^{(k)}(t)$ is the Rayleigh faded channel envelope's amplitude, $\varphi_{uv,ml}^{(k)}$ is a phase angle, which is the result of the channel-induced phase rotation, modelled by a random variable uniformly distributed in $[0, 2\pi]$, while $\tau_k$ is the signal's delay. Based on the assumption that all the $K$ users' signals are transmitted synchronously, we assume that we have $\tau_k = 0$, $k = 1,2,\ldots,K$, for simplicity. Based on (3.74), the ST-CIRs corresponding to the entire set of $M$ transmit antennas can be written as

$$\begin{aligned} \mathbf{h}_{uv}^{(k)}(t) &= \left[h_{uv,0}^{(k)}(t), h_{uv,1}^{(k)}(t), \ldots, h_{uv,(M-1)}^{(k)}(t)\right]^T \\ &= \mathbf{a}_{uv}^{(k)}(t)\delta(t) \\ &= \left[a_{uv,0}^{(k)}(t), a_{uv,1}^{(k)}(t), \ldots, a_{uv,(M-1)}^{(k)}(t)\right]^T \delta(t), \end{aligned} \tag{3.75}$$

which is an $M$-dimensional vector and has the same structure as (3.3) except that the term $L$ in (3.3) is replaced by the term $M$.

Assuming that the $K$ users' signals obeying the form of (3.68) are transmitted synchronously over dispersive Rayleigh fading channels characterized by the ST-CIR of (3.75), the complex-valued low-pass equivalent received signal can be expressed as

$$r(t) = \sum_{k=1}^{K} r_k(t) + n(t), \tag{3.76}$$

where $n(t)$ is the AWGN process having a zero mean and a variance described in Equation (3.6). In (3.76) $r_k(t)$ represents the $k$th user's transmitted signal received by the 1st user, which can be

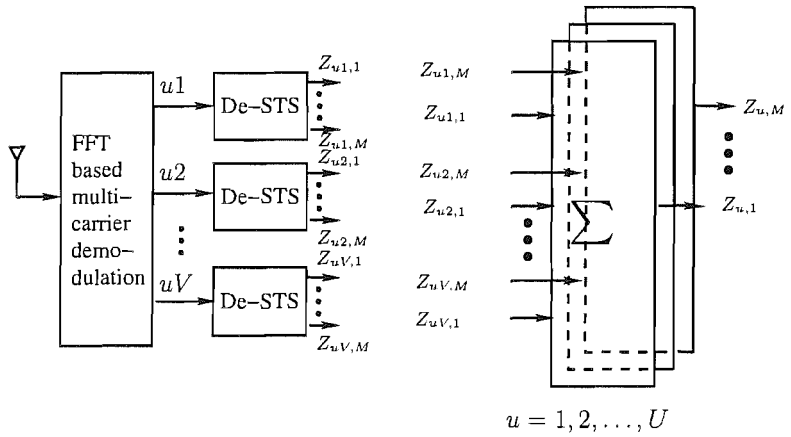


**Figure 3.9:** The receiver schematic of the generalized multicarrier DS-CDMA system associated with STTD. The only difference between this figure and Figure 3.2 of Section 3.2.2 is that the WH code despreading employed by the beamforming scheme in Figure 3.2 is replaced by space-time despreading carried out by the STTD scheme.

expressed as

$$\begin{aligned} r_k(t) &= \mathbf{s}_k^T(t) \otimes \mathbf{h}_{uv}^{(1)}(t) \\ &= \sum_{u=1}^{U}\sum_{v=1}^{V} \sqrt{\frac{2P_k}{V}\frac{1}{MM}}\mathbf{c}_k^T \mathbf{B}_{ku}^T \mathbf{h}_{uv}^{(1)}(t) \cos(2\pi f_{uv} t + \phi_{k,uv}). \end{aligned} \tag{3.77}$$

Specifically, for the case of $M = 2$, when the transmitted signal obeys (3.72), the complex-valued low-pass equivalent received signal can be expressed as

$$\begin{aligned} r(t) &= \sum_{k=1}^{K}\sum_{u=1}^{U}\sum_{v=1}^{V} \sqrt{\frac{2P_k}{4V}} \Big( a_{uv,0}^{(1)}[c_{k,1}(t)b_{k,u1} + c_{k,2}(t)b_{k,u2}] \\ &\quad + a_{uv,1}^{(1)}[c_{k,1}(t)b_{k,u2} - c_{k,2}(t)b_{k,u1}] \Big) \cos(2\pi f_{uv} t + \phi_{k,uv}) + n(t). \end{aligned} \tag{3.78}$$

Observing Equations (3.2), (3.5), (3.77) and (3.78) shows that the STTD scheme attains a transmit diversity gain by invoking STS processing, while the beamforming scheme attains an SNR gain as a benefit of its angular selectivity.

The receiver front-end of the STTD scheme in the downlink is shown in Figure 3.9, where the receiver first demodulates the received signal using Fast Fourier Transform (FFT) based multicarrier demodulation [9]. Hence we obtain $UV$ number of parallel streams corresponding to the signals transmitted on the $UV$ subcarriers. Each stream is then space-time de-spread using the approach of [8, 196], in order to obtain $M$ separate decision variables, $\{z_{uv,l}, z_{uv,2}, \ldots, z_{uv,M}\}$, corresponding to the $M$ data bits transmitted on the $uv$th stream, where we have $u = 1, 2, \ldots, U$; $v = 1, 2, \ldots, V$, respectively. The only difference between Figure 3.9 and Figure 3.2 of Section 3.2.2 is that the WH code despreading employed by the beamforming scheme in Figure 3.2 is replaced by space-time

de-spreading carried out by the STTD scheme.

For the case of $M = 2$, let $y_{uv,1}$, $y_{uv,2}$ represent the receiver correlator's output variables corresponding to the first two data bits transmitted on the $uv$th subcarrier, where

$$y_{uv,1} = \int_0^{2T_s} r(t)c_{1,1}(t)\exp\left(-j[2\pi f_{uv}t + \theta_{uv}]\right)dt, \tag{3.79}$$

$$y_{uv,2} = \int_0^{2T_s} r(t)c_{1,2}(t)\exp\left(-j[2\pi f_{uv}t + \theta_{uv}]\right)dt. \tag{3.80}$$

Since orthogonal multicarrier signals, orthogonal STS codes, synchronous transmission of the $K$ user signals as well as slow flat-fading of each subcarrier are assumed, there is no interference between the different users and the different subcarrier signals. Therefore, when substituting (3.78) into (3.79) and (3.80), it can be shown that we have

$$y_{uv,1} = \sqrt{\frac{2P}{V}}T_s\left[a_{uv,0}b_{1,u1} + a_{uv,1}b_{1,u2}\right] + n_{uv,1}, \tag{3.81}$$

$$y_{uv,2} = \sqrt{\frac{2P}{V}}T_s\left[a_{uv,0}b_{1,u2} - a_{uv,1}b_{1,u1}\right] + n_{uv,2}, \tag{3.82}$$

where $n_{uv,i}, i = 1, 2$ is due to the AWGN expressed as

$$n_{uv,i} = \int_0^{2T_s} n(t)c_{1,i}(t)\exp\left(-j[2\pi f_{uv}t + \theta_{uv}]\right)dt, \tag{3.83}$$

which is a complex Gaussian distributed variable having zero mean and a variance of $2N_0T_s$.

Assuming that the receiver has perfect knowledge of the fading parameters of $a_{uv,i}$, $i = 1, 2$, the decision variables corresponding to the data bits $b_{1,ui}, i = 1, 2$ associated with the $uv$th subcarrier can be expressed as

$$\begin{aligned} z_{uv,1} &= a^*_{uv,0}y_{uv,1} - a_{uv,1}y^*_{uv,2} \\ &= \sqrt{\frac{2P}{V}}T_s[\|a_{uv,0}\|^2 + \|a_{uv,1}\|^2]b_{1,u1} + n_{uv,1}a^*_{uv,0} - n^*_{uv,2}a_{uv,1}, \end{aligned} \tag{3.84}$$

$$\begin{aligned} Z_{uv,2} &= a^*_{uv,1}y_{uv,1} + a_{uv,0}y^*_{uv,2} \\ &= \sqrt{\frac{2P}{V}}T_s[\|a_{uv,0}\|^2 + \|a_{uv,1}\|^2]b_{1,u2} + n_{uv,1}a^*_{uv,1} + n^*_{uv,2}a_{uv,0}, \end{aligned} \tag{3.85}$$

for $u = 1, 2, \ldots, U$; $v = 1, 2, \ldots, V$. According to (3.84) and (3.85), it can be shown that a diversity order of two can be achieved, when two transmit antennas are employed. In contrast with (3.31), Equations (3.81), (3.82), (3.84) and (3.85) suggests that the STTD scheme obtains transmit diversity improvement by carrying out the STS processing, instead of a higher SNR gain by using the beamforming technique in (3.31).

Finally, after combining the identical replicas of the same signal transmitted on the independently fading $V$ subcarriers, the decision variables corresponding to the two bits in the $u$th sub-block can be

expressed as

$$z_{u,1} = \sum_{v=1}^{V} z_{uv,1}, \tag{3.86}$$

$$z_{u,2} = \sum_{v=1}^{V} Z_{uv,2}, \tag{3.87}$$

for $u = 1, 2, \ldots, U$, which show that a diversity order of $2V$ can now be achieved.

For the general case of $M = 2, 4, 8$, etc. the decision variable $z_{uv,m}$ corresponding to the $m$th bit in the sub-block $u$ can also be expressed as

$$z_{uv,m} = \sqrt{\frac{2P}{V}} T_s \sum_{l=1}^{M} \|a_{uv,l}\|^2 \times b_{1,um} + n'_{uv,m}, \; v = 1, 2, \ldots, V, \tag{3.88}$$

where $n'_{uv,m}$ is an AWGN process having a zero mean and a variance of $2N_0T_s \sum_{l=1}^{M} \|a_{uv,l}\|^2$. Hence, the benefit of STTD is that an $M$-fold diversity improvement can be attained. By contrast, Equation (3.32) shows that the beamforming scheme obtains a higher SNR gain, which is a function of $L$ - the number of array elements.

### 3.4.3 User-load Extension Using TF-Domain Spreading - Space Time Transmit Diversity

In Sections 3.4.1 and 3.4.2 the STS or the DS spreading operations used in the MC DS-CDMA systems were carried out in the T-domain only based on orthogonal WH DS-spreading codes. However, as proposed for the MC-CDMA schemes of [25, 80], additional spreading in the F-domain may also be employed to exploit the potential benefits of F-domain diversity. Let us assume that after the time-domain DS-spreading stage of Figure 3.8, the identical parallel data bits of the $V$ number of subcarriers are replaced by the $V$ number of chip values of $\{+1, -1, \ldots, +1\}$ of a F-domain spreading code invoked for spreading the data in the F-domain across $V$ number of different subcarriers. In this case the transmitted MC DS-CDMA signal benefits from the potential diversity gains of both the T-domain spreading and the F-domain spreading. At the receiver, the MC DS-CDMA signal is first STS despread using the T-domain STS code, then despread by the F-domain spreading code of length-$V$, as seen in Figure 3.8.

#### 3.4.3.1 System Model

The transmitter schematic of the STS assisted broadband MC DS-CDMA scheme using TF-domain spreading is similar to that seen in Figure 3.8, except that the $V$-depth repetition scheme of Figure 3.8 is now replaced by the F-domain spreading stage associated with an orthogonal spreading code of length $V$. Specifically, let $\{c'_k[0], c'_k[1], \ldots, c'_k[V-1]\}$ be the $k$th user's orthogonal code in discrete form, which will be used for F-domain spreading. By contrast, the $k$th user's T-domain orthogonal codes used for STS have been expressed in Section 3.4.1 as $c_{k,i}(t)$, $i = 1, 2, \ldots, M$ in continuous-

time form. Again, in the broadband MC DS-CDMA system using TF-domain spreading, instead of employing data repetition over $V$ subcarriers, the $U$ sub-block signals of user $k$ generated after STS are now further spread over the F-domain using the above-mentioned F-domain spreading codes. According to our analysis provided in Sections 3.4.1 and 3.4.2, the total number of orthogonal codes that can be used for STS is $UMN_e$ and the maximum number of users supported by these orthogonal codes is $K_{max} = UN_e$. By contrast, the total number of orthogonal codes that can be used for F-domain spreading is $V$. This implies that even if $V$ number of users share the same set of STS codes, these $V$ user signals might be distinguishable with the aid of the associated $V$ number of F-domain spreading codes. Explicitly, the total number of users supported is $VK_{max} = UVN_e$. Therefore, the orthogonal spreading codes can be assigned as follows. If the number of users is in the range of $0 \leq K \leq K_{max}$, these users will be assigned the required orthogonal STS codes and the same F-domain orthogonal spreading code. The resultant scheme is the same as the one we studied in Sections 3.4.1 as well as 3.4.2. However, when the number of users is in the range of $vK_{max} \leq K \leq (v+1)K_{max}$, $v = 1, 2 \ldots, V-1$, then the same set of $M$ STS orthogonal codes must be assigned to $v$ or $(v+1)$ users, but these $v$ or $(v+1)$ users are assigned different F-domain spreading codes. These $v$ or $(v+1)$ users employing the same set of $M$ STS codes are identified by their corresponding F-domain spreading codes. Since the subcarrier signals across which F-domain spreading takes place encounter independent fading, the orthogonality of the F-domain spreading codes cannot be retained in frequency-selective fading channels. Hence, multiuser interference is inevitably introduced, which degrades the BER performance, when increasing the number of users sharing the same set of $M$ STS orthogonal codes.

The signals transmitted from the $M$ transmitter antennas can be expressed as

$$\mathbf{s}_k(t) = \sum_{u=1}^{U} \sum_{v=1}^{V} \sqrt{\frac{2P_k}{V} \frac{1}{MM}} \mathbf{B}_{ku} \mathbf{c}_k c'_k[v-1] \cos(2\pi f_{uv} t + \phi_{k,uv}), \tag{3.89}$$

where $P_k/V$ represents the transmitted power of each subcarrier, while the factor of $MM$ in the denominator indicates that the total transmit power is now jointly conveyed by the STS using $M$ orthogonal codes and $M$ transmitter antennas. Furthermore, $\mathbf{s}_k(t) = [s_{k1}(t)\ s_{k2}(t)\ \ldots\ s_{kM}(t)]^T$ represents the transmitted signal vector of the $M$ transmitter antennas and $\mathbf{c}_k$ of (3.69) is an $M$-dimensional vector constituted by the orthogonal T-domain codes, while $\mathbf{B}_{ku}$ is an $(M \times M)$-dimensional matrix mapping the $u$th sub-block data bits to the $M$ transmit antennas, according to the requirements of STS [196]. Specifically, for $M = 2$, i.e. for MC DS-CDMA using two transmitter antennas, the MC

DS-CDMA signals transmitted by antenna 1 and 2 can be simply expressed as

$$\begin{aligned} \mathbf{s}_k(t) &= \begin{pmatrix} s_{k1}(t) \\ s_{k2}(t) \end{pmatrix} \\ &= \sqrt{\frac{2P_k}{4V}} \begin{pmatrix} \sum_{u=1}^{U}\sum_{v=1}^{V}[c_{k,1}b_{k,u1} + c_{k,2}b_{k,u2}]c'_k[v-1]\cos(2\pi f_{uv}t + \phi_{k,uv}) \\ \sum_{u=1}^{U}\sum_{v=1}^{V}[c_{k,1}b_{k,u2} - c_{k,2}b_{k,u1}]c'_k[v-1]\cos(2\pi f_{uv}t + \phi_{k,uv}) \end{pmatrix}. \end{aligned} \tag{3.90}$$

Equations (3.89) and (3.90) are similar to Equations (3.68) and (3.72), except for the F-domain spreading code $c'_k[v-1]$ seen in (3.89) and (3.90), which suggests that spreading in the F-domain is employed for the sake of attaining F-domain diversity.

Let $1 \leq K' \leq V$ be the number of users sharing the same set of $M$ STS orthogonal codes. We also assume that any set of $M$ STS orthogonal codes is shared by the same $K'$ number of users. Then, when the $K'\mathcal{K}_{max}$ signals expressed in the form of (3.90) are transmitted over frequency-selective fading channels, the complex-valued low-pass equivalent received signal can be expressed as

$$\begin{aligned} r(t) &= \sum_{k=1}^{K'\mathcal{K}_{max}} \mathbf{s}_k^T(t) \otimes \mathbf{h}_{uv}^{(1)}(t) + n(t) \\ &= \sum_{k=1}^{K'\mathcal{K}_{max}}\sum_{u=1}^{U}\sum_{v=1}^{V}\sqrt{\frac{2P_k}{V}\frac{1}{MM}}\mathbf{c}_k^T\mathbf{B}_{ku}^T c'_k[v-1]\mathbf{h}_{uv}^{(1)}(t)\cos(2\pi f_{uv}t + \phi_{k,uv}) + n(t). \end{aligned} \tag{3.91}$$

Specifically, for the case of $M = 2$, $r(t)$ can be expressed as

$$\begin{aligned} r(t) &= \sum_{k=1}^{K'\mathcal{K}_{max}}\sum_{u=1}^{U}\sum_{v=1}^{V}\sqrt{\frac{2P_k}{4V}}\Big(a_{uv,0}^{(1)}[c_{k,1}(t)b_{k,u1} + c_{k,2}(t)b_{k,u2}] \\ &\quad + a_{uv,1}^{(1)}[c_{k,1}(t)b_{k,u2} - c_{k,2}(t)b_{k,u1}]\Big)c'_k[v-1]\cos(2\pi f_{uv}t + \phi_{k,uv}) + n(t). \end{aligned} \tag{3.92}$$

Following the derivations in Section 3.4.2, for the general case of $M = 2, 4, 8$, etc. the decision variable $z_{uv,m}$ formulated in terms of the $m$th data bit in the sub-block $u$ and the subcarrier $uv$ can now be expressed as

$$z_{uv,m} = \sqrt{\frac{2P}{V}}T_s\sum_{k=1}^{K'}\left(\sum_{l=1}^{M}\|a_{uv,l}\|^2\right) \times c'_k[v-1]b_{k,um} + n'_{uv,m},\ v = 1, 2, \ldots, V, \tag{3.93}$$

where $n'_{uv,m}$ is an AWGN process having zero mean and a variance of $2N_0T_s\sum_{l=1}^{M}\|a_{uv,l}\|^2$. Comparing (3.93) to (3.35), we find that the term $\beta_{kv} = (\mathbf{w}_v^{(k)})^H\mathbf{a}_{uv}^{(1)}(t)$ in (3.35) is replaced by the term $\sum_{l=1}^{M}\|a_{uv,l}\|^2$ in (3.93), which means that the STTD scheme may be capable of achieving an $M$-fold diversity improvement. When comparing Equations (3.91), (3.92) and (3.93) with Equations (3.77), (3.78) and (3.88), again, the F-domain spreading code $c'_k[v-1]$ in (3.91), (3.92) and (3.93) represents

the spreading operation employed in the F-domain for the sake of achieving F-domain diversity.

Let

$$\mathbf{z}_{u,m} = [z_{u1,m}\ z_{u2,m}\ \ldots\ z_{uV,m}]^T, \tag{3.94}$$

$$\mathbf{A} = \text{diag}\left\{\sum_{l=1}^{M}\|a_{u1,l}\|^2, \sum_{l=1}^{M}\|a_{u2,l}\|^2, \ldots, \sum_{l=1}^{M}\|a_{uV,l}\|^2\right\}, \tag{3.95}$$

$$\mathbf{C} = \begin{pmatrix} c'_1[0] & c'_2[0] & \ldots & c'_{K'}[0] \\ c'_1[1] & c'_2[1] & \ldots & c'_{K'}[1] \\ \vdots & \vdots & \ddots & \vdots \\ c'_1[V-1] & c'_2[V-1] & \ldots & c'_{K'}[V-1] \end{pmatrix}, \tag{3.96}$$

$$\mathbf{b}_m = [b_{1,um}\ b_{2,um}\ \ldots\ b_{K',um}]^T, \tag{3.97}$$

$$\mathbf{n}_m = [n'_{u1,m}\ n'_{u2,m}\ \ldots\ n'_{uV,m}]^T. \tag{3.98}$$

Then (3.93) can be written in a matrix form as

$$\mathbf{z}_{u,m} = \sqrt{\frac{2P}{V}}T_s\mathbf{A}\mathbf{C}\mathbf{b}_m + \mathbf{n}_m. \tag{3.99}$$

Based on (3.99) the multiuser MC DS-CDMA signals can be detected by invoking different detection algorithms [195]. For simplicity, in this section, we investigate the single-user correlation based detector [195], where the vector $\mathbf{z}_m = \left[z_{u,m}^{(1)}\ z_{u,m}^{(2)}\ \ldots\ z_{u,m}^{(K')}\right]^T$ represents the decision variables. Then, these decision variables are obtained by multiplying both sides of (3.99) with $\mathbf{C}^T$, which can be expressed as

$$\mathbf{z}_m = \sqrt{\frac{2P}{V}}T_s\left(\sum_{v=1}^{V}\sum_{l=1}^{M}\|a_{uv,l}\|^2\right)\mathbf{R}\mathbf{b}_m + \mathbf{C}^T\mathbf{n}_m, \tag{3.100}$$

where

$$\mathbf{R} = \begin{pmatrix} 1 & \rho_{12} & \ldots & \rho_{1K'} \\ \rho_{21} & 1 & \ldots & \rho_{2K'} \\ \vdots & \vdots & \ddots & \vdots \\ \rho_{K'1} & \rho_{K'2} & \ldots & 1 \end{pmatrix} \tag{3.101}$$

is the correlation matrix of the $K'$ user signals, while $\rho_{ij}$ represents the correlation coefficient between the F-domain spreading codes of user $i$ and user $j$, which can be expressed as

$$\rho_{ij} = \frac{\sum_{v=1}^{V}\left(c'_i[v-1]c'_j[v-1]\sum_{l=1}^{M}\|a_{uv,l}\|^2\right)}{\sum_{v=1}^{V}\sum_{l=1}^{M}\|a_{uv,l}\|^2}. \tag{3.102}$$

Equation (3.100) suggests that the diversity gain contributed both by the transmit diversity and frequency diversity schemes can be retained, since we have a double sum of the components $\|a_{uv,l}\|^2$ corresponding to the STTD and frequency diversity orders of $M$ and $V$, respectively. However, multiuser interference is introduced by the channel's time-varying characteristics. Finally, the corresponding data bits, $b_{k,um}$, $k = 1, 2, \ldots, K'$, are decided according to $\hat{b}_{k,um} = \text{sgn}((\mathbf{z}_m)_k)$ for $k = 1, 2, \ldots, K'$, where $(\mathbf{z}_m)_k$ represents the $k$th row of $\mathbf{z}_m$ defined in Equation (3.100), while $\text{sgn}(\cdot)$ is the sign function [195]. Furthermore, it was shown that STS using $M$ transmitter antennas is capable of suppressing the multiuser interference without decreasing the achievable transmit diversity gain [197].

In the context of the multiuser decorrelating detector [195], the vector of decision variables derived for the $K'$ users $\mathbf{y}_m = \left[y_{u,m}^{(1)}, y_{u,m}^{(2)}, \ldots, y_{u,m}^{(K')}\right]^T$ are obtained by multiplying both sides of (3.100) with the inverse of the received signal's correlation matrix $\mathbf{R}$, which can be expressed as

$$\mathbf{y}_m = \sqrt{\frac{2P}{V}} T_s \left( \sum_{v=1}^{V} \sum_{l=1}^{M} \|a_{uv,l}\|^2 \right) \mathbf{b}_m + \mathbf{R}^{-1} \mathbf{C}^T \mathbf{n}_m. \tag{3.103}$$

It can be inferred from the right hand side term of Equation (3.103) that only the desired information and the noise are retained, while the multiuser interference is completely eliminated.

## 3.5 Steered Space-Time Spreading - Downlink

In [49], a hybrid technique designed for achieving both transmit diversity and beamforming, which is referred to steered space-time spreading (SSTS). The antenna architecture employed by the SSTS scheme of [49] has two antenna arrays spaced sufficiently far apart in order to achieve second-order transmit diversity. The $L$ number of elements of each of the two antenna arrays are spaced at a distance of $\lambda/2$ for the sake of achieving beamforming. Hence, the antenna architecture invoked here is the same as that described in Figure 2.4 in conjunction with $M = 2$. In [49], the SSTS scheme has been investigated in the context of DS-CDMA. By contrast, in this section we extend our study to the generalized MC DS-CDMA system. We will demonstrate in Section 3.7.4 that the achievable performance improvement of the generalized MC DS-CDMA system is a function of both the antenna spacing and the specific techniques used for achieving TD and beamforming. Moreover, it can be shown that TF-domain spreading can be invoked for supporting an increased number of users in comparison to F-domain repetition, while beamforming is capable of reducing the potentially increased interference caused by TF-domain spreading owing to supporting an increased number of users.

### 3.5.1 Transmitter Model - Steered Space-Time Spreading

Space-time block codes achieve diversity gains by simultaneously transmitting $M$ symbols on $M$ antenna arrays and using either orthogonal time slots or codes along with simple linear receiver combing techniques to advantageously combine the $M$ replicas of the transmitted signals. On the other hand,

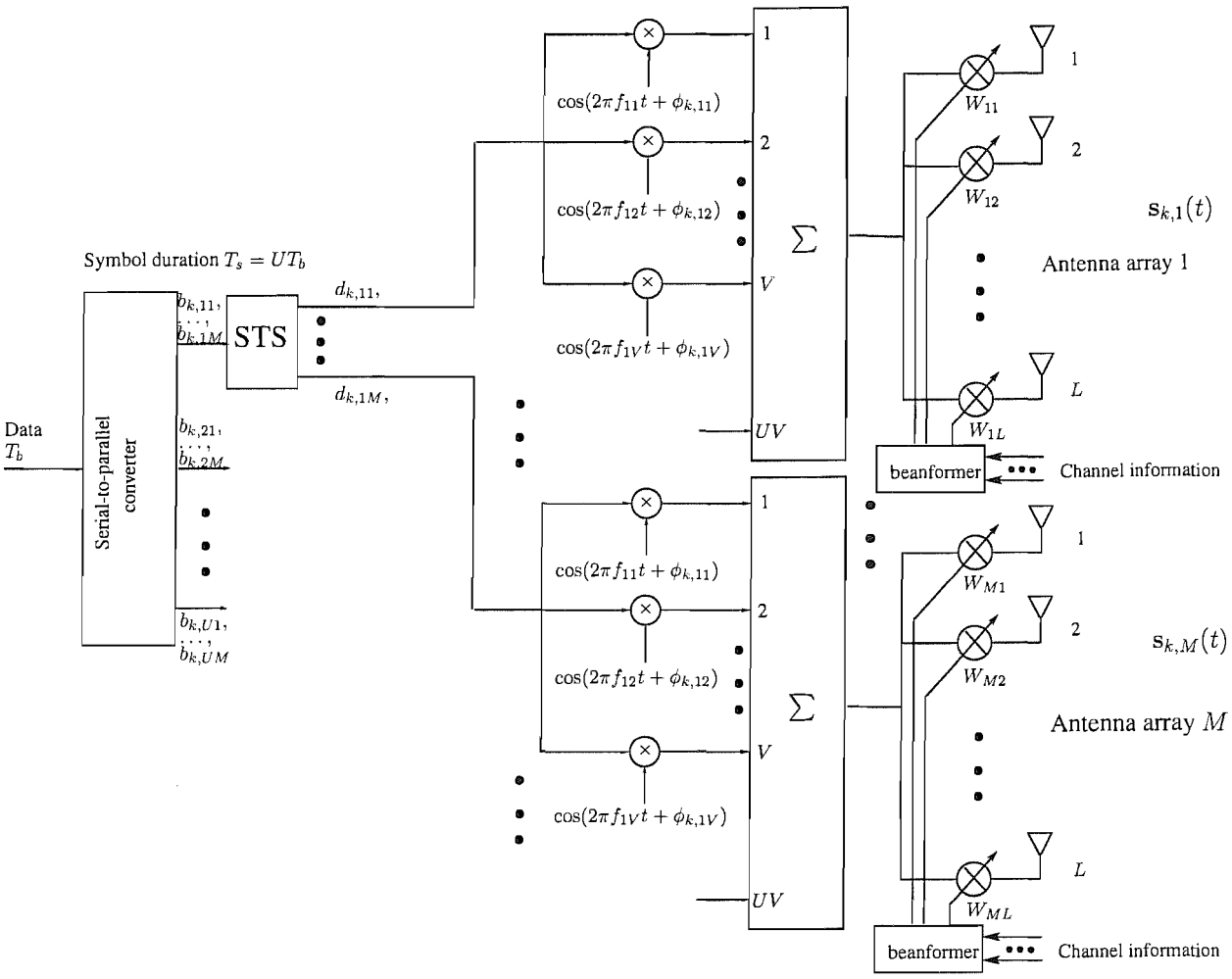


**Figure 3.10:** The $k$th user's transmitter schematic for the downlink of the SSTS assisted generalized multicarrier DS-CDMA system. Observing Figure 3.8 and this figure suggests that the only difference between these two figures is that the SSTS scheme employs $(M \times L)$-dimensional antenna arrays, while the STTD scheme employs a $(M \times 1)$-dimensional transmit antenna array. This difference confirms that the SSTS scheme not only employs STS to obtain transmit diversity, but additionally invokes beamforming to attain a higher SNR gain.

beamforming has the ability to direct the signal to the desired user with the aid of appropriately weighting the $L$ elements of each antenna array and suppressing the interfering signals. The system considered in this section is again the generalized MC DS-CDMA scheme of [40–42] using $U \cdot V$ number of subcarriers. The transmitter schematic of the BS's downlink configured for transmission to the $k$th user is shown in Figure 3.10, where real-valued data symbols using real-valued spreading [196] were considered. However, the analysis provided here may be extended to MC DS-CDMA systems using both complex-valued data symbols as well as complex-valued spreading. The F-domain arrangement of the $U \cdot V$ subcarriers in this system is the same as that shown in Figure 2.3. Thus, the subcarrier frequency arrangement obeying Equation (2.2) guarantees that the same STS signal is

copied to and transmitted by those specific $V$ subcarriers that have the maximum possible frequency spacings, so that they experience independent fading and hence achieve maximum frequency diversity. As shown in Figure 3.10, at the transmitter side a block of $(U \cdot M)$ data bits each having a bit duration of $T_b$ is S-P converted to $U$ parallel sub-blocks. The new bit duration of each sub-stream, which we refer to as the symbol duration becomes $T_s = UT_b$. Following the STS procedure described in Section 3.4.1, where the transmitted signal is spread to $M$ transmit antennas with the aid of the $M$ orthogonal spreading codes of $\{c_{k,1}(t), c_{k,2}(t), \ldots, c_{k,M}(t)\}$, $k = 1, 2, \ldots, K$, the $UM$ outputs of the $U$ STS blocks modulate a group of subcarrier frequencies $\{f_{u1}, f_{u2}, \ldots, f_{uV}\}$ using Binary Phase Shift Keying (BPSK) and then sent to the transmitter's beamformer. For the case of $M = 2$, we have two orthogonal spreading codes for the $k$th user, which are formulated as

$$\begin{aligned} c_{k,1}(t) &= [1, 1]c_k(t) = [c_k(t), c_k(t)], \\ c_{k,2}(t) &= [1, -1]c_k(t) = [c_k(t), -c_k(t)], \end{aligned} \tag{3.104}$$

Which is identical to Equation (3.66). The symbol duration of the STS signals is $MT_s$, and the discrete period of the orthogonal STS codes is $MT_s/T_c = MN_e$, where $N_e = T_s/T_c$ and $T_c$ represents the chip-duration of the orthogonal STS codes. Finally, according to the $k$th user's channel information, the $UMV$ signals of the $k$th user are weighted by the weight vector $\mathbf{w}_{v,m}^{(k)}$, as detailed in Section 3.3.1. Observing Figure 3.8 and Figure 3.10 suggests that the only difference between these two figures is that the SSTS scheme employs $(M \times L)$-dimensional antenna arrays, while the STTD scheme employs a $(M \times 1)$-dimensional transmit antenna array. This difference confirms that the SSTS scheme not only employs STS to obtain transmit diversity, but additionally invokes beamforming to attain a higher SNR gain.

The general form of the $k$th user's transmitted signal corresponding to the $M$ STS transmit antennas can be expressed as

$$\mathbf{s}_k(t) = \sum_{u=1}^{U} \sum_{v=1}^{V} \sqrt{\frac{2P_k}{VL} \frac{1}{MM}} \mathbf{W}_v^{(k)} \mathbf{B}_{ku} \mathbf{c}_k \cos(2\pi f_{uv} t + \phi_{k,uv}), \tag{3.105}$$

where $P_k/V$ represents the transmitted power of each subcarrier, while the factor of $MM$ in the denominator indicates that the total transmit power is jointly conveyed by the STS scheme using $M$ orthogonal codes and $M$ transmitter antenna arrays, while the factor of $L$ implies that each of the antenna arrays has $L$ elements which share the total transmit power. In (3.105) $\mathbf{s}_k(t) = \left[s_{k,00}(t), \ldots, s_{k,0(L-1)}(t), \ldots, s_{k,m0}(t), \ldots, s_{k,m(L-1)}(t), \ldots, s_{k,(M-1)0}(t), s_{k,(M-1)(L-1)}(t)\right]^T$ represents the transmitted signal vector of the $M$ transmitter antenna arrays, while $\mathbf{c}_k$ is an $M$-dimensional vector constituted by the orthogonal STS codes, which was expressed in (3.69). In (3.105) $\mathbf{B}_{ku}$ is an $(M \times M)$-dimensional matrix mapping the $u$th sub-block data bits to the $M$ STS antennas, according to the requirements of STS [196], as shown in (3.70). Finally, $\mathbf{W}_v^{(k)}$ in (3.105) is

the weight matrix derived from the weight vector $\mathbf{w}_{v,m}^{(k)}$, which can be expressed as

$$\mathbf{W}_v^{(k)} = \begin{bmatrix} (\mathbf{w}_{v,0}^{(k)})^* & \mathbf{0} & \dots & \mathbf{0} \\ \mathbf{0} & (\mathbf{w}_{v,1}^{(k)})^* & \dots & \mathbf{0} \\ \vdots & \vdots & \ddots & \vdots \\ \mathbf{0} & \mathbf{0} & \dots & (\mathbf{w}_{v,(M-1)}^{(k)})^* \end{bmatrix}, \tag{3.106}$$

where $\mathbf{0} = [0, 0, \dots, 0]^T$ is an $L$-dimensional vector, $\mathbf{w}_{v,m}^{(k)}$ is the $L$-dimensional weight vector of the $m$th antenna array and the $v$th subcarrier of the $k$th user. The weight matrix $\mathbf{W}_v^{(k)}$ in (3.105) shows that an $L$-dimensional beamforming technique is employed in the SSTS scheme, compared to the corresponding Equation (3.68) characterizing the STTD scheme.

Equation (3.105) represents the general form of the transmitted signals using SSTS, regardless of the value of $M$. However, the study conducted in [196] has shown that STS schemes using $M = 2, 4, 8$ constitute attractive schemes, since they are capable of achieving the maximal attainable transmit diversity without requiring extra STS codes. In this section, we only investigate these attractive STS schemes, and our results are mainly based on MC DS-CDMA systems using two antenna arrays. Specifically, for the case of $M = 2$, the MC DS-CDMA signals transmitted by antenna array 1 and 2 can be simply expressed as

$$\begin{aligned} \mathbf{s}_k(t) &= \begin{pmatrix} \mathbf{s}_{k,0}(t) \\ \mathbf{s}_{k,1}(t) \end{pmatrix} \\ &= \sqrt{\frac{2P_k}{4VL}} \begin{pmatrix} \sum_{u=1}^{U}\sum_{v=1}^{V}[c_{k,1}b_{k,u1} + c_{k,2}b_{k,u2}]\mathbf{w}_{v,0}^{(k)}\cos(2\pi f_{uv}t + \phi_{k,uv}) \\ \sum_{u=1}^{U}\sum_{v=1}^{V}[c_{k,1}b_{k,u2} - c_{k,2}b_{k,u1}]\mathbf{w}_{v,1}^{(k)}\cos(2\pi f_{uv}t + \phi_{k,uv}) \end{pmatrix}. \end{aligned} \tag{3.107}$$

Again, in contrast to (3.68), (3.107) explicitly indicates that the SSTS scheme uses an $L$-dimensional beamforming technique.

### 3.5.2 Receiver Model - Steered Space-Time Spreading

Based on the assumption that there are $M$ number of transmit antenna arrays at the BS, which are located sufficiently far apart from each other, having an antenna-spacing of about $10\lambda$, the ST-CIR vector $h_{uv,m}^{(k)}$ between the $uv$th subcarrier of the $k$th user and the $m$th antenna array can be expressed as

$$\begin{aligned} \mathbf{h}_{uv,m}^{(k)}(t) &= \left[h_{uv,m0}^{(k)}(t), h_{uv,m1}^{(k)}(t), \dots, h_{uv,m(L-1)}^{(k)}(t)\right]^T \\ &= \mathbf{a}_{uv,m}^{(k)}(t)\delta(t - \tau_k) \\ &= \left[a_{uv,m0}^{(k)}(t), a_{uv,m1}^{(k)}(t), \dots, a_{uv,m(L-1)}^{(k)}(t)\right]^T \delta(t - \tau_k), \end{aligned} \tag{3.108}$$

which is an $L$-dimensional vector and identical to (2.11), where $a_{uv,ml}^{(k)}(t)$ is the CIR with respect to the $uv$th subcarrier of the 1st user and the $l$th element of the $m$th antenna array. Based on the assumption that the array elements are separated by half a wavelength, i.e. that we have $d = \lambda/2$, we can simplify $\mathbf{a}_{uv,m}^{(k)}(t)$ of (3.108) to

$$\begin{aligned}\mathbf{a}_{uv,m}^{(k)}(t) &= \alpha_{uv,m}^{(k)}(t)\mathbf{d}_m^{(k)} \\ &= \alpha_{uv,m}^{(k)}(t)\,[1, \\ &\quad \exp\left(j\left[\pi\sin(\psi_m^{(k)} + \kappa_m^{(k)}B)\right]\right), \ldots, \\ &\quad \exp\left(j\left[(L-1)\pi\sin(\psi_m^{(k)} + \kappa_m^{(k)}B)\right]\right)\Big]^T, \end{aligned} \tag{3.109}$$

where $\mathbf{d}_m^{(k)} = \left[1, \exp\left(j\left[\pi\sin(\psi_m^{(k)} + \kappa_m^{(k)}B)\right]\right), \ldots, \exp\left(j\left[(L-1)\pi\sin(\psi_m^{(k)} + \kappa_m^{(k)}B)\right]\right)\right]^T$. (3.109) is identical to (2.12) in conjunction with $d = \lambda/2$.

Assuming that the $K$ users' signals expressed in the form of (3.106) are transmitted synchronously over dispersive Rayleigh fading channels characterized by the corresponding ST-CIRs, the complex-valued low-pass equivalent received signal can be expressed as

$$r(t) = \sum_{k=1}^{K} r_k(t) + n(t), \tag{3.110}$$

where $n(t)$ is the AWGN process having a zero mean and a variance given in Equation (3.6). In (3.110) $r_k(t)$ represents the $k$th user's transmitted signal received by the 1st user, which can be expressed as

$$\begin{aligned} r_k(t) &= \mathbf{s}_k^T(t) \otimes \mathbf{h}_{uv}^{(1)}(t) \\ &= \sum_{u=1}^{U}\sum_{v=1}^{V} \sqrt{\frac{2P_k}{VL}\frac{1}{MM}}\mathbf{c}_k^T\mathbf{B}_{ku}^T(\mathbf{W}_v^{(k)})^T\mathbf{h}_{uv}^{(1)}(t)\cos(2\pi f_{uv}t + \phi_{k,uv}), \end{aligned} \tag{3.111}$$

where $\mathbf{h}_{uv}^{(1)}(t) = \left[(\mathbf{h}_{uv,0}^{(1)}(t))^T, (\mathbf{h}_{uv,1}^{(1)}(t))^T, \ldots, (\mathbf{h}_{uv,(M-1)}^{(1)}(t))^T\right]^T$ is an $ML$-dimensional ST-CIR vector corresponding to the desired user.

Specifically, for the case of $M = 2$, when the transmitted signal obeys (3.106), the complex-valued low-pass equivalent received signal can be expressed as

$$\begin{aligned} r(t) &= \sum_{k=1}^{K}\sum_{u=1}^{U}\sum_{v=1}^{V}\sqrt{\frac{2P_k}{4VL}}\Big((\mathbf{w}_{v,0}^{(k)})^H\mathbf{a}_{uv,0}^{(1)}[c_{k,1}(t)b_{k,u1} + c_{k,2}(t)b_{k,u2}] \\ &\quad +(\mathbf{w}_{v,1}^{(k)})^H\mathbf{a}_{uv,1}^{(1)}[c_{k,1}(t)b_{k,u2} - c_{k,2}(t)b_{k,u1}]\Big)\cos(2\pi f_{uv}t + \phi_{k,uv}) + n(t). \end{aligned} \tag{3.112}$$

In the comparing (3.111) and (3.112) to (3.77) and (3.78), the weight matrix $\mathbf{W}_v^{(k)}$ in (3.111) and the weight vector $\mathbf{w}_{v,0}^{(k)}$ in (3.112) shows that the SSTS scheme employs an $l$-dimensional beamforming

technique to attain a higher SNR gain.

The receiver front-end is identical to that of the STTD receiver shown in Figure 3.9. After multicarrier demodulation, the $UV$ number of parallel streams corresponding to the signals transmitted on the $UV$ subcarriers are space-time de-spread using the approach of [196], in order to obtain the $M$ separate variables of $\{z_{uv,1}, z_{uv,2}, \ldots, z_{uv,M}\}$, corresponding to the $M$ number of data bits transmitted on the $uv$th stream, where we have $u = 1, 2, \ldots, U$; $v = 1, 2, \ldots, V$, respectively. For the case of $M = 2$, let $y_{uv,1}$, $y_{uv,2}$ represent the receiver correlator's output variables corresponding to the first two data bits transmitted on the $uv$th subcarrier. Since orthogonal multicarrier signals, orthogonal STS codes, synchronous transmission of the $K$ user signals as well as slow flat-fading of each subcarrier are assumed, there is no interference between the different users and the different subcarrier signals. Therefore, $y_{uv,1}$, $y_{uv,2}$ may be expressed as

$$y_{uv,1} = \sqrt{\frac{2P}{VL}} T_s \left[ (\mathbf{w}_{v,0}^{(1)})^H \mathbf{a}_{uv,0}^{(1)} b_{1,u1} + (\mathbf{w}_{v,1}^{(1)})^H \mathbf{a}_{uv,1}^{(1)} b_{1,u2} \right] + n_{uv,1}, \tag{3.113}$$

$$y_{uv,2} = \sqrt{\frac{2P}{VL}} T_s \left[ (\mathbf{w}_{v,0}^{(1)})^H \mathbf{a}_{uv,0}^{(1)} b_{1,u2} - (\mathbf{w}_{v,1}^{(1)})^H \mathbf{a}_{uv,1}^{(1)} b_{1,u1} \right] + n_{uv,2}, \tag{3.114}$$

where $n_{uv,i}, i = 1, 2$ is due to the AWGN and can be expressed as

$$n_{uv,i} = \int_0^{2T_s} n(t) c_{1,i}(t) \exp\left(-j[2\pi f_{uv} t + \theta_{uv}]\right) dt, \tag{3.115}$$

which is a complex Gaussian distributed variable having zero mean and a variance of $2N_0T_s$. In (3.113) and (3.114), $\mathbf{w}_{v,m}^{(1)}$, $m = 0, 1$, represents the weight matrix of the desired user derived for the $m$th antenna array, which is generated by the MRC beamformer [7] with the aid of the channel state information. In contrast with (3.81) and (3.82), (3.113) and (3.114) exhibit that the SSTS scheme not only employs the transmit diversity technique but also uses the beamforming technique. It can be shown that we have $(\mathbf{w}_{v,m}^{(1)}) = \mathbf{d}_m^{(1)}$, $m = 1, 2$, where $\mathbf{d}_m^{(1)}$ was defined in the context of (3.109). Consequently, (3.113) and (3.114) can be simplified to

$$y_{uv,1} = \sqrt{\frac{2PL}{V}} T_s \left[ \alpha_{uv,0} b_{1,u1} + \alpha_{uv,1} b_{1,u2} \right] + n_{uv,1}, \tag{3.116}$$

$$y_{uv,2} = \sqrt{\frac{2PL}{V}} T_s \left[ \alpha_{uv,0} b_{1,u2} - \alpha_{uv,1} b_{1,u1} \right] + n_{uv,2}. \tag{3.117}$$

Assuming that the receiver has perfect knowledge of the fading parameters of $\alpha_{uv,m}$, $m = 1, 2$, the decision variables corresponding to the data bits $b_{1,um}, m = 1, 2$ associated with the $uv$th subcar-

rier can be expressed as

$$z_{uv,1} = \alpha^*_{uv,0} y_{uv,1} - \alpha_{uv,1} y^*_{uv,2}$$
$$= \sqrt{\frac{2PL}{V}} T_s [\|\alpha_{uv,0}\|^2 + \|\alpha_{uv,1}\|^2] b_{1,u1} + n_{uv,1}\alpha^*_{uv,0} - n^*_{uv,2}\alpha_{uv,1}, \quad (3.118)$$

$$Z_{uv,2} = \alpha^*_{uv,1} y_{uv,1} + \alpha_{uv,0} y^*_{uv,2}$$
$$= \sqrt{\frac{2PL}{V}} T_s [\|\alpha_{uv,0}\|^2 + \|\alpha_{uv,1}\|^2] b_{1,u2} + n_{uv,1}\alpha^*_{uv,1} + n^*_{uv,2}\alpha_{uv,0}, \quad (3.119)$$

for $u = 1, 2, \ldots, U$; $v = 1, 2, \ldots, V$.

Finally, after combining the identical replicas of the same signal transmitted on the $V$ subcarriers, the decision variables corresponding to the two bits in the $u$th sub-block can be expressed as

$$z_{u,1} = \sum_{v=1}^{V} z_{uv,1}, \quad (3.120)$$

$$z_{u,2} = \sum_{v=1}^{V} Z_{uv,2}, \quad (3.121)$$

for $u = 1, 2, \ldots, U$.

Note that for the general case of $M = 2, 4, 8$, etc the decision variable $z_{uv,m}$ corresponding to the $m$th bit in the sub-block $u$ can be expressed as

$$z_{uv,m} = \sqrt{\frac{2PL}{V}} T_s \sum_{l=1}^{M} \|\alpha_{uv,l}\|^2 \times b_{1,um} + n'_{uv,m}, \; v = 1, 2, \ldots, V, \quad (3.122)$$

where $n'_{uv,m}$ is an AWGN process having a zero mean and a variance of $2N_0T_s \sum_{l=1}^{M} \|\alpha_{uv,l}\|^2$. Observing from Equations (3.122) and (3.88) shows that the factor of $L$ in the numerator of (3.122) is the result of an $L$-dimensional beamforming technique employed by SSTS, while the term $\sum_{l=1}^{M} \|\alpha_{uv,l}\|^2$ in both Equations exhibits that an $M$-fold diversity improvement is attained by both the SSTS scheme and the STTD scheme.

### 3.5.3 User-load Extension Using TF-Domain Spreading - Steered Space-Time Spreading

As described in Sections 3.2.4 and 3.4.3, spreading in the F-domain may also be employed for the sake of extending the system capacity of the generalized MC DS-CDMA aided by SSTS. The resultant bandwidth is again the same as that of the MC DS-CDMA scheme employing the time-domain only spreading, while the total number of users supported becomes $VK_{max} = VN_e$, which is $V$ times the number of the users supported by the MC DS-CDMA scheme employing the time-domain only spreading. This is an explicit benefit of using F-domain spreading, rather than F-domain repetition across $V$ subcarriers.

The transmitter schematic of the broadband MC DS-CDMA using TF-domain spreading is similar

to that of the generalized MC DS-CDMA system employing the time-domain only spreading seen in Figure 3.10, except that the $V$-depth data repetition scheme of Figure 3.10 is now replaced by the F-domain spreading associated with an orthogonal F-domain spreading code of length $V$. Similarly, let $\{c'_k[0], c'_k[1], \ldots, c'_k[V-1]\}$ be the $k$th user's orthogonal F-domain code in discrete form. The $k$th user's $M$ number of T-domain orthogonal STS spreading codes have been expressed in Section 3.4.1 as $\{c_{k,1}(t), c_{k,2}(t), \ldots, c_{k,M}(t)\}$, $k = 1, 2, \ldots, K$ in continuous-time form. Following the STS procedure described in Section 3.4.1, the $UM$ outputs of the $U$ STS blocks modulate a group of subcarrier frequencies $\{f_{u1}, f_{u2}, \ldots, f_{uV}\}$ using Binary Phase Shift Keying (BPSK) and they are then sent to the BS's downlink transmitter beamformer seen in Figure 3.10. The symbol duration of the STS signals is $MT_s$, and the discrete period of the orthogonal STS codes is $MT_s/T_c = MN_e$, where $N_e = T_s/T_c$ and $T_c$ represents the chip-duration of the orthogonal STS codes. Finally, according to the $k$th user's channel information, the $UMV$ signals of the $k$th user are weighted by the weight vector $\mathbf{w}_{v,m}^{(k)}$. Hence, the transmitted signal of the $k$th user can be expressed as

$$\mathbf{s}_k(t) = \sum_{u=1}^{U}\sum_{v=1}^{V}\sqrt{\frac{2P_k}{VL}\frac{1}{MM}}\mathbf{W}_v^{(k)}\mathbf{B}_{ku}\mathbf{c}_k c'_k[v-1]\cos(2\pi f_{uv}t + \phi_{k,uv}), \tag{3.123}$$

where $P_k/V$ represents the transmitted power of each subcarrier, while the factor of $MM$ in the denominator indicates that the transmitted signal is jointly conveyed by the STS scheme using $M$ orthogonal codes and $M$ transmitter antenna arrays, while the factor $L$ implies that each of the antenna arrays has $L$ elements sharing the total transmit power. In (3.123) $\mathbf{s}_k(t)$ represents the $ML$-dimensional transmitted signal vector of the $M$ transmitter antenna arrays, as defined in Section 3.5.1, while $\mathbf{c}_k$ is an $M$-dimensional vector constituted by the orthogonal STS codes, expressed in (3.69). The term $\mathbf{B}_{ku}$ denotes an $(M \times M)$-dimensional matrix mapping the $u$th sub-block data bits to the $M$ STS antennas, as outlined in (3.70). Finally, the matrix $\mathbf{W}_v^{(k)}$ is the BS's downlink weight matrix expressed in the form shown in (3.106).

In (3.123), the general form of the BS's downlink transmitted signals using both SSTS and TF-domain spreading was presented, regardless of the value of $M$. However, in our study, we will focus on the attractive family of STS schemes using $M = 2, 4, 8$, since they are capable of achieving the maximal attainable transmit diversity gain without requiring extra STS codes [196]. As in Section 3.5, we only investigate these attractive STS schemes, and our results are mainly based on MC DS-CDMA systems using two antenna arrays. For the case of $M = 2$, the MC DS-CDMA signals transmitted by antenna array 1 and 2 can be simply expressed as

$$\begin{aligned}\mathbf{s}_k(t) &= \begin{pmatrix} \mathbf{s}_{k,0}(t) \\ \mathbf{s}_{k,1}(t) \end{pmatrix} \\ &= \sqrt{\frac{2P_k}{4VL}}\begin{pmatrix} \sum_{u=1}^{U}\sum_{v=1}^{V}[c_{k,1}b_{k,u1} + c_{k,2}b_{k,u2}]\mathbf{w}_{v,0}^{(k)}c'_k[v-1]\cos(2\pi f_{uv}t + \phi_{k,uv}) \\ \sum_{u=1}^{U}\sum_{v=1}^{V}[c_{k,1}b_{k,u2} - c_{k,2}b_{k,u1}]\mathbf{w}_{v,1}^{(k)}c'_k[v-1]\cos(2\pi f_{uv}t + \phi_{k,uv}) \end{pmatrix}.\end{aligned} \tag{3.124}$$

Equation (3.124) is similar to (3.90) except the weight vector $\mathbf{w}_{v,m}^{(k)}, m = 0, 1$ in (3.124), which represents the effect of the $L$-dimensional beamforming technique employed by the SSTS scheme.

Let $1 \leq K' \leq V$ be the number of users sharing the same T-domain spreading code. We also assume that any T-domain spreading code is shared by the same $K'$ number of users. Then, when the $K'\mathcal{K}_{max}$ signals expressed in the form of (3.123) are transmitted over frequency-selective fading channels, the complex-valued low-pass equivalent received signal can be expressed as

$$\begin{aligned} r(t) &= \sum_{k=1}^{K'\mathcal{K}_{max}} \mathbf{s}_k^T(t) \otimes \mathbf{h}_{uv}^{(1)}(t) + n(t) \\ &= \sum_{k=1}^{K'\mathcal{K}_{max}} \sum_{u=1}^{U} \sum_{v=1}^{V} \sqrt{\frac{2P_k}{VL}\frac{1}{MM}} \mathbf{c}_k^T \mathbf{B}_{ku}^T (\mathbf{W}_v^{(k)})^T \mathbf{h}_{uv}^{(1)}(t) \\ &\quad \times c'_k[v-1] \cos(2\pi f_{uv} t + \phi_{k,uv}) + n(t), \end{aligned} \tag{3.125}$$

where $\mathbf{h}_{uv}^{(1)}(t) = \left[(\mathbf{h}_{uv,0}^{(1)}(t))^T, (\mathbf{h}_{uv,1}^{(1)}(t))^T, \ldots, (\mathbf{h}_{uv,(M-1)}^{(1)}(t))^T\right]^T$ is an $ML$-dimensional ST-CIR vector corresponding to the desired user, while $\mathbf{h}_{uv,m}^{(1)}(t)$ is an $L$-dimensional ST-CIR vector between the desired user and the $m$th antenna array at the BS's transmitter, and $\mathbf{h}_{uv,m}^{(1)}(t)$ is expressed in (3.108). In (3.125) $n(t)$ is the AWGN process having a zero mean and a variance expressed by Equation (3.6). Specifically, for the case of $M = 2$, when the transmitted signal obeys (3.124), the complex-valued low-pass equivalent received signal can be expressed as

$$\begin{aligned} r(t) &= \sum_{k=1}^{K'\mathcal{K}_{max}} \sum_{u=1}^{U} \sum_{v=1}^{V} \sqrt{\frac{2P_k}{4VL}} \Big( (\mathbf{w}_{v,0}^{(k)})^H \mathbf{a}_{uv,0}^{(1)} [c_{k,1}(t) b_{k,u1} + c_{k,2}(t) b_{k,u2}] \\ &\quad + (\mathbf{w}_{v,1}^{(k)})^H \mathbf{a}_{uv,1}^{(1)} [c_{k,1}(t) b_{k,u2} - c_{k,2}(t) b_{k,u1}] \Big) c'_k[v-1] \cos(2\pi f_{uv} t + \phi_{k,uv}) + n(t). \end{aligned} \tag{3.126}$$

Again, the weight vector $\mathbf{w}_{v,0}^{(k)}$ in (3.126) caused by the implementation of the beamforming technique in the SSTS scheme is the only difference between Equations (3.126) and (3.92), while the weight matrix in (3.125) is the only difference between Equations (3.125) and (3.91).

Since orthogonal multicarrier signals, orthogonal STS codes, synchronous transmission of the $K$ users' signals as well as slow flat-fading of each subcarrier are assumed, there is no interference between the users employing different T-domain STS spreading codes or using different subcarrier signals. Therefore, following the approach outlined in Section 3.5.2, the terms $y_{uv,1}$, $y_{uv,2}$, representing the receiver correlator's output variables corresponding to the first two data bits transmitted

on the $uv$th subcarrier for the case of $M = 2$, can be expressed as

$$y_{uv,1} = \sum_{k=1}^{K'} \sqrt{\frac{2P_k}{VL}} T_s \left[ (\mathbf{w}_{v,0}^{(k)})^H \mathbf{a}_{uv,0}^{(1)} b_{k,u1} + (\mathbf{w}_{v,1}^{(k)})^H \mathbf{a}_{uv,1}^{(1)} b_{k,u2} \right] c'_k[v-1] + n_{uv,1}, \tag{3.127}$$

$$y_{uv,2} = \sum_{k=1}^{K'} \sqrt{\frac{2P_k}{VL}} T_s \left[ (\mathbf{w}_{v,0}^{(k)})^H \mathbf{a}_{uv,0}^{(1)} b_{k,u2} - (\mathbf{w}_{v,1}^{(k)})^H \mathbf{a}_{uv,1}^{(1)} b_{k,u1} \right] c'_k[v-1] + n_{uv,2}, \tag{3.128}$$

where $n_{uv,i}, i = 1, 2$ is due to the AWGN, which is a complex Gaussian distributed variable having zero mean and a variance of $2N_0T_s$, as expressed in (3.83). In (3.127), $\mathbf{w}_{v,m}^{(k)}$, $m = 0, 1$, represents the BS's downlink weight matrix corresponding to the $k$th user and the $m$th transmit antenna array, which is generated by the MRC beamformer [7], as shown in Section 3.5.2. Consequently, we have $(\mathbf{w}_{v,m}^{(k)}) = \mathbf{d}_m^{(k)}$, $m = 0, 1$, and $\mathbf{d}_m^{(1)}$ was defined in the context of (3.109). In this case, (3.127) and (3.128) may be simplified to

$$y_{uv,1} = \sqrt{\frac{2PL}{V}} T_s \left[ \alpha_{uv,0} b_{1,u1} + \alpha_{uv,1} b_{1,u2} \right] c'_k[v-1] + n_{uv,1} + i_{uv,1}, \tag{3.129}$$

$$y_{uv,2} = \sqrt{\frac{2PL}{V}} T_s \left[ \alpha_{uv,0} b_{1,u2} - \alpha_{uv,1} b_{1,u1} \right] c'_k[v-1] + n_{uv,2} + i_{uv,2}, \tag{3.130}$$

where we have

$$i_{uv,1} = \sum_{k=2}^{K'} \sqrt{\frac{2P_k}{VL}} T_s \left[ \beta_{k,0} \alpha_{uv,0} b_{k,u1} + \beta_{k,1} \alpha_{uv,1} b_{k,u2} \right] c'_k[v-1], \tag{3.131}$$

$$i_{uv,2} = \sum_{k=2}^{K'} \sqrt{\frac{2P_k}{VL}} T_s \left[ \beta_{k,0} \alpha_{uv,0} b_{k,u2} - \beta_{k,1} \alpha_{uv,1} b_{k,u1} \right] c'_k[v-1], \tag{3.132}$$

and $\beta_{k,m} = (\mathbf{d}_m^{(k)})^H \mathbf{d}_m^{(1)}$.

Assuming that the receiver has perfect knowledge of the fading parameters of $\alpha_{uv,m}$, $m = 1, 2$, the decision variables corresponding to the data bits $b_{1,um}, m = 1, 2$ associated with the $uv$th subcarrier can be expressed as

$$\begin{aligned} z_{uv,1} &= \alpha_{uv,0}^* y_{uv,1} - \alpha_{uv,1} y_{uv,2}^* \\ &= \sqrt{\frac{2PL}{V}} T_s [\|\alpha_{uv,0}\|^2 + \|\alpha_{uv,1}\|^2] b_{1,u1} + n'_{uv,1} + i'_{uv,1}, \end{aligned} \tag{3.133}$$

$$\begin{aligned} z_{uv,2} &= \alpha_{uv,1}^* y_{uv,1} + \alpha_{uv,0} y_{uv,2}^* \\ &= \sqrt{\frac{2PL}{V}} T_s [\|\alpha_{uv,0}\|^2 + \|\alpha_{uv,1}\|^2] b_{1,u2} + + n'_{uv,2} + i'_{uv,2}, \end{aligned} \tag{3.134}$$

for $u = 1, 2, \ldots, U$; $v = 1, 2, \ldots, V$, where

$$n'_{uv,1} = n_{uv,1}\alpha^*_{uv,0} - n^*_{uv,2}\alpha_{uv,1}, \quad (3.135)$$

$$n'_{uv,2} = n_{uv,1}\alpha^*_{uv,1} + n^*_{uv,2}\alpha_{uv,0}, \quad (3.136)$$

$$i'_{uv,1} = i_{uv,1}\alpha^*_{uv,0} - i^*_{uv,2}\alpha_{uv,1}, \quad (3.137)$$

$$i'_{uv,2} = i_{uv,1}\alpha^*_{uv,1} + i^*_{uv,2}\alpha_{uv,0}. \quad (3.138)$$

Observing Equations (3.133), (3.134) and (3.93) suggests that the factor of $L$ in the numerator of (3.133) and (3.134) is the result of an $L$-dimensional beamforming technique employed by the SSTS scheme.

Finally, in the context of the single-user correlation based detector [195], the decision variable $z_{u,1}$ of the desired user is obtained by combining $\mathbf{z}_{u,1} = [z_{u1,1}, z_{u2,1}, \ldots, z_{uV,1}]$ with $\mathbf{c}'_1 = [c'_1[0], c'_1[1], \ldots, c'_1[V-1]]$, which can be expressed as

$$z_{u,1} = \sqrt{\frac{2PL}{V}} T_s \left[ \sum_{v=1}^{V} [\|\alpha_{uv,0}\|^2 + \|\alpha_{uv,1}\|^2] b_{1,u1} + \mathbf{c}'_1 \mathbf{i}'_{u,1} + \mathbf{c}'_1 \mathbf{n}'_{u,1} \right], \quad (3.139)$$

where $\mathbf{n}'_{u,1} = \left[n'_{u1,1}, n'_{u2,1}, \ldots, n'_{uV,1}\right]^T$ is the $V$-dimensional noise vector, while $\mathbf{i}'_{u,1} = \left[i'_{u1,1}, i'_{u2,1}, \ldots, i'_{uV,1}\right]^T$ is the $V$-dimensional interference vector. Then the interference term $\mathbf{c}'_1 \mathbf{i}'_{u,1}$ can be expressed as

$$\begin{aligned} \mathbf{c}'_1 \mathbf{i}'_{u,1} &= \sum_{v=1}^{V} c'_1[v-1] \left[ i_{uv,1}\alpha^*_{uv,0} - i^*_{uv,2}\alpha_{uv,1} \right] \quad (3.140) \\ &= \sum_{v=1}^{V} \sum_{k=2}^{K'} \sqrt{\frac{2P_k}{VL}} T_s c'_1[v-1] c'_k[v-1] \\ &\quad \times \left[ \left( \beta_{k,0} \|\alpha_{uv,0}\|^2 + \beta^*_{k,1} \|\alpha_{uv,1}\|^2 \right) b_{k,u1} + \left( \beta_{k,1}\alpha^*_{uv,0}\alpha_{uv,1} - \beta^*_{k,0}\alpha^*_{uv,0}\alpha_{uv,1} \right) b_{k,u2} \right]. \end{aligned}$$

We observe from Equation (3.139) that multiuser interference is inevitably encountered, since the orthogonality of the F-domain spreading codes cannot be retained over frequency-selective ST channels. However, the desired signal is not interfered by the signal of the users employing different orthogonal T-domain STS spreading codes, provided that synchronous transmission of all the $K'\mathcal{K}_{max}$ users' signals as well as slow flat-fading of each subcarrier may be assumed. Only the users sharing the same T-domain STS spreading code with the desired user will interfere with the desired user. Therefore, the interference $\mathbf{c}'_1 \mathbf{i}'_{u,1}$ may be reduced, if we carefully select the specific $K' - 1$ users, which have the lowest interference coefficient with respect to the desired user, from all the $K'\mathcal{K}_{max}$ users for the sake of sharing the same T-domain spreading code with the desired user. Let the interference coefficient be defined again as $\sqrt{P_k}\beta_{k,0}$ and $\sqrt{P_k}\beta_{k,1}$, which can be derived before transmission based on the assumption that $\mathbf{a}^{(1)}_{uv,m}(t)$ is perfectly estimated. We also assume that $\mathbf{w}^{(k)}_{v,m} = \mathbf{a}^{(k)}_{uv,m}(t)$ is perfectly estimated. With the advent of this user regrouping procedure, the effect

of the interfering signals imposed on the desired user is significantly reduced. Therefore, the BER performance is substantially improved. Note that when a new user joins or disjoins the system, the grouping has to be updated.

## 3.6 Differential Space-Time Spreading and Differential Steered Space-Time Spreading - Downlink

In [141], a DSCM scheme was proposed for flat fading channels by combining the merits of DSTM and spread spectrum techniques. It was shown that DSCM significantly outperforms DSTM in the presence of interference. Based on the DSCM technique, we extend our investigations to the DSTS and the DSSTS schemes invoked for the downlink of the generalized MC DS-CDMA system of [41]. As shown in Figure 2.4, the $M$ number of transmit antenna arrays are located sufficiently far apart so that the corresponding MC DS-CDMA signals experience independent fading. Each of the $M$ antenna arrays consists of $L$ number of elements separated by a distance of half a wavelength. When we have $L = 1$, the stand-alone DSTS scheme is employed. Otherwise, the more general DSSTS scheme is invoked and hence the DSTS scheme may be viewed as a special case of the generic DSSTS scheme in conjunction with $L = 1$.

### 3.6.1 Differential Space-Time Modulation

Before commencing our investigation of the DSTS and the DSSTS schemes, we provide a brief introduction to the unitary group code based DSTM of [138]. Let $\mathbf{X}_n$ be the $n$th $(M \times N_l)$-dimensional space-time code to be transmitted by the $M$ antennas over $N_l$ consecutive time-domain samples. For differential space-time coding we have [138]

$$\mathbf{X}_n\mathbf{X}_n^H = N_l\mathbf{I}_M,\ \mathbf{X}_n = \mathbf{X}_{n-1}\mathbf{G}_n,\ \mathbf{X}_0 = \mathbf{D},\ \forall n, \tag{3.141}$$

where the superscript $H$ denotes the conjugate transpose operation, $\mathbf{I}_M$ is an $(M \times M)$-dimensional identity matrix, $\mathbf{G}_n$ is the matrix representing the $n$th information bearing unitary group code and $\mathbf{D}$ is a known fixed matrix. For example, for $M = N_l = 2$, the pair [138]

$$\mathcal{G} = \left\{ \pm \begin{bmatrix} 1 & 0 \\ 0 & 1 \end{bmatrix}, \pm \begin{bmatrix} 0 & 1 \\ -1 & 0 \end{bmatrix} \right\}, \mathbf{D} = \begin{bmatrix} 1 & -1 \\ 1 & 1 \end{bmatrix}, \tag{3.142}$$

is a unitary group code designed for the BPSK constellation of $\{1, -1\}$ and $\mathbf{G}_n \in \mathcal{G}$. Each information bit pair in $\{00, 01, 10, 11\}$ corresponds to an element in $\mathcal{G}$.

The received data matrix $\mathbf{Y}_n \in \mathcal{C}^{N_r \times N_l}$ at the output of the $N_r$ receive antennas has the form of [138]

$$\mathbf{Y}_n = \sqrt{\frac{P}{M}}\mathbf{H}\mathbf{X}_n + \mathbf{N}_n, \tag{3.143}$$

where the variables $\mathbf{H} \in \mathcal{C}^{N_r \times M}$, $\mathbf{N}_n \in \mathcal{C}^{N_r \times N_l}$ and $P$ denote the unknown channel fading matrix in

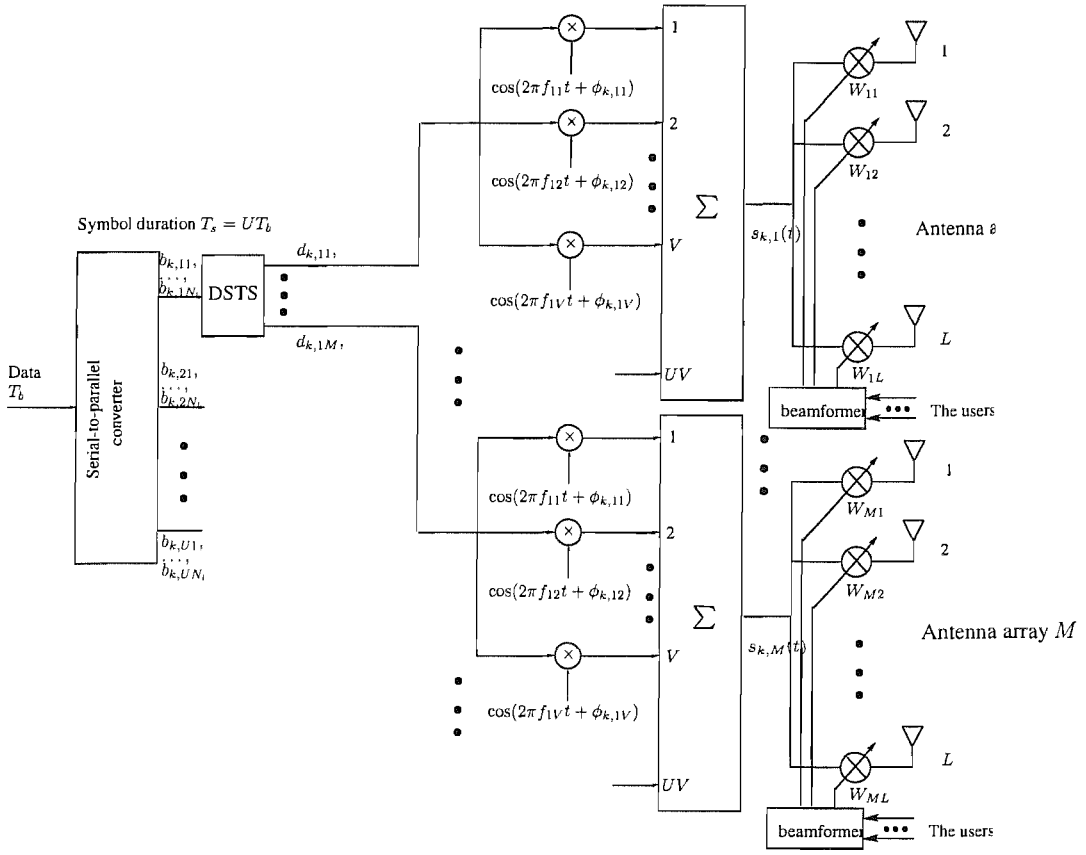


**Figure 3.11:** The $k$th user's transmitter schematic for the downlink of the DSSTS assisted generalized multi-carrier DS-CDMA system.

a flat fading environment, the additive noise matrix and the Signal-to-Noise Ratio (SNR) per receive antenna. Each of the elements of $\mathbf{H}$ and $\mathbf{N}_n$ is assumed to be an independently and identically distributed complex-valued Gaussian random variable with zero-mean and unit variance. Then, a simple differential receiver has the form of [138]

$$\hat{\mathbf{G}}_n = \arg \underbrace{\max}_{\mathbf{G}_n \in \mathcal{G}} \mathrm{ReTr}\left\{\mathbf{G}_n \mathbf{Y}_n^H \mathbf{Y}_{n-1}\right\}, \tag{3.144}$$

where "ReTr" denotes the real part of the trace of a matrix.

### 3.6.2 Transmitter Model

The system considered in this section is an evolutionary successor of the generalized MC DS-CDMA scheme [41] using $U \cdot V$ number of subcarriers. The transmitter schematic of the $k$th user is shown in Figure 3.11, where a block of $U \cdot N_l$ data bits each having a bit duration of $T_b$ is Serial-to-Parallel (S/P) converted to $U$ parallel sub-blocks. By using the mapping $\mathcal{G}$ described in Section 3.6.1, the transmitter maps the $N_l$ bits of each sub-stream to the information matrix $\mathbf{G}_{ku,n}$. Then, we attain

the $n$th $(M \times N_l)$-dimensional space-time code $\mathbf{X}_{ku,n} = \mathbf{X}_{ku,n-1}\mathbf{G}_{ku,n}$. After spreading $\mathbf{X}_{ku,n}$ with the aid of $N_l$ orthogonal Walsh-Hadamard spreading codes $\{c_{k,1}(t), c_{k,2}(t), \ldots, c_{k,N_l}(t)\}$, $k = 1, 2, \ldots, K$, the $UM$ outputs of the $U$ number of DSTS blocks are multicarrier modulated by a group of subcarrier frequencies $\{f_{u1}, f_{u2}, \ldots, f_{uV}\}$ and then forwarded to the transmitter's $M$ arrays. The symbol duration of the DSTS signals is $N_l T_s$, and the length of the orthogonal codes is $N_l T_s/T_c = N_l N_e$, where $N_e = T_s/T_c$ and $T_c$ represents the chip-duration of the orthogonal spreading codes. Finally, according to the $k$th user's Direction of Arrival (DOA), the $UMV$ signals of the $k$th user are weighted by the transmit weight vector $\mathbf{w}_{v,m}^{(k)}$ determined for the $v$th subcarrier of the $k$th user, which is generated for the $m$th array. It is reasonable to assume that the users' DOAs change slowly and hence may be estimated correctly.

The general form of the $k$th user's transmitted signal corresponding to the $M$ transmit antennas can be expressed as

$$\mathbf{s}_k(t) = \sum_{u=1}^{U}\sum_{v=1}^{V}\sqrt{\frac{2P_k}{VL}\frac{1}{M \cdot N_l}}\mathbf{W}^k\mathbf{X}_{ku,n}\mathbf{c}_k \cos(2\pi f_{uv}t + \phi_{k,uv}), \tag{3.145}$$

where $P_k/V$ represents the transmitted power of each subcarrier, $\mathbf{c}_k = [c_{k,1}(t), c_{k,2}(t), \ldots, c_{k,N_l}(t)]^T$ is an $N_l$-dimensional spreading sequence vector and $\mathbf{W}^{(k)}$ is the weight matrix, which can be expressed as

$$\mathbf{W}^k = \begin{bmatrix} (\mathbf{w}_0^k)^* & \mathbf{0} & \ldots & \mathbf{0} \\ \mathbf{0} & (\mathbf{w}_1^k)^* & \ldots & \mathbf{0} \\ \vdots & \vdots & \ddots & \vdots \\ \mathbf{0} & \mathbf{0} & \ldots & (\mathbf{w}_{M-1}^k)^* \end{bmatrix}, \tag{3.146}$$

where $\mathbf{0} = [0, 0, \ldots, 0]^T$ is an $L$-dimensional vector, while $\mathbf{w}_m^k$ is the $L$-dimensional weight vector of the $m$th beamformer antenna array of the $k$th user.

### 3.6.3 Receiver Model

In this section, we consider the case of a single receive antenna. The Spatio-Temporal (ST) Channel Impulse Response (CIR) vector $h_{uv,m}^{(k)}$ between the $uv$th subcarrier of the $k$th user and the $m$th antenna array can be expressed as

$$\begin{aligned} \mathbf{h}_{uv,m}^{(k)}(t) &= \mathbf{a}_{uv,m}^{(k)}(t)\delta(t - \tau_k) \\ &= \left[a_{uv,m0}^{(k)}(t), \ldots, a_{uv,m(L-1)}^{(k)}(t)\right]^T \delta(t - \tau_k), \end{aligned} \tag{3.147}$$

which is an $L$-dimensional vector, where $\tau_k$ is the signal's delay, $a_{uv,ml}^{(k)}(t)$ is the CIR with respect to the $uv$th subcarrier of the 1st user and the $l$th element of the $m$th antenna array. Based on the

assumption that the array elements are separated by half a wavelength, we can simplify $\mathbf{a}_{uv,m}^{(k)}(t)$ to

$$\mathbf{a}_{uv,m}^{(k)}(t) = \alpha_{uv,m}^{(k)}(t)\mathbf{d}^{(k)}, \tag{3.148}$$

where $\alpha_{uv,m}^{(k)}(t)$ is the Rayleigh faded envelope's amplitude. Furthermore, $\mathbf{d}^{(k)} = [1, \exp(j[\pi \sin(\psi^{(k)})]), \ldots, \exp(j[(L-1)\pi \sin(\psi^{(k)})])]^T$ and $\psi^{(k)}$ is the $k$th user's DOA.

Assuming that the $K$ users' signals expressed in the form of (3.145) are transmitted synchronously over Rayleigh fading channels, the baseband data matrix $\mathbf{Y}_{u,n} \in C^{V \times N_l N_e}$ received over $V$ number of subcarriers after multicarrier demodulation can be expressed as

$$\mathbf{Y}_{u,n} = \mathbf{H}_u \sum_{k=1}^{K} \sqrt{\frac{2P_k}{VL}\frac{1}{MN_l}}\mathbf{W}^k \mathbf{X}_{ku,n}\mathbf{C}_k + \mathbf{N}_n, \tag{3.149}$$

where $\mathbf{N}_n \in C^{V \times N_l N_e}$ denotes the AWGN matrix. In (3.149), the $V \times ML$-dimensional matrix of

$$\mathbf{H}_u = \begin{bmatrix} (\mathbf{h}_{u1,0}^{(1)}(t))^T & \ldots & (\mathbf{h}_{u1,(M-1)}^{(1)}(t))^T \\ (\mathbf{h}_{u2,0}^{(1)}(t))^T & \ldots & (\mathbf{h}_{u2,(M-1)}^{(1)}(t))^T \\ \vdots & \ddots & \vdots \\ (\mathbf{h}_{uV,0}^{(1)}(t))^T & \ldots & (\mathbf{h}_{uV,(M-1)}^{(1)}(t))^T \end{bmatrix} \tag{3.150}$$

is the unknown channel-fading matrix, while the spreading code matrix $\mathbf{C}_k$ is expressed as

$$\mathbf{C}_k = \begin{bmatrix} c_{k,1}[0] & c_{k,1}[1] & \ldots & c_{k,1}[N_l N_e - 1] \\ c_{k,2}[0] & c_{k,2}[1] & \ldots & c_{k,2}[N_l N_e - 1] \\ \vdots & \vdots & \ddots & \vdots \\ c_{k,N_l}[0] & c_{k,N_l}[1] & \ldots & c_{k,N_l}[N_l N_e - 1] \end{bmatrix}. \tag{3.151}$$

Based on the orthogonality of the spreading codes, we multiply both sides of (3.149) with the spreading code matrix $\mathbf{C}_1$ of the desired user and hence attain

$$\mathbf{Z}_{u,n} = \sqrt{\frac{2P_1}{VL}\frac{1}{MN_l}}\mathbf{H}_u \mathbf{W}^1 \mathbf{X}_{1u,n} + \mathbf{N}_n \mathbf{C}_1^H. \tag{3.152}$$

In this scenario, the MRC criterion based transmit beamformer, which constitutes an effective solution to maximizing the antenna gain in the direction of the desired user, is the optimum beamformer. Let us assign $\mathbf{w}_m^k = \mathbf{d}^{(k)}$ in (3.148). Then the term $\mathbf{Z}_{u,n}$ of Equation (3.152) can be expressed as

$$\mathbf{Z}_{u,n} = \sqrt{\frac{2P_1}{V}\frac{L}{MN_l}}\tilde{\mathbf{H}}_u \mathbf{X}_{1u,n} + \mathbf{N}_n \mathbf{C}_1^H, \tag{3.153}$$

where the $(V \times M)$-dimensional matrix $\tilde{\mathbf{H}}_u$ is given by

$$\tilde{\mathbf{H}}_u = \begin{bmatrix} h^{(1)}_{u1,0} & \cdots & h^{(1)}_{u1,(M-1)} \\ h^{(1)}_{u2,0} & \cdots & h^{(1)}_{u2,(M-1)} \\ \vdots & \ddots & \vdots \\ h^{(1)}_{uV,0} & \cdots & h^{(1)}_{uV,(M-1)} \end{bmatrix}. \tag{3.154}$$

Note that for $L = 1$, which corresponds to the stand-alone DSTS scheme, we have $\mathrm{w}^k_m = 1$. Hence no information is required about the user' DOAs by the DSTS scheme.

By invoking the differential receiver of [138], we attain the information matrix of

$$\hat{\mathbf{G}}_{ku,n} = \arg \underbrace{\max}_{\mathbf{G}_{ku,n} \in \mathcal{G}} \mathrm{ReTr}\left\{\mathbf{G}_{ku,n}\mathbf{Z}^H_{u,n}\mathbf{Z}_{u,n-1}\right\}. \tag{3.155}$$

### 3.6.4 User-load Extension Using Time-Frequency-Domain Spreading

As described in Sections 3.2.4 3.4.3 and 3.5.3, spreading in the F-domain may also be employed for the sake of extending the user-load of the generalized MC DS-CDMA system by DSTS and DSSTS. The resultant bandwidth is again the same as that of the MC DS-CDMA scheme employing time-domain-only spreading, while the total number of users supported becomes $VK_{max} = VN_e$, which is $V$ times the number of the users supported by the MC DS-CDMA scheme employing time-domain-only spreading. This is an explicit benefit of using F-domain spreading, rather than F-domain repetition across $V$ subcarriers.

The transmitter schematic of the broadband MC DS-CDMA system using TF-domain spreading is similar to that seen in Figure 3.11, except that the $V$-depth F-domain repetition scheme of Figure 3.11 is now replaced by F-domain spreading associated with an orthogonal spreading code of length $V$. Accordingly, let $\{c'_k[0], c'_k[1], \ldots, c'_k[V-1]\}$ be the $k$th user's orthogonal F-domain spreading code in discrete form. Following the approach of Section 3.6, the received baseband data matrix $\mathbf{Y}_{u,n}$ can be modified from (3.149) to

$$\mathbf{Y}_{u,n} = \sum_{k=1}^{K} \sqrt{\frac{2P_k}{VL}\frac{1}{MN_l}}\mathbf{C'}_k\mathbf{H}_u\mathbf{W}^k\mathbf{X}_{ku,n}\mathbf{C}_k + \mathbf{N}_n, \tag{3.156}$$

where the $(V \times V)$-dimensional F-domain spreading code matrix $\mathbf{C'}_k$ can be expressed as

$$\mathbf{C'}_k = \begin{bmatrix} c'_k[0] & 0 & \ldots & 0 \\ 0 & c'_k[1] & \ldots & 0 \\ \vdots & \vdots & \ddots & \vdots \\ 0 & 0 & \ldots & c'_k[V-1] \end{bmatrix}. \tag{3.157}$$

By multiplying both sides of (3.156) with the spreading code matrix $\mathbf{C}_1$ as well as with $\mathbf{C'}_1$ of the

desired user and letting $\mathbf{w}_m^k = \mathbf{d}^{(k)}$, we have

$$\begin{aligned}\mathbf{Z}_{u,n} &= \sqrt{\frac{2P_1}{V}\frac{L}{MN_l}}\tilde{\mathbf{H}}_u\mathbf{X}_{1u,n} + \mathbf{C}_1'^H\mathbf{N}_n\mathbf{C}_1^H \\ &\quad + \sum_{k=2}^{K'}\sqrt{\frac{2P_k}{VL}\frac{1}{MN_l}}\mathbf{C}_1'^H\mathbf{C}'_k\mathbf{d}^{(1)^T}\mathbf{d}^{(k)^*}\tilde{\mathbf{H}}_u\mathbf{X}_{ku,n}, \end{aligned} \tag{3.158}$$

where $K'$ is the number of users sharing the same T-domain spreading code matrix with the desired user, while the term $\sum_{k=2}^{K'}\sqrt{\frac{2P_k}{VL}\frac{1}{MN_l}}\mathbf{C}_1'^H\mathbf{C}'_k\mathbf{d}^{(1)^T}\mathbf{d}^{(k)^*}\tilde{\mathbf{H}}_u\mathbf{X}_{ku,n}$ is generated by the Multiuser Interference (MUI).

We know from Equation (3.158) that multiuser interference is inevitably introduced, since the orthogonality of the F-domain spreading codes cannot be retained over frequency-selective fading channels. However, the desired signal is not interfered by the transmitted signals of the users employing different orthogonal T-domain spreading codes, provided that synchronous transmission of all the $K'\mathcal{K}_{max}$ user signals as well as flat-fading of each subcarrier are assumed. Only the users sharing the same T-domain spreading code matrix with the desired user will impose interference on the desired user. Therefore, the MUI term can be reduced, if we carefully select the $(K'-1)$ users, namely those which have the lowest interference coefficient with respect to the desired user, from the set of all the $K'\mathcal{K}_{max}$ users for the sake of sharing the same T-domain spreading code with the desired user. Let the interference coefficient be defined as $\mathbf{d}^{(1)^T}\mathbf{d}^{(k)^*}$, which can be evaluated before transmission, based on the assumption that the users' DOAs are perfectly estimated. Following this user-grouping procedure, the effect of the interfering signals imposed on the desired user's signal becomes less pronounced. Therefore, the achievable BER performance is improved. Note that in the stand-alone DSTS scheme no beamforming is invoked and hence the interference coefficient becomes as high as $\mathbf{d}^{(1)^T}\mathbf{d}^{(k)^*} \equiv 1$. Therefore, the achievable BER performance cannot be improved in the DSTS scheme by employing the above-mentioned user-grouping procedure.

## 3.7 Comparison of Various Transmit Processing Schemes

### 3.7.1 Simulation Results - Beamforming

All the results provided in this section were based on evaluating the BER performance of the downlink of a generalized MC DS-CDMA system, when communicating over a dispersive ST Rayleigh fading channel contaminated by AWGN. We assumed that 32-chip WH codes were employed as the time-domain spreading sequences, while 4-chip WH codes were used as the frequency-domain spreading codes. The BS's downlink beamforming scheme was used to pre-process the transmitted signal, in order to maximize the received SNR value. Furthermore, perfect power control was assumed, which implies that we have $P_0 = P_1 = \ldots = P_K$.

In Figure 3.12 we used a $(1 \times 4)$-dimensional antenna array ($M = 1, L = 4$), having an element-spacing of $\lambda/2$. It transpires from Figure 3.12 that the performance of the system supporting 32 users is similar to that of the system supporting a single user. Recall the former assumptions of having

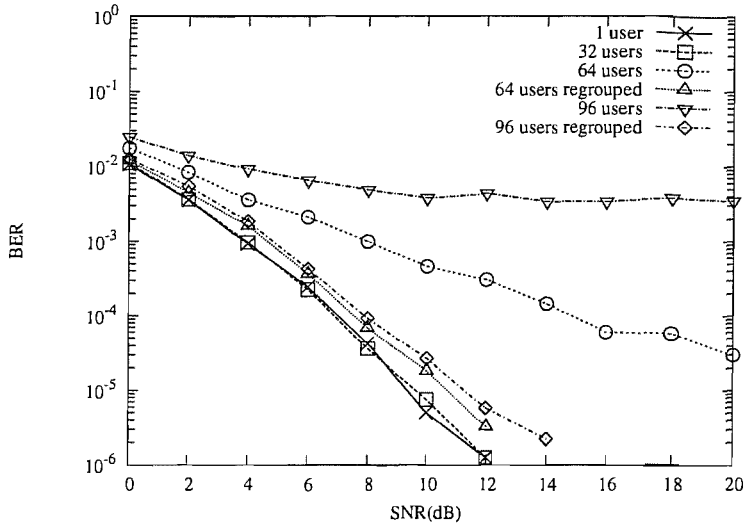


**Figure 3.12:** BER versus SNR performance of the downlink of a generalized MC DS-CDMA wireless system using 32-chip WH codes as T-domain spreading sequences and 4-chip WH codes as F-domain spreading sequences, using a $(1 \times 4)$-dimensional antenna array $(M = 1, L = 4)$. In these simulations, the beamforming scheme of Section 3.2 was used to pre-process the transmit signal. TF-domain spreading and user regrouping were used to extend the user-load of the system, while suppressing the interference.

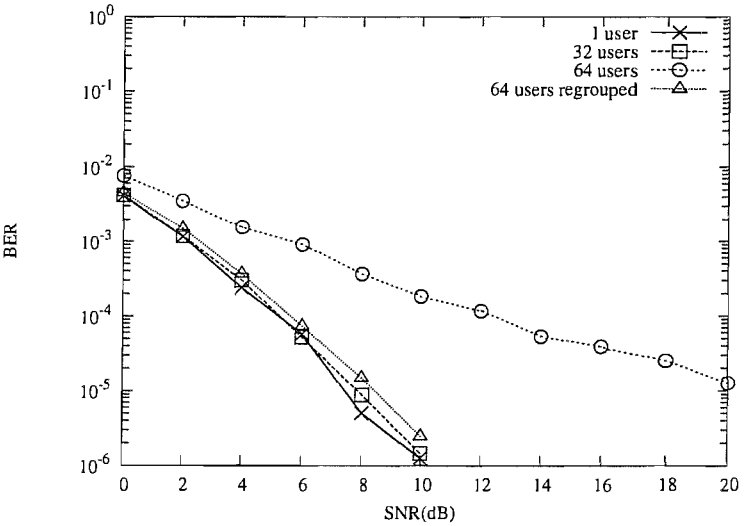


**Figure 3.13:** BER versus SNR performance of the downlink of a generalized MC DS-CDMA wireless system using 32-chip WH codes as T-domain spreading sequences and 4-chip WH codes as F-domain spreading sequences, using a $(1 \times 6)$-dimensional antenna array $(M = 1, L = 6)$. In these simulations, the beamforming scheme of Section 3.2 was used to pre-process the transmitted signal. TF-domain spreading and user regrouping were used to extend the user-load of the system, while suppressing the interference.

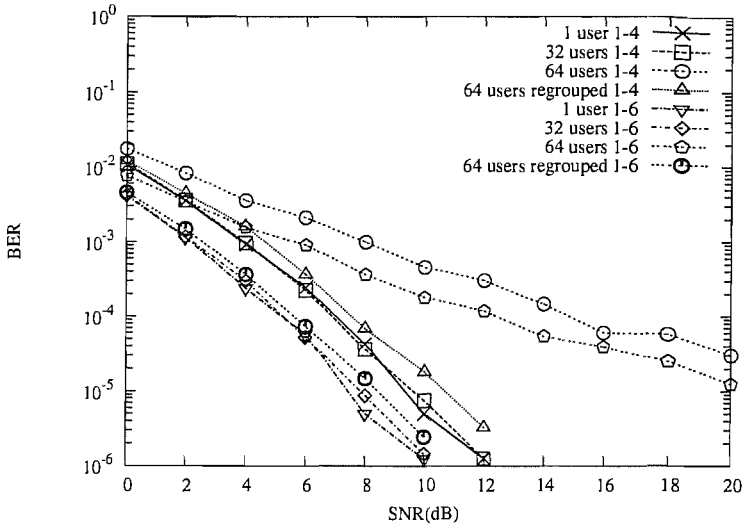


**Figure 3.14:** BER versus SNR performance of the downlink of a generalized MC DS-CDMA wireless system using 32-chip WH codes as T-domain spreading sequences and 4-chip WH codes as F-domain spreading sequences. the beamforming scheme of Section 3.2 was used to pre-process the transmitted signal. TF-domain spreading was used to extend the user-load of the system and the interference coefficient based user regrouping was used to reduce the interference between the users sharing the same 32-chip WH code as T-domain spreading code. In these simulations, two types of antenna arrays were employed, namely a $(1 \times 4)$-dimensional antenna array ($M = 1, L = 4$), and a $(1 \times 6)$-dimensional antenna array ($M = 1, L = 6$).

orthogonal multicarrier signals, synchronous transmission of the $K$ users' signals as well as slow flat-fading of each subcarrier. Hence there was no interference between the 32 users employing different orthogonal 32-chip WH codes as time-domain DS spreading codes. For the sake of extending the user-load of the system, TF-domain spreading was employed in the system supporting 64 and 96 users. Consequently, multiuser interference was inevitably introduced among the users sharing the same T-domain spreading code, since the orthogonality of the F-domain spreading codes cannot be retained in frequency-selective fading channels. We observe in Figure 3.12 that the BER performance of the system supporting 64 users is significantly worse than that of the system supporting a single user or 32 users, and naturally, the system supporting 96 users achieved the worst performance. After invoking the user regrouping technique of Section 3.2.4 by carefully selecting the $K' - 1$ users having the lowest interference coefficient with respect to the desired user from the entire population of $K'\mathcal{K}_{max}$ users to share the same T-domain spreading code with the desired user, the multiuser interference was substantially reduced. This is explicitly demonstrated in Figure 3.12, where the system employing the interference coefficient based user grouping technique was shown to outperform the system refraining from user grouping, regardless, whether 64 or 96 users were supported. However, the BER performance of the systems employing both TF-domain spreading and the user regrouping remained slightly worse than that of the system supporting a single user or 32 users, because the multiuser interference cannot be totally eliminated.

In Figure 3.13 we used a $(1 \times 6)$-dimensional antenna array ($M = 1, L = 6$), having an element-spacing of $\lambda/2$. Figure 3.13 shows that the performance of the system supporting 32 users is similar to that of the system supporting a single user for similar reasons as in Figure 3.12. When employing TF-domain spreading for the sake of increasing the user-load of the system by a factor of $V$ in comparison to the system employing F-domain repetition, the performance of the system supporting 64 users became significantly worse than that of the system supporting a single user or 32 users and again, the system serving 96 users achieved the worst performance. In Figure 3.13, the user regrouping was employed again for the sake of reducing the multiuser interference. Therefore, the system employing the interference coefficient based user grouping outperformed the system refraining from user grouping. Similarly, the performance of the systems employing TF-domain spreading and the user regrouping became slightly worse than that of the system serving a single user or 32 users. However, the performance difference between them became less pronounced, since a higher number of array elements was employed.

Finally, in Figure 3.14 the BER performance of the systems employing two different types of antenna arrays was compared, namely using a $(1 \times 4)$-dimensional antenna array ($M = 1, L = 4$) and a $(1 \times 6)$-dimensional antenna array ($M = 1, L = 6$). It is clearly seen from Figure 3.14 that the system using a $(1 \times 6)$-dimensional antenna array ($M = 1, L = 6$) achieves better performance than that of a $(1 \times 4)$-dimensional antenna array ($M = 1, L = 4$). This is because, when using a MRC assisted beamformer, the increased number of elements becomes capable of attaining a higher SNR gain, resulting in a better BER performance.

### 3.7.2 Simulation Results - Beam Selection Transmit Diversity

In this section the BER performance of the downlink of a generalized MC DS-CDMA system employing the BSTD scheme of Section 3.3, using 32-chip WH codes as time-domain spreading sequences and 4-chip WH codes as frequency-domain spreading codes was studied. As before, perfect power control was assumed, implying that $P_0 = P_1 = \ldots = P_K$.

In Figure 3.15 we used a $(2 \times 2)$-dimensional antenna array ($M = 2, L = 2$), having an element-spacing of $\lambda/2$ as well as an array-spacing of $10\lambda$. Figure 3.15 shows that the performance of the system supporting 32 users is similar to that of the system serving a single user, since there is no interference between the 32 users employing different orthogonal 32-chip WH codes as their time-domain DS spreading codes based on the assumption of having orthogonal multicarrier signals, synchronous transmission of the $K$ users' signals as well as slow flat-fading of each subcarrier. TF-domain spreading was also employed in the system to support an increased number of 64 or 96 users. Similarly to the scenario considered in Figure 3.12, multiuser interference was inevitably introduced, but it was mitigated by user grouping. Therefore, we observe in Figure 3.15 that the performance of the system supporting 64 users is significantly worse than that of the system serving a single user or 32 users, while the system supporting 96 users achieved the worst performance. Furthermore, the performance of the systems employing TF-domain spreading and the interference coefficient based user grouping remained slightly worse than that of the system supporting a single user or 32 users, because the

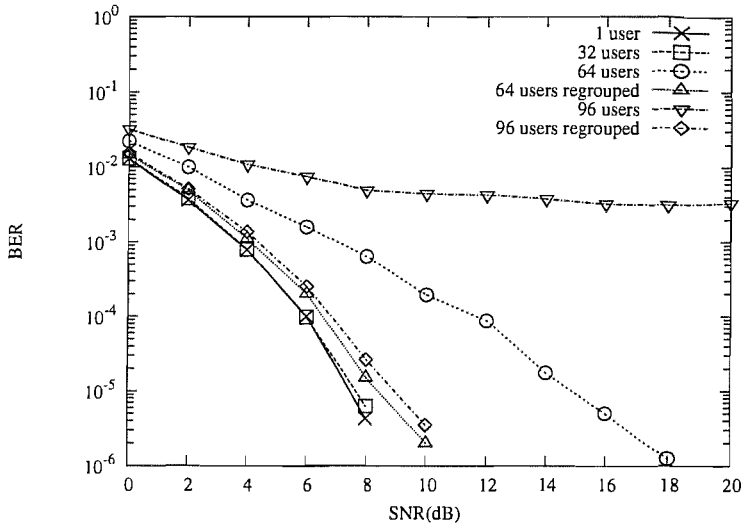


**Figure 3.15:** BER versus SNR performance of the downlink of a generalized MC DS-CDMA wireless system using 32-chip WH codes as T-domain spreading sequences and 4-chip WH codes as F-domain spreading sequences, using a $(2 \times 2)$-dimensional antenna array $(M = 2, L = 2)$. In these simulations, the BSTD scheme of Section 3.3 was used to pre-process the transmit signal. TF-domain spreading and user regrouping were used to extend the user-load of the system, while suppressing the interference.

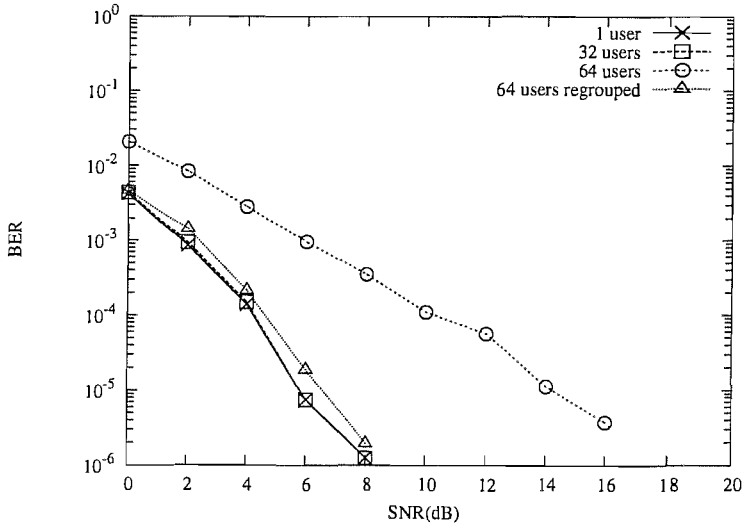


**Figure 3.16:** BER versus SNR performance of the downlink of a generalized MC DS-CDMA wireless system using 32-chip WH codes as T-domain spreading sequences and 4-chip WH codes as F-domain spreading sequences, using a $(2 \times 3)$-dimensional antenna array $(M = 2, L = 3)$. In these simulations, the BSTD scheme of Section 3.3 was used to pre-process the transmitted signal. TF-domain spreading and user regrouping were used to extend the user-load of the system, while suppressing the interference.

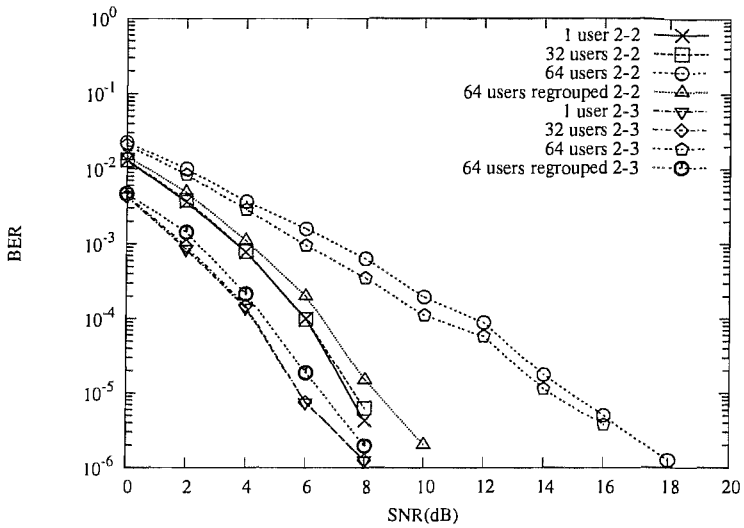


**Figure 3.17:** BER versus SNR performance of the downlink of a generalized MC DS-CDMA wireless system using 32-chip WH codes as T-domain spreading sequences and 4-chip WH codes as F-domain spreading sequences. The BSTD scheme of Section 3.3 was used to pre-process the transmitted signal. TF-domain spreading is used to extend the user-load of the system and the interference coefficient based user regrouping was used to reduce the interference between the users sharing the same 32-chip WH code as T-domain spreading code. In these simulations, two types of antenna arrays were employed, namely a $(2 \times 2)$-dimensional antenna array ($M = 2, L = 2$), and a $(2 \times 3)$-dimensional antenna array ($M = 2, L = 3$).

multiuser interference cannot be entirely eliminated.

In Figure 3.16 we used a $(2 \times 3)$-dimensional antenna array ($M = 2, L = 3$), having an element-spacing of $\lambda/2$ as well as an array-spacing of $10\lambda$. This figure demonstrates that the performance of the system supporting 32 users is similar to that of the system supporting a single user owing to similar reasons to those argued in the context of Figure 3.16. When employing TF-domain spreading for the sake of extending the user-load of the system, the performance of the system supporting 64 users became substantially worse than that of the system serving a single user or 32 users, and again, the system supporting 96 users achieved the poorest performance. In Figure 3.16, the user regrouping technique was employed again for the sake of reducing the multiuser interference, and it was demonstrated that the attainable performance was only marginally worse than that of the system supporting a single user or 32 users, which was a benefit of the increased number of array elements in comparison to Figure 3.15.

Finally, in Figure 3.17, the BER performance of the systems employing two different types of antenna arrays was compared, namely that of a $(2 \times 2)$-dimensional antenna array ($M = 2, L = 2$), and that of a $(2 \times 3)$-dimensional antenna array ($M = 2, L = 3$). It becomes explicit in Figure 3.17 that the system using a $(2 \times 3)$-dimensional antenna array ($M = 2, L = 3$) achieves better performance than that of the $(2 \times 2)$-dimensional antenna array ($M = 2, L = 2$). This is because, the MRC criterion based beamformer having an increased number of elements is capable of attaining a higher

SNR gain, resulting in an improved BER performance.

### 3.7.3 Simulation Results - Space Time Transmit Diversity

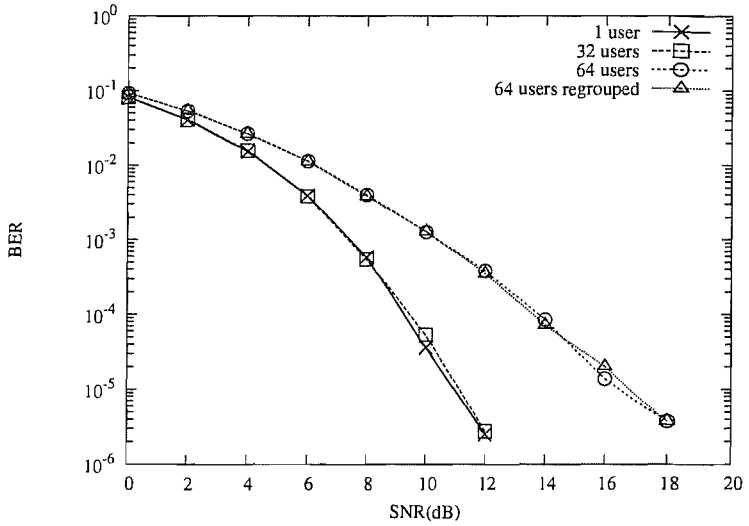


**Figure 3.18:** BER versus SNR performance of the downlink of a generalized MC DS-CDMA wireless system using 32-chip WH codes as T-domain spreading sequences and 4-chip WH codes as F-domain spreading sequences, using a $(4 \times 1)$-dimensional antenna array $(M = 4, L = 1)$. In these simulations, the STTD scheme of Section 3.4 was used to pre-process the transmit signal. TF-domain spreading was used to extend the user-load of the system.

All the results in this section were based on evaluating the BER performance of the downlink of a generalized MC DS-CDMA system employing the STTD scheme of Section 3.4, using 32-chip WH codes as time-domain spreading sequences and 4-chip WH codes as frequency-domain spreading codes. Again, perfect power control was assumed, implying that we had $P_0 = P_1 = \ldots = P_K$. In Figure 3.18 we used a $(4 \times 1)$-dimensional antenna array $(M = 4, L = 1)$ having an array-spacing of $10\lambda$. Observe in Figure 3.18 that the performance of the system supporting 32 users is similar to that of the system serving a single user. Recall that the former assumption of having orthogonal multicarrier signals, synchronous downlink transmission of the $K$ users' signals as well as slow flat-fading of each subcarrier was also adopted here and hence there is no interference between the 32 users employing different orthogonal 32-chip WH codes as their time-domain DS spreading codes. For the sake of extending the user-load of the system, TF-domain spreading was employed, when supporting 64 users. Consequently, multiuser interference was inevitably introduced among the users sharing the same T-domain spreading code, since the orthogonality of the F-domain spreading codes cannot be retained over frequency-selective fading channels. Observe in Figure 3.18 that the performance of the system supporting 64 users became slightly worse than that of the system supporting 1 or 32 users. However, without beamforming the user regrouping does not work for the system employing the STTD scheme of Section 3.4. As we can see from Figure 3.18, when

supporting 64 users, the system employing user regrouping achieves a similar performance to the system refraining from user grouping.

### 3.7.4 Simulation Results - Steered Space-Time Spreading

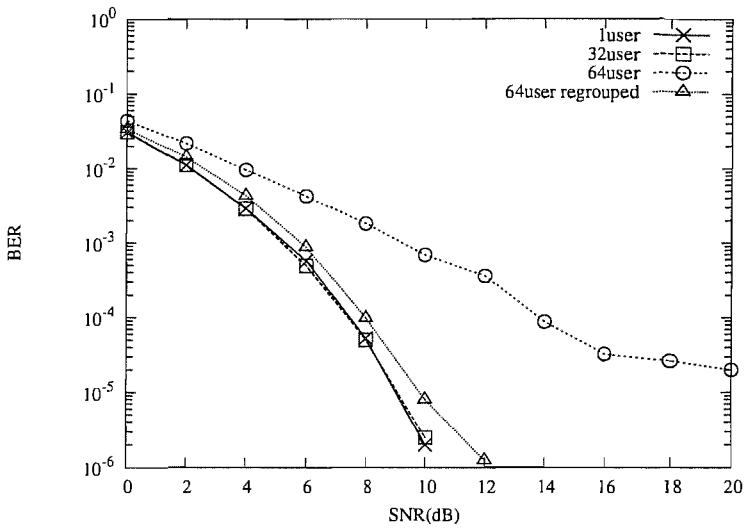


**Figure 3.19:** BER versus SNR performance of the downlink of a generalized MC DS-CDMA wireless system using 32-chip WH codes as T-domain spreading sequences and 4-chip WH codes as F-domain spreading sequences, using a $(2 \times 2)$-dimensional antenna array ($M = 2, L = 2$). In these simulations, the SSTS scheme of Section 3.5 was used to pre-process the transmit signal. TF-domain spreading and user regrouping were used to extend the user-load of the system, while suppressing the interference.

In this section the BER performance of the downlink of a generalized MC DS-CDMA system employing the SSTS scheme of Section 3.5, using 32-chip WH codes as time-domain spreading sequences and 4-chip WH codes as frequency-domain spreading codes was studied. Similarly to the other investigated scenarios, perfect power control was assumed, when we have $P_0 = P_1 = \ldots = P_K$.

In Figure 3.19 we used a $(2 \times 2)$-dimensional antenna array ($M = 2, L = 2$) having an element-spacing of $\lambda/2$ as well as an array-spacing of $10\lambda$. It may be observed in Figure 3.19 that the performance of the system supporting 32 users is close to that of the system serving a single user for the reasons discussed in Sections 3.7.1 and 3.7.2. This implies that in the downlink there is no interference between the 32 users employing different orthogonal 32-chip WH codes as time-domain DS spreading codes. As discussed in Sections 3.7.1 and 3.7.2, TF-domain spreading can be used for extending the user-load of the system, while the user regrouping technique may be employed for reducing the multiuser interference. Figure 3.19 also shows that the performance of the system supporting 64 users is substantially worse than that of the single-user or 32-user scenarios, while the system serving 96 users achieved the poorest performance. As before, the system employing user regrouping significantly outperformed the system refraining from user grouping. However, the per-

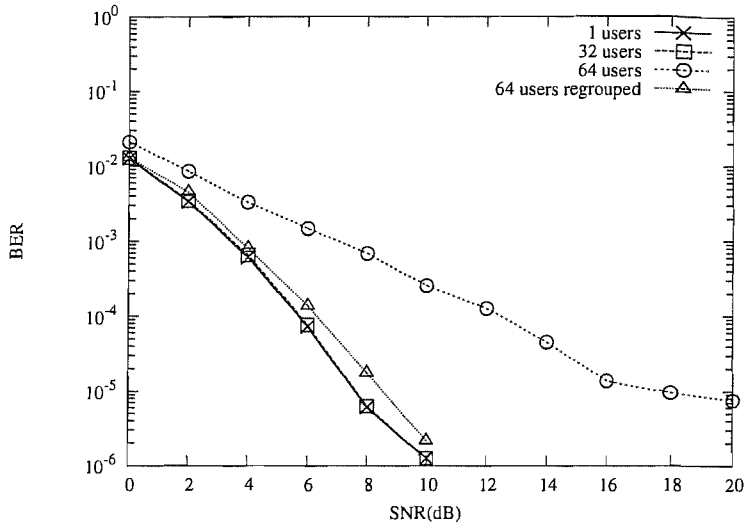


**Figure 3.20:** BER versus SNR performance of the downlink of a generalized MC DS-CDMA wireless system using 32-chip WH codes as T-domain spreading sequences and 4-chip WH codes as F-domain spreading sequences, using a $(2 \times 3)$-dimensional antenna array ($M = 2, L = 3$). In these simulations, the SSTS scheme of Section 3.5 was used to pre-process the transmitted signal. TF-domain spreading and user regrouping were used to extend the user-load of the system, while suppressing the interference.

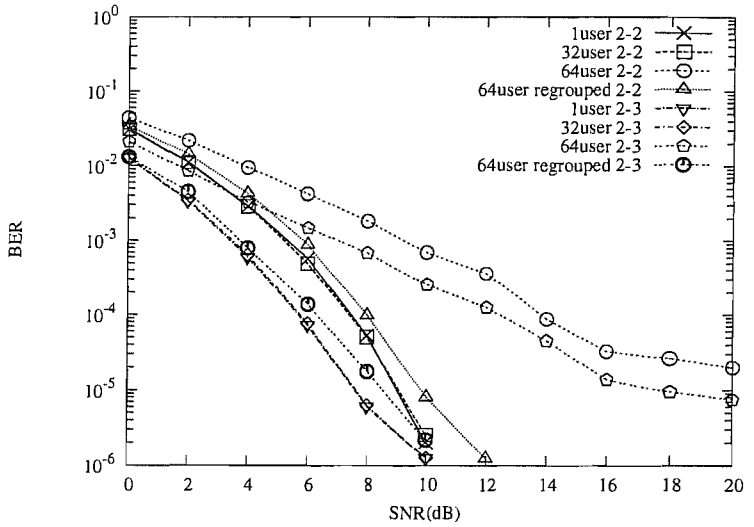


**Figure 3.21:** BER versus SNR performance of the downlink of a generalized MC DS-CDMA wireless system using 32-chip WH codes as T-domain spreading sequences and 4-chip WH codes as F-domain spreading sequences. The SSTS scheme of Section 3.5 was used to pre-process the transmitted signal. TF-domain spreading is used to extend the user-load of the system and the interference coefficient based user regrouping was used to reduce the interference between the users sharing the same 32-chip WH code as T-domain spreading code. In these simulations, two types of antenna arrays were employed, namely a $(2 \times 2)$-dimensional antenna array ($M = 2, L = 2$), and a $(2 \times 3)$-dimensional antenna array ($M = 2, L = 3$).

formance of the systems employing both TF-domain spreading and user regrouping remained slightly inferior in comparison to that of the system supporting one or 32 users, because the multiuser interference cannot be completely eliminated.

In order to investigate the performance of the SSTS scheme further, in Figure 3.20 we used a $(2 \times 3)$-dimensional antenna array ($M = 2, L = 3$), having an element-spacing of $\lambda/2$ as well as an array-spacing of $10\lambda$. It was found that the performance of the system supporting 32 users was virtually identical to that of the system serving a single user. When employing TF-domain spreading in order to extend the user-load of the system, the performance of the system supporting 64 users became inferior in comparison to that serving a single or 32 users and naturally, the system supporting 96 users achieved the poorest performance. When the user grouping technique of Section 3.5.3 was invoked, the achievable performance substantially improved, approaching the BER performance of the single-user system. Similar BER performance trends were observed also in Figure 3.21, where the benefits of increasing the dimension of the array from $(2 \times 2)$ to $(2 \times 3)$ were quantified.

Having studied the effects of different array dimensions in the context of the various transmission preprocessing techniques, in the rest of this section we will compare the BER performance of the generalized MC DS-CDMA systems employing the beamforming scheme of Section 3.2, the BSTD arrangement of Section 3.3, the STTD scheme of Section 3.4 and the SSTS technique of Section 3.5. As before, the generalized MC DS-CDMA system studied employs 32-chip WH codes as time-domain spreading sequences and 4-chip WH codes as frequency-domain spreading codes, communicating over a dispersive Rayleigh fading channel contaminated by AWGN, where all subcarriers experience flat fading. Based on the assumption of perfect power control, all the users have the same power, that is we have $P_0 = P_1 = \ldots = P_K$.

First we consider a generalized MC DS-CDMA system supporting 32 users, as seen in Figure 3.22, where three different types of antenna arrays were employed, namely a $(1 \times 4)$-dimensional antenna array ($M = 1, L = 4$) was used by the BS's downlink BeamForming (BF) scheme of Section 3.2, while a $(2 \times 2)$-dimensional antenna array ($M = 2, L = 2$) was employed by the BSTD and SSTS scheme of Section 3.3 and 3.5, respectively. Finally, a $(4 \times 1)$-dimensional antenna array ($M = 4, L = 1$) was invoked by the STTD scheme of Section 3.4. We observe from Figure 3.22 that when supporting 32 users, the system employing the BSTD scheme achieved the best BER performance, while the system employing the STTD scheme exhibited the poorest BER performance. The system employing the SSTS scheme outperformed that using the beamforming scheme for SNRs in excess of 8dB. However, when the SNR was below 8dB, the system employing the SSTS scheme achieved a worse BER performance than that using the beamforming scheme, while outperforming the system using the STTD scheme. Finally, the system employing the SSTS and the beamforming scheme achieved a worse performance than that of the BSTD scheme.

In Figure 3.23, a generalized MC DS-CDMA system supporting 64 users was studied. TF-domain spreading was used to extend the user-load of the system and the user grouping technique of Section 3.2.4 was employed for reducing the interference between the users sharing the same 32-chip WH code as their T-domain spreading code. The three different types of antenna arrays used in

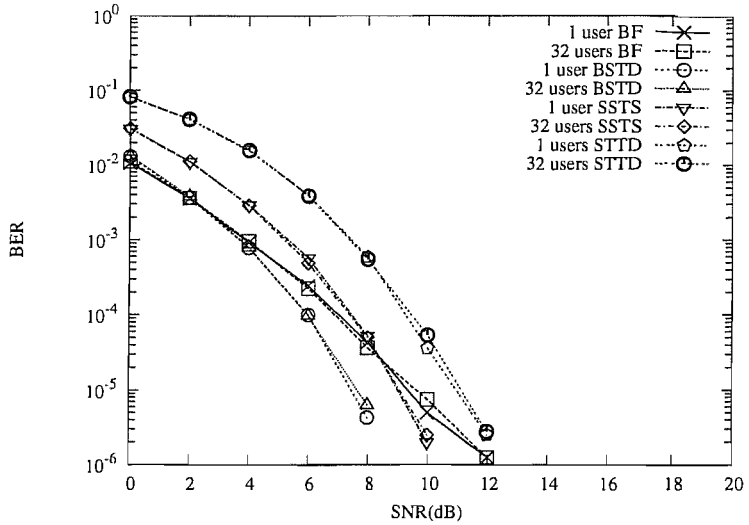


**Figure 3.22:** BER versus SNR performance of the downlink of a generalized MC DS-CDMA wireless system using 32-chip WH codes as T-domain spreading sequences and 4-chip WH codes as F-domain spreading sequences, supporting 32 users. In these simulations, three different types of antenna arrays were employed, namely a $(1 \times 4)$-dimensional antenna array $(M = 1, L = 4)$ employed for BeamForming (BF) scheme, a $(2 \times 2)$-dimensional antenna array $(M = 2, L = 2)$ used by the BSTD and SSTS schemes, and finally, a $(4 \times 1)$-dimensional antenna array $(M = 4, L = 1)$ employed for STTD scheme.

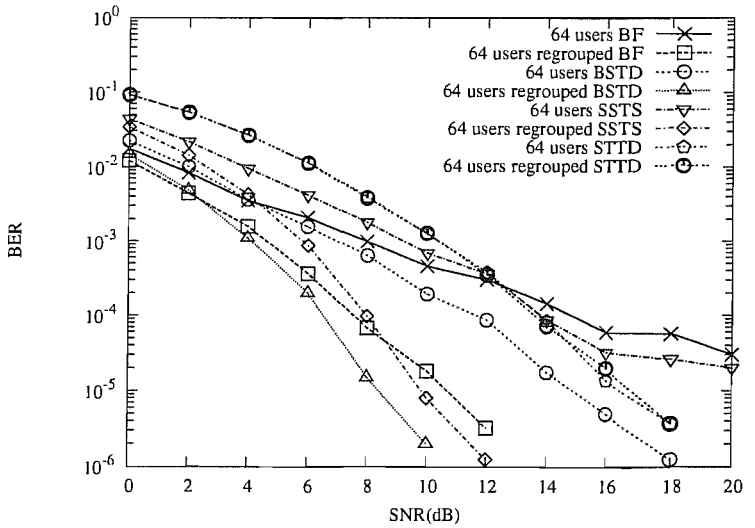


**Figure 3.23:** BER versus SNR performance of the downlink of a generalized MC DS-CDMA wireless system using 32-chip WH codes as T-domain spreading sequences and 4-chip WH codes as F-domain spreading sequences, supporting 64 users. In these simulations, three different types of antenna arrays were employed, namely a $(1 \times 4)$-dimensional antenna array $(M = 1, L = 4)$ employed for BF scheme, a $(2 \times 2)$-dimensional antenna array $(M = 2, L = 2)$ used by the BSTD and SSTS schemes, and finally, a $(4 \times 1)$-dimensional antenna array $(M = 4, L = 1)$ employed for STTD scheme.

the context of Figure 3.22 were employed again. Specifically, a $(1 \times 4)$-dimensional antenna array ($M = 1, L = 4$) was employed by the beamforming scheme, a $(2 \times 2)$-dimensional antenna array ($M = 2, L = 2$) was used by both the BSTD and the SSTS schemes, and finally, a $(4 \times 1)$-dimensional antenna array ($M = 4, L = 1$) was employed by the STTD scheme. When using both the user grouping technique of Section 3.2.4 and TF-domain spreading, the four systems exhibited a similar performance to that seen in Figure 3.22, except that the system employing the STTD scheme achieved a significantly worse BER performance than that of the other three systems using the BSTD scheme, as well as the SSTS and the beamforming arrangements. Again, the system employing the BSTD scheme achieved the best BER performance, while the SSTS scheme outperformed the beamforming arrangement for SNRs higher than 8dB, but it had an inferior performance for SNRs below 8dB. When employing TF-domain spreading but refraining from user grouping, the system using the BSTD scheme still achieved the best performance. At SNRs below 12dB the system employing the SSTS scheme was outperformed by the beamforming scheme, but it was superior in comparison to the system using the STTD scheme. In the SNR region above 12dB, the STTD scheme outperformed both the SSTS and the beamforming scheme and the latter had the poorest performance.

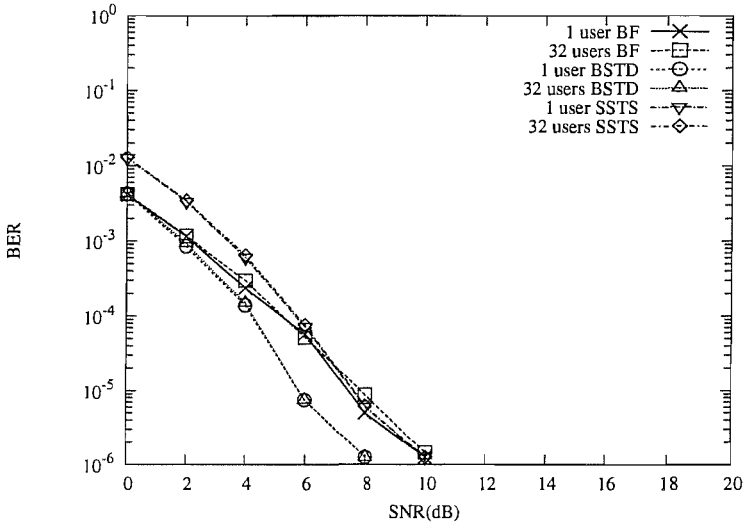


**Figure 3.24:** BER versus SNR performance of the downlink of a generalized MC DS-CDMA wireless system using 32-chip WH codes as T-domain spreading sequences and 4-chip WH codes as F-domain spreading sequences, supporting 32 users. In these simulations, two types of antenna arrays were employed, namely a $(1 \times 6)$-dimensional antenna array ($M = 1, L = 6$) employed for beamforming scheme, and a $(2 \times 3)$-dimensional antenna array ($M = 2, L = 3$) employed for BSTD scheme and SSTS scheme.

In Figure 3.24, a generalized MC DS-CDMA system supporting 32 users was studied, where two different types of antenna arrays were employed, one of which was a $(1 \times 6)$-dimensional antenna array ($M = 1, L = 6$) employed in the context of the beamforming scheme, while the other was a $(2 \times 3)$-dimensional antenna array ($M = 2, L = 3$) invoked by both the BSTD and the SSTS scheme. We observe from Figure 3.24 that when supporting 32 users, the system employing the BSTD scheme

achieved the best BER performance. The SSTS scheme achieved a slightly better performance than the beamforming scheme at SNRs higher than 6dB, while below this SNR threshold the opposite was true.

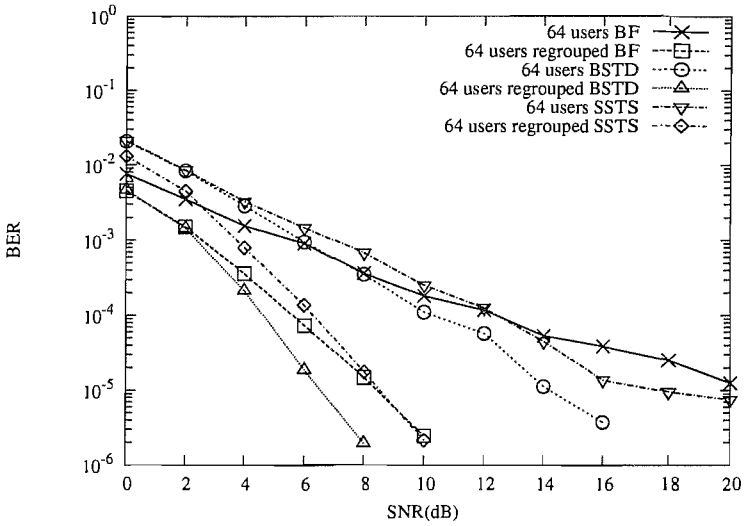


**Figure 3.25:** BER versus SNR performance of the downlink of a generalized MC DS-CDMA wireless system using 32-chip WH codes as T-domain spreading sequences and 4-chip WH codes as F-domain spreading sequences, supporting 64 users. In these simulations, two types of antenna arrays were employed, namely a $(1 \times 6)$-dimensional antenna array $(M = 1, L = 6)$ employed for beamforming scheme, and a $(2 \times 3)$-dimensional antenna array $(M = 2, L = 3)$ employed for BSTD scheme and SSTS scheme.

We continued our investigations in Figure 3.25, where a generalized MC DS-CDMA system supporting 64 users was studied. TF-domain spreading was used to improve the user-load of the system and the user regrouping technique of Section 3.2.4 was invoked for the sake of reducing the interference between the users sharing the same 32-chip WH code as their T-domain spreading code. The same two types of antenna arrays were employed again as in the context of Figure 3.24, namely a $(1 \times 6)$-dimensional antenna array $(M = 1, L = 6)$ was employed by the beamforming scheme, and a $(2 \times 3)$-dimensional antenna array $(M = 2, L = 3)$ was used by both the BSTD and the SSTS scheme. When employing both user grouping and TF-domain spreading, the three systems have a similar performance to that characterized in Figure 3.24.

In summary, upon observing Figures 3.22, 3.23, 3.24, 3.25, we infer that the beamforming scheme achieved a better performance at low SNRs, but a worse performance at high SNRs, in comparison to the BSTD and the SSTS schemes. It transpires from our discussions in Section 3.2 that the beamforming scheme was only used for pre-processing the transmitted signal. Therefore, when employing an antenna array having the same total number of elements as that of the BSTD and the SSTS schemes, the beamformer dedicates all of its elements to attaining the highest possible SNR gain. Hence, it achieves a better performance at low SNRs. However, without benefitting from transmit diversity, the BER performance of the beamforming scheme increases slowly, as the SNR increases. By contrast,

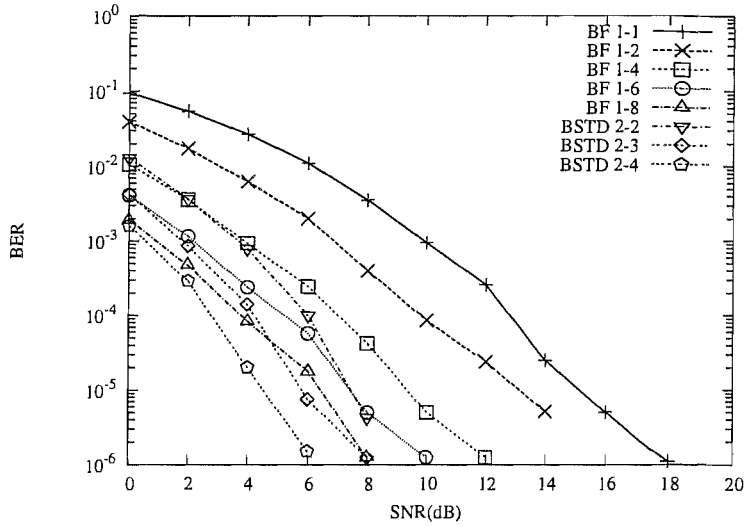


**Figure 3.26:** BER versus SNR performance of the downlink of a generalized MC DS-CDMA wireless system using 32-chip WH codes as T-domain spreading sequences and 4-chip WH codes as F-domain spreading sequences, supporting a single user. In these simulations, several types of antenna arrays were employed for the BF and the BSTD schemes.

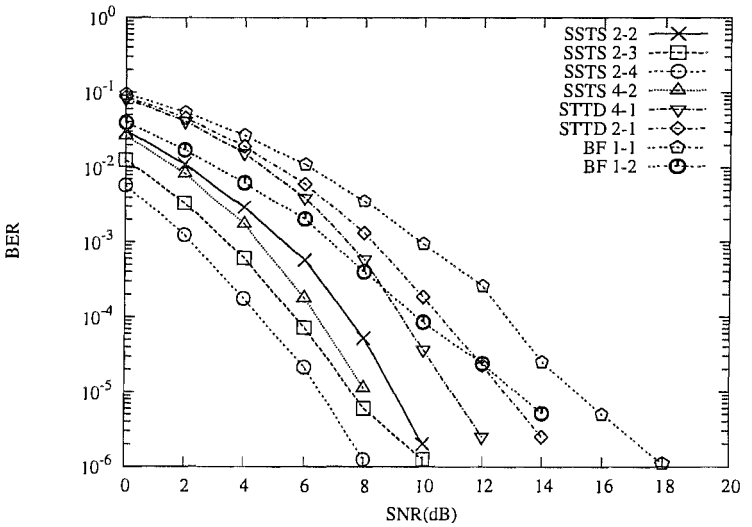


**Figure 3.27:** BER versus SNR performance of the downlink of a generalized MC DS-CDMA wireless system using 32-chip WH codes as T-domain spreading sequences and 4-chip WH codes as F-domain spreading sequences, supporting a single user. In these simulations, several types of antenna arrays were employed for the BF , the STTD and the SSTD schemes.

the BSTD and the SSTS schemes have a steeper BER reduction curve, implying a better performance at high SNRs, than that of the beamforming scheme as a benefit of the transmit diversity employed by them. In contrast to the SSTS scheme, which belongs to the family of open loop methods, the BSTD scheme is a representative of the class of closed loop proposals, activating the specific antenna array benefitting from the best instantaneous channel state and therefore its performance is superior in comparison to that of STTD in the investigated scenario. However, there is a sacrifice in terms of the achievable uplink user-load of the BSTD scheme, because the BSTD scheme requires that the channel information is promptly and correctly fed back from the mobile users to the BS. The STTD scheme achieves a higher transmit diversity gain than other three schemes, when the number of antenna array elements is fixed. However, as discussed in Section 3.4, the highest incremental diversity gains are achieved upon increasing the number of antennas from one to two antennas, while adding further additional antennas achieves modest further diversity gains on the downlink. Therefore, when employing more than $M = 2$ antenna arrays, the STTD scheme achieves the worst performance.

### 3.7.5 Simulation Results - DSTS and DSSTS

In Figure 3.28 we use three different types of antenna arrays, namely a $(2 \times 2)$-dimensional antenna array of $(M = 2, L = 2)$ corresponding to the DSSTS scheme, a $(4 \times 1)$-dimensional antenna array of $(M = 4, L = 1)$ and a $(2 \times 1)$-dimensional antenna array of $(M = 2, L = 1)$ corresponding to the stand-alone DSTS scheme. In these investigations $K = 4$ users are supported. Observe in Figure 3.28 that as expected, the attainable performance of the DSTS and the DSSTS schemes is about 3 dB worse than those of the STS and the SSTS schemes, respectively. The DSTS system using a $(4 \times 1)$-dimensional antenna array of $(M = 4, L = 1)$ achieved a slightly better performance than the DSTS system using a $(2 \times 1)$-dimensional antenna array of $(M = 2, L = 1)$, since the highest incremental diversity gains are achieved upon increasing the number of antennas from one to two, i.e. by 100%, while adding further additional antennas achieves modest extra diversity gains on the downlink. Furthermore, Figure 3.28 shows that the DSSTS system employing a $(2 \times 2)$-dimensional antenna array of $(M = 2, L = 2)$ outperforms the DSTS system using a $(4 \times 1)$-dimensional antenna array of $(M = 4, L = 1)$, suggesting that the DSSTS scheme employs DSTS for the sake of obtaining transmit diversity, but additionally invokes beamforming to attain a higher SNR gain.

In Figure 3.29, generalized MC DS-CDMA systems supporting $K = 1, 32$ and 64 users were studied. It transpires from Figure 3.29 that the performance of the system supporting 32 users is similar to that of the system serving a single user. Recall the assumptions of using orthogonal multicarrier signals, synchronous transmission of the $K$ user signals as well as slow flat-fading of each subcarrier, where no interference is encountered between the 32 users employing different orthogonal 32-chip Walsh codes as T-domain DS spreading codes. In order to extend the user-load of the system, TF-domain spreading is employed for the sake of supporting 64 users. Consequently, some multiuser interference is inevitably introduced among the users sharing the same T-domain spreading code, since the orthogonality of the F-domain spreading codes cannot be retained, when communicating over frequency-selective fading channels. Then a specific user grouping technique is employed by

the DSSTS system for the sake of reducing the multiuser interference imposed. Figure 3.29 demonstrates that the performance of the DSTS system supporting 64 users is significantly worse than that supporting a single user or even 32 users. By contrast, the DSSTS system supporting 64 users and employing the above-mentioned interference coefficient based user grouping technique achieves a slightly worse BER performance than that serving a single user, nonetheless, attaining a 5.7 dB SNR gain compared to the DSTS system at a BER of $10^{-5}$.

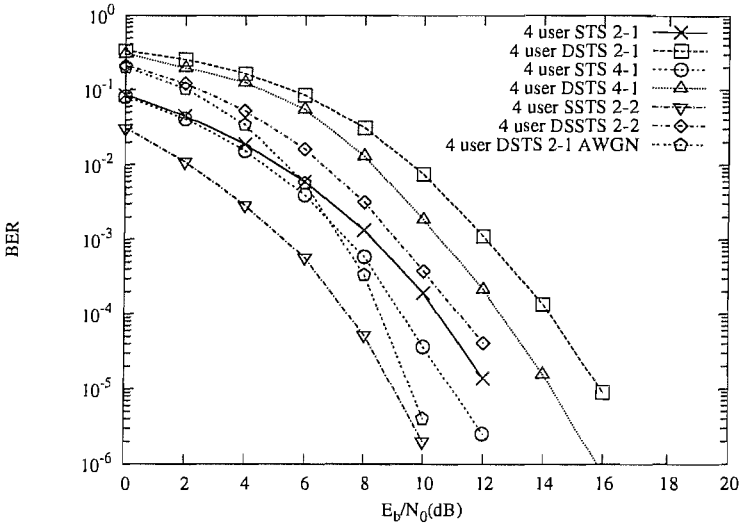


**Figure 3.28:** BER versus SNR performance of the downlink of a generalized MC DS-CDMA wireless system using 32-chip Walsh-Hadamard (WH) codes as T-domain spreading sequences and 4-chip WH codes as F-domain spreading sequences, employing three different types of antenna arrays, namely a $(2 \times 2)$-dimensional antenna array $(M = 2, L = 2)$ corresponding to the DSSTS scheme, a $(4 \times 1)$-dimensional antenna array $(M = 4, L = 1)$ and a $(2 \times 1)$-dimensional antenna array $(M = 2, L = 1)$ corresponding to the DSTS scheme.

## 3.8 Conclusions

In this chapter we have proposed four different downlink space-time transmitter processing schemes based on the principles of beamforming, BSTD, STTD and SSTS, in order to enhance the achievable performance of generalized MC DS-CDMA systems. In Section 3.1, various STTD schemes proposed in the literature [48, 126–134, 136] were briefly introduced. Then, in Section 3.1, the motivation of several beamforming schemes [6, 132–136] was outlined. Finally, some hybrid techniques, such as BSTD [47] and SSTS [49], were introduced in Section 3.1, respectively.

Our specific discussions concerning the downlink beamforming-aided generalized Multicarrier DS-CDMA system commenced in Section 3.2. The transmitter schematic for the downlink beamforming-aided generalized multicarrier DS-CDMA system was shown in Figure 3.1 and the corresponding receiver front-end of the downlink was shown in Figure 3.2. In Sections 3.2.1 and 3.2.2, we provided a general system model invoking a beamforming scheme. In Section 3.2.3 we

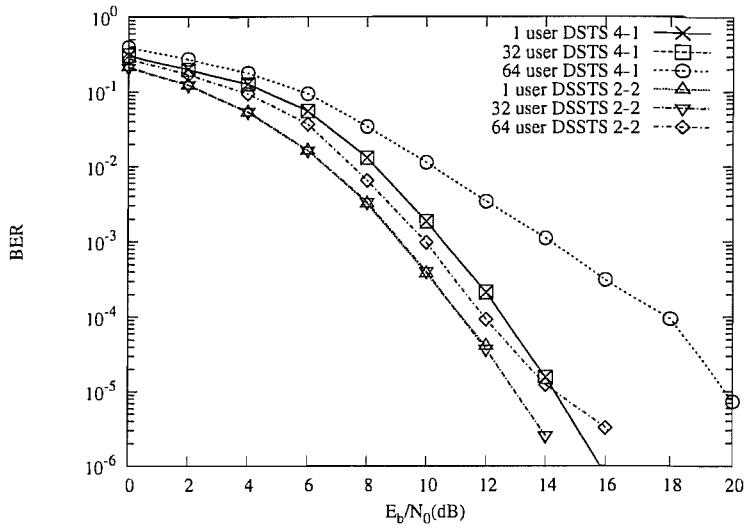


**Figure 3.29:** BER versus SNR performance of the downlink of a generalized MC DS-CDMA wireless system using 32-chip WH codes as T-domain spreading sequences and 4-chip WH codes as F-domain spreading sequences. TF-domain spreading was used to extend the user-load of the DSTS and the DSSTS systems, while an interference coefficient based user grouping technique was used in the DSSTS system to reduce the interference between the users sharing the same 32-chip WH code as T-domain spreading code. Two types of antenna arrays were employed, namely a $(2 \times 2)$-dimensional antenna array $(M = 2, L = 2)$, and a $(4 \times 1)$-dimensional antenna array $(M = 4, L = 1)$.

characterized the properties of the decision variable $z_{uv}$ in Equation (3.32). In order to exploit the attainable diversity gain in the F-domain and achieve user-load improvements, TF-domain spreading was employed by the generalized MC DS-CDMA system considered in Section 3.2.4. When using TF-domain spreading, the total processing gain becomes the product of the T-domain spreading code's processing gain and the F-domain spreading code's processing gain, yielding $N_e \cdot V$, which also determines the maximum number of users supported by the MC DS-CDMA system considered. In the context of our discussions in Section 3.2.4, we inferred that multiuser interference was inevitably introduced, since the orthogonality of the F-domain spreading codes cannot be retained in frequency-selective fading channels. However, we found that only the users sharing the same T-domain spreading code as the desired user would interfere with the desired user. In this scenario, we presented a user-grouping technique, which was employed for the sake of reducing the effects of multiuser interference caused by the employment of TF-domain spreading. The simulation results of Section 3.7.1 confirm that based on the assumptions of having orthogonal multicarrier signals, synchronous transmission of the $K$ users' signals as well as slow flat-fading of each subcarrier, there was no interference between the 32 users employing different orthogonal 32-chip WH codes as time-domain DS spreading codes. It was also shown in Figure 3.12 that the system employing the interference coefficient based user grouping technique outperformed the system refraining from user grouping, although the BER performance of the systems employing both TF-domain spreading

and the user regrouping procedure of Section 3.2.4 remained slightly worse than that of the system supporting a single user or 32 users. Furthermore, Figure 3.14 demonstrated that the system using a $(1 \times 6)$-dimensional antenna array ($M = 1, L = 6$) achieves a better performance than that of a $(1 \times 4)$-dimensional antenna array ($M = 1, L = 4$), suggesting that the increased number of elements was capable of attaining a higher SNR gain, resulting in a better BER performance.

A BSTD scheme constituted by an amalgam of beamforming and STD was discussed and analyzed in the context of the generalized MC DS-CDMA system in Section 3.3. The BSTD scheme was originally proposed by Zhou in [47]. We provided the generalized MC DS-CDMA system model invoking the BSTD scheme in Section 3.3.1. Figure 3.6 of Section 3.3.1 portrayed the downlink transmitter schematic of the system model using the BSTD scheme. The receiver of the BSTD scheme was the same as that seen in Figure 3.2 of Section 3.2. In Section 3.3.3 we employed TF-domain spreading for the sake of achieving both user-load improvements as well as F-domain diversity gain. Therefore, the maximum number of users supported by the MC DS-CDMA system was determined by the above product of $N_e \cdot V$. As a result of the employment of TF-domain spreading, multiuser interference was inevitably introduced. As detailed in Section 3.3.3, we employed the user-grouping processing technique advocated for the sake of reducing the effects of multiuser interference. Figures 3.15, 3.16 and 3.17 of Section 3.7.2 confirmed that the system employing the interference coefficient based user grouping technique of Section 3.3.3 outperformed the system refraining from user grouping. These figures also demonstrated that the increased number of array elements resulted in a better BER performance.

In Section 3.4, the STTD scheme [48] was introduced and its concept was extended for employment in the generalized MC DS-CDMA system considered. We first provided the general STTD system model invoked for the MC DS-CDMA system in Sections 3.4.1 and 3.4.2. Figure 3.8 of Section 3.4.1 portrayed the $k$th user's transmitter schematic for the downlink of the generalized multicarrier DS-CDMA system associated with STTD, while Figure 3.9 of Section 3.4.2 showed the receiver front-end of the STTD scheme in the downlink. Similar to the descriptions provided in Sections 3.2.4 and 3.3.3, we employed TF-domain spreading for the sake of achieving diversity gain in Section 3.4.3. However, without beamforming the user regrouping does not work for the system employing the STTD scheme of Section 3.4. As seen in Figure 3.18 of Section 3.7.3, when supporting 64 users, the system employing user regrouping achieved a similar performance to the system refraining from user grouping.

Based on both STTD and beamforming, SSTS, first proposed by Soni in [49], was adopted for employment in the generalized MC DS-CDMA system in Section 3.5. The SSTS system model was detailed in Sections 3.5.1 and 3.5.2, where Figure 3.10 portrayed the downlink transmitter schematic of the SSTS assisted generalized multicarrier DS-CDMA system. This figure suggests that the SSTS scheme not only employs STS to obtain transmit diversity, but additionally invokes beamforming to attain a higher SNR gain. In Section 3.5.3 TF-domain spreading was employed, while the user-grouping technique of Section 3.5.3 was invoked for the sake of reducing the effects of multiuser interference. Figures 3.19, 3.20 and 3.21 of Section 3.7.4 confirmed that the system employing the

| Scheme | Type of antenna arrays | $E_b/N_0$(dB) required at BER=$10^{-2}$ | $E_b/N_0$(dB) required at BER=$10^{-4}$ | $E_b/N_0$(dB) required at BER=$10^{-5}$ | Figure No. |
|---|---|---|---|---|---|
| Beamforming | $1 \times 4$ | 0.4 | 7.1 | 9.2 | Figure 3.22 |
| | $1 \times 6$ | -1.7 | 5.3 | 7.4 | Figure 3.24 |
| BSTD | $2 \times 2$ | 0.6 | 6.0 | 7.5 | Figure 3.22 |
| | $2 \times 3$ | -1.6 | 4.2 | 5.9 | Figure 3.24 |
| STTD | $4 \times 1$ | 4.9 | 9.5 | 10.9 | Figure 3.22 |
| SSTS | $2 \times 2$ | 2.4 | 7.5 | 9.0 | Figure 3.22 |
| | $2 \times 3$ | 0.4 | 5.9 | 7.6 | Figure 3.24 |

**Table 3.2:** Summary of the required $E_b/N_0$ values for the various schemes characterized in Figures 3.22 and 3.24 invoked for the downlink of the generalized MC DS-CDMA system supporting a single user, where five different types of antenna arrays were employed, namely a $(1 \times 4)$-dimensional antenna array ($M = 1, L = 4$) and a $(1 \times 6)$-dimensional antenna array ($M = 1, L = 6$) employed for the BF scheme, a $(2 \times 2)$-dimensional antenna array ($M = 2, L = 2$) and a $(2 \times 3)$-dimensional antenna array ($M = 2, L = 3$) used by the BSTD and SSTS schemes, and finally, a $(4 \times 1)$-dimensional antenna array ($M = 4, L = 1$) employed for the STTD scheme.

interference coefficient based user grouping technique outperformed the system refraining from user grouping.

In Section 3.6 we aimed for eliminating the need for channel estimation at the receiver, while retaining the desirable benefits of space-time coding techniques, we invoked two different DSTM schemes for improving the achievable performance in the downlink of a generalized MC DS-CDMA system communicating over rapidly fading channels, namely the DSTS scheme and the DSSTS scheme. Following a brief introduction to the unitary group code based DSTM of [138] in Section 3.6.1, we detailed the DSTS and DSSTS system model in Sections 3.6.2 and 3.6.3, where Figure 3.11 portrayed the downlink transmitter schematic of the DSTS and DSSTS assisted generalized multicarrier DS-CDMA system. Again, in Section 3.6.4 TF-domain spreading was employed, while the user-grouping technique of Section 3.2.4 was invoked for the sake of reducing the effects of multiuser interference. Figures 3.28 and 3.29 of Section 3.7.5 demonstrated that the attainable performance of the DSTS and that of the DSSTS schemes is about 3 dB worse than those of the corresponding non-differential STS and SSTS schemes, respectively, which is achieved, however, i.e. at a reduced complexity without having any CSI.

Finally, the performance of these schemes was studied and compared in Section 3.7. More explicitly, several different antenna array configurations have been investigated. Figures 3.22 and 3.23 showed that the beamforming scheme achieved a better performance at low SNRs, but a worse performance at high SNRs, when compared to the BSTD and the SSTS schemes. In contrast to the SSTS scheme, which belongs to the family of open-loop methods, the BSTD scheme is a representative of the class of closed loop proposals, activating the specific antenna array benefitting from the best instantaneous channel state and therefore in this scenario its performance is superior in comparison to that of SSTS. The STTD scheme achieves a higher transmit diversity gain than other three

schemes, when the number of antenna array elements is fixed. However, as discussed in Section 3.4, the highest incremental diversity gains are achieved upon increasing the number of antennas from one to two antennas, while adding further additional antennas achieves modest additional diversity gains on the downlink. Therefore, when employing more than $M = 2$ antenna arrays, the STTD scheme achieves the poorest performance. A summary of the associated results is provided in Table 3.2 for the sake of characterizing and comparing the attainable BER performance of all space-time processing schemes invoked for the downlink of the generalized MC DS-CDMA system supporting a single user. Figure 3.30 confirms that when a BER performance of $10^{-5}$ was required, the BSTD scheme achieved the highest $E_b/N_0$ gain and the SSTS scheme outperformed both the BF scheme and the STTD scheme. In contrast to the STTD scheme, the BF scheme attained a higher $E_b/N_0$ gain, when four or more transmit antennas were installed in the BS's transmitter. However, the STTD scheme outperformed the BF scheme when only two transmit antennas were invoked by the BS's transmitter. Furthermore, two different differential space-time processing schemes based on the principles of DSTS and DSSTS were invoked for the sake of enhancing the attainable performance of generalized MC DS-CDMA systems operating in rapidly fading channels. As expected, the attainable performance of both the DSTS and DSSTS schemes is about 3 dB worse than those of the corresponding non-differential STS and SSTS schemes, respectively, which can be achieved, however, i.e. at a reduced complexity without having any CSI. The DSSTS system employing a $(2 \times 2)$-dimensional antenna array $(M = 2, L = 2)$ outperforms the DSTS system using a $(4 \times 1)$-dimensional antenna array of $(M = 4, L = 1)$, suggesting that the DSSTS scheme employs DSTS for the sake of obtaining transmit diversity, but additionally also invokes beamforming to attain a higher SNR gain.

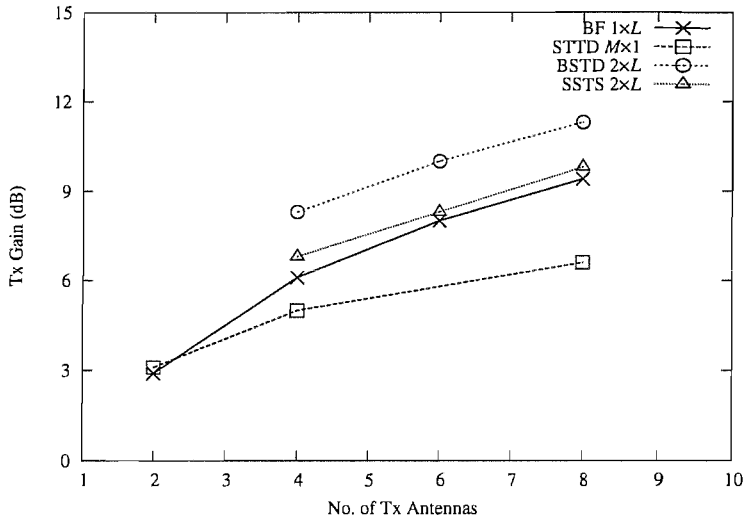


**Figure 3.30:** Transmit (Tx) gain versus the number of the transmit antennas for the various schemes invoked for the downlink of the generalized MC DS-CDMA system supporting a single user at a BER of $10^{-5}$, where ten different types of antenna arrays were employed, namely a $(1 \times 2)$-dimensional antenna array $(M = 1, L = 2)$, a $(1 \times 4)$-dimensional antenna array $(M = 1, L = 4)$, a $(1 \times 6)$-dimensional antenna array $(M = 1, L = 6)$ and a $(1 \times 8)$-dimensional antenna array $(M = 1, L = 8)$ employed for the BF scheme, a $(2 \times 2)$-dimensional antenna array $(M = 2, L = 2)$, a $(2 \times 3)$-dimensional antenna array $(M = 2, L = 3)$ and a $(2 \times 4)$-dimensional antenna array $(M = 2, L = 4)$ used by the BSTD and SSTS schemes, and finally, a $(2 \times 1)$-dimensional antenna array $(M = 2, L = 1)$, a $(4 \times 1)$-dimensional antenna array $(M = 4, L = 1)$ and a $(8 \times 1)$-dimensional antenna array $(M = 8, L = 1)$ employed for STTD scheme. These results were extracted from Figures 3.26 and 3.27.

# Chapter 4

# Multicarrier DS-CDMA Systems Using Smart Antennas - Adaptive Detection

## 4.1 Introduction

In this chapter we investigate adaptive space-time processing invoked in a generalized MC DS-CDMA system [41, 42] supported by smart antennas. In Chapter 2 we have proposed and investigated four different space-time processing schemes in the context of the generalized MC DS-CDMA system of [41, 42] supported by smart antennas. Specifically, the four types of space-time processing schemes employed are based on the MVDR, MSINR, MMSE and MPDR optimization criteria. Our study in Chapter 2 was based on the assumption that the receiver has either full knowledge or partial knowledge of the Direction of Arrival (DOA), of the channel amplitudes, the phases, as well as the timing of the interfering users. However, the estimation accuracy of the channel parameters has a grave impact on the attainable detection performance. Naturally, the estimation of these parameters increases the complexity imposed and typically requires channel sounding overhead, which wastes valuable bandwidth. Furthermore, when the Channel Impulse Response (CIR) fades rapidly, its estimation based on the previous symbols might be insufficiently accurate for the reliable detection of the forthcoming symbols. Hence it is beneficial to employ adaptive space-time processing, in order to track the space-time CIR in real time, while maintaining a modest receiver complexity.

Recently, adaptive Minimum Mean Square Error (MMSE) based space-time processing has received significant research attention [159–163, 199–202], since it offers an attractive tradeoff among the conflicting design factors of achievable performance, the complexity imposed and the associated side information transmission requirements. In [160, 199–201], an adaptive MMSE receiver was introduced for detecting DS-CDMA signals. The performance of various adaptive MMSE receivers has been investigated in diverse communications environments. More specifically, in [161] and [202] adaptive MMSE receivers have been investigated, when communicating over flat fading channels. By contrast, in [159] an adaptive MMSE receiver has been investigated when considering frequency-selective fading channels. Moreover, the performance of adaptive MMSE receivers has been investi-

gated, when considering both flat and frequency-selective fading channels in [162] and [163], where adaptive MMSE receivers were implemented based either on the principles of Least-Mean-Square (LMS) or Recursive-Least-Square (RLS) estimation. Moreover, most of the work related to adaptive MMSE detection has considered a DS-CDMA system using a single antenna. In the context of smart antenna aided systems, an adaptive MMSE based receiver has been investigated in [153], where an improved LMS algorithm was proposed for adaptive beamforming. By contrast, in [154, 155] an alternative adaptive beamforming algorithm imposing a lower detection complexity was proposed.

In this chapter, we focus our attention mainly on the design of adaptive linear filters [157]. The LMS and RLS algorithms are studied in the context of the generalized MC DS-CDMA system defined in Chapter 2. The LMS algorithm is a widely used technique, which was proposed by Widrow and Hoff in [156]. In [157] Haykin extended the employment of the steepest decent method to derive the LMS algorithm and studied its characteristics. An attractive feature of the LMS algorithm is its simplicity, although it has a low convergence speed. The RLS algorithm, developed from the least squares method is another well-known algorithm often used in adaptive filtering. Given the least-square estimate of the adaptive filter's tap-weight vector at iteration $(n-1)$, the updated estimate of this vector at iteration $n$ may be computed upon the arrival of new received data. An important feature of the RLS algorithm is that it utilizes not only information provided by the current received data, but also that of all past data, in order to update the weight vector of the adaptive filter. Therefore, the RLS algorithm converges faster than the LMS algorithm. However, this convergence rate improvement in the RLS algorithm is achieved at the expense of a higher computational complexity than that of the LMS algorithm. In practice, the adaptive receiver based on either the LMS or the RLS technique typically operates in two successive modes, the first being the training mode, during which a training sequence is used, while the second is the decision directed mode, where the adaptive filter is updated using the data decision. In order to reduce the transmission overhead introduced by the training sequence, iterative Interference Cancellation (IC) schemes may be employed for improving the attainable convergence rate of the LMS/RLS adaptive receiver. In [158] Hamouda presented a combined adaptive MMSE/PIC receiver designed for DS-CDMA systems. The proposed system made use of the available knowledge of the training sequences for all the users, so as to jointly suppress the MAI and increase the attainable convergence speed at the expense of a higher complexity. In this chapter adaptive MMSE/PIC space-time processing schemes imposing a lower complexity are invoked and analyzed in the context of the proposed MC DS-CDMA systems using multiple antenna arrays. In these schemes, only the strong interfering signals are subtracted from the received signal, while the weak interfering signals are treated as AWGN. The simulation results show that these schemes are capable of achieving the same convergence rate as that of the combined adaptive MMSE/PIC scheme presented in [158].

In this chapter, two adaptive space-time detectors having different structures are considered and analyzed in the context of the generalized MC DS-CDMA system [41, 42] of Chapter 2 employing smart antennas. The first adaptive space-time detector has $VML$ number of tap weights to be optimized, where $V$ is the number of the subcarriers and $ML$ is the total number of antenna elements of

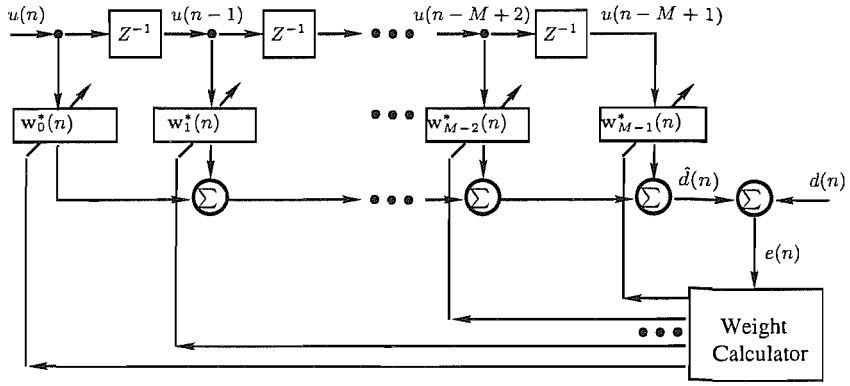


**Figure 4.1:** The block diagram of a transversal filter.

the $M$ antenna arrays. In the receiver using the above-mentioned adaptive detector, the received signals are first despread using the spreading code of the desired user and then combined by the adaptive detector. The second adaptive space-time detector considered is a joint adaptive space-time detector, which consists of two parts [203], the first part being an adaptive MMSE filter having $N_e$ number of taps, which depreads the received signals, while the second part is identical to the adaptive space-time detector discussed above.

The rest of this chapter has the following structure. In Section 4.2 the philosophy of the LMS algorithm is described and characterized. The RLS algorithm is defined and developed in Section 4.3. Then, the adaptive space-time processing scheme and the joint adaptive space-time processing scheme are described and their principles are extended for employment in the generalized MC DS-CDMA system considered in Section 4.4. In Section 4.5, the PIC technique is employed to accelerate the convergence rate of the adaptive beamformer. Finally, the performance of these schemes will be studied and compared in Section 4.6, again, in the context of the generalized MC DS-CDMA system concept advocated.

## 4.2 The Least-Mean-Square Algorithm

The LMS algorithm was proposed by Widrow and Hoff [156], while in [157] Haykin derived the LMS algorithm by using the steepest descent method. The block diagram of an adaptive transversal filter is shown in Figure 4.1, where the inputs $u(n), u(n-1), \ldots, u(n-M+1)$ represent samples drawn from a wide-sense stationary stochastic process having zero mean and a covariance matrix $\mathbf{R}$. The corresponding set of tap weights $w_0(n), w_1(n), \ldots, w_{M-1}(n)$ is updated by the weight calculator of Figure 4.1, which is supplied with the desired response $d(n)$, while $\hat{d}(n)$ is the estimate of the desired response at the adaptive filter's output. The method of steepest decent is summarized in Table 4.1.

Although it results in a slow convergence speed, the method of steepest decent is a low-complexity recursive algorithm. Accordingly, the LMS algorithm derived using the method of steepest decent is also a low-complexity algorithm. As shown in Figure 4.2(a), the transversal filter produces an estimate

| | |
|---|---|
| 1 | Initialize $\mathbf{w}(0)$. When no prior knowledge is available, $\mathbf{w}(0)$ is usually set to the null vector. |
| 2 | Compute the gradient vector $\nabla J(\mathbf{w}_n)$ with respect to the weight vector $\mathbf{w}(n)$. |
| 3 | Update the weight vector by adjusting its initial guess in a direction opposite to that of the gradient vector. |
| 4 | Repeat Steps 2 to 3. |

**Table 4.1:** The method of steepest decent.

$\hat{d}(n)$ of the desired response $d(n)$ based on the received signal vector $\mathbf{u}(n)$, which can be expressed as

$$\hat{d}(n) = \hat{\mathbf{w}}^H(n)\mathbf{u}(n). \tag{4.1}$$

After comparing the desired response estimate $\hat{d}(n)$ to the desired signal $d(n)$, we obtain the estimation error of

$$e(n) = d(n) - \hat{d}(n). \tag{4.2}$$

Upon forwarding the estimation error $e(n)$ and the input vector $\mathbf{u}(n)$ to the adaptive beamforming process, we can compute the weight adjustment $\Delta\hat{\mathbf{w}}(n) = \mu e^*(n)\mathbf{u}(n)$.

The scaling factor $\mu$ is referred to as the step-size parameter in the method of steepest decent. In practice we may let the step-size parameter $\mu$ satisfy the condition of

$$0 < \mu < \frac{2}{\sum_{k=0}^{M-1} E[|u(n-k)|^2]}. \tag{4.3}$$

As shown in [157], the recursive weight update formula of the LMS algorithm is expressed as

$$\begin{aligned} \hat{\mathbf{w}}(n+1) &= \hat{\mathbf{w}}(n) + \mu\mathbf{u}(n)[d^*(n) - \mathbf{u}^H(n)\hat{\mathbf{w}}(n)] \\ &= \hat{\mathbf{w}}(n) + \mu\mathbf{u}(n)e^*(n). \end{aligned} \tag{4.4}$$

According to (4.1), (4.2) and (4.4), it may be readily shown that the LMS algorithm requires only $(2M + 1)$ complex multiplications and $2M$ complex additions per iteration. Hence, the computational complexity of the LMS algorithm is $O(M)$. Finally, the procedure of the LMS algorithm is summarized in Table 4.2.

Having described the LMS algorithm, let us now turn our attention to the RLS algorithm.

## 4.3 The Recursive-Least-Square Algorithm

In this section, the RLS algorithm [157] is introduced, which utilizes information contained in the received data, extending back to the instant of time when the algorithm was initiated. Thus, at the expense of a substantial increase in computational complexity, the RLS technique is capable of achieving a significantly faster convergence rate than the lower-complexity LMS algorithm. Below we begin

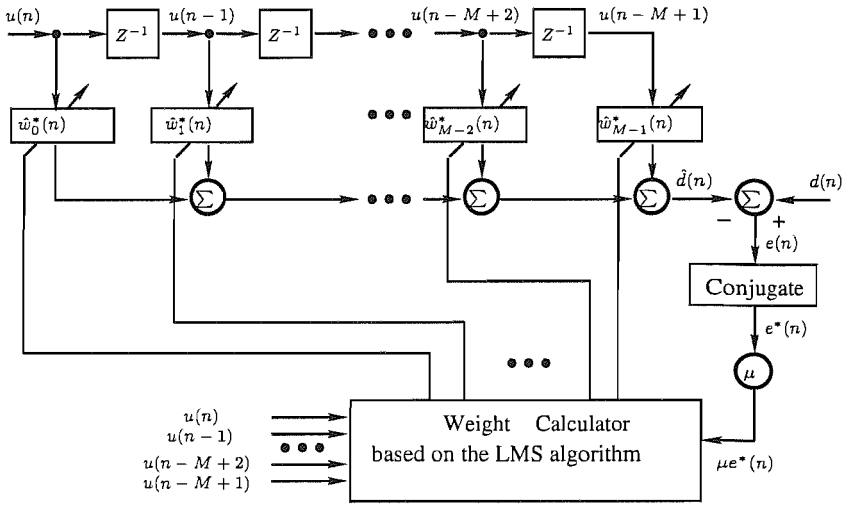


(a)

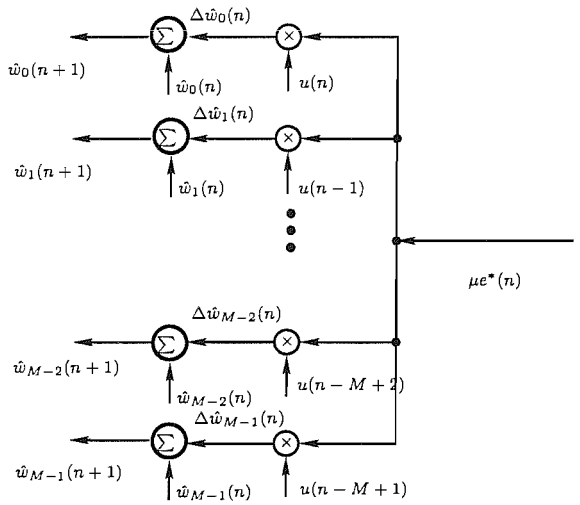


(b)

**Figure 4.2:** (a) The block diagram of an adaptive LMS filter. (b) Detailed structure of the adaptive LMS mechanism.

the development of the RLS algorithm by viewing some basic relations that pertain to the method of Least Squares (LS).

By using time averaging, the LS scheme minimizes the sum of the squared difference between the received data $u(n)$ and the array output data $\hat{d}(n)$ for $n = 1, 2, \ldots, N$. As shown in Figure 4.3, the desired signal $d(n)$ is a function of the $M$-dimensional input vector $\mathbf{u}(n) = [u(n), u(n-1), \ldots, u(n-M+1)]^T$, $\mathbf{w} = [w_0, w_1, \ldots, w_{M-1}]^T$ is the $M$-dimensional weight vector and $\hat{d}(n) = \mathbf{w}^H\mathbf{u}(n)$ is the filter output representing the estimate of $d(n)$, while $e(n)$ denotes the estimation error.

| | |
|---|---|
| 1 | Select a suitable step-size parameter $\mu$: $0 < \mu < \frac{2}{\text{tap-input power}}$, where the input power is $\sum_{k=0}^{M-1} E[\|u(n-k)\|^2]$. |
| 2 | Initialize $\hat{\mathbf{w}}(0)$. Without prior knowledge $\mathbf{w}(0)$ is usually set to the null vector. |
| 3 | Compute the estimation error $e(n) = d(n) - \hat{\mathbf{w}}^H(n)\mathbf{u}(n)$. |
| 4 | Update the weight vector $\hat{\mathbf{w}}(n+1) = \hat{\mathbf{w}}(n) + \mu\mathbf{u}(n)e^*(n)$. |
| 5 | Repeat Steps 3 to 4. |

**Table 4.2:** The procedure of the LMS algorithm.

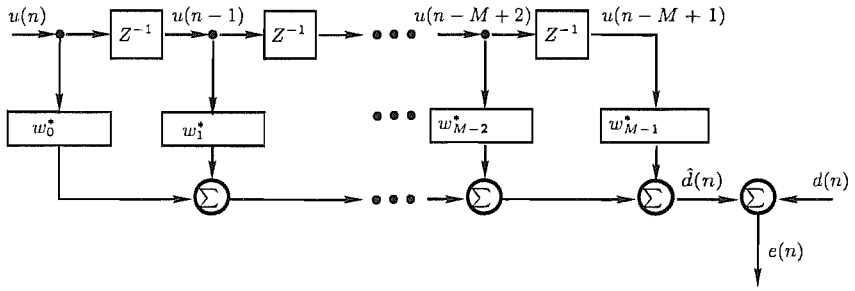


**Figure 4.3:** Linear transversal filter model.

The weight vector $\mathbf{w}$ of the LS scheme is chosen to minimize the cost function that consists of the sum of error squares [157], namely to minimize

$$J(\mathbf{w}) = \sum_{i=i_1}^{i_2} |e(i)|^2, \tag{4.5}$$

where $i_1$ and $i_2$ represent the index limits over which the error minimization occurs. The basic LS optimization problem is to minimize the cost function $J(\mathbf{w})$ of (4.5) with respect to the weight vector $\mathbf{w}$ of the transversal filter seen in Figure 4.3. Furthermore, it is assumed that during the interval $i_1 \leq i \leq i_2$ the weight vector $\mathbf{w}$ is held constant.

In contrast to the LS scheme, where the weight vector $\mathbf{w}$ is assumed to be constant during the interval $i_1 \leq i \leq i_2$, the RLS algorithm uses the information contained in each new received data symbol to update the weight vector $\mathbf{w}(n)$ at each iteration. Therefore, the length of observable data, corresponding to the interval $i_1 \leq i \leq i_2$ in the LS scheme, is variable.

The optimum weight vector $\mathbf{w}(n)$ at time $n$ can be expressed as

$$\hat{\mathbf{w}}(n) = \mathbf{\Phi}^{-1}(n)\mathbf{z}(n), \tag{4.6}$$

where we have $\mathbf{\Phi}(n) = \sum_{i=1}^{n} \lambda^{n-i}\mathbf{u}(i)\mathbf{u}^H(i)$ and $\mathbf{z}(n) = \sum_{i=1}^{n} \lambda^{n-i}\mathbf{u}(i)d^*(i)$. For convenience, let us define

$$\mathbf{P}(n) = \mathbf{\Phi}^{-1}(n), \tag{4.7}$$

| | |
|---|---|
| 1 | Initialize the algorithm by setting $\hat{\mathbf{w}}(0) = \mathbf{0}$ and $\mathbf{P}(0) = \delta^{-1}\mathbf{I}$, where $\delta$ is a small positive constant. |
| 2 | Update the gain vector $\mathbf{k}(n) = \frac{\lambda^{-1}\mathbf{P}(n-1)\mathbf{u}(n)}{1+\lambda^{-1}\mathbf{u}^H(n)\mathbf{P}(n-1)\mathbf{u}(n)}$. |
| 3 | Update the inverse correlation matrix $\mathbf{P}(n) = \lambda^{-1}\mathbf{P}(n-1) - \lambda^{-1}\mathbf{k}(n)\mathbf{u}^H(n)\mathbf{P}(n-1)$. |
| 4 | Compute the *a priori* estimation error $\xi(n) = d(n) - \hat{\mathbf{w}}^H(n-1)\mathbf{u}(n)$. |
| 5 | Update the weight vector $\hat{\mathbf{w}}(n) = \hat{\mathbf{w}}(n-1) + \mathbf{k}(n)\xi^*(n)$. |
| 6 | Repeat the steps 2 to 5. |

**Table 4.3:** Summary of the RLS algorithm.

which is referred to as the inverse autocorrelation matrix, and define furthermore the RLS gain vector as [157]

$$\mathbf{k}(n) = \frac{\lambda^{-1}\mathbf{P}(n-1)\mathbf{u}(n)}{1+\lambda^{-1}\mathbf{u}^H(n)\mathbf{P}(n-1)\mathbf{u}(n)}. \tag{4.8}$$

As shown in [157], we have

$$\mathbf{P}(n) = \lambda^{-1}\mathbf{P}(n-1) - \lambda^{-1}\mathbf{k}(n)\mathbf{u}^H(n)\mathbf{P}(n-1). \tag{4.9}$$

The recursive equation devised for updating the weight vector $\hat{\mathbf{w}}(n)$ is then given by [157]

$$\begin{aligned}\hat{\mathbf{w}}(n) &= \hat{\mathbf{w}}(n-1) + \mathbf{k}(n)[d^*(n) - \mathbf{u}(n)\hat{\mathbf{w}}(n-1)] \\ &= \hat{\mathbf{w}}(n-1) + \mathbf{k}(n)\xi^*(n),\end{aligned} \tag{4.10}$$

where the *a priori* estimation error $\xi(n)$ is given by [157]

$$\begin{aligned}\xi(n) &= d(n) - \mathbf{u}^T(n)\hat{\mathbf{w}}^*(n-1) \\ &= d(n) - \hat{\mathbf{w}}^H(n-1)\mathbf{u}(n).\end{aligned} \tag{4.11}$$

In order to carry out the RLS algorithm, a set of initial weight values has to be provided. As in [157], a soft-constrained initialization is employed in this section, which sets

$$\mathbf{P}(0) = \delta^{-1}\mathbf{I}, \tag{4.12}$$

where $\delta$ is recommended to be a small value compared to $0.01\sigma_u^2$, where $\sigma_u^2$ is the variance of a data sample $u(n)$ [157]. Furthermore, when no prior knowledge is available, the initial value of the weight vector $\hat{\mathbf{w}}(0)$ is typically set to be a null vector. Finally, the procedure of the RLS algorithm is summarized in Table 4.3.

Let us now invoke the LMS and RLS algorithms in the proposed generalized MC DS-CDMA system using smart antennas.

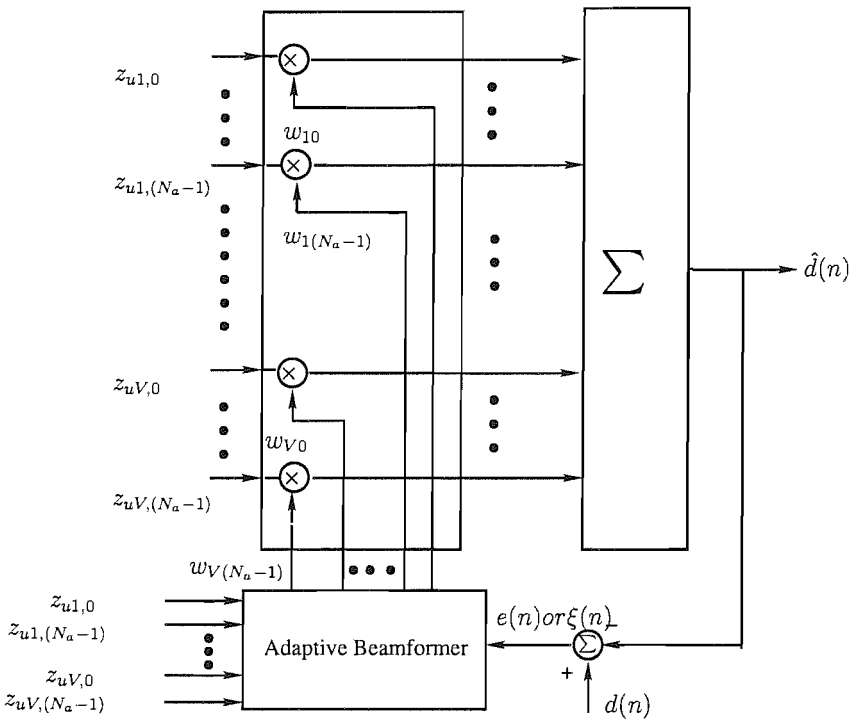


**Figure 4.4:** Block diagram of an Adaptive Space-Time Detector (ASTD).

## 4.4 Adaptive Detection in MC DS-CDMA Systems using Smart Antennas

Above we have provided a detailed introduction for both the LMS and RLS algorithms. In this section, we focus our attention on the application of these algorithms in the adaptive uplink detection of the generalized MC DS-CDMA system [41,42] supported by smart antennas. The smart antennas investigated in this section are identical to the antenna arrays shown in Figure 2.4. In contrast to the optimum detectors discussed in Chapter 2, which rely on perfect knowledge of the space-time channels, the adaptive detector considered is investigated without invoking the knowledge of the spatio-temporal channel as well as the users' DOAs. Two adaptive detection schemes having different structures are investigated and analyzed. The first adaptive detector, which is shown in Figure 4.4, has $VN_a$ number of weight taps, where $V$ represents the number of subcarriers, while $N_a = ML$ represents the total number of antenna elements in the $M$ antenna arrays. In this adaptive detection scheme, the received signals are first despread using the spreading code of the desired user, although this is not shown in Figure 4.4 and then combined by the adaptive detector. After weighting them by the beamformer weights $\mathbf{w}$, we attain the decision variable. The second adaptive detector, as shown in Figure 4.5, is a joint adaptive detector, which consists of two parts. The first part is an adaptive MMSE filter with $N_e$ number of taps, which are matched to the chip-based signals. By contrast, the second part is the same as the first adaptive space-time detector of Figure 4.4, which combines the space-time

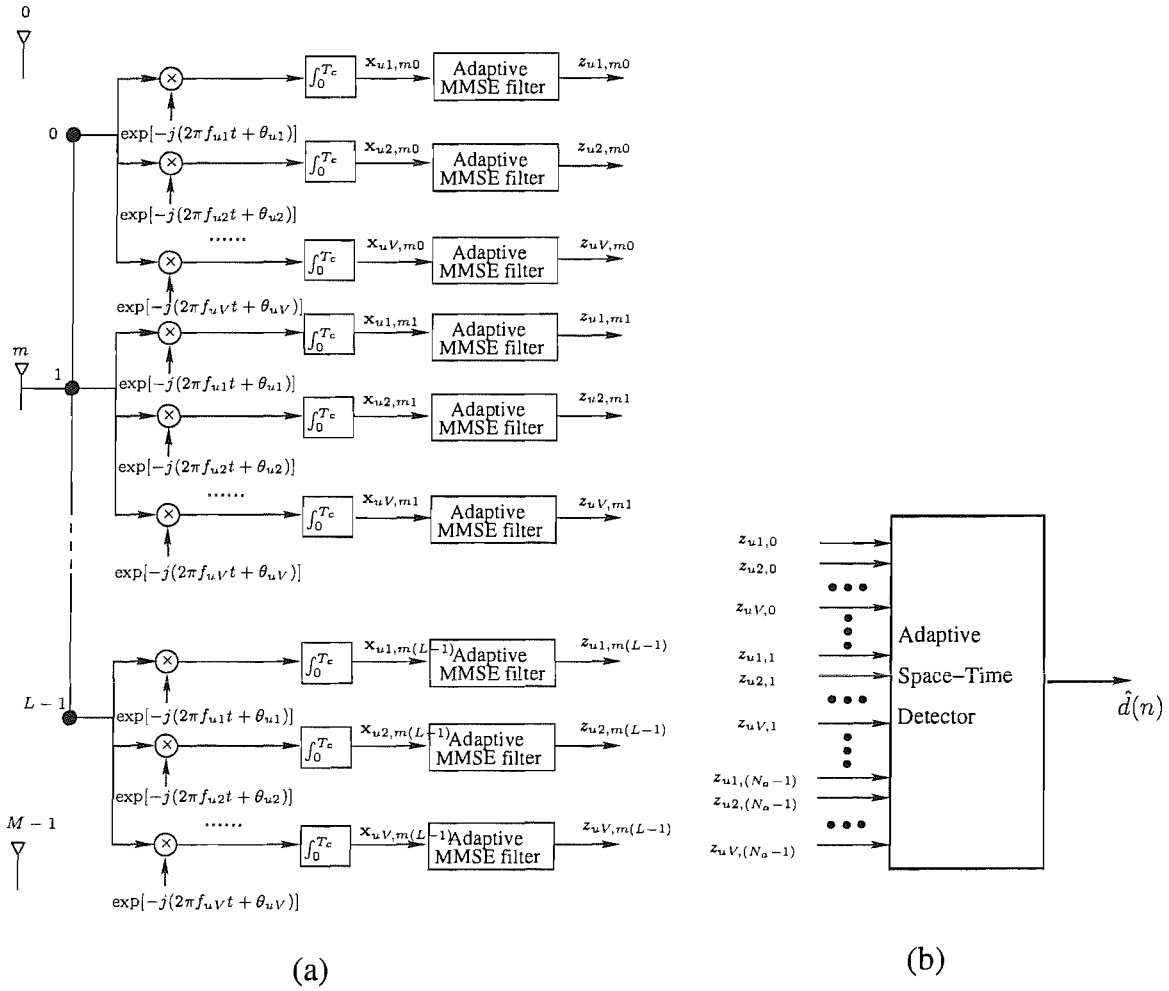


**Figure 4.5:** Block diagram of a joint adaptive detector. (a) An adaptive MMSE filter; (b) An ASTD.

subcarrier signals. Accordingly, the second part has $VN_a$ number of weight taps, where $V$ represents the number of subcarriers, while $N_a = ML$ represents the total number of antenna elements in the $M$ antenna arrays. In the second adaptive detector, an alternative adaptation algorithm is employed, in order to optimize the MMSE filter coefficients and the space-time filter's weights simultaneously, as will be detailed in Section 4.4.2 of our forthcoming discourse. Below the first adaptive detector is referred to as the adaptive space-time detector, while the second as the chip-based adaptive space-time detector.

### 4.4.1 Adaptive Space-Time Detector

In the context of the adaptive space-time detector (ASTD) of Figure 4.4, the received base-band equivalent signal at the output of the antenna arrays are identical to the signal $\mathbf{r}(t)$ of Equation (2.15). Following the derivation in Section 2.2, after the multicarrier demodulation and DS despreading stages shown in Figure 2.5, the $N_a$-dimensional signal vector $\mathbf{z}_{uv}(n) =$

$[z_{uv,0}(n), z_{uv,1}(n), \ldots, z_{uv,(N_a-1)}(n)]^T$ corresponding to the $n$th bit $b_u[n]$ and the $v$th subcarrier can be expressed as

$$\mathbf{z}_{uv}(n) = \sqrt{\frac{2P}{V}} T_s \left[ b_u[n]\tilde{\mathbf{a}}_{uv} + \tilde{\mathbf{n}}_{uv} + \underbrace{\sum_{u'=1}^{U}\sum_{v'=1}^{V}}_{v'\neq v, \text{ if } u'=u} \mathbf{i}_{u'v'}^{(s)} + \sum_{k=2}^{K} \mathbf{i}_{uv}^{(k)} + \sum_{k=2}^{K} \underbrace{\sum_{u'=1}^{U}\sum_{v'=1}^{V}}_{v'\neq v, \text{ if } u'=u} \mathbf{i}_{u'v'}^{(k)} \right], \tag{4.13}$$

which is identical to (2.22). In (4.13) $b_u[n]\tilde{\mathbf{a}}_{uv}$ represents the desired signal, while $\tilde{\mathbf{n}}_{uv}$, described in (2.23), is contributed by the AWGN. The term $\mathbf{i}_{u'v'}^{(s)}$ in (4.13) represents the self-interference contributed by the subcarrier indexed by $u'$, $v'$ of the reference signal, which has the form of (2.27). The MUI term $\mathbf{i}_{uv}^{(k)}$ in (4.13) is engendered by the subcarrier signal determined by $u$ and $v$ of the $k$th interfering user, which is expressed in (2.29). Finally, the MUI term $\mathbf{i}_{u'v'}^{(k)}$ in (4.13) is imposed by the subcarrier determined by $u'$ and $v'$ associated with the $k$th interfering user, which is described in (2.31). As shown in Figure 4.4, the $VN_a$-dimensional signal vector $\mathbf{z}_u(n) = \left[\mathbf{z}_{u1}^T(n), \mathbf{z}_{u2}^T(n), \ldots, \mathbf{z}_{uV}^T(n)\right]^T$ is the input vector of the ASTD, which has $VN_a$ number of weight taps.

When the LMS algorithm is invoked by the ASTD of Figure 4.4, a suitable step-size parameter $\mu$ has to be chosen according to the constraint of [157]

$$0 < \mu < \frac{2}{\sum_{v=1}^{V}\sum_{l=0}^{N_a-1} E[|z_{uv,l}(n)|^2]}. \tag{4.14}$$

According to the LMS principles, which have been analyzed in Section 4.2, when $\mu$ is too small, the adaption becomes slow. By contrast, if $\mu$ is excessive, the average excess mean-squared error after adaption will be high. Therefore a suitable $\mu$ value should be chosen in order to attain a good trade-off between the achievable convergence rate and the average excess mean-squared error. Additionally, according to the LMS algorithm, the $VN_a$-dimensional weight vector $\hat{\mathbf{w}}(0)$ is initialized to be a null vector, when we assume that the detector has no knowledge about the DOA and the CIR of the channel. In the ASTD of Figure 4.4, a training sequence is used and the corresponding estimation error can be expressed as

$$e(n) = d(n) - \hat{\mathbf{w}}^H(n)\mathbf{z}_u(n), \tag{4.15}$$

where $d(n)$ represent the training bits. The weight vector is updated according to

$$\hat{\mathbf{w}}(n+1) = \hat{\mathbf{w}}(n) + \mu\mathbf{z}_u(n)e^*(n) \tag{4.16}$$

with the aid of the estimation error $e(n)$. This process is repeated until the end of the training period. After the training stage, the ASTD will switch to a decision directed stage, where the estimation error $e(n)$ is computed with the aid of the decided data $\tilde{d}(n)$ fed back from the data decision unit of the

| | |
|---|---|
| 1 | Select a suitable step-size parameter $\mu$: $0 < \mu < \frac{2}{\text{tap-input power}}$, where the input power is $\sum_{v=1}^{V}\sum_{l=0}^{N_a-1} E[\|z_{uv,l}(n)\|^2]$. |
| 2 | Initialize $\hat{\mathbf{w}}(0)$. Without any prior knowledge, $\hat{\mathbf{w}}(0)$ is usually set to the null vector. |
| 3 | In the training period,<br>(a) Compute the estimation error: $e(n) = d(n) - \hat{\mathbf{w}}^H(n)\mathbf{z}_u(n)$;<br>(b) Update the weight vector: $\hat{\mathbf{w}}(n+1) = \hat{\mathbf{w}}(n) + \mu\mathbf{z}_u(n)e^*(n)$. |
| 4 | Repeat Step 3 until the decision directed period. |
| 5 | In the decision directed period,<br>(a) Data detection: $\tilde{d}(n) = \text{sgn}\left(\text{Re}\{\hat{\mathbf{w}}^H(n)\mathbf{z}_u(n)\}\right)$;<br>(b) Compute the estimation error: $e(n) = \tilde{d}(n) - \hat{\mathbf{w}}^H(n)\mathbf{z}_u(n)$;<br>(c) Update the weight vector: $\hat{\mathbf{w}}(n+1) = \hat{\mathbf{w}}(n) + \mu\mathbf{z}_u(n)e^*(n)$. |
| 6 | Repeat Step 5. |

**Table 4.4:** The LMS-based adaptive space-time detection algorithm invoked for the MC DS-CDMA system using multiple receive antenna arrays.

receiver. The decision is carried out according to

$$\tilde{d}(n) = \text{sgn}\left(\text{Re}\{\hat{\mathbf{w}}^H(n)\mathbf{z}_u(n)\}\right), \tag{4.17}$$

where $\text{Re}\{x\}$ represents the real part of $x$, while $\text{sgn}(x)$ is the sign function, defined in Equation (2.57). Accordingly, the estimation error may now be expressed as

$$e(n) = \tilde{d}(n) - \hat{\mathbf{w}}^H(n)\mathbf{z}_u(n), \tag{4.18}$$

and the weight vector is also updated using Equation (4.16). Finally, the entire procedure of the LMS-based ASTD is summarized in Table 4.4.

According to our discussions in the Section 4.3, the RLS algorithm may be employed in order to increase the convergence rate, but at the expense of a higher computation complexity. In the RLS-based ASTD, the $VN_a$-dimensional weight vector $\hat{\mathbf{w}}(0)$ can be initialized to be a null vector, when assuming no prior knowledge concerning the DOA and the CIR of the channel. The $(VN_a \times VN_a)$-dimensional inverse correlation matrix can be initialized as $\mathbf{P}(0) = \delta^{-1}\mathbf{I}$, where $\delta$ is chosen to be a small positive constant in comparison to $0.01\sigma_z^2$, where $\sigma_z^2 = \| \mathbf{z}_u(n) \|^2$. Furthermore, the parameter $\lambda$ in (**??**) is set to be a positive constant close to, but less than 1. Based on the above initialization, the $VN_a$-dimensional gain vector $\mathbf{k}(n)$ can be updated according to

$$\mathbf{k}(n) = \frac{\lambda^{-1}\mathbf{P}(n-1)\mathbf{z}_u(n)}{1 + \lambda^{-1}\mathbf{z}_u^H(n)\mathbf{P}(n-1)\mathbf{z}_u(n)}, \tag{4.19}$$

when the receiver receives $\mathbf{z}_u(n)$. Once $\mathbf{k}(n)$ has been obtained, the inverse correlation matrix $\mathbf{P}(n)$ can be updated according to

$$\mathbf{P}(n) = \lambda^{-1}\mathbf{P}(n-1) - \lambda^{-1}\mathbf{k}(n)\mathbf{z}_u^H(n)\mathbf{P}(n-1). \tag{4.20}$$

| | |
|---|---|
| 1 | Initialization: $\hat{\mathbf{w}}(0) = \mathbf{0}, \mathbf{P}(0) = \delta^{-1}\mathbf{I}$, where $\delta$ is a small positive constant. |
| 2 | Update the gain vector:<br>$\mathbf{k}(n) = \frac{\lambda^{-1}\mathbf{P}(n-1)\mathbf{z}_u(n)}{1+\lambda^{-1}\mathbf{z}_u^H(n)\mathbf{P}(n-1)\mathbf{z}_u(n)}$. |
| 3 | Update the inverse correlation matrix:<br>$\mathbf{P}(n) = \lambda^{-1}\mathbf{P}(n-1) - \lambda^{-1}\mathbf{k}(n)\mathbf{z}_u^H(n)\mathbf{P}(n-1)$. |
| 4 | In the training period:<br>(a) Compute the *a priori* estimation error: $\xi(n) = d(n) - \hat{\mathbf{w}}^H(n-1)\mathbf{z}_u(n)$;<br>(b) Update the weight vector: $\hat{\mathbf{w}}(n) = \hat{\mathbf{w}}(n-1) + \mathbf{k}(n)\xi^*(n)$. |
| 5 | Repeat Steps 2, 3 and 4 until the decision directed period is reached. |
| 6 | In the decision directed period:<br>(a) Data detection: $\tilde{d}(n) = \text{sgn}\left(\text{Re}\{\hat{\mathbf{w}}^H(n-1)\mathbf{z}_u(n)\}\right)$;<br>(b) Compute the *a priori* estimation error: $\xi(n) = \tilde{d} - \hat{\mathbf{w}}^H(n-1)\mathbf{z}_u(n)$;<br>(C) Update the weight vector: $\hat{\mathbf{w}}(n) = \hat{\mathbf{w}}(n-1) + \mathbf{k}(n)\xi^*(n)$. |
| 7 | Repeat Steps 2, 3 and 6. |

**Table 4.5:** The RLS-based ASTD algorithm invoked for the generalized MC DS-CDMA system using multiple receive antenna arrays.

According to the RLS principles, during the training stage the *a priori* estimation error can be expressed as

$$\xi(n) = d(n) - \hat{\mathbf{w}}^H(n-1)\mathbf{z}_u(n), \tag{4.21}$$

where $d(n)$ represents the desired signal generated using the training bits. Then, the corresponding weight vector can be updated using

$$\hat{\mathbf{w}}(n) = \hat{\mathbf{w}}(n-1) + \mathbf{k}(n)\xi^*(n). \tag{4.22}$$

Similar to the LMS algorithm, during the decision-directed stage, the *a priori* estimation error $\xi(n)$ is computed using the actual data decided according to $\tilde{d}(n) = \text{sgn}\left(\text{Re}\{\hat{\mathbf{w}}^H(n-1)\mathbf{z}_u(n)\}\right)$. Consequently, the *a priori* estimation error $\xi(n)$ may now be expressed as

$$\xi(n) = \tilde{d}(n) - \hat{\mathbf{w}}^H(n-1)\mathbf{z}_u(n). \tag{4.23}$$

Hence the RLS estimation based weight vector can be updated using (4.22), with the aid of (4.23). Finally, the entire procedure of the RLS-based ASTD is summarized in Table 4.5. In the context of the smart antennas aided generalized MC DS-CDMA system, the computational complexity of the LMS algorithm is on the order of $O(VN_a)$, while the computational complexity of the RLS algorithm is on the order of $O[(VN_a)^2]$.

### 4.4.2 Chip-Based Adaptive Space-Time Detector

Above we have provided a detailed derivation of the LMS-based and RLS-based ASTD of Figure 4.4, where the received signals are first despread using the spreading code of the desired user, and then

combined by the adaptive detector having $VN_a$ number of weight taps.

In the context of the chip-based ASTD, the received baseband equivalent signal vector $\mathbf{r}(t)$, which is expressed in (2.15), is first processed by a chip-matched-filter, as shown in Figure 4.5. The output of the chip-matched-filter is a $N_e$-dimensional signal vector, which is given by $\mathbf{x}_{uv,l} = [x_{uv,l1}(n), x_{uv,l2}(n), \ldots, x_{uv,lN_e}(n)]^T$ for the $l$th antenna element and the $v$th subcarrier. It can be shown that $x_{uv,li}, i = 1, 2, \ldots, N_e$, in $\mathbf{x}_{uv,l}$ may be expressed as

$$x_{uv,li} = \int_{(i-1)T_c}^{iT_c} \mathbf{r}(t) \exp\left(-j[2\pi f_{uv}t + \theta_{uv}]\right) p(t - iT_c))dt, \; v = 1, 2, \ldots, V, \tag{4.24}$$

where we assumed that the reference signal's transmission delay was $\tau_1 = 0$ for simplicity. In (4.24), $p(t)$ is the chip pulse shape, which is taken to be a rectangular pulse with amplitude $\frac{1}{\sqrt{N_e}}$. The $N_e$-dimensional signal vector $\mathbf{x}_{uv,l}$ is fed to an adaptive MMSE filter with $N_e$ number of coefficients, yielding

$$z_{uv,l}(n) = \mathbf{c}^H(n)\mathbf{x}_{uv,l}, \tag{4.25}$$

where $\mathbf{c}(n)$ contains the coefficients of the MMSE filter, which is given by

$$\mathbf{c}(n) = [c_1(n), c_2(n), \ldots, c_{N_e}(n)]^T. \tag{4.26}$$

After the chip-based MMSE filtering, the outputs of these MMSE filters are input to the ASTD unit, as shown in Figure 4.5. Finally, the $VN_a$-dimensional signal vector $\mathbf{z}_u(n) = [z_{u1,0}(n), \ldots, z_{uV,0}(n), \ldots, z_{u1,(N_a-1)}(n), \ldots, z_{uV,(N_a-1)}(n)$ is weighted by a $VN_a$-dimensional vector $\hat{\mathbf{w}}(n)$, yielding the decision variable of

$$\hat{d}(n) = \hat{\mathbf{w}}^H(n)\mathbf{z}_u(n). \tag{4.27}$$

Equation (4.27) implies that for a fixed $\mathbf{c}(n)$, updating the weight vector $\hat{\mathbf{w}}^H(n)$ to $\hat{\mathbf{w}}^H(n+1)$ can be implemented using the same procedure as described in Tables 4.4 or 4.5.

In order to update the coefficients of the adaptive MMSE filter of Figure 4.5, we use the updated weight vector $\hat{\mathbf{w}}^H(n+1)$ for appropriately weighting the output signal vector $\mathbf{x}_{uv,l}$ arriving from the chip matched filter. The resultant $N_e$-dimensional signal vector $\mathbf{z'}_u(n) = [z'_{u,1}, z'_{u,2}, \ldots, z'_{u,N_e}]^T$ can be expressed as

$$\mathbf{z'}_u(n) = \sum_{v=1}^{V} \sum_{l=0}^{N_a-1} w^*_{v,l}(n+1)\mathbf{x}_{uv,l}, \tag{4.28}$$

where the $N_e$-dimensional signal vector $\mathbf{z'}_u(n)$ is different from the $(VN_a)$-dimensional signal vector $\mathbf{z}_u(n)$ in (4.27), because the former is computed from the combination of signals received from the $N_a$ antenna elements and $V$ subcarriers.

When this adaptive MMSE filter is based on the LMS algorithm, we feed $\mathbf{z'}_u(n)$ to the adaptive MMSE filter of Figure 4.5 and arrive at the estimation error $e'(n)$ generated from the reference signal

| | |
|---|---|
| 1 | Initialize the coefficients of the LMS adaptive filter $\mathbf{c}(0)$. When we have no knowledge of the T-domain spreading code of the desired user, we set $\mathbf{c}(0) = \mathbf{0}$. Otherwise, $\mathbf{c}(0)$ is set to be the T-domain spreading code of the desired user. |
| 2 | Compute the the output signal of the adaptive LMS filter $z_{uv,l}(n) = \mathbf{c}^H(n)\mathbf{x}_{uv,l}$. |
| 3 | Compute the estimation error $e(n)$ and update the weight vector $\hat{\mathbf{w}}(n)$ according to the procedure described in Tables 4.4 or 4.5. |
| 4 | Use the updated weight vector $\hat{\mathbf{w}}(n+1)$ to compute the $N_e$-dimensional signal vector $\mathbf{z'}_u(n) = \sum_{v=1}^{V}\sum_{l=0}^{N_a-1} w^*_{v,l}(n+1)\mathbf{x}_{uv,l}$. |
| 5 | Select a suitable step-size parameter $\mu$: $0 < \mu < \frac{2}{\text{tap-input power}}$, where the input power is $\sum_{i=1}^{i=N_e} E[\|z'_{u,i}\|^2]$. |
| 6 | In the training stage:<br>(a) Compute the estimation error: $e'(n) = d(n) - \mathbf{c}^H(n)\mathbf{z'}_u(n)$;<br>(b) Update the weight vector $\mathbf{c}(n+1) = \mathbf{c}(n) + \mu\mathbf{z'}_u(n)e'^*(n)$. |
| 7 | Repeat Steps 2, 3, 4 and 6 until the decision directed stage is reached. |
| 8 | In the decision directed stage:<br>(a) Compute the actual data decision: $\tilde{d}(n) = \text{sgn}\left(\text{Re}\{\mathbf{c}^H(n)\mathbf{z'}_u(n)\}\right)$;<br>(b) Compute the estimation error: $e'(n) = \tilde{d}(n) - \mathbf{c}^H(n)\mathbf{z'}_u(n)$;<br>(c) Update the weight vector: $\mathbf{c}(n+1) = \mathbf{c}(n) + \mu\mathbf{z'}_u(n)e'^*(n)$. |
| 9 | Repeat Steps 2,3,4 and 8. |

**Table 4.6:** The procedure of the joint ASTD combined with a LMS-based adaptive filter.

$d(n)$ as follows:

$$e'(n) = d(n) - \mathbf{c}^H(n)\mathbf{z'}_u(n), \tag{4.29}$$

where $d(n)$ represents the training bits. Similarly, the MMSE beamformer coefficients are updated according to

$$\mathbf{c}(n+1) = \mathbf{c}(n) + \mu\mathbf{z'}_u(n)e'^*(n). \tag{4.30}$$

During the decision directed stage we compute the estimation error $e'(n)$ in the same way, as described during the training stage, where the estimation error may be expressed as

$$e'(n) = \tilde{d}(n) - \mathbf{c}^H(n)\mathbf{z'}_u(n), \tag{4.31}$$

and the term $\tilde{d}(n)$ represents the decision feedback based data decision. Similarly, the equation describing the update of the coefficients is the same as Equation (4.30). The procedure of the joint ASTD assisted by the LMS-based adaptive filter is summarized in Table 4.6.

When the adaptive MMSE filter is based on the RLS algorithm, we can update the coefficients of the filter in the same way as described in the RLS-based ASTD. The procedure of the joint ASTD assisted by the RLS-based adaptive filter is summarized in Table 4.7.

| | |
|---|---|
| 1 | Initialize the coefficients of the LMS adaptive filter $\mathbf{c}(0)$. When we have no knowledge of the T-domain spreading code of the desired user, we set $\mathbf{c}(0) = \mathbf{0}$. Otherwise, $\mathbf{c}(0)$ is set to be the T-domain spreading code of the desired user. |
| 2 | Compute the the output signal of the adaptive LMS filter $z_{uv,l}(n) = \mathbf{c}^H(n)\mathbf{x}_{uv,l}$. |
| 3 | Compute the estimation error $e(n)$ and update the weight vector $\hat{\mathbf{w}}(n)$ according to the procedure described in Tables 4.4 or 4.5. |
| 4 | Use the updated weight vector $\hat{\mathbf{w}}(n+1)$ to compute the $N_e$-dimensional signal vector $\mathbf{z'}_u(n) = \sum_{v=1}^{V}\sum_{l=0}^{N_a-1} w^*_{v,l}(n+1)\mathbf{x}_{uv,l}$. |
| 5 | Initialize the algorithm by setting $\mathbf{P}(0) = \delta^{-1}\mathbf{I}$, where $\delta$ is a small positive constant. |
| 6 | Update the gain vector $\mathbf{k}(n) = \frac{\lambda^{-1}\mathbf{P}(n-1)\mathbf{z'}_u(n)}{1+\lambda^{-1}\mathbf{z'}_u^H(n)\mathbf{P}(n-1)\mathbf{z'}_u(n)}$. |
| 7 | Update the inverse correlation matrix $\mathbf{P}(n) = \lambda^{-1}\mathbf{P}(n-1) - \lambda^{-1}\mathbf{k}(n)\mathbf{z'}_u^H(n)\mathbf{P}(n-1)$. |
| 8 | In the training stage:<br>(a) Compute the *a priori* estimation error: $\xi(n) = d(n) - \mathbf{c}^H(n-1)\mathbf{z'}_u(n)$;<br>(b) Update the weight vector: $\mathbf{c}(n) = \mathbf{c}(n-1) + \mathbf{k}(n)\xi^*(n)$. |
| 9 | Repeat Steps 2, 3, 4, 6, 7 and 8 until the decision directed stage is reached. |
| 10 | In the decision directed stage:<br>(a) Compute the actual data decision: $\tilde{d}(n) = \text{sgn}\left(\text{Re}\{\mathbf{c}^H(n-1)\mathbf{z'}_u(n)\}\right)$;<br>(b) Compute the *a priori* estimation error: $\xi(n) = \tilde{d} - \mathbf{c}^H(n-1)\mathbf{z'}_u(n)$;<br>(c) Update the weight vector: $\mathbf{c}(n) = \mathbf{c}(n-1) + \mathbf{k}(n)\xi^*(n)$. |
| 11 | Repeat Steps 2, 3, 4, 6, 7 and 10 . |

**Table 4.7:** The procedure of the joint ASTD combined with a RLS-based adaptive filter.

## 4.5 Combined MMSE/PIC Space-Time Processing

As stated in Section 4.4, the ASTD commences its operation with the aid of a training period invoking a training sequence. It is plausible that using a shorter training period results in a higher spectral efficiency, provided that the associated performance degradation of the system is affordable. As a further performance enhancement, iterative Interference Cancellation (IC) techniques may be employed [8], in order to improve the convergence rate of the LMS/RLS algorithms, while maintaining the required BER performance. The principle behind interference cancellation is that the interference can be estimated and removed from the received signal before the signal detection stage. Either Successive IC (SIC) [204, 205], or Parallel IC (PIC) [206, 207] may be used. In [158], Hamouda presented a combined adaptive MMSE/PIC receiver, which is capable of increasing the attainable convergence rate, while maintaining the required BER performance. In the MMSE/PIC scheme of [158] the knowledge of the training sequence available to all the users was exploited for jointly cancelling the Multiple Access Interference (MAI), and for ultimately increasing the attainable convergence rate at the expense of an increased complexity. In this section a modified adaptive MMSE/PIC space-time processing scheme imposing a lower complexity was developed and analyzed. In this adaptive MMSE/PIC space-time processing scheme, partial PIC was employed for improving the achievable convergence

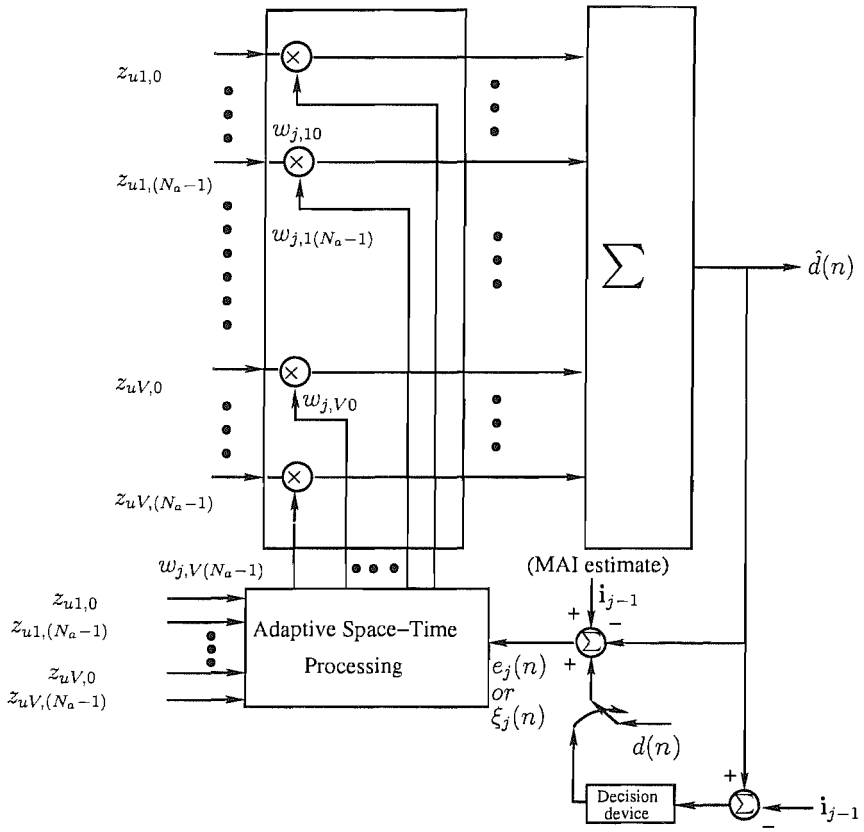


**Figure 4.6:** The block diagram of the adaptive MMSE/PIC beamformer.

speed of the adaptive filter, which attempts to subtract the strong interfering signals from the received signal.

The block diagram of the adaptive space-time processing scheme is shown in Figure 4.6, where the MMSE/PIC ASTD uses a training sequence for both removing the MAI and for updating its weight vector during the training mode. After the training mode, the MMSE/PIC ASTD switches to the decision-directed mode. It removes the MAI and updates its weight vector using the data decisions. The weight vector of the adaptive MMSE/PIC scheme is iteratively adjusted once in every bit interval. However, during a bit interval several PIC iterations might be invoked. Specifically, during each PIC iteration, the receiver determines the estimation error, which is proportional to the difference between the space-time processed output produced by the partial PIC and either the reference signal or the data decisions. This estimation error is then used for updating the weight vector employing either the LMS or the RLS algorithm, as described in Section 4.4.1. This process is repeated for every received bit, until convergence is attained. Below we will outline the principles of the proposed MMSE/PIC scheme using the block diagram of Figure 4.6.

### 4.5.1 LMS-based MMSE/PIC Adaptive Space-Time Processing

In the LMS-based MMSE/PIC ASTD of Figure 4.6, the weight vector is denoted by $\hat{\mathbf{w}}_{kj}(n)$, which is now indexed by the $j$th PIC iteration during the $n$th bit interval of the $k$th user. The input signal of the adaptive LMS-based MMSE/PIC scheme proposed in this section is identical to that of the ASTD characterized in Equation (4.13). As described in the context of the LMS-based ASTD of Section 4.4.1, an appropriate step-size parameter $\mu$ is chosen according to Equation (4.14). As shown in Figure 4.6, the output signal $y_j(n)$ of the LMS-based MMSE/PIC ASTD of Figure 4.6 at the $j$th PIC iteration during $n$th bit interval can be expressed as

$$y_j(n) = \hat{\mathbf{w}}_{j-1}^H(n)\mathbf{z}_u(n) - \hat{i}_{j-1}(n), \tag{4.32}$$

where $\hat{\mathbf{w}}_{j-1}^H(n)$ is the beamformer's weight vector corresponding to the $(j-1)$th PIC iteration and to the $n$th bit interval of the desired user. Note that in (4.32) the superscript and subscript denoting the reference user of $k = 1$ have been omitted for notational convenience. Furthermore, in (4.32) the term of $\hat{i}_{j-1}(n)$ represents the estimate of the MAI during the $(j-1)$th iteration of the $n$th received bit, which is expressed as

$$\hat{i}_{j-1}(n) = \sum_{k=2}^{K} \rho_k \hat{\mathbf{w}}_{j-1}^H(n) d_k(n) \hat{\mathbf{w}}_{k(j-1)}(n) = \sum_{k=2}^{K} \beta_k d_k(n), \tag{4.33}$$

where $K$, $d_k(n)$ and $\hat{\mathbf{w}}_{k(j-1)}^H(n)$ represent the number of active users in the system, the $k$th user's reference signal and the beamformer's weight vector corresponding to the $(j-1)$th PIC iteration during the $n$th bit interval of the $k$th user, respectively. The variable $\rho_k$ in (4.33) represents the cross-correlation between the T-domain (TD) spreading sequence of the desired user and the $k$th user. Furthermore, the term $\beta_k$ in (4.33) may be defined as the interference coefficient quantifying the interference imposed by the $k$th user, which is expressed as

$$\beta_k = \rho_k \hat{\mathbf{w}}_{j-1}^H(n) \hat{\mathbf{w}}_{k(j-1)}(n). \tag{4.34}$$

In ST-spread systems employing beamforming some users' signal may impose strong interference on the desired user, while some other users' signals might inflict relatively low interference on the desired signal, depending on the DOAs of the interfering signals. Hence, the interfering users may be classified into two categories according to their DOAs. The MMSE/PIC ASTD only removes the strong interfering signal from the output signal, while treats the weak interference as additional background noise. Based on the above principles, in our LMS-based MMSE/PIC ASTD, we distinguish the interfering signals according to their interference coefficient $\beta_k$. Hence, the number of strong interfering users is $\kappa \leq K-1$, which implies a proportionate reduction of the implementation complexity of the LMS-based MMSE/PIC ASTD, because only the significant interferers have to be removed by the PIC detector.

The LMS-based MMSE/PIC ASTD is implemented as follows. Firstly, the interference estimate

of (4.33) is modified to

$$\hat{i}_{j-1}(n) = \sum_{k=1}^{\kappa} \rho_k \hat{\mathbf{w}}_{j-1}^H(n) d_k(n) \hat{\mathbf{w}}_{k(j-1)}(n) = \sum_{k=1}^{\kappa} \beta_k d_k(n), \tag{4.35}$$

where $\beta_k$ represents the interference coefficients corresponding to the strong interfering signals. Then, during the training period, the estimation error corresponding to the $j$th PIC iteration during the $n$th bit interval is given by

$$e_j(n) = d(n) - y_j(n), \tag{4.36}$$

where $y_j(n)$ is expressed in (4.32) and $d(n)$ is one of the training bits. Finally, the weight vector is updated according to

$$\hat{\mathbf{w}}_j(n) = \hat{\mathbf{w}}_{j-1}(n) + \mu \mathbf{z}_u(n) e_j^*(n). \tag{4.37}$$

During the data transmission stage, when a new data bit is received, the weight vector of the LMS-based MMSE/PIC ASTD is adapted using (4.32), (4.36) and (4.37), commencing from the initial weight vector given by

$$\hat{\mathbf{w}}_0(n+1) = \hat{\mathbf{w}}_F(n), \tag{4.38}$$

where $\hat{\mathbf{w}}_F(n)$ represents the final weight vector during the $n$th bit interval. In the decision directed mode, we compute the estimation error $e_j(n)$ based on the feedback of the actual data decision $\tilde{d}_j(n)$ generated during the $j$th PIC iteration, which is expressed as

$$\tilde{d}_j(n) = \text{sgn}\left(\text{Re}\{y_j(n)\}\right). \tag{4.39}$$

Accordingly, the estimation error may be expressed as

$$e_j(n) = \tilde{d}_j(n) - y_j(n). \tag{4.40}$$

The weight vector update formula is the same as Equation (4.37).

### 4.5.2 RLS-based MMSE/PIC Adaptive Space-Time Processing

In the RLS-based MMSE/PIC ASTD of Figure 4.6, the weight vector $\hat{\mathbf{w}}_{kj}(n)$ has the same form as that of the LMS-based MMSE/PIC ASTD described in Section 4.5.1. The initial weight vector $\hat{\mathbf{w}}_{k0}(0)$ of the $k$th user is set to be a null vector, when having no *a priori* knowledge concerning the DOAs and CIRs of the channel. Furthermore, the input signal $\mathbf{z}_u(n)$ of the RLS-based MMSE/PIC ASTD is identical to that in (4.19). The $(VN_a \times VN_a)$-dimensional inverse correlation matrix is initialized to $\mathbf{P}(0) = \delta^{-1}\mathbf{I}$, which is identical to $\mathbf{P}(0)$ described in (4.12). Furthermore, the update formula of the the $VN_a$-dimensional gain vector $\mathbf{k}(n)$ is the same as (4.19). The inverse correlation matrix $\mathbf{P}(n)$ is updated by using (4.20). At the $j$th PIC iteration invoked in the $n$th bit interval the

output signal $y_j(n)$ can be expressed as

$$y_j(n) = \hat{\mathbf{w}}_{j-1}^H(n-1)\mathbf{z}_u(n) - \hat{i}_{j-1}(n), \tag{4.41}$$

where the interference estimate $\hat{i}_{j-1}(n)$ has the same form as (4.33). Similar to the LMS-based MMSE/PIC ASTD of Section 4.5.1, only the strong interfering signals having a high interference coefficient $\beta_k$ will be removed from the received signal, in order to reduce the PIC's detection complexity.

During the training period a training sequence is used for computing the *a priori* estimation error in the $j$th PIC iteration, yielding

$$\xi_j(n) = d(n) - y_j(n), \tag{4.42}$$

where $y_j(n)$ is given by (4.41) and $d(n)$ is a training bit. Finally, the weight vector is updated according to

$$\hat{\mathbf{w}}_j(n-1) = \hat{\mathbf{w}}_{j-1}(n-1) + \mathbf{k}(n)\xi_j^*(n). \tag{4.43}$$

Similarly, in the decision directed mode, the *a priori* estimation error $\xi_j(n)$ is computed in the $j$th PIC iteration based on the data decision $\tilde{d}_j(n) = \text{sgn}\left(\text{Re}\{y_j(n)\}\right)$. Consequently, the *a priori* estimation error $\xi_j(n)$ may be expressed as

$$\xi_j(n) = \tilde{d}(n) - y_j(n). \tag{4.44}$$

Finally, by using a similar approach as in the context of the LMS-based MMSE/PIC ASTD, the weight vector update formula is the same as Equation (4.43).

## 4.6 Comparison of Various Adaptive Detectors

All investigations of this section were based on evaluating the performance of an adaptive detector employed in the uplink of a generalized MC DS-CDMA system aided by smart antennas. We assumed that 31-chip Gold codes were employed as TD spreading sequences, while 4-chip Walsh codes were used as F-Domain (FD) spreading codes.

In Figure 4.7, the LMS-based stand-alone ASTD, which we refer to as the standard ASTD of Figure 4.4 detailed in Section 4.4.1 was used to adjust the beamformer weights. By contrast, the RLS-based ASTD of Section 4.4.1 was employed in Figure 4.8, which exhibits a more rapid convergence. In Figure 4.9, the joint LMS-based ASTD of Figure 4.5 discussed in Section 4.4.2 was compared to the standard LMS-based ASTD of Figure 4.4, which was outlined in Section 4.4.1. Moreover, in Figure 4.10 the learning curves of all the adaptive detectors considered are shown. In Figures 4.7, 4.8, 4.9 and 4.10, a $(1 \times 3)$-dimensional antenna array ($M = 1, L = 3$) was employed. The SNR was 10dB and the length of the training period was fixed to 100 symbols, while the length of the transmission frame was 1000 symbols. The learning curves seen in Figures 4.7, 4.8, 4.9 and 4.10 are

the results of ensemble-averaging the instantaneous squared error "$e^2(n)$ versus $n$" curve over 800 independent experiments.

In Figures 4.7 and 4.9, the step-size parameter $\mu$ was assigned one of three different values: 0.5, 1.0, 2.0. Figure 4.7 confirms that the convergence rate of the LMS-based ASTD is heavily dependent on the step-size parameter $\mu$. For a large step-size parameter of $\mu = 2.0$, the adaptive detector converged to its steady-state value in approximately 350 iterations. On the other hand, when $\mu$ is small, for example 0.5, the convergence rate was reduced by more than an order of magnitude. The results also show that the steady-state value of the mean squared error slightly increased upon increasing $\mu$. The joint LMS-based ASTD employed in Figure 4.9 has a similar performance to that of the standard LMS-based ASTD outlined in Figure 4.7. Figure 4.9 confirms that the convergence rate of the joint LMS-based ASTD is also heavily dependent on the step-size parameter $\mu$. Furthermore, Figure 4.9 shows that the joint LMS-based ASTD of Figure 4.5 achieved a slightly slower convergence rate than the standard LMS-based ASTD of Figure 4.4, which was discussed in Section 4.4.1. Since the standard LMS-based ASTD only updates one weight vector at each iteration, while the joint LMS-based ASTD has to update two weight vectors at each iteration, the misadjustment of one of the weight vectors will affect the convergence rate of the other one. However, the BER performance of the joint LMS-based ASTD of Figure 4.5 is better than that of the standard LMS-based ASTD outlined in Figure 4.4. This will be explicitly shown in Figures 4.15 and 4.16.

In Figure 4.8, the parameter $\delta$ was assigned one of the following three different values: 50, 100, 200. Figure 4.8 shows that the convergence rate of the RLS-based ASTD is strongly dependent on the parameter $\delta$. For a small value of $\delta = 50$, the adaptive detector converged to its steady-state solution in approximately 150 iterations, which was significantly faster than the convergence of the LMS-based ASTD using a step-size parameter of $\mu = 2.0$. On the other hand, when $\delta$ was large, such as 200, the convergence rate was reduced. The detector converged to its steady-state solution in approximately 250 iterations.

In Figure 4.10, the step-size parameter of the LMS-based ATSD of Figure 4.4 detailed in Section 4.4.1 was fixed to $\mu = 2$. The number of PIC iterations during each bit interval was set to one of the following three values: 0, 2, 4. Naturally, the performance of the LMS-based MMSE/PIC ASTD of Section 4.5.1 using 0 PIC iterations is identical to that of the LMS-based ASTD of Section 4.4.1. On the other hand, the performance of the RLS-based MMSE/PIC ASTD of Section 4.5.2 employing 0 PIC iterations is identical to that of the RLS-based ASTD of Section 4.4.1. Figure 4.10 confirms that the RLS-based ASTD converges to its steady-state solution faster than the LMS-based ASTD, which is achieved at the expense of a higher computational complexity. Again, when having the same number of PIC iterations, the RLS-based MMSE/PIC ASTD outperforms the LMS-based MMSE/PIC ASTD. Figure 4.10 demonstrates that by using the PIC technique in the context of the LMS-based ASTD, the achievable convergence speed increases by more than an order of magnitude. When the number of PIC iterations in each bit interval was 4 and the step-size parameter was $\mu = 2.0$, the LMS-based MMSE/PIC ASTD converged to its steady-state solution in approximately 75 iterations. Similarly, when using the PIC technique, the RLS-based ASTD converged to its steady-state solution

at a significantly faster rate. When the number of PIC iterations used in each bit interval was 4 and we had $\delta = 50$, the RLS-based MMSE/PIC ASTD converged to its steady-state solution in approximately 25 iterations. It can be shown that the achievable rate of convergence increased, when more PIC iterations were carried out during each bit interval. Finally, we concluded from Figure 4.10 that all adaptive detectors had a similar steady-state misadjustment.

Figure 4.11 describes the BER performance of a generalized MC DS-CDMA system employing the LMS-based ASTD of Figure 4.4 outlined in Section 4.4.1. Here, the step-size parameter $\mu$ was fixed to 2.0. By contrast, Figure 4.12 denotes the BER performance of the corresponding RLS-based ASTD of Section 4.4.1 also obeying the structure of Figure 4.4, where the parameter $\delta$ was fixed to 100. Furthermore, Figure 4.13 portrays the attainable BER performance of an LMS-based MMSE/PIC ASTD of Figure 4.6 discussed in Section 4.5.1, where the parameter $\mu$ was fixed to 2, and 2 PIC iterations were carried out during each bit interval. Figure 4.14 characterizes the BER performance of the RLS-based MMSE/PIC ASTD of Figure 4.6 detailed in Section 4.5.2 in conjunction with the parameter $\delta$ fixed to 100, where 2 PIC iterations were employed during each bit interval. Observe from Figures 4.11, 4.12, 4.13 and 4.14 that as expected, the performance of the system supporting 31 users is worse than that supporting 4 users. Furthermore, the systems benefitting from a longer training period tend to achieve a better performance than those having a shorter training period, when the length of the transmission frame is fixed. On the other hand, the systems having a longer transmission frame achieve a better performance than those using a shorter frame, when the duration of the training period is fixed.

In Figure 4.15, a generalized MC DS-CDMA system supporting 31 users is studied, while in Figure 4.16 a generalized MC DS-CDMA system supporting 4 users is investigated. The simulation results shown in Figures 4.15 and 4.16 were obtained using a frame constituted by a training period of 100 bits and a decision-directed period of 900 bits. As observed from comparing Figures 4.15 and 4.16, the BER performance of the LMS-based MMSE/PIC and the RLS-based MMSE/PIC detector are similar to that of the LMS-based and the RLS-based ASTD. This confirms that having the same steady-state misadjustment MSE for the different adaptive detectors results in a similar BER performance. Furthermore, Figures 4.15 and 4.16 confirm that the BER performance of the joint LMS-based ASTD is better than that of the standard LMS-based ASTD.

Below three types of antenna array models are studied in conjunction with the LMS-based ASTD of Section 4.4.1 and the RLS-based ASTD of Section 4.4.1, namely a $(1 \times 4)$-dimensional antenna array $(M = 1, L = 4)$, a $(2 \times 2)$-dimensional antenna array $(M = 2, L = 2)$, and finally a $(4 \times 1)$-dimensional antenna array $(M = 4, L = 1)$. Again, Figure 4.17 confirms that the RLS-based ASTD of Figure 4.4 detailed in Section 4.4.1 converges to its steady-state solution faster than the LMS-based ASTD of Section 4.4.1 for all these different types of antenna arrays. Furthermore, we observe from Figure 4.17 that the ASTD employing the $(4 \times 1)$-dimensional antenna array $(M = 4, L = 1)$ converges to its steady-state solution faster than the ASTD employing the $(2 \times 2)$-dimensional antenna array $(M = 2, L = 2)$, while the ASTD employing the $(1 \times 4)$-dimensional antenna array $(M = 1, L = 4)$ has the lowest convergence rate. As depicted in Figure 4.18, all adaptive detectors

achieve a similar BER performance, when using the same type of antenna arrays. Again, this confirms that having the same steady-state misadjustment MSE for the different adaptive detectors results in a similar BER performance. Figure 4.18 shows that the ASTD of Figure 4.4 outlined in Section 4.4 employing the $(4 \times 1)$-dimensional antenna array $(M = 4, L = 1)$ achieves the best BER performance, followed by the ASTD employing a $(2 \times 2)$-dimensional antenna array $(M = 2, L = 2)$, whilst the ASTD employing a $(1 \times 4)$-dimensional antenna array $(M = 1, L = 4)$ has the worst BER performance. From Figures 4.17 and 4.18 we observe that when the spatial signals arriving at the different elements of the antenna array become less correlated, the spatial diversity gain becomes higher, hence the achievable BER performance improves.

Figure 4.19 characterizes the BER performance of the various systems supporting $K = 4$ users, employing either the LMS-based ASTD or the LMS-based MMSE/PIC ASTD of Sections 4.4.1 and 4.5.1. Furthermore, the BER performance of the conventional LMS/PIC adaptive detector proposed in [158] was provided as a benchmark. Figure 4.19 indicates that the ASTD systems were robust against the near-far effect. Three scenarios were considered. In the first scenario, the power of the interfering users was equal to that of the desired user, that is, we had $P_0 = P_1 = P_2 = P_3$. In the second scenario, we had $4P_0 = P_1 = P_2 = P_3$. By contrast, we had $16P_0 = P_1 = P_2 = P_3$ in the third scenario. As observed from Figure 4.19, the ASTD systems achieved a slightly worse BER versus $E_b/N_0$ performance in the second scenario than the ASTD systems in the first scenario, while the ASTD systems in the third scenario achieved the worst BER performance.

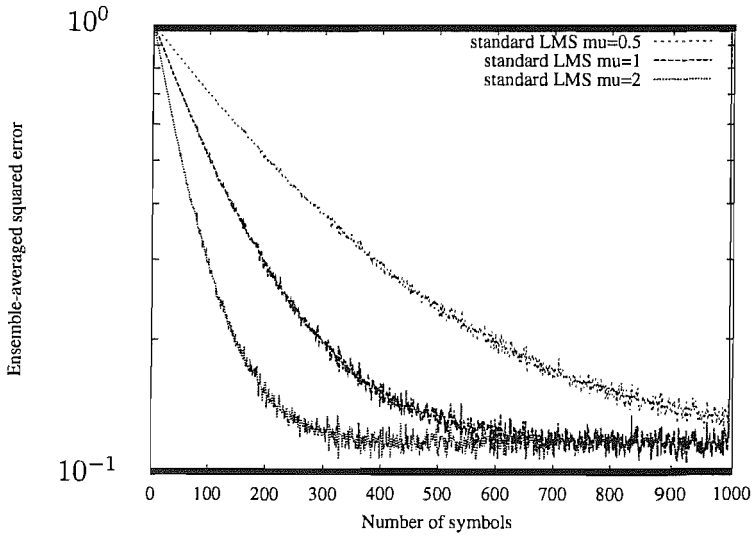


**Figure 4.7:** Learning curves of the **standard LMS-based** ASTD seen in Figure 4.4 invoked for the uplink of a generalized MC DS-CDMA wireless system supporting $K = 4$ users and using 31-chip Gold codes as time-domain spreading sequences and 4-chip Walsh codes as frequency-domain spreading sequences, as well as a $(1 \times 3)$-dimensional antenna array $(M = 1, L = 3)$. Here, mu= $\mu$.

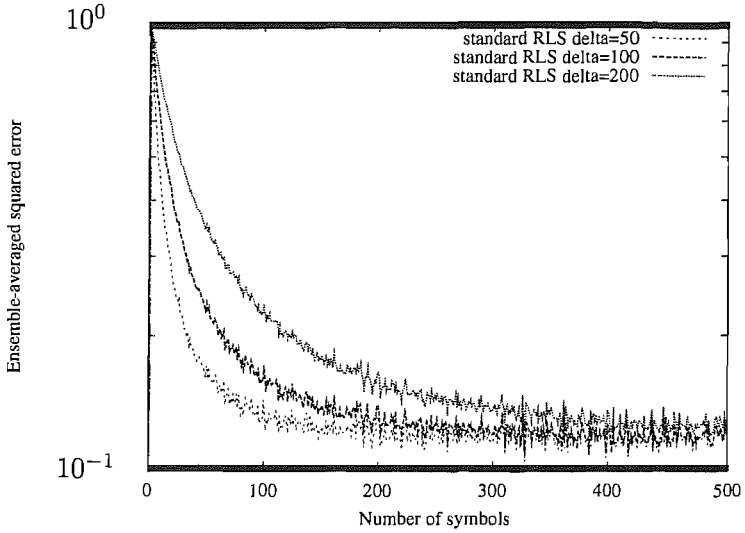


**Figure 4.8:** Learning curves of the **standard RLS-based** ASTD outlined in Figure 4.4 invoked for the uplink of a generalized MC DS-CDMA wireless system supporting $K = 4$ users and using 31-chip Gold codes as time-domain spreading sequences and 4-chip Walsh codes as frequency-domain spreading sequences, as well as a $(1 \times 3)$-dimensional antenna array $(M = 1, L = 3)$, where we have delta= $\delta$.

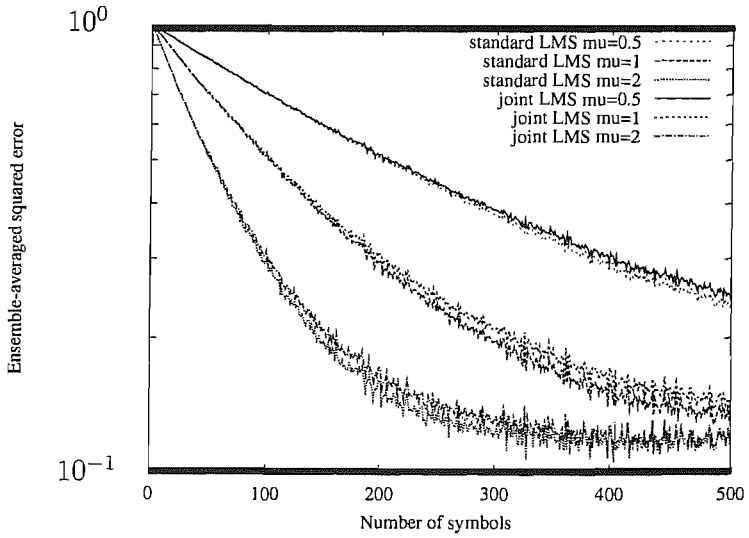


**Figure 4.9:** Learning curves of the **joint LMS-based** ASTD outlined in Figure 4.5 and the **standard LMS-based** ASTD seen in Figure 4.4 invoked for the uplink of a generalized MC DS-CDMA wireless system supporting $K = 4$ users and using 31-chip Gold codes as time-domain spreading sequences and 4-chip Walsh codes as frequency-domain spreading sequences, as well as a $(1 \times 3)$-dimensional antenna array $(M = 1, L = 3)$. Here, mu= $\mu$.

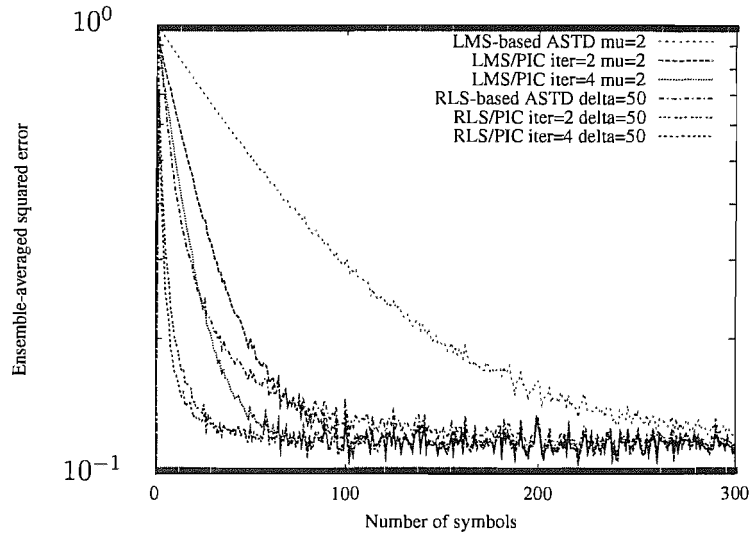


**Figure 4.10:** Learning curves of **all** adaptive detectors invoked for the uplink of a generalized MC DS-CDMA wireless system supporting $K = 4$ users and using 31-chip Gold codes as time-domain spreading sequences and 4-chip Walsh codes as frequency-domain spreading sequences, as well as a $(1 \times 3)$-dimensional antenna array $(M = 1, L = 3)$, where we have mu= $\mu$ and delta= $\delta$.

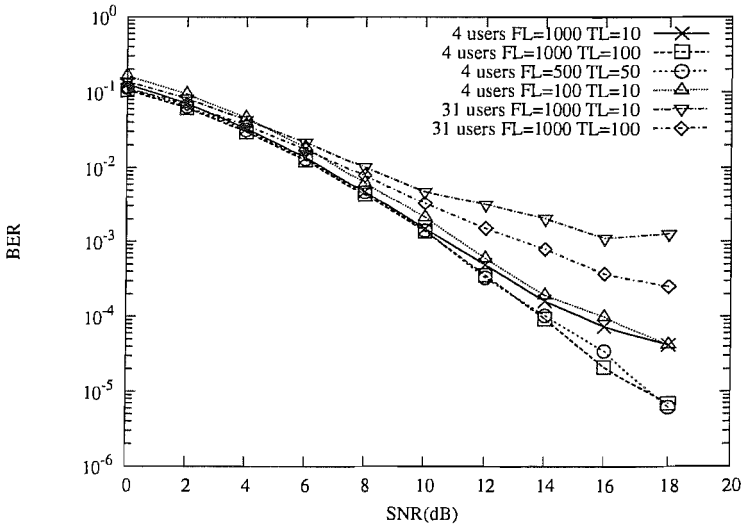


**Figure 4.11:** BER versus SNR performance of the uplink of a generalized MC DS-CDMA wireless system using 31-chip Gold codes as time-domain spreading sequences and 4-chip Walsh codes as frequency-domain spreading sequences, as well as a $(1 \times 3)$-dimensional antenna array $(M = 1, L = 3)$, where the **LMS-based ASTD** is used to process the received signal.

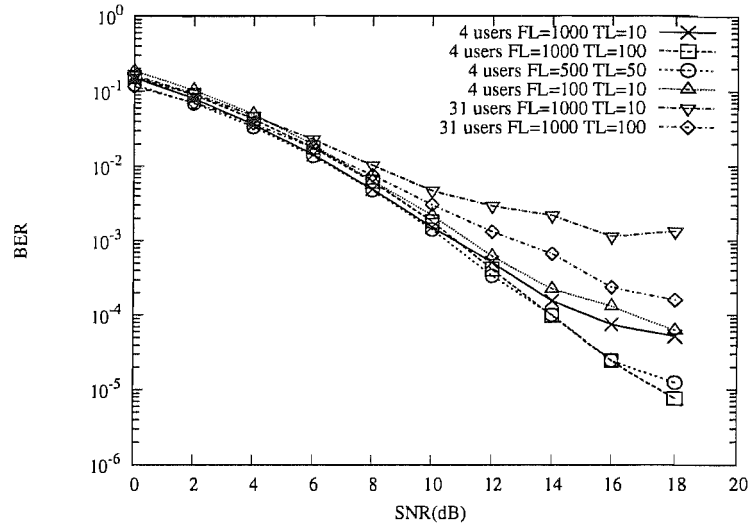


**Figure 4.12:** BER versus SNR performance of the uplink of a generalized MC DS-CDMA wireless system using 31-chip Gold codes as time-domain spreading sequences and 4-chip Walsh codes as frequency-domain spreading sequences, using a $1 \times 3$-dimensional antenna array ($M = 1, L = 3$), where the **RLS-based ASTD** is used to process the received signal.

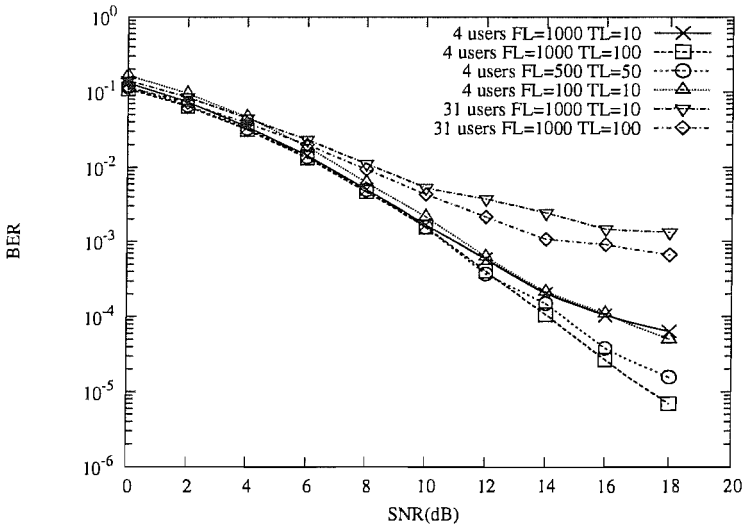


**Figure 4.13:** BER versus SNR performance of the uplink of a generalized MC DS-CDMA wireless system using 31-chip Gold codes as time-domain spreading sequences and 4-chip Walsh codes as frequency-domain spreading sequences, as well as a $1 \times 3$-dimensional antenna array ($M = 1, L = 3$), where the **LMS-based MMSE/PIC ASTD** is used to process the received signal.

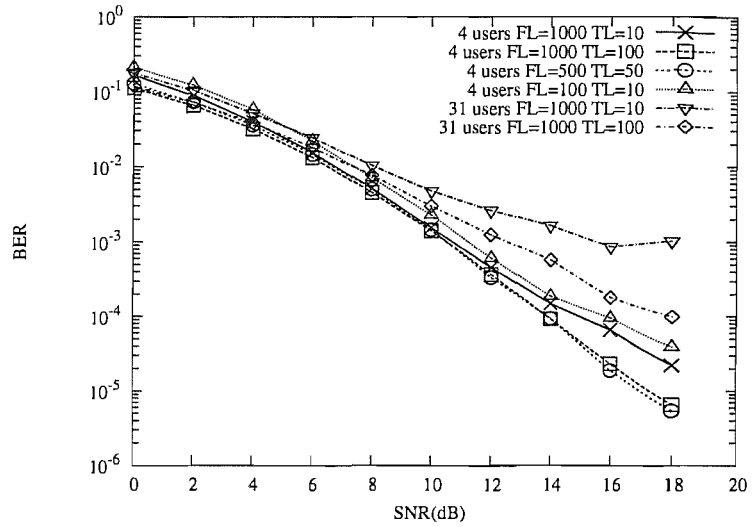


**Figure 4.14:** BER versus SNR performance of the uplink of a generalized MC DS-CDMA wireless system using 31-chip Gold codes as time-domain spreading sequences and 4-chip Walsh codes as frequency-domain spreading sequences, as well as a $1 \times 3$-dimensional antenna array ($M = 1, L = 3$), where the **RLS-based MMSE/PIC ASTD** is used to process the received signal.

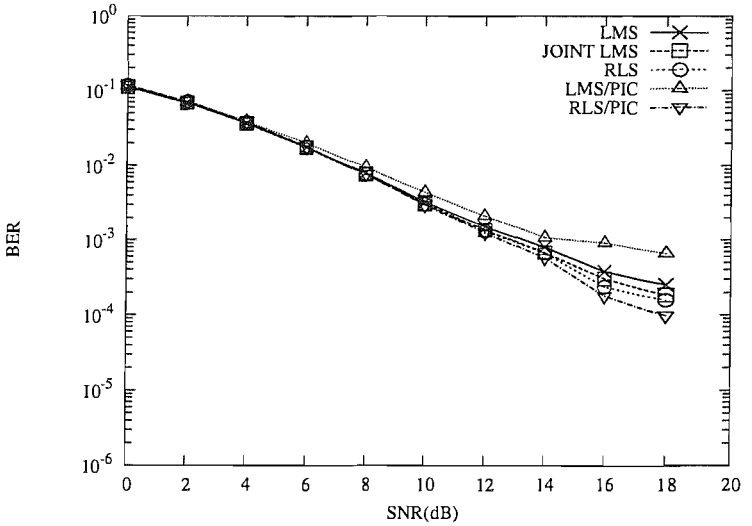


**Figure 4.15:** BER versus SNR performance of the uplink of a generalized MC DS-CDMA wireless system supporting **31 users**, using 31-chip Gold codes as time-domain spreading sequences and 4-chip Walsh codes as frequency-domain spreading sequences, as well as a $(1 \times 3)$-dimensional antenna array ($M = 1, L = 3$), where the performances of **all** the adaptive detectors are evaluated and compared.

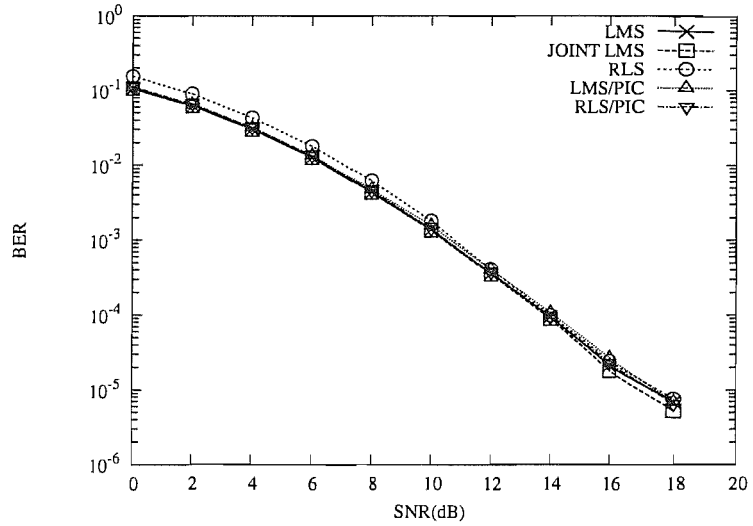


**Figure 4.16:** BER versus SNR performance of the uplink of a generalized MC DS-CDMA wireless system supporting **4 users**, using 31-chip Gold codes as time-domain spreading sequences and 4-chip Walsh codes as frequency-domain spreading sequences, as well as a $(1 \times 3)$-dimensional antenna array $(M = 1, L = 3)$, where the performances of **all** the adaptive detectors are evaluated and compared.

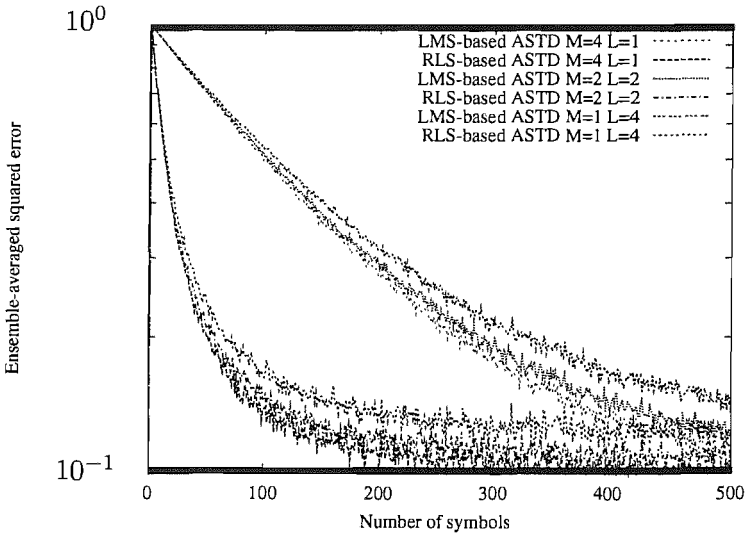


**Figure 4.17:** Learning curves of LMS-based and RLS-based ASTD invoked for the uplink of a generalized MC DS-CDMA wireless system supporting $K = 4$ users and using 31-chip Gold codes as time-domain spreading sequences and 4-chip Walsh codes as frequency-domain spreading sequences. In this simulation, **three types of antenna array are employed, namely a $(1 \times 4)$-dimensional antenna array $(M = 1, L = 4)$, a $(2 \times 2)$-dimensional antenna array $(M = 2, L = 2)$, and a $(4 \times 1)$-dimensional antenna array $(M = 4, L = 1)$.**

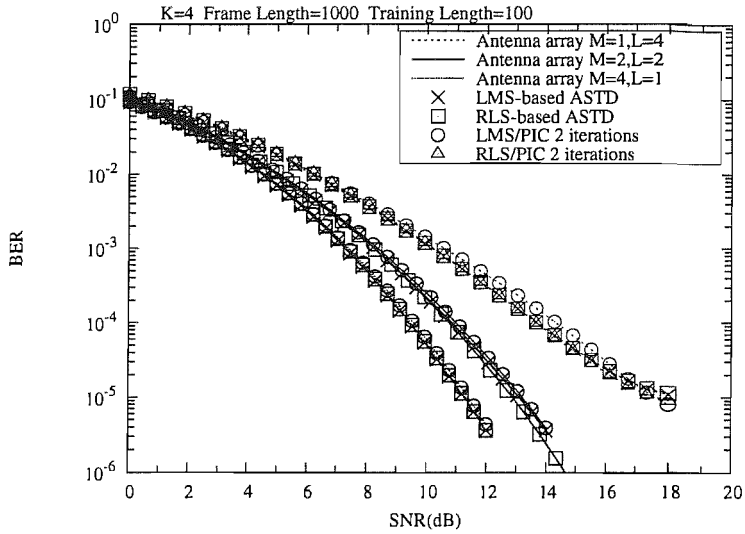


**Figure 4.18:** BER versus SNR performance of the uplink of a generalized MC DS-CDMA wireless system supporting 4 users, using 31-chip Gold codes as time-domain spreading sequences and 4-chip Walsh codes as frequency-domain spreading sequences, Where the performances of all adaptive detectors are evaluated and compared. **Three types of antenna array are employed, namely a** $(1 \times 4)$**-dimensional antenna array** $(M = 1, L = 4)$**, a** $(2 \times 2)$**-dimensional antenna array** $(M = 2, L = 2)$**, and a** $(4 \times 1)$**-dimensional antenna array** $(M = 4, L = 1)$**.**

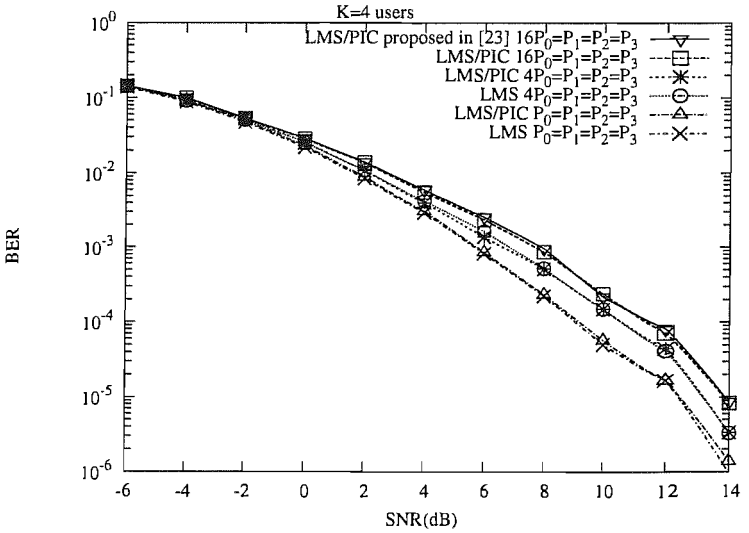


**Figure 4.19:** BER versus SNR performance of the uplink of a generalized MC DS-CDMA wireless system serving 4 users, using 31-chip Gold codes as time-domain spreading sequences and 4-chip Walsh codes as frequency-domain spreading sequences, as well as a $(1 \times 3)$-dimensional antenna array $(M = 1, L = 3)$, where LMS-based ASTD and LMS-based MMSE/PIC ASTD are used to process the received signal.

## 4.7 Conclusions

In this chapter we studied the performance of a range of adaptive space-time processing schemes invoked for a generalized MC DS-CDMA system supported by a $(M \times L)$-dimensional antenna array. In Section 4.1, a brief introduction to various literatures on adaptive space-time processing was first presented, followed by a rudimentary overview of the LMS and RLS algorithms. Furthermore, combined adaptive MMSE/PIC receivers and two adaptive space-time detectors having different structures were outlined and introduced for the sake of improving the attainable convergence rate or the BER performance of the LMS/RLS adaptive receiver.

In Section 4.2 the philosophy of the LMS algorithm is described and characterized. Following our study by reviewing the steepest decent adaptive algorithm, we detailed the LMS algorithm derived using the method of steepest decent. The method of steepest decent was summarized in Table 4.1, while the procedure of the LMS algorithm was summarized in Table 4.2. Finally, the block diagram of an adaptive LMS filter was portrayed in Figure 4.2. The RLS algorithm was defined and developed in Section 4.3. We commenced our study by reviewing the method of least squares, from which the RLS algorithm was developed. After a detailed description and derivation of the RLS algorithm, we provided a comparison between the RLS and the LMS algorithm. The summary of the RLS algorithm was provided in Table 4.3.

We then focused our attention on the application of these algorithms in the adaptive uplink of the generalized MC DS-CDMA system in Section 4.4. The block diagram of the adaptive space-time detector was portrayed in Figure 4.4, while the schematic structure of the joint adaptive space-time detector was shown in Figure 4.5. The LMS-based ASTD was first developed in Section 4.4.1, followed by the derivation of the RLS-based ASTD. The procedures of the LMS-based ASTD and the RLS-based ASTD were summarized in Tables 4.4 and 4.5, respectively. Finally, the joint adaptive space-time processing scheme was described and its principles were extended for employment in the generalized MC DS-CDMA system considered. Tables 4.6 and 4.7 summarized the procedures of the joint ASTD assisted by the LMS-based adaptive filter and the joint ASTD assisted by the RLS-based adaptive filter, respectively.

In Section 4.5, the PIC technique was employed for improving the convergence rate of the adaptive beamformer. The block diagram of the adaptive space-time processing scheme was portrayed in Figure 4.6, where the MMSE/PIC ASTD used a training sequence for both removing the MAI and for updating its weight vector during the training mode. Then, in Section 4.5.1 the LMS-based MMSE/PIC ASTD was derived, followed by the development of the RLS-based MMSE/PIC ASTD in Section 4.5.2.

Finally, the performance of these schemes was comparatively studied in Section 4.6 in the context of the generalized MC DS-CDMA system concept advocated. The convergence rate of the LMS-based ASTD of Figure 4.4 outlined in Section 4.4.1 was shown to be heavily dependent on the step-size parameter $\mu$, while that of the RLS-based ASTD also outlined in Section 4.4.1 was seen to be largely dependent on the parameter $\delta$. The simulation results confirm that the RLS-based ASTD has

| Scheme | Type of antenna arrays | Number of iterations required for converging to steady-state value | Figure No. |
|---|---|---|---|
| LMS-based ASTD | $1 \times 3$ | 350 | Figure 4.10 |
| | $1 \times 4$ | 550 | Figure 4.17 |
| | $2 \times 2$ | 510 | Figure 4.17 |
| | $4 \times 1$ | 495 | Figure 4.17 |
| RLS-based ASTD | $1 \times 3$ | 150 | Figure 4.10 |
| | $1 \times 4$ | 230 | Figure 4.17 |
| | $2 \times 2$ | 210 | Figure 4.17 |
| | $4 \times 1$ | 200 | Figure 4.17 |
| LMS/PIC iter=2 | $1 \times 3$ | 110 | Figure 4.10 |
| LMS/PIC iter=4 | $1 \times 3$ | 75 | Figure 4.10 |
| RLS/PIC iter=2 | $1 \times 3$ | 35 | Figure 4.10 |
| RLS/PIC iter=4 | $1 \times 3$ | 25 | Figure 4.10 |

**Table 4.8:** Summary of the learning curves for the various adaptive space-time processing schemes characterized in Figures 4.10 and 4.17 invoked for the uplink of the generalized MC DS-CDMA system supporting four users, employing several different antenna arrays, where we have $\mu = 2.0$ and $\delta = 50$.

a higher convergence rate than that of the LMS-based ASTD, which is achieved at the expense of a higher computational complexity. The joint LMS-based ASTD of Figure 4.5 outperforms the standard LMS-based ASTD seen in Figure 4.4 in terms of its BER performance, although it has a slightly slower convergence rate than the standard LMS-based ASTD. With the advent of the proposed PIC technique we are able to increase the achievable convergence rate of the ASTD, while maintaining the required BER performance. The BER performances of all the adaptive detectors were found to be similar, when they have the same misadjustment MSE. Having investigated a range of different antenna array models, we conclude that when the spatial signals arriving at the different elements of the antenna array become less correlated, the spatial diversity gain becomes higher, hence the achievable BER performance improves.

A summary of the associated results is provided in Table 4.8 for the sake of characterizing and comparing the convergence rate of all adaptive space-time processing schemes invoked for the uplink of the generalized MC DS-CDMA system supporting four user. By contrast, the comparison of the BER performance of all adaptive space-time processing schemes invoked for the systems employing several different antenna arrays as well as supporting four users is provided in Table 4.9. The four users employ the same Gold code as their time-domain spreading sequence, while using different Walsh codes as their frequency-domain spreading sequences. Finally, Figure 4.20(b) portrays the computational complexity of the corresponding ASTD aided generalized MC DS-CDMA systems.

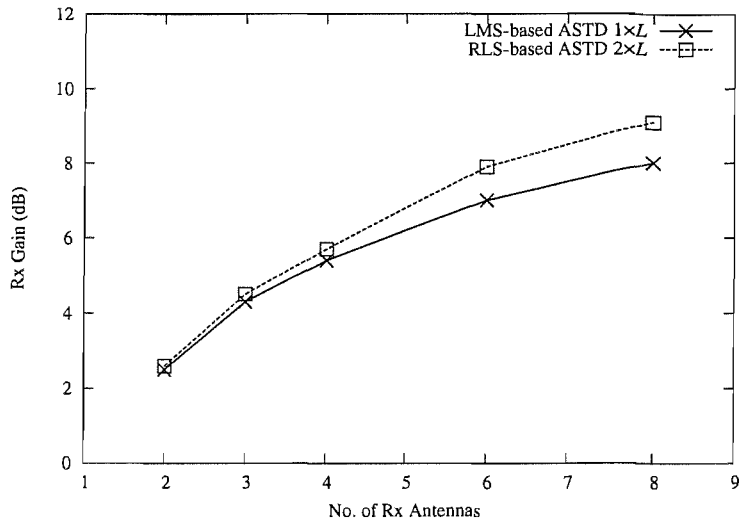


(a)

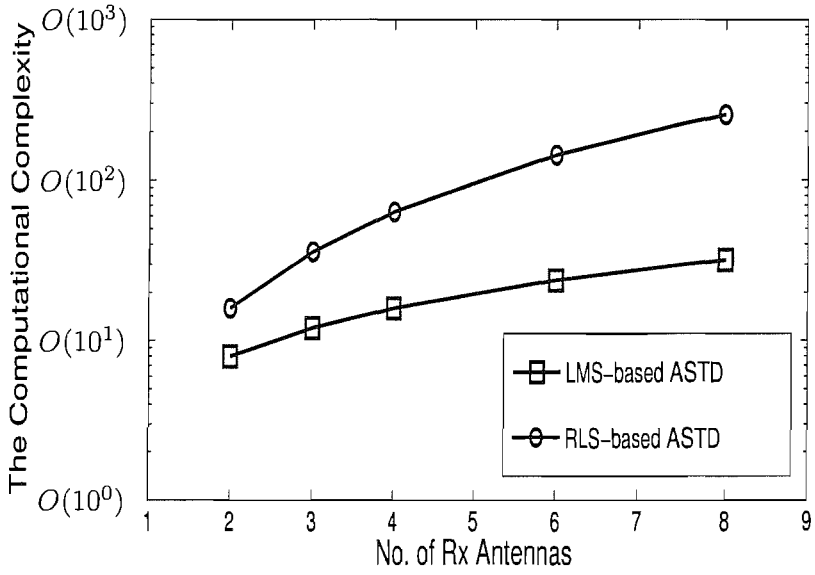


(b)

**Figure 4.20:** (a) Receive (Rx) gain versus the number of the receive antennas for the uplink of the ASTD-aided generalized MC DS-CDMA system supporting four users at a BER performance of $10^{-4}$. Note that the computational complexity of the LMS-based ASTD is on the order of $O(VML)$, while the computational complexity of the RLS-based ASTD is on the order of $O[(VML)^2]$. (b) The computational complexity versus the number of receive antennas for the various antenna array types of Section 4.6 employed for the uplink of the ASTD-aided generalized MC DS-CDMA system employing $V = 4$ subcarriers based on both the LMS-based ASTD and the RLS-based ASTD as outlined in Section 4.4.1. Figure 4.20(a) suggests that when more antennas are employed, the performance gap between the RLS-based ASTD and the LMS-based ASTD becomes larger, since the former has a faster convergence rate.

| Scheme | Type of antenna arrays | $E_b/N_0$(dB) required at BER=$10^{-4}$ | $E_b/N_0$(dB) required at BER=$10^{-5}$ | Figure No. |
|---|---|---|---|---|
| LMS-based ASTD | $1 \times 4$ | 13.9 | 18.0 | Figure 4.18 |
| | $2 \times 2$ | 10.8 | 13.0 | Figure 4.18 |
| | $4 \times 1$ | 9.4 | 11.3 | Figure 4.18 |
| RLS-based ASTD | $1 \times 4$ | 13.9 | 18.1 | Figure 4.18 |
| | $2 \times 2$ | 10.8 | 12.9 | Figure 4.18 |
| | $4 \times 1$ | 9.4 | 11.3 | Figure 4.18 |
| LMS/PIC iter=2 | $1 \times 4$ | 13.9 | 18.0 | Figure 4.18 |
| | $2 \times 2$ | 10.8 | 13.0 | Figure 4.18 |
| | $4 \times 1$ | 9.4 | 11.3 | Figure 4.18 |
| RLS/PIC iter=4 | $1 \times 4$ | 13.8 | 18.0 | Figure 4.18 |
| | $2 \times 2$ | 10.7 | 12.8 | Figure 4.18 |
| | $4 \times 1$ | 9.3 | 11.3 | Figure 4.18 |

**Table 4.9:** Summary of the required $E_b/N_0$ values for the various adaptive space-time processing schemes characterized in Figure 4.18 invoked for the uplink of the generalized MC DS-CDMA system supporting four users, as well as employing several different antenna arrays, where we have $\mu = 2.0$ and $\delta = 50$.

Chapter 5

# Multicarrier DS-CDMA Systems Using Smart Antennas - Blind Detection

## 5.1 Introduction

Over the past decade, numerous research contributions have appeared on the topic of Multi-User Detection (MUD), which is capable of dealing with the demodulation of digitally modulated signals in the presence of multiuser interference and hence can substantially increase the user-load of CDMA systems [8, 35]. In [195, 208], Verdu's optimum MUD was presented for asynchronous multiple-access Gaussian channels, where the receiver was shown to attain a near-single-user performance by exploiting prior knowledge, namely that of the signature waveform of the desired user, the signature waveforms of the interfering users, the timing information of the desired user, the timing information of the interfering users and the received amplitudes of the interfering users. In contrast to the conventional single-user CDMA receiver, which only requires the signature waveform and the timing information of the desired user, the optimum MUD is capable of overcoming the near-far problem, which severely degrades the achievable performance of the conventional CDMA receiver even in the presence of perfect power control [168]. The decorrelating detector presented in [209, 210] avoids the exponentially increasing complexity of the optimum MUD [195, 208] imposed by increasing the number of users supported and does not require any knowledge of the received amplitudes of the interfering users, although this is achieved at the expense of a slight increase of the BER. Recently, considerable amount of research has been carried out on adaptive multiuser detection [211–214], which only requires the signature waveform and the timing information of the desired user. The adaptive decorrelating detector, zero-forcing detector and linear detector proposed in [211–214] require the employment of training sequences, which significantly reduces the achievable spectrum efficiency. In order to overcome this problem, the Minimum-Output-Energy (MOE) based blind adaptive detector was proposed in [168], which does not require any training sequence. The MOE based blind detector was then extended in [215], where the effects of multipath distortions are considered and compensated for. However, the performance of MOE based blind detectors is suboptimum in the high SNR

region.

Subspace-based methods [216] play an important role in sensor array processing, spectrum analysis and general parameter estimation [216], but they have been also invoked for delay estimation [217, 218] and channel estimation [217, 219] in CDMA systems. A novel blind MUD based on signal subspace estimation was proposed by Wang and Poor in [1] for single-carrier DS-CDMA systems communicating over synchronous AWGN channels, which benefits from a lower computational complexity and a better performance compared to the MOE based blind MUD. In [2], subspace based blind MUDs were developed for the joint suppression of MAI and ISI in dispersive CDMA channels. Furthermore, in [169, 220], group-blind MUDs having the prior knowledge of all known signature waveforms were proposed for the uplink of a single-carrier DS-CDMA system, which exhibited a significant performance improvement over that of the blind MUDs advocated in [1, 2].

In [26], an adaptive algorithm was proposed in the context of MC-CDMA for exploiting the correlation between the noise and the interference for the sake of rejecting the MAI. However, this frequency-domain MMSE MUD performs well only in situations, where the number of subcarriers is low and only a few dominant interferers exist [173]. A subspace-based MMSE receiver was proposed in [173] for a MC DS-CDMA system, which is similar to that advocated in [1, 174], where the orthogonality between the noise subspace and the desired signal vector was exploited for blindly extracting both the timing and channel information.

The rest of this chapter has the following structure. In Section 5.2 the philosophy of subspace-based blind and group-blind MUDs was detailed and characterized. Two low-complexity subspace tracking algorithms, namely the Projection Approximation Subspace Tracking deflation (PASTd) algorithm and the Noise-Averaged Hermitian-Jacobi Fast Subspace Tracking (NAHJ-FST) algorithm are investigated in Section 5.2.4. Then, we concentrate our investigations on the blind and group-blind MUDs invoked for a generalized MC DS-CDMA system in Section 5.3, where the space-time blind and group-blind MUDs were further investigated for a smart antennas aided MC DS-CDMA system. Finally, the performance of these blind and group-blind MUDs was investigated in the context of smart antenna aided MC DS-CDMA systems in Section 5.4. Our conclusions are provided in Section 5.5.

## 5.2 The Philosophy of Subspace-Based Blind and Group-Blind Multiuser Detection

Before commencing our investigations of subspace-based blind and group-blind multiuser detection in the context of smart antenna aided generalized MC DS-CDMA systems, we provide an introduction to the philosophy of subspace-based blind MUDs. Subspace-based blind MUDs were first proposed for synchronous DS-CDMA systems [1] and then were extended to dispersive asynchronous DS-CDMA environments [2] as well as Multicarrier CDMA systems [173]. It is worth commencing by contrasting blind MUDs to their more conventional non-blind counterparts, where the latter schemes require both channel estimation and the knowledge of all users' unique signatures. Blind MUDs

dispense with this knowledge and only require the knowledge of the desired user's signature. By contrast, group-blind MUDs assume the knowledge of all the intracell users' spreading codes, but no knowledge about the intercell interfering users.

### 5.2.1 Blind Multiuser Detection for Synchronous DS-CDMA [1]

Consider a synchronous DS-CDMA system supporting $K$ users. The $N$-dimensional received signal vector defined within a symbol interval $T$ can be expressed as [1]

$$\mathbf{r} = \sum_{k=1}^{K} A_k b_k \mathbf{c}_k + \sigma \mathbf{n}, \tag{5.1}$$

where $A_k$, $b_k$ and $\mathbf{c}_k = \frac{1}{\sqrt{N}}[c_1, c_2, \ldots, c_N]^T$ represent the received signal's amplitude, the transmitted bit and the normalized signature waveform of the $k$th user, respectively, while $\mathbf{n}$ is a white Gaussian noise vector having a zero mean and covariance matrix of $\mathbf{I}_N$, where $\mathbf{I}_N$ denotes the $(N \times N)$-dimensional identity matrix and $N$ is the spreading factor.

Without loss of generality, we assume that the signature waveforms $\{\mathbf{c}_k\}_{k=1}^{K}$ of the $K$ users are linearly independent. Then the autocorrelation matrix $\mathbf{R}$ of the $N$-dimensional received signal vector $\mathbf{r}$ can be expressed as

$$\mathbf{R} \triangleq E\{\mathbf{r}\mathbf{r}^T\} = \sum_{k=1}^{K} A_k^2 \mathbf{c}_k \mathbf{c}_k^T + \sigma^2 \mathbf{I}_N = \mathbf{C}\mathbf{A}\mathbf{C}^T + \sigma^2 \mathbf{I}_N, \tag{5.2}$$

where we have $\mathbf{C} \triangleq [\mathbf{c}_1, \mathbf{c}_2, \ldots, \mathbf{c}_K]$ and $\mathbf{A} \triangleq \text{diag}[A_1^2, A_2^2, \ldots, A_K^2]$. Physically the autocorrelation matrix $\mathbf{R}$ of the received signal vector $\mathbf{r}$ in (5.2) is the sum of the composite multiuser signal's autocorrelation matrix $\mathbf{C}\mathbf{A}\mathbf{C}^T$ and the identity matrix $\sigma^2\mathbf{I}_N$ contributed by the AWGN.

According to [1], the eigen-decomposition of the received signal's autocorrelation matrix $\mathbf{R}$ is given by

$$\mathbf{R} = \mathbf{U}\Lambda\mathbf{U}^T = [\mathbf{U}_s \ \mathbf{U}_n] \begin{bmatrix} \mathbf{\Lambda}_s & 0 \\ 0 & \mathbf{\Lambda}_n \end{bmatrix} \begin{bmatrix} \mathbf{U}_s^T \\ \mathbf{U}_n^T \end{bmatrix}, \tag{5.3}$$

where we have $\mathbf{U} = [\mathbf{U}_s \ \mathbf{U}_n]$ and $\Lambda = \text{diag}(\mathbf{\Lambda}_s, \mathbf{\Lambda}_n)$. Specifically, $\mathbf{\Lambda}_s = \text{diag}\{\lambda_1, \ldots, \lambda_K\}$ and $\mathbf{U}_s = [\mathbf{u}_1, \ldots, \mathbf{u}_K]$ contain the largest $K$ eigenvalues of the autocorrelation matrix $\mathbf{R}$ stored in descending order and the corresponding orthonormal eigenvectors, while the matrix $\mathbf{U}_n = [\mathbf{u}_{K+1}, \ldots, \mathbf{u}_N]$ contains the $(N-K)$ orthonormal eigenvectors corresponding to the smallest eigenvalues in $\mathbf{\Lambda}_n$, all of which are $\sigma^2$. The range space of $\mathbf{U}_s$ is referred to as the *signal space*, while its orthogonal complement, the *noise space*, is spanned by $\mathbf{U}_n$ [1]. Equation (5.3) physically states that the received signal's autocorrelation matrix $\mathbf{R}$ may be diagonalized by a unitary matrix $\mathbf{U}$, resulting in a diagonal matrix $\mathbf{\Lambda}$, where the entries are the eigenvalues of $\mathbf{R}$. Furthermore, the unitary matrix $\mathbf{U}$ that is used to diagonalize $\mathbf{R}$ has constituting columns an orthonormal set of eigenvectors of $\mathbf{R}$.

Below we will demonstrate the EigenValue-Decomposition (EVD) of the received signal's auto-

correlation matrix $\mathbf{R}$ with the aid of an example. Let us consider a system having the parameters of $N = 4$, $K = 2$, $A_1 = A_2 = 1$, and $\mathbf{c}_1 = [1/2, 1/2, 1/2, 1/2]^T$, $\mathbf{c}_2 = [-1/2, 1/2, 1/2, 1/2]^T$. In order to exemplify these quantities, we conducted simulations at $E_b/N_0 = 20dB$ and recorded the corresponding autocorrelation matrix $\mathbf{R}$ after we received $M_F = 256$ number of multiuser received signal samples, which is given by:

$$\mathbf{R} = [\mathbf{c}_1, \mathbf{c}_2] \times \begin{bmatrix} \mathbf{c}_1 \\ \mathbf{c}_2 \end{bmatrix} + \sigma^2 \mathbf{I}_4 = \begin{bmatrix} 0.51 & 0 & 0 & 0 \\ 0 & 0.51 & 0.50 & 0.50 \\ 0 & 0.50 & 0.51 & 0.50 \\ 0 & 0.50 & 0.50 & 0.51 \end{bmatrix}. \tag{5.4}$$

The corresponding eigendecomposition can be expressed as:

$$\mathbf{R} = \mathbf{U}\Lambda\mathbf{U}^T = \left[\begin{array}{cc|cc} 0 & 1.00 & 0 & 0 \\ 0.58 & 0 & -0.52 & 0.63 \\ 0.58 & 0 & 0.80 & 0.14 \\ 0.58 & 0 & -0.28 & -0.77 \end{array}\right] \times \begin{bmatrix} 0.51 & 0 & 0 & 0 \\ 0 & 0.51 & 0 & 0 \\ 0 & 0 & 0.01 & 0 \\ 0 & 0 & 0 & 0.01 \end{bmatrix} \times \left[\begin{array}{cccc} 0 & 0.58 & 0.58 & 0.58 \\ 1.00 & 0 & 0 & 0 \\ \hline 0 & -0.52 & 0.80 & -0.28 \\ 0 & 0.63 & 0.14 & -0.77 \end{array}\right]. \tag{5.5}$$

The first two columns of $\mathbf{U}$ in (5.5) constitute the *signal subspace*, while the 3rd and 4th columns of $\mathbf{U}$ are referred to as the *noise subspace*, which correspond to the smallest eigenvalues of $\sigma^2 = 0.01$ in (5.5).

The Singular Value Decomposition (SVD) is another decomposition technique, which is typically invoked for decomposing a non-square matrix. For the received signal matrix $\mathbf{X} = \frac{1}{\sqrt{M_F}}[\mathbf{r}_1, \ldots, \mathbf{r}_{M_F}]$, which is constituted by the $M_F$ number of multiuser received signal samples $\mathbf{r}_i \in \mathcal{R}^N, i = 1, \ldots M_F$, the corresponding SVD can be expressed as $\text{SVD}(\mathbf{X}) = \mathbf{V}\Lambda\mathbf{U}^T$, where again, $\mathbf{U}$ is constituted by the eigenvectors and $\Lambda$ contains the corresponding eigenvalues. Again, we will exemplify the SVD of the received signal matrix $\mathbf{X}$ based on the same system as the one used in EVD, which has the parameters of $N = 4$, $K = 2$, $A_1 = A_2 = 1$, and $\mathbf{c}_1 = [1/2, 1/2, 1/2, 1/2]^T$, $\mathbf{c}_2 = [-1/2, 1/2, 1/2, 1/2]^T$. After we received $M_F = 80$ number of multiuser signal samples at $E_b/N_0 = 20dB$, we have the received signal matrix $\mathbf{X} = \frac{1}{\sqrt{80}}[\mathbf{r}_1, \ldots, \mathbf{r}_{80}]$ in the form of

$$\mathbf{X} = \frac{1}{\sqrt{80}} \begin{bmatrix} -0.949 & 0.038 & \ldots & -0.108 \\ 0.169 & -1.101 & \ldots & -1.113 \\ 0.059 & -1.002 & \ldots & -0.826 \\ -0.064 & -1.005 & \ldots & -0.806 \end{bmatrix}. \tag{5.6}$$

The corresponding SVD can be expressed as:

$$
\begin{aligned}
\mathbf{X} &= \mathbf{V}\Lambda\mathbf{U}^T \\
&= \begin{bmatrix} -0.006 & -0.120 & 0.152 & 0.018 \\ 0.132 & 0.006 & -0.058 & -0.046 \\ \vdots & \vdots & \vdots & \vdots \\ 0.173 & -0.018 & -0.261 & -0.207 \end{bmatrix} \times \begin{bmatrix} 1.024 & 0 & 0 & 0 \\ 0 & 0.591 & 0 & 0 \\ 0 & 0 & 0.085 & 0 \\ 0 & 0 & 0 & 0.073 \end{bmatrix} \\
&\times \left[\begin{array}{cccc} -0.007 & -0.577 & -0.574 & -0.580 \\ 0.999 & 0.000 & 0.000 & -0.012 \\ \hline -0.009 & 0.634 & 0.131 & -0.761 \\ 0.003 & 0.513 & -0.808 & 0.288 \end{array}\right].
\end{aligned}
$$

The first two rows of $\mathbf{U}^T$ constitute the *signal subspace*, while the 3rd and 4th rows of $\mathbf{U}^T$ are referred to as the *noise subspace*, which correspond to the smallest eigenvalues.

From (5.2) and (5.3), we attain

$$\mathbf{CAC}^T = \mathbf{U}_s(\mathbf{\Lambda}_s - \sigma^2\mathbf{I}_K)\mathbf{U}_s^T = \mathbf{U}\Lambda_0\mathbf{U}^T, \tag{5.7}$$

where $\Lambda_0$ is an $(N \times N)$-dimensional diagonal matrix given by $\Lambda_0 \triangleq \Lambda - \sigma^2\mathbf{I}_N = \text{diag}(\lambda_1 - \sigma^2, \ldots, \lambda_K - \sigma^2, 0, \ldots, 0)$. Physically the composite multiuser signal's autocorrelation matrix $\mathbf{CAC}^T$ may be diagonalized by a unitary matrix $\mathbf{U}_s$ and $\mathbf{U}$ to a diagonal matrix $(\mathbf{\Lambda}_s - \sigma^2\mathbf{I}_K)$ and $\mathbf{\Lambda}_0$, respectively.

The linear MUD designed for demodulating the $k$th user's data bit in (5.1) is then given by [1]

$$\hat{b}_k = \text{sgn}(\mathbf{w}_k^T\mathbf{r}), \tag{5.8}$$

where the $N$-dimensional vector $\mathbf{w}_k$ denotes the MUD's weight vector optimized for detecting user $k$. Below, we will derive expressions for the decorrelating detector [209] and the linear MMSE detector [168] in terms of the signal subspace parameters $\mathbf{U}_s$, $\mathbf{\Lambda}_s$ and $\sigma$.

#### 5.2.1.1 Decorrelating Detector

The decorrelating detector proposed in [209] is capable of completely eliminating the MAI imposed by the interfering users at the expense of enhancing the effects of noise. Let us denote the correlation matrix of the signature waveforms [1] as $\mathcal{R} \triangleq \mathbf{C}^T\mathbf{C}$, which is invertible, since we have $rank(\mathbf{C}) = K$. Then, for the first user, the weight vector $\mathbf{w}_1 = \mathbf{d}_1$ of the decorrelating detector may be expressed as [1]

$$\mathbf{d}_1 = \sum_{k=1}^{K} [\mathcal{R}^{-1}]_{1k}\mathbf{c}_k, \tag{5.9}$$

[1] Please observe that the autocorrelation matrix of the received signal was denoted by bold, rather than calligraphic R

where $[\mathcal{R}^{-1}]_{ij}$ is the $(i,j)$th element of the matrix $\mathcal{R}^{-1}$. Physically the multiplication of $\mathbf{c}_k$ by $[\mathcal{R}^{-1}]_{1k}$ corresponds to the product of the $(1,k)$th element of the inverse of the signature waveforms' correlation matrix $\mathcal{R}^{-1}$ and the $k$th user's signature waveform $\mathbf{c}_k$. We characterize the properties of the decorrelating detector having a weight vector $\mathbf{d}_1$ during our forthcoming discussion.

*Lemma 1* [1]: The decorrelating detector $\mathbf{d}_1$ defined in (5.9) is the unique vector expressed as $\mathbf{d} \in range(\mathbf{U}_s)$, which satisfies $\mathbf{d}_1{}^T\mathbf{c}_1 = 1$ and $\mathbf{d}_1^T\mathbf{c}_k = 0$, for $k = 2, \ldots, K$.

*Proof:* Observe from Equation (5.9) that we have $\mathbf{d}_1 \in range(C) \in range(\mathbf{U}_s)$ and

$$\mathbf{d}_1^T\mathbf{c}_k = \sum_{i=1}^{K}[\mathcal{R}^{-1}]_{1i}\mathbf{c}_i^T\mathbf{c}_k = \sum_{i=1}^{K}[\mathcal{R}^{-1}]_{1i}[\mathcal{R}]_{ik} = [\mathcal{R}^{-1}\mathcal{R}]_{1k} = \begin{cases} 1, & \text{for } k = 1, \\ 0, & \text{for } k = 2, \ldots, K. \end{cases} \tag{5.10}$$

Since we have $rank(U_s) = K$, the MUD's weight vector $\mathbf{d} = \mathbf{d}_1$ is unique.

*Lemma 2* [1]: The decorrelating detector's weight vector $\mathbf{d}_1$ is defined with the aid of the unique vector $\mathbf{d} \in range(\mathbf{U}_s)$ that minimizes the following expected value expression:

$$\Omega(\mathbf{d}) = E\left[\mathbf{d}^T\left(\sum_{k=1}^{K} A_k b_k \mathbf{c}_k\right)\right]^2 \tag{5.11}$$

subject to the constraint of $\mathbf{d}^T\mathbf{c}_1 = 1$. In physically tangible terms Equation (5.11) corresponds to minimizing the expected value of the MUD's output, given by the product of the composite multiuser signal and the MUD's weight vector $\mathbf{d}$.

*Proof*: Since we have

$$\begin{aligned} \Omega(\mathbf{d}) &= \mathbf{d}^T E\left[\left(\sum_{k=1}^{K} A_k b_k \mathbf{c}_k\right)\left(\sum_{k=1}^{K} A_k b_k \mathbf{c}_k\right)^T\right]\mathbf{d} \\ &= \mathbf{d}^T E\left[\sum_{k=1}^{K} A_k^2 \mathbf{c}_k \mathbf{c}_k^T\right]\mathbf{d} \\ &= A_1^2(\mathbf{d}^T\mathbf{c}_1)^2 + \sum_{k=2}^{K} A_k^2(\mathbf{d}^T\mathbf{c}_k)^2 \\ &= A_1^2 + \sum_{k=2}^{K} A_k^2(\mathbf{d}^T\mathbf{c}_k)^2, \end{aligned} \tag{5.12}$$

then for $\mathbf{d} \in range(\mathbf{U}_s) = range(C)$, $\Omega(\mathbf{d})$ is minimized if and only if we have $\mathbf{d}^T\mathbf{c}_k = 0$, for $k = 2, \ldots, K$. From *Lemma 1*, we have a weight vector $\mathbf{d} = \mathbf{d}_1$, which is unique in the range space of $\mathbf{U}_s$ [1].

*Proposition 1* [1]: The decorrelating detector's weight vector $\mathbf{d}_1$ defined in Equation (5.9) can be alternatively expressed in terms of the signal subspace parameters $\mathbf{U}_s$, $\mathbf{\Lambda}_s$ and $\sigma$ as [1]

$$\mathbf{d}_1 = \frac{1}{\mathbf{c}_1^T\mathbf{U}_s(\mathbf{\Lambda}_s - \sigma^2\mathbf{I}_K)^{-1}\mathbf{U}_s^T\mathbf{c}_1}\mathbf{U}_s(\mathbf{\Lambda}_s - \sigma^2\mathbf{I}_K)^{-1}\mathbf{U}_s^T\mathbf{c}_1. \tag{5.13}$$

The physically motivated interpretation of Equation (5.13) will be provided after its proof.

*Proof:* For some $\mathbf{s} \in \mathcal{R}^K$, the vector $\mathbf{d}$ falls in the range space of $\mathbf{U}_s$ if and only if we have $\mathbf{d} = \mathbf{U}_s\mathbf{s}$. Then, according to Lemma 2, the decorrelating detector's weight vector $\mathbf{d}_1$ can be written as $\mathbf{d}_1 = \mathbf{U}_s\mathbf{s}_1$, where we have [1]:

$$\begin{aligned}
\mathbf{s}_1 &= \arg\min_{\mathbf{s}\in\mathcal{R}^K} (\mathbf{U}_s\mathbf{s})^T \left(\sum_1^K A_k^2 \mathbf{c}_k\mathbf{c}_k^T\right)(\mathbf{U}_s\mathbf{s}), \\
&\quad s.t.\ \ (\mathbf{U}_s\mathbf{s})^T\mathbf{c}_1 = 1 \\
&= \arg\min_{\mathbf{s}\in\mathcal{R}^K} \mathbf{s}^T[\mathbf{U}_s^T(\mathbf{C}\mathbf{A}\mathbf{C}^T)\mathbf{U}_s]\mathbf{s}, \\
&\quad s.t.\ \ \mathbf{s}^T(\mathbf{U}_s^T\mathbf{c}_1) = 1 \\
&= \arg\min_{\mathbf{s}\in\mathcal{R}^K} \mathbf{s}^T(\mathbf{\Lambda}_s - \sigma^2\mathbf{I}_k)\mathbf{s} \\
&\quad s.t.\ \ \mathbf{s}^T(\mathbf{U}_s^T\mathbf{c}_1) = 1,
\end{aligned} \tag{5.14}$$

where the second equality follows from (5.2) and the third equality follows from Eq.(5.7). Then, by employing the method of Lagrange multipliers [1], the function to be optimized can be expressed as

$$\Omega(\mathbf{s}) = \mathbf{s}^T(\mathbf{\Lambda}_s - \sigma^2\mathbf{I}_k)\mathbf{s} - 2\mu[\mathbf{s}^T(\mathbf{U}_s^T\mathbf{c}_1) - 1], \tag{5.15}$$

which is a convex function of $\mathbf{s}$, since the matrix $(\mathbf{\Lambda}_s - \sigma^2\mathbf{I}_k)$ is positive definite. In (5.15), the second term represents the optimization constraints and $\mu$ is the Lagrange multiplier. Hence, we may attain the unique minimum of $\Omega(\mathbf{s})$ at the specific value of $\mathbf{s}_1$, where we have $\bigtriangledown\Omega(\mathbf{s_1}) = 0$, which leads to

$$(\mathbf{\Lambda}_s - \sigma^2\mathbf{I}_k)\mathbf{s}_1 = \mu\mathbf{U}_s^T\mathbf{c}_1. \tag{5.16}$$

Then we arrive at $\mathbf{s}_1 = \mu(\mathbf{\Lambda}_s - \sigma^2\mathbf{I}_k)^{-1}\mathbf{U}_s^T\mathbf{c}_1$, where $\mu = \frac{1}{\mathbf{c}_1^T\mathbf{U}_s(\mathbf{\Lambda}_s - \sigma^2\mathbf{I}_k)^{-1}\mathbf{U}_s^T\mathbf{c}_1}$ is determined from the constraint of $(\mathbf{U}_s\mathbf{c}_1)^T\mathbf{s}_1 = 1$ seen in (5.14). Finally, the decorrelating detector's weight vector is given by [1]:

$$\mathbf{d}_1 = \mathbf{U}_s\mathbf{s}_1 = \frac{1}{\mathbf{c}_1^T\mathbf{U}_s(\mathbf{\Lambda}_s - \sigma^2\mathbf{I}_K)^{-1}\mathbf{U}_s^T\mathbf{c}_1}\mathbf{U}_s(\mathbf{\Lambda}_s - \sigma^2\mathbf{I}_K)^{-1}\mathbf{U}_s^T\mathbf{c}_1, \tag{5.17}$$

which physically implies that the projection of the decorrelating detector's weight vector $\mathbf{d}_1$ in the signal subspace $\mathbf{U}_s$ is obtained by projecting the desired user's signature waveform $\mathbf{c}_1$ onto the signal subspace $\mathbf{U}_s$, followed by scaling the $k$th component of this projection by a factor of $(\lambda_k - \sigma^2)^{-1}$.

Above, the decorrelating detector's weight vector was derived in terms of its signal subspace parameters. In the next section we consider the linear MMSE detector [168].

#### 5.2.1.2 Linear MMSE Detector

The MMSE weight vector is defined in form of (5.8), employing the weight vector $\mathbf{w}_1 = \mathbf{m}_1$ for the first user, where $\mathbf{m}_1 \in \mathcal{R}^N$ minimizes the Mean-Square Error (MSE) between the MUD's output vector $\mathbf{m}_1\mathbf{r}$ and the legitimate channel output given by the product of the transmitted bit $b_1$ and the

channel's complex-valued transfer factor $A_1$, namely by $A_1 b_1$, which is defined as [1]

$$\begin{aligned} \text{MSE}(\mathbf{m}_1) &= E\big[A_1 b_1 - \mathbf{m}_1^T \mathbf{r}\big]^2 \\ & \quad s.t.\ \mathbf{m}_1^T \mathbf{c}_1 = 1. \end{aligned} \tag{5.18}$$

*Proposition 2:* Based on the signal space parameters $\mathbf{U}_s$ and $\mathbf{\Lambda}_s$ in (5.3), the linear MMSE detector's weight vector $\mathbf{m}_1$ can be expressed as [1]

$$\mathbf{m}_1 = \frac{1}{\mathbf{c}_1^T \mathbf{U}_s \mathbf{\Lambda}_s^{-1} \mathbf{U}_s^T \mathbf{c}_1} \mathbf{U}_s \mathbf{\Lambda}_s^{-1} \mathbf{U}_s^T \mathbf{c}_1. \tag{5.19}$$

*Proof:* By employing again the method of Lagrange multipliers used in (5.14) during the derivation of the decorrelating detector, we arrive at the optimization function of the MMSE detector, which has the form of [1]

$$\begin{aligned} \Omega(\mathbf{m}) &= \text{MSE}(\mathbf{m}) - 2\mu(\mathbf{m}^T \mathbf{c}_1 - 1) \\ &= \mathbf{m}^T E\{\mathbf{r}\mathbf{r}^T\}\mathbf{m} - 2A_1 \mathbf{m}^T E\{b_1 \mathbf{r}\} + A_1^2 - 2\mu(\mathbf{m}^T \mathbf{c}_1 - 1) \\ &= \mathbf{m}^T \mathbf{R}\mathbf{m} - 2(A_1^2 + \mu)\mathbf{m}^T \mathbf{c}_1 + (A_1^2 + 2\mu), \end{aligned} \tag{5.20}$$

where $E\{\mathbf{r}\mathbf{r}^T\} = \mathbf{R}$ and $E\{b_1 \mathbf{r}\} = \mathbf{c}_1$ were invoked for attaining the third equality in (5.20). Since $\mathbf{R}$ is positive definite, $\Omega(\mathbf{m})$ is a strictly convex function of $\mathbf{m}$. Hence, by solving the equation $\bigtriangledown \Omega(\mathbf{m}_1) = 0$ with respect to $\mathbf{m}_1$, we arrive at the linear MMSE detector's weight vector in the form of [1]

$$\begin{aligned} \mathbf{m}_1 &= (A_1^2 + \mu)\mathbf{R}^{-1}\mathbf{c}_1 \\ &= (A_1^2 + \mu)(\mathbf{U}_s \mathbf{\Lambda}_s^{-1} \mathbf{U}_s^T)\mathbf{c}_1 + (A_1^2 + \mu)\sigma^{-2}(\mathbf{U}_n \mathbf{U}_n^T)\mathbf{c}_1 \\ &= (A_1^2 + \mu)\mathbf{U}_s \mathbf{\Lambda}^{-1} \mathbf{U}_s^T \mathbf{c}_1, \end{aligned} \tag{5.21}$$

where the second equality of (5.21) follows from the eigen-decomposition (5.3) of $\mathbf{R}$, and the third equality follows from the fact that $\mathbf{c}_1 \in range(\mathbf{U}_s)$ is orthogonal to the noise space, *i.e.* from the fact that we have $\mathbf{U}_n^T \mathbf{c}_1 = 0$. Equations (5.19) and (5.21) physically imply that the projection of the linear MMSE detector's weight vector $\mathbf{m}_1$ in the signal subspace $\mathbf{U}_s$ is obtained by projecting the desired user's signature waveform $\mathbf{c}_1$ onto the signal subspace $\mathbf{U}_s$, followed by scaling the $k$th component of this projection by a factor of $\lambda_k^{-1}$. Observe from Equations (5.17) and (5.19), together with their physical interpretations, that a factor of $(\lambda_k - \sigma^2)^{-1}$ is employed for the sake of attaining the decorrelating detector, while a factor of $\lambda_k^{-1}$ is used in order to arrive at the linear MMSE detector. Hence, in contrast to the decorrelating detector that is designed to completely eliminate the MAI at the expense of enhancing the noise, the linear MMSE detector is capable of jointly minimizing the effect of the MAI and the noise at the detector's output.

Finally, we obtain

$$(A_1^2 + \mu) = \frac{1}{\mathbf{c}_1^T \mathbf{U}_s \mathbf{\Lambda}_s^{-1} \mathbf{U}_s^T \mathbf{c}_1} \tag{5.22}$$

according to the constraint of $\mathbf{m}_1^T \mathbf{c}_1 = 1$. In (5.22), $(A_1^2 + \mu)$ is a constant scalar, physically used for satisfying the constraint of $\mathbf{m}_1^T \mathbf{c}_1 = 1$. By using (5.21) and (5.22), we obtain the MMSE detector's weight vector $\mathbf{m}_1$, having the form of (5.19).

From the above derivations of the decorrelating detector's weight vector $\mathbf{d}_1$ and the linear MMSE detector's weight vector $\mathbf{m}_1$, we observe that both of them can be estimated from the received signal $\mathbf{r}$ with the aid of the prior knowledge of the signature waveform and the timing of the user of interest, since the received signal's autocorrelation matrix $\mathbf{R}$ and the components of its eigendecomposition $\mathbf{U}_s, \mathbf{\Lambda}_s, \sigma$ can be estimated from the received signal $\mathbf{r}$. In other words, the MUD's weight vectors $\mathbf{d}_1, \mathbf{m}_1$ can be obtained blindly [1].

### 5.2.2 Blind and Group-Blind Multiuser Detection for Dispersive DS-CDMA Channels [2]

In DS-CDMA systems, the delay-spread-induced ISI, aggravated by the MAI which results in a substantial degradation of the overall system performance [2]. In this section, we extend our investigations of blind MUDs to dispersive channels for the sake of jointly combatting the effects of both MAI and ISI.

Let us consider a dispersive DS-CDMA system serving $K$ users, where the transmitted signals of the $K$ users propagate over their respective dispersive multipath channels contaminated by the AWGN. The CIR corresponding to the $k$th user can be expressed as:

$$h_k(t) = \sum_{l=1}^{L_k} h_{kl} \delta(t - \tau_{kl}), \tag{5.23}$$

where $h_{kl}$ is the complex-valued channel gain experienced by the signal of the $k$th user in the $l$th path, which obeys Rayleigh fading, while $L_k$ and $\tau_{kl}$ denote the total number of paths in the channel and the delay of the $l$th path of the $k$th user. The transmitted signal of the $k$th user is given by [169]

$$s_k(t) = \sum_{i=0}^{M_F - 1} A_k b_k[i] \mathbf{c}_k(t - iT - \tau_k), \tag{5.24}$$

where $T$ denotes the symbol duration and $M_F$ is the number of data bits in the transmitted data frame, while $A_k$, $\{b_k[i]\}$ and $0 \leq \tau_k < T$ represent the amplitude, symbol stream and the delay of the $k$th user, respectively. Furthermore, the spreading sequence $\mathbf{c}_k(t) = \sum_{j=0}^{N-1} c_k(j) \psi(t - jT_c)$ denotes the signature waveform of the $k$th user, where $c_k(j)$ assumes values of +1 or -1 with equal probability, while $\psi(t)$ is a normalized chip waveform of duration $T_c = T/N$. Then, the response of the $k$th

user's dispersive channel to the transmitted signal $s_k(t)$ can be expressed as

$$\begin{aligned} y_k(t) &= s_k(t) \otimes h_k(t) \\ &= \sum_{i=0}^{M_F-1} b_k[i][A_k \mathbf{c}_k(t - iT - \tau_k) \otimes h_k(t)] \\ &= \sum_{i=0}^{M_F-1} b_k[i]\bar{h}_k(t - iT), \end{aligned} \tag{5.25}$$

where $\otimes$ represents convolution and

$$\begin{aligned} \bar{h}_k(t) &\triangleq A_k \mathbf{c}_k(t - \tau_k) \otimes h_k(t) \\ &= \sum_{j=0}^{N-1} c_k(j) \left[ A_k \sum_{l=1}^{L_k} h_{kl} \psi(t - jT_c - \tau_k - \tau_{kl}) \right] \end{aligned} \tag{5.26}$$

is the composite signature waveform of the $k$th user, which is constituted by the convolution of the user's signature waveform and the CIR. This composite CIR is zero outside the interval $[\tau_k + \tau_{k1}, \tau_k + \tau_{kL_k} + T]$, taking into account the effects of the transmitted signal's amplitude $A_k$, the user's delay and those of the multipath channel represented by $h_k(t)$. The total received signal is the superposition of all the $K$ users' transmissions plus the AWGN, hence we have

$$r(t) = \sum_{k=1}^{K} y_k(t) + n(t), \tag{5.27}$$

where $n(t)$ is a zero mean AWGN process, having a power spectral density of $\sigma^2$.

The received signal $r(t)$ is first filtered by a chip-matched filter and then sampled at a chip-rate of $\frac{1}{T_c}$, yielding the discrete-time received signal $r[i,n]$ during the $n$th chip period of the $i$th symbol interval expressed as

$$\begin{aligned} r[i,n] &= r(iT + nT_c) \\ &= \sum_{k=1}^{K} \underbrace{y_k(iT + nT_c)}_{y_k[i,n]} + \underbrace{n(iT + nT_c)}_{n[i,n]}. \end{aligned} \tag{5.28}$$

Let us define the total delay spread experienced by the symbols of the $k$th user as $\iota_k = \lceil (\tau_k + \tau_{kL_k} +$

$T_c)/T]$. Then, we have

$$\begin{aligned} y_k[i,n] &= y_k(iT+nT_c) = \sum_{j=0}^{M_F-1} b_k[j]\bar{h}_k(iT+nT_c-jT) \\ &= \sum_{j=i-\iota_k}^{i} b_k[j]\bar{h}_k(iT+nT_c-jT) \\ &= \sum_{j=0}^{\iota_k} \bar{h}_k[j,n]b_k[i-j], \end{aligned} \tag{5.29}$$

since $\bar{h}_k(t)$ is zero outside the interval $[0,(\iota_k+1)T]$. Hence, (5.28) can be rewritten for the $k$th user as

$$r[i,n] = \underbrace{\bar{h}_k[0,n]b_k[i]}_{\text{Desired signal}} + \underbrace{\sum_{j=1}^{\iota_k} \bar{h}_k[j,n]b_k[i-j]}_{\text{ISI}} + \underbrace{\sum_{k'\neq k} y_{k'}[i,n]}_{\text{MAI}} + \underbrace{n[i,n]}_{\text{noise}}. \tag{5.30}$$

Let us furthermore introduce the notation

$$\underbrace{\bar{\mathbf{r}}[i]}_{N\times 1} = \begin{bmatrix} r[i,0] \\ \vdots \\ r[i,N-1] \end{bmatrix}, \tag{5.31}$$

$$\underbrace{\bar{\mathbf{n}}[i]}_{N\times 1} = \begin{bmatrix} n[i,0] \\ \vdots \\ n[i,N-1], \end{bmatrix} \tag{5.32}$$

$$\underbrace{\bar{\mathbf{b}}[i]}_{K\times 1} = \begin{bmatrix} b[i,0] \\ \vdots \\ b[i,K-1] \end{bmatrix} \tag{5.33}$$

and

$$\underbrace{\bar{\mathbf{H}}[i]}_{N\times K} = \begin{bmatrix} \bar{h}_1[i,0] & \bar{h}_2[i,0] & \dots & \bar{h}_K[i,0] \\ \vdots & \vdots & \vdots & \vdots \\ \bar{h}_1[i,N-1] & \bar{h}_2[i,N-1] & \dots & \bar{h}_K[i,N-1] \end{bmatrix}. \tag{5.34}$$

Then (5.30) can be written in a matrix form as

$$\bar{\mathbf{r}}[i] = \bar{\mathbf{H}}[i] \otimes \bar{\mathbf{b}}[i] + \bar{\mathbf{n}}[i]. \tag{5.35}$$

For the sake of converting the convolution operation to a product operation, we introduce the nota-

tion of $\iota \triangleq \max_{1\leq k\leq K}\{\iota_k\}$, and stack $m$ number of successive received sample vectors, by further defining

$$\underbrace{\mathbf{r}[i]}_{Nm\times 1} = \begin{bmatrix} \bar{\mathbf{r}}[i+0] \\ \vdots \\ \bar{\mathbf{r}}[i+m-1] \end{bmatrix}, \tag{5.36}$$

$$\underbrace{\mathbf{n}[i]}_{Nm\times 1} = \begin{bmatrix} \bar{\mathbf{n}}[i+0] \\ \vdots \\ \bar{\mathbf{n}}[i+m-1] \end{bmatrix}, \tag{5.37}$$

$$\underbrace{\mathbf{b}[i]}_{r\times 1} = \begin{bmatrix} \bar{\mathbf{b}}[i-\iota] \\ \vdots \\ \bar{\mathbf{b}}[i+m-1] \end{bmatrix} \tag{5.38}$$

and

$$\underbrace{\mathbf{H}}_{Nm\times r} = \begin{bmatrix} \bar{\mathbf{H}}[\iota] & \dots & \bar{\mathbf{H}}[0] & \dots & 0 \\ \vdots & \ddots & \ddots & \ddots & \vdots \\ 0 & \dots & \bar{\mathbf{H}}[\iota] & \dots & \bar{\mathbf{H}}[0] \end{bmatrix}, \tag{5.39}$$

where we have $r = K(m+\iota)$. Hence, Equation (5.35) may be rewritten as:

$$\mathbf{r}[i] = \mathbf{H}\mathbf{b}[i] + \mathbf{n}[i]. \tag{5.40}$$

According to [169], the smoothing factor $m$ introduced in Equations (5.36), (5.37), (5.38) and (5.39) is chosen to satisfy $m = \lceil (N+K)/(N-K) \rceil \iota$, so that the matrix $\mathbf{H}$ becomes a "tall" matrix, i.e. that we have $Nm \geq K(m+\iota)$ and hence the matrix $\mathbf{H}$ has the rank of $K(m+\iota)$.

### 5.2.2.1 Blind Channel Estimation

Following the approach presented in Equation (5.3) of Section 5.2.1, we can express the eigendecomposition of the received signal's autocorrelation matrix $\mathbf{R}$ as

$$\begin{aligned} \mathbf{R} &= E\{\mathbf{r}[i]\mathbf{r}[i]^H\} = \mathbf{H}\mathbf{H}^H + \sigma^2\mathbf{I}_{Nm} \\ &= \mathbf{U}\mathbf{\Lambda}\mathbf{U}^H = [\mathbf{U}_s \ \mathbf{U}_n] \begin{bmatrix} \mathbf{\Lambda}_s & 0 \\ 0 & \mathbf{\Lambda}_n \end{bmatrix} \begin{bmatrix} \mathbf{U}_s^H \\ \mathbf{U}_n^H \end{bmatrix}, \end{aligned} \tag{5.41}$$

where we have $\mathbf{U} = [\mathbf{U}_s \ \mathbf{U}_n]$, $\mathbf{\Lambda} = \text{diag}(\mathbf{\Lambda}_s, \mathbf{\Lambda}_n)$. Since the matrix $\mathbf{H}$ has the full column rank of $r = K(m+\iota)$, the matrix $\mathbf{H}\mathbf{H}^H$ in (5.41) also has a rank of $r$. Therefore, in (5.41) $\mathbf{\Lambda}_s = \text{diag}\{\lambda_1, \dots, \lambda_{K(m+\iota)}\}$ contains the largest $K(m+\iota)$ number of eigenvalues of the matrix $\mathbf{R}$, which

are strictly larger than $\sigma^2$. The column space of the eigenvectors $\mathbf{U}_s = [\mathbf{u}_1, \ldots, \mathbf{u}_{K(m+\iota)}]$, which correspond to the largest $K(m+\iota)$ number of eigenvalues, is referred to as the *signal space*, while the *noise space* is spanned by the columns of $\mathbf{U}_n = [\mathbf{u}_{K(m+\iota)+1}, \ldots, \mathbf{u}_{Nm}]$ which contain the $[Nm - K(m+\iota)]$ orthogonal eigenvectors corresponding to the smallest eigenvalues of $\sigma^2$ in $\mathbf{\Lambda}_n$. Physically, Equation (5.41) suggests that the received signal's autocorrelation matrix $\mathbf{R}$ may be diagonalized by a unitary matrix $\mathbf{U}$ to a diagonal matrix $\mathbf{\Lambda}$, where the entries are the eigenvalues of $\mathbf{R}$. Furthermore, Equation (5.41) has a form similar to (5.3), except that the composite signature waveform matrix $\mathbf{H}$ that is contributed by the spreading code matrix $\mathbf{C}_k$ and the channel response $\mathbf{h}_k$ is used in (5.41).

Define $\mathbf{1}_l$ as a $K(m+\iota)$-dimensional vector having all-zero elements, except for the $l$th element, which is one, and $\bar{\mathbf{h}}_k = \mathbf{H}\mathbf{1}_{K\iota+k}$, which is the column space of $\mathbf{H}$. Based on the assumption that the channel dispersion is limited to the delay range of $[0, (\iota_k + 1)T]$, $\bar{\mathbf{h}}_k$ can be expressed as the product of the spreading code matrix $\mathbf{C}_k$ and the channel response $\mathbf{h}_k$, which physically corresponds to their convolution given by

$$\bar{\mathbf{h}}_k = \underbrace{\mathbf{C}_k}_{Nm\times\iota N}\underbrace{\mathbf{h}_k}_{\iota N\times 1} = \begin{bmatrix} c_k[0] & & \\ c_k[1] & \ddots & \\ \vdots & \ddots & c_k[0] \\ \vdots & \ddots & c_k[1] \\ c_k[N-1] & \ddots & \vdots \\ & & c_k[N-1] \\ \vdots & \vdots & \vdots \end{bmatrix} \begin{bmatrix} h_k[0] \\ \vdots \\ h_k[\iota N] \end{bmatrix}, \tag{5.42}$$

where we have

$$\underbrace{\mathbf{C}_k}_{2N\times N} = \begin{bmatrix} c_k[0] & & \\ c_k[1] & \ddots & \\ \vdots & \ddots & c_k[0] \\ \vdots & \ddots & c_k[1] \\ c_k[N-1] & \ddots & \vdots \\ & & c_k[N-1] \end{bmatrix} \tag{5.43}$$

for the case of $m = 2, \iota = 1$.

The channel response $\mathbf{h}_k$ can be estimated by exploiting the orthogonality between the signal subspace and the noise space as shown in [2, 169]. More specifically, $\mathbf{U}_n$ is orthogonal to the column space of $\mathbf{H}$ and $\bar{\mathbf{h}}_k$ represents the column space of $\mathbf{H}$ [2, 169]. Hence we have

$$\mathbf{U}_n^H \bar{\mathbf{h}}_k = \mathbf{U}_n^H \mathbf{C}_k \mathbf{h}_k = 0. \tag{5.44}$$

As shown in [2, 169], an estimate of the channel response $\mathbf{h}_k$ can be generated by computing the minimum eigenvector of the matrix $\mathbf{C}_k^H \mathbf{U}_n \mathbf{U}_n^H \mathbf{C}_k$. Note that the minimum eigenvector in this chapter

is referred to as the eigenvector corresponding to the minimum eigenvalue. A necessary condition for such a channel estimate to be unique is that the rank of the matrix $\mathbf{U}_n^H \mathbf{C}_k$ is higher than $\iota N$ [169]. Since the rank of this matrix can be expressed as $\min\{Nm - K(m+\iota), \iota N\}$, value of the smoothing factor $m$ defined in Equation (5.36) must be chosen to satisfy

$$Nm - K(m+\iota) \geq \iota N, \tag{5.45}$$

which implies that the number of stacked received vector components $m$ should be selected as

$$m = \frac{N+K}{N-K}\iota. \tag{5.46}$$

Similarly, the maximum number of users supported must obey

$$K \leq N\frac{m-\iota}{m+\iota}, \tag{5.47}$$

given an arbitrary value of $m$.

Since the estimated channel vector $\mathbf{h}_k$ contains the information of both the delays and complex gains of the multipath channels of the $k$th user, this channel estimation technique requires no other information than the prior knowledge of the spreading waveform and the delay spread, where the latter is typically limited to a single symbol interval in practical CDMA systems.

#### 5.2.2.2 Decorrelating Detector and Linear MMSE Detector

In the context of DS-CDMA systems communicating over dispersive channels, the linear MUD's $Nm$-dimensional weight vector $\mathbf{w}_k \in \mathcal{R}^{Nm}$ optimized for the $k$th user is applied to the received signal $\mathbf{r}[i]$ expressed in (5.40), yielding the estimate of the $i$th bit of the $k$th user

$$\hat{b}_k[i] = \text{sgn}\{\Re(\mathbf{w}_k^H \mathbf{r}[i])\}. \tag{5.48}$$

The decorrelating detector's $Nm$-dimensional weight vector $\mathbf{w}_k = \mathbf{d}_k$ optimized for the $k$th user completely eliminates both the MAI and ISI, yielding $\mathbf{d}_k^H \mathbf{H} = 1_{K\iota+k}^T$. Hence, the decorrelating detector's weight vector $\mathbf{d}_k$ can be expressed as

$$\mathbf{d}_k = \mathbf{H}(\mathbf{H}^H \mathbf{H})^{-1} 1_{K\iota+k}. \tag{5.49}$$

Once we obtained the subspace parameters $\mathbf{U}_s, \mathbf{\Lambda}_s$ and $\sigma^2$ from the eigendecomposition of $\mathbf{R}$ in (5.41), as well as the composite signature waveform $\bar{\mathbf{h}}_k$ by performing blind channel estimation as described in Section 5.2.2.1, the weight vector $\mathbf{d}_k$ of the decorrelating detector can be expressed as [2]

$$\mathbf{d}_k = \mathbf{U}_s(\mathbf{\Lambda}_s - \sigma^2 \mathbf{I}_r)^{-1} \mathbf{U}_s^H \bar{\mathbf{h}}_k. \tag{5.50}$$

The linear MMSE detector's weight vector of $\mathbf{w}_k = \mathbf{m}_k$ optimized for the $k$th user is determined

by minimizing the MSE at its output, which is formulated as

$$\mathbf{m}_k = \arg \min_{\mathbf{w} \in \mathcal{R}^{Nm}} E\{|b_k[i] - \mathbf{w}^H \mathbf{r}[i]|^2\} = \mathbf{R}^{-1} \bar{\mathbf{h}}_k. \tag{5.51}$$

Similar to the decorrelating detector, the linear MMSE detector $\mathbf{m}_k$ can be expressed in terms of the signal subspace components as [2]

$$\mathbf{m}_k = \mathbf{U}_s \mathbf{\Lambda}_s^{-1} \mathbf{U}_s^H \bar{\mathbf{h}}_k. \tag{5.52}$$

Physically, Equations (5.50) and (5.52) show that the projection of the decorrelating detector's weight vector $\mathbf{d}_k$ and the linear MMSE detector's weight vector $\mathbf{m}_k$ in the signal subspace $\mathbf{U}_s$ is obtained by projecting the desired user's composite signature waveform $\bar{\mathbf{h}}_k$ onto the signal subspace $\mathbf{U}_s$, followed by scaling the $r'$th component of this projection by a factor of $(\lambda_{r'} - \sigma^2)^{-1}, 1 \leq r' \leq r$ for the decorrelating detector and $\lambda_{r'}^{-1}, 1 \leq r' \leq r$ for the linear MMSE detector, respectively. In contrast to Equations (5.17) and (5.19), where the signature waveform $\mathbf{c}_1$ is used, Equations (5.50) and (5.52) employ the composite signature waveform $\bar{\mathbf{h}}_k$ that is contributed by the spreading code matrix $\mathbf{C}_k$ and the estimate of the CIR $\mathbf{h}_k$.

Since both the signal subspace components $\mathbf{U}_s$, $\mathbf{\Lambda}_s$, $\sigma^2$ and the composite signature waveform $\bar{\mathbf{h}}_k$ can be estimated from the received signal $\mathbf{r}[i]$ using the procedures outlined in Section 5.2.2.1 and require only limited prior knowledge, namely that of the spreading sequence of the $k$th user, both the decorrelating detector (5.50) and the linear MMSE detector (5.52) are capable of operating blindly.

#### 5.2.2.3 Group-Blind Multiuser Detection

In [169] a range of group-blind techniques were developed for multiuser detection in the CDMA uplink, where the base station receiver has explicit knowledge of the spreading sequences of all the users within the serving cell, but not that of the users from other cells. It has been demonstrated that the proposed group-blind MUD substantially outperformed the totally blind MUD in a CDMA uplink environment at the cost of a moderate increase in the computational complexity imposed [169]. In contrast to the blind multiuser detection scheme discussed in Sections 5.2.1.1 and 5.2.1.2, where only the knowledge of the desired user's signature waveform and timing was exploited, the group-blind MUDs of [169, 220] make use of the known spreading sequences of all users roaming in the serving cell in order to suppress the intracell interference, while blindly suppressing the intercell interference. Several forms of group-blind linear detectors may be developed based on different optimization criteria, such as the group-blind linear zero-forcing detector-form I [169], the group-blind linear hybrid detector-form I [169], the group-blind linear MMSE detector-form I [169], the group-blind linear zero-forcing detector-form II [169], the group-blind linear hybrid detector-form II [169] and the group-blind linear MMSE detector-form II [169]. Their derivation and the related proofs are detailed in [169]. Based on the conclusion that the form II group-blind linear hybrid detectors exhibit a low computational complexity and a good performance [169], we only consider this form of group-blind MUD in our investigations. Furthermore, we will show that this form of

group-blind MUD requires a slight modification of the blind MUDs of Sections 5.2.1.1 and 5.2.1.2.

We assume that the receiver has the knowledge of the signature waveforms of the first $\tilde{K}(\tilde{K} \leq K)$ users communicating within the cell of the reference user, whereas the spreading sequences of the $(K - \tilde{K})$ intercell users are unknown to the receiver. Let us define $\tilde{\mathbf{H}} \in \mathcal{R}^{Nm \times \tilde{r}}$ as the matrix consisting of the first $\tilde{r}$ columns of $\mathbf{H}$, where $\tilde{r} = \tilde{K}(m + \iota)$ represents the dimension of the subspace of the intracell users. It is readily seen that the matrix $\tilde{\mathbf{H}}$ has a full column rank of $\tilde{r}$. The linear group-blind hybrid detector of user $k$, $k = 1, \ldots, \tilde{K}$ is given by the solution of the following constrained optimization problem [169]:

$$\begin{aligned} \bar{\mathbf{w}}_k &= \arg \min_{\mathbf{w}_k \in range(\bar{\mathbf{H}})} E\{|b_k[i] - \mathbf{w}_k^H \mathbf{r}[i]|^2\}, \\ &\quad \text{subject to } \mathbf{w}_k^H \tilde{\mathbf{H}} = 1_{\tilde{K}\iota+k}^T, \quad k = 1, \ldots, \tilde{K}. \end{aligned} \tag{5.53}$$

Generally speaking, this detector forces the interference caused by the $\tilde{K}$ intracell users to zero and suppresses the interference imposed by the intercell users with the aid of the MMSE criterion.

By applying the Lagrange multiplier based optimization of [169] to (5.53), we arrive at

$$\begin{aligned} \bar{\mathbf{w}}_k &= \arg \min_{\mathbf{w}_k \in \mathcal{R}^{Nm}} E\{|b_k[i] - \mathbf{w}_k^H \mathbf{r}[i]|^2\} + \Re\{\tilde{\underline{\lambda}}^H (\tilde{\mathbf{H}}^H \mathbf{w}_k - 1_{\tilde{K}\iota+k})\} \\ &= \arg \min_{\mathbf{w}_k \in \mathcal{R}^{Nm}} \mathbf{w}_k^H \mathbf{R} \mathbf{w}_k - \Re\{2\bar{\mathbf{h}}_k^H \mathbf{w}_k\} + \Re\{\tilde{\underline{\lambda}}^H (\tilde{\mathbf{H}}^H \mathbf{w}_k - 1_{\tilde{K}\iota+k})\} \\ &= \arg \min_{\mathbf{w}_k \in \mathcal{R}^{Nm}} \mathbf{w}_k^H \mathbf{R} \mathbf{w}_k + \Re\{\underline{\lambda}^H (\tilde{\mathbf{H}}^H \mathbf{w}_k - 1_{\tilde{K}\iota+k})\} \\ &= \mathbf{R}^{-1} \tilde{\mathbf{H}} \underline{\lambda}, \end{aligned} \tag{5.54}$$

where we have $\underline{\lambda} \triangleq \tilde{\underline{\lambda}} - 21_{\tilde{K}\iota+k}$. Based on the constraint that $\tilde{\mathbf{H}}^H \bar{\mathbf{w}}_k = 1_{\tilde{K}\iota+k}$, we obtain $\underline{\lambda} = (\tilde{\mathbf{H}}^H \mathbf{R}^{-1} \tilde{\mathbf{H}})^{-1} 1_{\tilde{K}\iota+k}$ and hence

$$\begin{aligned} \bar{\mathbf{w}}_k &= \mathbf{R}^{-1} \tilde{\mathbf{H}} (\tilde{\mathbf{H}}^H \mathbf{R}^{-1} \tilde{\mathbf{H}})^{-1} 1_{\tilde{K}\iota+k} \\ &= \mathbf{U}_s \mathbf{\Lambda}_s^{-1} \mathbf{U}_s^H \tilde{\mathbf{H}} (\tilde{\mathbf{H}}^H \mathbf{U}_s \mathbf{\Lambda}_s^{-1} \mathbf{U}_s^H \tilde{\mathbf{H}})^{-1} 1_{\tilde{K}\iota+k} \end{aligned} \tag{5.55}$$

where the second equality follows from (5.41) and $\mathbf{U}_n^H \tilde{\mathbf{H}} = \mathbf{0}$. For the group-blind hybrid detector of (5.55), the interfering signals arriving from known users are nulled by a projection of the received signal onto the orthogonal subspace of these users' signal subspace. The unknown interfering users' signals are suppressed by identifying the subspace spanned by these users, followed by a linear transformation in this subspace based on the MMSE criterion.

As seen in Figure 5.1, the subspace parameters $\mathbf{U}_s, \mathbf{\Lambda}_s, \mathbf{U}_n$ and $\sigma^2$ are obtained by computing the EVD of the received signal's autocorrelation matrix $\mathbf{R} = \frac{1}{M_F} \sum_{i=0}^{M_F - 1} \mathbf{r}[i]\mathbf{r}[i]^H$, followed by carrying out the blind channel estimation according to $\tilde{\mathbf{h}}_k = \text{min-eigenvector}(\mathbf{C}_k^H \mathbf{U}_n \mathbf{U}_n^H \mathbf{C}_k)$ and $\bar{\mathbf{h}}_k = \mathbf{C}_k \tilde{\mathbf{h}}_k$, $k = 1 \ldots \tilde{K}$. Then the estimate of the composite signature waveform matrix $\tilde{\mathbf{H}}$ is generated by using $\bar{\mathbf{h}}_k$, $k = 1 \ldots \tilde{K}$. Finally, we arrive at the blind and group-blind MUDs according to (5.50), (5.52) and (5.55) based on the subspace parameters $\mathbf{U}_s, \mathbf{\Lambda}_s, \sigma^2$ and the estimate of the composite signature waveform matrix $\tilde{\mathbf{H}}$.

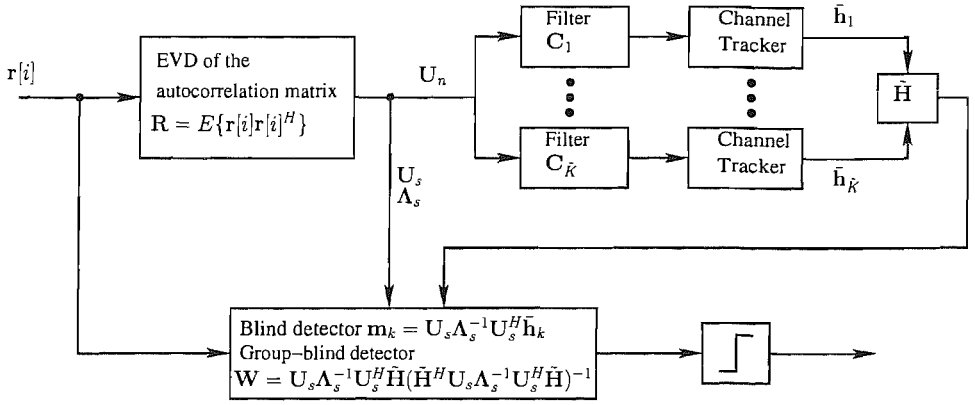


**Figure 5.1:** Subspace-based blind and group-blind receiver structure.

### 5.2.3 Blind and Group-Blind Multiuser Detection for the MC-CDMA Uplink

In this section, we extend our investigations and develop subspace-based blind MUDs for the uplink of MC-CDMA systems, where $K$ number of users are supported. The first $\tilde{K}(\tilde{K} \leq K)$ users are within the reference cell, while the spreading sequences of the $(K-\tilde{K})$ intercell users are unknown to the receiver. Without loss of generality, BPSK modulation is invoked in this section. The modulating symbols of $b_k \in \{-1, +1\}$ having a duration of $T_b$ are first spread using a user-specific frequency-domain spreading sequence $\mathbf{c}_k = [c_{k,0}, c_{k,1}, \ldots, c_{k,V-1}]$ of length $V$, where we have $\mathbf{c}_k \cdot \mathbf{c}_k^H = 1$. In our investigations we assume that OFDM using $V$ subcarriers was invoked [9], where $V$ consecutive chips of the MC-CDMA frequency-domain spreading sequences were mapped to $V$ different subcarriers during an OFDM symbol and hence the OFDM symbol duration was $T_s = T_b$. The spread OFDM symbol-vector of $V$ subcarriers can be expressed as $\mathbf{s}_k = \mathbf{c}_k b_k = [s_1, s_2, \ldots s_V]$. The Inverse Fast Fourier Transform (IFFT) is then invoked for modulating the $V$ subcarriers by using the spread OFDM symbol-vector $\mathbf{s}_k$ [9]. The output signal of the IFFT-based demodulator is a block of $V$ number of time domain samples generated in a parallel form. After Parallel to Serial (P/S) conversion, these time domain signals are transmitted through a multipath fading channel, which is assumed to have $L$ paths. We assume that the CIR encountered is time-invariant during consecutive OFDM symbols, which can be expressed as:

$$h_k(t) = \sum_{l=0}^{L-1} h_{kl}\delta(t - lT_c), \tag{5.56}$$

where $h_{kl}$ is the complex-valued channel gain experienced by the signal of the $k$th user in the $l$th path, which obeys Rayleigh fading, while $T_c = T_s/N$ is the chip-duration. For the sake of compensating for both the asynchronous delay differences of the different users as well as for the delay-spread-induced ISI imposed by the dispersive channel [9], a cyclic prefix of length $(L-1)$ then is inserted in the OFDM symbol prior to transmission.

At the receiver, the time-domain samples of the received signal corresponding to the cyclic prefix

are first removed and $V$-point FFT is invoked for demodulating the remaining $V$ samples and generating the demodulated subcarrier signals in the frequency-domain [9]. Consequently, the received signal $\mathbf{r} \in \mathcal{R}^V$ can be expressed in vectorial form as

$$\mathbf{r} = \sum_{k=1}^{K} \mathbf{C}_k \mathbf{H}_k b_k + \mathbf{n} = \mathbf{G}\mathbf{b} + \mathbf{n}, \tag{5.57}$$

where $\mathbf{H}_k = [H_{k0}, H_{k1}, \ldots, H_{k(V-1)}]^T$ denotes the Frequency-Domain Channel Transfer Function (FDCTF), and $\mathbf{C}_k = diag\{\mathbf{c}_k\}$. The matrix $\mathbf{G}$ in (5.57) is an $(V \times K)$-dimensional matrix comprising both the channel's complex-valued frequency-domain fading factors and the frequency domain spreading signatures of all the $K$ users, hence we have $\mathbf{G} = [\mathbf{g}_1, \mathbf{g}_2, \ldots, \mathbf{g}_K]$, where the effective Frequency Domain (FD) signature waveform of the $k$th user becomes $\mathbf{g}_k = \mathbf{C}_k \mathbf{H}_k$. More explicitly, the effective FD signature waveform is the product of their signature waveform and their FDCTF. Furthermore, the vector $\mathbf{b} = [b_1, b_2, \ldots, b_K]^T$ is the transmitted BPSK data vector and $\mathbf{n}$ is the AWGN vector having a covariance matrix of $\sigma^2 \mathbf{I}_V$.

Since we assume that a cyclic prefix of length $(L-1)$ was inserted and we have $V \geq L$, each subcarrier experiences flat fading and hence no OFDM ISI is incurred. Therefore, the FDCTF $\mathbf{H}_k$ in (5.57) can be expressed as the $V$-point DFT of $\mathbf{h}_k = [h_{k0}, \ldots, h_{k(L-1)}]^T$. More explicitly, we have $\mathbf{H}_k = \mathbf{F}_L \cdot \mathbf{h}_k$, where $\mathbf{F}_L$ is an $(V \times L)$-dimensional matrix, which is given by the first $L$ columns of the DFT matrix $\mathbf{F}$ formulated as:

$$\mathbf{F} = \begin{pmatrix} 1 & 1 & \ldots & 1 \\ 1 & e^{-j2\pi/V} & \ldots & e^{-j2\pi(V-1)/V} \\ \vdots & \vdots & \ddots & \vdots \\ 1 & e^{-j2\pi(V-1)/V} & \ldots & e^{-j2\pi(V-1)(V-1)/V} \end{pmatrix}. \tag{5.58}$$

#### 5.2.3.1 Blind Channel Estimation

As in Section 5.2.2.1, we commence our investigations of blind channel estimation from the eigenanalysis of the autocorrelation matrix $\mathbf{R}$ of the received MC-CDMA signal vector $\mathbf{r}$ formulated in (5.57). The corresponding eigendecomposition of the autocorrelation matrix $\mathbf{R}$ can be expressed as

$$\begin{aligned} \mathbf{R} &= E\{\mathbf{r}\mathbf{r}^H\} = \mathbf{G}\mathbf{G}^H + \sigma^2 \mathbf{I}_V \\ &= \mathbf{U}_s \mathbf{\Lambda}_s \mathbf{U}_s^H + \sigma^2 \mathbf{U}_n \mathbf{U}_n^H, \end{aligned} \tag{5.59}$$

where the matrix $\mathbf{G}\mathbf{G}^H$ has a rank of $K$, since the matrix $\mathbf{G}$ has a full column rank of $K$. Therefore, $\mathbf{\Lambda}_s = diag(\lambda_1, \lambda_2, \ldots, \lambda_K)$ in (5.59) contains the $K$ largest eigenvalues of $\mathbf{R}$ in descending order, all of which are strictly larger than $\sigma^2$, $\mathbf{U}_s = [\mathbf{u}_1 \ldots \mathbf{u}_K]$ contains the corresponding orthonormal eigenvectors and $\mathbf{U}_n = [\mathbf{u}_{K+1} \ldots \mathbf{u}_V]$ contains the remaining $(V-K)$ number of orthonormal eigenvectors that correspond to the eigenvalue of $\sigma^2$.

Following the approach of Section 5.2.2.1, we estimate the CIR $\mathbf{h}_k$ by exploiting the orthogo-

nality between the signal space and the noise space as suggested in [169]. Since the column space of $\mathbf{G}$ belongs to signal space, the noise space $\mathbf{U}_n$ is orthogonal to the column space of $\mathbf{G}$ [169]. Furthermore $\mathbf{g}_k$ is in the column space of $\mathbf{G}$, therefore we have:

$$\mathbf{U}_n^H \mathbf{g}_k = \mathbf{U}_n^H \mathbf{C}_k \mathbf{H}_k = \mathbf{U}_n^H \mathbf{C}_k \mathbf{F}_L \mathbf{h}_k = 0. \tag{5.60}$$

Hence, we obtain an estimate of the composite CIR $\bar{\mathbf{h}}_k$ by computing the minimum eigenvector of the matrix $(\mathbf{F}_L^H \mathbf{C}_k^H \mathbf{U}_n \mathbf{U}_n^H \mathbf{C}_k \mathbf{F}_L)$. A necessary condition for such a channel estimate to be unique is that the matrix $\mathbf{U}_n^H \mathbf{C}_k \mathbf{F}_L$ has a rank of $L$, which requires this matrix be "tall" [2]. Hence, we have $L \leq V - K$. Furthermore, with the aid of the cyclic prefix, we can remove the phase ambiguity encountered during the blind channel estimation process by using the techniques proposed in [221].

#### 5.2.3.2 Rank Estimation

Based on the estimated eigenvalues $\Lambda = [\lambda_1, \lambda_2, \ldots, \lambda_V]$ of the received signal's autocorrelation matrix $\mathbf{R}$, we can adaptively estimate the rank of the signal space, or equivalently, the number of active users in the system by using information-theoretic criteria such as the Akaike Information Criterion (AIC) [222] or the Minimum Description Length (MDL) Criterion [222]. The quantities invoked in the AIC and MDL Criteria are defined as follows:

$$\text{AIC}(k) \triangleq (V-k)M_F \cdot \ln\alpha(k) + k(2V-k), \tag{5.61}$$

$$\text{MDL}(k) \triangleq (V-k)M_F \cdot \ln\alpha(k) + \frac{k}{2}(2V-k) \cdot \ln M_F, \tag{5.62}$$

respectively, where $M_F$ is the number of data bits used during the estimation of the number of active users $K$ and is conveniently chosen to be the transmission burst length in our investigations. Furthermore, $\alpha(k)$ in (5.61) and (5.62) is given by [222]

$$\alpha(k) = \frac{(\sum_{i=k+1}^{V} \lambda_i)/(V-k)}{(\Pi_{i=k+1}^{V} \lambda_i)^{1/(V-k)}}, \tag{5.63}$$

which is the ratio of the arithmetic mean to the geometric mean of the smallest $V-k$ eigenvalues. The estimate $\hat{K}$ of the rank $K$ of the signal space is given by that particular value of $k$, which minimizes the quantities outlined in (5.61) or (5.62) [222], which can be expressed as

$$\hat{K} = \arg \min_{0 \leq k \leq V-1} \{\text{AIC}(k)\} \text{ or } \hat{K} = \arg \min_{0 \leq k \leq V-1} \{\text{MDL}(k)\}. \tag{5.64}$$

[2] "The matrix $\mathbf{A}$ is a "tall" matrix, when the number of its rows is higher than that of its columns. For example, when $L \leq V - K$, the matrix $\mathbf{U}_n^H \mathbf{C}_k \mathbf{F}_L$ becomes "tall" and has a rank of $L$."

#### 5.2.3.3 Blind and Group-Blind Multiuser Detection

In order to attain an estimate $\hat{b}_k$ for the bits of the $k$th user, the linear MUD's weight vector $\mathbf{w}_k \in \mathcal{R}^V$ of the $k$th user is applied to the received signal $\mathbf{r}$ formulated in (5.57), yielding

$$\hat{b}_k = \text{sgn}\{\Re(\mathbf{w}_k^H \mathbf{r})\}. \tag{5.65}$$

Given the prior knowledge of the desired user's signature waveform, we attain the decorrelating detector's weight vector $\mathbf{w}_k = \mathbf{d}_k$ as [2]

$$\mathbf{d}_k = \mathbf{U}_s(\mathbf{\Lambda}_s - \sigma^2 \mathbf{I}_K)^{-1} \mathbf{U}_s^H \bar{\mathbf{g}}_k, \tag{5.66}$$

where $\bar{\mathbf{g}}_k = \mathbf{C}_k \mathbf{F}_L \bar{\mathbf{h}}_k$ is the estimate of the composite frequency domain signature waveform of the $k$th user.

Similar to the decorrelating detector outlined in (5.66), the linear MMSE detector's weight vector $\mathbf{w}_k = \mathbf{m}_k$ can be expressed in terms of its signal subspace components and the estimate of the composite frequency domain signature waveform $\bar{\mathbf{g}}_k$ as [2]

$$\mathbf{m}_k = \mathbf{U}_s \mathbf{\Lambda}_s^{-1} \mathbf{U}_s^H \bar{\mathbf{g}}_k, \tag{5.67}$$

which minimizes the following MUD output MSE expression

$$\mathbf{m}_k = \arg \min_{\mathbf{w} \in \mathcal{R}^V} E\{|b_k - \mathbf{w}^H \mathbf{r}|^2\} = \mathbf{R}^{-1} \bar{\mathbf{g}}_k. \tag{5.68}$$

Physically, Equations (5.66) and (5.67) show that the projection of the decorrelating detector's weight vector $\mathbf{d}_k$ and the linear MMSE detector's weight vector $\mathbf{m}_k$ in the signal subspace $\mathbf{U}_s$ is obtained by projecting the desired user's composite signature waveform $\bar{\mathbf{g}}_k$ onto the signal subspace $\mathbf{U}_s$, followed by scaling the $k$th component of this projection by a factor of $(\lambda_k - \sigma^2)^{-1}$ for the decorrelating detector and $\lambda_k^{-1}$ for the linear MMSE detector, respectively. In contrast to Equations (5.17), (5.19), (5.50) and (5.52), Equations (5.66) and (5.67) employ the composite signature waveform $\bar{\mathbf{g}}_k$ that is contributed by the frequency-domain spreading code matrix $\mathbf{C}_k$ and the estimate of the FDCTF $\mathbf{H}_k$.

Furthermore, the so-called form-II linear hybrid group-blind MUD [169] $\bar{\mathbf{w}}_k$, which exploits the knowledge of a group of $\tilde{K}$ composite frequency domain signature waveforms corresponding to $\tilde{K}(\tilde{K} \leq K)$ intracell users, is given by the solution of the following constrained optimization problem [169]

$$\begin{aligned} \bar{\mathbf{w}}_k \quad = \quad & \arg \min_{\mathbf{w}_k \in range(\mathbf{G})} E\{|b_k - \mathbf{w}_k^H \mathbf{r}|^2\}, \\ & \text{subject to} \quad \mathbf{w}_k^H \tilde{\mathbf{G}} = \mathbf{1}_k^T, \quad k = 1, \ldots, \tilde{K}, \end{aligned} \tag{5.69}$$

where $\tilde{\mathbf{G}} = [\bar{\mathbf{g}}_1, \ldots, \bar{\mathbf{g}}_{\tilde{K}}]$ is an $(V \times \tilde{K})$-dimensional matrix comprising the CIRs and the spreading signature waveforms of all the $\tilde{K}$ intracell users. Observe from (5.69) that this detector forces the interference caused by the $\tilde{K}$ intracell users to zero and suppresses the interference imposed by the

intercell users with the aid of the MMSE criterion. Applying the method of Lagrange multipliers to (5.69), we finally arrive at the form-II linear hybrid group-blind MUD's weight vector, which is formulated as [169]

$$\bar{\mathbf{w}}_k = \mathbf{U}_s \mathbf{\Lambda}_s^{-1} \mathbf{U}_s^H \tilde{\mathbf{G}} (\tilde{\mathbf{G}}^H \mathbf{U}_s \mathbf{\Lambda}_s^{-1} \mathbf{U}_s^H \tilde{\mathbf{G}})^{-1} \mathbf{1}_k. \tag{5.70}$$

The blind multiuser detection and the group-blind multiuser detection algorithms invoked for an MC-CDMA system communicating over a dispersive AWGN channel are summarized in Table 5.1.

| The received signals<br>$\mathbf{X} = [\mathbf{r}_1, \mathbf{r}_2, \ldots, \mathbf{r}_{M_F}]$ |
|---|
| 1. Compute the sample autocorrelation<br>$\mathbf{R} = \frac{1}{M_F} \mathbf{X}\mathbf{X}^H$; |
| 2. Compute the eigen-decomposition of<br>$\mathbf{R} = \mathbf{U}_s \mathbf{\Lambda}_s \mathbf{U}_s^H + \sigma^2 \mathbf{U}_n \mathbf{U}_n^H$; |
| 3. Rank Estimation<br>$\hat{K} = \arg \min_{0 \le k \le V-1} \{\text{AIC}(k)\}$ or<br>$\hat{K} = \arg \min_{0 \le k \le V-1} \{\text{MDL}(k)\}$; |
| 4. Blind Channel Estimation<br>$\bar{\mathbf{h}}_k = \text{min-eigenvector}(\mathbf{F}_L^H \mathbf{C}_k^H \mathbf{U}_n \mathbf{U}_n^H \mathbf{C}_k \mathbf{F}_L)$<br>$\tilde{\mathbf{g}}_k = \mathbf{C}_k \mathbf{F}_L \bar{\mathbf{h}}_k, \ k = 1 \ldots \tilde{K}$,<br>generating $\tilde{\mathbf{G}}$ using $(\tilde{\mathbf{g}}_1, \ldots, \tilde{\mathbf{g}}_{\tilde{K}})$; |
| 5. Form the detectors according to<br>(5.66), (5.67) and (5.70); |

**Table 5.1:** Summary of the blind and group-blind MC-CDMA MUDs communicating over a dispersive AWGN channel [2, 169].

### 5.2.4 Subspace Tracking Algorithms

#### 5.2.4.1 Eigenvalue Decomposition and Singular Value Decomposition

The EVD decomposes a square-shaped matrix into an orthogonal matrix constituted by its eigenvectors and a diagonal matrix containing its eigenvalues. In our investigations, the EVD is invoked for decomposing the autocorrelation matrix $\mathbf{R}$ of the superimposed received signals $\mathbf{r}$. Based on $M_F$ number of received samples $\mathbf{r}_i \in \mathcal{R}^N, i = 1, \ldots M_F$, the corresponding autocorrelation matrix $\mathbf{R}$ can be estimated as

$$\mathbf{R} = \frac{1}{M_F} \sum_{i=1}^{M_F} \mathbf{r}_i \mathbf{r}_i^H. \tag{5.71}$$

As shown in Equations (5.3), (5.41) and (5.59), the eigen-decomposition of the autocorrelation matrix can be expressed as $\text{EVD}(\mathbf{R}) = \mathbf{U}\Lambda\mathbf{U}^T$, where the diagonal matrix $\Lambda$ contains the eigenvalues and

the matrix $\mathbf{U}$ is constituted by the corresponding eigenvectors. The eigenvectors corresponding to the largest $K$ eigenvalues and eigenvectors span the corresponding *signal subspace*.

The SVD is another decomposition technique, which is typically invoked for decomposing a non-square matrix. For the received signal matrix $\mathbf{X} = \frac{1}{\sqrt{M_F}}[\mathbf{r}_1, \ldots, \mathbf{r}_{M_F}]$, which is constituted by the $M_F$ number of multiuser received signal sample vectors $\mathbf{r}_i \in \mathcal{R}^N, i = 1, \ldots M_F$ and $N$ is the number of samples in one received signal vector, the corresponding SVD can be expressed as $\text{SVD}(\mathbf{X}) = \mathbf{V}\Lambda\mathbf{U}^T$, where again, $\mathbf{U}$ is constituted by the eigenvectors and $\Lambda$ is related to the eigenvalues of the matrix $\mathbf{X}\mathbf{X}^H$.

However, carrying out the EVD and the SVD in the context of adaptive applications is computationally expensive, since the number of operations to be carried out at each update is on the order of $O(N^3)$. Hence in the forthcoming section, low-complexity algorithms will be introduced, which aim for directly tracking the components of the EVD, rather than having to carry out the EVD for each block of the received signal samples.

#### 5.2.4.2 PASTd Algorithm [3]

The classic approach to subspace based channel and/or data estimation is centered around the above-mentioned EVD of the sample autocorrelation matrix $\mathbf{R}$, or the SVD of the data matrix $\mathbf{X}$. However, again, both the EVD and the SVD exhibit a high complexity, since the number of operations to be carried out is on the order of $O(N^3)$, which becomes particularly problematic in agile adaptive applications. In practical applications, we are interested in efficient subspace tracking algorithms, which are capable of recursively updating the subspace on a sample-by-sample fashion. Various subspace tracking algorithms have been proposed in the literature [3, 223–227]. The Projection Approximation Subspace Tracking deflation (PASTd) algorithm [1, 3] was first proposed by Yang for the sake of recursively tracking the signal subspace. The advantage of this algorithm includes almost guaranteed global convergence to the true eigenvectors and eigenvalues of the received signal, a low computational complexity, which is on the order of $O(N \cdot K)$, where $N$ is the dimension of the received signal sample space $\mathbf{r}(t)$ and $K$ is the number of eigencomponents to be updated. Furthermore, based on the estimated eigenvalues, the rank of the signal subspace can be estimated adaptively by using the AIC or MDL criterion [228], which directly gives the number of users supported.

The PASTd algorithm of [1, 3] designed for signal subspace tracking is summarized in Table 5.2, where $\mathbf{r}(n)$ is the $n$th $K$-component received signal sample vector, while $\lambda_k(n)$ and $\mathbf{u}_k(n)$ represent the $k$th eigenvalue and $k$th eigenvector at the $n$th time instant, and finally, $\sigma^2(n)$ is the noise vector recorded at the $n$th time instant. Table 5.2 summarizes the operations of the PASTd algorithm, which is based on the so-called deflation technique [3] and its basic philosophy is that of the sequential estimation of the so-called principal components [3]. The most dominant eigenvector is updated first by applying the PAST algorithm at 1st iteration [3]. Then the projection of the current signal sample vector $\mathbf{r}(n)$ onto this eigenvector is removed from $\mathbf{r}(n)$ itself. Now the second most dominant eigenvector becomes the most dominant one in the updated signal sample vector and can be extracted in the same way as before. This procedure is applied repeatedly, until all desired eigencomponents

have been estimated.

| Operation procedure of PASTd algorithm<br>Updating the eigenvalues and eigenvectors of signal space $\lambda_k, \mathbf{u}_k$. |
|---|
| $\mathbf{x}_1(n) = \mathbf{r}(n)$ |
| FOR $k = 1 : K$ DO |
| $y_k(n) = \mathbf{u}_k^H(n-1)\mathbf{x}_k(n)$; projection operation |
| $\lambda_k(n) = \beta\lambda_k(n-1) + \lvert y_k(n)\rvert^2$; updating eigenvalue |
| $\mathbf{u}_k(n) = \mathbf{u}_k(n-1) + \frac{[\mathbf{x}_k(n) - \mathbf{u}_k(n-1)y_k(n)]y_k^*(n)}{\lambda_k(n)}$; updating eigenvectors |
| $\mathbf{x}_{k+1}(n) = \mathbf{x}_k(n) - \mathbf{u}_k(n)y_k(n)$; |
| END |
| $\sigma^2(n) = \beta\sigma^2(n-1) + \frac{\lVert\mathbf{x}_{K+1}(n)\rVert^2}{N-K}$; updating noise variance |

**Table 5.2:** The PASTd algorithm designed for tracking the signal subspace components of the received signal vector $\mathbf{r}$.

### 5.2.4.3 NAHJ-FST Algorithm [4]

As described in Section 5.2.4.2, the PASTd algorithm uses the iterative deflation technique of [3] for sequentially estimating the principal components, starting with the largest eigenvalues and eigenvectors. The accumulation of the roundoff estimation errors imposed by this procedure may however lead to poor estimates of the highly attenuated, low-power signals' eigenvalues and their corresponding eigenvectors. Furthermore, the blind and group-blind MUDs of [1, 2, 169, 220] require the inversion of the signals' eigenvalues, which exacerbates the effect of estimation errors for the low-power signals' eigenvalues, resulting in a degraded output SINR.

In [4], a low-complexity, high-performance subspace tracking algorithm, namely the Noise-Averaged Hermitian-Jacobi Fast Subspace Tracking (NAHJ-FST) algorithm was invoked for adaptive group-blind multiuser detection in asynchronous multipath CDMA channels, which is capable of tracking changes in the number of users and their composite signature waveforms. As in [4], let us denote $\mathbf{R}(l) = [\mathbf{r}(1)\ldots\mathbf{r}(l)]$ as an $(N \times l)$-dimensional matrix, whose columns contain the first $l$ snapshots of the received signal vector, and define the matrix $\mathbf{\Gamma}(l) = diag\{\sqrt{\gamma}^{l-1}, \ldots, \sqrt{\gamma}, 1\}$, where $\gamma$ is the forgetting factor. Then we arrive at the exponentially windowed sample correlation matrix in the form of [4]

$$\begin{aligned}\mathbf{C}(l) &= \frac{1}{M(l)}\mathbf{R}(l)\mathbf{\Gamma}(l)\cdot[\mathbf{R}(l)\mathbf{\Gamma}(l)]^H \\ &= \frac{1}{M(l)}\mathbf{C}'(l),\end{aligned} \tag{5.72}$$

where $M(l) = \frac{1-\gamma^l}{1-\gamma}$ is the effective window length and the EVD of $\mathbf{C}'(l)$ can be expressed as

$$\mathbf{C}'(l) = \mathbf{U}\Lambda\mathbf{U}^T = [\mathbf{U}_s\ \mathbf{U}_n]\begin{bmatrix}\mathbf{\Lambda}_s & 0\\ 0 & \mathbf{\Lambda}_n\end{bmatrix}\begin{bmatrix}\mathbf{U}_s^T\\ \mathbf{U}_n^T\end{bmatrix}. \tag{5.73}$$

The SVD-based subspace tracking algorithms are capable of tracking the SVD of a growing data matrix, recursively defined as [4]

$$\Gamma(l+1)\mathbf{R}^H(l+1) = \begin{bmatrix} \sqrt{\gamma}\Gamma(l)\mathbf{R}^H(l) \\ \mathbf{r}^H(l+1) \end{bmatrix}, \tag{5.74}$$

which may be rewritten as

$$\begin{aligned} \Gamma(\mathrm{l}+\mathbf{1})\mathbf{R}^H(l+1) &= \mathbf{V}(l+1)\mathbf{\Lambda}(l+1)\mathbf{U}^H(l+1) \\ &= \mathbf{V}(l+1)\begin{bmatrix} \mathbf{\Lambda}_s(l+1) & 0 \\ 0 & \mathbf{\Lambda}_n(l+1) \end{bmatrix}\begin{bmatrix} \mathbf{U}_s^H(l+1) \\ \mathbf{U}_n^H(l+1) \end{bmatrix}, \end{aligned} \tag{5.75}$$

where the column space of the matrix $\mathbf{U}_s(l+1)$ corresponds to the signal subspace, $\mathbf{\Lambda}_s(l+1)$ contains the square-root of the corresponding eigenvalues, and $\mathbf{V}(l+1)$ does not have to be tracked. Since calculating the SVD at each iteration is time consuming and expensive, the NAHJ-FST algorithm having a low complexity of $O(NK)$ may be employed to update the eigenvectors $\mathbf{U}_s(l+1)$ and eigenvalues $\Lambda_s(l+1)$ by using the new received sample vector $\mathbf{r}(l+1)$.

First, we project the new sample vector $\mathbf{r}(l+1)$ on to the noise subspace

$$\mathbf{r}_s = \mathbf{U}_s(l)^H\mathbf{r}(l+1), \tag{5.76}$$

then the noise-average vector can be written as

$$\mathbf{u}_n = \frac{\mathbf{r}(l+1) - \mathbf{U}_s(l)\mathbf{r}_s}{\beta}, \tag{5.77}$$

where $\beta = \| \mathbf{r}(l+1) - \mathbf{U}_s(l)\mathbf{r}_s \|$. Then, according to (5.75), (5.76) and (5.77) we attain the SVD operation of the $l+1$ received sample matrix in the form of [4]

$$\begin{bmatrix} \sqrt{\gamma}\Gamma(l)\mathbf{R}^H(l) \\ \mathbf{r}^H(l+1) \end{bmatrix} = \mathbf{V}(l+1)\begin{bmatrix} \sqrt{\gamma}\mathbf{\Lambda}_s(l+1) \\ \mathbf{r}_s \quad \beta \end{bmatrix}\begin{bmatrix} \mathbf{U}_s^H(l+1) \\ \mathbf{u}_n^H(l+1) \end{bmatrix}. \tag{5.78}$$

Based on (5.72) and (5.78), the correlation matrix $\mathbf{C}'(l+1)$ can be written as:

$$\mathbf{C}'(l+1) = \begin{bmatrix} \mathbf{U}_s(l+1) \\ \mathbf{u}_n(l+1) \end{bmatrix}\left(\begin{bmatrix} \gamma\mathbf{\Lambda}_s^2(l) & 0 \\ 0 & \gamma\sigma^2(l) \end{bmatrix} + [[\mathbf{r}_s^H|\beta]^H[\mathbf{r}_s^H|\beta]]\right)\begin{bmatrix} \mathbf{U}_s^H(l+1) \\ \mathbf{u}_n^H(l+1) \end{bmatrix} \tag{5.79}$$

where we have

$$\mathbf{R}_s = \left(\begin{bmatrix} \gamma\mathbf{\Lambda}_s^2(l) & 0 \\ 0 & \gamma\sigma^2(l) \end{bmatrix} + [[\mathbf{r}_s^H|\beta]^H[\mathbf{r}_s^H|\beta]]\right), \tag{5.80}$$

where the matrix $\mathbf{\Lambda}_s^2(l)$ is Hermitian and a strongly diagonal matrix. At each iteration, we directly update $\mathbf{\Lambda}_s^2(l)$ and $\mathbf{U}_s(l)$ of (5.79) by diagonalizing the matrix $\mathbf{R}_s$. The diagonalization of $\mathbf{R}_s$ employs

the well-known symmetric Jacobi SVD algorithm [157], which uses a series of Givens rotations [157] for diagonalizing the matrix $\mathbf{R}_s$. However, we do not perform the full series of $r(r-1)/2$ number of Givens rotations required for the symmetric Jacobi algorithm, only a carefully selected $r$ number of rotations [157]. The reason for this is described as follows. Upon introducing $\mathbf{z} = [\mathbf{r}_s^H|\beta]^H$ and assuming that $i_0$, obeying $1 < i_0 \leq r+1$, is the index of that particular element in $\mathbf{z}$ that has the largest magnitude, we choose to eliminate those elements of $(\mathbf{R}_s)_{i_0,j}$, which are associated with $j = 1 \ldots r+1$, corresponding to $(r+1)$ number of Givens rotations. This suboptimal alternative [4] is implementationally simple but effective, hence the diagonalization of $\mathbf{R}_s$ can be expressed as:

$$\mathbf{R}_a = \Theta_{r+1}^T \ldots \Theta_1^T \mathbf{R}_s \Theta_1 \ldots \Theta_{r+1}, \tag{5.81}$$

where $\Theta$ represents a Givens rotation. Hence the update of $\Lambda_s^2(l+1)$ and $\mathbf{U}_s(l+1)$ can be expressed as:

$$\Lambda_s^2(l+1) = \mathbf{R}_a. \tag{5.82}$$

Then the matrix $\mathbf{U}_s$ can be updated as follows:

$$\begin{bmatrix} \mathbf{U}_s(l+1) \\ \mathbf{u}_n \end{bmatrix} = \begin{bmatrix} \mathbf{U}_s(l) \\ \mathbf{u}_n \end{bmatrix} \Theta_1 \ldots \Theta_{r+1} \tag{5.83}$$

and we re-evaluate the average of the noise power as:

$$\sigma^2(l+1) = \frac{(N-r-1)(\sqrt{\gamma}\sigma^2(l)) + \hat{\sigma}^2}{N-r}, \quad \hat{\sigma}^2 = [\mathbf{R}_a]_{r+1,r+1}. \tag{5.84}$$

The operation of the NAHJ-FST algorithm is summarized in Table 5.3, where $\gamma$ is the forgetting factor.

Finally, the schematic of the adaptive subspace-based blind and group-blind receiver is portrayed in Figure 5.2, where we update the signal subspace components $\mathbf{U}_s[i], \mathbf{\Lambda}_s[i]$ and $\sigma^2[i]$ by using the PASTd algorithm of Section 5.2.4.2 or the NAHJ-FST algorithm of Section 5.2.4.3. Based on the updated signal subspace $\mathbf{U}_s[i]$ and the received signal $\mathbf{r}[i]$, we attain $\mathbf{z}[i]$, the projection of the received signal $\mathbf{r}[i]$ onto the noise space, in the form of [229]

$$\mathbf{z}[i] \triangleq \mathbf{r}[i] - \mathbf{U}_s[i]\mathbf{U}_s[i]^H\mathbf{r}[i] = \mathbf{U}_n[i]\mathbf{U}_n[i]^H\mathbf{r}[i]. \tag{5.85}$$

From (5.85) we may conclude that $\mathbf{z}[i]$ lies in the noise subspace and hence it is orthogonal to any signal in the signal subspace. More explicitly, $\mathbf{z}[i]$ is orthogonal to the composite signature waveform, i.e. we have $\bar{\mathbf{h}}_k[i] = \mathbf{C}_k\tilde{\mathbf{h}}_k[i]$ in (5.42) of Section 5.2.2.1. Hence we arrive at the blind channel estimation procedure formulated as $\tilde{\mathbf{h}}_k[i] = \text{min-eigenvector}(\mathbf{C}_k^H\mathbf{z}[i]\mathbf{z}[i]^H\mathbf{C}_k)$ and $\bar{\mathbf{h}}_k[i] = \mathbf{C}_k\tilde{\mathbf{h}}_k[i]$, $k = 1 \ldots \tilde{K}$. Then the estimate of the composite signature waveform matrix $\tilde{\mathbf{H}}[i]$ is generated by using $\bar{\mathbf{h}}_k[i]$, $k = 1 \ldots \tilde{K}$. Finally, we attain the blind and group-blind MUDs according to (5.50), (5.52) and (5.55) based on the subspace parameters $\mathbf{U}_s[i], \mathbf{\Lambda}_s[i], \sigma^2[i]$ and on the estimate of the composite signature waveform matrix $\tilde{\mathbf{H}}[i]$ at the $i$th iteration.

| Operation procedure of NAHJ-FST algorithm<br>Updating the eigenvalues and eigenvectors of signal space $\mathbf{\Lambda}_s, \mathbf{U}_s$. |
|---|
| 1. Projecting the received signal vector $\mathbf{r}(l+1)$ to signal subspace:<br>$\mathbf{r}_s = \mathbf{U}_s^H(l)\mathbf{r}(l+1)$, Generating $\beta = \|\mathbf{r}(l+1) - \mathbf{U}_s(l)\mathbf{r}_s\|$ and the noise-average vector $\mathbf{u}_n = \frac{\mathbf{r}(l+1)-\mathbf{U}_s(l)\mathbf{r}_s}{\beta}$;<br>2. Generating $\mathbf{R}_s = \left( \begin{bmatrix} \gamma\mathbf{\Lambda}_s^2(l) & 0 \\ 0 & \gamma\sigma^2(l) \end{bmatrix} + [[\mathbf{r}_s^H\|\beta]^H[\mathbf{r}_s^H\|\beta]] \right)$;<br>3. Diagonalizing the matrix $\mathbf{R}_s$ to $\mathbf{R}_a$ with $r+1$ Givens rotations:<br>$\mathbf{R}_a = \Theta_{r+1}^T \ldots \Theta_1^T \mathbf{R}_s \Theta_1 \ldots \Theta_{r+1}$;<br>4. Let $\mathbf{\Lambda}_s(l+1)$ be the diagonal matrix whose diagonal elements is equal to the largest $r$ elements of the diagonal elements of $\mathbf{R}_a$;<br>5. Updating $\mathbf{\Lambda}_s^2(l+1)$ to be the $r+1$ principal submatrix of $\mathbf{R}_a$.<br>6. Updating $\mathbf{U}_s(l+1)$ to be the first $r+1$ columns of<br>$\begin{bmatrix} \mathbf{U}_s(l+1) \\ \mathbf{u}_n \end{bmatrix} = \begin{bmatrix} \mathbf{U}_s(l) \\ \mathbf{u}_n \end{bmatrix} \Theta_1 \ldots \Theta_{r+1}$;<br>7. Reaveraging the noise power: $\sigma^2(l+1) = \frac{(N-r-1)(\sqrt{\gamma}\sigma^2(l))+\hat{\sigma}^2}{N-r}$, where<br>$\hat{\sigma}^2 = [\mathbf{R}_a]_{r+1,r+1}$. |

**Table 5.3:** The NAHJ-FST algorithm for fast tracking the signal subspace components of the received signal vector $\mathbf{r}$.

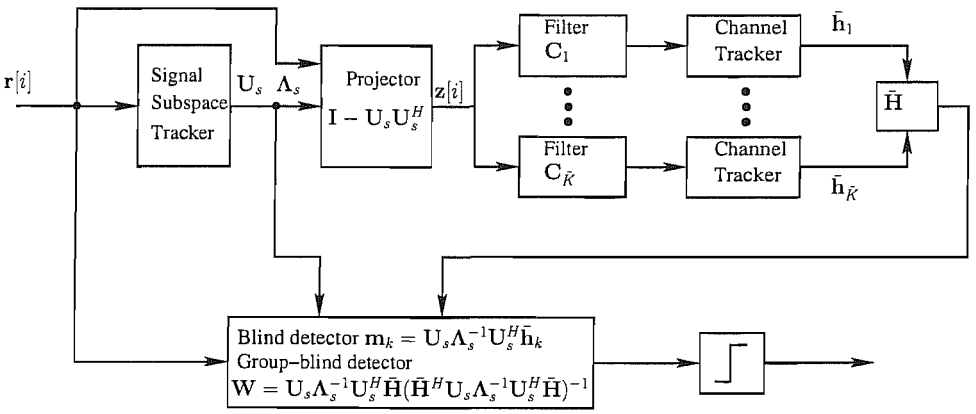


**Figure 5.2:** Adaptive subspace-based blind and group-blind receiver structure.

## 5.3 Subspace-Based Blind and Group-Blind Multiuser Detection for the Generalized MC DS-CDMA Uplink

In this section, we concentrate our investigations on the blind and group-blind multiuser detection invoked for a generalized MC DS-CDMA system, where $K$ simultaneous users are supported and each user modulates the same $V$ subcarriers.

### 5.3.1 System Model

The transmitter of the generalized MC DS-CDMA system is portrayed in Fig.5.3. At the transmitter side, the binary data stream $b_k(t)$ having bit duration $T_b$ is spread using an $N$-chip time domain DS

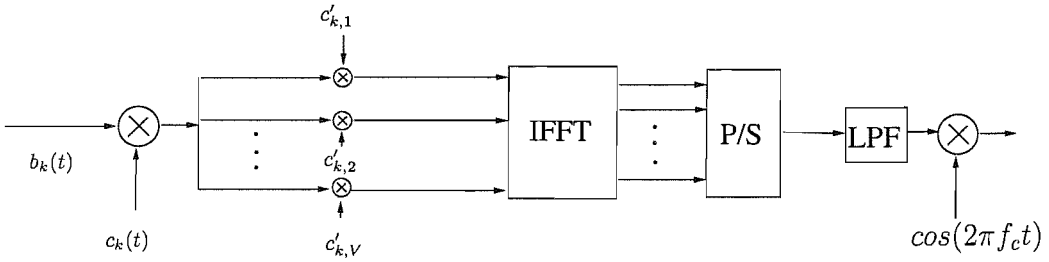


**Figure 5.3:** Transmitter schematic of MC DS-CDMA using both time-domain and frequency-domain spreading

spreading waveform $c_k(t)$. The DS spread signals are simultaneously modulated using BPSK and then spread using a frequency domain orthogonal spreading sequence $\mathbf{c'}_k = [c'_{k,0}, c'_{k,1}, \ldots, c'_{k,V-1}]$ of length $V$, where we have $\mathbf{c'}_k \cdot \mathbf{c'}_k^H = 1$. In this section we assume that OFDM using $V$ subcarriers was invoked [9], where $V$ consecutive chips of the MC DS-CDMA spreading sequences were mapped to $V$ different subcarriers during an OFDM symbol and hence the OFDM symbol duration was $T_c = T_b/N$. The spread OFDM chip-vector of $V$ subcarriers can be expressed as $\mathbf{s}_k(t) = \mathbf{c'}_k b_k(t) c_k(t) = [s_1(t), s_2(t), ..., s_V(t)]$. The IFFT is then invoked for modulating the $V$ subcarriers by using the spread OFDM chip-vector $\mathbf{s}_k(t)$ [9]. The output signal of the IFFT-based demodulator is a block of $V$ number of time domain samples in parallel form. After P/S conversion, a sufficiently long cyclic prefix is inserted in the OFDM symbol for the sake of compensating for the delay-spread-induced ISI imposed by the dispersive channel [9]. Then, these time domain signals are transmitted through a multipath fading channel, which is assumed to have $L$ paths for all the $K$ users. When assuming a time-invariant channel magnitude and phase during consecutive bits, the CIR corresponding to the $k$th user can be expressed as:

$$h_k(t) = \sum_{l=0}^{L-1} h_{kl} \delta(t - lT_{c'}), \tag{5.86}$$

where $h_{kl}$ is the complex channel gain experienced by the signal of the $k$th user in the $l$th path, which obeys Rayleigh fading, while $T_{c'} = \frac{T_b}{NV}$ denotes the OFDM-chip-duration.

At the receiver, the time domain samples of the received signal corresponding to the cyclic prefix are first removed and $V$-point FFT is invoked for demodulating the remaining $V$ samples and for generating the demodulated subcarrier signals in the frequency domain [9]. Consequently, the received signal can be written as $\mathbf{r}(t) = [r_0(t), r_1(t), \ldots, r_{V-1}(t)]^T$,

$$\mathbf{r}(t) = \sum_{k=1}^{K} \mathbf{C'}_k \mathbf{H}_k \sum_{i=0}^{M_F-1} A_k b_k[i] \mathbf{c}_k(t - iT_b - \tau_k) + \mathbf{n}(t) = \mathbf{G}\mathbf{b}(t) + \mathbf{n}(t), \tag{5.87}$$

where $\mathbf{H}_k = [H_{k0}, H_{k1}, \ldots, H_{k(V-1)}]^T$ denotes the FDCTF and $\mathbf{C'}_k = diag\{\mathbf{c'}_k\}$. The matrix $\mathbf{G}$ in (5.87) is a $(V \times K)$-dimensional matrix comprising both the channel's complex-valued frequency domain fading factors and the frequency domain spreading signatures of all the $K$ users, hence we

have $\mathbf{G} = [\mathbf{g}_1, \mathbf{g}_2, \ldots, \mathbf{g}_K]$, where $\mathbf{g}_k = \mathbf{C'}_k\mathbf{H}_k$. In (5.87), the $K$-dimensional vector $\mathbf{b}(t) = [x_1(t), \ldots, x_k(t), \ldots, x_K(t)]^T$ is the data vector and we have $x_k(t) = \sum_{i=0}^{M_F-1} A_k b_k[i]\mathbf{c}_k(t - iT_b - \tau_k)$, where $M_F$ is the length of the transmitted data frame, while $A_k$, $\{b_k[i]\}$ and $0 \leq \tau_k < T_b$ represent the amplitude, symbol stream and the delay of the $k$th user, respectively. The spreading sequence $\mathbf{c}_k(t) = \sum_{j=0}^{N-1} c_k(j)\psi(t - jT_c)$ in (5.87) denotes the signature waveform of the $k$th user, where $c_k(j)$ assumes values of +1 or -1 with equal probability, while $\psi(t)$ is a normalized chip waveform of duration $T_c$. Furthermore, $\mathbf{n}(t)$ is the AWGN vector associated with the covariance matrix of $\sigma^2\mathbf{I}_V$, where $\mathbf{I}_V$ denotes the $(V \times V)$-dimensional identity matrix. Since we assume that a sufficiently long cyclic prefix was inserted and we have $V \geq L$, every subcarrier experiences flat fading and hence no OFDM ISI is incurred. Therefore, the FDCTF $\mathbf{H}_k$ in (5.87) can be expressed as the $V$-point DFT of $\mathbf{h}_k = [h_{k0}, \ldots, h_{k(L-1)}]^T$. More explicitly, we have $\mathbf{H}_k = \mathbf{F}_L \cdot \mathbf{h}_k$, where $\mathbf{F}_L$ is a $(V \times L)$-dimensional matrix defined in (5.58).

A set of $V$ chip-matched filters are used for sampling the received signal $\mathbf{r}(t)$ at a rate of $\frac{1}{T_c}$. Since the delay spread is often assumed to be less than one symbol interval in practical CDMA systems [2], we observe the chip-matched filter outputs for a duration of $2T_b$ so that despite the channel-induced dispersion a complete symbol of the desired user is guaranteed to be observed. Hence the $n$th received signal sample of the $v$th chip-matched filter corresponding to the $v$th subcarrier during the $l$th symbol can be expressed as

$$\begin{aligned} r_v[l,n] &= r_v(lT_b + nT_c) \\ &= \sum_{k=1}^{K} y_{k,v}[l,n] + n_v[l,n], \end{aligned} \tag{5.88}$$

where $n_v[l,n]$ denotes the component due to the AWGN and

$$y_{k,v}[l,n] = A_k H_{kv} c'_{k,v} \sum_{i=0}^{M_F-1} \sum_{j=0}^{N-1} b_k[i]c_k(j)\hat{\psi}((lN + n - j - iN)T_c - \tau_k) \tag{5.89}$$

is the component engendered by the $k$th user's signal. The function $\hat{\psi}(t) = \int_{-\infty}^{\infty} \psi(s)\psi^*(s-t)ds$ in (5.89) represents the of the chip-matched filter.

Let us define

$$\underbrace{\bar{\mathbf{r}}_v[l]}_{2N\times 1} = \begin{bmatrix} r_v[l,0] \\ \vdots \\ r_v[l,2N-1] \end{bmatrix}, \tag{5.90}$$

$$\underbrace{\bar{\mathbf{n}}_v[l]}_{2N\times 1} = \begin{bmatrix} n_v[l,0] \\ \vdots \\ n_v[l,2N-1] \end{bmatrix}, \tag{5.91}$$

$$\underbrace{\bar{\mathbf{y}}_{k,v}[l]}_{2N\times 1} = \begin{bmatrix} y_{k,v}[l,0] \\ \vdots \\ y_{k,v}[l,2N-1] \end{bmatrix}, \tag{5.92}$$

for $v = 0,1,\ldots,V-1$ and $k = 1,2,\ldots,K$. Then, by concatenating these vectors corresponding to the $V$ subcarriers, we obtain the following $2NV$-dimensional vectors, $\mathbf{r}[l] = [\bar{\mathbf{r}}_0^T[l],\bar{\mathbf{r}}_1^T[l],\ldots,\bar{\mathbf{r}}_{V-1}^T[l]]^T$, $\mathbf{n}[l] = [\bar{\mathbf{n}}_0^T[l],\bar{\mathbf{n}}_1^T[l],\ldots,\bar{\mathbf{n}}_{V-1}^T[l]]^T$ and $\mathbf{y}_k[l] = [\bar{\mathbf{y}}_{k,0}^T[l],\bar{\mathbf{y}}_{k,1}^T[l],\ldots,\bar{\mathbf{y}}_{k,V-1}^T[l]]^T$. Hence, (5.88) can be rewritten as

$$\mathbf{r}[l] = \sum_{k=1}^{K} \mathbf{y}_k[l] + \mathbf{n}[l], \tag{5.93}$$

where $\mathbf{n}[l]$ is a zero mean AWGN process having a covariance of $\sigma^2\mathbf{I}_{2NV}$.

Without loss of generality, let $b_k[l]$ represent the bit of the $k$th user that falls completely in the $l$th symbol period and denote the delay of this bit relative to the left edge of the $l$th symbol period by $\tau_k = (n_k+\delta_k)T_c$, which is based on the assumption of $\tau_k \in T_b$, where $n_k$ is an integer between zero and $N-1$, while $\delta_k \in [0,1)$. Let $\mathbf{c}_k = [c_k(0),c_k(1),\ldots,c_k(N-1),\underbrace{0,\ldots,0}_{N}]^T$ denote a vector of length $2N$, consisting of the $N$ elements of the spreading sequence of the $k$th user followed by $N$ zeros. Following the notation in [214], we define $\mathbf{T}_L$ and $\mathbf{T}_R$ as the acyclic left shift operator and the acyclic right shift operator processing vectors of length $2N$, respectively. For example, for a vector $\mathbf{x} = [x_0,\ldots,x_{2N-1}]^T$, we have $\mathbf{T}_L\mathbf{x} = [x_1,\ldots,x_{2N-1},0]^T$ and $\mathbf{T}_R\mathbf{x} = [0,x_0,\ldots,x_{2N-2}]^T$. Then, we use $\mathbf{T}_L^n$ and $\mathbf{T}_R^n$ to denote $n$ applications of these operators, resulting in $n$ left and right shifts, respectively. Based on these operators, we define, for $k = 1,2,\ldots,K$

$$\begin{aligned} \underline{\mathbf{v}}_k^{-1} &= (1-\delta_k)\mathbf{T}_L^{N-n_k}\mathbf{c}_k + \delta_k\mathbf{T}_L^{N-n_k-1}\mathbf{c}_k, \\ \underline{\mathbf{v}}_k^{0} &= (1-\delta_k)\mathbf{T}_R^{n_k}\mathbf{c}_k + \delta_k\mathbf{T}_R^{n_k+1}\mathbf{c}_k, \\ \underline{\mathbf{v}}_k^{1} &= (1-\delta_k)\mathbf{T}_R^{N+n_k}\mathbf{c}_k + \delta_k\mathbf{T}_R^{N+n_k+1}\mathbf{c}_k. \end{aligned} \tag{5.94}$$

For each asynchronous user, three consecutive bit intervals overlap with a given observation interval of length $2T_b$. Furthermore, since the system is chip asynchronous, two adjacent chips contribute to each chip sample. The contribution of the $k$th user $\mathbf{y}_k[l]$ to the received vector $\mathbf{r}[l] \in \mathcal{R}^{2NV}$ in (5.93) for the $l$th symbol is therefore given by

$$\mathbf{y}_k[l] = \mathbf{D}_k(b_k[l-1]\mathbf{v}_k^{-1} + b_k[l]\mathbf{v}_k^{0} + b_k[l+1]\mathbf{v}_k^{1}), \tag{5.95}$$

where $\mathbf{D}_k = \mathrm{diag}\left(\underbrace{A_kH_{k0}c'_{k,0},\ldots,A_kH_{k0}c'_{k,0}}_{2N},\ldots,\underbrace{A_kH_{k(V-1)}c'_{k,V-1},\ldots,A_kH_{k(V-1)}c'_{k,V-1}}_{2N}\right)$,

$\mathbf{v}_k^{-1} = [\underbrace{(\underline{\mathbf{v}}_k^{-1})^T, \ldots, (\underline{\mathbf{v}}_k^{-1})^T}_{V}]^T$, $\mathbf{v}_k^0 = [\underbrace{(\underline{\mathbf{v}}_k^0)^T, \ldots, (\underline{\mathbf{v}}_k^0)^T}_{V}]^T$ and $\mathbf{v}_k^1 = [\underbrace{(\underline{\mathbf{v}}_k^1)^T, \ldots, (\underline{\mathbf{v}}_k^1)^T}_{V}]^T$. Upon substituting (5.95) into (5.93), we arrive at

$$\mathbf{r}[l] = \mathbf{D}_1 b_1[l]\mathbf{v}_1^0 + \sum_{k=2}^{K} \mathbf{D}_k b_k[l]\mathbf{v}_k^0 + \sum_{k=1}^{K} \mathbf{D}_k (b_k[l-1]\mathbf{v}_k^{-1} + b_k[l+1]\mathbf{v}_k^1) + \mathbf{n}[l],$$

which, for notational convenience, can be rewritten as

$$\mathbf{r}[l] = b_1[l]\mathbf{p}_1 + \sum_{j=2}^{J} b_j[l]\mathbf{p}_j + \mathbf{n}[l] \tag{5.96}$$

by using the equivalent synchronous model described in [214], where $b_1[l]$ is the desired bit and $\mathbf{p}_1 = \mathbf{D}_1\mathbf{v}_1^0$, while other vectors correspond to the intersymbol interference and MAI vectors in (5.96). Note that we have $2K \leq J \leq 3K$.

### 5.3.2 Blind Channel Estimation for Generalized MC DS-CDMA

The autocorrelation matrix $\mathbf{R}$ of the received MC DS-CDMA signal vector $\mathbf{r}$ can be expressed as

$$\begin{aligned} \mathbf{R} &= E\{\mathbf{r}\mathbf{r}^H\} = \mathbf{P}\mathbf{P}^H + \sigma^2 I_{2NV} \\ &= \mathbf{U}\mathbf{\Lambda}\mathbf{U}^H = [\mathbf{U}_s \ \mathbf{U}_n] \begin{bmatrix} \mathbf{\Lambda}_s & 0 \\ 0 & \mathbf{\Lambda}_n \end{bmatrix} \begin{bmatrix} \mathbf{U}_s^H \\ \mathbf{U}_n^H \end{bmatrix}, \end{aligned} \tag{5.97}$$

where we have $\mathbf{P} = [\mathbf{p}_1, \ldots, \mathbf{p}_J]$, $\mathbf{U} = [\mathbf{U}_s \ \mathbf{U}_n]$ and $\mathbf{\Lambda} = \text{diag}(\mathbf{\Lambda}_s, \mathbf{\Lambda}_n)$. Without loss of generality, we assume that the vectors $\mathbf{p}_1, \ldots, \mathbf{p}_J$ are linearly independent [173] and that we have $J < 2NV$. Hence, the matrix $\mathbf{P}$ is a "tall" matrix having a rank of $\text{rank}(\mathbf{P}) = \text{rank}(\mathbf{P}\mathbf{P}^H) = J$. Therefore, $\mathbf{\Lambda}_s = \text{diag}\{\lambda_1, \ldots, \lambda_J\}$ in (5.97) contains the largest $J$ eigenvalues of the autocorrelation matrix $\mathbf{R}$, which are strictly larger than $\sigma^2$. The column space of the eigenvectors $\mathbf{U}_s = [\mathbf{u}_1, \ldots, \mathbf{u}_J]$, which correspond to the largest $J$ eigenvalues, is referred to as the *signal space*, while the *noise space* is spanned by the columns of $\mathbf{U}_n = [\mathbf{u}_{J+1}, \ldots, \mathbf{u}_{2NV}]$, which contains the $(2NV - J)$ number of orthogonal eigenvectors corresponding to the smallest eigenvalues $\sigma^2$ in $\mathbf{\Lambda}_n$. Physically, Equation (5.97) suggests that the received signal's autocorrelation matrix $\mathbf{R}$ may be diagonalized by a unitary matrix $\mathbf{U}$ to a diagonal matrix $\mathbf{\Lambda}$, where the entries are the eigenvalues of $\mathbf{R}$. Furthermore, Equation (5.97) has a form similar to (5.3) and (5.41), except that the composite signature waveform matrix $\mathbf{P}$ that is contributed by the T-domain spreading code matrix $\mathbf{V}_k^0$, $\mathbf{V}_k^1$ or $\mathbf{V}_k^{-1}$, F-domain spreading code matrix $\mathbf{C}'_k$ and the FDCTF $\mathbf{H}_k$ is used in (5.97).

As discussed in the context of Equations (5.44) and (5.60) of Sections 5.2.2.1 and 5.2.3.1, the CIR $\mathbf{h}_1$ of the desired user can be estimated by exploiting the orthogonality between the signal subspace and the noise space. Since the matrix $\mathbf{U}_n$ is orthogonal to $\mathbf{p}_1$, we have

$$\mathbf{U}_n^H \mathbf{p}_1 = \mathbf{U}_n^H \mathbf{V}_1^0 \mathbf{d}_1 = A_1 \mathbf{U}_n^H \mathbf{V}_1^0 \mathbf{C}'_1 \mathbf{F}_L \mathbf{h}_1 = 0, \tag{5.98}$$

where

$$\underbrace{\mathbf{V}_1^0}_{2NV\times V} = \begin{bmatrix} \underline{\mathbf{v}}_1^0 & & & \\ & \underline{\mathbf{v}}_1^0 & & \\ & & \ddots & \\ & & & \underline{\mathbf{v}}_1^0 \end{bmatrix} \tag{5.99}$$

and $\mathbf{d}_1 = A_1\mathbf{C'}_1\mathbf{F}_L\mathbf{h}_1 = [A_1H_{10}c'_{1,0}, A_1H_{11}c'_{1,1}, \ldots, A_1H_{1(V-1)}c'_{1,V-1}]^T$.

The estimate $\bar{\mathbf{h}}_1$ of the channel response $\mathbf{h}_1$ can be generated by computing the minimum eigenvector of the matrix $\mathbf{F}_L^H\mathbf{C'}_1^H(\mathbf{V}_1^0)^H\mathbf{U}_n\mathbf{U}_n^H\mathbf{V}_1^0\mathbf{C'}_1\mathbf{F}_L$. Again, the necessary condition for such a channel estimate to be unique is that the rank of the matrix $\mathbf{U}_n^H\mathbf{V}_1^0\mathbf{C'}_1\mathbf{F}_L$ is higher than $L$, which requires that this matrix be tall. Hence, we have $L \leq 2NV - J$. For the worst case scenario of $J = 3K$, a necessary condition imposed on the number of users for the sake of uniquely determining $\mathbf{h}_1$ is then $K \leq \frac{2NV-L}{3}$. Even for the best-case scenario of $J = 2K$, the necessary condition imposed on the number of users is $K \leq \frac{2NV-L}{2}$, which implies that the system considered cannot be fully loaded, i.e. we have $K < NV$. Again, with the aid of the cyclic prefix, we can remove the phase ambiguity encountered in the blind channel estimation process by using the techniques proposed in [221].

If the value of $\tau_1$ is not available, joint timing and channel estimation must be carried out for the desired user, which is summarized as follows:

1) Hypothesize a value for $\tau_1 < T_b$ and construct the matrix $\mathbf{V}_1^0(\tau_1)$ based on this hypothesized value;

2) obtain the best estimate $\bar{\mathbf{h}}_1(\tau_1)$ by computing the minimum eigenvector of the matrix $\mathbf{F}_L^H\mathbf{C'}_1^H(\mathbf{V}_1^0)^H\mathbf{U}_n\mathbf{U}_n^H\mathbf{V}_1^0\mathbf{C'}_1\mathbf{F}_L$ for this value of $\tau_1$;

3) Repeat Steps 1) to 2) for different values of $\tau_1$;

4) Attain the best timing estimate $\bar{\tau}_1$ by solving the minimization problem of [173]

$$\bar{\tau}_1 = \arg\min_{\tau_1\in[0,T_b)} \Omega(\tau_1) = \arg\min_{\tau_1\in[0,T_b)} \frac{\|\mathbf{U}_n^H\mathbf{V}_1^0(\tau_1)\mathbf{C'}_1\mathbf{F}_L\bar{\mathbf{h}}_1(\tau_1)\|^2}{\|\mathbf{V}_1^0(\tau_1)\mathbf{C'}_1\mathbf{F}_L\bar{\mathbf{h}}_1(\tau_1)\|^2}. \tag{5.100}$$

5) Arrive at the best channel estimate $\bar{\mathbf{h}}_1(\bar{\tau}_1)$ based on $\bar{\tau}_1$.

In practice, we have to quantize the infinite number of possible hypothesized values of $\tau_1$ in the interval $[0, T_b)$ to a finite set. In our investigations, the value of $\tau_k$ is normalized to the chip duration $T_c$. Since the optimization problem in (5.100) is one-dimensional, not all choices of the pair $(\tau_1, \mathbf{h}_1)$ are legitimate. The procedure described above leads to the best estimate $\bar{\mathbf{h}}_1(\tau_1)$ for a hypothesized value of $\tau_1$. Therefore, the search space is substantially reduced, rendering the above method more practical. Furthermore, since $\Omega(\tau_1)$ is a continuous function of $\tau_1$, it must have a minimum within the closed interval $[0, T_b)$, which hence guarantees the optimal choice of $\tau_1$ that minimizes the cost function, provided that we search on a sufficiently fine grid.

### 5.3.3 Blind and Group-Blind Multiuser Detection for Generalized MC DS-CDMA

In order to obtain an estimate $\hat{b}_1[l]$ for the $l$th bit of the desired user, the linear MUD weights $\mathbf{w}_1 \in \mathcal{R}^{2NV}$ of the desired user are applied to the received signal $\mathbf{r}[l]$ in (5.96), yielding

$$\hat{b}_1[l] = \text{sgn}\{\Re(\mathbf{w}_1^H \mathbf{r}[l])\}. \tag{5.101}$$

Given the prior knowledge of the desired user's spreading code and timing information, we obtain the decorrelating detector $\mathbf{w}_1 = \mathbf{d}_1$ as

$$\mathbf{d}_1 = \mathbf{U}_s(\mathbf{\Lambda}_s - \sigma^2 \mathbf{I}_J)^{-1} \mathbf{U}_s^H \bar{\mathbf{p}}_1, \tag{5.102}$$

where $\bar{\mathbf{p}}_1 = \mathbf{V}_1^0 \mathbf{C'}_1 \mathbf{F}_L \bar{\mathbf{h}}_1$ is the estimated composite signature waveform of the desired user.

Similar to the decorrelating MUD [169], the linear MMSE MUD weights $\mathbf{w}_1 = \mathbf{m}_1$ can be expressed in terms of the signal subspace components and the estimated composite signature waveform $\bar{\mathbf{p}}_1$ as

$$\mathbf{m}_1 = \mathbf{U}_s \mathbf{\Lambda}_s^{-1} \mathbf{U}_s^H \bar{\mathbf{p}}_1, \tag{5.103}$$

which is obtained by solving the following optimization problem [169]

$$\mathbf{m}_1 = \arg \min_{\mathbf{w} \in \mathcal{R}^{2NV}} E\{|b_1 - \mathbf{w}^H \mathbf{r}|^2\} = \mathbf{R}^{-1} \bar{\mathbf{p}}_1. \tag{5.104}$$

Physically, Equations (5.102) and (5.103) show that the projection of the decorrelating detector's weight vector $\mathbf{d}_1$ and the linear MMSE detector's weight vector $\mathbf{m}_1$ in the signal subspace $\mathbf{U}_s$ is obtained by projecting the desired user's composite signature waveform $\bar{\mathbf{p}}_1$ onto the signal subspace $\mathbf{U}_s$, followed by scaling the $j$th component of this projection by a factor of $(\lambda_j - \sigma^2)^{-1}$ for the decorrelating detector and $\lambda_j^{-1}$ for the linear MMSE detector, respectively. In contrast to Equations (5.50), (5.52), (5.66) and (5.67), Equations (5.102) and (5.103) employ the composite signature waveform $\bar{\mathbf{p}}_1$ that is contributed by the T-domain spreading code matrix $\mathbf{V}_k^0, \mathbf{V}_k^1 or \mathbf{V}_k^{-1}$, F-domain spreading code matrix $\mathbf{C'}_k$ and the FDCTF $\mathbf{H}_k$.

Furthermore, the so-called form-II linear hybrid group-blind MUD $\bar{\mathbf{w}}_1$ [169], which exploits the knowledge of a group of $\tilde{K}$ composite signature waveforms corresponding to $\tilde{K}(\tilde{K} \leq K)$ intracell users, is given by the solution of the following constrained optimization problem [169]

$$\begin{aligned} \bar{\mathbf{w}}_1 \quad = \quad & \arg \min_{\mathbf{w}_1 \in range(\mathbf{P})} E\{|b_1 - \mathbf{w}_1^H \mathbf{r}|^2\}, \\ & \text{subject to} \quad \mathbf{w}_1^H \tilde{\mathbf{P}} = \mathbf{1}_1^T, \end{aligned} \tag{5.105}$$

where $\tilde{\mathbf{P}} = [\bar{\mathbf{p}}_1, \ldots, \bar{\mathbf{p}}_{\tilde{J}}]$ is a $(2NV \times \tilde{J})$-dimensional matrix constructed based on the estimated CIRs, timing information and the spreading signature waveforms of all the $\tilde{K}$ intracell users. Hence we have $2\tilde{K} \leq \tilde{J} \leq 3\tilde{K}$. Again, this detector forces the ISI caused by the desired user and the MAI caused by the $\tilde{K}$ intracell users to zero, while suppressing the interference imposed by the intercell

users with the aid of the MMSE criterion. Using the method of Lagrange multipliers [169] in (5.105), we obtain the form-II linear hybrid group-blind MUD's weight vector in the form of [169]

$$\bar{\mathbf{w}}_1 = \mathbf{U}_s\mathbf{\Lambda}_s^{-1}\mathbf{U}_s^H\tilde{\mathbf{P}}(\tilde{\mathbf{P}}^H\mathbf{U}_s\mathbf{\Lambda}_s^{-1}\mathbf{U}_s^H\tilde{\mathbf{P}})^{-1}\mathbf{1}_1. \tag{5.106}$$

For the group-blind hybrid detector of (5.106), the interfering signals arriving from known users are nulled by a projection of the received signal onto the orthogonal subspace of these users' signal subspace. The unknown interfering users' signals are suppressed by identifying the subspace spanned by these users, followed by a linear transformation in this subspace based on the MMSE criterion.

The blind multiuser detection and the group-blind multiuser detection algorithms invoked for a generalized MC DS-CDMA system communicating over a dispersive AWGN channel are summarized in Table 5.4.

| The received signals<br>$\mathbf{X} = [\mathbf{r}_1, \mathbf{r}_2, \ldots, \mathbf{r}_{M_F}]$ |
|---|
| 1. Compute sample autocorrelation<br>$\mathbf{R} = \frac{1}{M_F}\mathbf{X}\mathbf{X}^H$;<br>2. Compute the eigen-decomposition of<br>$\mathbf{R} = \mathbf{U}_s\mathbf{\Lambda}_s\mathbf{U}_s^H + \sigma^2\mathbf{U}_n\mathbf{U}_n^H$;<br>3. Blind Channel Estimation<br>$\bar{\mathbf{h}}_k = \text{min-eigenvector}(\mathbf{F}_L^H\mathbf{C}'^H_k(\mathbf{V}_k^0)^H\mathbf{U}_n\mathbf{U}_n^H\mathbf{V}_k^0\mathbf{C}'_k\mathbf{F}_L)$<br>$\bar{\mathbf{p}}_k = \mathbf{V}_k^0\mathbf{C}'_k\mathbf{F}_L\bar{\mathbf{h}}_k$ $\bar{\mathbf{p}}_{\tilde{K}+k} = \mathbf{V}_k^1\mathbf{C}'_k\mathbf{F}_L\bar{\mathbf{h}}_k$ $\bar{\mathbf{p}}_{2\tilde{K}+k} = \mathbf{V}_k^{-1}\mathbf{C}'_k\mathbf{F}_L\bar{\mathbf{h}}_k$<br>$k = 1 \ldots \tilde{K}$ when $\tau_k = 0$, we have $\bar{\mathbf{p}}_{2\tilde{K}+k} = \mathbf{0}$.<br>Excluding these zero vectors, we have $2\tilde{K} \leq \tilde{J} \leq 3\tilde{K}$ non-null vectors.<br>form $\tilde{\mathbf{P}}$ using $(\bar{\mathbf{p}}_1, \ldots, \bar{\mathbf{p}}_{\tilde{J}})$;<br>4. Form the detectors according to<br>(5.102), (5.103) and (5.106); |

**Table 5.4:** Summary of the blind and group-blind generalized MC DS-CDMA MUDs communicating over a dispersive AWGN channel.

### 5.3.4 Blind and Group-Blind Space-Time Multiuser Detection for Generalized MC DS-CDMA

In this section, we consider an asynchronous MC DS-CDMA system employing smart antennas. We assume that at the Base-Station (BS) there are $M$ number of receiver antenna elements and the Spatio-Temporal CIR (ST-CIR) $h_{km}(t)$ between the $k$th user and the $m$th Antenna Element (AE) can be expressed as

$$h_{km}(t) = \sum_{l=0}^{L-1} h_{km,l}\delta(t - lT_{c'}), \tag{5.107}$$

where $h_{km,l}$ is the complex channel gain experienced by the signal of the $k$th user in the $l$th path impinging on the $m$th AE, while $L$ and $T_{c'} = \frac{T_b}{NV}$ denote the number of paths and the OFDM-chip-duration for all $K$ users, respectively.

Hence, we can rewrite the received signal as $\mathbf{r}(t) = [\mathbf{r}_0^T(t), \mathbf{r}_1^T(t), \ldots, \mathbf{r}_{M-1}^T(t)]^T$, where $\mathbf{r}_m(t) \in \mathcal{R}^V$ has a similar form to (5.87), which is given by

$$\mathbf{r}_m(t) = \sum_{k=1}^{K} \mathbf{C'}_k \mathbf{H}_{km} \sum_{i=0}^{M_F-1} A_k b_k[i] \mathbf{c}_k(t - iT_b - \tau_k) + \mathbf{n}_m(t), \tag{5.108}$$

and $\mathbf{H}_{km} = [H_{km,0}, H_{km,1}, \ldots, H_{km,V-1}]^T$ denotes the FDCTF between the $k$th user and the $m$th AE, which can be expressed as the $V$-point DFT of $\mathbf{h}_{km} = [h_{km,0}, \ldots, h_{km,L-1}]^T$ in the form of $\mathbf{H}_{km} = \mathbf{F}_L \cdot \mathbf{h}_{km}$. In (5.108), $\mathbf{n}_m(t)$ represents the AWGN vector associated with the covariance matrix of $\sigma^2 \mathbf{I}_V$.

Consequently, the $n$th received signal sample of the $v$th chip-matched filter corresponding to the $m$th AE during the $l$th symbol has the form of

$$\begin{aligned} r_{m,v}[l,n] &= r_{m,v}(lT_b + nT_c) \\ &= \sum_{k=1}^{K} y_{km,v}[l,n] + n_{m,v}[l,n], \end{aligned} \tag{5.109}$$

where $n_{m,v}[l,n]$ is the AWGN component and

$$y_{km,v}[l,n] = A_k H_{km,v} c'_{k,v} \sum_{i=0}^{M_F-1} \sum_{j=0}^{N-1} b_k[i] c_k(j) \hat{\psi}((lN + n - j - iN)T_c - \tau_k)$$

is the component due to the $k$th user's signal received at the $m$th AE. Following the approach described in Section 5.3.1, we concatenate the vectors corresponding to the $M$ AEs and obtain the following $2NVM$-dimensional vectors

$$\mathbf{r}[l] = \Big[\underbrace{\bar{\mathbf{r}}_{00}^T[l], \ldots, \bar{\mathbf{r}}_{(M-1)(V-1)}^T[l]}_{V}, \ldots, \underbrace{\bar{\mathbf{r}}_{(M-1)0}^T[l], \ldots, \bar{\mathbf{r}}_{(M-1)(V-1)}^T[l]}_{V}\Big]^T,$$

$$\mathbf{n}[l] = \Big[\underbrace{\bar{\mathbf{n}}_{00}^T[l], \ldots, \bar{\mathbf{n}}_{(M-1)(V-1)}^T[l]}_{V}, \ldots, \underbrace{\bar{\mathbf{n}}_{(M-1)0}^T[l], \ldots, \bar{\mathbf{n}}_{(M-1)(V-1)}^T[l]}_{V}\Big]^T \quad \text{and}$$

$$\mathbf{y}_k[l] = \Big[\underbrace{\bar{\mathbf{y}}_{k0,0}^T[l], \ldots, \bar{\mathbf{y}}_{k(M-1),V-1}^T[l]}_{V}, \ldots, \underbrace{\bar{\mathbf{y}}_{k(M-1),0}^T[l], \ldots, \bar{\mathbf{y}}_{k(M-1),V-1}^T[l]}_{V}\Big]^T,$$

where $\bar{\mathbf{r}}_{mv}[l]$ has the same form as (5.90), $\bar{\mathbf{n}}_{mv}[l]$ has the same form as (5.91), and $\bar{\mathbf{y}}_{km,v}[l]$ has the same form as (5.92). The relationship among the vectors $\mathbf{r}[l]$, $\mathbf{n}[l]$ and $\mathbf{y}_k[l]$ is given by (5.93).

Moreover, as in Section 5.3.1, the $2NVM$-dimensional output signal vector $\mathbf{r}[l]$ of the $M$ AEs

during the $l$th symbol period can also be expressed as

$$\mathbf{r}[l] = \check{\mathbf{D}}_1 b_1[l]\check{\mathbf{v}}_1^0 + \sum_{k=2}^{K} \check{\mathbf{D}}_k b_k[l]\check{\mathbf{v}}_k^0 + \sum_{k=1}^{K} \check{\mathbf{D}}_k (b_k[l-1]\check{\mathbf{v}}_k^{-1} + b_k[l+1]\check{\mathbf{v}}_k^1) + \mathbf{n}[l],$$

where $\check{\mathbf{D}}_k = \text{diag}\left(\mathbf{D}_{k0}, \mathbf{D}_{k1} \ldots, \mathbf{D}_{k(M-1)}\right)$ is a $(2NVM \times 2NVM)$-dimensional matrix and $\mathbf{D}_{km} = \text{diag}(A_k H_{km,0} c'_{k,0}, \ldots, A_k H_{km,0} c'_{k,0}, \ldots, A_k H_{km,V-1} c'_{k,V-1}, \ldots,$ $A_k H_{km,V-1} c'_{k,V-1})$. Furthermore, we have $\check{\mathbf{v}}_k^{-1} = [\underbrace{(\underline{\mathbf{v}}_k^{-1})^T, \ldots, (\underline{\mathbf{v}}_k^{-1})^T}_{VM}]^T$, $\check{\mathbf{v}}_k^0 = [\underbrace{(\underline{\mathbf{v}}_k^0)^T, \ldots, (\underline{\mathbf{v}}_k^0)^T}_{VM}]^T$ and $\check{\mathbf{v}}_k^1 = [\underbrace{(\underline{\mathbf{v}}_k^1)^T, \ldots, (\underline{\mathbf{v}}_k^1)^T}_{VM}]^T$. Finally, we arrive at

$$\mathbf{r}[l] = b_1[l]\check{\mathbf{p}}_1 + \sum_{j=2}^{J} b_j[l]\check{\mathbf{p}}_j + \mathbf{n}[l], \tag{5.110}$$

where $b_1[l]$ is the desired bit and $\check{\mathbf{p}}_1 = \check{\mathbf{D}}_1\check{\mathbf{v}}_1^0$, while the remaining vectors correspond to the ISI and MAI vectors in (5.110). Again, we have $2K \leq J \leq 3K$.

Now, the eigen-decomposition of the autocorrelation matrix $\mathbf{R}$ of the received MC DS-CDMA signal vector $\mathbf{r}$ is given by

$$\begin{aligned} \mathbf{R} &= E\{\mathbf{r}\mathbf{r}^H\} = \check{\mathbf{P}}\check{\mathbf{P}}^H + \sigma^2 I_{2NVM} \\ &= \mathbf{U}\mathbf{\Lambda}\mathbf{U}^H = [\mathbf{U}_s \ \mathbf{U}_n] \begin{bmatrix} \mathbf{\Lambda}_s & 0 \\ 0 & \mathbf{\Lambda}_n \end{bmatrix} \begin{bmatrix} \mathbf{U}_s^H \\ \mathbf{U}_n^H \end{bmatrix}, \end{aligned} \tag{5.111}$$

where we have $\check{\mathbf{P}} = [\check{\mathbf{p}}_1, \ldots, \check{\mathbf{p}}_J]$ and $\text{rank}(\mathbf{P}) = \text{rank}(\mathbf{P}\mathbf{P}^H) = J$. Hence $\mathbf{\Lambda}_s = \text{diag}\{\lambda_1, \ldots, \lambda_J\}$ contains the largest $J$ number of eigenvalues of the received signal's autocorrelation matrix $\mathbf{R}$. In contrast to the *signal space* $\mathbf{U}_s = [\mathbf{u}_1, \ldots, \mathbf{u}_J]$, the *noise space* $\mathbf{U}_n = [\mathbf{u}_{J+1}, \ldots, \mathbf{u}_{2NVM}]$ contains the $(2NVM - J)$ orthogonal eigenvectors corresponding to the smallest eigenvalues $\sigma^2$ in $\mathbf{\Lambda}_n$.

Since the noise space $\mathbf{U}_n$ is orthogonal to $\check{\mathbf{p}}_1$, we have

$$\mathbf{U}_n^H \check{\mathbf{p}}_1 = \mathbf{U}_n^H \check{\mathbf{V}}_1^0 \check{\mathbf{d}}_1 = 0, \tag{5.112}$$

where

$$\underbrace{\check{\mathbf{V}}_1^0}_{2NVM \times VM} = \begin{bmatrix} \underline{\mathbf{v}}_1^0 & & & \\ & \underline{\mathbf{v}}_1^0 & & \\ & & \ddots & \\ & & & \underline{\mathbf{v}}_1^0 \end{bmatrix} \tag{5.113}$$

and $\check{\mathbf{d}}_1 = [\mathbf{d}_{1,0}^T, \mathbf{d}_{1,1}^T, \ldots, \mathbf{d}_{1,M-1}^T]^T$, where $\mathbf{d}_{1,m} = A_1 \mathbf{C'}_1 \mathbf{F}_L \mathbf{h}_{1m} = [A_1 H_{1m,0} c'_{1,0},$ $A_1 H_{1m,1} c'_{1,1}, \ldots, A_1 H_{1m,V-1} c'_{1,V-1}]^T$. After obtaining the estimate $\bar{\mathbf{d}}_1$ by computing the minimum eigenvector of the matrix $(\check{\mathbf{V}}_1^0)^H \mathbf{U}_n \mathbf{U}_n^H \check{\mathbf{V}}_1^0$, we arrive at the composite signature waveform

$\bar{\mathbf{p}}_1 = \check{\mathbf{V}}_1^0 \bar{\mathbf{d}}_1$. As discussed in Section 5.3.2, the necessary condition for such an estimate to be unique is that we have $J \leq 2NVM - LM$. For the worst-case scenario of $J = 3K$, a necessary condition imposed on the number of users for the sake of uniquely determining $\mathbf{h}_1$ is then $K \leq \frac{(2NV-L)M}{3}$. Since we have $M \geq 2$ in our smart antenna aided system, the number of users supported can be as high as $K = NV$, provided that the condition of $\frac{(2M-3)NV}{M} \geq L$ is met, which can be readily satisfied by appropriately choosing $M$, $N$ and $V$. Compared to the generalized MC DS-CDMA system using a single antenna, the smart antenna aided system is capable of supporting more users, because generally speaking, increasing the number of AEs has the potential of providing a higher degree of freedom and hence it is capable of improving both the achievable system performance and the user-load.

With the aid of the subspace parameters $\mathbf{U}_s$, $\mathbf{\Lambda}_s$, $\sigma^2$ and the composite signature waveform $\bar{\mathbf{p}}_1$, the decorrelating detector's weight vector $\mathbf{w}_1 = \mathbf{d}_1$ is given by

$$\mathbf{d}_1 = \mathbf{U}_s(\mathbf{\Lambda}_s - \sigma^2\mathbf{I}_J)^{-1}\mathbf{U}_s^H\bar{\mathbf{p}}_1. \tag{5.114}$$

The linear MMSE detector's weight vector $\mathbf{w}_1 = \mathbf{m}_1$ has the form of

$$\mathbf{m}_1 = \mathbf{U}_s\mathbf{\Lambda}_s^{-1}\mathbf{U}_s^H\bar{\mathbf{p}}_1. \tag{5.115}$$

By exploiting the knowledge of a group of $\tilde{K}$ composite signature waveforms corresponding to $\tilde{K}(\tilde{K} \leq K)$ intracell users, we arrive at the form-II linear hybrid group-blind MUD's weight vector $\bar{\mathbf{w}}_1$ as

$$\bar{\mathbf{w}}_1 = \mathbf{U}_s\mathbf{\Lambda}_s^{-1}\mathbf{U}_s^H\tilde{\mathbf{P}}(\tilde{\mathbf{P}}^H\mathbf{U}_s\mathbf{\Lambda}_s^{-1}\mathbf{U}_s^H\tilde{\mathbf{P}})^{-1}1_1, \tag{5.116}$$

where $\tilde{\mathbf{P}} = [\bar{\mathbf{p}}_1, \ldots, \bar{\mathbf{p}}_J]$ is a $(2NVM \times \tilde{J})$-dimensional matrix constructed based on the estimated CIRs, the timing information and the TF-domain spreading signature waveforms of all the $\tilde{K}$ intracell users. The blind multiuser detection and the group-blind multiuser detection algorithms invoked for a generalized MC DS-CDMA system employing smart antennas are summarized in Table 5.5.

## 5.4 Performance of Blind and Group-Blind Multiuser Detection

All investigations of this section were based on evaluating the performance of the subspace-based blind and group-blind MUDs employed in the uplink of a smart antenna aided generalized MC DS-CDMA system, when communicating over a dispersive ST Rayleigh fading channel contaminated by AWGN. More specifically, the multipath Rayleigh fading channel of all the $K$ users supported has $L = 3$ paths, while the fading factors of each complex-valued path are generated according to the Rayleigh distribution, where the paths are normalized so that each user's signal arrives at the receiver with an equal power, *i.e.* we have $\| \mathbf{h}_k \|^2 = 1$. In each transmission burst, $M_F = 256$ number of MC DS-CDMA modulated bits are transmitted. We assumed that $m$-sequences having a length of $N = 15$ were employed as Time-Domain (TD) spreading sequences, while 4-chip Walsh codes were

| The received signals<br>$\mathbf{X} = [\mathbf{r}_1, \mathbf{r}_2, \ldots, \mathbf{r}_{M_F}]$ |
|---|
| 1. Compute sample autocorrelation<br>$\mathbf{R} = \frac{1}{M_F}\mathbf{X}\mathbf{X}^H$;<br>2. Compute the eigen-decomposition of<br>$\mathbf{R} = \mathbf{U}_s\mathbf{\Lambda}_s\mathbf{U}_s^H + \sigma^2\mathbf{U}_n\mathbf{U}_n^H$;<br>3. Blind Channel Estimation<br>$\bar{\mathbf{d}}_k = \text{min-eigenvector}((\check{\mathbf{V}}_k^0)^H\mathbf{U}_n\mathbf{U}_n^H\check{\mathbf{V}}_k^0)$<br>$\bar{\mathbf{p}}_k = \check{\mathbf{V}}_k^0\bar{\mathbf{d}}_k\ \bar{\mathbf{p}}_{\tilde{K}+k} = \check{\mathbf{V}}_k^1\bar{\mathbf{d}}_k\ \bar{\mathbf{p}}_{2\tilde{K}+k} = \check{\mathbf{V}}_k^{-1}\bar{\mathbf{d}}_k$<br>$k = 1 \ldots \tilde{K}$ when $\tau_k = 0$, we have $\bar{\mathbf{p}}_{2\tilde{K}+k} = \mathbf{0}$.<br>Excluding these zero vectors, we have $2\tilde{K} \leq \tilde{J} \leq 3\tilde{K}$ non-null vectors.<br>form $\tilde{\mathbf{P}}$ using $(\bar{\mathbf{p}}_1, \ldots, \bar{\mathbf{p}}_{\tilde{J}})$;<br>4. Form the detectors according to<br>(5.114), (5.115) and (5.116); |

**Table 5.5:** Summary of the blind and group-blind MC DS-CDMA MUDs employing smart antennas.

used as Frequency-Domain (FD) spreading codes. An antenna array having $M$ number of AEs is considered in our investigations. The cross-correlation coefficient among the AEs is defined as $\rho$. When the AEs are located sufficiently far apart, the MC DS-CDMA signal experiences independent fading upon reaching the different AEs, hence we have $\rho = 0$. By contrast, when the AEs are separated by a distance of half a wavelength, we have $\rho = 1$, which implies that these AEs are fully correlated. The basic parameters of the blind and group-blind MUDs invoked for the generalized MC DS-CDMA system considered are summarized in Table 5.6, where 4-chip Walsh codes were used as FD spreading sequences, corresponding to $V = 4$ subcarriers. Employing more subcarriers, i.e. $V = 256$, will increase the attainable frequency diversity gain and hence improve the achievable performance. However, employing more subcarriers potentially imposes higher peak-to average ratios and hence requires a perfectly linear transmit amplifier having a higher dynamic range [230, 231]. Furthermore, employing more subcarriers implies a higher system complexity. Without loss of generality, we use $V = 4$ subcarriers in our generalized MC DS-CDMA system.

| **Parameters** | **Value** |
|---|---|
| Chips-spaced CIR length $L$ | 3 |
| Normalized Dopper frequency | 0.01 |
| Short cyclic prefix | 2 chips |
| Burst length $M_F$ | 256 |
| Number of subcarriers $V$ | 4 |
| FD Spreading gain | 4 |
| TD Spreading gain | 15 |

**Table 5.6:** Basic simulation parameters for the blind and group-blind MUDs invoked for the generalized MC DS-CDMA system considered.

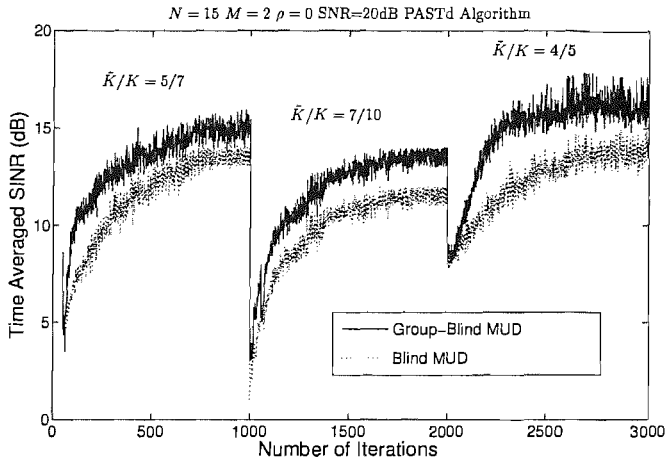


**Figure 5.4:** Performance of both the blind and group-blind MUDs of Section 5.3.4 using the PASTd subspace tracking algorithm invoked for a generalized MC DS-CDMA system communicating over a dispersive ST Rayleigh fading channel contaminated by AWGN. The SNR was 20dB. An antenna array having $M = 2$ uncorrelated AEs was employed and hence we have $\rho = 0$. At $t = 0$, a total of $K = 7$ users are activated and we have $\tilde{K} = 5$ intracell users. At $t = 1000$ iterations corresponding to 1000 symbols three more users engage in communications, hence we have $K = 10$ and $\tilde{K} = 7$. Finally, at $t = 2000$, five users exit the system and hence we have $K = 5$ as well as $\tilde{K} = 4$. The forgetting factor is 0.995. The curves plotted are averaged over 100 simulation runs and the remaining parameters are summarized in Table 5.6.

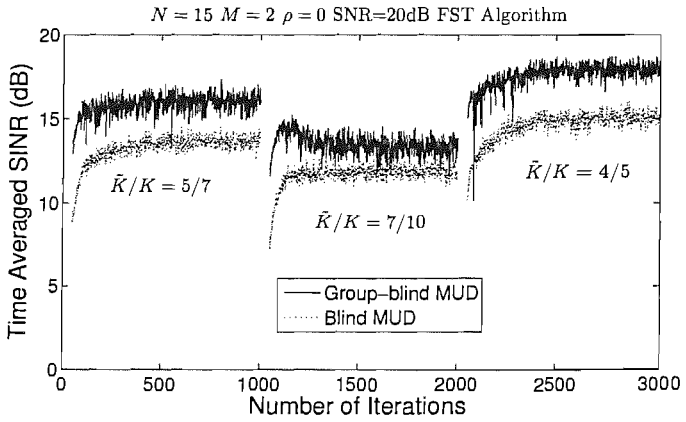


**Figure 5.5:** Performance of both the blind and group-blind MUDs of Section 5.3.4 using the FST algorithm invoked for a generalized MC DS-CDMA system communicating over a dispersive ST Rayleigh fading channel contaminated by AWGN. The SNR was 20dB. An antenna array having $M = 2$ uncorrelated AEs was employed and hence we have $\rho = 0$. At $t = 0$, a total of $K = 7$ users are activated and we have $\tilde{K} = 5$ intracell users. At $t = 1000$ iterations corresponding to 1000 symbols three more users engage in communications, hence we have $K = 10$ and $\tilde{K} = 7$. Finally, at $t = 2000$, five users exit the system and hence we have $K = 5$ as well as $\tilde{K} = 4$. The forgetting factor is 0.995. The curves plotted are averaged over 100 simulation runs and the remaining parameters are summarized in Table 5.6.

In Figures 5.4 and 5.5, the PASTd algorithm of Section 5.2.4.2 and the NAHJ-FST algorithm of Section 5.2.4.3 were invoked for both blind and group-blind multiuser detection in the context of generalized MC DS-CDMA, where an antenna array having $M = 2$ uncorrelated AEs was employed and we have $\rho = 0$.

Figure 5.4 characterizes the achievable performance of the blind and group-blind MUDs of Section 5.3.4, when the PASTd tracking algorithm was invoked for communicating over a dispersive ST Rayleigh fading channel contaminated by AWGN. the MUDs employing the PASTd algorithm converged to their steady-state solutions in approximately 800 iterations corresponding to 800 MC DS-CDMA symbols. Furthermore, the group-blind MUD significantly outperforms the blind MUD. For example, when we supported a total of $K = 5$ users and the signature sequences of $\tilde{K} = 4$ intracell users were known, the group-blind MUD had a 3dB higher output SINR than that of the blind MUD. By contrast, Figure 5.5 characterizes the MUDs of Section 5.3.4, when the FST algorithm was employed for transmission over a dispersive ST Rayleigh fading channel contaminated by AWGN. As seen in Figure 5.5, the NAHJ-FST algorithm converged after receiving approximately 200 symbols, substantially outperforming the PASTd algorithm characterized in Figure 5.4. Furthermore, the FST tracking algorithm featuring in Figure 5.4 exhibited a better steady-state performance than that of the PASTd tracking algorithm of Figure 5.4.

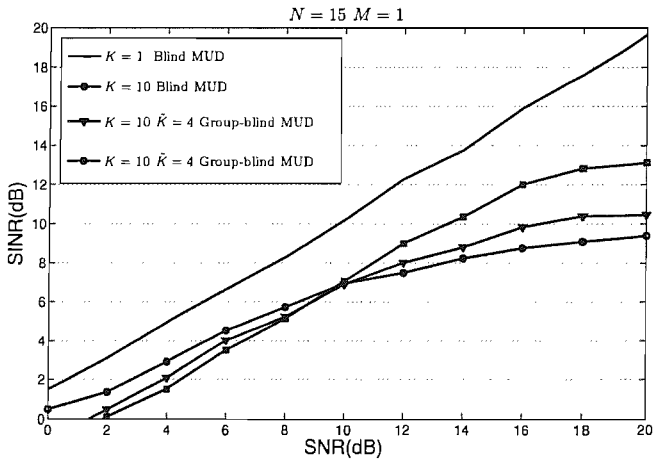


**Figure 5.6:** SINR versus SNR performance of the blind and group-blind MUDs invoked for a generalized MC DS-CDMA system. A single antenna was employed in our simulations, a total of $K = 10$ users were supported and the spreading codes of $\tilde{K}$=4 and 8 intracell users were known to the group-blind MUD. The remaining system parameters are summarized in Table 5.6.

Figures 5.6, 5.7, 5.8 and 5.9 characterize the output SINR performance of the blind and group-blind MUDs of Sections 5.3.3 and 5.3.4 as a function of the SNR, when the total number of users supported is $K = 10$ and the spreading codes of $\tilde{K}$=4 and 8 intracell users were known to the group-blind MUD. Three different types of antenna arrays were studied in these four figures, namely a single antenna, an antenna array having $M = 2$ number of correlated AEs and an antenna array

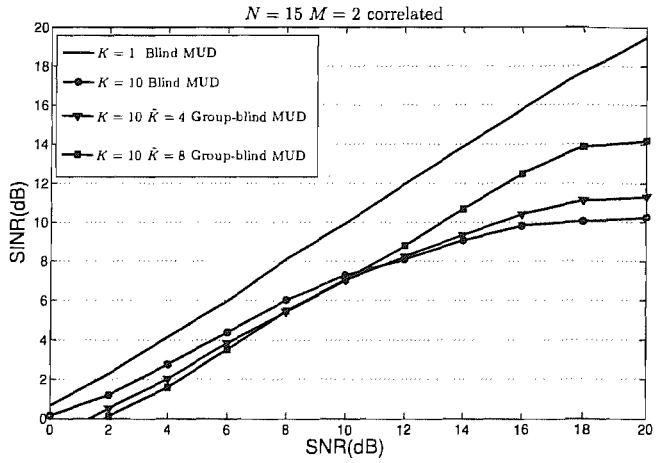


**Figure 5.7:** SINR versus SNR performance of the blind and group-blind MUDs invoked for a generalized MC DS-CDMA system. An antenna array having $M = 2$ number of correlated AEs was employed in our simulations and we have $\rho = 1$. A total of $K = 10$ users were supported and the spreading codes of $\tilde{K}$=4 and 8 intracell users were known to the group-blind MUD. The remaining system parameters are summarized in Table 5.6.

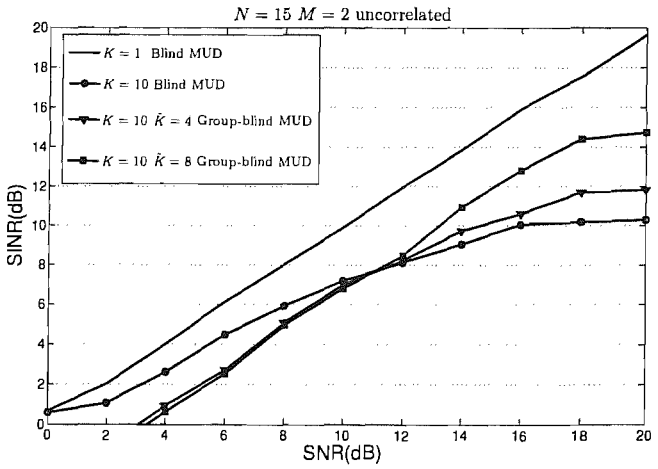


**Figure 5.8:** SINR versus SNR performance of the blind and group-blind MUDs invoked for a generalized MC DS-CDMA system. An antenna array having $M = 2$ number of uncorrelated AEs was employed in our simulations and we have $\rho = 0$. A total of $K = 10$ users were supported and the spreading codes of $\tilde{K}$=4 and 8 intracell users were known to the group-blind MUD. The remaining system parameters are summarized in Table 5.6.

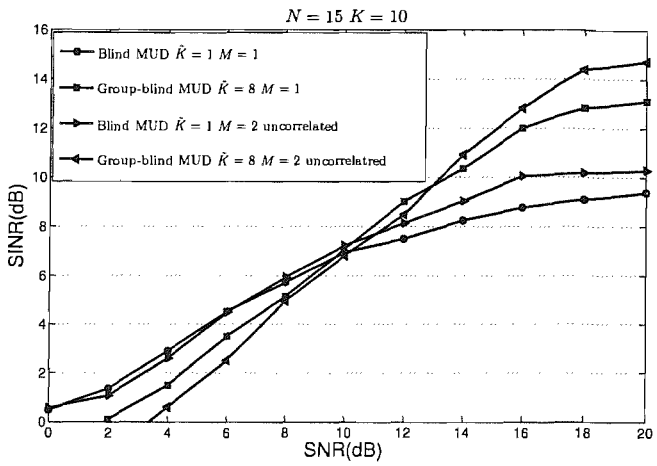


**Figure 5.9:** SINR versus SNR performance of the blind and group-blind MUDs invoked for a generalized MC DS-CDMA system. Three different types of antenna array were studied, namely a single antenna, an antenna array having $M = 2$ number of correlated AEs and an antenna array having $M = 2$ number of uncorrelated AEs. A total of $K = 10$ users were supported and the spreading codes of $\tilde{K}$=4 and 8 intracell users were known to the group-blind MUD. The remaining system parameters are summarized in Table 5.6.

having $M = 2$ uncorrelated AEs.

Figures 5.6, 5.7 and 5.8 demonstrated that the more users' signature waveforms are known, the better the group-blind MUD's achievable performance. Again, the group-blind MUD significantly outperformed the blind MUD. Furthermore, Figure 5.9 demonstrated that the blind MUD operating in conjunction with an antenna array having $M = 2$ uncorrelated AEs achieved a better performance than that having $M = 2$ correlated AEs, which confirmed that when the spatial signals arriving at the elements of an antenna array are less correlated, the attainable spatial diversity gain becomes higher. As expected, the blind MUD employing a single antenna attained the worst performance.

To elaborate a little further, Figure 5.10 portrays the achievable performance of both blind and group-blind MUDs at SNR of 20dB, when different cross-correlation coefficients $\rho$ between the two AEs were recorded. As shown in Figure 5.10, the performance of blind and group-blind MUDs slightly degraded upon increasing the AEs' cross-correlation coefficient $\rho$. By contrast, Figure 5.11 exhibits the SINR performance of both blind and group-blind MUDs at SNR of 20dB, when different number of users were supported. As expected, when the number of users supported is increased, the achievable performance of both the blind and group-blind MUDs is degraded. Furthermore, we may conclude from this figure that the higher the value of higher the value of $\tilde{K}/K$, the better the group-blind MUDs.

In Figures 5.12, 5.13 and 5.14 the near-far performance of the blind and group-blind MUDs is investigated. All these figures confirmed that the blind and group blind MUDs were resistant to the near-far phenomenon, regardless of the type of the antenna array employed.

In Figures 5.15 and 5.16, both timing and channel estimation were considered in the context of

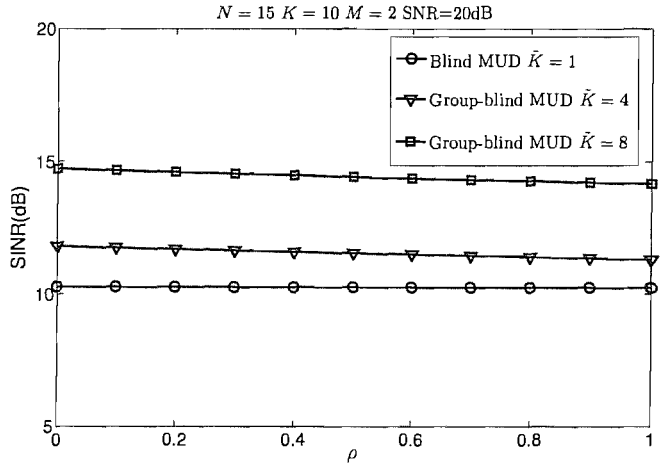


**Figure 5.10:** SINR versus the cross-correlation coefficient, $\rho$, performance of both the blind and group-blind MUDs. An antenna array having $M = 2$ AEs was employed. The SNR was fixed to 20dB. A total of $K = 10$ users were supported and the spreading codes of $\tilde{K} = 4$ and 8 intracell users were known to the group-blind MUD. The remaining system parameters are summarized in Table 5.6.

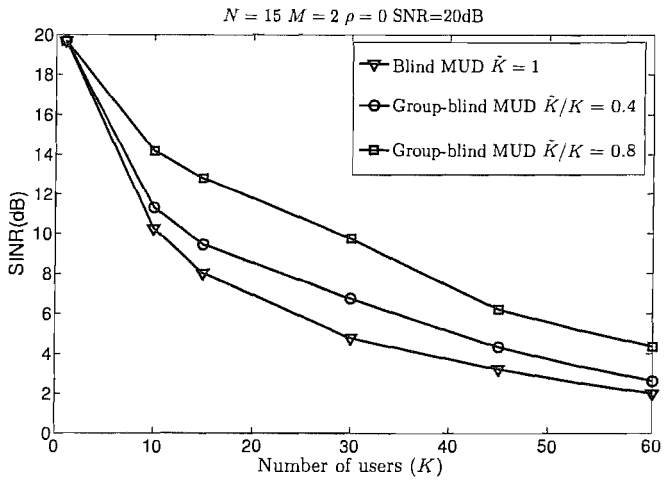


**Figure 5.11:** SINR versus the number of users, $K$, performance of the blind and group-blind MUDs invoked for a generalized MC DS-CDMA system, when an antenna array having $M = 2$ uncorrelated AEs is used. The SNR was fixed to 20dB. When considering the group-blind MUDs, the ratio of $\tilde{K}/K$ was assigned to 0.4 or 0.8. The remaining system parameters are summarized in Table 5.6.

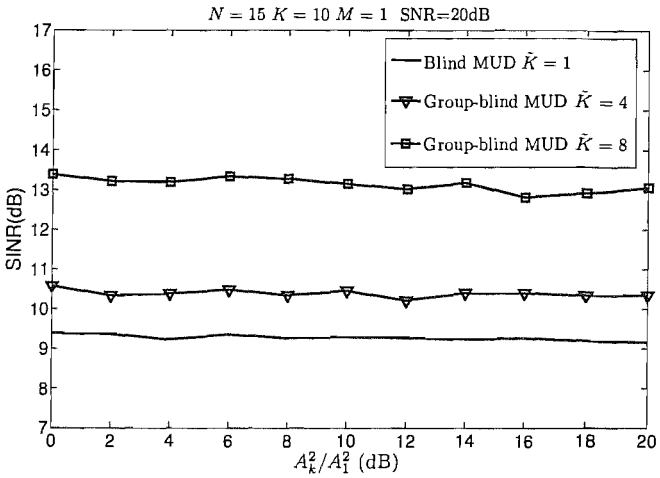


**Figure 5.12:** Near-far performance of both the blind and group-blind MUDs supporting a total of $K = 10$ users, when employing a single antenna and having an SNR of 20dB. The group-blind MUDs benefitted from the knowledge of $\tilde{K} = 4$ or 8 intracell users' spreading codes. The remaining system parameters are summarized in Table 5.6.

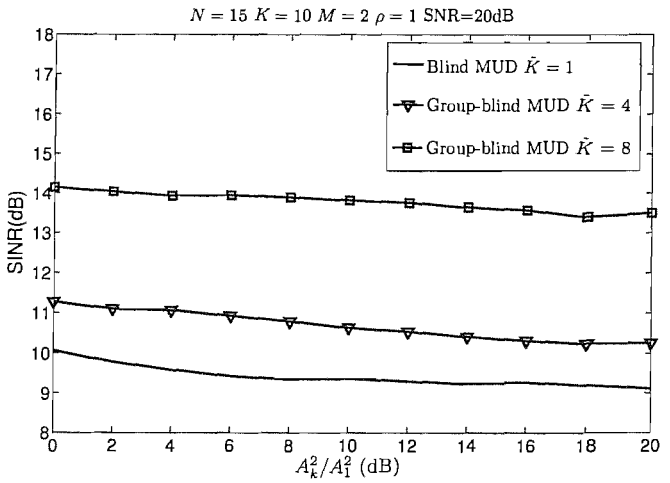


**Figure 5.13:** Near-far performance of both the blind and group-blind MUDs supporting a total of $K = 10$ users, when employing an antenna array having $M = 2$ correlated AEs and $\rho = 1$. The SNR was fixed to 20dB. The group-blind MUDs benefitted from the knowledge of $\tilde{K} = 4$ or 8 intracell users' spreading codes. The remaining system parameters are summarized in Table 5.6.

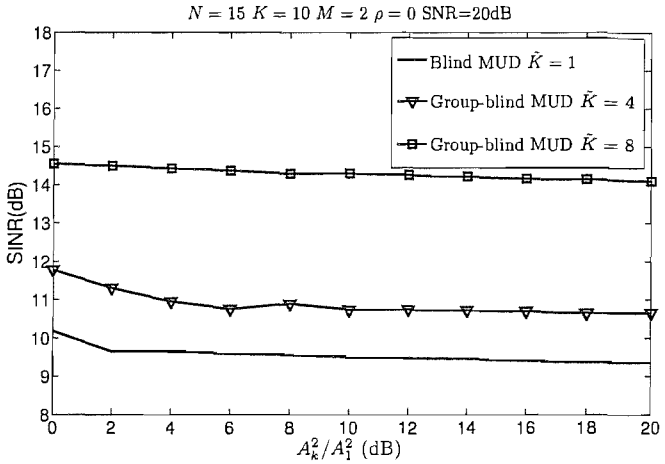


**Figure 5.14:** Near-far performance of both the blind and group-blind MUDs supporting a total of $K = 10$ users, when employing an antenna array having $M = 2$ uncorrelated AEs and $\rho = 0$. The SNR was fixed to 20dB. The group-blind MUDs benefitted from the knowledge of $\tilde{K} = 4$ or 8 intracell users' spreading codes. The remaining system parameters are summarized in Table 5.6.

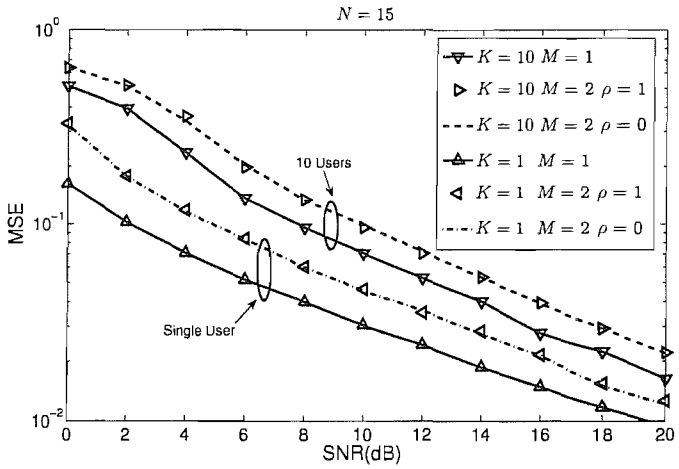


**Figure 5.15:** MSE performance of the subspace-based blind channel estimator in the context of generalized MC DS-CDMA systems supporting $K = 1$ or 10 users. Three different types of antenna arrays were investigated, namely a single antenna as well as an antenna array having $M = 2$ correlated or $M = 2$ uncorrelated AEs. The remaining system parameters are summarized in Table 5.6.

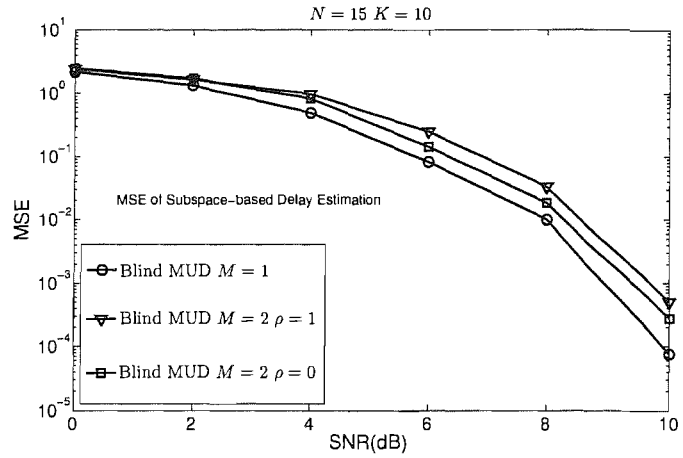


**Figure 5.16:** MSE performance of the subspace-based timing estimator in the context of generalized MC DS-CDMA systems supporting $K = 1$ or 10 users. Three different types of antenna arrays were investigated, namely a single antenna as well as an antenna array having $M = 2$ correlated or $M = 2$ uncorrelated AEs. The remaining system parameters are summarized in Table 5.6.

a generalized MC DS-CDMA system, where either $K = 1$ or 10 users were served. Three different types of antenna arrays were investigated, namely a single antenna and an antenna array having $M = 2$ correlated or $M = 2$ uncorrelated AEs. Fig. 5.15 portrays the MSE performance of the subspace-based blind channel estimator of Sections 5.3.2 and 5.3.4, while Fig. 5.16 characterizes the MSE performance of the subspace-based blind timing estimator of Sections 5.3.2 and 5.3.4. Figures 5.15 and 5.16 demonstrated that the subspace based timing and channel estimator is capable of accurately tracking the timing drifts and the CIRs.

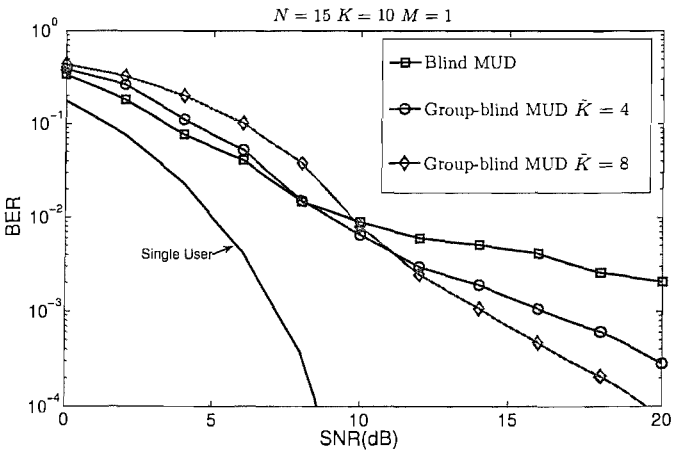


**Figure 5.17:** BER performance of the various MC DS-CDMA MUDs considered. A single antenna was invoked. Both the scenario of a single user and $K = 10$ users were considered. The group-blind MUDs benefitted from the knowledge of $\tilde{K} = 4$ or 8 intracell users' spreading codes. The remaining system parameters are summarized in Table 5.6.

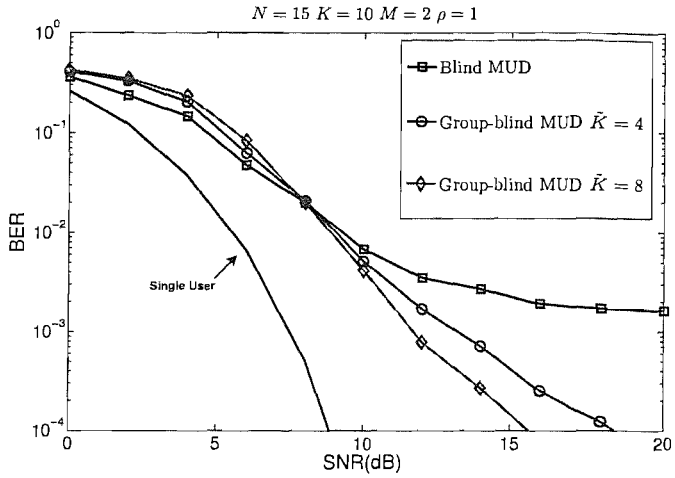


**Figure 5.18:** BER performance of the various MC DS-CDMA MUDs considered. An antenna array having $M = 2$ correlated AEs was employed and we had $\rho = 1$. Both the scenario of a single user and $K = 10$ users were considered. The group-blind MUDs benefitted from the knowledge of $\tilde{K} = 4$ or 8 intracell users' spreading codes. The remaining system parameters are summarized in Table 5.6.

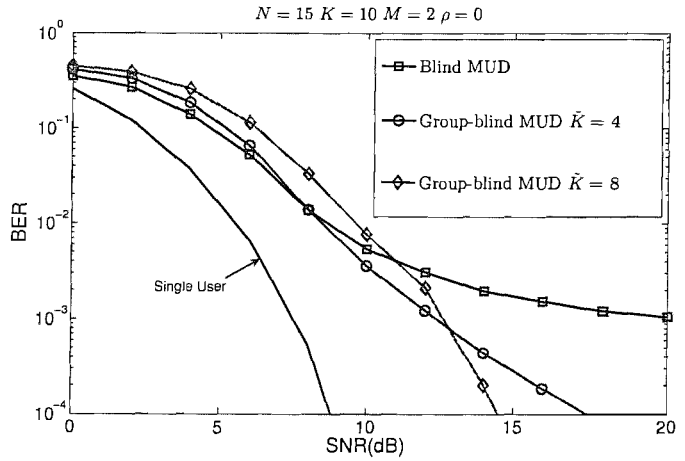


**Figure 5.19:** BER performance of the various MC DS-CDMA MUDs considered. An antenna array having $M = 2$ uncorrelated AEs was employed and we had $\rho = 0$. Both the scenario of a single user and $K = 10$ users were considered. The group-blind MUDs benefitted from the knowledge of $\tilde{K} = 4$ or 8 intracell users' spreading codes. The remaining system parameters are summarized in Table 5.6.

Below, let us consider the BER performance of the proposed blind and group-blind MUDs in the context of generalized MC DS-CDMA. In Figures 5.17, 5.18 and 5.19, three different types of antenna arrays, namely a single antenna as well as an array having $M = 2$ correlated AEs or $M = 2$ uncorrelated AEs were employed, respectively. The simulation results showed that the group-blind MUD benefitting from the knowledge of more users' signature waveforms attained a better BER

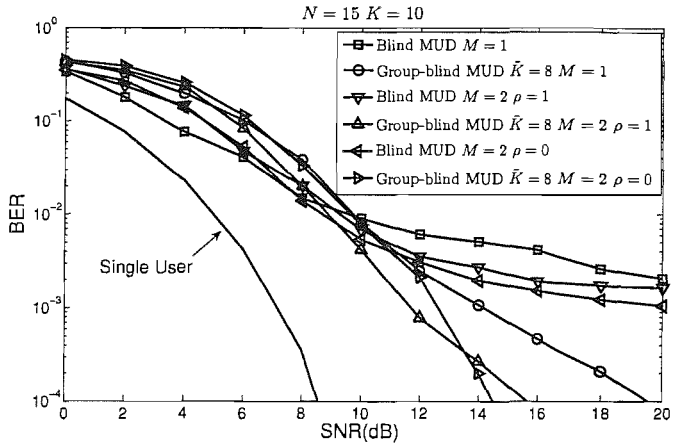


**Figure 5.20:** BER performance of the various MC DS-CDMA MUDs considered. Three different types of antenna array were studied, namely a single antenna as well as an antenna array having $M = 2$ correlated and uncorrelated AEs. A total of $K = 10$ users were supported and the group-blind MUDs benefitted from the knowledge of $\tilde{K} = 8$ intracell users' spreading codes. The remaining system parameters are summarized in Table 5.6.

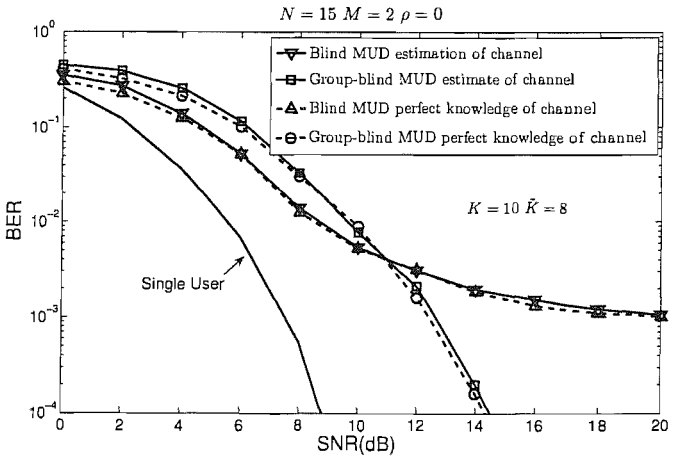


**Figure 5.21:** BER performance of the various MC DS-CDMA MUDs considered. An antenna array having $M = 2$ uncorrelated AEs was employed and we had $\rho = 0$. Both the scenario of having the perfect knowledge of the complex-valued CIRs and their realistic estimation were considered. The group-blind MUDs benefitted from the knowledge of $\tilde{K} = 8$ intracell users' spreading codes. The remaining system parameters are summarized in Table 5.6.

performance. Again, it can be seen from Figure 5.20 that as expected the blind MUD operating in conjunction with an antenna array having $M = 2$ uncorrelated AEs achieved a better BER performance than that having $M = 2$ correlated AEs. Naturally, the blind MUD employing a single antenna attained the worst BER performance. In Figure 5.21 we observe that the space-time blind and group-blind MUDs equipped with the subspace based CIRs estimator perform estimator perform only slightly worse than the estimator exploiting the perfect knowledge of the CIRs, which implied that the associated performance degradation imposed by the channel estimator error is negligible.

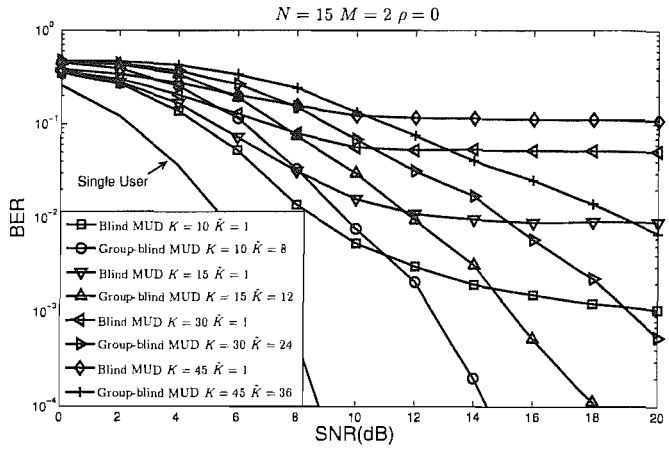


**Figure 5.22:** BER performance of the various MC DS-CDMA MUDs considered, where different number of users were activated. An antenna array having $M = 2$ uncorrelated AEs was employed and we had $\rho = 0$. When considering the group-blind MUDs, the ratio of $\tilde{K}/K$ was assigned to 0.8. The remaining system parameters are summarized in Table 5.6.

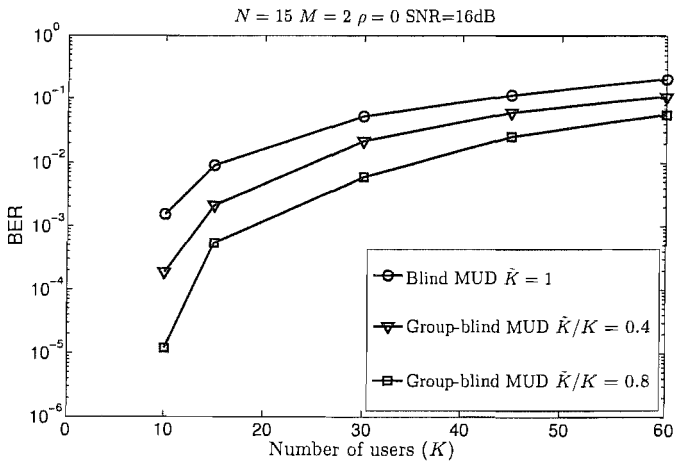


**Figure 5.23:** BER versus the number of users, $K$, performance of the various MC DS-CDMA MUDs considered. An antenna array having $M = 2$ uncorrelated AEs was employed and we had $\rho = 0$. The SNR was fixed to 16dB. When considering the group-blind MUDs, the ratio of $\tilde{K}/K$ was assigned to 0.4 or 0.8. The remaining system parameters are summarized in Table 5.6.

In Figures 5.22 and 5.23, an antenna array having $M = 2$ uncorrelated AEs was employed and we had $\rho = 0$, where the BER performance of the blind and the group-blind MUDs was presented as a function of the number of users supported. Note that the system serving $K = 60$ users was full loaded. Finally, Figure 5.24 characterizes the SNR gains achieved by increasing the number of AEs, where a total of $K = 10$ users were supported and the group-blind MUDs benefitted from the knowledge of $\tilde{K} = 8$ intracell users' spreading codes.

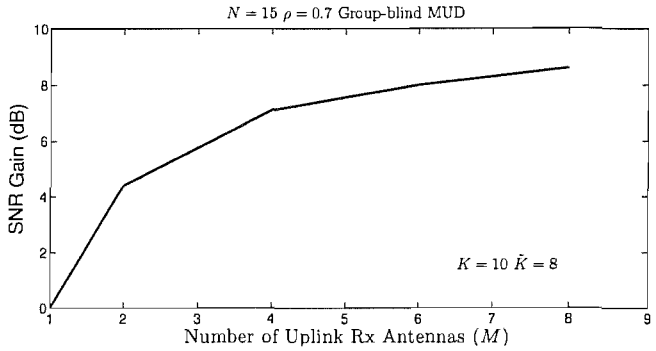


**Figure 5.24:** SNR gain versus the number of the receive antennas, $M$, performance of group-blind MUDs at a BER of $10^{-4}$. Antenna arrays having a cross-correlation coefficient of $\rho = 0.7$ were used. A total of $K = 10$ users were supported and the group-blind MUDs benefitted from the knowledge of $\tilde{K} = 8$ intracell users' spreading codes. The remaining system parameters are summarized in Table 5.6.

## 5.5 Conclusions

In this chapter we studied the performance of subspace-based blind and group-blind MUDs invoked for a generalized MC DS-CDMA system, where an antenna array having $M$ AEs was employed. In Section 5.1, a brief introduction to the literature of conventional MUD [195, 209, 210] was provided, followed by an overview of adaptive MUDs [211–214] in Section 5.1. Then, subspace-based blind MUD [1, 2, 169, 220] was discussed in Section 5.1.

In Section 5.2 the philosophy of subspace-based blind and group-blind MUDs was detailed. Subspace-based blind MUDs designed for synchronous DS-CDMA were first introduced in Section 5.2.1. Then in Section 5.2.2, we extended our investigations of blind MUDs to dispersive DS-CDMA channels for the sake of jointly combatting the effects of both MAI and ISI. Group-blind MUDs [169, 220] were introduced in Section 5.2.2.3, which make use of the known spreading sequences of all users roaming in the serving cell in order to suppress the intracell interference, while blindly suppressing the intercell interference. In Section 5.2.2, subspace-based blind and group-blind MUDs were further developed for the uplink of MC-CDMA systems. The summary of blind and group-blind MC-CDMA MUDs communicating over a dispersive AWGN channel was provided in Table 5.1.

In Section 5.2.4, after a brief introduction to EVD and SVD, which exhibit a relatively high

complexity, we investigated two low-complexity subspace tracking algorithms, namely the PASTd algorithm and the NAHJ-FST algorithm. Both of the PASTd and the NAHJ-FST algorithm have a computational complexity on the order of $O(NK)$. The operations of the PASTd algorithm and the NAHJ-FST algorithm were summarized in Table 5.2 and Table 5.3, respectively.

Then, we concentrated our investigations on blind and group-blind multiuser detection invoked for a generalized MC DS-CDMA system in Section 5.3. Our system model was characterized in Section 5.3.1, followed by the discussion of subspace-based blind channel estimation in Section 5.3.2. Based on the signal subspace components and the estimated signature waveform, Section 5.3.3 outlined the expressions characterizing the blind and group-blind MUDs considered. The operations of the blind and group-blind MUDs invoked for an MC DS-CDMA system communicating over a dispersive AWGN channel were then summarized in Table 5.4. Furthermore, the space-time blind and group-blind MUDs were considered in the context of a smart antenna aided MC DS-CDMA system in Section 5.3.4. Table 5.5 summarized the operations of the corresponding space-time blind and group-blind MUD algorithms.

Finally, the performance of these blind and group-blind MUDs was characterized in the context of smart antenna aided MC DS-CDMA systems in Section 5.4. As seen in Figures 5.4 and 5.5, when more signature waveforms were known to the receiver, the group-blind MUD significantly outperformed the blind MUD. Furthermore, the FST tracking algorithm exhibited a faster convergence and better steady-state performance than that of the PASTd tracking algorithm. When considering the space-time blind and group-blind MUDs, the system using an antenna array having uncorrelated AEs achieved a better performance than that associated with correlated AEs, which was confirmed by Figure 5.10. As expected, the blind MUD employing a single antenna attained the worst performance. Figures 5.12, 5.13 and 5.14 demonstrated the robustness of the family of blind and group-blind MUDs against the near-far effects, since they are capable of efficiently suppressing the MAI. Furthermore, Figure 5.21 shows that the space-time blind and group-blind MUDs of Section 5.3.4 are capable of achieving a performance close to that attained with the aid of perfect knowledge of the CIRs. The comparison of the BER performance of blind and group-blind MUDs invoked for the generalized MC DS-CDMA system supporting $K = 10$ users is provided in Table 5.7.

| Scheme | Type of antenna arrays | $E_b/N_0$(dB) required at BER=$2 \times 10^{-3}$ | $E_b/N_0$(dB) required at BER=$3 \times 10^{-4}$ | Figure No. |
|---|---|---|---|---|
| Blind MUD $\tilde{K} = 1$ | $M = 1$ | 20.0 | | Figure 5.17 |
| | $M = 2,\ \rho = 1$ | 15.9 | | Figure 5.18 |
| | $M = 2,\ \rho = 0$ | 14.0 | | Figure 5.19 |
| Group-blind MUD $\tilde{K} = 4$ | $M = 1$ | 13.9 | 19.9 | Figure 5.17 |
| | $M = 2,\ \rho = 1$ | 11.8 | 15.7 | Figure 5.18 |
| | $M = 2,\ \rho = 0$ | 11.0 | 14.8 | Figure 5.19 |
| Group-blind MUD $\tilde{K} = 8$ | $M = 1$ | 12.5 | 17.1 | Figure 5.17 |
| | $M = 2,\ \rho = 1$ | 10.9 | 13.8 | Figure 5.18 |
| | $M = 2,\ \rho = 0$ | 12.1 | 13.7 | Figure 5.19 |

**Table 5.7:** Summary of the required $E_b/N_0$ values for blind and group-blind MUDs invoked for the uplink of the generalized MC DS-CDMA system supporting $K = 10$ users.

# Chapter 6

# Conclusions and Future Work

In this concluding chapter, a summary of the thesis will be presented. This will be followed by our suggestions for future work.

## 6.1 Conclusions

This thesis has considered a generalized MC DS-CDMA system using smart antennas, including:

1) optimum beamforming schemes invoked for the uplink of generalized MC DS-CDMA systems;

2) space-time transmitter processing schemes employed for the downlink of generalized MC DS-CDMA systems considered;

3) adaptive space-time processing schemes;

4) subspace-based blind and group-blind space-time MUDs invoked for the proposed smart antenna aided generalized MC DS-CDMA systems.

We combined the generalized MC DS-CDMA system with smart antennas for the sake of improving the performance of the system by suppressing the multiuser interference, while achieving frequency, time and spatial diversity.

Before commencing our investigations of a generalized MC DS-CDMA system supported by smart antennas, a brief introduction to mobile radio channels was provided in Chapter 1, followed by a comprehensive overview of contributions on spatial channel models, which is summarized in Tables 1.1 and 1.2. Since the study of generalized MC DS-CDMA techniques requires the understanding of DS-CDMA, MC CDMA, MT-CDMA, and orthogonal MC DS-CDMA, these four techniques were reviewed in Sections 1.2.1, 1.2.2, 1.2.3 and 1.2.4, respectively. The corresponding historical perspective on Multicarrier CDMA techniques was provided in Tables 1.4 and 1.5, while Table 1.3 compared the features of various CDMA systems. In Section 1.3, smart antenna techniques including optimum beamforming and transmit processing were briefly introduced. The contributions on the topic of smart antenna techniques were summarized in Tables 1.6, 1.7, 1.8 and 1.9. Then, adaptive detection was

discussed in Section 1.3.3, which requires the knowledge of the signature waveform and the timing information of the desired user. Finally, Section 1.3.4 introduced blind detection for the sake of achieving a relatively high spectrum efficiency, while maintaining the required system performance. Historical perspectives on adaptive detection and blind detection were provided in Tables 1.10 and 1.11.

In Chapter 2, we have characterized the philosophy of the generalized MC DS-CDMA system using smart antennas and developed a detailed system model of the considered MC DS-CDMA system. In the context of the uplink of the proposed MC DS-CDMA system, we invoked a range of linear optimum combining based antenna array weight optimization schemes for the sake of mitigating the effects of the interfering signals and hence improving both the achievable performance and user-load. In Chapter 2 our study was based on the assumption that the receiver either has full knowledge or partial knowledge of the Direction of Arrival (DOA), of the channel amplitudes, the phases, as well as the timing of the interfering users. In Section 2.3.6, the BER performance of these optimum combining schemes was comparatively studied in the context of a DS-CDMA system, a MC-CDMA system and a generalized MC DS-CDMA system. From the simulation results of Figure 2.11-Figure 2.19 and the accompanying analysis we concluded that the MVDR optimum combiner is the best one in the context of a DS-CDMA system, while the individual subcarrier-based optimum MVDR combiner exhibits the poorest performance in the context of the MC-CDMA system of Figure 2.7 or in the generalized MC DS-CDMA system of Figure 2.2. When the number of the users increases, the correlation matrix $\mathbf{R}_{uu}$ or $\mathbf{R}_{zz}$ becomes reminiscent of an identity matrix. Therefore, the weighting process becomes reminiscent of the MRC scheme. Having investigated a range of different antenna array models in Figure 2.20(a), we found that when the spatial signals arriving at the different elements of the antenna array become less correlated, the achievable spatial diversity gain becomes higher, hence the achievable performance improves. Furthermore, when the correlation of the signals arriving at the different elements of the antenna array decreases, the performance difference between the MRC scheme and the optimum combiners will reduce. A summary of the associated results was provided in Table. 2.1 for the sake of characterizing and comparing the attainable BER performance of all optimum combining schemes invoked for the uplink of the generalized MC DS-CDMA system supporting four users. As expected, the generalized MC DS-CDMA uplink system employing $V = 4$ subcarriers significantly outperformed the single-carrier DS-CDMA system, attaining a 6.7 dB SNR gain at a BER of $10^{-3}$. However, this implies a higher computational complexity, which is increased from the order of $O(L^3) = O(3^3)$ to $O[(VL)^3] = O(12^3)$, when a $(1 \times 3)$-dimensional receive antenna array ($M = 1, L = 3$) and any of the joint subcarrier processing based optimum combiners of Section 2.3 are employed. Observe from Figure 6.1(a) that when increasing the number of receive antenna elements $L$ in each of the $M$ arrays, the attainable directional gain becomes higher. For example, the system employing a $(1 \times 2)$-dimensional beamforming uplink receive array ($M = 1, L = 2$) achieved a 2.9 dB SNR gain at a BER of $10^{-4}$ compared to that employing a single receive antenna and this was achieved by increasing the computational complexity from $O[V^3]$ to $O[(2V)^3]$. Furthermore, increasing the number of receive antenna arrays $M$ from 1

| MSINR Scheme Normalized User-load | $E_b/N_0$(dB) required at BER=$10^{-4}$ | $E_b/N_0$(dB) required at BER=$10^{-5}$ | Figure No. |
|---|---|---|---|
| 1/124 ($K = 1$) | 14.2 | 16.7 | Figure 2.13 |
| 1/31 ($K = 4$) | 14.6 | 17.8 | Figure 2.13 |
| 1/4 ($K = 31$) | 15.0 | 18.0 | N/A |
| 1/2 ($K = 62$) | 16.2 | 18.8 | Figure 2.15 |

**Table 6.1:** Summary of the required $E_b/N_0$ values for the MSINR scheme of Section 2.3.3 using no channel coding and characterized in Figures 2.13 and 2.15 invoked for the uplink of the generalized MC DS-CDMA system, employing a $(1 \times 3)$-dimensional antenna array ($M = 1, L = 3$).

to 2, is capable of improving the achievable spatial diversity gain, resulting in a 5.3 dB SNR gain at the expense of increasing the computational complexity from $O[(2V)^3]$ to $O[(4V)^3]$. However, with the aid of individual subcarrier based processing schemes, we are capable of substantially reducing the computational complexity from $O[(VML)^3]$ to $O[V(ML)^3]$, while maintaining a similar BER performance. A summary of the associated results is provided in Table. 6.1 for the sake of characterizing and comparing the attainable BER performance of the MSINR scheme invoked for the uplink of the generalized MC DS-CDMA system supporting a different number of users. Finally, the computational complexity of the corresponding optimum beamforming aided generalized MC DS-CDMA systems is provided in Figure 6.1(b).

For a downlink scenario, Chapter 3 has provided four downlink space-time transmitter processing schemes based on the principles of beamforming, BSTD, STTD and SSTS, which were outlined in Sections 3.2-3.5. Four corresponding downlink system models were also provided and developed. It has been shown that the achievable downlink performance improvements are a function of both the antenna spacing and the specific techniques used for attaining TD and beamforming. TF-domain spreading was employed for the sake of achieving both user-load improvements as well as F-domain diversity gain, while a novel interference coefficient based user-grouping technique was employed in order to mitigate the effects of multiuser interference caused by the employment of TF-domain spreading. The performance of these schemes was studied and compared in Section 3.7. More explicitly, several different antenna array configurations have been investigated. Figures 3.22 and 3.23 demonstrated that the beamforming scheme achieved a better performance at low SNRs, but a worse performance at high SNRs, when compared to the BSTD and the SSTS schemes. In contrast to the SSTS scheme of Section 3.5 of Section 3.3, which belongs to the family of open-loop methods, the BSTD scheme is a representative of the class of closed loop proposals, activating the specific antenna array benefitting from the best instantaneous channel state and therefore in this scenario its performance is superior in comparison to that of SSTS. The STTD scheme of Section 3.4 achieves a higher transmit diversity gain than other three schemes, when the number of downlink transmit antenna array elements is fixed. However, as discussed in Section 3.4, the highest incremental diversity gains are achieved upon increasing the number of downlink transmit antennas from one to two,

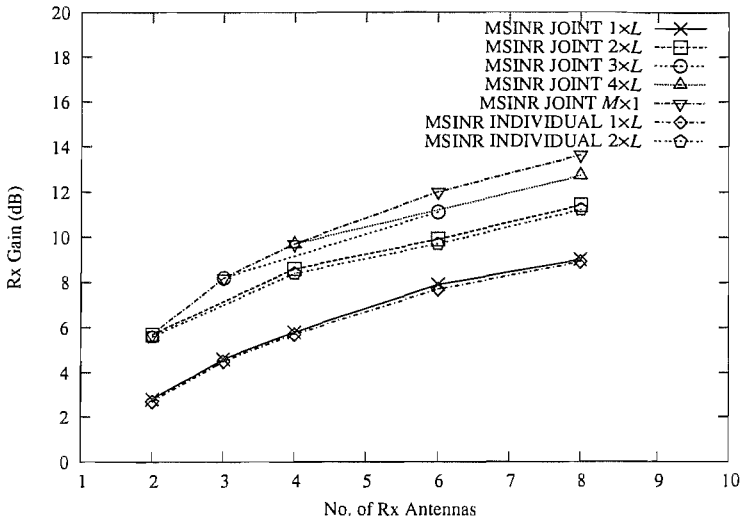


(a)

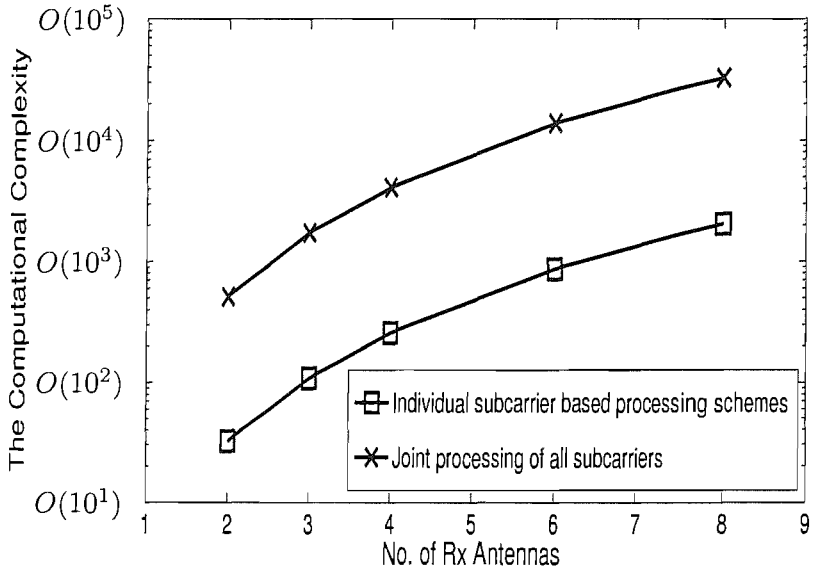


(b)

**Figure 6.1:** (a) Receive (Rx) gain versus the number of receive antennas for the various antenna array types employed for the uplink of the MSINR-aided generalized MC DS-CDMA system supporting four users at a BER of $10^{-4}$. These results were extracted from Figures 2.17, 2.18 and 2.19. (b) The computational complexity versus the number of receive antennas for the various antenna array types employed for the uplink of the optimum beamforming-aided generalized MC DS-CDMA system employing $V = 4$ subcarriers based on both individual subcarrier based processing and on using joint processing of all subcarriers, as outlined in Section 2.3.1.4. Since the corresponding Rx gain recorded in Figure 6.1(a) for the joint processing of all subcarriers is only marginally better than that of the substantially less complex individual subcarrier processing, the latter is recommended for practical implementations.

while adding further additional antennas achieves modest additional diversity gains on the downlink. Therefore, when employing more than $M = 2$ downlink transmit antenna arrays, the STTD scheme of Section 3.4 achieves the poorest performance. A summary of the associated results was provided in Table 3.2 for the sake of characterizing and comparing the attainable BER performance of all transmit space-time processing schemes invoked for the downlink of the generalized MC DS-CDMA system. This summary is repeated in Table 6.2 for the reader's convenience. Figure 6.2 confirmed that when a BER performance of $10^{-5}$ was required, the downlink BSTD scheme achieved the highest $E_b/N_0$ gain, while the SSTS scheme outperformed both the BF scheme and the STTD scheme. In contrast to the STTD scheme, the BF scheme attained a higher $E_b/N_0$ gain, when four or more transmit antennas were installed in the BS's transmitter. However, the downlink STTD scheme outperformed the downlink BF scheme, when only two transmit antennas were invoked by the BS's downlink transmitter. Figure 6.2 demonstrated that the STTD system using a $(2 \times 1)$-dimensional downlink transmit antenna array ($M = 2, L = 1$) and hence benefitting from $2^{\text{nd}}$-order transmit diversity outperformed the system employing a single antenna ($M = 1, L = 1$), attaining a 2.9 dB SNR gain at a BER of $10^{-5}$. By additionally invoking downlink beamforming, the SSTS system using a $(2 \times 2)$-dimensional transmit antenna array ($M = 2, L = 2$) achieved a 4.0 dB SNR gain compared to the STTD system employing a $(2 \times 1)$-dimensional antenna array ($M = 2, L = 1$) and a 2.6 dB SNR gain compared to the STTD system using a $(4 \times 1)$-dimensional antenna array ($M = 4, L = 1$) at a BER of $10^{-5}$. Furthermore, two downlink differential space-time processing schemes based on the principles of DSTS and DSSTS were proposed in Section 3.6 for the sake of enhancing the attainable downlink performance of generalized MC DS-CDMA systems operating in fast fading channels. As expected, the attainable performance of both the DSTS and DSSTS schemes is about 3 dB worse than those of the corresponding non-differential STS and SSTS schemes, respectively, which can be achieved however without any CSI, i.e. at a reduced complexity. The DSSTS system employing a $(2 \times 2)$-dimensional downlink transmit antenna array ($M = 2, L = 2$) outperforms the DSTS system using a $(4 \times 1)$-dimensional antenna array ($M = 4, L = 1$), suggesting that the DSSTS scheme employs DSTS for the sake of obtaining transmit diversity, but additionally also invokes beamforming to attain a higher SNR gain. Table. 6.3 characterized the attainable BER performance of the SSTS scheme invoked for the downlink of the generalized MC DS-CDMA system supporting different users.

Our study in Chapter 2 was based on the assumption that the receiver has either full knowledge or partial knowledge of the DOA, of the channel amplitudes, the phases, as well as the timing of the interfering users. However, the estimation accuracy of the channel parameters has a grave impact on the attainable detection performance. Naturally, the estimation of these parameters increases the complexity imposed and typically requires channel sounding overhead, which wastes valuable bandwidth. Furthermore, when the CIR fades rapidly, its estimation based on the previous symbols might be insufficiently accurate for the reliable detection of the forthcoming symbols. Hence in Chapter 4, adaptive space-time processing schemes were invoked for the proposed generalized MC DS-CDMA uplink, which are capable of tracking the space-time CIR in real time, while maintaining a modest receiver complexity. The convergence rate of the LMS-based ASTD of Figure 4.4 was shown to be

| Scheme | Type of antenna arrays | $E_b/N_0$(dB) required at BER=$10^{-2}$ | $E_b/N_0$(dB) required at BER=$10^{-4}$ | $E_b/N_0$(dB) required at BER=$10^{-5}$ | Figure No. |
|---|---|---|---|---|---|
| Beamforming | 1 × 4 | 0.4 | 7.1 | 9.2 | Figure 3.22 |
| | 1 × 6 | -1.7 | 5.3 | 7.4 | Figure 3.24 |
| BSTD | 2 × 2 | 0.6 | 6.0 | 7.5 | Figure 3.22 |
| | 2 × 3 | -1.6 | 4.2 | 5.9 | Figure 3.24 |
| STTD | 4 × 1 | 4.9 | 9.5 | 10.9 | Figure 3.22 |
| SSTS | 2 × 2 | 2.4 | 7.5 | 9.0 | Figure 3.22 |
| | 2 × 3 | 0.4 | 5.9 | 7.6 | Figure 3.24 |

**Table 6.2:** Summary of the required $E_b/N_0$ values for the various schemes characterized in Figures 3.22 and 3.24 invoked for the downlink of the generalized MC DS-CDMA system supporting a single user, where five different types of antenna arrays were employed, namely a $(1 \times 4)$-dimensional antenna array $(M = 1, L = 4)$ and a $(1 \times 6)$-dimensional antenna array $(M = 1, L = 6)$ employed for the BF scheme, a $(2 \times 2)$-dimensional antenna array $(M = 2, L = 2)$ and a $(2 \times 3)$-dimensional antenna array $(M = 2, L = 3)$ used by the BSTD and SSTS schemes, and finally, a $(4 \times 1)$-dimensional antenna array $(M = 4, L = 1)$ employed for the STTD scheme.

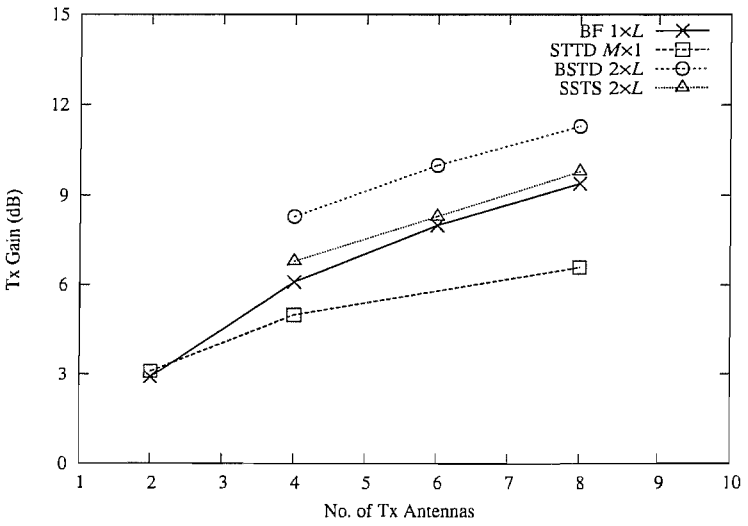


**Figure 6.2:** Transmit (Tx) gain versus the number of the transmit antennas for the various schemes invoked for the downlink of the generalized MC DS-CDMA system supporting a single user at a BER of $10^{-5}$, where ten different types of antenna arrays were employed, namely a $(1 \times 2)$-dimensional antenna array $(M = 1, L = 2)$, a $(1 \times 4)$-dimensional antenna array $(M = 1, L = 4)$, a $(1 \times 6)$-dimensional antenna array $(M = 1, L = 6)$ and a $(1 \times 8)$-dimensional antenna array $(M = 1, L = 8)$ employed for the BF scheme, a $(2 \times 2)$-dimensional antenna array $(M = 2, L = 2)$, a $(2 \times 3)$-dimensional antenna array $(M = 2, L = 3)$ and a $(2 \times 4)$-dimensional antenna array $(M = 2, L = 4)$ used by the BSTD and SSTS schemes, and finally, a $(2 \times 1)$-dimensional antenna array $(M = 2, L = 1)$, a $(4 \times 1)$-dimensional antenna array $(M = 4, L = 1)$ and a $(8 \times 1)$-dimensional antenna array $(M = 8, L = 1)$ employed for STTD scheme. These results were extracted from Figures 3.26 and 3.27.

| SSTS Scheme Normalized User-load | $E_b/N_0$(dB) required at BER=$10^{-4}$ | $E_b/N_0$(dB) required at BER=$10^{-5}$ | Figure No. |
|---|---|---|---|
| 1/128 ($K = 1$) | 7.5 | 9.0 | Figure 3.19 |
| 1/4 ($K = 32$) | 7.5 | 9.0 | Figure 3.19 |
| 1/2 ($K = 64$) | 13.8 | 22.1 | Figure 3.19 |
| 1/2 ($K = 64$) user-grouping | 8.1 | 9.8 | Figure 3.19 |

**Table 6.3:** Summary of the required $E_b/N_0$ values for the SSTS scheme characterized in Figure 3.19 invoked for the downlink of the generalized MC DS-CDMA system, employing a $(2 \times 2)$-dimensional antenna array ($M = 2, L = 2$).

heavily dependent on the step-size parameter $\mu$, while that of the RLS-based ASTD was seen to be largely dependent on the parameter $\delta$ of Section 4.4. As expected, the RLS-based uplink ASTD has a higher convergence rate than that of the LMS-based ASTD, which is achieved by increasing the computational complexity from the order of $O(VN_a)$ to $O[(VN_a)^2]$. Furthermore, the joint uplink LMS-based ASTD of Figure 4.5 outperformed the standard LMS-based ASTD seen in Figure 4.4 in terms of its BER performance, although it has a slightly slower convergence rate than the standard LMS-based ASTD. By using the proposed PIC technique of Section 4.5, we increased the achievable convergence rate of the uplink ASTD, while maintaining the required BER performance. The BER performances of all the adaptive detectors characterized in Figure 4.11 - Figure 4.16 were found to be similar, when they have the same misadjustment MSE. Having investigated a range of different antenna array models, we concluded that when the spatial signals arriving at the different elements of the uplink antenna array become less correlated, the spatial diversity gain becomes higher, hence the achievable BER performance improves. Table 6.4 suggests that at a BER of $10^{-5}$, the uplink ASTDs employing a $(4 \times 1)$-dimensional antenna array ($M = 4, L = 1$) achieve a 5.0 dB SNR gain compared to that using a $(2 \times 2)$-dimensional antenna array ($M = 2, L = 2$), a 6.7 dB SNR gain in comparison to a $(1 \times 4)$-dimensional antenna array ($M = 1, L = 4$) and a 7.1 dB SNR gain in comparison to that employing a $(1 \times 3)$-dimensional antenna array ($M = 1, L = 3$). The computational complexity of the corresponding ASTD aided generalized MC DS-CDMA systems is portrayed in Figure 6.3(b). Finally, Table. 6.5 summarized the attainable BER performance of the RLS-based ASTD invoked for the uplink of the generalized MC DS-CDMA system supporting different number of users.

Finally, subspace-based blind and group-blind space-time MUDs are invoked as joint space-time-frequency domain MUDs for the smart antenna aided generalized MC DS-CDMA uplink outlined in Chapter 5, since subspace-based estimation techniques are capable of extracting the channel estimates required. Furthermore, these blind and group-blind MUDs do not require any training sequence and hence achieve an increased spectral efficiency. The performance of these blind and group-blind MUDs was characterized in Section 5.4. As seen in Figures 5.4 and 5.5, when more signature waveforms were known to the receiver, the group-blind MUD significantly outperformed the blind MUD.

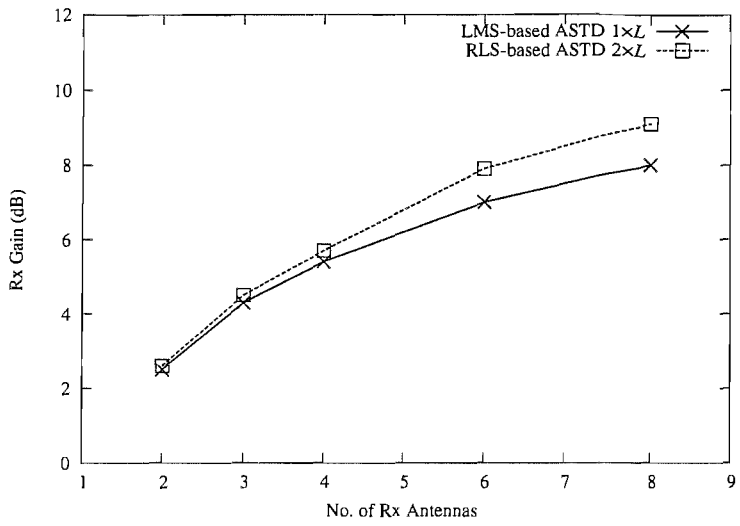


(a)

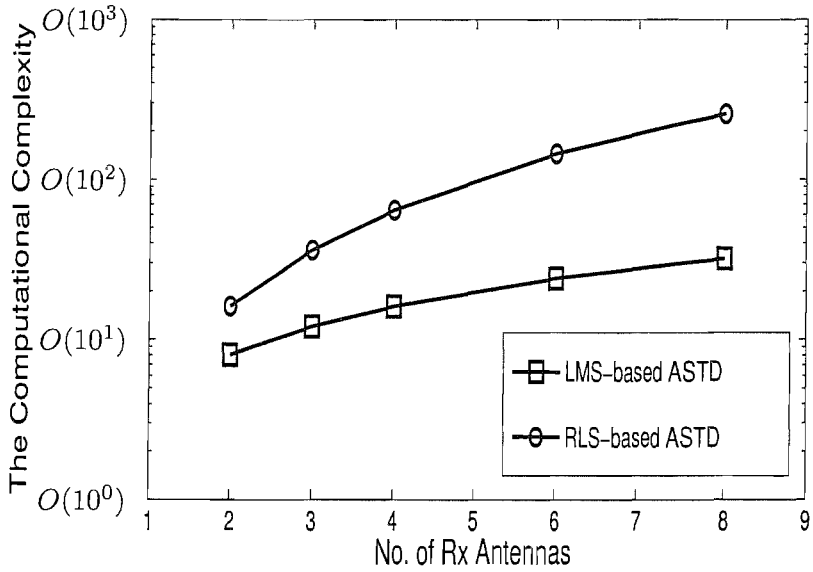


(b)

**Figure 6.3:** (a) Receive (Rx) gain versus the number of the receive antennas for the uplink of the ASTD-aided generalized MC DS-CDMA system supporting four users at a BER performance of $10^{-4}$. Note that the computational complexity of the LMS-based ASTD is on the order of $O(VML)$, while the computational complexity of the RLS-based ASTD is on the order of $O[(VML)^2]$. (b) The computational complexity versus the number of receive antennas for the various antenna array types of Section 4.6 employed for the uplink of the ASTD-aided generalized MC DS-CDMA system employing $V = 4$ subcarriers based on both the LMS-based ASTD and the RLS-based ASTD as outlined in Section 4.4.1. Figure 6.3(a) suggests that when more antennas are employed, the performance gap between the RLS-based ASTD and the LMS-based ASTD becomes larger, since the former has a faster convergence rate.

| Scheme | Type of antenna arrays | $E_b/N_0$(dB) required at BER=$10^{-4}$ | $E_b/N_0$(dB) required at BER=$10^{-5}$ | Figure No. |
|---|---|---|---|---|
| LMS-based ASTD | 1 × 4 | 13.9 | 18.0 | Figure 4.18 |
| | 2 × 2 | 10.8 | 13.0 | Figure 4.18 |
| | 4 × 1 | 9.4 | 11.3 | Figure 4.18 |
| RLS-based ASTD | 1 × 4 | 13.9 | 18.1 | Figure 4.18 |
| | 2 × 2 | 10.8 | 12.9 | Figure 4.18 |
| | 4 × 1 | 9.4 | 11.3 | Figure 4.18 |
| LMS/PIC iter=2 | 1 × 4 | 13.9 | 18.0 | Figure 4.18 |
| | 2 × 2 | 10.8 | 13.0 | Figure 4.18 |
| | 4 × 1 | 9.4 | 11.3 | Figure 4.18 |
| RLS/PIC iter=2 | 1 × 4 | 13.8 | 18.0 | Figure 4.18 |
| | 2 × 2 | 10.7 | 12.8 | Figure 4.18 |
| | 4 × 1 | 9.3 | 11.3 | Figure 4.18 |

**Table 6.4:** Summary of the $E_b/N_0$ values required by the various adaptive space-time processing schemes characterized in Figure 4.18 invoked for the uplink of the generalized MC DS-CDMA system supporting four users, as well as employing the different antenna arrays outlined in Section 4.6, where we have $\mu = 2.0$ and $\delta = 50$.

| RLS-based ASTD Normalized User-load | $E_b/N_0$(dB) required at BER=$10^{-3}$ | $E_b/N_0$(dB) required at BER=$10^{-4}$ | Figure No. |
|---|---|---|---|
| $1/124$ $(K = 1)$ | 9.8 | 14.3 | N/A |
| $1/31$ $(K = 4)$ | 10.2 | 14.7 | Figure 4.16 |
| $1/4$ $(K = 31)$ | 12.4 | 18.3 | Figures 4.15 |
| $1/2$ $(K = 62)$ | 14.3 | 23.7 | N/A |

**Table 6.5:** Summary of the required $E_b/N_0$ values for the RLS-based ASTD characterized in Figures 4.15 and 4.16 invoked for the uplink of the generalized MC DS-CDMA system, employing a (1 × 3)-dimensional antenna array ($M = 1, L = 3$).

Furthermore, the FST tracking algorithm of Section 5.2.4 exhibited a faster convergence and better steady-state performance than that of the PASTd tracking algorithm of Section 5.2.4. When considering the space-time blind and group-blind MUDs, the system using an antenna array having AEs exposed to uncorrelated fading achieved a better performance than that associated with correlated AEs, which was confirmed by Figure 5.10. As expected, the blind MUD employing a single antenna attained the worst performance. Figures 5.12, 5.13 and 5.14 demonstrated the robustness of the family of blind and group-blind MUDs against the near-far effects, since they are capable of efficiently suppressing the MAI. Furthermore, Figure 5.21 showed that the space-time blind and group-blind MUDs of Section 5.3.4 are capable of achieving a performance close to that attained with the aid of perfect knowledge of the CIRs, which implied that the associated performance degradation imposed by channel estimator errors is negligible. Our simulation results also suggested that increasing the number

of AEs is capable of providing an increased degree of freedom and hence of substantially improving the attainable performance at the expense of a higher system complexity. Similarly, increasing the number of subcarriers employed has the potential of offering an increased degree of freedom. Furthermore, employing more subcarriers will increase the attainable frequency diversity gain and hence improve the achievable performance. However, employing more subcarriers typically implies a higher system complexity. Observe in Figure 5.17 that when employing a single antenna, the group-blind MUD benefitting from the knowledge of $\tilde{K} = 8$ intracell users' signature waveforms and hence carrying out blind channel estimation for these $\tilde{K} = 8$ users outperformed the totally blind MUD exploiting the signature waveform of the desired user only, attaining a 2.9 dB SNR gain at a BER of $5 \times 10^{-3}$. As documented in Figure 5.20, when using the NAHJ-FST algorithm of Section 5.2.4, the group-blind MUD employing an antenna array having $M = 2$ AEs exposed to uncorrelated fading achieved a 4.2 dB SNR gain at a BER of $10^{-4}$ compared to that employing a single antenna, which is attained at the cost of increasing the computational complexity from the order of $O(2NV \cdot J)$ to $O(4NV \cdot J)$. Furthermore, the NAHJ-FST algorithm based group-blind MUD attained a similar BER performance to that employing EVD algorithm of Section 5.2.4, while significantly reducing the computational complexity, namely from the order of $O[(2NVM)^3]$ to $O(2NVM \cdot J)$. Table 5.7 provids a comparison of the BER performance of blind and group-blind MUDs invoked for the generalized MC DS-CDMA system supporting $K = 10$ users. It was shown that when employing an antenna array having $M = 2$ correlated AEs, the Group-blind space-time MUD benefitting from the knowledge of $\tilde{K} = 8$ intracell users' spreading codes attained a 5.0 dB SNR gain at a BER of $2 \times 10^{-3}$, compared to the blind space-time MUD. Figure 6.4(a) characterizes the SNR gains achieved by increasing the number of AEs, where a total of $K = 10$ users were supported and the group-blind MUDs benefitted from the knowledge of $\tilde{K} = 8$ intracell users' spreading codes. Finally, in Figure 6.5, where an antenna array having $M = 2$ uncorrelated AEs was employed and we had $\rho = 0$, the BER performance of the blind and the group-blind MUDs was presented as a function of the number of users supported. Note that the system serving $K = 60$ users was fully loaded.

## 6.2 Future Work

There are several possible extensions to the work presented in this thesis.

In Chapter 2, our investigations focused on the optimum combining schemes invoked for the uplink of the proposed generalized MC DS-CDMA. Channel coding schemes, including turbo coding [7, 232, 233], Trellis Coded Modulation (TCM) [7, 234] and Turbo Trellis Coded Modulation (TTCM) [7, 235], would be employed in our future study, since these channel coding schemes have the potential of further improving the performance of the generalized MC DS-CDMA system considered. Turbo codes were pioneered by Berrou, Glavieux and Thitimajshima [232, 233] in 1993, which facilitate the operation of communications systems near the Shannonian limits. TCM [234] was originally proposed for communicating over Gaussian channels and it was later further developed for applications in mobile communications [236]. TTCM [235] is a more recent joint coding

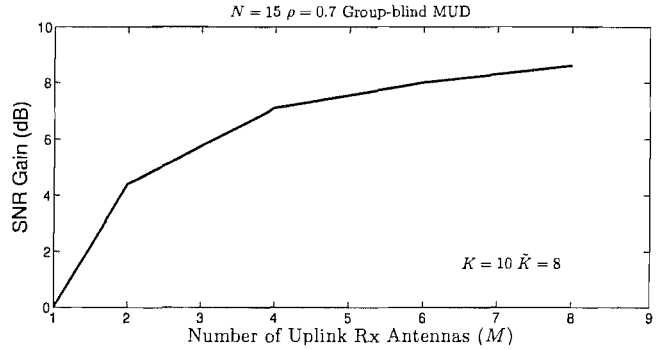


(a)

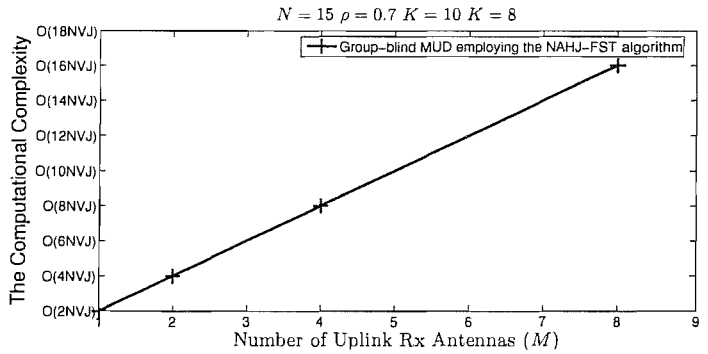


(b)

**Figure 6.4:** (a) SNR gain versus the number of receive antennas, $M$, performance of group-blind MUDs at a BER of $10^{-4}$. (b) The computational complexity imposed versus the number of the receive antennas, $M$, performance of group-blind MUDs employing the NAHJ-FST algorithm of Section 5.2.4. Antenna arrays having a cross-correlation coefficient of $\rho = 0.7$ were used. A total of $K = 10$ users were supported and the group-blind MUDs benefitted from the knowledge of $\tilde{K} = 8$ intracell users' spreading codes. The remaining system parameters are summarized in Table 5.6. Note that we have $2K \leq J \leq 3K$. Observe by comparing Figures 6.4(a) and 6.4(b) that most of the SNR gain was achieved by the uplink MUD employing $M = 4$ receive antennas at a moderate complexity.

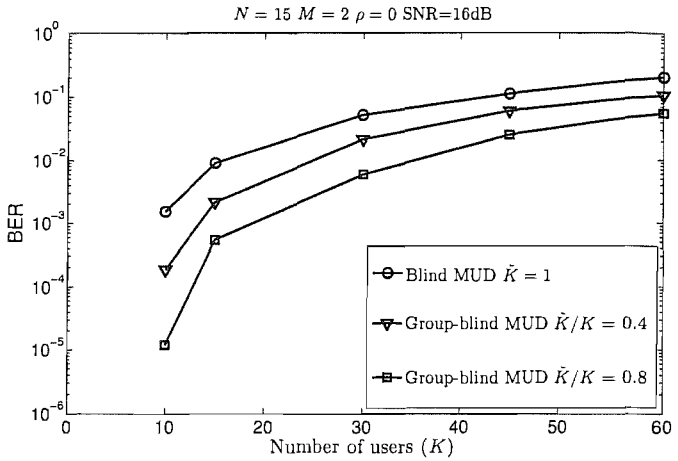


**Figure 6.5:** BER versus the number of users, $K$, performance of the various MC DS-CDMA MUDs considered. An antenna array having $M = 2$ uncorrelated AEs was employed and we had $\rho = 0$. The SNR was fixed to 16dB. When considering the group-blind MUDs, the ratio of $\tilde{K}/K$ was assigned to 0.4 or 0.8. The remaining system parameters are summarized in Table 5.6.

and modulation scheme that has a structure similar to that of the family of power-efficient binary turbo codes [232, 233], but employs TCM schemes as component codes. Both TCM and TTCM use symbol interleavers for the sake of achieving time diversity, when communicating over Rayleigh fading channels. Furthermore, three types of rank reduction schemes [237, 238] based on the principles of Principal Components (PC) [237, 238], on the so-called Cross-Spectral Metric (CSM) [237, 238], or on the Taylor Polynomial Approximation (TPA) [237, 238] would be studied, which are capable of substantially reducing the computational complexity.

In Chapter 3, the four downlink space-time transmitter processing schemes of Sections 3.2 - 3.5 were based on pure beamforming, pure spatial diversity and a combination of diversity as well as beamforming. However, Space Division Multiple Access (SDMA) [9] techniques and Bell Laboratory's Layered Space-Time (BLAST) [116–118] techniques and their hybrids can also be used to improve the proposed MC DS-CDMA system's coverage, capacity and link quality. As a third application of smart antennas, SDMA schemes exploiting the unique, user-specific "spatial signature" of the individual users for the sake of differentiating amongst them will be studied. In the downlink of the generalized MC DS-CDMA systems considered, SDMA schemes can be employed in conjunction with a range of performance enhancement schemes, such as the user-grouping technique of Chapter 3, where users are grouped according to the interference coefficients that are derived from the user-specific "spatial signature" of the individual users. Finally, BLAST schemes also employ smart antennas for the sake of increasing the throughput of a wireless system in terms of the number of bits per symbol.

The above-mentioned channel coding schemes can also be combined with the adaptive space-time processing schemes of Chapter 4, for the sake of further improving the achievable performance at the expense of a higher computational complexity. However, the increased computational complexity can

be counteracted by using rank reduction schemes. Furthermore, for a fast fading scenario, long range CIR-tap prediction techniques [239] can be invoked.

Two adaptive subspace tracking algorithms, namely the PASTd algorithm and the NAHJ-FST algorithm, were investigated in Chapter 5 for the sake of reducing the computational complexity. Both of them have a low computational complexity on the order of $O(N \cdot K)$, where $N$ is the dimension of the received signal sample space $\mathbf{r}(t)$ and $K$ is the number of eigencomponents to be updated. We can further reduce the computational complexity by invoking the Expectation-Maximization (EM) algorithm [172], which exhibited a lower computational complexity on the order of $O(K^2)$. Multi-Stage Wiener Filtering (MSWF) [237, 238] based adaptive reduced-rank interference suppression algorithms can also be employed to reduced the computational complexity. Once we achieve a modest complexity by employing above-mentioned algorithms, channel coding schemes can be used in order to improve the attainable performance.

# Bibliography


[1] X. Wang and H. V. Poor, "Blind Multiuser Detection: A Subspace Approach," *IEEE Transactions on Information Theory*, vol. 44, pp. 677–690, March 1998.

[2] X. Wang and H. V. Poor, "Blind Equalization and Multiuser Detection in Dispersive CDMA Channels," *IEEE Transactions on Communications*, vol. 6, pp. 91–103, January 1998.

[3] B. Yang, "Projection Approximation Subspace Tracking," *IEEE Transactions on Signal Processing*, vol. 44, pp. 95–107, January 1995.

[4] D. Reynolds and X. Wang, "Adaptive Transmitter Optimization for Blind and Group-Blind Multiuser Detection," *IEEE Transactions on Signal Processing*, vol. 51, pp. 825–832, March 2003.

[5] L. Hanzo, W. T. Webb, and T. Keller, *Single- and Multi-carrier Quadrature Amplitude Modulation: Principles and Applications for Personal Communications, WLANs and Broadcasting.* London: IEEE Press, and John Wiley & Sons, 2nd ed., 1999.

[6] J. Blogh and L. Hanzo, *Third-generation systems and intelligent wireless networking: smart antennas and adaptive modulation.* John Wiley & Sons - IEEE Press, 2002.

[7] L. Hanzo, C. H. Wong, and M. S. Yee, *Adaptive Wireless Transceivers : Turbo-Coded, Turbo-Equalised and Space-Time Coded TDMA, CDMA, MC-CDMA and OFDM Systems.* John Wiley & Sons - IEEE Press, 2002.

[8] L. Hanzo, L. L. Yang, E. L. Kuan, and K. Yen, *Single- and Multi- Carrier DS-CDMA.* John Wiley & Sons - IEEE Press, 2003, 1060 pages.

[9] L. Hanzo, M. Munster, B. J. Choi, and T. Keller, *OFDM and MC-CDMA.* John Wiley & Sons - IEEE Press, 2003, 960 pages.

[10] R. Steele and L. Hanzo, eds., *Mobile Radio Communications.* IEEE Press-John Wiley, 2 ed., 1999.

[11] A. J. Viterbi, *CDMA: Principles of Spread Spectrum Communications*. New York: Addison-Wesley Publishing Company, 1995.

[12] E. A. Sourour and M. Nakagawa, "Performance of orthogonal multicarrier CDMA in a multipath fading channel," *IEEE Transactions on Communications*, vol. 44, pp. 356–367, March 1996.

[13] S. B. Slimane, "MC-CDMA with quadrature spreading for wireless communication systems," *European Transactions on Telecommunications*, vol. 9, pp. 371–378, July–August 1998.

[14] I. Kalet, "The multitone channel," *IEEE Transactions on Communications*, vol. 37, pp. 119–124, February 1989.

[15] R. Li and G. Stette, "Time-limited orthogonal multicarrier modulation schemes," *IEEE Transactions on Communications*, vol. 43, pp. 1269–1272, February/March/April 1995.

[16] L. Goldfeld and D. Wulich, "Multicarrier modulation system with erasures-correcting decoding for nakagami fading channels," *European Trans. on Telecommunications*, vol. 8, pp. 591–595, November–December 1997.

[17] E. S. Sousa, "Performance of a direct sequence spread spectrum multiple access system utilizing unequal carrier frequencies," *IEICE Transactions on Communications*, vol. E76-B, pp. 906–912, August 1993.

[18] B. R. Saltzberg, "Performance of an efficient parallel data transmission system," *IEEE Transactions on Communication Technology*, vol. 15, pp. 805–811, December 1967.

[19] C. W. Baum and K. F. Conner, "A multicarrier transmission scheme for wireless local communications," *IEEE Journal on Selected Areas in Communications*, vol. 14, pp. 512–529, April 1996.

[20] V. M. Dasilva and E. S. Sousa, "Multicarrier orthogonal CDMA signals for quasi-synchronous communication systems," *IEEE Journal on Selected Areas in Communications*, vol. 12, pp. 842–852, June 1994.

[21] L. Vandendorpe and O. V. de Wiel, "MIMO DEF equalization for multitone DS/SS systems over multipath channels," *IEEE Journal on Selected Areas in Communications*, vol. 14, pp. 502–511, April 1996.

[22] N. Al-Dhahir and J. M. Cioffi, "A bandwidth-optimized reduced-complexity equalized multicarrier transceiver," *IEEE Transactions on Communications*, vol. 45, pp. 948–956, August 1997.

[23] S. Hara and R. Prasad, "Design and performance of multicarrier CDMA system in frequency-selective Rayleigh fading channels," *IEEE Transactions on Vehicular Technology*, vol. 48, pp. 1584–1595, September 1999.

[24] Y. H. Kim, I. Song, Seokho, and S. R. Park, "A multicarrier CDMA system with adaptive subchannel allocation for forward links," *IEEE Transactions on Vehicular Technology*, vol. 48, pp. 1428–1436, September 1999.

[25] X. Gui and T. S. Ng, "Performance of asynchronous orthogonal multicarrier CDMA system in frequency selective fading channel," *IEEE Transactions on Communications*, vol. 47, pp. 1084–1091, July 1999.

[26] T. M. Lok, T. F. Wong, and J. S. Lehnert, "Blind adaptive signal reception for MC-CDMA systems in Rayleigh fading channels," *IEEE Transactions on Communications*, vol. 47, pp. 464–471, March 1999.

[27] B. J. Rainbolt and S. L. Miller, "Multicarrier CDMA for cellular overlay systems," *IEEE Journal on Selected Areas in Communications*, vol. 17, pp. 1807–1814, October 1999.

[28] S.-M. Tseng and M. R. Bell, "Asynchronous multicarrier DS-CDMA using mutually orthogonal complementary sets of sequences," *IEEE Transactions on Communications*, vol. 48, pp. 53–59, January 2000.

[29] D. N. Rowitch and L. B. Milstein, "Convolutionally coded multicarrier DS-CDMA systems in a multipath fading channel – Part I: Performance analysis," *IEEE Transactions on Communications*, vol. 47, pp. 1570–1582, October 1999.

[30] D. N. Rowitch and L. B. Milstein, "Convolutionally coded multicarrier DS-CDMA systems in a multipath fading channel – Part II: Narrow-band interference suppression," *IEEE Transactions on Communications*, vol. 47, pp. 1729–1736, November 1999.

[31] D. Lee and L. B. Milstein, "Comparison of multicarrier DS-CDMA broadcast systems in a multipath fading channel," *IEEE Transactions on Communications*, vol. 47, pp. 1897–1904, December 1999.

[32] N. Yee, J.-P. Linnartz, and G. Fettweis, "Multi-carrier CDMA in indoor wireless radio network," *IEICE Transactions on Communications*, vol. E77-B, pp. 900–904, July 1994.

[33] K. Fazel and S. Kaiser, *Multi-Carrier Spread-Spectrum Proceedings of the 5th International Workshop, Oberpfaffenhofen, Germany.* P.O. Box 17, 3300 AA Dordrecht, The Netherlands: Springer, 2006, 502 pages.

[34] L. L. Yang and L. Hanzo, "Slow frequency-hopping multicarrier DS-CDMA for transmission over Nakagami multipath fading channels," *IEEE Journal on Selected Areas in Communications*, vol. 19, pp. 1211–1221, July 2001.

[35] L. L. Yang, W. Hua, and L. Hanzo, "Multiuser Detection Assisted Time- and Frequency-Domain Spread Multicarrier Code-Division Multiple-Access," *IEEE Transactions on Vehicular Technology*, vol. 55, pp. 397–405, Jan. 2006.

[36] H. Wei, L. L. Yang, and L. Hanzo, "Interference-free broadband single- and multicarrier DS-CDMA," *IEEE Communications Magazine*, vol. 43, pp. 68–73, Feb. 2005.

[37] R. W. Chang, "Synthesis of band-limited orthogonal signals for multichannel data transmission," *Bell Systems Technical Journal*, vol. 45, pp. 1775–1796, December 1966.

[38] L. J. C. Jr., "Analysis and simulation of a digital mobile channel using orthogonal frequency division multiplexing," *IEEE Transactions on Communications*, vol. 33, pp. 665–675, July 1985.

[39] S. Hara and R. Prasad, "Overview of multicarrier cdma," *IEEE Communications Magazine*, pp. 126–133, December 1997.

[40] L.-L. Yang and L. Hanzo, "A unified approach to the analysis of multicarrier DS-CDMA over Nakagami-$m$ fading channels," in *Proceedings of IEEE GLOBECOM*, vol. 6, (San Antonio, Texas, USA), pp. 3429–3433, November 25-29, 2001.

[41] L.-L. Yang and L. Hanzo, "Performance of generalized multicarrier DS-CDMA over Nakagami-$m$ fading channels," *IEEE Transactions on Communications*, vol. 50, pp. 956 – 966, June 2002.

[42] L.-L. Yang and L. Hanzo, "Performance of generalized multicarrier DS-CDMA using various chip waveforms," *IEEE Transactions on Communications*, vol. 51, pp. 748–752, May 2003.

[43] L. Vandendorpe, "Multitone spread spectrum multiple access communications system in a multipath Rician fading channel," *IEEE Transactions on Vehicular Technology*, vol. 44, no. 2, pp. 327–337, 1995.

[44] H. L. V. Trees, *Optimum array processing Part IV of detection, estimation, and modulation theory*. New York: John Wiley & Sons, 2002.

[45] S. Affes and P. Mermelstein, "A new receiver structure for asynchronous CDMA: STAR - the spatio-temporal array-receiver," *IEEE Journal on Selected Areas in Communications*, vol. 16, pp. 1411 – 1422, October 1998.

[46] M. Dell'Anna and A. H. Aghvami, "Performance of optimum and suboptimum combining at the antenna array of a W-CDMA system," *IEEE Journal on Selected Areas in Communications*, vol. 17, pp. 1030–1039, Dec. 1999.

[47] Y. Zhou, F. Chin, Y. C. Liang, and C. C. Ko, "A novel beam selection transmit diversity scheme for DS-CDMA system," *IEICE Transaction on Communications*, vol. E84-B, pp. 2178–2185, Aug. 2001.

[48] Proposed TDOC: 662/98 to ETSI SMG2 UMTS Standards, *Space-time block coded transmit antenna diversity for WCDMA*, December 1998.

[49] R. A. Soni, R. M. Buehrer, and R. D. Benning, "Intelligent antenna system for cdma2000," *IEEE Signal Processing Magazine*, pp. 54–67, July 2002.

[50] T. S. Rappaport, *Wireless communications: principle and practice*. New Jersey, USA: Prentice Hall, 1996.

[51] J. D. Parsons, *The Mobile Radio Propagation Channel*. London: Pentech Press, 1992.

[52] S. R. Saunders, *Antennas and Propagation for Wireless Communication Systems*. John Wiley & Sons, 1999.

[53] W. C. Jakes, *Microwave Mobile Communications*. New York: Wiley, 1974.

[54] B. Sklar, *Digital Communications*. Englewood Cliffs, New Jersey: Prentice Hall, 1988, 766 pages.

[55] M. J. Gans, "A Powerful Spectral Theory of Propagation in the Mobile Radio Environment," *IEEE Transactions on Vehicular Technology*, vol. VT-21, pp. 27–38, Feb. 1972.

[56] A. M. Saleh and R. A. Valenzuela, "A statistical model for indoor multipath propagation," *IEEE JSAC*, vol. SAC-5, Feb. 1987.

[57] S. Y. Seidel and T. S. Rappaport, "Site-specific propagation prediction for wireless in-building personal communication system design," *IEEE Transactions on Vehicular Technology*, vol. 43, pp. 879–891, Nov. 1994.

[58] S. Y. Seidel, T. S. Rappaport, S. Jain, M. Lord, and R. Singh, "Path Loss, Scattering and Multipath Delay Statistics in Four European Cities for Digital Celluar and Microcelluar Radiotelephone," *IEEE Transactions on Vehicular Technology*, vol. 40, pp. 721–730, Nov. 1991.

[59] S. Y. Seidel and T. S. Rappaport, "914 MHz path loss prediction models for indoor wireless communications in multifloored buildings," *IEEE Transactions on Antennas and Propagation*, vol. 40, pp. 207–217, Feb. 1992.

[60] W. C. Y. Lee, *Mobile Communications Engineering*. New York: McGraw-Hill, 2nd ed., 1998.

[61] O. Norklit and J. B. Anderson, "Mobile radio environments and adaptive arrays," *Proceeding IEEE PIMRC*, pp. 725–728, 1994.

[62] P. Zetterberg and B. Ottersten, "The spectrum efficiency of a base station antenna array system for spatially selective transmission," *IEEE Transactions on Vehicular Technology*, vol. 44, pp. 651–660, Aug. 1995.

[63] G. G. Raleigh and A. Paulraj, "Time varying vector channel estimation for adaptive spatial equalization," *GLOBECOM '95., IEEE*, vol. 1, pp. 218–224, Nov. 1995.

[64] D. Aszetly, *On antenna arrays in mobile communication systems: Fast fading and GSM base station receiver algorithm.* Royal Inst. Technology: Ph.D. dissertation, Mar. 1996.

[65] P. Petrus, J. H. Reed, and T. S. Rappaport, "Geometrically based statistical channel model for macrocellular mobile environments," *IEEE Global Telecommunications Conference, 1996*, vol. 2, pp. 1197–1201, Nov. 1996.

[66] J. C. Liberti and T. S. Rappaport, "A geometrically based model for line-of-sight multipath radio channels," *IEEE Vehicular Technology Conference, 1996*, vol. 2, pp. 844–848, April 1996.

[67] P. Mogensen, "Algorithms and antenna array recommendations," *Tech. rep. A020/AUC/A12/DR/P/1/xx-D2.1.2*, Sept. 1996.

[68] A. Klein and W. Mohr, "A statistical wideband mobile radio channel model including the direction of arrival," *Proceeding IEEE 4th International Symposium on Spread Spectrum Techniques and Applications*, vol. 1, pp. 102–106, Sept. 1996.

[69] J. Litva and T. Lo, *Digital beamforming in wireless communications.* Artech, 1996.

[70] M. Lu, T. Lo, and J. Litva, "A physical spatio-temporal model of multipath propagation channels," *Proceeding IEEE VTC*, vol. 2, pp. 810–814, May 1997.

[71] R. B. Ertel, P. Cardieri, K. W. Sowerby, T. S. Rappaport, and J. Reed, "Overview of spatial channel models for antenna array communication systems," *IEEE Personal Communications*, vol. 5, pp. 10–22, Feb. 1998.

[72] T. Zwick, C. Fischer, D. Didascalou, and W. Wiesbeck, "A stochastic spatial channel model based on wave-propagation modeling," *IEEE Journal on Selected Areas in Communications*, vol. 18, pp. 6–15, Jan. 2000.

[73] T. Zwick, C. Fischer, and W. Wiesbeck, "A stochastic multipath channel model including path directions for indoor environments," *IEEE Journal on Selected Areas in Communications*, vol. 20, pp. 1178–1192, Aug. 2002.

[74] D. Reed, J. Smith, A. Rodriguez, and G. Calcev, "Spatial channel models for multi-antenna systems," *IEEE Vehicular Technology Conference, 2003*, vol. 1, pp. 99–103, Oct. 2003.

[75] F. Simpson and J. M. holtzman, "Direct sequence CDMA power control, interleaving, and coding," *IEEE Journal on Selected Areas in Communications*, vol. 11, pp. 1085–1095, Sept. 1993.

[76] S. Ariyavisitakul and L. F. Chang, "Signal and interference statistics of a CDMA system with feedback power control," *IEEE Transactions on Communications*, vol. 41, pp. 1626–1634, Nov. 1993.

[77] S. Ariyavisitakul, "Signal and interference statistics of a CDMA system with feedback power control ii," *IEEE Transactions on Communications*, vol. 42, pp. 597–605, February/March/April 1994.

[78] K. S. Gilhousen, I. M. Jacobs, R. Padovani, A. J. Viterbi, L. A. Weaver, and C. E. Wheatley, "On the capacity of a cellular CDMA system design," *IEEE Transactions on Vehicular Technology*, vol. 40, pp. 303–312, May 1991.

[79] R. Kohno, R. Median, and L. B. Milstein, "Spread spectrum access methods for wireless communications," *IEEE Communications Magazine*, pp. 58–67, Jan. 1995.

[80] S. Hara and R. Prasad, "Overview of multicarrier CDMA," *IEEE Communications Magazine*, pp. 126–133, December 1997.

[81] N. Yee, J.-P. Linnartz, and G. P. Fettweis, "Multicarrier CDMA in indoor wireless radio networks," in *Proceedings of PIMRC'93*, pp. 109–113, 1993.

[82] K. Fazel and L. Papke, "On the performance of convolutionally-coded CDMA/OFDM for mobile communication systems," in *Proceedings of PIMRC'93*, pp. 468–472, IEEE, September 1993.

[83] A. Chouly, A. Brajal, and S. Jourdan, "Orthogonal multicarrier techniques applied to direct sequence spread spectrum CDMA systems," in *Proceedings of the IEEE GLOBECOM '93*, (Houston, USA), pp. 1723–1728, November 1993.

[84] L. Vandendorpe, "Multitone direct sequence CDMA system in an indoor wireless environment," in *Proceedings of IEEE First Symposium of Communications and Vehicular Technology in the Benelux, Delft, The Netherlands*, pp. 4.1–1–4.1–8, Oct. 1993.

[85] H. H. Nguyen, "Effect of chip waveform shaping on the performance of multicarrier CDMA systems," *IEEE Transactions on Vehicular Technology*, vol. 54, pp. 1022–1029, May 2005.

[86] D. J. Sadler and A. Manikas, "MMSE multiuser detection for array multicarrier DS-CDMA in fading channels," *IEEE Transactions on Signal Processing*, vol. 53, pp. 2348–2358, July 2005.

[87] N. K. Bose, C. R. Rao, Lal, and C. Godara, *Handbook of statistics 10, signal processing and its applications: constrained beamforming and adaptive algorithms*. Amsterdam: Amsterdam, The Netherlands: North Hollands, 1993.

[88] D. H. Johnson and D. E. Dudgeon, *Array signal processing: concepts and techniques*. Englewood Cliffs: Englewood Cliffs, NJ:prentice-Hall, 1993.

[89] T. K. Sarkar, M. C. Wicks, M. Salazar-Palma, and R. J. Bonneau, *Smart-Antennas*. John Wiley & Sons - IEEE Press, 2003, 472 pages.

[90] R. A. Monzingo and T. W. Miller, *Introduction to adaptive arrays*. New York: Wiley, 1980.

[91] V. J. Garg and L. Huntington, "Application of adaptive array antenna to a tdma cellular/pcs system," *IEEE Communications Magazine*, vol. 35, pp. 148–152, Oct. 1997.

[92] Y. Li and N. R. Sollenberger, "Adaptive antenna arrays for OFDM systems with cochannel interference," *IEEE Transaction on Communications*, vol. 47, pp. 217–229, Feb 1999.

[93] J. B. Schodorf and D. B. Williams, "Array processing techniques for multiuser detection," *IEEE Transactions on Communications*, vol. 45, pp. 1375–1378, Nov. 1997.

[94] L. C. Godara, "Applications of antenna arrays to mobile communications. I. Performance improvement, feasibility, and system considerations," *Proceedings of the IEEE*, vol. 85, pp. 1031–1060, July 1997.

[95] A. J. Paulraj and C. B. Papadias, "Space-time processing for wireless communications," *IEEE Signal Processing Magazine*, vol. 14, pp. 49–83, Nov. 1997.

[96] N. Herscovici and C. Christodoulou, "Potentials of smart antennas in cdma systems and uplink improvements," *IEEE Antennas and Propagation Magazine*, vol. 43, pp. 172–177, Oct. 2001.

[97] S. A. Zekavat, C. R. Nassar, and S. Shattil, "Oscillating-beam smart antenna arrays and multicarrier systems: Achieving transmit diversity, frequency diversity, and directionality," *IEEE Transactions on Vehicular Technology*, vol. 51, pp. 1030–1039, Sep. 2002.

[98] S. A. Zekavat and C. R. Nassar, "Smart antenna arrays with oscillating beam patterns: characterization of transmit diversity in semi-elliptic coverage," *IEEE Transactions on Communications*, vol. 50, pp. 1549–1556, Oct. 2002.

[99] S. A. Zekavat, C. R. Nassar, and S. Shattil, "Merging multicarrier CDMA and oscillating-beam smart antenna arrays: exploiting directionality, transmit diversity, and frequency diversity," *IEEE Transactions on Communications*, vol. 52, pp. 110–119, Jan. 2004.

[100] S. C. Swales, M. A. Beach, D. J. Edwards, and J. P. McGeehan, "The performance enhancement of multibeam adaptive base-station antennas for cellular land mobile radio systems," *IEEE Transactions on Vehicular Technology*, vol. 39, pp. 56–67, Feb. 1990.

[101] S. Anderson, M. Millnert, M. Viberg, and B. Wahlberg, "An adaptive array for mobile communication systems," *IEEE Transactions on Vehicular Technology*, vol. 40, pp. 230–236, Feb. 1991.

[102] L. L. Yang, "MIMO-Assisted Space-Code-Division Multiple-Access: Linear Detectors and Performance Over Multipath Fading Channels," *IEEE Journal on Selected Areas in Communications*, vol. 24, pp. 121–131, Jan. 2006.

[103] Y. S. Song, H. M. Kwon, and B. J. Min, "Computationally efficient smart antennas for CDMA wireless communications," *IEEE Transactions on Vehicular Technology*, vol. 50, pp. 1613–1628, Nov. 2001.

[104] S.-S. Jeng, G. T. Okamoto, G. Xu, H.-P. Lin, and W. J. Vogel, "Experimental evaluation of smart antenna system performance for wireless communications," *IEEE Transactions on Antennas and Propagation*, vol. 46, pp. 749–757, June 1998.

[105] J. J. Blanz, A. Papathanassiou, M. Haardt, I. Furio, and P. W. Baier, "Smart antennas for combined DOA and joint channel estimation in time-slotted CDMA mobile radio systems with joint detection," *IEEE Transactions on Vehicular Technology*, vol. 49, pp. 293–306, March 2000.

[106] G. V. Tsoulos, G. E. Athanasiadou, and R. J. Piechocki, "Low-complexity smart antenna methods for third-generation W-CDMA systems," *IEEE Transactions on Vehicular Technology*, vol. 49, pp. 2382–2396, Nov. 2000.

[107] M. Ghavami, "Wideband smart antenna theory using rectangular array structures," *IEEE Transactions on Signal Processing*, vol. 50, pp. 2143–2151, Sept. 2002.

[108] A. O. Boukalov and S.-G. Haggman, "System aspects of smart-antenna technology in cellular wireless communications-an overview," *IEEE Transactions on Microwave Theory and Techniques*, vol. 48, pp. 919–929, June 2000.

[109] A. T. Alastalo and M. Kahola, "Smart-antenna operation for indoor wireless local-area networks using OFDM," *IEEE Transactions on Wireless Communications*, vol. 2, pp. 392–399, March 2003.

[110] I.-M. Kim, R. Yim, and H. Chaskar, "Optimum scheduling for smart antenna systems in Rayleigh fading channels," *IEEE Transactions on Communications*, vol. 53, pp. 1210–1219, July 2005.

[111] H. Liu and G. Xu, "Smart antennas in wireless systems: uplink multiuser blind channel and sequence detection," *IEEE Transactions on Communications*, vol. 45, pp. 187–199, Feb. 1997.

[112] T. Baumgartner and E. Bonek, "On the optimum number of beams for fixed beam smart antennas in UMTS FDD," *IEEE Transactions on Wireless Communications*, vol. 5, pp. 560–567, March 2006.

[113] J. H. Winters, "Smart antennas for wireless systems," *Personal Communications, IEEE*, vol. 5, pp. 23–27, February 1998.

[114] A. F. Naguib, A. Paulraj, and T. Kailath, "Capacity improvement with base-station antenna arrays in cellular cdma," *IEEE Transactions on Vehicular Technology*, vol. 43, pp. 691–698, Aug. 1994.

[115] L. C. Godara, "Application of antenna arrays to mobile communications. II. Beam-forming and direction-of-arrival considerations," *Proceedings of the IEEE*, vol. 85, pp. 1195–1245, Aug. 1997.

[116] G. J. Foschini, "Layed Space-Time architecture for wireless communication in a fading environment when using multiple antennas," *Bell Laboratories Technical Journal*, vol. 1, pp. 41–59, Aut. 1996.

[117] P. W. Wolniansky, G. J. Foschini, G. D. Golden, and R. A. Valenzuela, "V-BLAST: an architecture for realizing very high data rates over the rich-scattering wireless channel," *Proceeding IEEE ISSSE-98.*, pp. 295–300, (Pisa, Italy) Sept. 1998.

[118] S. Da-Shan and M. Kahn, "Layered space-time codes for wireless communications using multiple transmit antennas," *1999 IEEE International Conference on Communications*, vol. 1, pp. 436–440, June 1999.

[119] T. F. Wong, T. M. Lok, J. S. Lehnert, and M. D. Zoltowski, "A linear receiver for direct-sequence spread-spectrum multiple-access systems with antenna arrays and blind adaptation," *IEEE Transactions on Information Theory*, vol. 44, pp. 659–676, March 1998.

[120] E. N. Onggosanusi, A. M. Sayeed, and B. D. V. Veen, "Canonical space-time processing for wireless communications," *IEEE Transactions on Communications*, vol. 48, pp. 1669–1680, October 2000.

[121] J. D. Fredrick, Y. Wang, and T. Itoh, "Smart antennas based on spatial multiplexing of local elements (SMILE) for mutual coupling reduction," *IEEE Transactions on Antennas and Propagation*, vol. 52, pp. 106–114, Jan. 2004.

[122] P. Ioannides and C. A. Balanis, "Uniform circular arrays for smart antennas," *IEEE Antennas and Propagation Magazine*, vol. 47, pp. 192–206, Aug. 2005.

[123] M. Uthansakul and M. E. Bialkowski, "Fully spatial wide-band beamforming using a rectangular array of planar monopoles," *IEEE Transactions on Antennas and Propagation*, vol. 54, pp. 527–533, Feb. 2006.

[124] M. Wax and Y. Anu, "Performance analysis of the minimum variance beamformer," *IEEE Transactions on Signal Processing*, vol. 44, pp. 928–937, April 1996.

[125] A. F. Naguib, "Adaptive antennas for CDMA wireless networks," *Ph.D. Thesis*, August 1996.

[126] Y. Zhou, F. Chin, Y. C. Liang, and C. C. Ko, "Performance comparison of transmit diversity and beamforming for the downlink of DS-CDMA system," *IEEE Transactions on Wireless Communications*, vol. 2, pp. 320–334, Mar. 2003.

[127] A. Hottinen and R. Wichman, "Transmit diversity techniques for WCDMA," *Presented at the 5th Annual Smart Antenna Workshop*, July 1998.

[128] D. Rajan and S. D. Gray, "Transmit diversity schemes for CDMA-2000," *Proceeding IEEE Wireless Communications and Networking Conference*, pp. 669–673, Sept. 1999.

[129] A. Correia, A. Hottinen, and R. Wichman, "Space-time transmitter diversity schemes for wideband WCDMA," *Proceeding IEEE 51th Vehicular Technology Conference*, pp. 313–317, Spring 2000.

[130] J. S. Thompson, P. M. Grant, and B. Mulgrew, "Downlink transmit diversity schemes for CDMA networks," *Proceeding IEEE 50th Vehicular Technology Conference*, pp. 1382–1386, Fall 1999.

[131] A. Dabak, S. Hosur, and R. Negi, "Space time block coded transmit antenna diversity scheme for WCDMA," *Proceeding IEEE Wireless Communications and Networking Conference*, pp. 1466–1469, Sept. 1999.

[132] D. Gerlach and A. Paulraj, "Adaptive transmitting antenna methods for multipath environments," *Proceeding IEEE GLOBECOM*, pp. 425–429, Nov. 1994.

[133] M. J. Ho, G. L. Stüber, and M. D. Austin, "Performance of switched-beam smart antennas for cellular radio systems," *IEEE Transactions on Vehicular Technology*, vol. 47, pp. 10–19, Feb. 1998.

[134] J. Choi, "A semiblind method for transmit antenna arrays in WCDMA systems," *IEEE Transactions on Vehicular Technology*, vol. 51, pp. 624–635, July 2002.

[135] A. F. Naguib and A. Paulraj, "Performance of wireless CDMA with $M$-ary orthogonal modulation and cell site antenna arrays," *IEEE Journal on Selected Areas in Communications*, vol. 14, pp. 1770–1783, December 1996.

[136] Y. C. Liang and F. Chin, "Transmit antenna array techniques for celluar WCDMA systems," *Proceeding IEEE 9th PIMRC*, pp. 1396–1400, Sept. 1998.

[137] V. Tarokh and H. Jafarkhani, "A differential detection scheme for transmit diversity," *IEEE Journal on Selected Areas in Communications*, vol. 18, pp. 1169–1174, July 2000.

[138] B. L. Hughes, "Differential space-time modulation," *IEEE Transactions on Information Theory*, vol. 46, pp. 2567–2578, Nov. 2000.

[139] B. M. Hochwald and W. Sweldens, "Differential unitary space-time modulation," *IEEE Transactions on Communications*, vol. 48, pp. 2041–2052, Dec. 2000.

[140] S. M. Alamouti, "A simple ransmit diversity technique for wireless communications," *IEEE Journal on Selected Areas in Communications*, vol. 16, pp. 1451–1458, October 1998.

[141] J. H. Liu, J. Li, H. B. Li, and E. G. Larsson, "Differential space-code modulation for interference suppression," *IEEE Transactions on Signal Processing*, vol. 49, pp. 1786–1795, Aug. 2001.

[142] R. A. Soni and R. M. Buehrer, "On the performance of open-loop transmit diversity techniques for IS-2000 systems: a comparative study," *IEEE Transactions on Wireless Communications*, vol. 53, pp. 1602–1615, Sept. 2004.

[143] X. Cai, G. B. Giannakis, and M. D. Zoltowski, "Space-time spreading and block coding for correlated fading channels in the presence of interference," *IEEE Transactions on Communications*, vol. 53, pp. 515–525, March 2005.

[144] J. Wang and X. Wang, "Optimal linear space-time spreading for multiuser MIMO communications," *IEEE Journal on Selected Areas in Communications*, vol. 24, pp. 113–120, Jan. 2006.

[145] Z. Liu, G. B. Giannakis, and B. L. Hughes, "Double Differential Space¨CTime Block Coding for Time-Selective Fading Channels," *IEEE Transactions on Communications*, vol. 49, pp. 1529–1539, Sept. 2001.

[146] L. H.-J. Lampe and R. Schober, "Bit-Interleaved Coded Differential Space-Time Modulation," *IEEE Transactions on Communications*, vol. 50, pp. 1429–1439, Sept. 2002.

[147] H. B. Li and J. Li, "Differential and Coherent Decorrelating Multiuser Receivers for Space-Time-Coded CDMA Systems," *IEEE Transactions on Signal Processing*, vol. 50, pp. 2529–2537, Oct. 2002.

[148] R. Schober and L. H.-J. Lampe, "Differential Modulation Diversity," *IEEE Transactions on Vehicular Technology*, vol. 51, pp. 1431–1444, Nov. 2002.

[149] L. H.-J. Lampe, R. Schober, and R. F. H. Fischer, "Coded Differential Space¨CTime Modulation for Flat Fading Channels," *IEEE Transactions on Wireless Communications*, vol. 2, pp. 582–590, May 2003.

[150] R. T. Compton and Jr., *Adaptive antennas: Concepts and performance*. Prentice Hall, 1988.

[151] B. D. V. Veen and K. M. Buckley, "Beamforming: A versatile approach to spatial filtering," *IEEE ASSP Magazine*, vol. 5, pp. 4–24, April 1998.

[152] J. S. Thompson, P. M. Grant, and B. Mulgrew, "Smart antenna arrays for CDMA systems," *IEEE Personal Communications*, vol. 3, pp. 16–25, Oct. 1996.

[153] L. C. Godara, "Improved lms algorithm for adaptive beamforming," *IEEE Transactions on Antennas and Propagation*, vol. 38, pp. 1631–1635, Oct. 1990.

[154] S. Choi, "A novel adaptive beamforming algorithm for a smart antenna system in a CDMA mobile communications environment," *IEEE Transactions on Vehicular Technology*, vol. 49, pp. 1793–1806, Sept. 2000.

[155] S. Sigdel, K. M. Ahmed, and A. Fernando, "Performance of multicarrier-cdma uplink with antenna arrays and multiuser detection," *Journal of Communications and Network*, vol. 5, pp. 150–155, Jun. 2003.

[156] B. Widrow and M. E. Hoff, "Adaptive switching circuits," *1960 IRE WESCON Convention Record, New York IRE*, pp. 96–104, 1960.

[157] S. Haykin, *Adaptive filter theory*. New Jersey, USA: Prentice Hall, 3rd ed., 1996.

[158] W. A. Hamouda and P. J. Mclane, "Multiuser interference cancellation aided adaptation of a MMSE receiver for direct-sequence code-division multiple-access systems," *GLOBECOM '01. IEEE*, vol. 2, pp. 723–727, Nov. 25-29 2001.

[159] C. Pateros and G. Saulnier, "Adaptive correlator receiver performance in fading multipath channels," *Proceeding 1993 IEEE Vehicular Technology Conference*, pp. 746–749, 1993.

[160] S. Miller, "An adaptive direct-sequence code-division multiple-access receiver for multi-user interference rejection," *IEEE Transactions on Communications*, vol. 43, pp. 1746–1755, Apr. 1995.

[161] M. Honig, M. Shensa, S. Miller, and L. B. Milstein, "Performance of adaptive linear interference suppression for DS-CDMA in the presence of flat Rayleigh fading," *Proceeding 1997 IEEE Vehicular Technology Conference*, vol. 3, pp. 2191–2195, May 1997.

[162] A. N. Barbosa and S. Miller, "Adaptive detection of DS/CDMA signals in fading channels," *IEEE Transactions on Commmunications*, vol. 46, pp. 115–124, Jan. 1998.

[163] S. Miller, M. Honig, and L. B. Milstein, "Performance analysis of MMSE receivers for DS-CDMA in frequency-selective fading channels," *IEEE Transactions on Commmunications*, vol. 48, pp. 1919–1929, Nov. 2000.

[164] G. G. Joshi, J. C. B. Dietrich, and W. L. Stutzman, "Adaptive beamforming measurements using four-element portable and mobile arrays," *IEEE Transactions on Antennas and Propagation*, vol. 53, pp. 4065–4072, Dec. 2005.

[165] Y. Chen and S. S. Chi, "A RAKE receiver design for WCDMA FDD uplink with an RLS-based adaptive beamforming scheme," *IEEE Transactions on Vehicular Technology*, vol. 54, pp. 508–515, March 2005.

[166] A. El-Keyi, T. Kirubarajan, and A. B. Gershman, "Robust adaptive beamforming based on the Kalman filter," *IEEE Transactions on Signal Processing*, vol. 53, pp. 3032–3041, Aug. 2005.

[167] S. Chen, N. N. Ahmad, and L. Hanzo, "Adaptive minimum bit-error rate beamforming," *IEEE Transactions on Wireless Communications*, vol. 4, pp. 341–348, March 2005.

[168] M. Honig, U. Madhow, and H. V. Poor, "Blind Adaptive Multiuser Detection," *IEEE Transactions on Information Theory*, vol. 41, pp. 944–960, July 1995.

[169] X. Wang and A. Host-Madsen, "Group-Blind Multiuser Detection for Uplink CDMA," *IEEE Journal on Selected Areas in Communications*, vol. 17, pp. 1971–1984, November 1999.

[170] P. Spasojevic, X. Wang, and A. Host-Madsen, "Nonlinear Group-Blind Multiuser Detection," *IEEE Transactions on Communications*, vol. 49, pp. 1631 – 1641, September 2001.

[171] K. Yen and L. Hanzo, "Genetic algorithm assisted joint multiuser symbol detection and fading channel estimation for synchronous CDMA systems," *IEEE Journal on Selected Areas in Communications*, vol. 19, pp. 985 –998, June 2001.

[172] Q. Li, C. Georghiades, and X. Wang, "Blind multiuser detection in uplink CDMA with multipath fading: a sequential EM approach," *IEEE Transactions on Communications*, vol. 52, pp. 71–81, January 2004.

[173] J. Namgoong, T. F. Wong, and J. S. Lehnert, "Subspace multiuser detection for multicarrier DS-CDMA," *IEEE Transactions on Communications*, vol. 48, pp. 1897–1908, Nov. 2000.

[174] M. Torlak and G. Xu, "Blind multiuser channel estimation in asynchronous CDMA systems," *IEEE Transactions on Signal Processing*, vol. 45, pp. 137–147, Jan. 1997.

[175] D. Reynolds and X. Wang, "Adaptive Transmitter Optimization for Blind and Group-Blind Multiuser Detection," *IEEE Transactions on Signal Processing*, vol. 51, pp. 825–838, March 2003.

[176] Z. Ding and D. B. Ward, "Subspace approach to blind and semi-blind channel estimation for space-time block codes," *IEEE Transactions on Wireless Communications*, vol. 4, pp. 357–362, March 2005.

[177] W. Kang and B. Champagne, "Subspace-based blind channel estimation: generalization and performance analysis," *IEEE Transactions on Signal Processing*, vol. 53, pp. 1151–1162, March 2005.

[178] D. Kotoulas, P. Koukoulas, and N. Kalouptsidis, "Subspace projection based blind channel order estimation of MIMO systems," *IEEE Transactions on Signal Processing*, vol. 54, pp. 1351–1363, April 2006.

[179] J. K. Tugnait and W. Luo, "Blind space-time multiuser channel estimation in time-varying DS-CDMA systems," *IEEE Transactions on Vehicular Technology*, vol. 55, pp. 207–218, Jan. 2006.

[180] B. Hu, L. L. Yang, and L. Hanzo, "Performance of the Smart Antenna Aided Multicarrier DS-CDMA Uplink," *IEEE Vehicular Technology Conference, Fall 2004*, vol. 1, pp. 191–195, 26-29 Sept. 2004.

[181] B. Hu, L. L. Yang, and L. Hanzo, "Time-frequency-space diversity aided generalized multicarrier ds-cdma," *submitted to IEE Proc. Communications*, March 2006.

[182] B. Hu, L. L. Yang, and L. Hanzo, "Downlink beamforming, beam-selection transmit diversity and steered space-time spreading aided mc ds-cdma," *submitted to IEEE Transactions on Vehicular Technology*, March 2006.

[183] B. Hu, L. L. Yang, and L. Hanzo, "Performance of the Smart Antenna Aided Generalized Multicarrier DS-CDMA Downlink Using Both Time-Domain Spreading and Steered Space-Time Spreading," *IEEE Vehicular Technology Conference, Fall 2005*, vol. 1, pp. 458 – 462, 25-28 Sept. 2005.

[184] B. Hu, L. L. Yang, and L. Hanzo, "Differential Space-Time Modulation Schemes for Smart Antenna Aided Generalized Multicarrier DS-CDMA Systems," *to appear in Proceedings of IEEE Wireless Communications and Networking Conference 2006*, 3-6 April 2006.

[185] B. Hu, L. L. Yang, and L. Hanzo, "Downlink Differential Space-Time Spreading and Space-Time Steering Aided Generalized Multicarrier DS-CDMA," *submitted to IEEE Transactions on Wireless Communications*, October 2005.

[186] B. Hu, L. L. Yang, and L. Hanzo, "Adaptive Detection of Generalized Multicarrier DS-CDMA Employing Smart Antennas," *In Proceedings of the IEE International Conference on 3G Mobile Communication Technologies 2005*, 7-9 November 2005.

[187] B. Hu, L. L. Yang, and L. Hanzo, "Adaptive Detection in the Generalized Multicarrier DS-CDMA Uplink Using Both Receiver Diversity and Receiver Beamforming," *submitted to IEEE Transactions on Vehicular Technology*, January 2006.

[188] B. Hu, L. L. Yang, and L. Hanzo, "Subspace-Based Blind and Group-Blind Space-Time Multiuser Detection for the Generalized Multicarrier DS-CDMA Uplink," *submitted to IEEE Vehicular Technology Conference, Fall 2006*, 25-28 Sept. 2006.

[189] B. Hu, L. L. Yang, and L. Hanzo, "Time- and Frequency-Domain Spread Generalized Multicarrier DS-CDMA Using Subspace-Based Blind and Group-Blind Space-Time Multiuser Detection," *submitted to IEEE Transactions on Vehicular Technology*, February 2006.

[190] J. G. Proakis, *Digital Communications*. McGraw Hill, 3rd ed., 1995.

[191] J. H. Winters, "Optimum combining in digital mobile radio with cochannel interference," *Selected Areas in Communications*, vol. SAC-2, July 1984.

[192] L.-L. Yang and L. Hanzo, "Performance of Broadband Multicarrier DS-CDMA Using Space-Time Spreading-Assisted Transmit Diversity," *IEEE Transactions on Wireless Communications*, vol. 4, pp. 885–894, May 2005.

[193] T. Kailath, *Linear Systems*. Englewood Cliffs, N.J. USA: Prentice-Hall, 1981.

[194] C. Brunner, W. Utschick, and J. A. Nossek, "Exploiting the short-term and long-term channel properties in space and time: Eigenbeamforming concepts for the BS in WCDMA," *European Transactions on Telecommunications*, vol. 12, pp. 371–378, Aug. 1991.

[195] S. Verdu, *Multiuser Detection*. Cambridge University Press, 1998, 474 pages.

[196] B. Hochwald, T. L. Marzetta, and C. B. Papadias, "A transmitter diversity scheme for wideband CDMA systems based on space-time spreading," *IEEE Journal on Selected Areas in Communications*, vol. 19, pp. 48–60, January 2001.

[197] L.-L. Yang and L. Hanzo, "A space-time spreading assisted broadband multicarrier DS-CDMA scheme: System design and performance analysis," *Submitted for Possible Publication (http://www-mobile.ecs.soton.ac.uk/lly)*, July 2001.

[198] L.-L. Yang and L. Hanzo, "Performance analysis of space-time spreading assisted wideband CDMA systems communicating over multipath Nakagami fading channels," *Submitted for Possible Publication (http://www-mobile.ecs.soton.ac.uk/lly)*, May 2001.

[199] M. Abdulrahman, A. U. H. Sheikh, and D. D. Falconer, "Decision feed-back equalization for CDMA in indoor wireless communications," *IEEE Journal on Selected Areas in Communications*, vol. 12, pp. 698–706, May 1994.

[200] U. Madhow and M. L. Honig, "MMSE interference suppression for direct-sequence spread-spectrum cdma," *IEEE Transactions on Communications*, vol. 42, pp. 3178–3188, Dec. 1994.

[201] P. Rapajic and B. Vucetic, "Adaptive receiver structures for asynchronous CDMA systems," *IEEE Journal on Selected Areas in Communications*, vol. 12, pp. 685–697, May 1994.

[202] S. Miller and A. N. Barbosa, "A modified MMSE receiver for detection of DS-CDMA signals in fading channels," *Proceeding 1996 IEEE Military Communications Conference*, pp. 898–902, 1996.

[203] Z. Guo and K. B. Letaief, "Adaptive MMSE receiver with beamforming for DS/CDMA systems," *IEEE Transactions on Wireless Commmunications*, vol. 2, pp. 605–610, Jul. 2003.

[204] A. J. Viterbi, "Very low rate convolutional codes for maximum theoretical performance of spread-spectrum multiple-access channels," *IEEE Journal on Selected Areas in Communications*, vol. 8, pp. 641–649, May 1990.

[205] P. Patel and J. Holtzman, "Analysis of a simple successive interference cancellation scheme in DS/CDMA system," *IEEE Journal on Selected Areas in Communications*, vol. 12, pp. 796–807, June 1994.

[206] M. K. Varanasi and B. Aazhang, "Multistage detection in asychronous code-division multiple-access communications," *IEEE Transactions on Communications*, vol. 38, pp. 509–519, Apr. 1990.

[207] M. K. Varanasi and B. Aazhang, "Near-optimum detection in synchronous code-division multiple-access systems," *IEEE Transactions on Communications*, vol. 39, pp. 725–736, May 1991.

[208] S. Verdu, "Minimum Probability of Error for Asynchronous Gaussian Multiple-access Channels," *IEEE Transactions on Information Theory*, vol. IT-32, pp. 85–96, Jan. 1986.

[209] R. Lupas and S. Verdú, "Linear Mulituser Detectors for Synchronous Code Division Multiple Access Channel," *IEEE Transactions on Communications*, vol. 35, pp. 123–136, January 1989.

[210] R. Lupas and S. Verdú, "Near-Far Resistance of Multiuser Detectors in Asynchronous Channels," *IEEE Transactions on Communications*, vol. 38, pp. 509–519, April 1990.

[211] D. S. Chen and S. Roy, "An Adaptive Multiuser Receiver for CDMA Systems," *IEEE Journal on Selected Areas in Communications*, vol. 12, pp. 808–816, June 1994.

[212] G. Woodward and B. S. Vucetic, "Adaptive detection for DS-CDMA," *Proceedings of the IEEE*, vol. 86, pp. 1413–1434, July 1998.

[213] U. Mitra and H. V. Poor, "Adaptive receiver algorithms for near-far resistant CDMA," *IEEE Transactions on Communications*, vol. 43, pp. 1713–1724, 1995.

[214] U. Madhow, "MMSE interference suppression for timing acquisition and demodulation in direct-sequence CDMA systems," *IEEE Transactions on Communications*, vol. 46, pp. 1065–1075, August 1998.

[215] M. K. Tsatsanis, "Inverse filtering criteria for CDMA systems," *IEEE Transactions on Signal Processing*, vol. 45, pp. 102–112, Jan. 1997.

[216] A. J. Van Der Veen, E. F. Deprettere, and A. L. Swindlehurst, "Subspace-based signal analysis using singular value decomposition," *Proceedings of the IEEE*, vol. 81, pp. 1277–1308, Sept. 1993.

[217] S. E. Bensley and B. Aazhang, "Subspace-based channel estimation for code division multiple access communication systems," *IEEE Transactions on Communications*, vol. 44, pp. 1009–1020, Aug. 1996.

[218] E. G. Strom, S. Parkvall, S. L. Miller, and B. E. Ottersten, "Propagation Delay Estimation in Asynchronous Direct-Sequence Code-Division Multiple Access Systems," *IEEE Transactions on Communications*, vol. 44, pp. 84–93, Jan. 1996.

[219] H. Liu and G. Xu, "A subspace method for signal waveform estimation in synchronous CDMA systems," *IEEE Transactions on Communications*, vol. 44, pp. 1346–1354, Oct. 1996.

[220] A. Host-Madsen and X. Wang, "Performance of Blind and Group-Blind Multiuser Detection," *IEEE Transactions on Information Theory*, vol. 48, pp. 1849–1872, July 2002.

[221] S. Zhou, B. Muquet, and G. B. Giannakis, "Subspace-Based (Semi-) Blind Channel Estimation for Block Precoded Space-Time OFDM," *IEEE Transactions on Signal Processing*, vol. 50, pp. 1215–1228, May 2002.

[222] M. Wax and T. Kailath, "Detection of Signals by Information Theoretic Criteria," *IEEE Transactions on Acoustics, Speech and Signal Processing*, vol. 33, pp. 387 –392, April 1985.

[223] C. H. Bischof and G. M. Shroff, "On updating signal subspaces," *IEEE Transactions on Signal Processing*, vol. 40, pp. 1009–1020, August 1996.

[224] P. Comon and G. H. Golub, "Tracking a few extreme singular values and vectors in signal processing," *Proceedings of the IEEE*, vol. 78, pp. 1327–1343, August 1990.

[225] R. D. DeGroat, "Noniterative subspace tracking," *IEEE Transactions on Signal Processing*, vol. 40, pp. 571–577, March 1992.

[226] G. W. Stewart, "An updating algorithm for subspace tracking," *IEEE Transactions on Signal Processing*, vol. 40, pp. 1535–1541, June 1992.

[227] D. W. Tufts and C. D. Melissinos, "Simple, effective computation of principle eigenvectors and their eigenvalues and application to high resolution estimation of frequencies," *IEEE Transactions on Signal Processing*, vol. 34, pp. 1046–1053, Oct. 1986.

[228] B. Yang, "An extension of the PASTd algorithm to both rank and subspace tracking," *IEEE Transactions on Signal Processing*, vol. 2, pp. 179–182, Sept. 1995.

[229] X. Wang and H. V. Poor, *Wireless Communication Systems: Adavanced Techniques for Signal Reception*. Pearson Education, Inc., N.J. : Prentice Hall, 1st ed., 2003.

[230] A. E. Jones, T. A. Wilkinson, and S. K. Barton, "Block coding scheme for reduction of peak to mean envelope power ratio of multicarrier transmission schemes," *Electronics Letters*, vol. 30, pp. 2098–2099, December 1994.

[231] P. V. Eetvelt, S. J. Shepherd, and S. K. Barton, "The distribution of peak factor in QPSK multicarrier modulation," *Wireless Personal Communications*, vol. 2, pp. 87–96, 1995.

[232] C. Berrou, A. Glavieux, and P. Thitimajshima, "Near Shannon limit error-correcting coding and decoding: Turbo-codes," in *IEEE Int. Conference Communications ICC'93*, pp. 1064–1071, May 1993.

[233] C. Berrou and A. Glavieux, "Near optimum error correcting coding and decoding: turbo codes," *IEEE Transactions on Communications*, vol. 44, pp. 1261–1271, October 1996.

[234] G. Ungerböck, "Channel coding with multilevel/phase signals," *IEEE Transactions on Information Theory*, vol. 28, pp. 55–67, January 1982.

[235] P. Robertson and T. Wörz, "Bandwidth-Efficient Turbo Trellis-Coded Modulation Using Punctured Component Codes," *IEEE Journal on Selected Areas in Communications*, vol. 16, pp. 206–218, February 1998.

[236] D. Divsalar and M. K. Simon, "The Design of Trellis Coded MPSK for Fading Channel: Performance Criteria," *IEEE Transactions on Communications*, vol. 36, pp. 1004–1012, September 1988.

[237] J. S. Goldstein, I. S. Reed, and L. L. Scharf, "A multistage representation of the Wiener filter based on orthogonal projections," *IEEE Transactions on Information Theory*, vol. 44, pp. 2943–2959, Nov. 1998.

[238] M. L. Honig and J. S. Goldstein, "Adaptive reduced-rank interference suppression based on the multistage Wiener filter," *IEEE Transactions on Communications*, vol. 50, pp. 986–994, June 2002.

[239] A. Duel-Hallen, S. Hu, and H. Hallen, "Long range prediction of fading signals: enabling adaptive transmission for mobile radio channels," *IEEE Signal Processing Magzine*, vol. 17, pp. 62–75, May 2000.

# Glossary

| | |
|---|---|
| 2G | Second Generation |
| AE | Antenna Element |
| AIC | Akaike Information Criterion |
| ASTD | Adaptive Space-Time Detector |
| AWGN | Additive White Gaussian Noise |
| BER | Bit Error Ratio |
| BF | BeamForming |
| BLAST | Bell Laboratory's Layered Space-Time |
| BPSK | Binary Phase Shift Keying |
| BS | Base Station |
| BSTD | Beam Selection Transmit Diversity |
| BU | Bad Urban |
| CDMA | Code-Division Multiple-Access |
| CIR | Channel Impulse Response |
| CSI | Channel State Information |
| CSM | Cross-Spectral Metric |
| DD | Delay Diversity |
| DL | DownLink |
| DOA | Direction-Of-Arrival |
| DPSK | Differential Phase Shift Keying |
| DS-CDMA | Direct Sequence Code Division Multiple Access |
| DSCM | Differential Space-Code Modulation |
| DSSTS | Differential Steered Space-Time Spreading |
| DSTM | Differential Space-Time Modulation |

| | |
|---|---|
| DSTS | Differential Space-Time Spreading |
| EM | Expectation-Maximization |
| EVD | EigenValue-Decomposition |
| F-domain | Frequency-Domain |
| FD | F-Domain |
| FDCTF | Frequency-Domain Channel Transfer Function |
| FDD | Frequency Division Duplex |
| FFT | Fast Fourier Transform |
| FIR | Finite-duration Impulse Response |
| GA | Genetic Algorithm |
| GBSBEM | Geometrically Based Single Bounce Elliptical Model |
| GBSBM | Geometrically Based Single Bounce Microcell |
| GPRS | Generic Packet Radio System |
| GSM | Global System for Mobile Communication |
| IC | Interference Cancellation |
| IFFT | Inverse Fast Fourier Transform |
| ISI | Inter-Symbol Interference |
| LMS | Least-Mean-Square |
| LS | Least Squares |
| MAI | Multiple Access Interference |
| MC | MultiCarrier |
| MC CDMA | MultiCarrier Code Division Multiple Access |
| MC DS-CDMA | MultiCarrier Direct Sequence Code Division Multiple Access |
| MDL | Minimum Description Length |
| ML | Maximum Likelihood |
| MMSE | Minimum Mean-Square Error |
| MMSE/PIC | Minimum Mean Square Error/Parallel Interference Canceller |
| MOE | Minimum-Output-Energy |
| MPDR | Minimum Power Distortionless Response |
| MRC | Maximal Ratio Combining |
| MSE | Mean-Square Error |
| MSINR | Maximum Signal-to-Interference-plus-Noise Ratio |

| | |
|---|---|
| MSWF | Multi-Stage Wiener Filtering |
| MT CDMA | MultiTone CDMA |
| MUD | Multi-User Detection |
| MUI | Multi-User Interference |
| MVDR | Minimum Variance Distortionless Response |
| NAHJ-FST | Noise-Averaged Hermitian-Jacobi Fast Subspace Tracking |
| OFDM | Orthogonal Frequency Division Multiplexing |
| OTD | Orthogonal Transmit Diversity |
| P/S | Parallel to Serial |
| PASTd | Projection Approximation Subspace Tracking deflation |
| PC | Principal Components |
| PIC | Parallel Interference Canceller |
| PSTD | Phase Sweeping Transmit Diversity |
| RLS | Recursive-Least-Square |
| Rx | Receive |
| S/P | Serial-to-Parallel |
| SDMA | Space Division Multiple Access |
| SINR | Signal-to-Interference-plus-Noise Ratio |
| SNR | Signal-to-Noise Ratio |
| SSTS | Steered Space-Time Spreading |
| ST | Spatio-Temporal |
| ST-CIR | Spatio-Temporal CIR |
| STAR | Spatio-Temporal Array-Receiver |
| STD | Selection Transmit Diversity |
| STS | Space-Time Spreading |
| STTD | Space-Time Transmit Diversity |
| SVD | Singular Value-Decomposition |
| T-domain | Time-Domain |
| TCM | Trellis Coded Modulation |
| TD | T-domain |
| TD | Transmit Diversity |
| TDMA | Time-Division Multiple-Access |

| | |
|---|---|
| TF | Time and Frequency |
| TPA | Taylor Polynomial Approximation |
| TS | Time Slots |
| TSTD | Time Switched Transmit Diversity |
| TTCM | Turbo Trellis Coded Modulation |
| TU | Typical Urban |
| UL | Uplink |
| USD | Uniform Sectored Distribution |
| WH | Walsh-Hadamard |

# Index

## T



## U



## W

# Author Index